

ИНСТИТУТ ЗА ФИЗИКУ

ПРИМЉЕНО:		03. 02. 2022	
Ред.јед.	број	Арх.шифра	Прилог
0801	15211		

НАУЧНОМ ВЕЋУ  
ИНСТИТУТА ЗА ФИЗИКУ  
У БЕОГРАДУ

Предмет: Молба за покретање поступка за избор у звање виши научни сарадник

МОЛБА

Молим Научно веће Института за физику у Београду да у складу са Правилником о поступку, начину вредновања и квантитативном исказивању научноистраживачких резултата Министарства за просвету, науку и технолошки развој покрене поступак за мој избор у звање виши научни сарадник.

У прилогу достављам:

- Мишљење руководиоца са предлогом чланова комисије;
- Биографске податке;
- Преглед научне активности;
- Елементе за квалитативну оцену научног доприноса;
- Елементе за квантитативну оцену научног доприноса;
- Списак објављених научних радова и фотокопије радова објављених након претходног избора у звање;
- Податке о цитираности;
- Копију решења о претходном избору у звање;
- Додатне прилоге са доказима.

У Београду,  
3.02.2022.

С поштовањем

  
Сања Тошић

**НАУЧНОМ ВЕЋУ  
ИНСТИТУТА ЗА ФИЗИКУ  
У БЕОГРАДУ**

**Предмет: Мишљење руководиоца за избор др Сање Тошић у звање виши научни сарадник**

Др Сања Тошић запослена је у Лабораторији за атомске сударне процесе Института за физику у Београду од 2001. године. У претходном периоду била је ангажована на пројектима основних истраживања Министарства просвете, науке и технолошког развоја као и на неколико међународних пројеката у оквиру којих је учествовала у експерименталним истраживањима судара електрона са атомима метала и мањим молекулима, као и у истраживањима интеракције електрона и фотона са биомолекулима.

С обзиром да испуњава све критеријуме прописане Правилником о поступку, начину вредновања и квантитативном исказивању научноистраживачких резултата Министарства просвете, науке и технолошког развоја, сагласан сам са покретањем поступка за избор др Сање Тошић у звање виши научни сарадник.

Предлажем да комисију за избор др Сање Тошић у звање виши научни сарадник чине:

1. др Ненад Симоновић, научни саветник, Институт за физику у Београду,
2. др Владимир Срећковић, научни саветник, Институт за физику у Београду,
3. др Братислав Маринковић, научни саветник у пензији, Институт за физику у Београду и
4. проф. др Горан Попарић, редовни професор, Физички факултет, Универзитет у Београду

У Београду,  
03.02.2022

Руководилац лабораторије,



Др Ненад Симоновић

научни саветник

Институт за физику у Београду

## 1. БИОГРАФСКИ ПОДАЦИ

Сања Тошић рођена је у Зајечару 04. 06. 1973. године. Физички факултет – смер Примењена физика завршила је на Универзитету у Београду 2000. године са средњом оценом 9,08. Последипломске студије је уписала 2001. године на Физичком факултету Универзитета у Београду – смер Експериментална физика атома и молекула. Магистарску тезу је комплетирала у Лабораторији за атомске сударе Института за физику у Београду под руководством др Братислава Маринковића. Магистарску тезу под називом "*Еластично и нееластично расејање електрона на атому калцијума*" је одбранила 30. 06. 2006. године на Физичком факултету у Београду. Докторску тезу под називом "*Расејање електрона средњих енергија на атомима олова и сребра*" је такође урадила у Лабораторији за атомске сударе Института за физику под руководством др Братислава Маринковића и одбранила је 23. 03. 2012. година на Физичком факултету Универзитета у Београду.

У радном односу је од септембра 2001. године у Институту за физику у Београду. 30. 01. 2007. године изабрана је у звање истраживач сарадник а од 31.10.2012. је у звању научни сарадник. У исто звање реизабрана је 26.04.2018. године.

Била је ангажована на више националних пројеката финансираних од стране Министарства просвете, науке и технолошког развоја. Такође је била ангажована на пројекту „Nanoscale insights in radiation damage“ (2014-2015) под руководством др Братислава Маринковића. У питању је истраживачки пројекат од посебног значаја (Grande Rilevanza) изабран у оквиру извршног програма научне и технолошке сарадње између Републике Италије и Републике Србије. Била је руководилац другог Grande Rilevanza билатералног пројекта (Research area: Mathematics, Physics, Chemistry and Biology ) између Републике Италије и Републике Србије под насловом „A nanoview of radiation-biomatter interaction“ (2016 – 2018).

У периоду од 2014. године, учествовала је и на више пројеката на синхротронском извору зрачења Elettra у Трсту, Италија (на једном од њих као главни предлагач):

- “Energy flow in halogenated pyrimidines studied by site- and state-selective fragmentation” (2014, Proposal 20135431, Beamline GASPHASE Elettra synchrotron Trieste; Principal investigator: Paola Bolognesi, CNR-ISM, Roma, Italy);
- “Investigation of the fragmentation mechanisms of nitroimidazole radio sensitisers” (2015, Proposal 20150216, Beamline GASPHASE Elettra synchrotron Trieste ; Principal investigator: Paola Bolognesi, , CNR-ISM, Roma, Italy);
- “Investigation of the radiation damage mechanisms of chemotherapeutically active nitro compounds” (2016, Proposal 20160070, Beamline GASPHASE, Elettra synchrotron Trieste ; Principal nvestigator: Paola Bolognesi, CNR-ISM, Roma, Italy);
- “ Investigation of the fragmentation mechanisms of halogenated anesthetics” (2018, Proposal 20180158, Beamline GASPHASE Elettra synchrotron Trieste; Principal investigator: Sanja Tošić, IPB, Serbia);

Активно је учествовала на пројектима у оквиру 4 акције Европског програма за сарадњу у домену научних и технолошких истраживања - COST (European Cooperation in Science and Technology):

- MP1002 Nano - IBCT “Nanoscale insights into Ion Beam Cancer Therapy” (2010-2014);

- CM-1204 XLIC “XUV/X-ray light and fast ions for ultrafast chemistry” (2013-2017);
- CA-18222 AttoChem “Attosecond Chemistry” (2019-2023)
- CA18212 MD-GAS “Molecular Dynamics in the GAS phase” (2019-2023) - национални представник у менаџмент комитету, члан core групе, STSM (Short term scientific missions) координатор и ITC conference grants менаџер.

Сања Тошић је добитница награде *Проф. др Љубомир Ћирковић* за најбољи магистарски рад одбрањен на Физичком факултету 2006. године као и Студентске награде Института за физику 2007. године. Аутор/коаутор је 18 радова објављених у међународним часописима (од чега 15 у категорији M21, 2 у категорији M22, и један у категорији M23) као и већег броја саопштења на домаћим и међународним конференцијама. Резултати су презентовани и у склопу предавања по позиву на међународним и домаћим скуповима.

## 2. ПРЕГЛЕД НАУЧНЕ АКТИВНОСТИ

Научна активност др Сање Тошић везана је за област атомске, молекулске и хемијске физике, пре свега за експериментална истраживања основне феноменологије судара електрона са атомима и молекулима као и интеракције фотона из синхротронског радијационог извора са молекулима, првенствено биомолекулима у гасном стању.

Сударне интеракције електрона са различитим атомима и молекулима имају велику улогу у развоју модерне физике, и то не само атомске и молекулске већ и физике плазме, физике кондензованог стања, физике површина, физике атмосфере, астрофизике, биофизике али и многих других области где се управо помоћу механизма елементарних реакција у судару као и микроскопског понашања електрона, атома и молекула објашњавају неки макроскопски феномени.

Истраживање процеса интеракције синхротронског зрачења и нискоенергијских електрона са биомолекулима има како фундаментални значај тако и значај у примени где пружа важне податке за истраживања у научним областима, као што су биомедицина и истраживања радијационог оштећења живе материје.

У наставку су укратко описане активности кандидата у оквиру истраживачких тема.

*Напомена: Звездицом (\*) су означени радови публиковани у периоду након претходног избора у звање. У једном периоду научног рада, кандидаткиња је објављивала радове под презименом Милисављевић.*

### 2.1. Расејање електрона на атомима метала

Истраживање интеракција електрона са изолованим атомима под добро дефинисаним експерименталним условима има за циљ да се прошири знање о атомским процесима (разумевање структуре и динамике атомских честичних система) како би се исти могли карактеризовати у теоријским прорачунима атомских система. Налажење вероватноће, тј. диференцијалног пресека је од пресудног значаја за опис сударног процеса и у експерименталним и у теоријским истраживањима. Сам пресек је повезан са амплитудом



ресејања која је опет одређена типом интеракције, тј. интеракционим потенцијалом, структуром и физичким особинама честица, њиховом релативном брзином, таласним функцијама, углом ресејања. Избором одговарајућих параметара за посматрани систем и применом одговарајуће апроксимације, теорисјким путем се може израчунати прво амплитуда ресејања а преко ње и диференцијални пресек. Експериментално одређивање диференцијалног пресека заснива се на мерењу интензитета, тј. броја ресејаних електрона у функцији угла или енергије при чему између мереног сигнала и траженог пресека постоји директна зависност.

Од примарног интереса истраживања електронских сударних процеса је било еластично ресејање електрона средњих енергија, спектри губитака енергије и диференцијални пресеци за ексцитацију атома метала (Са, Рб, Аг, Ин). Сва мерења су извршена у режиму бинарних судара техником укрупњених млазева – електронског млаза произведеног у електронском топу и ефузионог млаза атома метала.

У циљу добијања поузданих вредности пресека било је потребно развити методологију мерења и унапредити низ експерименталних техника у електронској спектрометрији. У оквиру ове тематике Сања Тошић је радила на:

- анализи режима рада пећи за метале (захваљујући детаљном познавању рада са металним парама дала је значајан допринос конструисању система пећи за топљење метала у условима високог вакуума);
- калибрацији и тестирању експерименталног уређаја;
- методологији добијања атомског млаза мете атома метала који имају високу температуру топљења;
- методологији мерења релативних пресека и добијању апсолутних вредности диференцијалних пресека применом технике нормализације на оптичку јачину осцилатора.

Резултати до којих је дошла кандидаткиња у оквиру ове тематике представљају значајан научни допринос разумевању интеракције електрона са атомима метала, посебно тешким атомима (Аг и Рб) и у исто време представљају ригорозан тест за нове и квалитетније прорачуне интеракције електрона са атомима који имају релативно велики број електрона.

Резултати истраживања приказани су у следећим радовима:

(M21) \* B. P. Marinković, **S. D. Тошић**, D. Šević, R. P. McEachran, F. Blanco, G. Garcia and M. J. Brunger

Electron-impact excitation of the  $(4d^{10}5s) \ ^2S_{1/2} - (4d^95s^2) \ ^2D_{3/2}$  and  $(4d^{10}5s) \ ^2S_{1/2} - (4d^{10}6s) \ 2S_{1/2}$  transitions in silver: Experiment and theory

*Physical Review A*, **104** 022808 (2021)

doi: 10.1103/PhysRevA.104.022808

(M21)\* **S. D. Тошић**, V. Pejčev, D. Šević, R. P. McEachran, A. D. Stauffer and B. P. Marinković  
Electron-impact excitation of silver

*Physical Review A*, **91** 052703 (2015)

doi: 10.1103/PhysRevA.91.052703

(M21) **S. D. Тошић**, V. Pejčev, D. Šević, R. P. McEachran, A. D. Stauffer and B. P. Marinković  
Absolute differential cross sections for electron excitation of silver at small scattering angles

*Nuclear instruments & Methods in Physics Research Section B-Beam Interactions with Materials and Atoms*, **279** 53 (2012)

doi:10.1016/j.nimb.2011.10.066

(M21) **S. D. Tošić**, V. I. Kelemen, D. Šević, V. Pejčev, D. M. Filipović, E. Yu. Remeta and B. P. Marinković

Elastic electron scattering by silver atoms

*Nuclear instruments & Methods in Physics Research Section B-Beam Interactions with Materials and Atoms*, **267** 283 (2009)

doi:10.1016/j.nimb.2008.10.060

(M21) M. S. Rabasović, **S. D. Tošić**, D. Šević, V. Pejčev, D. M. Filipović and B. P. Marinković

Electron impact excitation of the  $6s\ ^2S_{1/2}$  state of In atom at small scattering angles

*Nuclear instruments & Methods in Physics Research Section B-Beam Interactions with Materials and Atoms*, **267** 279 (2009)

doi:10.1016/j.nimb.2008.10.056

(M21) M. S. Rabasović, V. I. Kelemen, **S. D. Tošić**, D. Šević, M. M. Dovahnych, V. Pejčev, D. M. Filipović, E. Yu. Remeta and B. P. Marinković

Experimental and theoretical study of the elastic electron-indium atom scattering in the intermediate energy range

*Physical Review A*, **77** 062713 (2008)

doi: 10.1103/PhysRevA.77.062713

(M21) **S. D. Tošić**, M. S. Rabasović, D. Šević, V. Pejčev, D. M. Filipović, Lalita Sharma, A. N. Tripathi, Rajesh Srivastava and B. P. Marinković

Elastic electron scattering by a Pb atom

*Physical Review A*, **77** 012725 (2008)

doi: 10.1103/PhysRevA.77.012725

(M21) **S. Milisavljević**, M. S. Rabasović, D. Šević, V. Pejčev, D. M. Filipović, Lalita Sharma, Rajesh Srivastava, A. D. Stauffer and B. P. Marinković

Excitation of the  $6p7s\ ^3P_{0,1}$  states of Pb atoms by electron impact: Differential and integrated cross sections

*Physical Review A*, **76** 022714 (2007)

doi: 10.1103/PhysRevA.76.022714

(M21) **S. Milisavljević**, M. S. Rabasović, D. Šević, V. Pejčev, D. M. Filipović, Lalita Sharma, Rajesh Srivastava, A. D. Stauffer and B. P. Marinković

Electron-impact excitation of the  $6p7s\ ^3P_1$  state of Pb atom at small scattering angles

*Physical Review A*, **75** 052713 (2007)

doi: 10.1103/PhysRevA.76.052713

(M22) B. P. Marinković, V. Pejčev, D. M. Filipović, D. Šević, **S. Milisavljević** and B. Predojević

Electron collisions by metal atom vapour

*Radiation Physics and Chemistry*, **76** 455 (2007).

(M21) **S. Milisavljević**, D. Šević, R. K. Chauhan, V. Pejčev, D. M. Filipović, R. Srivastava and B. P. Marinković

Differential and integrated cross sections for the elastic electron scattering by calcium atom

*Journal of Physics B: Atomic Molecular and Optical Physics*, **38** 2371 (2005)  
doi: 10.1088/0953-4075/38/14/004

(M21) S. Milisavljević, D. Šević, V. Pejčev, D. M. Filipović and B. P. Marinković  
Differential and integrated cross sections for the electron excitation of the  $4^1P_0$  state of calcium atom  
*Journal of Physics B: Atomic Molecular and Optical Physics*, **37** 3571 (2004)  
doi: 10.1088/0953-4075/37/18/002

## 2.2. Интеракција фотона са биомолекулима

Истраживање процеса интеракције синхротронског зрачења са биомолекулима има фундаментални значај и пружа важне податке за истраживања, пре свега у биомедицини где се последњих година посебна пажња поклања проучавању радијационог оштећења живе материје у циљу проналажења нових ефикаснијих метода у лечењу неких тешких болести као што је нпр. рак. У радиотерапији се користе различити извори зрачења, од фотона до електрона и јонских снопова при чему се свака врста зрачења различито понаша у интеракцији са биолошким материјалом тј. са ћелијама. Међутим, заједничко за све њих јесте недостатак селективности у смислу разликовања здравих од оболелих ћелија. Селективна, тј. „циљана“ радиотерапија омогућава смањење дозе зрачења којој се излаже пацијент и усто време повећава своје „штетно“ дејство на ћелије захваћене раком штедећи при томе здраве ћелије. Зато се у клиничким применама у комбинацији са зрачењем користе и специјални лекови, тзв. радиосенситизери. Проучавање физичких и хемијских механизма одговорних за особине ових молекула је од пресудног значаја за избор одговарајућег ефикасног радиосенситизера.

У оквиру ове тематике, а у сарадњи са колегама из Италије, кандидаткиња је проучавала могуће механизме радијационог оштећења као директну последицу апсорпцију X зрачења у халогеним дериватима пиримидина који представљају значајну класу радиосенситизер молекула. У експериментима је коришћена коинцидентна техника где су коначни производи карактеристичног фотојонизационог процеса у коелацији са временом при чему се добијају јединствене информације о фотофрагментацији посматраног молекула. Показано је да у молекулу пиримидина  $C_4H_4N_2$  фрагментација значајно зависи од енергије фотона тј. зависи од тога да ли је у питању резонантна електронска ексцитација  $1s$  електрона из најниже љуске три нееквивалентна угљеникова атома или једног атома азота у вишу непопуњену везивну молекулску  $\pi^*$  орбиталу. Резултати мерења на молекулима 2Br-пиримидина и 5Br-пиримидина такође указују да је фрагментација молекула функција супституената и њиховог положаја у прстену пиримидина.

Комбинован експериментални и теорисјки приступ је коришћен и у проучавању механизма фрагментације молекула имидазола ( $C_3H_4N_2$ ), нитроимидазола ( $C_3H_3N_3O_2$ ) и његова три изомера (4-, 5- и 2-нитроимидазол). Резултати масене спектрометрије и електрон-јон коинцидентне спектроскопије и овде показују битне разлике у фрагментацији индукованој VUV зрачењем. У експерименту је показано да постоје механизми који доводе до ослобађања неутрала као што су NO, CO и HCN који имају снажан утицај на биолошки материјал (ћелије) па као такви могу да имају значајну улогу у механизму деловања радиосенситизер молекула у току радиотерапије.

Резултати истраживања приказани су у следећим радовима:

(M22) \* P. Bolognesi, A. Kettunen, P. O’Keeffe, R. Richter, A. Cartoni, A. Casavola, M. Castrovilli, **S. Tosic**, B. Marinkovic and L. Avaldi

Inner shell photofragmentation of 2Cl-pyrimidine studied by mass spectrometry and electron-ion coincidence experiments

*Journal of Physics B: Atomic, Molecular and Optical Physics - Special issue on Frontiers of AMO Science with FELs and Synchrotron Radiation*, **53** 244004 (2020)

<https://doi.org/10.1088/1361-6455/abc146>

(M21) \* J. Chiarinelli, A. R. Casavola, M. C. Castrovilli, P. Bolognesi, A. Cartoni, Feng Wang, R. Richter, D. Catone, **S. Tosic**, B. P. Marinkovic and L. Avaldi

Radiation Damage Mechanisms of Chemotherapeutically Active Nitroimidazole Derived Compounds  
*Frontiers in Chemistry*, **7** 329 (2019)

(M21) \* P. Bolognesi, V. Carravetta, L. Sementa, G. Barcaro, S. Monti, P. M. Mishra, A. Cartoni, M. C. Castrovilli, J. Chiarinelli, **S. Tošić**, B.P. Marinković, R. Richter and L. Avaldi

Core Shell Investigation of 2-nitroimidazole

*Frontiers in Chemistry*, **7** 151 (2019)

(M21) \* P. Bolognesi, A. R. Casavola, A. Cartoni, R. Richter, P. Markus, S. Borocci, J. Chiarinelli, **S. Tošić**, H. Sa’adeh, M. Masič, B.P. Marinković, K.C. Prince and L. Avaldi

Communication: “Position” does matter: The photofragmentation of the nitroimidazole isomers  
*Journal of Chemical Physics*, **145** 191102 (2017)

doi: 10.1063/1.4967770

(M21) \* P. Bolognesi, J. A. Kettunen, A. Cartoni, R. Richter, **S. Tosic**, S. Maclot, P. Rousseau, R. Delaunay and L. Avaldi

Site- and state- selected photofragmentation of 2Br-pyrimidine

*Physical Chemistry Chemical Physics*, **17** 24063 (2015)

doi: 10.1039/C5CP02601F

### 2.3. Истраживање механизма фрагментације халогених анестетика

Постоји много фактора који диктирају правац и величину климатских промена. Пре свега, људске активности резултирају испуштањем велике количине различитих хемијских једињења у атмосферу која утичу на животну средину и здравље људи. С обзиром да су дугоживећа једињења која садрже хлор и бром директно одговорна за уништавање стратосферског озонског омотача, последњих година посебна пажња посвећена је халогеним анестетикима и њиховом доприносу и утицају на климатске промене. Наиме, инхалациони анестетици се веома мало метаболички мењају приликом клиничке употребе, остају у непромењеном облику и као такви могу заврше у атмосфери док молекули неких анестетика са дугим временом живота могу стићи и у стратосферу у значајним количинама. Као резултат фотојонизације тих молекула настају радикали који везују озон и на тај начин директно утичу на уништавање озонског омотача.

У оквиру ове истраживачке теме коју је Сања Тошић покренула, у сарадњи са колегама из CNR-ISM, извршена је опсежна и детаљна студија о механизму фотофрагментације

молекула халотена ( $C_2HBrClF_3$ ) једног од најчешће коришћених халогених анестетика (у поређењу са другим испарљивим анестетикима из исте групе (халогенизовани хлорофлуороугљеници) овај агенс који садржи бром је један од најактивнијих агенаса у смањењу озонског омотача). Прелиминарни добијени резултати показују неколико различитих путева фрагментације који садрже фрагменте уочене у атмосфери.

Такође је испитивана фрагментација и других халогених анестетика, односно молекула севофлурана ( $C_4H_3F_7O$ ), енфлурана ( $C_3H_2ClF_5O$ ) и изофлурана ( $C_3H_2ClF_5O$ ). Анализа добијених масених спектра, спектра добијених из коинциденције фотоелектрон-фотојон и NEXAFS (near edge X-ray absorption fine structure) спектра ових молекула је у току. Прелиминарни резултати су презентовани у виду неколико саопштења на конференцијама.

### 3. ЕЛЕМЕНТИ ЗА КВАЛИТАТИВНУ ОЦЕНУ НАУЧНОГ ДОПРИНОСА

#### 3.1. Квалитет научних резултата

##### 3.1.1. Научни ниво и значај научних резултата, утицај научних радова

Сања Тошић је у свом досадашњем научном раду објавила укупно 18 радова у међународним часописима са ISI листе, од чега 15 категорије M21 (врхунски међународни часописи), 2 категорије M22 (истакнути међународни часописи) и 1 рад у категорији M23 (међународни часописи). Такође је објавила 1 рад категорије M52 (рад у истакнутом националном часопису), 1 категорије M31 (предавање по позиву са међународног скупа штампано у целини), 1 категорије M32 (предавање по позиву са међународног скупа штампано у изводу), 9 категорије M33 (саопштење са међународног скупа штампано у целини), 28 категорије M34 (саопштење са међународног скупа штампано у изводу), 2 категорије M61 (предавање по позиву са скупа националног значаја штампано у целини), 2 категорије M63 (саопштење са скупа националног значаја штампано у целини), 3 категорије M64 (саопштење са скупа националног значаја штампано у изводу). У једном периоду научног рада објављивала је радове под презименом Милисављевић.

Кандидаткиња је након претходног избора у звање научни сарадник објавила 8 радова у међународним часописима са ISI листе. Од тога, 6 радова су категорије M21 (врхунски међународни часописи), 1 рад је категорије M22 (истакнути међународни часописи) и 1 рад у категорији M23 (међународни часописи). Поред тога, објавила је 1 рад категорије M31 (предавање по позиву са међународног скупа штампано у целини), 1 рад категорије M32 (предавање по позиву са међународног скупа штампано у изводу), 2 категорије M33 (саопштење са међународног скупа штампано у целини), 16 радова категорије M34 (саопштење са међународног скупа штампано у изводу). Такође, била је један од уредника зборника саопштења међународног скупа (M36).

Пет најзначајнијих радова:

1. (M21) P. Bolognesi, A. R. Casavola, A. Cartoni, R. Richter, P. Markus, S. Borocci, J. Chiarinelli, **S. Tošić**, H. Sa'adeh, M. Masič, B.P. Marinković, K.C. Prince and L. Avaldi  
Communication: "Position" does matter: The photofragmentation of the nitroimidazole isomers  
*Journal of Chemical Physics*, **145** 191102 (2017)

doi: 10.1063/1.4967770  
(ИФ 2.965, цитиран 15 пута)

2. (M21) P. Bolognesi, J. A. Kettunen, A. Cartoni, R. Richter, **S. Tosic**, S. Maclot, P. Rousseau, R. Delaunay and L. Avaldi  
Site- and state- selected photofragmentation of 2Br-pyrimidine  
*Physical Chemistry Chemical Physics*, **17** 24063 (2015)  
doi: 10.1039/C5CP02601F  
(ИФ 4.493, цитиран 22 пута)

3. (M21) **S. D. Tošić**, V. I. Kelemen, D. Šević, V. Pejčev, D. M. Filipović, E. Yu. Remeta and B. P. Marinković  
Elastic electron scattering by silver atoms  
*Nuclear instruments & Methods in Physics Research Section B-Beam Interactions with Materials and Atoms*, **267** 283 (2009)  
doi:10.1016/j.nimb.2008.10.060  
(ИФ 1.156, цитиран 19 пута)

4. (M21) **S. D. Tošić**, M. S. Rabasović, D. Šević, V. Pejčev, D. M. Filipović, Lalita Sharma, A. N. Tripathi, Rajesh Srivastava and B. P. Marinković  
Elastic electron scattering by a Pb atom  
*Physical Review A*, **77** 012725 (2008)  
doi: 10.1103/PhysRevA.77.012725  
(ИФ 2.908, цитиран 17 пута)

5. (M21) **S. Milisavljević**, D. Šević, V. Pejčev, D. M. Filipović and B. P. Marinković  
Differential and integrated cross sections for the electron excitation of the  $4^1P_0$  state of calcium atom  
*Journal of Physics B: Atomic Molecular and Optical Physics*, **37** 3571 (2004)  
doi: 10.1088/0953-4075/37/18/002  
(ИФ 1.969, цитиран 14 пута)

Први рад (*Journal of Chemical Physics*, **145** 191102 (2017)) урађен је на синхротрону Elettra у Трсту на гасној линији (GASPHASE). Комбинован експериментални и теорисјки приступ је коришћен у проучавању механизма фрагментације молекула имидазола ( $C_3H_4N_2$ ), нитроимидазола ( $C_3H_3N_3O_2$ ) и његова три изомера (4-, 5- и 2-нитроимидазола). Резултати масене спектрометрије и електрон-јон коинцидентне спектроскопије показују битне разлике у фрагментацији индукованој VUV зрачењем. У експерименту је показано да постоје механизми који доводе до ослобађања неутрала као што су NO, CO и HCN који имају снажан утицај на билошки материјал (ћелије) па као такви могу да имају значајну улогу у механизму деловања радиосенситајзер молекула у току радиотерапије. Конкретни научни допринос кандидаткиње у реализацији резултата се огледа у анализи масених и NEXAFS спектра што је самостално урадила. Елементи примењивости добијених научних резултата постоје, посебно у примени радиотерапије и употребе радиосенситајзера (потврђена разлика у делотворности изомера 4-нитроимидазола у односу на изомере истог молекула који се у медицини користи као радиосенситајзер).

Експериментална истраживања презентована у другом раду (*Physical Chemistry Chemical Physics*, **17** 24063 (2015)) су добијена на синхротрону Elettra и Лабораторији Института за истраживање материје у Риму. У овом раду кандидаткиња је проучавала могуће механизме

радијационог оштећења као директну последицу апсорпцију X зрачења у халогеним дериватима пиримидина (2Br-пиримидина и 5Br-пиримидина) који представљају значајну класу радиосенситивних молекула. У експериментима је коришћена коинцидентна техника где су коначни производи карактеристичног фотојонизационог процеса у корелацији са временом при чему се добијају јединствене информације о фотофрагментацији посматраног молекула. Показано је да у молекулу пиримидина  $C_4H_4N_2$  фрагментација значајно зависи од енергије фотона тј. зависи од тога да ли је у питању резонантна електронска ексцитација 1s електрона из најниже љуске три нееквивалентна угљеникова атома или једног атома азота у вишу непопуњену везивну молекулску  $\pi^*$  орбиталу. Резултати мерења на молекулима 2Br-пиримидина и 5Br-пиримидина такође указују да је фрагментација молекула функција супституената и њиховог положаја у прстену пиримидина. Као и у мерењима на молекулу нитроимидазола (први рад) , и овде се степен учешћа Сање Тошић у реализацији резултата огледа у равноправном учешћу у експерименталном делу рада и самосталној анализи дела добијених резултата (масени, NEXAFS, XPS спектри).

У трећем раду (*Nuclear instruments & Methods in Physics Research Section B-Beam Interactions with Materials and Atoms*, **267** 283 (2009)) презентована су експериментална и теоријска истраживања еластичног расејања електрона средњих енергија на атомима сребра, при чему је Сања Тошић дала кључни допринос експерименталном делу (мерења, анализа и тумачење измерених резултата). Угаоне зависности диференцијалних пресека за посматрани процес су измерене на апаратури ESMA у Институту за физику у Београду. Сва мерења су извршена у режиму бинарних судара техником укрштених млазева – електронског млаза произведеног у електронском топу и ефузионог млаза атома метала за електроне у опсегу енергија од 10eV до 100eV. Теоријски прорачуни су урађени коришћењем комплексног оптичког потенцијала (укључена спин-орбитна интеракција) са и без апсорције. Експерименталне апсолутне вредности пресека добијене су из односа интензитета еластичног и нееластичног сигнала (нераздвојена резонантна линија сребра  $4d^{10}5p^2P_{1/2, 3/2}$ ) на углу  $10^\circ$  на свакој упадној енергији електрона.

Експериментални резултати представљени у четвртном раду (*Physical Review A*, **77** 012725 (2008)) су такође добијени у Институту за физику у Београду. Поред тога, приказани су и резултати теоријских студија еластичног расејања електрона на атомима олова. Измерена је угаона расподела еластично расејаних електрона у средњем енергетском опсегу до 100 eV на угловима расејања од  $10^\circ$  до  $150^\circ$  (на угловима расејања мањим од  $10^\circ$  мерења нису одрађена због могућег утицаја примарног електронског снопа) и израчунати су одговарајући интегрални пресеци (интегрални, за пренос импулса, за вискозност). За теорисјко моделовање коришћен је метод релативистичког оптичког потенцијала коришћењем Hartree-Fock и Dirac-Fock таласних функција. Добијени резултати су представљали наставак наших ранијих истраживања процеса нееластичног расејања у систему електрон-атом олова. И у овом случају кандидаткиња је дала кључни допринос експерименталном делу рада. Радила је на развијању методологије мерења, пре свега на конструисању система пећи за топљење метала у условима високог вакуума и добијању атомског млаза мете атома метала који имају високу температуру топљења.

Пети рад (*Journal of Physics B: Atomic Molecular and Optical Physics*, **37** 3571 (2004)) даје приказ експерименталног проучавања електронске ексцитације  $4^1P$  стања атома калцијума.

Сања Тошић је учествовала у мерењу, радила је на анализи режима рада пећи за метале, калибрацији и тестирању експерименталног уређаја, на методологији мерења релативних пресека и добијању апсолутних вредности диференцијалних пресека применом одговарајуће технике нормализације. Такође је дала кључан допринос и у обради и тумачењу експерименталних резултата. По први пут су измерени диференцијални пресеци у процесу бинарних судара електрона средњих енергија (до 100eV) са атомима калцијума коришћењем методе укрштених млазева. Одрађена су мерења на малим угловима расејања (од 1° до 10°) и на угловима од 10° до 150°. Прва група мерења на малим угловима је посебно значајна због процеса нормирања. Наиме, прво су апсолутне вредности диференцијалног пресека на малим угловима добијене нормирањем генералисане јачине осцилатора на оптичку јачину осцилатора за дато стање а затим су пресеци на већим угловима једноставно „зашивени“ на тако добијене апсолутне пресеке. Диференцијални пресеци су екстраполирани до 180° и израчунати су и интегрални пресек, пресек за пренос импулса и за вискозност. Резултати су поређени са постојећим теоријским прорачуном (релативистички метод изобличених таласа).

Резултати до којих је дошла кандидаткиња и који су представљени у радовима 3, 4 и 5 представљају значајан научни допринос разумевању интеракције електрона са атомима метала, посебно тешким атомима (Ag и Pb) а у исто време представљају ригорозан тест за нове и квалитетније прорачуне интеракције електрона са атомима који имају релативно велики број електрона.

### **3.1.2. Позитивна цитираност научних радова**

Према Web of Science/Scopus цитатним базама, научни радови др Сање Тошић цитирани су 171/210 пута, односно 134 пута без самоцитата (h-index=9).

### **3.1.3. Параметри квалитета радова и часописа**

За процену квалитета часописа у којима су радови публиковани у наставку су приказане категорије часописа и њихов фактор утицаја, односно импакт фактор – ИФ (наведена је најбоља вредност из периода до две године уназад од када је рад објављен). Подвучени су фактори утицаја часописа у којима су објављени радови након претходног избора у звање.

Категорија M21

6 радова у *Physical Review A* (ИФ 3.140, ИФ 2.991, ИФ 2.908 за два рада, ИФ 3,047 за два рада);

2 рада у *Frontiers in Chemistry* (ИФ 4.155 за оба рада);

1 рад у *Journal of Chemical Physics* (ИФ 2.969);

1 рад у *Physical Chemistry Chemical Physics* (ИФ 4.493);

3 рада у *Nuclear instruments & Methods in Physics Research Section B-Beam Interactions with Materials and Atoms* (ИФ 1.266, ИФ 1.156 за два рада)

2 рада у *Journal of Physics B: Atomic Molecular and Optical Physics* (ИФ 1.913, ИФ 1,969)

Категорија M22



1 рад у *Journal of Physics B: Atomic, Molecular and Optical Physics - Special issue on Frontiers of AMO Science with FELs and Synchrotron Radiation* (ИФ 1.917)

1 рад у *Radiation Physics and Chemistry* (ИФ 0.934)

Категорија М23

1 рад у *Topical Review - Molecular Physics and Chemical Physics. Eur. Phys. J. D* (ИФ 1.425)

Укупан импакт-фактор радова др Сања Тошић износи 45.549, а фактор утицаја радова у периоду након избора у претходно звање је 25.245. Научни ниво и значај резултата је исказан кроз чињеницу да су радови публиковани у реномираним часописима који представљају референтне часописе у области атомске, молекулске и хемијске физике.

Додатни библиометријски показатељи према Упутству о начину писања извештаја о изборима у звања које је усвојио Матични научни одбор за физику приказани су у следећој табели:

	ИФ	М	СНИП
Укупно	25.245	56	7.452
Усредњено по чланку	3.156	7	0.931
Усредњено по аутору	2.596	5.89	1.44

### **3.1.4. Степен самосталности и степен учешћа у реализацији радова у научним центрима у земљи и иностранству**

Др Сања Тошић је након одбране докторске дисертације започела самосталан научни рад у оквиру Лабораторије за атомске сударне процесе Института за физику у Београду. Након боравка у CNR-ISM (Istituto di Struttura della Materia) у Риму, развила је и међународну сарадњу са истраживачком групом др Паоле Болоњези. Сарадња је реализована кроз учешће на неколико Beamline GASPHASE Elettra synchrotrone Trieste пројеката (#20135431 “Energy flow in halogenated pyrimidines studied by site- and state-selective fragmentation”; #20150216 “Investigation of the fragmentation mechanisms of nitroimidazole radio sensitizers”; #20160070 “Investigation of the radiation damage mechanisms of chemotherapeutically active nitro compounds”). Захваљујући овој сарадњи, Сања Тошић стиче експериментално искуство и покреће истраживачку тему Интеракција фотона са молекулима халогених анестетика. Била је главни истраживач на пројекту #20180158 “Investigation of the fragmentation mechanisms of halogenated anesthetics” (Beamline GASPHASE Elettra synchrotron Trieste). Резултат ове сарадње је 6 радова категорије М21, једно предавање по позиву (М32) и више саопштења на међународним конференцијама (М34).

Руководила је са српске стране заједничким пројектом у билатералној сарадњи са Италијом од посебног значаја - Research projects of particular relevance (Grande Rilevanza) selected within the frame of the executive programme of scientific and technological cooperation between

Italian Republic and Republic of Serbia – Research area: Mathematics, Physics, Chemistry and Biology: “A nanoview of radiation-biomatter interaction” (2016 – 2018). Такође је у претходном периоду била ангажована на пројекту „Nanoscale insights in radiation damage“ (Grande Rilevanza 2014-2015) под руководством др Братислава Маринковића.

Као члан core групе COST акције CA18212 MD-GAS “Molecular Dynamics in the GAS phase” (2019-2023), активно учествује у њеном раду и активностима. Најважнији резултати сарадње која је остварена у оквиру ове акције, представљени су у прегледном раду “Roadmap on dynamics of molecules and clusters in the gas phase”, *Topical Review - Molecular Physics and Chemical Physics. Eur. Phys. J. D 75*, 152 (2021).

### **3.1.5. Награде**

Сања Тошић је добитница награде *Проф. др Љубомир Ђирковић* за најбољи магистарски рад одбрањен на Физичком факултету 2006. године као и Студентске награде Института за физику 2007. Године

### **3.1.6. Елементи применљивости научних резултата**

Генерално, истраживање процеса интеракције синхротронског зрачења са биомолекулима има фундаментални значај и пружа важне податке за истраживања, пре свега у биомедицини где се последњих година посебна пажња поклања проучавању радијационог оштећења живе материје у циљу проналажења нових ефикаснијих метода у лечењу неких тешких болести. Елементи примењивости конкретних научних резултата добијених у оквиру ове тематике постоје, посебно у примени радиотерапије и употребе радиосенситизера (потврђена разлика у делотворности изомера 4-нитроимидазола у односу на изомере истог молекула који се у медицини користи као радиосенситизер).

Резултати добијени у оквиру тематике расејања електрона на атомима метала представљају улазне податке за експертске програме EELS анализе и као такви значајни су елементи одговарајућих база података. EELS (Electron energy loss spectroscopy) техника се користи за одређивање атомске структуре и хемијских својстава узорка, укључујући тип и количину присутних атома, хемијско стање атома и ефекте који настају као последица интеракције атома са суседним атомима.

## **3.2. Ангажованост у формирању научних кадрова**

Сања Тошић је била члан Комисије за такмичења из физике ученика средњих школа (школске 2011/2012, 2012/2013).

## **3.3. Нормирање броја коауторских радова, патената и техничких решења**

У периоду након претходног избора у звање Сања Тошић је објавила 8 радова, од којих се 2 рачунају са пуном тежином док је на 6 радова више од 7 аутора. Нормирање М бодова урађено је по правилнику а остварен и нормиран број М поена приказан је у табели у делу **4. Елементи за квантитативну оцену научног доприноса кандидата.** Укупан број М поена је 72.7, нормираних поена има 51.58 што је изнад захтеваног броја бодова за избор у звање виши научни сарадник.

### 3.4. Руковођење пројектима, потпројектима и пројектним задацима

Сања Тошић је била руководицац билатералног пројекта Republic of Serbia – Italy, 2016 – 2018: Research projects of particular relevance (Grande Rilevanza) selected within the frame of the executive programme of scientific and technological cooperation between Italian Republic and Republic of Serbia – Research area: Mathematics, Physics, Chemistry and Biology “A nanoview of radiation-biomatter interaction“.

Такође, била је главни истраживач на пројекту #20180158 “Investigation of the fragmentation mechanisms of halogenated anesthetics” (Beamline GASPHASE Elettra synchrotron Trieste).

На пројекту ОИ 171020 „Физика судара и фото процеса у атомским, (био)молекуларним и нано системима” руководила је задатком интеракција VUV зрачења са молекулом халотена на теми 3.1 истраживања интеракција синхротронског зрачења са (био)молекулима.

### 3.5. Активност у научним и научно-стручним друштвима

- Члан Одељења Друштва физичара Србије за научна истраживања и високо образовање у Одсеку за атомску и молекулску физику.
- Члан Комисије за такмичења из физике ученика средњих школа (школске 2011/2012, 2012/2013).
- Члан научног комитета међународних научних конференција:
  - SPIG 2018 (<http://www.spig2018.ipb.ac.rs/committee.html>),
  - SPIG 2020 (<http://spig2020.ipb.ac.rs/committee.html>)
- Члан научног комитета 2nd general meeting of the COST Action CA18212 ([https://mdgas.eu/single\\_event.php?post-slug=2nd-general-meeting-of-the-cost-action-ca18212](https://mdgas.eu/single_event.php?post-slug=2nd-general-meeting-of-the-cost-action-ca18212))
- Члан core групе COST акције Molecular Dynamics in the GAS phase MD-GAS CA18212 (STSM и ИТC grants координатор). ([https://mdgas.eu/core\\_group.php](https://mdgas.eu/core_group.php))
- Члан организационих комитета међународних научних конференција:
  - POSMOL 2019, XX International Workshop on Low-Energy Positron and Positronium Physics, XXI International Symposium on Electron-Molecule Collisions and Swarms 18 - 20 July 2019, Belgrade, Serbia.
  - COST Action CM1204 (XUV/X-ray light and fast ions for ultrafast chemistry) Working Group 2 Expert Meeting on Biomolecules, April 27-30, 2015, Fruška gora, Serbia
  - 27<sup>th</sup> Summer School and International Symposium on the Physics of Ionized Gases - SPIG 2014, 26 – 29 August 2012, Belgrade, Serbia.
  - 5<sup>th</sup> International Conference on Elementary Processes in Atomic Systems - CEPAS, 22-24 June 2011, Belgrade, Serbia.
  - 23<sup>rd</sup> Summer School and International Symposium on the Physics of Ionized Gases - SPIG 2006, 28 August - 1 September 2006, Kopaonik, Serbia.
- Уредник зборника радова са међународне конференције POSMOL 2019, XX International Workshop on Low-Energy Positron and Positronium Physics, XXI International Symposium on Electron-Molecule Collisions and Swarms 18 - 20 July 2019, Belgrade, Serbia ([http://posmol2019.ipb.ac.rs/\\_files/Book\\_POSMOL2019\\_Online.pdf](http://posmol2019.ipb.ac.rs/_files/Book_POSMOL2019_Online.pdf))

### 3.6. Утицај научних резултата

Утицајност научних радова кандидаткиње је наведена у одељцима **3.1. Квалитет научних резултата**. Пун списак радова дат је у одељку 5, док су подаци о цитираности наведени након списка свих радова.

### 3.7. Конкретан допринос кандидата у реализацији радова у научним центрима у земљи и иностранству

За више детаља о доприносу кандидаткиње у реализацији радова у научним центрима у земљи и иностранству погледати одељак **3.1.1. Научни ниво и значај научних резултата, утицај научних радова** и **3.1.4. Степен самосталности и степен учешћа у реализацији радова у научним центрима у земљи и иностранству**.

### 3.8. Уводна предавања на конференцијама, друга предавања и активности

#### - Sanja D. Tošić

Measurements of differential cross sections for elastic electron scattering and electronic excitation of silver and lead atoms

26th Summer School and International Symposium on the Physics of Ionized Gases – SPIG 2012, 27-31 August 2012, Zrenjanin, Serbia

#### - S. Tošić, P. Bolognesi, L. Avaldi, R. Richter and B. P. Marinković

Fragmentation of halothane molecule by synchrotron radiation

The Workshop on X-ray Interaction with Biomolecules in Gas Phase (XiBiGP), 28th Summer School and International Symposium on the Physics of Ionized Gases – SPIG 2016, August 29th-Sept 2nd 2016, Belgrade, Serbia.

## 4. ЕЛЕМЕНТИ ЗА КВАНТИТАТИВНУ ОЦЕНУ НАУЧНОГ ДОПРИНОСА КАНДИДАТА

### Остварени М-бодови кандидата у периоду након претходног избора у звање

Категорија	М бодова по раду	Број радова	Укупно М бодова	Нормирано М бодова
M21	8	6	48	33.43
M22	5	1	5	3.125
M23	3	1	3	0.357
M31	3.5	1	3.5	3.5
M32	1.5	1	1.5	1.5
M33	1	2	2	2
M34	0.5	16	8	5.97

M36	1.5	1	1.5	1.5
M64	0.2	1	0.2	0.2

**Поређење оствареног броја М-бодова са минималним условима потребним за избор у звање виши научни сарадник:**

Минималан број М бодова		Остварено	Остварено нормирано
Укупно	50	72.7	51.58
M10+M20+M31+M32+M33+M41+M42+M90	40	63	43.912
M11+M12+M21+M22+ M23	30	56	36.912

## 5. СПИСАК ОБЈАВЉЕНИХ НАУЧНИХ РАДОВА

### Радови у врхунским међународним часописима (M21)

*Радови објављени након претходног избора у звање*

1. B. P. Marinkovic, **S. D. Tosić**, D. Sevic, R. P. McEachran, F. Blanco, G. Garcia and M. J. Brunger  
Electron-impact excitation of the  $(4d^{10}5s) \ ^2S_{1/2} - (4d^95s^2) \ ^2D_{3/2}$  and  $(4d^{10}5s) \ ^2S_{1/2} - (4d^{10}6s) \ 2S_{1/2}$  transitions in silver: Experiment and theory  
*Physical Review A*, **104** 022808 (2021)  
<https://doi.org/10.1103/PhysRevA.104.022808>  
IF 3.140, M = 8

2. J. Chiarinelli, A. R. Casavola, M. C. Castrovilli, P. Bolognesi, A. Cartoni, Feng Wang, R. Richter, D. Catone, **S. Tosić**, B. P. Marinkovic and L. Avaldi  
Radiation Damage Mechanisms of Chemotherapeutically Active Nitroimidazole Derived Compounds  
*Frontiers in Chemistry*, **7** 329 (2019)  
<https://doi.org/10.3389/fchem.2019.00329>  
IF 4.155,  $M_{norm} = 4.44$

3. P. Bolognesi, V. Carravetta, L. Sementa, G. Barcaro, S. Monti, P. M. Mishra, A. Cartoni, M. C. Castrovilli, J. Chiarinelli, **S. Tošić**, B.P. Marinković, R. Richter and L. Avaldi  
Core Shell Investigation of 2-nitroimidazole  
*Frontiers in Chemistry*, **7** 151 (2019)  
<https://doi.org/10.3389/fchem.2019.00151>  
IF 4.155,  $M_{norm} = 3.64$

4. P. Bolognesi, A. R. Casavola, A. Cartoni, R. Richter, P. Markus, S. Borocci, J. Chiarinelli, **S. Tošić**, H. Sa'adeh, M. Masić, B.P. Marinković, K.C. Prince and L. Avaldi  
Communication: "Position" does matter: The photofragmentation of the nitroimidazole isomers  
*Journal of Chemical Physics*, **145** 191192 (2017)  
doi: 10.1063/1.4967770  
IF 2.965,  $M_{norm} = 3.64$

5. P. Bolognesi, J. A. Kettunen, A. Cartoni, R. Richter, **S. Tosic**, S. Maclot, P. Rousseau, R. Delaunay and L. Avaldi  
Site- and state- selected photofragmentation of 2Br-pyrimidine  
*Physical Chemistry Chemical Physics*, **17** 24063 (2015)  
doi: 10.1039/C5CP02601F  
IF 4.493,  $M_{\text{norm}} = 5.71$

6. **S. D. Tošić**, V. Pejčev, D. Šević, R. P. McEachran, A. D. Stauffer and B. P. Marinković  
Electron-impact excitation of silver  
*Physical Review A*, **91** 052703 (2015)  
doi: 10.1103/PhysRevA.91.052703  
IF 2.991,  $M = 8$

Радови објављени пре претходног избора у звање

1. **S. D. Tošić**, V. Pejčev, D. Šević, R. P. McEachran, A. D. Stauffer and B. P. Marinković  
Absolute differential cross sections for electron excitation of silver at small scattering angles  
*Nuclear instruments & Methods in Physics Research Section B-Beam Interactions with Materials and Atoms*, **279** 53 (2012)

doi:10.1016/j.nimb.2011.10.066

2. **S. D. Tošić**, V. I. Kelemen, D. Šević, V. Pejčev, D. M. Filipović, E. Yu. Remeta and B. P. Marinković

Elastic electron scattering by silver atoms

*Nuclear instruments & Methods in Physics Research Section B - Beam Interactions with Materials and Atoms*, **267** 283 (2009)

doi:10.1016/j.nimb.2008.10.060

3. M. S. Rabasović, **S. D. Tošić**, D. Šević, V. Pejčev, D. M. Filipović and B. P. Marinković  
Electron impact excitation of the  $6s^2S_{1/2}$  state of In atom at small scattering angles

*Nuclear instruments & Methods in Physics Research Section B - Beam Interactions with Materials and Atoms*, **267** 279 (2009)

doi:10.1016/j.nimb.2008.10.056

4. M. S. Rabasović, V. I. Kelemen, **S. D. Tošić**, D. Šević, M. M. Dovhanych, V. Pejčev, D. M. Filipović, E. Yu. Remeta and B. P. Marinković

Experimental and theoretical study of the elastic electron-indium atom scattering in the intermediate energy range

*Physical Review A*, **77** 062713 (2008)

doi: 10.1103/PhysRevA.77.062713

5. **S. D. Tošić**, M. S. Rabasović, D. Šević, V. Pejčev, D. M. Filipović, Lalita Sharma, A. N. Tripathi, Rajesh Srivastava and B. P. Marinković

Elastic electron scattering by a Pb atom

*Physical Review A*, **77** 012725 (2008)

doi: 10.1103/PhysRevA.77.012725

6. **S. Milisavljević**, M. S. Rabasović, D. Šević, V. Pejčev, D. M. Filipović, Lalita Sharma, Rajesh Srivastava, A. D. Stauffer and B. P. Marinković

Excitation of the  $6p7s^3P_{0,1}$  states of Pb atoms by electron impact: Differential and integrated cross sections

*Physical Review A*, **76** 022714 (2007)

doi: 10.1103/PhysRevA.76.022714

7. **S. Milisavljević**, M. S. Rabasović, D. Šević, V. Pejčev, D. M. Filipović, Lalita Sharma, Rajesh Srivastava, A. D. Stauffer and B. P. Marinković

Electron-impact excitation of the  $6p7s\ ^3P_1$  state of Pb atom at small scattering angles  
*Physical Review A*, **75** 052713 (2007)

doi: 10.1103/PhysRevA.76.052713

8. **S. Milisavljević**, D. Šević, R. K. Chauhan, V. Pejčev, D. M. Filipović, R. Srivastava and B. P. Marinković

Differential and integrated cross sections for the elastic electron scattering by calcium atom  
*Journal of Physics B: Atomic Molecular and Optical Physics*, **38** 2371 (2005)

doi: 10.1088/0953-4075/38/14/004

9. **S. Milisavljević**, D. Šević, V. Pejčev, D. M. Filipović and B. P. Marinković

Differential and integrated cross sections for the electron excitation of the  $4^1P_0$  state of calcium atom  
*Journal of Physics B: Atomic Molecular and Optical Physics*, **37** 3571 (2004)

doi: 10.1088/0953-4075/37/18/002

### Радови у истакнутим међународним часописима (M22)

Рад објављени након претходног избора у звање

1. P. Bolognesi, A. Kettunen, P. O’Keeffe, R. Richter, A. Cartoni, A. Casavola, M. Castrovilli, **S. Tosić**, B. Marinković and L. Avaldi

Inner shell photofragmentation of 2Cl-pyrimidine studied by mass spectrometry and electron-ion coincidence experiments

*Journal of Physics B: Atomic, Molecular and Optical Physics - Special issue on Frontiers of AMO Science with FELs and Synchrotron Radiation*, **53** 244004 (2020)

<https://doi.org/10.1088/1361-6455/abc146>

IF 1.917,  $M_{\text{norm}} = 3.125$

Рад објављени пре претходног избора у звање

2. B. P. Marinković, V. Pejčev, D. M. Filipović, D. Šević, **S. Milisavljević** and B. Predojević

Electron collisions by metal atom vapour

*Radiation Physics and Chemistry*, **76** 455 (2007).

<https://doi.org/10.1016/j.radphyschem.2006.01.018>

### Рад у међународном часопису (M23)

Рад објављени након претходног избора у звање

1. H. Zettergren, A. Domaracka, T. Schlathölter, P. Bolognesi, S. Díaz-Tendero, M. Łabuda, **S. Tosić et al.**

Roadmap on dynamics of molecules and clusters in the gas phase.

Topical Review - Molecular Physics and Chemical Physics. *Eur. Phys. J. D* **75**, 152 (2021).

<https://doi.org/10.1140/epjd/s10053-021-00155-y>

IF 1.425,  $M_{\text{norm}} = 0.357$

### Предавање по позиву са међународног скупа штампано у целини (M31)

Рад објављени након претходног избора у звање

**1. S. D. Tošić**

Measurements of differential cross sections for elastic electron scattering and electronic excitation of silver and lead atoms

26<sup>th</sup> Summer School and International Symposium on Physics of Ionized Gases SPIG, 27<sup>th</sup> – 30<sup>th</sup> Aug. 2012, Zrenjanin, Serbia

*Journal of Physics: Conference Series*, **399** 012004 (2012).

**Предавање по позиву са међународног скупа штампано у изводу (M32)**

Рад објављени након претходног избора у звање

**1. S. Tošić, P. Bolognesi, L. Avaldi, R. Richter and B. P. Marinković**

Fragmentation of halothane molecule by synchrotron radiation

The Workshop on X-ray Interaction with Biomolecules in Gas Phase (XiBiGP), August 29<sup>th</sup> 2016, Belgrade, Serbia

**Саопштења са међународног скупа штампана у целини (M33)**

Радови објављени након претходног избора у звање

**1. Paola Bolognesi, Sanja Tosic, Bratislav Marinkovic and Lorenzo Avaldi**

A nanoscale insight in radiation damage

in e-Book Serbia - Italia: Italian - Serbian Bilateral Cooperation on Science, Technology and Humanities, Eds. P. R. Andjus and P. Battinelli, 16th November 2015, University of Belgrade, Section I: Research Projects of Particular Relevance 2013 – 2015, pp.33-37.

Association of Italian and Serbian Scientists and Scholars (AIS3)

**2. S. D. Tošić, V. Pejčev, D. Šević, R. P. McEachran, A. D. Stauffer and B. P. Marinković**

Integrated cross sections for electron excitation of the 4d105p state of the Ag atom

27<sup>th</sup> Summer School and Int. Symp. on Physics of Ionized Gases – SPIG 2014, 26th - 29th August 2014, Belgrade, Serbia, pp.46-49.

Радови објављени пре претходног избора у звање

**1. S. D. Tošić, D. Šević, V. Pejčev, D. M. Filipović and B. P. Marinković**

Electron impact excitation of Ag atom: energy-loss spectroscopy

24<sup>th</sup> Symposium on Physics of Ionized Gases – SPIG 2008, 25 – 29 August 2008, Novi Sad, Serbia, pp. 45 – 48.

**2. B. P. Marinković, V. Pejčev, D. M. Filipović, D. Šević, A. R. Milosavljević, S. Milisavljević, M. S. Rabasović, D. Pavlović and J. B. Maljković,**

“Cross section data for electron collisions in plasma physics”,

5<sup>th</sup> EU-Japan Joint Symposium on Plasma Processing (*Radicals and Non-Equilibrium Processes in Low-Temperature Plasmas*), 7 – 9 March 2007, Belgrade, Serbia, Abstracts of Invited Lectures, Progress Reports and Contributed Papers, Eds. Z. Lj. Petrović, N. Mason, S. Hamaguchi, M. Radmilović-Radjenović, (Serbian Academy of Sciences and Arts, Institute of Physics: Belgrade, 2007) Invited Lecture p.I-12.

*Journal of Physics: Conference Series*, **86**, 012006 (2007).

doi: 10.1088/1742-6596/86/1/012006



3. B. P. Marinković, D. M. Filipović, V. Pejčev, D. Šević, A. R. Milosavljević, D. Pavlović, **S. Milisavljević**, P. Kolarž and M. Pardjovska  
Low energy interactions with bio-molecules  
XXIV ICPEAC Int. Conf. Photonic, Electronic and Atomic Collisions, Rosario, Argentina, Eds. P D Fainstein, M A P Lima, J E Miraglia, E C Montenegro and R D Rivarola, World Scientific 2006, ISBN 981-270-412-4, Progress Report, pp. 336 – 342.
4. **S. Milisavljević**, M. Pardjovska, D. Šević, V. Pejčev, D.M. Filipović and B.P. Marinković  
Electron impact excitation of the  $6p7s\ ^3P_1$  state of Pb atom at Small Scattering Angles: Generalized Oscillator Strengths  
23<sup>rd</sup> Symposium on the Physics of Ionized Gases – SPIG 2006, August 28<sup>th</sup>- September 1<sup>st</sup> 2006, Kopaonik, Serbia, pp. 55 – 58.
5. M. Pardjovska, **S. Milisavljević**, V. Pejčev, D. Šević, D.M. Filipović, B.P. Marinković, V. I. Kelemen, E. Yu. Remeta and E. P. Sabad  
Differential Cross Section for Elastic Electron Scattering by In Atom  
23<sup>rd</sup> Symposium on the Physics of Ionized Gases – SPIG 2006, August 28<sup>th</sup>- September 1<sup>st</sup> 2006, Kopaonik, Serbia, pp. 71 – 74.
6. **S. Milisavljević**, M. Pardjovska, D. Šević, V. Pejčev, D. M. Filipović and B. P. Marinković  
Differential Cross Section for Elastic Electron Scattering by Pb Atom  
22<sup>nd</sup> Symposium on Physics of Ionized Gases – SPIG 2004, 23-27 August 2004, National Park Tara, Bajna Bašta, Serbia and Montenegro, pp. 73 – 75.
7. **S. Tošić**, D. Šević, V. Pejčev, D. M. Filipović and B. P. Marinković  
Differential cross sections for elastic electron scattering by Ca atom  
21<sup>st</sup> Symposium on Physics of Ionized Gases – SPIG 2002, 26-30 August 2002, Soko Banja, Yugoslavia, pp. 26 – 29.

**Саопштења са међународног скупа штампана у изводу (M34)**

*Радови објављени након претходног избора у звање*

1. **S. D. Tošić**, D. Šević and B. P. Marinković  
Excitation of silver atoms from the ground S state to the first excited P state by electron impact  
BOOK OF ABSTRACTS AND CONTRIBUTED PAPERS, III Meeting on Astrophysical Spectroscopy - A&M DATA December 6 to 9, 2021, Palić, Serbia, p.13
2. **S. D. Tošić**, D. Šević and B. P. Marinković  
Integrated cross sections for electron impact excitation of atomic silver  
BOOK OF ABSTRACTS AND CONTRIBUTED PAPERS, III Meeting on Astrophysical Spectroscopy - A&M DATA December 6 to 9, 2021, Palić, Serbia, p.14
3. B. P. Marinković, D. Šević, S. Ivanović, N. Uskoković, **S. D. Tošić**, M. S. Rabasović and B. Predojević  
Electron-metal atom vapor cross sections maintained within BEAM database  
BOOK OF ABSTRACTS AND CONTRIBUTED PAPERS, III Meeting on Astrophysical Spectroscopy - A&M DATA December 6 to 9, 2021, Palić, Serbia, p.11
4. H. Delibašić Marković, V. Petrović, I. Petrović and **S. Tošić**

Investigation and modeling of the free-electron density and temperature during the formation of laser-induced breakdown of plasma in air at various laser parameters  
BOOK OF ABSTRACTS AND CONTRIBUTED PAPERS, III Meeting on Astrophysical Spectroscopy - A&M DATA December 6 to 9, 2021, Palić, Serbia, p.50

5. **S. D. Tošić**, M. Radibratović, J. Chiarinelli, M. Milčić, P. Bolognesi, L. Avaldi, R. Richter, M. Coreno and B. P. Marinković

Photo-induced fragmentation of the titanium (IV) iso-propoxide molecule  
Proc. Twenty-first International Summer School on Vacuum, Electron and Ion Technologies (VEIT 2019), 23 – 27 September 2019, Sozopol, Bulgaria, Poster contribution PC14, p.128.

6. **S. D. Tošić**, M. Radibratović, J. Chiarinelli, M. Milčić, P. Bolognesi, L. Avaldi, R. Richter, M. Coreno and B. P. Marinković

Inner-shell spectroscopy of titanium (IV) iso-propoxide  
Proc. PHOTONICA2019 - The Seventh International School and Conference on Photonics, 26 August – 30 August 2019, Belgrade, Serbia & Machine Learning with Photonics Symposium (ML-Photonica 2019) & ESUO Regional Workshop & COST action CA16221, Book of Abstracts, print:p.167; on-line: p.183

7. M. Radibratović, **S. D. Tošić**, M.C. Castrovilli, J. Chiarinelli, P. Bolognesi, L. Avaldi, R. Richter, M. Coreno, B. P. Marinković and M. K. Milčić

Computational tools for studying X-ray-molecule interactions: photofragmentation of halothane  
Proc. The Workshop on X-ray Interaction with Biomolecules in Gas Phase (XiBiGP), August 28th 2018, Belgrade, Serbia: In the book: 29th Summer School and Int. Symp. on Physics of Ionized Gases – SPIG 2018, August 28th – Sept 1st. 2018, Belgrade, Serbia Invited Talk, p.326. ISBN 978-86-7306-146-7

8. **S. D. Tošić**, M. Radibratović, M. Milčić, P. Bolognesi, L. Avaldi, R. Richter, M. Coreno and B. P. Marinković

The photofragmentation of the core excited halothane molecule  
7th Conference on Elementary Processes in Atomic Systems (CEPAS), 03-06 September 2017, Pruhonice, Czech Republic, Poster presentation, M-25.

9. J. Chiarinelli, P. Bolognesi, A. Casavola, A. Cartoni, M. C. Castrovilli, D. Catone, R. Richter, S. Borocci, **S. Tošić**, H. Sa'adeh, M. Masič, B. P. Marinković, K. C. Prince, and L. Avaldi

“Position” does matter: The photofragmentation of the nitroimidazole isomers  
XXX International Conference on Photonic, Electronic, and Atomic Collisions (ICPEAC2017), 26 July- 1 August 2017, Cairns, Queensland, Australia, Abstracts, TH-40  
*Journal of Physics: Conf. Series* **875** 032007 (2017)  
doi:10.1088/1742-6596/875/4/032007

10. P. Bolognesi, A. R. Casavola, A. Cartoni, R. Richter, P. Markus, S. Borocci, J. Chiarinelli, **S. Tošić**, H. Sa'adeh, M. Masič, B. P. Marinković, K. C. Prince, and L. Avaldi

“Position” does matter: The photofragmentation of the nitroimidazole isomers  
4<sup>th</sup> XLIC General Meeting COST Action CM1204, 14-16 March 2017, Prague, Czech Republic, Book of Abstracts, Editors: Miroslav Polasek, Vera Krizova (J. Heyrovsky Institute of Physical Chemistry of the CAS, v.v.i., Prague, 2017) Poster presentation, p.68.  
ISSN: 978-80-87351-41-3

11. P. Bolognesi, A. Kettunen, A. Cartoni, R. Richter, **S. Tošić**, S. Maclot, P. Rousseau,

R. Delaunay, P. Markus, H. Sa'adeh, Maša Masič, B. Marinković, K. Prince, L. Avaldi  
Search for the ‘molecular scissor’ via site- and state selected molecular fragmentation studies  
3rd General Meeting of XLIC (XUV/X-ray light and fast ions for ultrafast chemistry) COST Action

CM1204, 2-4 November 2015 Debrecen, Hungary, Programme and Book of Abstracts, Editor: P. Badankó, Poster presentation, p.64.  
ISBN: 978-963-832-51-0 (Károly Tökési,, Atomki, Hungary)

12. P. Bolognesi, M.C. Castrovilli, A. Kettunen, A. Cartoni, R. Richter, **S. Tosic**, S. Maclot, P. Rousseau, R. Delaunay, A. Domaracka, B. Huber and L. Avaldi  
Fragmentation of halopyrimidines and halouraciles by photoionization and ion impact  
Proc. WG2 Expert Meeting on Biomolecules, COST Action CM1204, XLIC - XUV/X-ray Light and fast Ions for ultrafast Chemistry, April 27- 30, 2015, Book of Abstracts, Eds. P Bolognesi and A Milosavljevic, Invited Talk, p.41.

13. P. Bolognesi, A. Kettunen, A. Cartoni, R. Richter, **S. Tosic**, S. Maclot, P. Rousseau, R. Delaunay, A. Domaracka and L. Avaldi  
Selectivity in the photofragmentation of halo-pyrimidines  
XXIX International Conference on Photonic, Electronic, and Atomic Collisions (ICPEAC2015), 22–28 July 2015, Toledo, Spain, Abstracts, MO-074.  
*Journal of Physics: Conference Series*, **635** 112041 (2015)  
doi:10.1088/1742-6596/635/11/112041

14. **S. D. Tošić**, V. Pejčev , D. Šević and B. P. Marinković  
Electron scattering by silver: excitation of the  $4d^9 5s^2 \ ^2D_{3/2}$  and  $4d^{10} 6s \ ^2S_{1/2}$  states  
S. D. Tošić, V. Pejčev , D. Šević and B. P. Marinković  
XXIX International Conference on Photonic, Electronic, and Atomic Collisions (ICPEAC2015), 22–28 July 2015, Toledo, Spain, Abstracts, MO-117.  
*Journal of Physics: Conference Series*, **635** 052054 (2015)  
doi:10.1088/1742-6596/635/5/052054

15. Z. M. Raspopović, Ž. D. Nikitović, **S. D. Tošić** and V. D. Stojanović  
Cross section set and transport properties of Ne<sup>+</sup> in CF<sub>4</sub>  
XXIX International Conference on Photonic, Electronic, and Atomic Collisions (ICPEAC2015), 22–28 July 2015, Toledo, Spain, Abstracts, WE-048.  
*Journal of Physics: Conference Series*, **635** 022099 (2015)  
doi:10.1088/1742-6596/635/5/022099

16. P. Bolognesi, A. Kettunen, A. Cartoni, R. Richter, **S. Tošić**, S. Maclot, P. Rousseau, R. Delaunay, A. Domaracka and L. Avaldi,  
Selectivity in the Photofragmentation of Halo-pyrimidines  
Proc. 3<sup>rd</sup> Int. Conf. “Radiation Damage in Biomolecular Systems: Nanoscale Insights into Ion-Beam Cancer Therapy” – Nano-IBCT 2014, October 27 – 31, 2014, Boppard am Rhein, Germany, Book of Abstracts, Eds. G. García, N. Mason and A. V. Solov’ov, Poster presentation PS04, p.84-85. ISBN: N/A, (COST Action MP1002, DFG and MBN Research Centre, Frankfurt am Main, Germany)

Радови објављени пре претходног избора у звање

1. **S. D. Tošić**, V. Pejčev , D. Šević, B. P. Marinković, R. P. McEachran and A. D. Stauffer  
Excitation of silver by electron impact  
XXVII ICPEAC 2011 International Conference on Photonic, Electronic and Atomic Collisions, 27 July - 2 August 2011, Belfast, United Kingdom, Poster presentation We015.  
*Journal of Physics: Conference Series*, **388** 042015 (2012)  
doi:10.1088/1742-6596/388/4/042015

2. **S. D. Tošić**, D. Šević, V. Pejčev, D. M. Filipović and B. P. Marinković  
Electron scattering by Ag atom at small scattering angles  
Proc. 10<sup>th</sup> European Conf. on Atoms, Molecules, and Photons – ECAMP X, 4 – 9 July 2010, Salamanca, Spain.
3. B. P. Marinković, **S. D. Tošić**, M. S. Rabasović, D. Šević, V. Pejčev, B. Predojević and D. M. Filipović  
Measurements of electron interactions with metal vapour atoms  
Proc. 2<sup>nd</sup> Meeting on Electron Controlled Chemical Lithography (ECCL 2009), 4 – 9 June 2009, Sabanci Üniversitesi, Istanbul, Turkey, Abstract Booklet, Oral Presentation, p.34. Book of Abstracts I-19.
4. **S. D. Tošić**, V. I. Kelemen, D. Šević, V. Pejčev, D. M. Filipović, E. Yu. Remeta and B. P. Marinković  
Elastic electron scattering by silver atoms  
Proc. CEPAS 2008 Conference (4<sup>th</sup> Conf. on Elementary Processes in Atomic Systems) 18-20 June 2008, Babes-Bolyai University, Cluj-Napoca, Romania, Book of Abstracts, Eds. K. Póra, V. Chis and L. Nagy. ISBN 978-973-647-596-2, Poster presentation We-17, p.75.
5. M. S. Rabasović, **S. D. Tošić**, V. Pejčev, D. Šević, D. M. Filipović and B. P. Marinković  
Generalized oscillator strengths for electron scattering by In atom at small angles  
Proc. CEPAS 2008 Conference (4<sup>th</sup> Conf. on Elementary Processes in Atomic Systems) 18-20 June 2008, Babes-Bolyai University, Cluj-Napoca, Romania, Book of Abstracts, Eds. K. Póra, V. Chis and L. Nagy. ISBN 978-973-647-596-2, Poster presentation We-16, p.74.
6. **S. Milisavljević**, M. Pardžovska, D. Šević, V. Pejčev, D. M. Filipović and B. P. Marinković  
Electron Energy-Loss Spectroscopy of Pb Atom  
Proc. 15<sup>th</sup> Int. Symp. “Spectroscopy in Theory and Practice”, 18-21 April 2007, Nova Gorica, Slovenia, Book of Abstracts (Knjiga povzetkov), Eds. M. Bavcon Kralj and P. Trebše, ISBN: 978-961-6311-44-1. Poster P17 - p.78.
7. **S. Milisavljević**, M. S. Rabasović, B. Predojević, D. Šević, V. Pejčev, D. M. Filipović and B. P. Marinković  
Electron collisions by metal atoms  
Proc. 5<sup>th</sup> EU-Japan Joint Symposium on Plasma Processing (Radicals and Non-Equilibrium Processes in Low-Temperature Plasmas), 7-9.03.2007 Belgrade, Serbia, Abstracts of Invited Lectures, Progress Reports and Contributed Papers, Eds. Z. Lj. Petrovic, N. Mason, S. Hamaguchi, M. Radmilovic-Radjenovic, (Serbian Academy of Sciences and Arts, Institute of Physics: Belgrade, 2007) Contributed Paper p.Po-11.
8. **S. Milisavljević**, M. Pardžovska, D. Šević, V. Pejčev, D. M. Filipović, B. P. Marinković  
Electron impact excitation of the  $6p7s\ ^3P_1$  state of Pb atom,  
Proc. CEPAS 2005 Conference (3rd Conf. on Elementary Processes in Atomic Systems) 31 Aug. - 2 Sept. 2005. University of Miskolc, Hungary, Book of Abstracts, Poster presentation P-25, p.73
9. B. P. Marinković, D. M. Filipović, V. Pejčev, D. Šević, **S. Milisavljević**, B. Predojević and M. Pardžovska  
Electron collisions by metal atom vapours  
Progress Report at CEPAS 2005 Conference (3rd Conf. on Elementary Processes in Atomic Systems), 31 Aug. - 2 Sept. 2005. University of Miskolc, Hungary, Book of Abstracts I-19
10. B. P. Marinković, D. M. Filipović, J. Jureta, V. Pejčev, D. Šević, M.-J. Hubin-Franskin, A. Giuliani, A. R. Milosavljević, P. Kolarž, **S. Milisavljević**, M. Pardžovska, D. Pavlović and N. J. Mason

Electron Interaction with Small and “Little Larger” Molecules  
RADAM Conference (RADIATION DAMAGE in Biomolecular Systems), June 24 – 27, 2004, Lyone, France,  
Working – Group invited talk, COST action P9, Ed. M. Farizon, Abstract S1\_2

11. **S. Tošić**, D. Šević, V. Pejčev, D. M. Filipović and B. P. Marinković  
Differential cross sections for inelastic electron scattering by calcium atom  
Proc. of the Fifth Gen. Conf. of Balkan Physical Union BPU-5, Vrnjčka Banja, Serbia and Montenegro,  
August 25 – 29, 2003, Eds. S. Jokic, I. Milosevic, A. Balaz and Z. Nikolic, (Belgrade: Serbian Physical  
Society) CD-ROM Abstract SO04 – 002, pp. 241 – 244.

12. **S. Tošić**, D. Šević, V. Pejčev, D. M. Filipović and B. P. Marinković  
Generalized oscillator strengths for electron scattering by Ca atom at small angles,  
Proc 23<sup>rd</sup> Int. Conf. on Photonic Electronic and Atomic Collisions ICPEAC 2003, July 23 – 29, 2003,  
Stockholm, Sweden, Eds: J. Anton, H. Cederquist, M.Larsson, E. Lindroth, S. Mannervik, H. Schmidt and  
R. Schuch, Abstracts of Contributed Papers, Vol. II, Tu050

### **Уређивање зборника саопштења међународног скупа (M36)**

Зборник објављен након претходног избора у звање

1. Eds. D. Cassidy, M.J. Brunger, Z.Lj. Petrović, S. Dujko, B.P. Marinković, D. Marić and  
**S. Tošić**,  
Proc. XX International Workshop on Low-Energy Positron and Positronium Physics, XXI International  
Symposium on Electron-Molecule Collisions and Swarms and V Workshop on Non-Equilibrium  
Processes – POSMOL2019, 18 - 20 July 2019 Belgrade, Serbia, Book of Abstracts, (Serbian Academy of  
Sciences and Arts and Institute of Physics Belgrade, Serbia, 2019).  
ISBN 978-86-7025-819-8

### **Рад у истакнутом националном часопису (M52)**

Рад објављен пре претходног избора у звање

1. M. S. Rabasović, **S. D. Tošić**, V. Pejčev, D. Šević, D. M. Filipović and B. P. Marinković  
Volume correction factor in electron-indium atom scattering experiments  
*Facta Universitatis, Series Phys. Chem. Technol.*, **6** 119 (2008)

### **Предавање по позиву са скупа националног значаја штампано у целини (M61)**

Радови објављени пре претходног избора у звање

1. **S. D. Tošić**, D. Šević, V. Pejčev and B. P. Marinković  
Diferencijalni preseki za rasejanje elektrona na atomima srebra i olova  
Zbornik radova “Fizika 2010 BL”, Banja Luka, Republika Srpska, BiH, 22-24 septembar 2010. Urednik:  
B. Predojević, Sekcijsko predavanje Sudari elektrona sa atomima i molekulima, str. 181 – 189.

2. B. P. Marinković, D. Šević, B. Predojević, V. Pejčev, **S. D. Tošić**, M. S. Rabasović, V. D. Bočvarski,  
B. A. Petruševski, N. S. Nikolić and D. Radosavljević  
Elektron - metal atom sudari i baze podataka  
Zbornik radova “Fizika 2010 BL”, Banja Luka, Republika Srpska, BiH, 22-24 septembar 2010. Urednik:  
B. Predojević, Plenarno predavanje, str. 13 – 46.

### Саопштење са скупа националног значаја штампано у целини (M63)

#### Радови објављени пре претходног избора у звање

1. M. S. Rabasović, **S. D. Tošić**, V. Pejčev, D. Šević, D. M. Filipović and B. P. Marinković  
Effective Path Length Correction Factor in Electron-Indium Atom Scattering Experiments  
Proc. 1<sup>st</sup> National Conference on Electronic, Atomic, Molecular and Photonic Physics, 15-18 May 2008, Zaječar, Serbia, Book of Contributed Papers and Abstracts of Invited Lectures and Progress Reports, Eds. A. R. Milosavljević, D. Šević and B. P. Marinković, (Institute of Physics, Belgrade 2008) ISBN: 978-86-82441-22-9, Contributed Paper, pp.42-44.

2. **S. Milisavljević**, D. Šević, V. Pejčev, D. M. Filipović and B. P. Marinković  
Integral Cross-Sections for Electron Excitation of the  $4^1P$  State of Calcium Atom,  
*Proc. XI Congress of Physicists of Serbia and Montenegro*, Petrovac na Moru, 3 – 5 June 2004, Eds. Nikola Konjevic, Borko Vujicic and Predrag Miranovic, CD Contribution [s2\_10] pp. 2.67 – 69 (in Serbian)

### Саопштење са скупа националног значаја штампано у изводу (M64)

#### Рад објављени након претходног избора у звање




1. Bratislav P. Marinković, **Sanja D. Tošić**,  
“Photon interaction with (bio)molecules - Near-edge X-ray absorption fine-structure (NEXAFS) spectroscopy”,  
Proc. 11th Photonics Workshop, Kopaonik, 11-14 March 2018, Book of Abstracts, Ed. D. Lukić, (Institute of Physics Belgrade, Belgrade, 2018) Invited Lecture, p.36.  
Konferencija Jedanaesta radionica fotonike (2018), Kopaonik 11-14.03.2018, Zbornik apstrakata, Urednik: D. Lukić, (Institut za fiziku Beograd, 2018) Uvodno predavanje, str.36.  
ISBN: 978-86-82441-47-2  
<http://photonicsworkshop.ipb.ac.rs/11/index.php>

#### Радови објављени пре претходног избора у звање

1. **S. D. Tošić**, V. Pejčev, D. Šević and B. P. Marinković  
Absolute cross sections for electron excitation of silver  
Proc. 2<sup>nd</sup> National Conference on Electronic, Atomic, Molecular and Photonic Physics, 21-25 June 2011, Belgrade, Serbia, Book of Contributed Papers and Abstracts of Invited Lectures, Eds. A. R. Milosavljević, S. Dujko and B. P. Marinković, (Institute of Physics, Belgrade 2012) ISBN: 978-86-82441-32-8, p.112.

2. **S. D. Tošić**, D. Šević, V. Pejčev, D. M. Filipović and B. P. Marinković  
Electron Energy-Loss Spectroscopy of Ag Atom  
Proc. 1<sup>st</sup> National Conference on Electronic, Atomic, Molecular and Photonic Physics, 15-18 May 2008, Zaječar, Serbia, Book of Contributed Papers and Abstracts of Invited Lectures and Progress Reports, Eds. A. R. Milosavljević, D. Šević and B. P. Marinković, (Institute of Physics, Belgrade 2008) ISBN: 978-86-82441-22-9, p.16.


# Electron-impact excitation of the $(4d^{10}5s) \ ^2S_{1/2} \rightarrow (4d^95s^2) \ ^2D_{3/2}$ and $(4d^{10}5s) \ ^2S_{1/2} \rightarrow (4d^{10}6s) \ ^2S_{1/2}$ transitions in silver: Experiment and theory

B. P. Marinković , S. D. Tošić , and D. Šević 

*Institute of Physics Belgrade, University of Belgrade, Pregrevica 118, 11080 Belgrade, Serbia*

R. P. McEachran

*Laser Physics Centre, The Research School of Physics, Australian National University, Canberra, ACT 0200, Australia*

F. Blanco 

*Departamento de Estructura de la Materia, Física Térmica y Electrónica e IPARCOS, Universidad Complutense de Madrid, Avienda Complutense, E-28040 Madrid, Spain*

G. García

*Instituto de Física Fundamental, CSIC, Serrano 113-bis, E-28006 Madrid, Spain*

M. J. Brunger \*

*College of Science and Engineering, Flinders University, GPO Box 2100, Adelaide, SA 5001, Australia  
and Department of Actuarial Science and Applied Statistics, Faculty of Business and Management,  
UCSI University, Kuala Lumpur 56000, Malaysia*



(Received 15 April 2021; accepted 22 July 2021; published 10 August 2021)

We present angle-differential and angle-integrated cross sections for electron-impact excitation of the  $(4d^{10}5s) \ ^2S_{1/2} \rightarrow (4d^95s^2) \ ^2D_{3/2}$  and  $(4d^{10}5s) \ ^2S_{1/2} \rightarrow (4d^{10}6s) \ ^2S_{1/2}$  transitions in atomic silver. Experimental data for four incident electron energies between 10 and 60 eV are compared with predictions from our relativistic distorted wave (RDW) and nonrelativistic atomic optical potential models. Agreement between our measured and calculated data is only fair, although in the case of the RDW it is seen to improve with increasing incident electron energy. However, only for the  $(4d^{10}6s) \ ^2S_{1/2}$  excitation process, agreement of our measured data with earlier relativistic convergent close coupling results from McNamara *et al.* [*J. Phys. B* **51**, 085203 (2018)] was, with a few exceptions, typically observed to be very good, to within the uncertainties on the data.

DOI: [10.1103/PhysRevA.104.022808](https://doi.org/10.1103/PhysRevA.104.022808)

## I. INTRODUCTION

Silver (Ag) is a fairly heavy atom ( $Z = 47$ ) with, similar to the alkali metals, one valence electron ( $e$ ) in an outer ( $5s$ ) orbital leading to a  $^2S_{1/2}$  ground state. It sits in the Group IB elements of the periodic table. Silver possesses high thermal and electric conductivity, and is extensively employed in various technological applications including printed circuit boards in mobile phones and computers and in conventional switches such as those used for controlling room lights. Understanding electron interactions with Ag atoms is important for improving our knowledge of laser techniques [1], in plasma diagnostics [2], astrophysics [3,4], in the development of atomic frequency standards [5,6], and most recently it may be an avenue in searching for new physics beyond the standard model [7].

It is therefore a little surprising to see the paucity of cross-section data for the  $e$ -Ag scattering system in the literature. We are aware of measurements for elastic scattering angle-

differential cross sections (DCSs) and angle-integrated cross sections (ICSSs) from Tošić *et al.* [8]. That work also included corresponding theoretical optical potential (OP) results. An initial relativistic distorted wave (RDW) computation for excitation of the  $(4d^{10}5p) \ ^2P_{1/2,3/2}$  levels was reported by Zeman *et al.* [9], with subsequent experimental cross sections, although the  $J = 1/2$  and  $3/2$  states were not energetically resolved in their work, being given by Tošić *et al.* [10,11]. Note that in that latter work [10,11], updated RDW results from an improved code were also reported. Perhaps the most comprehensive investigation conducted so far was the relativistic convergent close coupling (RCCC) computation by McNamara *et al.* [12]. Here DCSs and ICSSs were reported for the elastic channel and eight excited electronic states of Ag, as well as for ionization [12], for incident electron energies ( $E_0$ ) up to 200 eV. Nonetheless, excitation of core-excited levels, such as the energetically low-lying  $(4d^95s^2) \ ^2D_{5/2}$  and  $(4d^95s^2) \ ^2D_{3/2}$  states, were not considered by McNamara *et al.* [12]. To quantitatively undertake Monte Carlo simulations or multiterm Boltzmann equation modeling (see, e.g., Refs. [13–16]) of a given system, Tanaka *et al.* [17] and Brunger [18] noted that a comprehensive and complete

\*Corresponding author: michael.brunger@flinders.edu.au

cross-section database is required. Therefore, we surmise that further work on  $e$ -Ag collisional behavior is required and this forms one rationale for the present investigation. A further rationale behind this study is to provide a more detailed set of experimental data, against which theory might be benchmarked. This is particularly the case for the present ( $4d^{10}6s$ )  $^2S_{1/2}$  cross-section measurements, which are the first against which the RCCC(80) results [12] may be compared.

The structure of the remainder of this paper is as follows. In Sec. II, a description of our experimental methodology, including the uncertainties in making our measurements, is provided. The approaches we adopted to extrapolate our DCS data to  $0^\circ$  and  $180^\circ$ , in order to generate the corresponding ICS at that energy, are also described in this section. Thereafter, in Sec. III, we provide computational details of our RDW and nonrelativistic OP calculations. In Sec. IV, the current experimental and theoretical DCSs and ICSs are described and discussed, and compared to the earlier RCCC(80) results [12] where possible. Finally, some conclusions from the present investigation are given in Sec. V.

## II. EXPERIMENTAL CONSIDERATIONS

In the present experimental study of some of the higher-lying excited states in Ag, we used the same spectrometer that had been specifically designed for electron–metal-atom scattering investigations [19]. It is the same spectrometer we employed in our earlier elastic scattering [8] and excitation of the unresolved ( $4d^{10}5p$ )  $^2P_{1/2,3/2}$  levels [10,11] in silver. As a consequence, only a brief description of its utility need be given here, with an emphasis on any experimental procedures that differed from those used previously. A quasimonochromatic beam of electrons was produced through thermionic emission from a thoriated iridium filament, which in conjunction with appropriate electrostatic lenses and apertures and a hemispherical dispersion element, formed a well-focused beam at the interaction region of typical energy spread  $\sim 110$  meV (FWHM). This electron beam was perpendicularly crossed by an atomic silver beam, that was produced by a Knudsen-type oven heated to temperatures in the range 1300–1320 K which gave rise to vapor pressures of 1.3–1.9 Pa [20]. Inelastically scattered electrons were then transported and energy analyzed by a hemispherical analyzer identical to the one in the monochromator stage, before ultimately being detected by a single channel electron multiplier.

The incident electron energies ( $E_0$ ) of the present study were 10, 20, 40, and 60 eV, while the scattered electron angular range ( $\theta$ ) varied between  $10^\circ$  and  $150^\circ$  in  $10^\circ$  increments. Energy loss spectra (see Fig. 1 for a typical example) were measured at each  $\theta$ , before being analyzed. For many years we calibrated, often using a variety of resonance or Wigner-cusp features for the species in question (e.g., [21–23]), our incident electron beam energy. In all that time the correction to the value of  $E_0$  read on the relevant voltage supply was never worse than  $\pm 0.1$  eV. We therefore relied on the same calibration we employed in our recent work on indium [23] and we believe it to again be accurate to  $\pm 0.1$  eV. Note that this is something of a moot point in this case as away from the effects of resonance behavior the cross section only varies very slowly with  $E_0$ . While McNamara *et al.* [12] did note

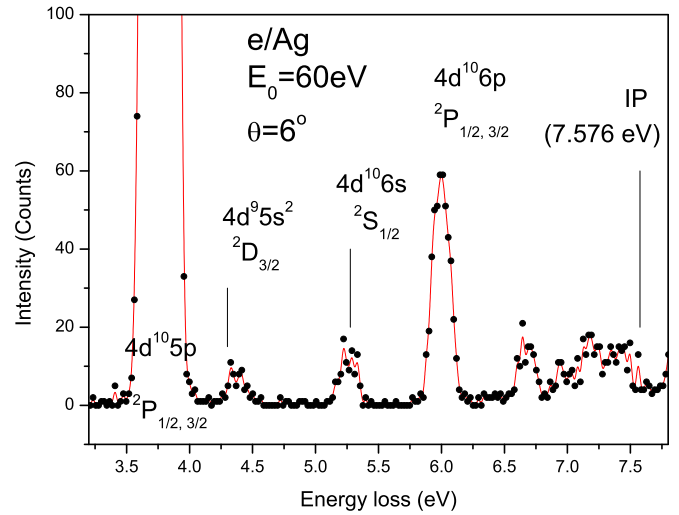


FIG. 1. Typical energy loss spectrum for electron scattering from silver. The incident electron energy was  $E_0 = 60$  eV and the scattered electron angle was  $\theta = 6^\circ$ . Spectroscopic notation for the main features we observe is denoted on this figure. Note that the elastic peak has been suppressed for clarity, while the solid red line is simply a weighted cubic spline interpolation between the data points.

some near-threshold resonances in some of the states they investigated, those resonances were always lower in energy than the 10–60 eV energy regime of this work. The energy loss range in this investigation was from  $\sim 3.2$  to 7.8 eV, thereby covering the whole range of the excited states up to and a little beyond the ionization threshold (see Fig. 1). Some of those states are explicitly labeled in Fig. 1, with only the lower-lying ( $4d^9 5s^2$ )  $^2D_{5/2}$  missing as it is unresolved from the ( $4d^{10}5p$ )  $^2P_{1/2,3/2}$  levels. Note that Tošić *et al.* [10,11] and McNamara *et al.* [12] both assumed that the contribution of the  $4d_{5/2}$  state to the  $5p_{1/2,3/2}$  states would be very small, and so could be ignored. The present RDW calculation (see next section), although we do not explicitly show its results, confirms the validity of that assumption. The overall energy resolution of the energy loss spectral features was  $\sim 160$  meV (FWHM), as determined from a Gaussian fit to the isolated  $4d_{3/2}$  and  $6s_{1/2}$  features.

The intensity ratios for the respective areas under the ( $4d^9 5s^2$ )  $^2D_{3/2}$  and ( $4d^{10}6s$ )  $^2S_{1/2}$  peaks, relative to that under the unresolved ( $4d^{10}5p$ )  $^2P_{1/2,3/2}$  peak, were determined at each  $\theta$  in the range  $10^\circ$ – $150^\circ$  and at each  $E_0$ . From those ratios at each  $\theta$  and  $E_0$  the corresponding absolute ( $4d^9 5s^2$ )  $^2D_{3/2}$  and ( $4d^{10}6s$ )  $^2S_{1/2}$  DCS were simply determined by multiplying the relevant ratio by the corresponding  $DCS(E_0, \theta)$  for the unresolved ( $4d^{10}5p$ )  $^2P_{1/2,3/2}$  state from Tošić *et al.* [10,11]. The  $5p_{1/2,3/2}$  DCSs of Tošić *et al.* [10,11], in the energy range 20–100 eV, were placed on an absolute scale using a generalized oscillator strength formalism [24–26], in conjunction with the known optical oscillator strength for the  $5s_{1/2} \rightarrow 5p_{1/2,3/2}$  excitation [27]. At 10 eV, however, Tošić *et al.* [10,11] normalized their  $5p_{1/2,3/2}$  scattered electron intensities against the corresponding RDW result at  $5^\circ$ . Therefore, at 10 eV, our measured  $4d_{3/2}$  and  $6s_{1/2}$  data are restricted to testing the shapes (angular distributions) of the corresponding RDW results, and the ratios, as a function of



TABLE I. Differential electron excitation cross sections, DCS ( $10^{-16}$  cm<sup>2</sup>/sr), and their uncertainties for the ( $4d^9 5s^2$ )  $^2D_{3/2}$  state of Ag. The stated uncertainties are at the one standard deviation level.

Energy Scattering angle (°)	10 eV		20 eV		40 eV		60 eV	
	DCS	Uncertainty	DCS	Uncertainty	DCS	Uncertainty	DCS	Uncertainty
	$(10^{-16}$ cm <sup>2</sup> /sr)							
10	0.20040	0.06690	0.11319	0.04928	0.05269	0.01904	0.03745	0.01666
20	0.08280	0.04430	0.04256	0.02236	0.00625	0.00338	0.02149	0.01562
30	0.03718	0.02343	0.03795	0.02081	0.00303	0.00194	0.01583	0.01444
40	0.01351	0.00816	0.02388	0.01569	0.00256	0.00208	0.01091	0.01037
50	0.01395	0.00707	0.00423	0.00333	0.00146	0.00126	0.00197	0.00181
60	0.01188	0.00822	0.00674	0.00606	0.00165	0.00147	$9.71 \times 10^{-4}$	$8.44 \times 10^{-4}$
70	0.00595	0.00445	0.00332	0.00263	0.00209	0.00187	0.00132	0.00115
80	0.00497	0.00352	0.00234	0.00180	0.00269	0.00237	0.00153	0.00129
90	0.00548	0.00382	0.00517	0.00418	0.00222	0.00200	0.00166	0.00131
100	0.00497	0.00376	0.00437	0.00344	0.00424	0.00398	0.00480	0.00394
110	0.00202	0.00165	0.00360	0.00284	0.00565	0.00476	0.00843	0.00700
120	0.00181	0.00137	0.00703	0.00560	0.00512	0.00411	0.00695	0.00560
130	0.00232	0.00186	0.01092	0.00893	0.00562	0.00424	0.00570	0.00477
140	0.00681	0.00521	0.00960	0.00803	0.00866	0.00694	0.00297	0.00254
150	0.01333	0.00857	0.02154	0.01761	0.01595	0.01315	0.00156	0.00135

the scattered electron angle, of the  $4d_{3/2}/5p_{1/2,3/2}$  intensities and  $6s_{1/2}/5p_{1/2,3/2}$  intensities from the RDW. Note that our ratios normalization procedure is only valid if the analyser transmission remains constant across the energy-loss range 3.2–5.5 eV, at each  $E_0$ . Our steps for ensuring this can be found, for example, in Hamilton *et al.* [23]. We should further note that McNamara *et al.* [12] raised queries as to the validity of the  $5p_{1/2,3/2}$  DCSs of Tošić *et al.* [10,11]. As a result, we have reanalyzed the earlier  $5p_{1/2,3/2}$  DCS data. In performing that reanalysis we found an error in the earlier work [11], which was caused at 20 and 40 eV by Tošić *et al.* incorrectly splicing their very forward-angular distributions onto their middle and backward-angular distributions. The appropriate renormalization factor to be applied to the published 20 eV  $5p_{1/2,3/2}$  DCSs of Tošić *et al.* is 0.76, in reasonable accord with that suggested by McNamara *et al.* [12], while that at 40 eV is 0.42. No renormalization was needed at 10 and 60 eV, for the  $5p_{1/2,3/2}$  DCSs of Tošić *et al.*, with the latter result also being consistent with that found by McNamara *et al.* [12]. A table of the corrected  $5p_{1/2,3/2}$  DCSs, which we use in this work, can be obtained directly from Marinković [28], while a summary of the present ( $4d^9 5s^2$ )  $^2D_{3/2}$  DCSs is given in Table I, and the present ( $4d^{10} 6s$ )  $^2S_{1/2}$  DCSs are listed in Table II.

There are many factors which contribute to the overall uncertainties in cross-section measurements such as those performed here. These include uncertainties related to the electron and atomic beam stabilities throughout the measurements. Both our electron and silver beam fluxes were highly stable during the course of these experiments, with uncertainties due to their fluctuations being less than 1.5%. By far the two largest sources of uncertainty in our determination of the present DCSs were the error associated with the  $5p_{1/2,3/2}$  cross sections (in the range 10%–49% depending on the actual  $E_0$  and  $\theta$  being considered), which we inherit in the normalization procedure, and the relatively small signal intensity of both the  $4d_{3/2}$  (again, depending on the actual  $E_0$  and  $\theta$  being studied, the error on the  $4d_{3/2}/5p_{1/2,3/2}$  ratio lay in the range

19%–66%) and  $6s_{1/2}$  (the error on the  $6s_{1/2}/5p_{1/2,3/2}$  ratio lay in the range 9%–67%, depending on  $E_0$  and  $\theta$ ) states (see Fig. 1). When all those factors are taken into account, the overall errors on our  $4d_{3/2}$  DCSs (in the range 33%–94%) can also be found in Table I, while those for the  $6s_{1/2}$  state (in the range 22%–94%) are listed in Table II.

ICSs, for both the  $4d_{3/2}$  and  $6s_{1/2}$  states, can, at each  $E_0$ , be derived from the corresponding DCSs. To achieve this we need to extrapolate our DCSs to  $0^\circ$  and  $180^\circ$ , perform an interpolation, and then undertake the appropriate integration. Two approaches were used to enable that aim. In the first, we took the angular dependence of the RCCC(80) results [12] to derive the  $6s_{1/2}$  ICSs, while our own RDW calculations were employed to derive the  $4d_{3/2}$  ICSs. In the second approach, the fitting analysis of Allen and co-workers [29,30] provided an independent self-consistency check. In all cases, the  $4d_{3/2}$  and  $6s_{1/2}$  ICSs we obtained, from each of the aforementioned approaches, were found to be consistent with one another to within our uncertainty estimates on the ICS. A summary of our measured ICSs and their associated uncertainties can be found in Table III. Note that our uncertainty estimates on those ICSs include all the uncertainties on the DCSs, but weighted for the  $\sin \theta$  term in the integrand when calculating them, and an additional uncertainty due to the extrapolation of our DCS to  $0^\circ$  and  $180^\circ$  in order to perform the integration for each state at each  $E_0$ .

### III. THEORETICAL DETAILS

#### A. RDW theory

In this work the differential cross sections and integral cross sections for electron-impact excitation were calculated using the RDW method. This method was originally developed for closed-shell atoms by Zuo *et al.* [31] and then successfully applied to the heavy noble gases [32], as well as cadmium [33] and mercury [34]. It was then modified by Zeman *et al.* [35] in order to treat the electron-impact

TABLE II. Differential electron excitation cross sections, DCS ( $10^{-16}$  cm<sup>2</sup>/sr), and their uncertainties for the  $(4d^{10}6s) {}^2S_{1/2}$  state of Ag. The stated uncertainties are at the one standard deviation level.

Energy	10 eV		20 eV		40 eV		60 eV	
	DCS	Uncertainty	DCS	Uncertainty	DCS	Uncertainty	DCS	Uncertainty
Scattering angle (°)	( $10^{-16}$ cm <sup>2</sup> /sr)							
10	0.22770	0.07300	0.50650	0.11130	0.18640	0.04970	0.08800	0.03230
20	0.12040	0.06190	0.13380	0.05370	0.01810	0.00810	0.01610	0.01260
30	0.04577	0.02854	0.04818	0.02451	0.00336	0.00307	0.03800	0.02870
40	0.02110	0.01170	0.01069	0.00713	0.00766	0.00501	0.01745	0.01499
50	0.01078	0.00577	0.00501	0.00317	0.00555	0.00356	0.00592	0.00435
60	0.01088	0.00767	0.00721	0.00586	0.00824	0.00532	0.00340	0.00284
70	0.00891	0.00621	0.00408	0.00337	0.00628	0.00441	0.00158	0.00138
80	0.00456	0.00329	0.00234	0.00193	0.00592	0.00565	0.00189	0.00172
90	0.00585	0.00402	0.00409	0.00385	0.00296	0.00281	0.00181	0.00160
100	0.00538	0.00401	0.00403	0.00376	0.00660	0.00542	0.00384	0.00336
110	0.00238	0.00223	0.00499	0.00437	0.00690	0.00589	0.00763	0.00661
120	0.00326	0.00231	0.00402	0.00291	0.00717	0.00669	0.00833	0.00641
130	0.00182	0.00152	0.00286	0.00256	0.00750	0.00681	0.00505	0.00421
140	0.00386	0.00322	0.01976	0.01730	0.01444	0.01397	0.00233	0.00213
150	0.01194	0.00778	0.03525	0.02751	0.00957	0.00814	0.00222	0.00205

excitation of cesium and other alkali-metal atoms. Subsequently, this latter RDW approach was applied to the alkali-metal-like atoms silver and gold [9,36] in order to excite the resonance transitions. The reader is referred to the above papers, in particular Ref. [31], for the overall details of the RDW method.

### 1. Inner-shell excitation

Here the above alkali-like code was further modified to allow for the electron-impact excitation of inner-shell electrons, namely, the  $(n-1)d_{3/2,5/2}$  electrons from the valence  $ns_{1/2}$  shell in copper, silver, and gold; for silver we have  $n=5$ . In this application the ground- and excited-state wavefunctions of silver were determined in single configuration calculations using the multiconfiguration Dirac-Fock program of Grant *et al.* [37]. The distorted waves in the initial and final channels were determined by the usual procedure of electron scattering from the ground- and excited-state static potentials. These static potentials were determined in the standard manner from the ground- and excited-state Dirac-Fock orbitals of silver. The nonlocal exchange interaction was included by antisymmetrizing the total scattering wave function.

TABLE III. ICSs ( $10^{-16}$  cm<sup>2</sup>) and their uncertainties for the  $(4d^9 5s^2) {}^2D_{3/2}$  and  $(4d^{10} 6s) {}^2S_{1/2}$  states of Ag. The stated uncertainties are at the one standard deviation level.

Energy (eV)	$(4d^9 5s^2) {}^2D_{3/2}$		$(4d^{10} 6s) {}^2S_{1/2}$	
	ICS	Uncertainty	ICS	Uncertainty
10	0.179	0.063	0.304	0.106
20	0.159	0.026	0.326	0.114
40	0.0744	0.0261	0.163	0.057
60	0.0687	0.0241	0.130	0.045

### 2. Excitation of the 6s state

In this case the usual RDW code of Zeman *et al.* [35] for the alkali atoms was used. However, the ground and excited state wave functions were now determined by a polarized frozen-core model with a nonempirical polarization potential [38]. In particular, the valence orbitals were determined in the field of the  $Ag^+$  core plus a “scaled” polarized orbital dipole potential [39]. Here the dipole polarization potential is scaled by a constant factor which is adjusted such that the energy of valence orbitals agrees with experiment. For the 5s orbital this factor was 0.97867 and for the 6s orbital it was 1.04279. A Gram-Schmidt procedure was then used to ensure the orthogonality of the 5s and 6s orbitals. Finally, the distorted waves in the initial and final channels were determined in the same manner as that given above for inner-shell excitation. Once again, the nonlocal exchange interaction was included by antisymmetrizing the total scattering wave function.

### B. Atomic optical potential model

We have recently described our standard nonrelativistic optical potential approach in our studies of the electron-beryllium [40], electron-magnesium [41], electron-zinc [42], and electron-indium [43] scattering systems. The generic details of this atomic OP method were given in those papers, so only the key points of this method are summarized below.

The electron-atom interaction is described by a local complex potential given by

$$V(r) = V_s(r) + V_{ex}(r) + V_{pol}(r) + iV_{abs}(r), \quad (1)$$

where the real part comprises the following three terms. The static term  $V_s$  is derived from a Hartree-Fock calculation [44] of the atomic charge distribution. An exchange term  $V_{ex}$  accounts for the indistinguishability of the incident and target electrons; it is given by the semiclassical energy dependent formula derived by Riley and Truhlar [45]. A polarization potential  $V_{pol}$  is used for the long-range interactions which

depend on the target dipole polarizability, in the form given by Zhang *et al.* [46].

The imaginary absorption potential accounts for the electronically inelastic scattering events. It is based on the quasifree model by Staszewska *et al.* [47], but incorporates some improvements to the original formulation, such as the inclusion of screening effects, local velocity corrections, and the description of the electron indistinguishability [48] leading to a model which provides a realistic approximation for electron-atom scattering over a broad energy range [49]. We used here a standard partial wave expansion procedure. In order to obtain the  $l$ th complex partial-wave phase shift  $\eta_l$ , the scattering equation for the radial wave functions has been numerically integrated and the details of such a procedure can be obtained from Refs. [48,50,51]. Once the corresponding  $\eta_l$  phase shifts are obtained for the above potential, the elastic differential  $d\sigma_{\text{elas}}/d\Omega$  and integral  $\sigma_{\text{elas}}$  cross sections result from the expressions

$$\frac{d\sigma_{\text{elas}}}{d\Omega} = \frac{1}{4k^2} \left| \sum_{l=0}^{l_{\text{max}}} (2l+1)(e^{2i\eta_l} - 1)P_l(\cos\theta) \right|^2 \quad (2)$$

and

$$\sigma_{\text{elas}}(E_0) = \frac{4\pi}{k^2} \sum_{l=0}^{l_{\text{max}}} (2l+1) \sin^2 \eta_l, \quad (3)$$

respectively, and the total scattering cross section ( $\sigma_{\text{total}}$ ) results from the optical theorem  $\sigma_{\text{total}}(E_0) = \frac{4\pi}{k^2} \text{Im}(f_{\theta=0})$ . The total inelastic cross section  $\sigma_{\text{inelas}}(E_0)$  therefore corresponds to

$$\sigma_{\text{inelas}}(E_0) = \sigma_{\text{total}}(E_0) - \sigma_{\text{elas}}(E_0). \quad (4)$$

In order to calculate the electron-impact ionization cross section,  $\sigma_{\text{ion}}(E_0)$ , the above calculation procedure was repeated, but using the ionization energy (IE) as the gap energy parameter, as described in Ref. [52]. In these conditions, only excitation to continuum states above the ionization threshold is considered. By combining the respective results for both gap energy parameters, summed electronic excitation cross sections ( $\sigma_{\text{exci}}$ ) can also be derived from the expression  $\sigma_{\text{exci}}(E_0) = \sigma_{\text{inelas}}(E_0) - \sigma_{\text{ion}}(E_0)$ . Repeating this procedure for the threshold excitation energies, corresponding to the different excited states, their respective excitation cross sections can be extracted from the integral inelastic cross section.

While our OP calculations cannot in general compete, in terms of accuracy (except perhaps in the elastic channel [49]) and the breadth of information provided, with state-of-the-art  $B$ -spline  $R$ -matrix [53] and RCCC [12] methods, in this case no  $B$ -spline  $R$ -matrix results for electron scattering from Ag are available and the RCCC results are limited to the excitation of the  $6s_{1/2}$  state. Therefore, under these circumstances, the present OP calculation results add to the story we are telling and, just as importantly, add to the available database for this scattering system.

#### IV. RESULTS AND DISCUSSION

In Table I and Figs. 2(a)–2(d), we present our measured ( $4d^9 5s^2$ )  $^2D_{3/2}$  excitation DCSs for the incident electron energies (a) 10 eV, (b) 20 eV, (c) 40 eV, and (d) 60 eV. Also shown in Fig. 2 are the corresponding results from our current RDW

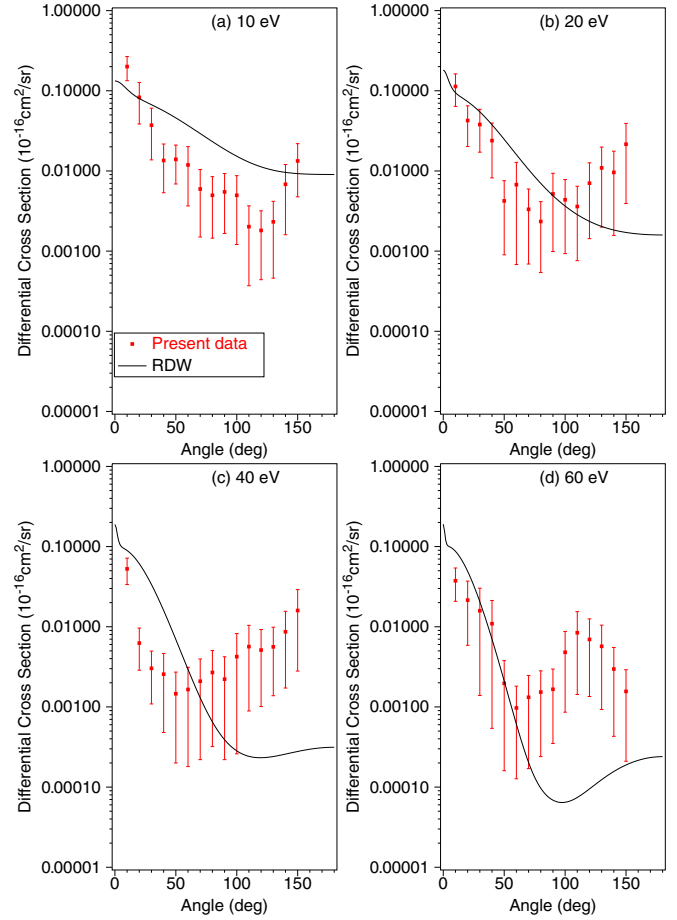


FIG. 2. Differential cross sections ( $\times 10^{-16}$  cm<sup>2</sup>/sr) for electron-impact excitation of the ( $4d^9 5s^2$ )  $^2D_{3/2}$  state of silver. The present data (■) are compared against theoretical results from our RDW calculations (—).

computations. There are several general observations we can make with regard to Fig. 2. Firstly, it is clear that there are no other experimental or theoretical data currently available in the literature to compare against. In particular, we note that McNamara *et al.* [12] did not consider any core-excited processes in their otherwise detailed study of Ag. Thus our results for this excitation process are unique. The second point we can glean from Fig. 2 is that the agreement between our measured DCS and RDW computed DCS, at each  $E_0$ , is only fair. This level of accord probably improves somewhat as the incident electron energy is increased, as one might anticipate with the RDW method, but a more quantitative description is difficult here given the measurement uncertainties. Inner-shell quadrupole transitions present a real challenge to theory, so that in the present application more elaborate (multiconfiguration) wave functions will probably be needed in order to better describe the collision dynamics of this excitation process. Finally, with the possible exception of the 60-eV experimental angular distribution, we note that both our measured and calculated ( $4d^9 5s^2$ )  $^2D_{3/2}$  differential cross sections display little or no angular structure. As we shall shortly see, this is in marked contrast to the angular distributions for excitation of the ( $4d^{10} 6s$ )  $^2S_{1/2}$  state. Note that as the  $4d_{3/2}$  quadrupole

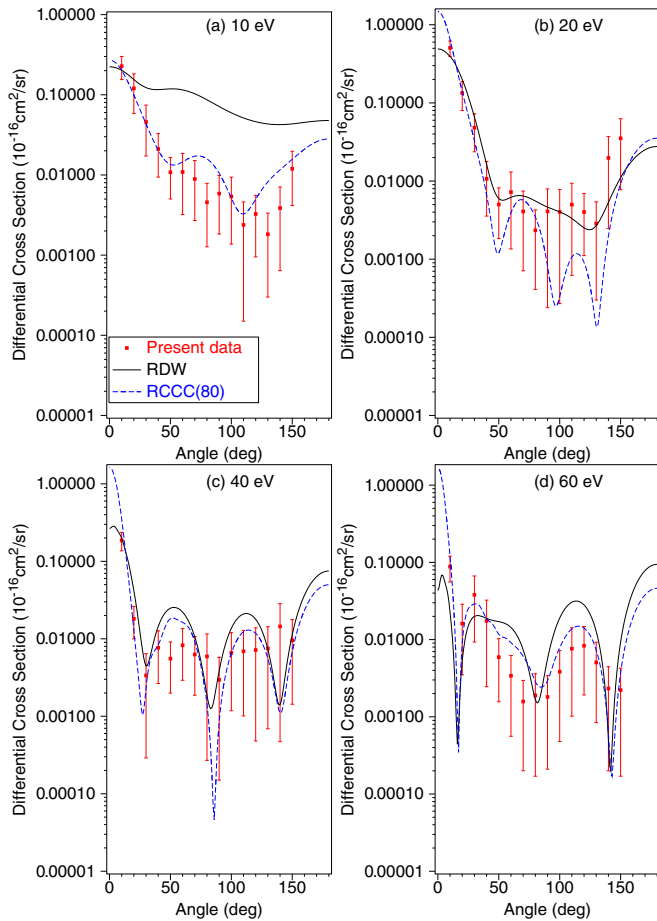


FIG. 3. Differential cross sections ( $\times 10^{-16}$  cm<sup>2</sup>/sr) for electron-impact excitation of the  $(4d^{10}6s) ^2S_{1/2}$  state of silver. The present data (■) are compared against theoretical results from our RDW calculations (—) and the RCCC(80) computations of McNamara *et al.* [12] (---).

transition is very weak compared to the  $6s_{1/2}$  excitation and, in particular, the unresolved  $5p_{1/2,3/2}$  transitions, it is likely that only very few of the initial partial waves are important in describing that quadrupole transition. Consequently, the “interference” effects between the partial waves are reduced so that the  $4d_{3/2}$  angular distribution exhibits less structure.

In Table II and Figs. 3(a)–3(d) we present our measured  $(4d^{10}6s) ^2S_{1/2}$  excitation DCSs, again for the incident electron energies (a) 10 eV, (b) 20 eV, (c) 40 eV, and (d) 60 eV. Also shown in Fig. 3 are the corresponding results from our RDW computation and the RCCC(80) calculation of McNamara *et al.* [12]. Agreement between the present measured DCSs and the RCCC(80) results [12] is seen to be very good, in terms of both the shapes and absolute cross-section values, at each  $E_0$  studied. This provides further evidence for the efficacy of the RCCC(80) theory to be used as a good starting point to construct a complete database for Ag in modeling applications of its behavior in low-temperature plasmas and gaseous electronics in general. On the other hand, the comparison between our present measured and RDW calculated DCSs is not as impressive as that just described. Nonetheless, the RDW does improve, certainly in terms of the shapes of

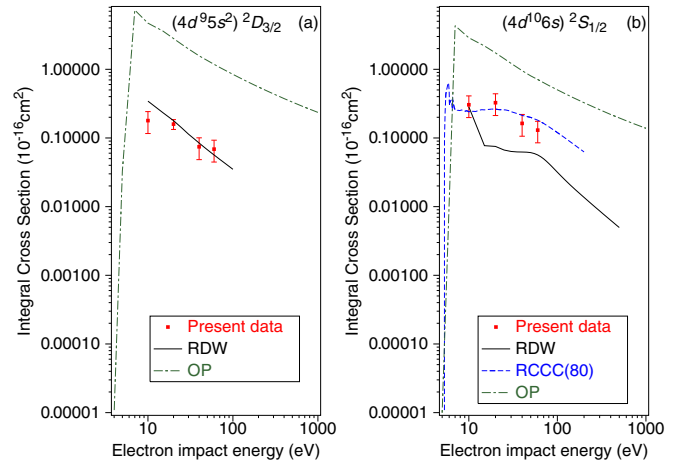


FIG. 4. Integral cross sections ( $\times 10^{-16}$  cm<sup>2</sup>) for electron-impact excitation of the (a)  $(4d^9 5s^2) ^2D_{3/2}$  and (b)  $(4d^{10}6s) ^2S_{1/2}$  states of silver. The present data (■) are compared against theoretical results from our RDW calculations (—), OP calculations (---), and the RCCC(80) computations of McNamara *et al.* [12] (---).

the  $6s_{1/2}$  angular distributions and their magnitude, as  $E_0$  is increased. One of the key features from the present study is the strong oscillatory nature of the  $(4d^{10}6s) ^2S_{1/2}$  angular distributions in Fig. 3. Indeed this behavior appears to be ubiquitous in electron-metal-vapor scattering, for both the elastic and discrete inelastic channels, with a few examples supporting that assertion being bismuth [22], zinc [21], indium [23], sodium [54], and magnesium [55]. The oscillatory nature of any differential cross section arises from the interference between the various partial waves that describe the collisional behavior. In the present case of inelastic scattering, the details depend in a complex way on the interference between  $T$ -matrix elements that need to be combined with spherical harmonics in order to generate the scattering amplitudes [56] and, subsequently, the angle-differential cross section [57]. It is, therefore, generally not possible to predict either the number or the positions of the minima (maxima) in the DCS. Even though in some special circumstances and models a resemblance to elastic scattering may appear in inelastic collisions [58], and the DCS generally exhibits less structure in the angular dependence with decreasing projectile energy, drawing truly quantitative conclusions is not possible.

In Table III and Figs. 4(a) and 4(b), we present our respective derived  $4d_{3/2}$  and  $6s_{1/2}$  experimental excitation ICSs. Also shown, where possible, in Fig. 4 are the corresponding results from our RDW and OP calculations, and those from the RCCC(80) computation of McNamara *et al.* [12]. Considering first the  $4d_{3/2}$  state [see Fig. 4(a)], we find that with the exception of the 10 eV ICS, there is a very good level of agreement between our measured and RDW calculated ICSs. Given our previous discussion, for the excitation of the  $4d_{3/2}$  level at the DCS level, that degree of accord can only be due to a happy cancellation of divergences in the integrand, coupled with roughly the same theory and experimental DCS magnitudes, and so must be considered to be somewhat fortuitous. Our atomic OP calculation clearly overestimates the magnitude of the experimental ICSs over the entire 10–60 eV energy



range. However, the functional dependence (shape) of our OP integral cross section corresponds quite well with that of the experimental data, so that an appropriately scaled OP ICS might be used, in the context of assembling a complete Ag database, to extend the measured cross sections to larger energies and down to threshold. For the  $6s_{1/2}$  ICSs [see Fig. 4(b) and Table III], we find a very good level of accord between our measured cross sections and those calculated within the RCCC(80) approach [12]. Furthermore, that statement holds across the entire common energy range. Figure 4(b) also clearly indicates that our RDW ICS typically underestimates the magnitude of the measured data, between 20 and 60 eV, which, even allowing for the  $\sin \theta$  term in the integrand, probably reflects its inability to describe the very forward angle DCSs which are strongly peaked at small scattering angles (see Fig. 3). Finally, we note that our present atomic optical potential ICS overestimates significantly the magnitude of the  $6s_{1/2}$  experimental ICS [see Fig. 4(b)]. This result, and that for the  $4d_{3/2}$  state, reflect difficulties in our semiphenomenological approach to extracting individual integral excitation cross sections from the total inelastic cross section that is calculated *ab initio*.

## V. CONCLUSIONS

We have reported on experimental and theoretical DCS and ICS results for electron-impact excitation of the  $(4d^{10}5s) \ ^2S_{1/2} \rightarrow (4d^95s^2) \ ^2D_{3/2}$  and  $(4d^{10}5s) \ ^2S_{1/2} \rightarrow (4d^{10}6s) \ ^2S_{1/2}$  transitions in silver, and in doing so we have extended the available cross-section database for this scattering system. Neither of those transitions are electric-dipole allowed, so that the corresponding measured scattering intensities were relatively low which in turn led to higher statistical uncertainties than were normally found to be the case [10,11,23]. Nonetheless, all our measured data were observed to be consistently reproducible, to within the stated one standard deviation uncertainties, so that we are confident in their validity.

For the excitation of the  $(4d^95s^2) \ ^2D_{3/2}$  state, at the DCS level only the present RDW calculation could be compared to our experimental data. Here the level of accord between them was found to be only fair, with more elaborate (multiconfiguration) wave functions probably being required to improve

our description of this inner-shell quadrupole transition. At the ICS level, however, our RDW and OP computations could now be compared to our data. Here the OP calculation was found to overestimate the magnitude of the ICS across the common energy range, although its energy dependence was in good qualitative accord with our measurements. The excellent agreement between our RDW calculation and experimental data, across 20–60 eV, was undoubtedly somewhat fortuitous given the behavior at the DCS level.

For the excitation of the  $(4d^{10}6s) \ ^2S_{1/2}$  state, a very good level of accord was found between our measured DCSs and the RCCC(80) calculated DCSs at all common incident electron energies. For this state the RDW computation also provided a fair description for this scattering process, with the level of accord between our measured and calculated DCS improving as  $E_0$  increased. This was no real surprise, as based on our experience the RDW method becomes quite reliable above two to three times the ionization energy of the target in question (for silver the ionization energy = 7.576 eV). Strong interference effects, both constructive and destructive, in the partial waves describing the  $5s \rightarrow 6s$  scattering process were clearly observed in our measured and calculated angular distributions, as was their energy dependence. Finally, we note the excellent agreement between our measured ICS and the RCCC(80) ICS for this transition. Agreement with our RDW and OP ICS was found to be less satisfactory, although the qualitative energy dependence of the OP calculation was again in good accord with the experimental ICS.

## ACKNOWLEDGMENTS

This work was financially supported, in part, by the Australian Research Council (Project No. DP180101655), the Institute of Physics Belgrade through the Ministry of Education, Science and Technological Development (MESTD) of Serbia, and the Spanish Ministerio de Ciencia e Innovación - MICNN (Project No. PID2019–104727RB-C21) and CSIC (Project No. LINKA 20085). We thank Dr. L. Campbell for his help with some aspects of this paper, and Professor D. V. Fursa for providing us with tables of his RCCC(80) results. R.P.M. acknowledges very valuable discussions with Professor A. D. Stauffer in the early stages of the development of the inner-shell RDW method.

- 
- [1] B. Wernsman, T. Prabhuran, K. Lewis, F. Gonzales, M. Villagran, and J. J. Rocca, *IEEE J. Quantum Electron.* **24**, 1554 (1988).
  - [2] P. Choi and M. B. Favre, *J. Phys. D* **20**, 169 (1987).
  - [3] J. A. Johnson and M. Boltz, *Astrophys. J.* **579**, 616 (2002).
  - [4] D. Kasen, B. Metzger, J. Barnes, E. Quataert, and E. Ramirez-Ruiz, *Nature (London)* **551**, 80 (2017).
  - [5] G. Uhlenberg, J. Dirscherl, and H. Walther, *Phys. Rev. A* **62**, 063404 (2000).
  - [6] T. Badr, M. D. Plimmer, P. Juncar, M. E. Himbert, Y. Louyer, and D. J. E. Knight, *Phys. Rev. A* **74**, 062509 (2006).
  - [7] V. A. Dzuba, S. O. Allehabi, V. V. Flambaum, J. Li, and S. Schiller, *Phys. Rev. A* **103**, 022822 (2021).
  - [8] S. D. Tošić, V. I. Kelemen, D. Šević, V. Pejčev, D. M. Filipović, E. Yu. Remeta, and B. P. Marinković, *Nucl. Instrum. Methods B* **267**, 283 (2009).
  - [9] V. Zeman, R. P. McEachran, and A. D. Stauffer, *Can. J. Phys.* **74**, 889 (1996).
  - [10] S. D. Tošić, V. Pejčev, D. Šević, R. P. McEachran, A. D. Stauffer, and B. P. Marinković, *Nucl. Instrum. Methods B* **279**, 53 (2012).
  - [11] S. D. Tošić, V. Pejčev, D. Šević, R. P. McEachran, A. D. Stauffer, and B. P. Marinković, *Phys. Rev. A* **91**, 052703 (2015).

- [12] K. McNamara, D. V. Fursa, and I. Bray, *J. Phys. B* **51**, 085203 (2018).
- [13] A. I. Lozano, K. Krupa, F. Ferreira da Silva, P. Limão-Vieira, F. Blanco, A. Munõz, D. B. Jones, M. J. Brunger, and G. García, *Eur. Phys. J. D* **71**, 226 (2017).
- [14] F. Costa, A. Traoré-Dubuis, L. Álvarez, A. I. Lozano, X. Ren, A. Dorn, P. Limão-Vieira, F. Blanco, J. C. Oller, A. Muñoz, A. García-Abenza, J. D. Gorfinkiel, A. S. Barbosa, M. H. F. Bettega, P. Stokes, R. D. White, D. B. Jones, M. J. Brunger, and G. García, *Int. J. Mol. Sci.* **21**, 6947 (2020).
- [15] P. W. Stokes, M. J. E. Casey, D. G. Cocks, J. de Urquijo, G. García, M. J. Brunger, and R. D. White, *Plasma Sources Sci. Technol.* **29**, 105008 (2020).
- [16] P. W. Stokes, S. P. Foster, M. J. E. Casey, D. G. Cocks, O. González-Magaña, J. D. Urquijo, G. García, M. J. Brunger, and R. D. White, *J. Chem. Phys.* **154**, 084306 (2021).
- [17] H. Tanaka, M. J. Brunger, L. Campbell, H. Kato, M. Hoshino, and A. R. P. Rau, *Rev. Mod. Phys.* **88**, 025004 (2016).
- [18] M. J. Brunger, *Int. Rev. Phys. Chem.* **36**, 333 (2017).
- [19] B. P. Marinković, V. Pejčev, D. M. Filipović, D. Šević, S. Milisavljević, and B. Predojević, *Radiat. Phys. Chem.* **76**, 455 (2007).
- [20] C. B. Alcock, V. P. Itkin, and M. Y. Harrigan, *Can. Metall. Q.* **23**, 309 (1984).
- [21] B. P. Marinković, R. Panajotović, D. Šević, R. P. McEachran, G. García, F. Blanco, and M. J. Brunger, *Phys. Rev. A* **99**, 062702 (2019).
- [22] B. Predojević, D. Šević, B. P. Marinković, R. P. McEachran, F. Blanco, G. García, and M. J. Brunger, *Phys. Rev. A* **101**, 032704 (2020).
- [23] K. R. Hamilton, O. Zatsarinny, K. Bartschat, M. S. Rabasović, D. Šević, B. P. Marinković, S. Dujko, J. Atić, D. V. Fursa, I. Bray, R. P. McEachran, F. Blanco, G. García, P. W. Stokes, R. D. White, and M. J. Brunger, *Phys. Rev. A* **102**, 022801 (2020).
- [24] E. N. Lassetre, *J. Chem. Phys.* **43**, 4479 (1965).
- [25] L. Vriens, *Phys. Rev.* **160**, 100 (1967).
- [26] H. Kato, H. Kawahara, M. Hoshino, H. Tanaka, M. J. Brunger, and Y.-K. Kim, *J. Chem. Phys.* **126**, 064307 (2007).
- [27] J. R. Fuhr and W. L. Wiese, in *CRC Handbook of Chemistry and Physics*, 89th ed., edited by D. R. Lide (CRC, Boca Raton, FL, 2009).
- [28] bratislav.marinkovic@ipb.ac.rs.
- [29] L. J. Allen, M. J. Brunger, I. E. McCarthy, and P. J. O. Teubner, *J. Phys. B* **20**, 4861 (1987).
- [30] M. J. Brunger, S. J. Buckman, L. J. Allen, I. E. McCarthy, and K. Ratnavelu, *J. Phys. B* **25**, 1823 (1992).
- [31] T. Zuo, R. P. McEachran, and A. D. Stauffer, *J. Phys. B* **24**, 2853 (1991).
- [32] T. Zuo, R. P. McEachran, and A. D. Stauffer, *J. Phys. B* **25**, 3393 (1992).
- [33] R. Srivastava, T. Zuo, R. P. McEachran, and A. D. Stauffer, *J. Phys. B* **25**, 1073 (1992).
- [34] R. Srivastava, T. Zuo, R. P. McEachran, and A. D. Stauffer, *J. Phys. B* **25**, 2409 (1992).
- [35] V. Zeman, R. P. McEachran, and A. D. Stauffer, *J. Phys. B* **27**, 3175 (1994).
- [36] M. Maslov, M. J. Brunger, P. J. O. Teubner, O. Zatsarinny, K. Bartschat, D. V. Fursa, I. Bray, and R. P. McEachran, *Phys. Rev. A* **77**, 062711 (2008).
- [37] I. P. Grant, B. J. McKenzie, P. H. Norrington, D. F. Mayer, and N. C. Pyper, *Comput. Phys. Commun.* **21**, 207 (1980).
- [38] R. P. McEachran and M. Cohen, *J. Phys. B* **16**, 3125 (1983).
- [39] R. P. McEachran, D. L. Morgan, A. G. Ryman, and A. D. Stauffer, *J. Phys. B* **10**, 663 (1977).
- [40] R. P. McEachran, F. Blanco, G. García, and M. J. Brunger, *J. Phys. Chem. Ref. Data* **47**, 033103 (2018).
- [41] R. P. McEachran, F. Blanco, G. García, P. W. Stokes, R. D. White, and M. J. Brunger, *J. Phys. Chem. Ref. Data* **47**, 043104 (2018).
- [42] R. P. McEachran, B. P. Marinković, G. García, R. D. White, P. W. Stokes, D. B. Jones, and M. J. Brunger, *J. Phys. Chem. Ref. Data* **49**, 013102 (2020).
- [43] K. R. Hamilton, O. Zatsarinny, K. Bartschat, M. S. Rabasović, D. Šević, B. P. Marinković, S. Dujko, J. Atić, D. V. Fursa, I. Bray, R. P. McEachran, F. Blanco, G. García, P. W. Stokes, R. D. White, D. B. Jones, L. Campbell, and M. J. Brunger, *J. Phys. Chem. Ref. Data* **50**, 013101 (2021).
- [44] R. D. Cowan, *The Theory of Atomic Structure and Spectra* (University of California Press, Berkeley, 1981).
- [45] M. E. Riley and D. G. Truhlar, *J. Chem. Phys.* **63**, 2182 (1975).
- [46] X. Zhang, J. Sun, and Y. Liu, *J. Phys. B* **25**, 1893 (1992).
- [47] G. Staszewska, D. W. Schwenke, D. Thirumalai, and D. G. Truhlar, *Phys. Rev. A* **28**, 2740 (1983).
- [48] F. Blanco and G. García, *Phys. Rev. A* **67**, 022701 (2003).
- [49] O. Zatsarinny, K. Bartschat, G. García, F. Blanco, L. R. Hargreaves, D. B. Jones, R. Murrie, J. R. Brunton, M. J. Brunger, M. Hoshino, and S. J. Buckman, *Phys. Rev. A* **83**, 042702 (2011).
- [50] F. Blanco and G. García, *Phys. Lett. A* **255**, 147 (1999).
- [51] F. Blanco and G. García, *Phys. Lett. A* **295**, 178 (2002).
- [52] L. Chiari, A. Zecca, G. García, F. Blanco, and M. J. Brunger, *J. Phys. B* **46**, 235202 (2013).
- [53] O. Zatsarinny and K. Bartschat, *Phys. Rev. A* **79**, 042713 (2009).
- [54] P. J. O. Teubner, J. L. Riley, M. J. Brunger, and S. J. Buckman, *J. Phys. B* **19**, 3313 (1986).
- [55] M. J. Brunger, J. L. Riley, R. E. Scholten, and P. J. O. Teubner, *J. Phys. B* **21**, 1639 (1988).
- [56] K. Bartschat and N. S. Scott, *Comput. Phys. Commun.* **30**, 369 (1983).
- [57] K. Bartschat, *Comput. Phys. Commun.* **30**, 383 (1983).
- [58] C. K. Bartschat and K. Blum, *J. Phys. B* **15**, 2747 (1982).



# Radiation Damage Mechanisms of Chemotherapeutically Active Nitroimidazole Derived Compounds

Jacopo Chiarinelli<sup>1,2</sup>, Anna Rita Casavola<sup>1</sup>, Mattea Carmen Castrovilli<sup>1</sup>, Paola Bolognesi<sup>1</sup>, Antonella Cartoni<sup>1,3</sup>, Feng Wang<sup>4</sup>, R. Richter<sup>5</sup>, Daniele Catone<sup>6</sup>, Sanja Tosic<sup>7</sup>, Bratislav P. Marinkovic<sup>7</sup> and Lorenzo Avaldi<sup>1\*</sup>

<sup>1</sup> CNR-Istituto di Struttura Della Materia (CNR-ISM), Area della Ricerca di Roma 1, Monterotondo Scalo, Italy, <sup>2</sup> Dipartimento di Scienze, Università di Roma Tre, Rome, Italy, <sup>3</sup> Dipartimento di Chimica, Sapienza Università di Roma, Rome, Italy, <sup>4</sup> Molecular Modelling Discovery Laboratory, Department of Chemistry and Biotechnology, Faculty of Science, Engineering and Technology, Swinburne University of Technology, Melbourne, VIC, Australia, <sup>5</sup> Elettra-Sincrotrone Trieste, Trieste, Italy, <sup>6</sup> CNR-Istituto di Struttura Della Materia, Area della Ricerca di Tor Vergata, Rome, Italy, <sup>7</sup> Institute of Physics, Laboratory for Atomic Collision Processes, University of Belgrade, Belgrade, Serbia

## OPEN ACCESS

### Edited by:

Antonio Aguilar,  
University of Barcelona, Spain

### Reviewed by:

Radha Gobinda Bhui,  
University of Erlangen  
Nuremberg, Germany  
Yujun Shi,  
University of Calgary, Canada

### \*Correspondence:

Lorenzo Avaldi  
lorenzo.avaldi@ism.cnr.it

### Specialty section:

This article was submitted to  
Physical Chemistry and Chemical  
Physics,  
a section of the journal  
Frontiers in Chemistry

Received: 22 February 2019

Accepted: 24 April 2019

Published: 14 May 2019

### Citation:

Chiarinelli J, Casavola AR, Castrovilli MC, Bolognesi P, Cartoni A, Wang F, Richter R, Catone D, Tosic S, Marinkovic BP and Avaldi L (2019) Radiation Damage Mechanisms of Chemotherapeutically Active Nitroimidazole Derived Compounds. *Front. Chem.* 7:329. doi: 10.3389/fchem.2019.00329

Photoionization mass spectrometry, photoelectron-photoion coincidence spectroscopic technique, and computational methods have been combined to investigate the fragmentation of two nitroimidazole derived compounds: the metronidazole and misonidazole. These molecules are used in radiotherapy thanks to their capability to sensitize hypoxic tumor cells to radiation by “mimicking” the effects of the presence of oxygen as a damaging agent. Previous investigations of the fragmentation patterns of the nitroimidazole isomers (Bolognesi et al., 2016; Cartoni et al., 2018) have shown their capacity to produce reactive molecular species such as nitric oxide, carbon monoxide or hydrogen cyanide, and their potential impact on the biological system. The results of the present work suggest that different mechanisms are active for the more complex metronidazole and misonidazole molecules. The release of nitric oxide is hampered by the efficient formation of nitrous acid or nitrogen dioxide. Although both metronidazole and misonidazole contain imidazole ring in the backbone, the side branches of these molecules lead to very different bonding mechanisms and properties.

**Keywords:** nitroimidazole, radiosensitizers, mass spectrometry, PEPICO experiments, appearance energy, DFT

## INTRODUCTION

The use of “high-throughput screening” methods for drug discovery allows to rapidly conduct a very broad and random screening over an enormous number of chemicals. However, in these procedures the very fundamental chemical and physical mechanisms that determine the activity of these compounds at the molecular level remain unknown. On the other hand, highly sensitive experimental techniques and accurate computational methods have been developed to provide a detailed description of model molecules and to link their electronic and geometric structure to their functions. This, in particular, is of paramount importance in the case of the molecular response of cells and their building blocks to radiosensitising drugs used to increase the potential of radiotherapy. Despite the fact that the typical energies used in radiotherapy are in the keV to MeV range it is well-documented (García Gómez-Tejedor and Fuss, 2012) that a large fraction of the radiation damage on biological systems is due to secondary processes releasing particles (electrons, ions, radicals) with a broad energy distribution, which can subsequently trigger the

damaging of DNA and its surrounding environment. Slow electrons with energy of a few eV have been considered among the most active species (Boudaiffa et al., 2000; Michael and O'Neill, 2000). Thus, the potential impact of VUV based techniques is due to their possibility to provide detailed information on the electronic structure and fragmentation of valence orbitals, which are the ones mainly involved in the processes induced by low energy electrons. Photoelectron-photoion coincidence, PEPICO, experiments then, due to their energy selectivity, provide detailed insights on state-selected fragmentation, and therefore are particularly suited to identify the states involved in the production of specific fragments and the release of radicals.

The question is whether the fragmentation mechanisms and properties identified in the model systems are still active at macroscopic level in more complex and realistic systems.

In this work we present the results of a bottom-up approach, which goes from the model molecule to the real drugs used in therapy. Photoionization mass spectrometry (PIMS), photoelectron spectroscopy and photoelectron-photoion spectroscopic (PEPICO) technique, and computational methods

have been combined to investigate nitroimidazole (NI) derived molecules. These molecules are used in radiotherapy thanks to their capability to sensitize hypoxic tumor cells to radiation by “mimicking” the effects of the presence of oxygen as a damaging agent (Wardman et al., 2007; Rockwell et al., 2009; Sonveaux et al., 2009; Wilson and Hay, 2011; Higgins et al., 2015). However, the detailed mechanisms of their operation at molecular levels are still unknown, making difficult any rationale in the design of more efficient and less toxic drugs for treatment. In our bottom-up approach we have investigated the building blocks of the molecules used in therapy: the 2- and 4(5)-NI molecules (Bolognesi et al., 2016; Cartoni et al., 2018). The main results of the investigation of the fragmentation patterns of the NI isomers are summarized in **Figure 1** where the mass spectra (bottom panel) of the 2-NI and 4(5)-NI and the potential energy surfaces (top panels) for the NO loss and further fragmentations are shown.

At first glance, the most evident observation in **Figure 1** is that the fragment at  $m/z$  83 is one of the leading fragmentation channels in 2-NI, while it is almost absent in the 4(5)-NI sample. The  $m/z$  83 fragment can be unambiguously attributed to the

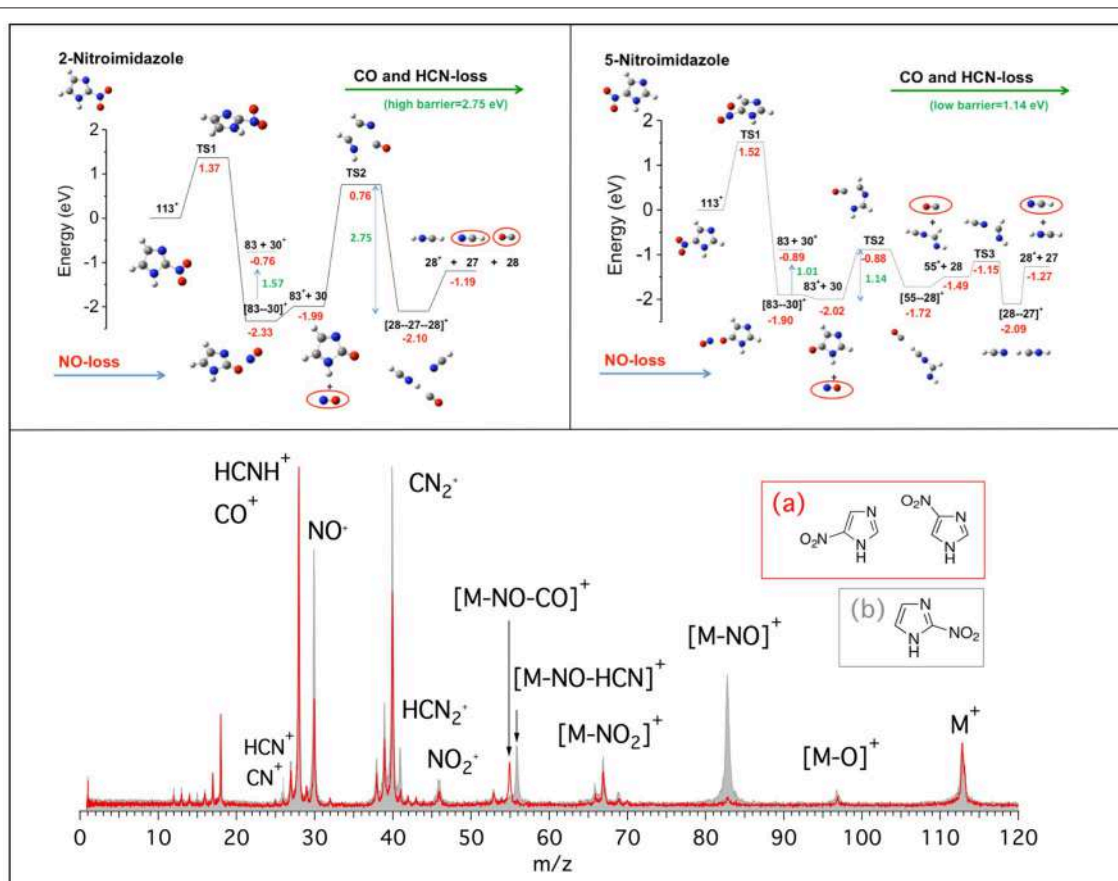
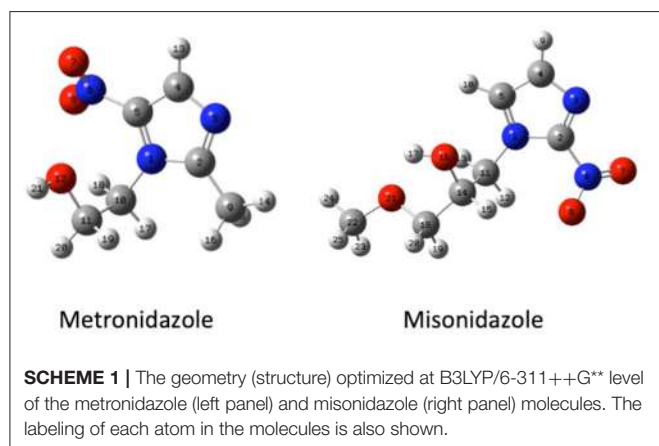


**FIGURE 1** | (Bottom panel) Mass spectra of 4(5)-NI [red line and inset (A)] and 2-NI molecules [gray, full area, and inset (B)] measured at 60 eV photon energy. The assignment of the main fragments is reported. (Top panels) Potential energy surfaces of the 2-NI and 5-NI, respectively, for the fragmentation of their corresponding molecular ions  $M^+$  ( $m/z$  113) calculated at the CCSD/6-311++G\*\*//B3LYP/6-311++G\*\* level of theory (Bolognesi et al., 2016). The molecular ion  $M^+$  as well as the fragments  $[M-O]^+$ ,  $NO_2^+$ ,  $HCN_2^+$ ,  $NO^+$ , and  $HCNH^+$  are all radical ions; the radical symbol  $\bullet$  as been omitted here and all over the paper for sake of simplicity.



loss of nitric oxide, which is particularly relevant for its potential implications in the biological context due to the well-recognized action of NO as a radiosensitizer and vasodilator (Wardman et al., 2007; Rockwell et al., 2009; Sonveaux et al., 2009). This may suggest that 2-NI is able to release a significantly larger amount of NO than 4(5)-NI, hence supporting the observation of its higher efficiency as radiosensitizer (Wardman et al., 2007). The quantum mechanical calculations (Figure 1, top panels) at the B3LYP/6-311++G\*\* level of theory for the geometry optimization and at the CCSD/6-311++G\*\* level for single-point energy calculation show that all of the nitroimidazole isomers are likely to release NO. However, in 4(5)-NI the subsequent fragmentation of the residual *m/z* 83 intermediate breaks the imidazole ring releasing HCN and CO molecules, while in 2-NI the higher kinetic stability of the ring leaves the intermediate intact. These results explain the different intensity of the fragments at *m/z* 83, 55, 30, and 28 observed in the mass spectra of both 2-NI and 4(5)-NI, respectively. From these evidences we determined that all the nitroimidazole isomers release the NO fragment with similar mechanisms. The released NO, being active for a short period of time after irradiation, could act by fixing dangling bonds in damaged DNA, making the damage permanent and by “favoring either drug delivery or the therapeutic efficacy of irradiation through transient tumor reoxygenation,” as suggested by Sonveaux et al. (2009). In addition to the redox mechanism, this could provide explanation for the potential of all nitroimidazoles as radiosensitizers active on hypoxic tumors (Higgins et al., 2015). On the other hand, the release of carbon monoxide, CO, and hydrogen cyanide, HCN, more pronounced in 4(5)-NI isomers, may induce an opposite effect by efficiently attaching to hemoglobin (Berg et al., 2012) and inhibiting the *cytochrome c* oxidase in mitochondria (Yoshikawa and Caughey, 1990), respectively. Therefore, this effectively reduces the needed oxygenation and the overall radiosensitizing effect.

Guided by these former results, in this work we have studied both experimentally and theoretically the fragmentation mechanisms of metronidazole [IUPAC name: 2-(2-methyl-5-nitro-1H-imidazol-1-yl) ethanol] and misonidazole [IUPAC name (RS)-1-methoxy-3-(2-nitroimidazol-1-yl)propan-2-ol]



(Scheme 1), the two radiosensitizers built on the 5-NI and 2-NI compounds, respectively, which are used in radiotherapy.

The experimental methods are described in section Experimental, while the theoretical ones are summarized in section Theoretical Methods. The experimental results are analyzed in section Results and discussed/interpreted with the support of the DFT theoretical calculations in section Discussion. Finally some conclusions are presented in section Conclusion. In the following the radical symbol • has been omitted for the sake of simplicity.

## EXPERIMENTAL

The experiments have been performed at the Circular Polarized (CIPO) and Gas Phase Photoemission (GAPH) beamlines of the Elettra synchrotron radiation source, Trieste (Italy). The characteristics of the beamlines have been described in details elsewhere (Derossi et al., 1995; Blyth et al., 1999) and will not be repeated here.

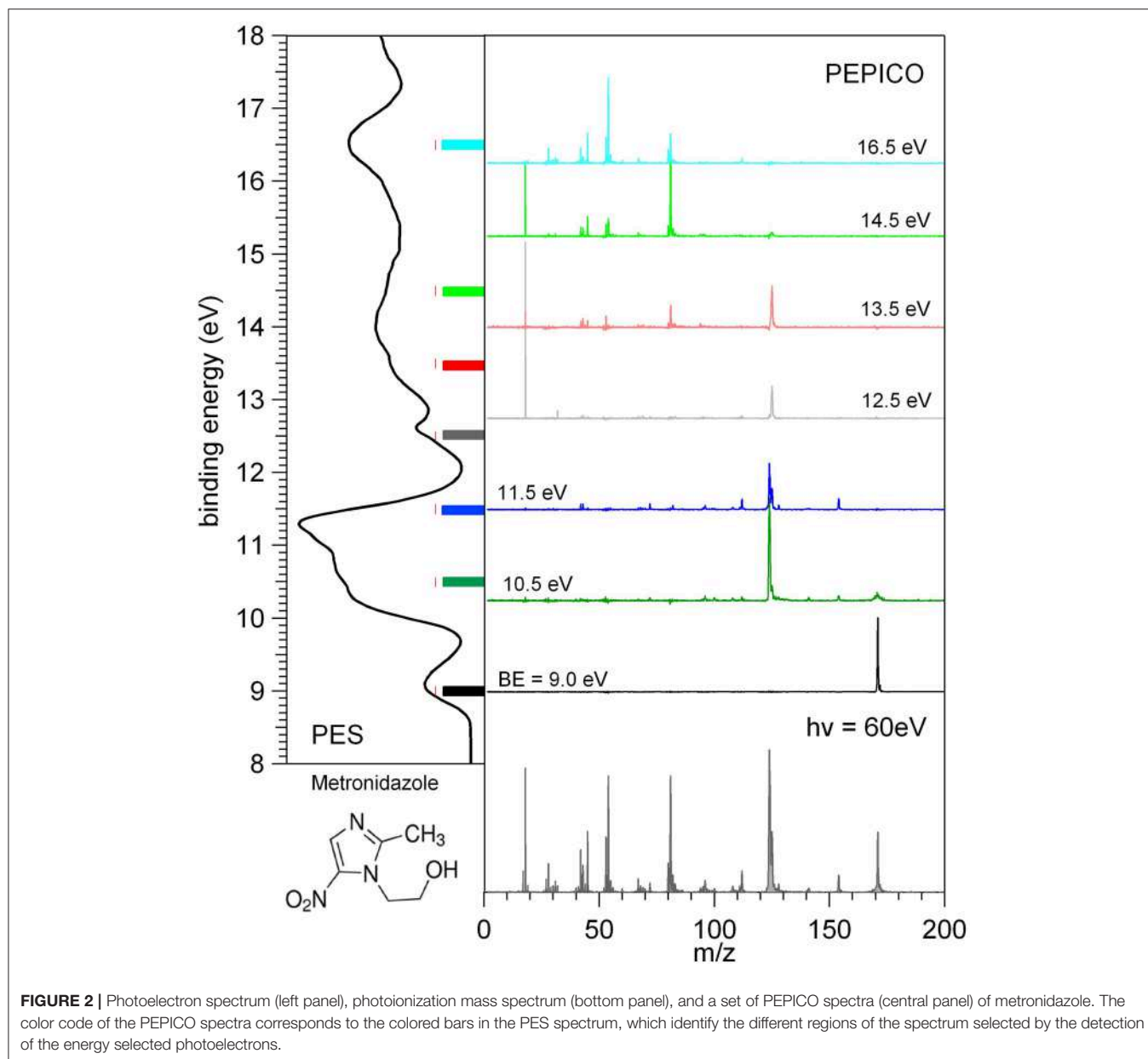
The metronidazole sample of analytical standard was purchased from Sigma-Aldrich, while the misonidazole one with 95% purity by Vinci-Biochem Srl. Both samples have been used without further purification. They are in the form of powders at standard ambient temperature and pressure, and they are evaporated in a furnace at about 150°C. No evidence of sample dissociation is observed.

The Appearance Energy, AE, of the different fragments has been obtained by the measurement of the photoionization efficiency curves of the parent ion and selected fragments at the CIPO beamline using the aluminum normal incidence monochromator (NIM), that covers the photon energy range 5–17 eV with a resolving power of about 1,000. The setup consists of five electrostatic lenses that focus and accelerate the ions from the region of interaction to the quadrupole mass spectrometer (QMS). This is a commercial QMS (10–4000 u, Extrel 150-QC 0.88 MHz) with a mass resolution  $M/\Delta M$  of about 500. It is mounted perpendicularly to the photon beam and to the gas source. The photoionization efficiency curves were normalized to the photon intensity, measured simultaneously by a photodiode located at the end of the beamline. The photon energy was calibrated against the autoionization features observed in the Ar total photoionization spectrum between the 3p spin orbit components. In the photon energy scans up to 11.7 eV, a lithium fluoride filter was used to remove the second order radiation. Above this energy, the contribution of the second order radiation was evaluated by comparing the Ar<sup>+</sup> ion yield measured as a function of the photon energy to its ionization cross section (Marr and West, 1976). This second order contribution has been taken into account in the extraction of the photoionization efficiency curves (Castrovilli et al., 2014).

The photoelectron and mass spectra as well as the photoelectron-photoion coincidence, PEPICO, spectra have been measured at the GAPH beamline using a high vacuum chamber hosting a hemispherical analyzer (VG 220i) equipped with six channeltron detectors and a custom made Wiley McLaren (Wiley and McLaren, 1955) time-of-flight (TOF)

mass spectrometer mounted opposite to each other at the magic angle with respect to the polarization axis of the photon beam. The TOF mass spectrometer, working in conjunction with the “virtually” continuous ionization source provided by the multibunch operation mode of the synchrotron radiation, is operated in pulsed extraction mode. The repeller and extractor electrodes are polarized with antisymmetric voltages (manufacturer Directed Energy Inc., model PVM4210) driven by an external trigger, which provides a typical extraction field of 700 V/cm. The electron and ion mass analyzers can be operated independently, for photoelectron spectroscopy and photoionization mass spectrometry, respectively. In these operation modes (i) the hemispherical analyzer is normally operated with pass energy of 5 eV, corresponding to a kinetic

energy resolution of about 150 meV or (ii) the extraction field of the TOF spectrometer is triggered using a 1 kHz pulse generator (Stanford Research Systems DG535) to extract the ions. The two analyzers can also be operated simultaneously for coincidence measurements. In this mode a residual penetration field from the drift tube of the TOF produces a kinetic energy shift of the photoelectron spectrum (easily taken into account by the calibration procedure) and a degradation of the energy resolution of the electron analyzer. Therefore, in the coincidence mode the electron energy analyzer has been operated at pass energy of 20 eV, with a gain in efficiency, but no further loss of resolution. The final energy resolution is estimated to be around 0.5 eV. In order to perform photoelectron-photoion coincidence spectroscopic measurements, the electronic chain



schematically reported in Figure 1 of Plekan et al. (2008) has been used for all detectors of the VG analyser. The three different types of measurement, that can be performed by this set-up, are illustrated in Figure 2 where the photoelectron spectrum, the photoionization mass spectrum and a few PEPICO spectra of metronidazole measured at 60 eV photon energy are shown.

In the PEPICO measurements the selection of the kinetic energy of the detected photoelectron allows to make a state selected investigation of the fragmentation of the molecule as clearly shown in the central panel of Figure 2. From the spectra measured at different binding energies, BE, the branching ratio for the formation of a selected fragment vs. photon energy can be obtained. The procedures for the treatment of the PEPICO spectra, with the subtraction of the background due to the random coincidence and relative normalization have been described recently elsewhere (Chiarinelli et al., 2018) and therefore will not be repeated here.

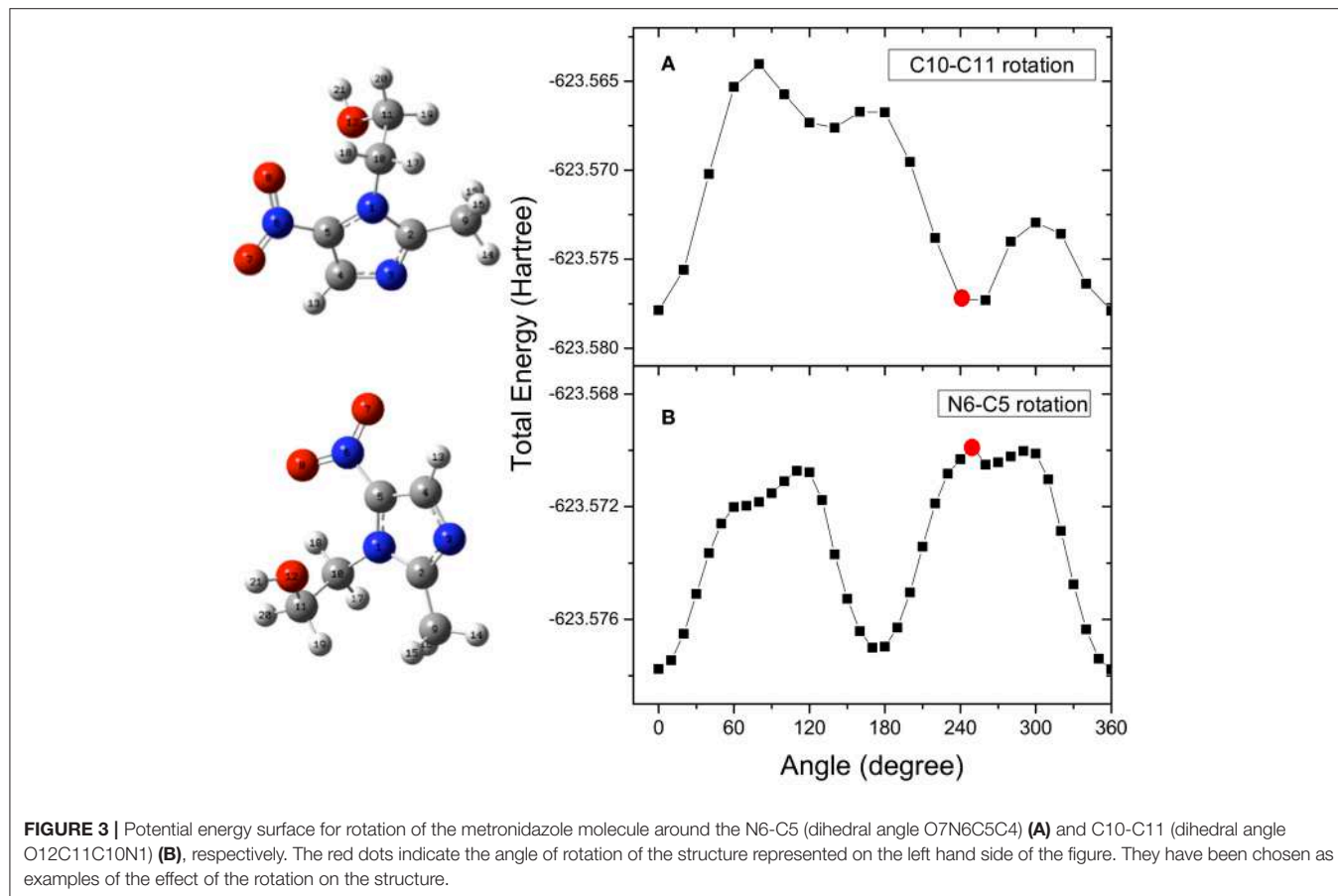
In Figure 2 each energy selected mass spectrum is characterized by only a few fragments as compared to the unselected mass spectrum (see bottom panel in Figure 2); the parent ion is observed only near the ionization energy of the molecule; only a few fragmentation channels at a time are associated with a selected electronic state of the cation although lower energy fragmentation channels are already energetically open.

## THEORETICAL METHODS

Quantum chemical calculations have been performed with Density Functional Theory (DFT). The geometries were optimized using the Becke, three-parameter, Lee-Yang-Parr (B3LYP) functional with the 6-311++G\*\* basis set. The frequency analysis was based on the normal mode harmonic approximation (Wong, 1996). All critical points were characterized as energy minima or transition state structures (TS) by calculating the harmonic vibrational frequencies at the same level of theory. They were also used to compute the zero-point and thermal energy corrections. The TS were unambiguously related to their interconnected energy minima by intrinsic reaction coordinates (IRC) calculations (Gonzalez and Schlegel, 1989, 1990).

The outer valence vertical ionization energies were calculated using the outer valence Green function OVGF/6-311++G\*\* methods (von Niessen et al., 1984; Ortiz, 1988), based on the optimized geometries using B3LYP/6-311++G\*\*.

The determination of the potential energy surfaces for the two flexible metronidazole and misonidazole compounds is very challenging, because rotations of their single C-N, C-C, and C-O bonds may produce a number of local minimum structures, i.e., conformers on their potential energy surfaces. All the possible stable conformers of a molecule may contribute



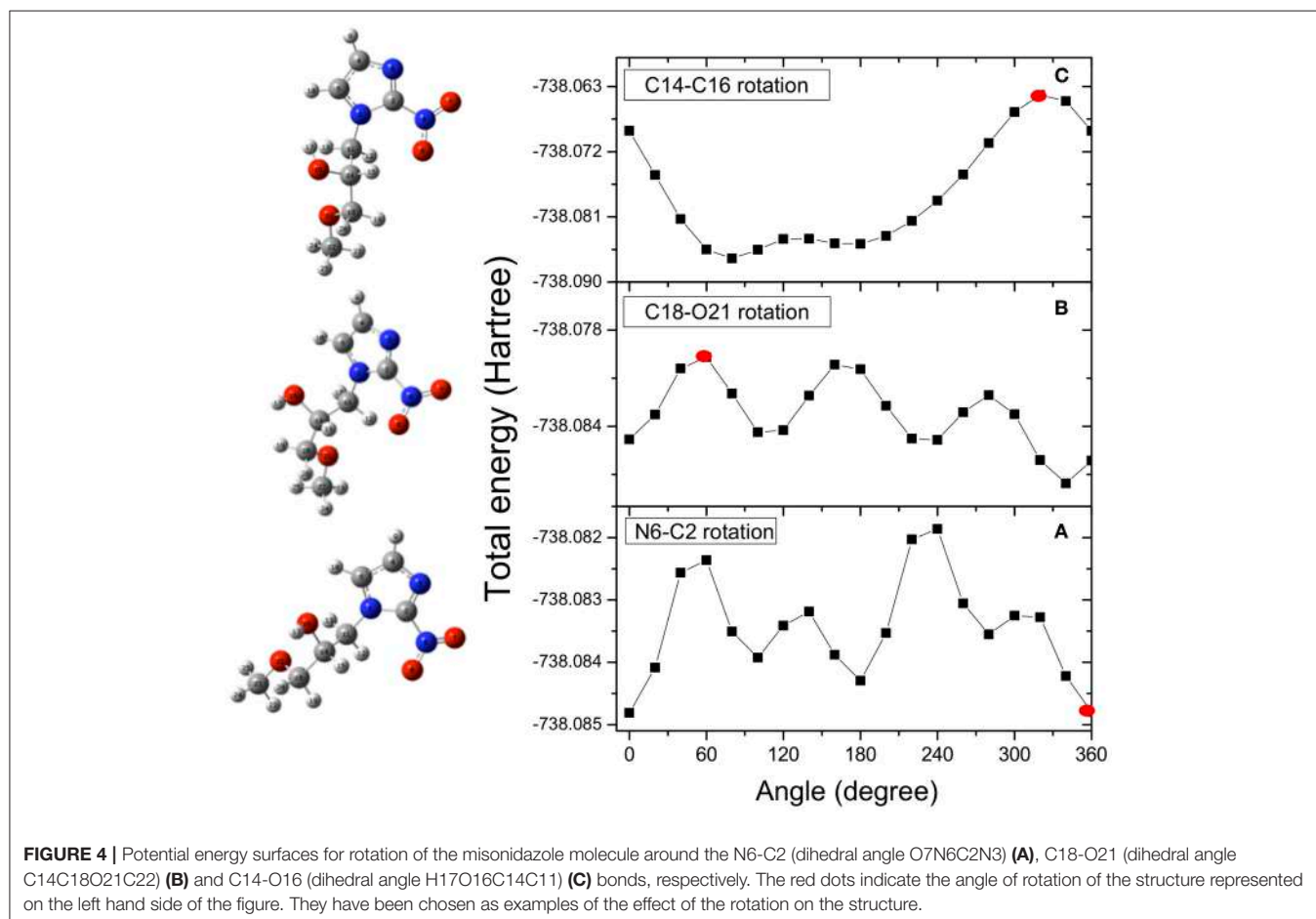
to the measurement, based on Boltzmann's distribution at the temperature of the measurement. The search for all possibly stable conformers can be a daunting task. The structures and vibrational frequencies of the different structures in the potential energy surface of metronidazole and misonidazole for the electronic ground state were calculated using the Gaussian 09 program package (Frisch et al., 2009). High-level ab initio calculations have been done to map the potential energy surface for internal rotation of the molecules. Among the several rotational paths that the molecule can follow, here we have considered the ones which, leading to large potential energy barriers, are able to produce stable local minimum structures, i.e., conformers of the compounds. These rotational pathways are represented in the following figures. In the case of metronidazole the rotations around the N6-C5, which is the nitro and imidazole N-C bond and C10-C11 which is the ethanol backbone C-C bond, exhibit apparent energy barriers due to formation of the intramolecular hydrogen bonding. The relative potential energy scans were calculated rotating these two bonds, N6-C5 (dihedral angle O7N6C5C4), and C10-C11 (dihedral angle O12C11C10N1), respectively. The potential energy scans as a function of the dihedral angles are reported in **Figure 3**.

Optimizations of the structures are performed again at the local minima structures on the potential energy surface and

the stable local minimum structures (conformers) are then found. The selected parameters which characterize the minimum structures conformer I (C10-C11) and conformer II (N6-C5) are collected in **Table 1SM**. We found that although conformers I and II obtained from rotation of the N6-C5 and C10-C11 bonds, respectively, are almost energy degenerate with a difference of 0.085 KJ/mol, they are different conformers as other properties such as dipole moments are very different. Vibrational frequency calculations were performed at the same level of the geometry optimization to characterize the stationary points as either minima or transition state structures (first-order saddle points). The frequencies calculated for the minimum structure conformers are all positive confirming that they are true minimum structures.

In the case of misonidazole the same high-level ab-initio calculations have been performed to map out the potential energy surface for internal rotation of the NO<sub>2</sub> group around the N6-C2 bond (**Figure 4A**), of the OCH<sub>3</sub> group around the C18-O21 bond (**Figure 4B**) and of the OH group around the C14-O16 bond (**Figure 4C**).

Once the minimum in the potential energy surface is found, we optimized it for the most stable structure. Due to intramolecular hydrogen bonding, the rotation of the OH group produces a conformer more stable than the rotation around



the other bonds. As in the case of metronidazole, the energy differences between the analyzed conformers are in the range of few Kcal/mol. It means that already at room temperature there is a mix of different conformers. In the calculations only one structure, the most stable one resulting from the rotation of the C14-C16 bond (dihedral angle H17O16C14C11), is chosen as starting point of the fragmentation pathway. This may represent a strong limit, because some pathways might not be identified due to a different initial structure.

## RESULTS

The mass spectra of the metronidazole and misonidazole molecules measured at 60 eV photon energy are shown in **Figure 5**.

The metronidazole molecule is built on the 5-NI where the H bound to C2 is replaced by the methyl group CH<sub>3</sub> and the one bound to the N1 in the imidazole ring by a “short” ethanol tail (T<sub>1</sub> = CH<sub>2</sub>CH<sub>2</sub>OH, m = 45 Da) terminated by a OH group. In its

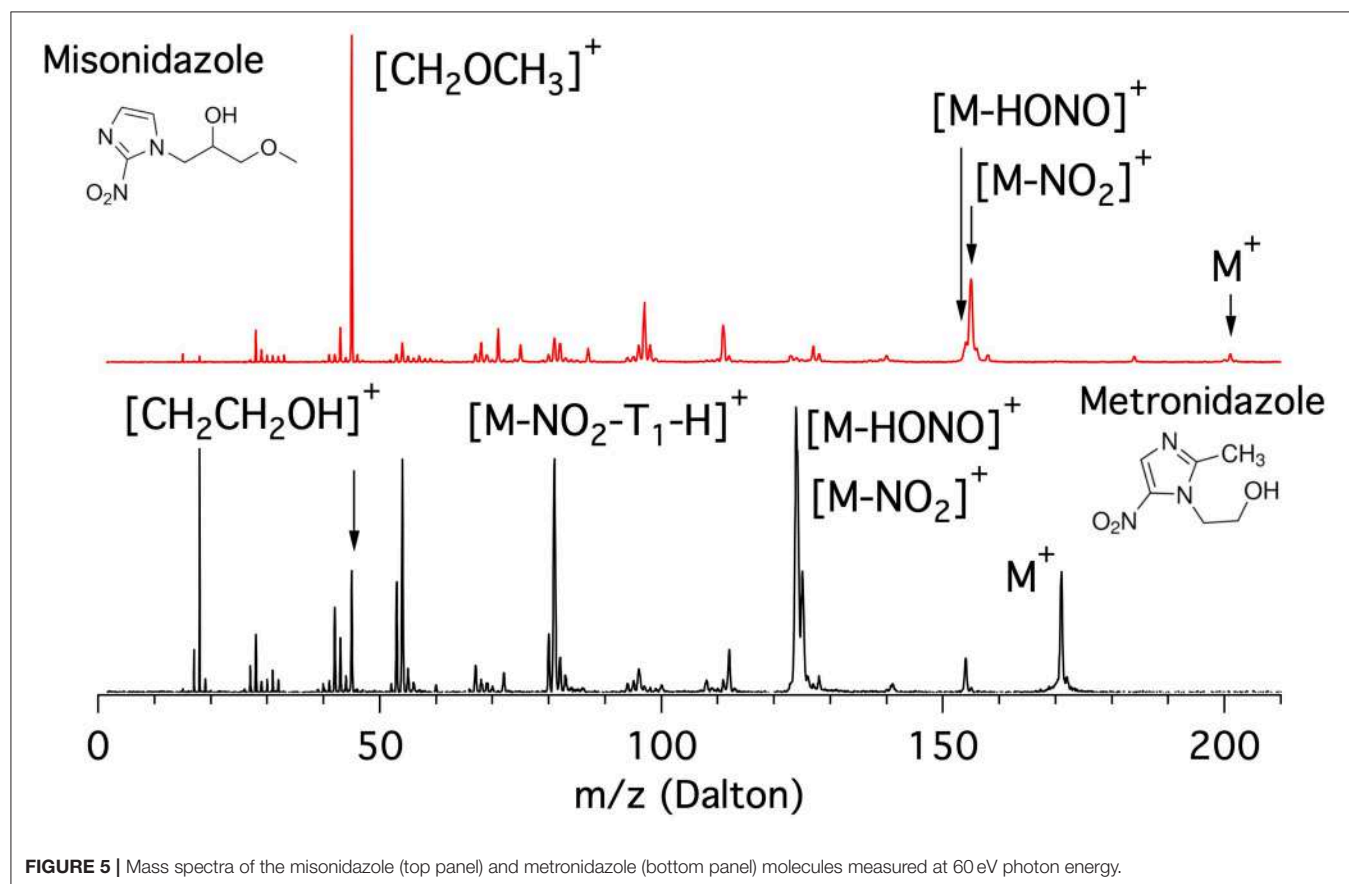


**FIGURE 5** | Mass spectra of the misonidazole (top panel) and metronidazole (bottom panel) molecules measured at 60 eV photon energy.

**TABLE 1** | Experimental and theoretical values calculated at the B3LYP6-311++G\*\* level of the ionization potential, IP, of the parent ion and AE of some fragments of the metronidazole, and misonidazole.

Metronidazole				Misonidazole				
m/z	Assignment fragments	Exp.	Exp*	Theory	m/z	Assignment	Exp.	Theory
171	M = C <sub>6</sub> H <sub>9</sub> N <sub>3</sub> O <sub>3</sub>	8.57 ± 0.05	8.84 ± 0.1	8.6	201	M = C <sub>7</sub> H <sub>11</sub> N <sub>3</sub> O <sub>4</sub>	8.55 ± 0.03	8.77
125	M-NO <sub>2</sub>	9.33 ± 0.07	10.02 ± 0.1	9.59	155	M-NO <sub>2</sub>	8.90 ± 0.04	9.1
124	M-HONO	9.14 ± 0.10	9.96 ± 0.1		154	M-HONO	8.91 ± 0.04	
81	M-NO <sub>2</sub> -(T <sub>1</sub> -H)	12.22 ± 0.10						
54	M-NO <sub>2</sub> -(T <sub>1</sub> -H)-HCN	13.42 ± 0.10		13.55				
45	T <sub>1</sub> = CH <sub>2</sub> CH <sub>2</sub> OH	12.09 ± 0.10		11.34	45	CH <sub>2</sub> OCH <sub>3</sub>	10.21 ± 0.10	10.40

In the case of metronidazole also the experimental data by Guo et al. (2012) have been reported. \*(Guo et al., 2012)



mass spectrum (bottom panel of **Figure 5**) the main features are at  $m/z$  171 (parent ion  $M^+$ ),  $m/z$  125, and 124 ( $[M-NO_2]^+$  and  $[M-HONO]^+$ , respectively), around  $m/z$  81 ( $[M-NO_2-(T_1-H)]^+$  group),  $m/z$  53 (corresponding to the opening of the imidazole ring following a further fragmentation of  $m/z$  81), and around  $m/z$  42 with the peak at  $m/z$  45 assigned to the ethanol cation tail  $[T_1]^+$ . Below  $m/z$  20 the peaks due to smaller fragments such as  $H_2O$  and  $CH_3$  are also observed.

The misonidazole molecule is built on the 2-NI where the H bound to the N1 of the imidazole ring is replaced by a “longer” tail ( $T_2 = CH_2CH(OH)CH_2OCH_3$ ,  $m = 89$  Da) in which the propanol-2 is terminated by a methoxy group. The inspection of the mass spectra of misonidazole (top, red) and metronidazole (bottom, black) given in **Figure 5** shows that, although the two molecules share some common fragment groups, the relative intensities of the different fragments are very different. Two major differences are observed. One major difference in the two spectra is represented by the near absence of the parent ion in misonidazole; the other is that the very limited number of relevant fragments in the misonidazole spectrum or the number of intensive fragments in the metronidazole spectrum (bottom, black) indicate this molecule is more fragile. Therefore, the radiosensitizers engage with very different bonding mechanism. The parent ion  $M^+$  at  $m/z$  201 of misonidazole represents only a minor contribution to the mass spectrum and the main feature at  $m/z$  45 can be assigned to the  $[CH_2OCH_3]^+$  fragment and

corresponds to a part of the tail  $T_2$ . The other noticeable feature is represented by the group at about  $m/z$  155 assigned to the  $[M-NO_2]^+$  fragment. All in all the  $[CH_2OCH_3]^+$  fragment and the group at about  $m/z$  155 contribute to about 50% of the spectrum at this photon energy.

As for as the comparison with the 2-NI and 4(5)-NI spectra reported in **Figure 1**, it is noticeable that the loss of the NO group ( $[M-NO]^+$  with  $m/z$  141 and 171 in the metronidazole and misonidazole, respectively) or the correlated product  $NO^+$  ( $m/z$  30) appear to be, if any, a minor channel.

Based on the observations from the mass spectra in **Figure 5**, in the PEPICO and AE measurements we concentrated our attention on the parent ion, the fragments corresponding to  $[M-NO_2]^+$  and  $[M-HONO]^+$  and the  $m/z$  45 fragment which may correspond to the tail  $[HOCH_2CH_2]^+$  in metronidazole and a section of the tail  $[CH_2OCH_3]^+$  in the misonidazole. In the case of the metronidazole we also investigated two other fragments at  $m/z$  81 and 54. A detailed report of the AE and PEPICO measurements relative to all the fragments observed in the mass spectra will be reported in a separate publication (Bolognesi, in preparation).

The experimental and calculated AE values are collected in **Table 1**, while the branching ratio of the parent ion and different fragments derived from the PEPICO measurements are shown in **Figure 6**. In the bottom panel of the same figures the photoelectron spectrum of each molecule measured at 60 eV

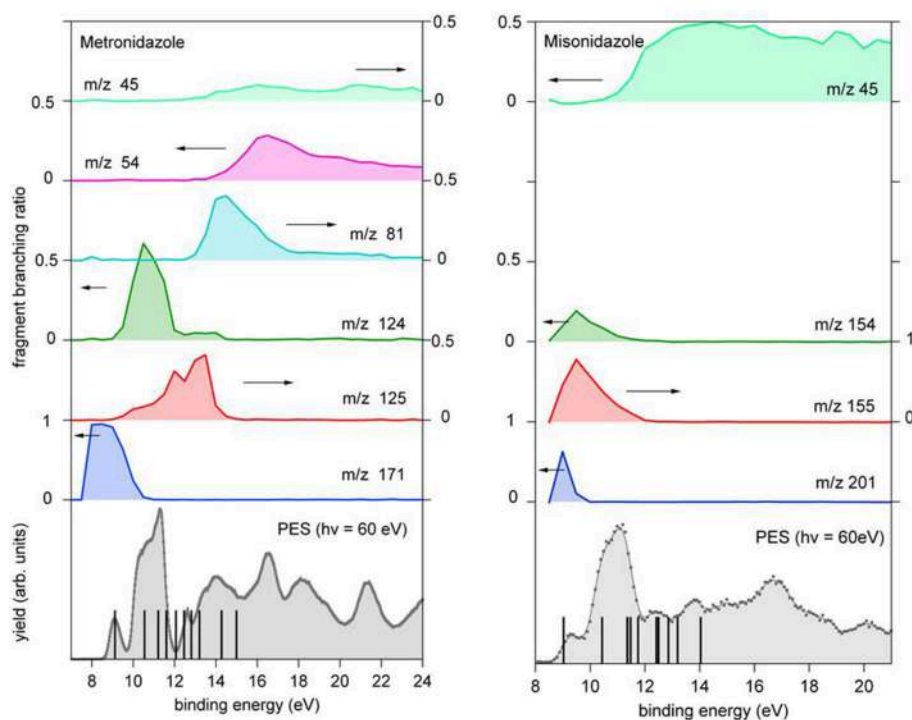


**FIGURE 6** | Branching ratio for the parent ion and a few fragments of metronidazole (left panel) and misonidazole (right panel) reported vs. the binding energy. The scale of the different branching ratios is indicated by the arrows. At the bottom of each figure the photoelectron spectrum of the molecule is reported. The vertical bars represent the binding energy of the cation states calculated using the outer valence Green function OVG76-311++G\*\* method (von Niessen et al., 1984), see **Supplementary Material**.

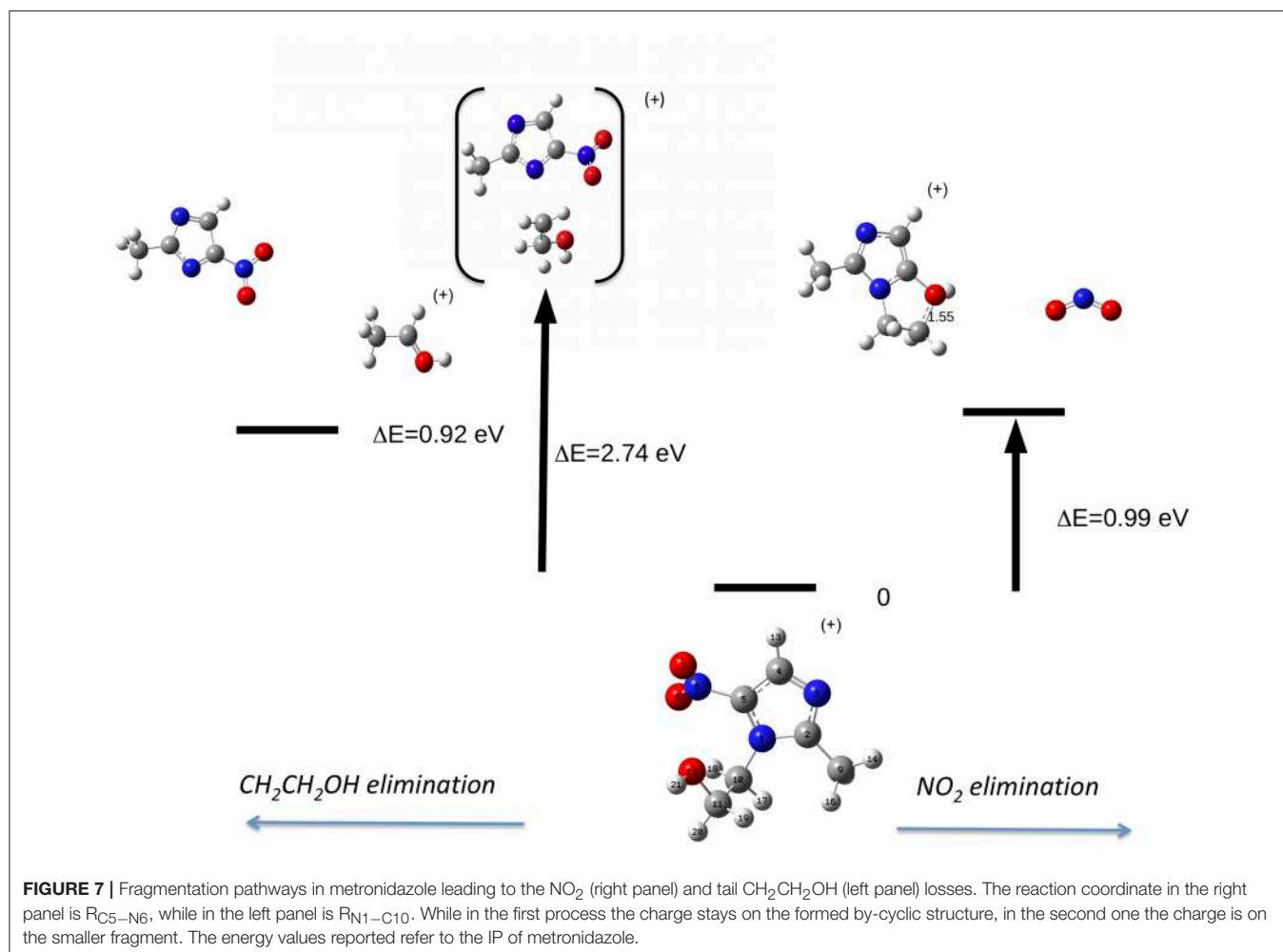
is reported. The energies of the cation states calculated by the outer valence Green function OVG6-311++G\*\* method (von Niessen et al., 1984) up to 15 eV are reported in **Figure 6** and tabulated in **Table 2SM**. The spectroscopic pole strengths calculated in the Green's function model are in the range of 0.85–0.91, suggesting that the independent particle picture is a good approximation in this energy region. In the region of BEs higher than 15 eV electronic configurations with relaxation, two-hole-one-particle (2h-1p) and higher excitations may dominate the cationic states. These contributions, which represent the electronic correlation and relaxation, make the one-particle picture of the cationic states and/or vertical ionization process no more good approximations in this region. As a result, we concentrate on the outer valence region of the compounds in this section.

In both molecules the parent ions are possibly produced only via the ionization of the electrons on their highest occupied molecular orbital (HOMO) states. In the case of misonidazole the production of the parent ion competes already at threshold with dissociation channels involving the NO<sub>2</sub> and HONO losses, see also **Table 1**. The same channels are observed in the metronidazole at about 1 eV above the ionization threshold with

the HONO fragment loss having its maximum branching ratio in the energy region of HOMO-1 to HOMO-3 orbitals. The NO<sub>2</sub> loss channel is characterized by an AE very close to the one of the HONO loss, but becomes more effective at BE > 12 eV. The channel leading to the formation of the [CH<sub>2</sub>OCH<sub>3</sub>]<sup>+</sup> fragment, which appears to be the dominant channel in the fragmentation of misonidazole, has a measured AE in the proximity of the BE of the HOMO-1 state and already at a BE of 12 eV its branching ratio is about 0.5. The channel leading to the m/z 45 fragment in metronidazole, which corresponds to the loss of the tail bound to N1 in the imidazole ring, displays a higher AE (about 12.09 eV), but a lower branching ratio (maximum value of about 0.1). The AE of m/z 124 and 125 fragments measured by Guo et al. (2012) are also reported in **Table 1**. The two sets of experimental data agree within their respective uncertainties.

## DISCUSSION

The mass spectrum of the metronidazole molecule has been previously measured by 75 eV electron impact (Linstrom and Mallard, 2008) and at a few photon energies between 9.5 and



13 eV by Guo et al. (2012) in the  $m/z$  range 100–180. All the previously observed fragments of metronidazole in the electron impact spectrum are also present in **Figure 5**. However, we noted that slightly different intensities for the bands centered at approximately  $m/z$  125 and 81, respectively, are observed in this spectrum. In the outer valence region, the measurements by Guo et al. (2012) are consistent with the present PEPICO experiments. At 9.5 eV only the parent ion is produced in the photoionization event, while at 11 eV fragments corresponding to the NO<sub>2</sub> and HONO losses at  $m/z$  124 and 125 are observed as well as at the highest photon energy used (13 eV) also the fragments corresponding to  $m/z = 126$  and 127. Pandeti et al. (2017) observed the loss of C<sub>2</sub>H<sub>4</sub>O (44 Da) at position N1 followed by the NO<sub>2</sub> loss as the dominant fragmentation channels in a collision induced dissociation experiment of protonated metronidazole. Such a process in the present case would lead to prominent features at  $m/z$  127 and 81, respectively. While the feature at  $m/z$  81 is clearly observed in the mass spectrum in **Figure 5**, the other one seems to give a minor contribution to our spectrum.

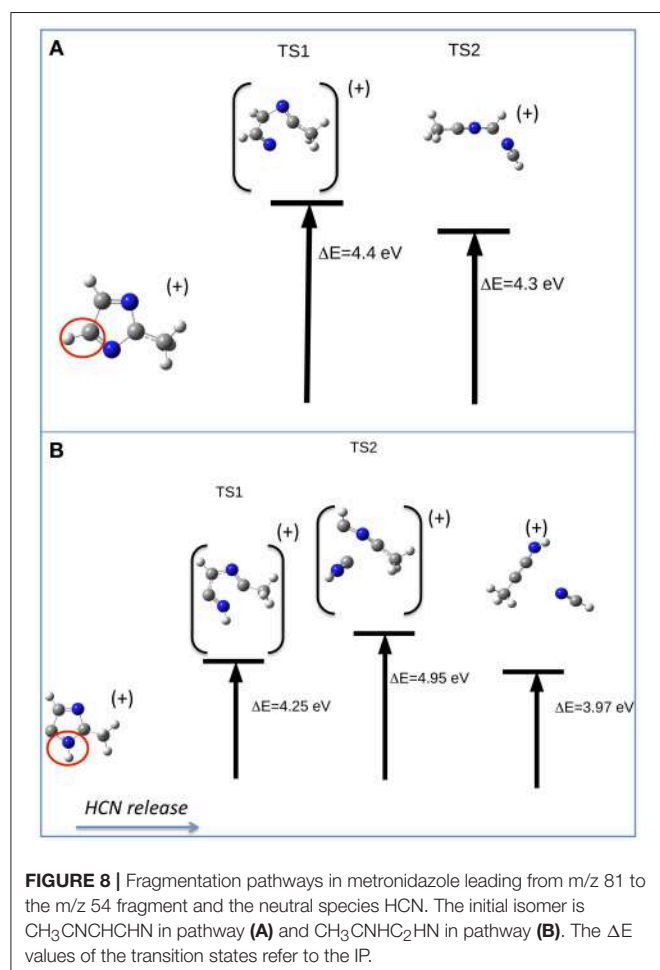
Less information is available for the mass spectrum of misonidazole. Recently Feketeova et al. (2014) presented fragmentation spectra of protonated misonidazole in the  $m/z$

range 60–205 obtained by collision and electron induced dissociation experiments. The assignment of the features observed in **Figure 5** has been done according to that work and for the low  $m/z$  region not covered by the study of Feketeova et al. (2014) the results of the competitive fragmentation modeling method (Allen et al., 2014) have been employed to assist the analysis.

Very rare photoelectron spectrum (PES) studies are available for metronidazole and misonimidazole. The PES of metronidazole was measured and interpreted by a comparison with a series of spectra of simpler methylnitroimidazoles by Kajfez et al. (1979). The spectrum was measured with a HeI discharge lamp with a resolution of about 35 meV. Despite the lower resolution all the features assigned by Kajfez et al. (1979) are also visible in the present study as given in **Figure 6** (see **Table 3SM**). The present measurement extends over a broader binding energy range up to 25 eV. To our knowledge no previous photoelectron spectrum of misonimidazole has been reported in the literature. The charge densities of the molecular orbitals in **Table 4SM** indicate that the HOMO is a  $\pi$  orbital located above and below the imidazole ring plane, while in the case of the HOMO-1 a contribution of  $\sigma$  type between C14 and C18 exists. In the comparison of the two experimental spectra the HOMO of the misonidazole appears to be stabilized (the BE being about 200 meV higher than in the metronidazole) while the theoretical predictions sets the BE of the HOMO of misonidazole about 100 meV below the metronidazole one, see **Table 2SM**. However, the differences are well within the accuracy of the approximation of the used theoretical method and the experimental uncertainties.

Let's now discuss the AEs and the ion yields determined in the energy selected PEPICO experiments. In the case of the metronidazole the parent ion ( $m/z$  171) is observed (**Figure 6**) only in the region of the HOMO orbital. Already at about 1 eV above the ionization potential, IP, the state selected mass spectrum is dominated by the  $m/z$  125 and 124 fragments, which correspond to the NO<sub>2</sub> and HONO losses, respectively. The process leading to the NO<sub>2</sub> elimination has been simulated. In this simulation as well as in all the others discussed later on in the text the full potential energy surface along the possible reaction coordinate has been explored. To simplify the representation in the figures only the transition states (TS) and the final optimized geometries of the products have been reported together with the relevant energies referred to the calculated adiabatic IP. The simulations summarized in **Figure 7**, right panel, shows that the process leading from the parent ion in its ground state to a charged fragment with  $m/z$  125 and the NO<sub>2</sub> elimination needs to overcome a barrier of about 1 eV. The calculated AE is in satisfactory agreement with the measured value. The simulation also indicates that the NO<sub>2</sub> elimination leads to the formation of a by-cyclic structure in which O12 is bound to C5. This can be explained by considering as a starting configuration the conformer II (see **Table 1SM**) with the O12H group oriented toward the nitril group.

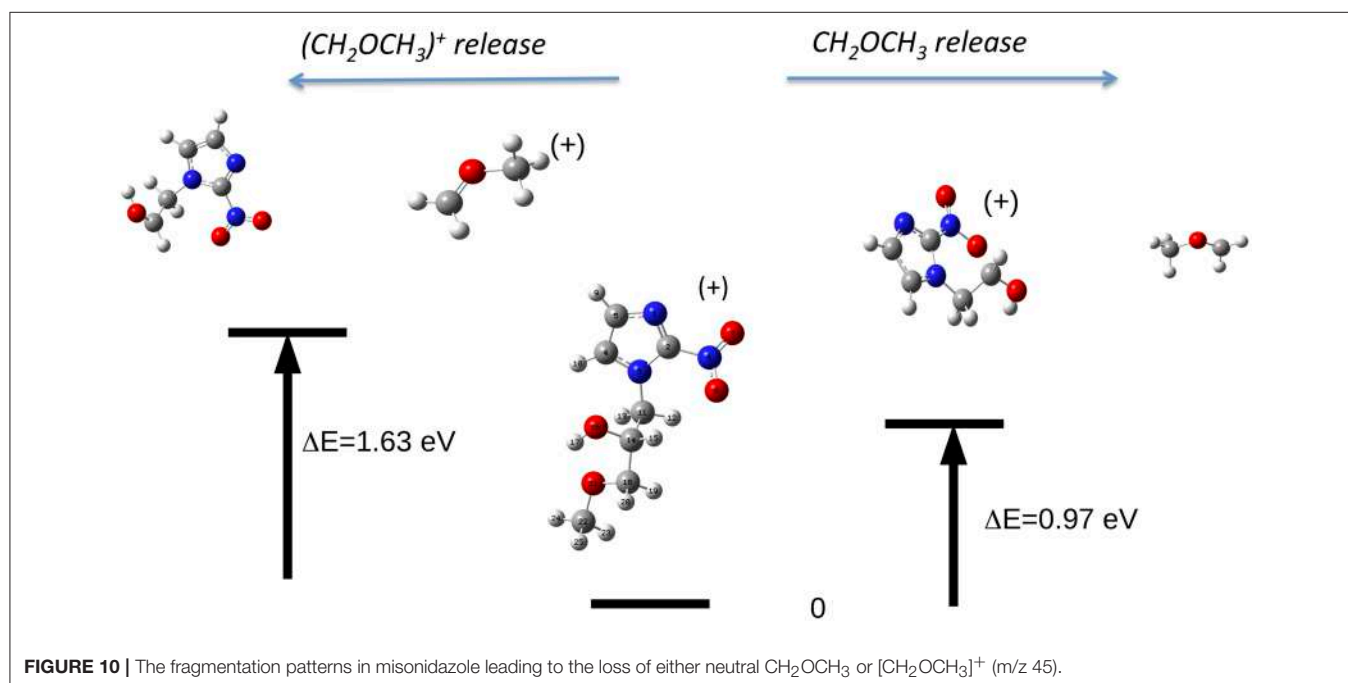
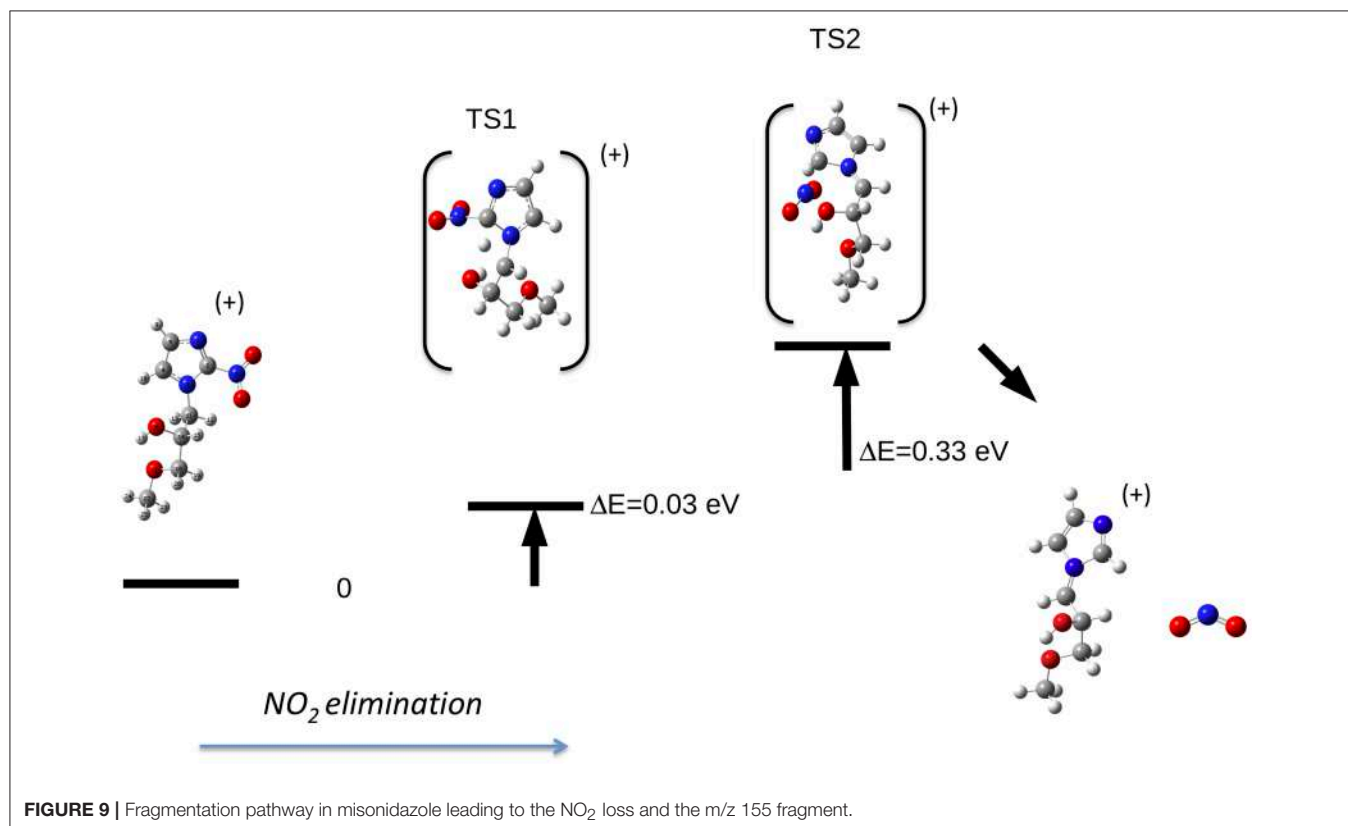
This can be rationalized considering that the scans that lead to the identification of the conformer of minimum energy (see **Figure 3**), indicate that within an energy range of a few meV several conformers exist. As already mentioned, this





represents a severe challenge for the simulations, because the use of a conformer as a starting point of a scan may strongly influence the reaction path. Guo et al. (2012) studied the  $\text{NO}_2$  loss and found that the cleavage of the C5-N6 bond is

accompanied by an intramolecular hydrogen transfer. These authors considered three different formation pathways starting by two conformations of the parent ion, which differ by the orientation of the O12H hydroxyl group with respect to the nitril



group. In all cases the transition states involve the formation of a by-cyclic structure with energy barriers between 1.1 and 1.3 eV, which is consistent with the one calculated in the present work.

The same authors (Guo et al., 2012) proposed similar reactions for the HONO loss. When the hydroxyl group is located at the same side of the nitril one the H atom of the hydroxyl group is transferred to the nitril one and an intramolecular ring-closing reaction occurs via the formation of the C11O12-C5 bond. When the hydroxyl group is located at the other side one H atom migrates from C10 to the nitril group. The calculated energy barrier of 0.72 eV and AE=9.20 eV for the first route are closer to the observed experimental value, thus it has been suggested as the most likely (Guo et al., 2012). Our extensive search for the transition state leading the HONO loss failed. The formation of the fragment at m/z 124 via the two successive losses of NO<sub>2</sub> and H lead to a calculated AE of about 17 eV, i.e., more than 7 eV higher than the experimental observation. Thus, while our experimental observation is in agreement with the one by Guo et al. (2012) and consistent with the predicted value by the same authors we can't confirm theoretically the reaction pathway they proposed.

On the left part of **Figure 7** the path leading to the loss of the tail T<sub>1</sub> (CH<sub>2</sub>CH<sub>2</sub>OH, 45 Da) by the C10-N1 rupture is illustrated. The simulation shows that at the rupture of the bond the formed structure is CH<sub>3</sub>CHOH, i.e., a H migration occurred. In this process the charge might be localized either on the heavier fragment, which includes the imidazole ring, or on the tail. Considering the relative intensity of the peaks at m/z 126 and 45 in **Figure 5**, it seems that the process leading to the CH<sub>3</sub>CHOH<sup>+</sup> fragment is the most likely one. The appearance energy of this latter process has been calculated to be 11.34 eV, i.e., 2.74 eV above the IP. The predicted value is about 1 eV lower than the observed one. Guo et al. (2012) in the measurement at photon energy of 13 eV observed a tiny feature assigned to m/z 126 and calculated the AE of that fragment at 12.21 eV. Even though in our experiment the branching ratio for that fragment is vanishing, we calculated its AE and found a value of 12.16 eV consistent with the one by Guo et al. (2012).

It is interesting to note that in the scan of the potential energy surface no paths leading to the isomerization of the NO<sub>2</sub> and the following NO loss, as observed in the 2- and 4(5)-NI, have been found. This is consistent with the experimental observation and represents a major difference in the fragmentation of the molecules studied here and their nitroimidazole model systems.

The other relevant fragment in the mass spectrum of metronidazole is at m/z 81, which results from the successive losses of NO<sub>2</sub> and CH<sub>2</sub>CHOH. Starting from the fragment m/z 125, the migration of H from the CH<sub>2</sub>OH group to the ring occurs, leading to a break of the double ring and subsequent elimination of CH<sub>2</sub>CHOH. The m/z 81 fragment, which can have two configurations with a H atom either bound to C5 or to N1 (**Figures 8A,B**, respectively), will further evolve with the formation of the fragment m/z 54 and the neutral species HCN (27 Da). Depending on the initial structure two interesting paths have been observed on the potential energy surface. In the first case (**Figure 8A**) a transition state at about 4.4 eV above the IP leads to the opening of the ring at the N3-C2 bond with the

release of the HC4N3 group. In the second case (**Figure 8B**) one could have foreseen a direct elimination of HNC, but theoretical calculations demonstrate instead an unexpected mechanism. This involves two bond ruptures along the ring leading to HNC elimination as a first step. Then a closed structure with C4-C2 and C4-C5 bonds is formed (transition state at about 4.95 eV above the IP) and finally the HC5N1 group is lost. The predicted AEs for the m/z 54 fragment in both pathways are consistent with the experimental value, but the second one is closer to the experiment. Thus, it seems the most likely one.

In the case of the misonidazole fragmentation the NO<sub>2</sub> loss leading to fragment m/z 155 occurs via two transition states (see **Figure 9**) in which a H atom bond to C11 migrates from the tail to C2. The calculated AE is in satisfactory agreement with the measured value.

The reaction, that leads to the C<sub>5</sub>H<sub>6</sub>N<sub>3</sub>O<sub>3</sub> (156 Da) and H<sub>3</sub>COCH<sub>2</sub> (45 Da) moieties, can occur via two different paths of concerted mechanisms (**Figure 10**) depending on where the charge is localized. The path with the lower barrier (<1 eV) leaves the charge on the m/z 156 fragment, while the other path with a transition state of about 1.63 eV has the charge localized on the m/z 45 fragment. The mass spectrum at 60 eV (**Figure 5**) is dominated by this latter fragment and in the PEPICO spectra (**Figure 6**) the largest branching ratio is associated to this fragment, too. The observation that a channel not favored from an energetic point of view appears to be the dominant one in the experiment is unusual. It may be explained by the structure of the orbitals of the misonidazole. As seen in the bottom panel of **Figure 6** and in **Table 2SM** no ionic states exist at about 1 eV above the IP and the charge of the π HOMO is mainly distributed above and below the ring (**Table 4SM**). Vice versa the HOMO-1 binding energy is calculated to be at about 1.4 eV above the IP and its charge distribution displays a contribution along the C14-C16 σ bond (**Table 4SM**). Thus, the removal of one electron from this orbital may weaken the bond and lead to the release of the charged tail H<sub>3</sub>COCH<sub>2</sub><sup>+</sup>.

It is interesting to observe that while in misonidazole the fragmentation channel leading to the [CH<sub>2</sub>OCH<sub>3</sub>]<sup>+</sup> m/z 45, i.e., the loss of a charged part of the tail T<sub>2</sub>, appears to be the dominant channel with an AE close to the energy of the HOMO-1 orbital, the loss of the tail, [CH<sub>2</sub>CH<sub>2</sub>OH]<sup>+</sup>, in metronidazole has a definitely higher AE (>12 eV) and it is characterized by a small branching ratio in the PEPICO measurements. This indicates that this low-lying fragmentation channel in misonidazole represents the most efficient channel for energy dissipation.

## CONCLUSION

The photoinduced fragmentation of metronidazole and misonidazole molecules has been studied. The combination of photoionization mass spectrometry, photoelectron spectroscopy, photoelectron-photoion coincidence spectroscopy, and computational spectroscopy has been used to investigate and characterize the main reaction/fragmentation channels observed in the mass spectra, which correspond to the elimination of the NO<sub>2</sub> and HONO group in both molecules

and the formation of the  $[\text{CH}_2\text{OCH}_3]^+$  ion in misonidazole. The preferential elimination of the nitro-group ( $-\text{NO}_2$ ) in both molecules supports the hypothesis (Adams et al., 2012) that the radiosensitizer effect is due to the complex redox chemistry, which, occurring after the selective binding of the nitroaromatic compounds to hypoxic cells, involves the reduction of the nitro-group to an amine ( $-\text{NH}_2$ ).

The message that can be derived from the present results is that although both metronidazole and misonidazole contain imidazole ring in the backbone, the side branches of these molecules lead to different bonding mechanisms and properties. Metronidazole is very fragile and a complex fragmentation process follows the initial ionization. Misonidazole on the other hand is relatively robust. Ionization and fragmentation may occur simultaneously, as the intensity of the molecular ion in the mass spectrum is very small. Then the preferential loss of the  $[\text{CH}_2\text{OCH}_3]^+$  fragment, i.e., a part of the tail  $T_2$ , acts as a protection of the ring against its opening and successive fragmentations. Therefore, if the therapeutic effect is linked to the nitroimidazole building block, then the efficient formation of the  $[\text{CH}_2\text{OCH}_3]^+$  fragment may help to protect the ring and to preserve the therapeutic effect of the compound.

More complex fragmentation can be linked to toxicity, thus from this point of view metronidazole, which displays a very rich mass spectrum, seems to have a higher toxicity than misonidazole.

The observation that the NO loss, the most relevant channel discussed in the previous studies (Bolognesi et al., 2016; Cartoni et al., 2018) in the 2-NI and 4(5)-NI molecules, is a minor, if any, channel in these compounds used in radiotherapy, prevents a direct extension of the chemical physics mechanisms identified in the building block molecules to the real drugs adopted in the clinical use. However the complex metabolism, that determines the biotransformation of NO and its related oxides *in vivo* (Kelm, 1999) does not allow to make definitive conclusions.

The results of our study, which has followed a bottom-up approach, indicate that translating the findings of chemical physics experiment to chemotherapeutic compounds

is not an easy task. However considering that nitro compounds have found and are finding clinical application (Overgaard, 2011; Wang et al., 2018) the understanding of their chemical physics properties, of the specific mechanisms of the interaction between radiation and chemotherapy and of how the chemical radiosensitizers actually work at the molecular level is a challenge that cannot be neglected.

## DATA AVAILABILITY

The datasets generated for this study are available on request to the corresponding author.

## AUTHOR CONTRIBUTIONS

PB, JC, RR, ST, BM, and LA performed the PEPICO experiments, while PB, MCC, and DC performed the AE measurements. ARC and AC performed the theoretical calculations and FW provided advices on the computational spectroscopy and interpretation of the spectra. PB, AC, JC, and MCC participated to the data analysis and interpretation. ARC, PB, and LA prepared the manuscripts. All the authors contributed to the interpretation of the results and the revision of the manuscript.

## ACKNOWLEDGMENTS

We gratefully acknowledge the support from the Progetto di Grande Rilevanza of the Italian Ministero degli Affari Esteri e della Cooperazione Internazionale (MAECI) Italia-Serbia A nanoview of radiation-biomatter interaction. ST and BM acknowledge the support from MESTD project OI 171020.

## SUPPLEMENTARY MATERIAL

The Supplementary Material for this article can be found online at: <https://www.frontiersin.org/articles/10.3389/fchem.2019.00329/full#supplementary-material>

## REFERENCES

- Adams, G. E., Flockhart, I. R., Smithern, C. E., Stratford, I. J., Wardman, P., and Watts, M.E. (2012). Electron affinity sensitization: VII. A correlation between structure, one electron reduction potentials and efficiencies of nitroimidazoles as hypoxic cell radiosensitizers. *Radiat. Res.* 178, AV183-AV189. doi: 10.1667/RRAV14.1
- Allen, F., Pon, A., Wilson, M., Greiner, R., and Wishart, D. (2014). CFM-ID: a web server for annotation, spectrum prediction, and metabolite identification from tandem mass spectra. *Nucleic Acids Res.* 42, W94–W99. doi: 10.1093/nar/gku436
- Berg, J. M., Tymoczko, J. L., and Stryer, L. (2012). *Biochemistry, 7th Edn.* New York, NY: W. H. Freeman and Company.
- Blyth, R., Delaunay, R., Zitnik, M., Krempasky, J., Krempaska, R., Slezak, J., et al. (1999). The high resolution gas phase photoemission beamline at Elettra. *J. Electron. Spectrosc. Relat. Phenom.* 101, 959–964. doi: 10.1016/S0368-2048(98)00381-8
- Bolognesi, P., Casavola, A. R., Cartoni, A., Richter, R., Markus, P., Borocci, S., et al. (2016). Communication: Position does matter: the photofragmentation of the nitroimidazole isomers. *J. Chem. Phys.* 145:191102. doi: 10.1063/1.4967770
- Boudaiffa, B., Cloutier, P., Hunting, D., and Huels, M. A., Sanche, L. (2000). Resonant formation of DNA strand breaks by low-energy (3 to 20 eV) electrons. *Science* 287, 1658–1660. doi: 10.1126/science.287.5458.1658
- Cartoni, A., Casavola, A. R., Bolognesi, P., Castrovilli, M. C., Catone, D., Chiarinelli, J., et al. (2018). Insights into 2- and 4 (5)-Nitroimidazole decomposition into relevant ions and molecules induced by VUV ionization. *J. Phys. Chem. A* 122, 4031–4041. doi: 10.1021/acs.jpca.8b01144
- Castrovilli, M. C., Bolognesi, P., Cartoni, A., Catone, D., O'Keeffe, P., Casavola, A., et al. (2014). Photofragmentation of halogenated pyrimidine molecules in the VUV range. *J. Am. Soc. Mass Spect.* 25:351. doi: 10.1007/s13361-013-0783-x
- Chiarinelli, J., Bolognesi, P., Domaracka, A., Rousseau, P., Castrovilli, M. C., Richter, R., et al. (2018). Insights in the dissociative ionization of glycine by PEPICO experiment. *Phys. Chem. Chem. Phys.* 20, 22841–22848. doi: 10.1039/C8CP03473G
- Derossi, A., Lama, F., Piacentini, M., Prospero, T., and Zema, N. (1995). High flux and high resolution beamline for elliptically polarized radiation in the

- vacuum ultraviolet and soft x-ray regions. *Rev. Sci. Instrum.* 66, 1718–1720. doi: 10.1063/1.1145828
- Feketeova, K., Albright, A. L., Sørensen, B. S., Horman, M. R., Whit, J., O'Hair, R. A. J., et al. (2014). Formation of radical anions of radiosensitizers and related model compounds via electrospray ionization. *Int. J. Mass Spectr.* 56, 365–366. doi: 10.1016/j.ijms.2013.12.014
- Frisch, M. J., Trucks, G., Schlegel, H. B., Scuseria, G. E., Robb, M. A., Cheeseman, J. R., et al. (2009). *Gaussian 09, Revision A.1*. Wallingford: Gaussian, Inc.,
- García Gómez-Tejedor, G., and Fuss, M. C. (2012). "Radiation damage in biomolecular systems," in *Series: Biological and Biomedical Physics, Biomedical Engineering* (Springer Netherland), 2012. doi: 10.1007/978-94-007-2564-5
- Gonzalez, C., and Schlegel, H. B. (1989). An improved algorithm for reaction path following. *J. Chem. Phys.* 90, 2154–2161. doi: 10.1063/1.456010
- Gonzalez, C., and Schlegel, H. B. (1990). Reaction path following in mass-weighted internal coordinates. *J. Phys. Chem.* 94, 5523–5527. doi: 10.1021/j100377a021
- Guo, H., Zhang, L., Jia, L., and Qi, F. (2012). Photon induced side-chain elimination of metronidazole: photoionization mass spectrometric and theoretical studies. *J. Spectrosc. Dyn.* 2:2.
- Higgins, G. S., O'Cathail, S. M., Muschel, R. J., and McKenna, W. G. (2015). Drug radiotherapy combinations: review of previous failures and reasons for future optimism. *Cancer Treat. Rev.* 41, 105–113. doi: 10.1016/j.ctrv.2014.12.012
- Kajfez, F., Klansic, and Šunjic, V. L. (1979). Application of photoelectron spectroscopy to biologically active molecules and their constituent parts IV. methylnitroimidazoles. *J. Heterocyclic Chem.* 16, 529–531. doi: 10.1002/jhet.5570160325
- Kelm, M. (1999). Nitric oxide metabolism and breakdown. *Biochim. Biophys. Acta* 1411, 273–289. doi: 10.1016/S0005-2728(99)00020-1
- Linstrom, P. J., and Mallard, W. G. (2008). *NIST Chemistry Webbook, Number 69*. Gaithersburg, MD. Available online at: <http://webbook.nist.gov>
- Marr, G. V., and West, J. B. (1976). Absolute photoionization cross-section tables for helium, neon argon, and krypton in the VUV spectral regions. *At. Data Nucl. Data Tables* 18, 497–508. doi: 10.1016/0092-640X(76)90015-2
- Michael, B. D., and O'Neill, P. A. (2000). A sting in the tail of electron tracks *Science* 287, 1603–1604. doi: 10.1126/science.287.5458.1603
- Ortiz, J. V. (1988). Electron binding energies of anionic alkali metal atoms from partial fourth order electron propagator theory calculations. *J. Chem. Phys.* 89, 6348–6352. doi: 10.1063/1.455401
- Overgaard, J. (2011). Hypoxic modification of radiotherapy in squamous cell carcinoma of the head and neck a systematic review and meta-analysis. *Radiother. Oncol.* 100, 22–32. doi: 10.1016/j.radonc.2011.03.004
- Pandeti, S., Feketeova, L., Reddy, T. J., Abdoul-Carime, H., Farizon, B., Farizon, M., et al. (2017). Nitroimidazolic radiosensitizers investigated by electrospray ionization time-of-flight mass spectrometry and density functional theory. *RSC Adv.* 7, 45211–45221. doi: 10.1039/C7RA08312B
- Plekan, O., Coreno, M., Feyer, V., Moise, A., Richter, R., De Simone, M., et al. (2008). Electronic state resolved PEPICO spectroscopy of pyrimidine. *Phys. Scripta* 78:058105. doi: 10.1088/0031-8949/78/05/058105
- Rockwell, S., Dobrucki, I. T., Kim, E. Y., Marrison, S. T., and Vu, V. T. (2009). Hypoxia and radiation therapy: past history, ongoing research, and future promise. *Curr. Mol. Med.* 9, 442–458. doi: 10.2174/156652409788167087
- Sonveaux, P., Jordan, B. F., Gallez, B., and Feron, O. (2009). Nitric oxide delivery to cancer: Why and how? *Eur. J. Cancer* 45, 1352–1369. doi: 10.1016/j.ejca.2008.12.018
- von Niessen, W., Schirmer, J., and Cederbaum, L. S. (1984). Computational methods for the one-particle green's function. *Comput. Phys. Rep.* 1, 57–125. doi: 10.1016/0167-7977(84)90002-9
- Wang, H., Mu, X., He, H., and Zhan, X. D. (2018). Cancer Radiosensitizers. *Trends Pharmacol. Sci.* 39, 24–28. doi: 10.1016/j.tips.2017.11.003
- Wardman, P., Rothkamm, K., Folkes, L. K., Woodcock, M., and Johnston, P. J. (2007). Radiosensitization by nitric oxide at low radiation doses. *Radiat. Res.* 167, 475–484. doi: 10.1667/RR0827.1
- Wiley, W., and McLaren, I. H. (1955). Time-of-flight mass spectrometer with improved resolution. *Rev. Sci. Instrum.* 26, 1150–1157. doi: 10.1063/1.1715212
- Wilson, W. R., and Hay, M. P. (2011). Targeting hypoxia in cancer therapy. *Nat. Rev. Cancer* 11, 393–410. doi: 10.1038/nrc3064
- Wong, M. W. (1996). Vibrational frequency prediction using density functional theory. *Chem. Phys. Lett.* 256, 391–399. doi: 10.1016/0009-2614(96)00483-6
- Yoshikawa, S., and Caughey, W. S. (1990). Infrared evidence of cyanide binding to iron and copper sites in bovine heart cytochrome c oxidase. Implications regarding oxygen reduction. *J. Biol. Chem.* 265, 7945–7958.

**Conflict of Interest Statement:** The authors declare that the research was conducted in the absence of any commercial or financial relationships that could be construed as a potential conflict of interest.

Copyright © 2019 Chiarinelli, Casavola, Castrovilli, Bolognesi, Cartoni, Wang, Richter, Catone, Tosic, Marinkovic and Avaldi. This is an open-access article distributed under the terms of the Creative Commons Attribution License (CC BY). The use, distribution or reproduction in other forums is permitted, provided the original author(s) and the copyright owner(s) are credited and that the original publication in this journal is cited, in accordance with accepted academic practice. No use, distribution or reproduction is permitted which does not comply with these terms.



# Core Shell Investigation of 2-nitroimidazole

Paola Bolognesi<sup>1\*</sup>, Vincenzo Carravetta<sup>2</sup>, Luca Sementa<sup>2</sup>, Giovanni Barcaro<sup>2</sup>, Susanna Monti<sup>3</sup>, Preeti Manjari Mishra<sup>4</sup>, Antonella Cartoni<sup>1,5</sup>, Mattea C. Castrovilli<sup>1</sup>, Jacopo Chiarinelli<sup>1,6</sup>, Sanja Tosic<sup>7</sup>, Bratislav P. Marinkovic<sup>7</sup>, Robert Richter<sup>8</sup> and Lorenzo Avaldi<sup>1</sup>

<sup>1</sup> CNR-Istituto di Struttura della Materia, Area della Ricerca di Roma 1, Montelibretti, Italy, <sup>2</sup> CNR-Istituto per i Processi Chimico Fisici, Pisa, Italy, <sup>3</sup> CNR-Istituto di Chimica dei Composti Organo Metallici, Pisa, Italy, <sup>4</sup> Stored and Cooled Ions Division, Max Planck Institute for Nuclear Physics, Heidelberg, Germany, <sup>5</sup> Dipartimento di Chimica, Sapienza Università di Roma, Rome, Italy, <sup>6</sup> Dipartimento di Scienze, Università degli Studi di Roma 3, Rome, Italy, <sup>7</sup> Institute of Physics, University of Belgrade, Belgrade, Serbia, <sup>8</sup> Elettra Sincrotrone Trieste, Area Science Park, Trieste, Italy

Tunability and selectivity of synchrotron radiation have been used to study the excitation and ionization of 2-nitroimidazole at the C, N, and O K-edges. The combination of a set of different measurements (X-ray photoelectron spectroscopy, near-edge photoabsorption spectroscopy, Resonant Auger electron spectroscopy, and mass spectrometry) and computational modeling have successfully disclosed local effects due to the chemical environment on both excitation/ionization and fragmentation of the molecule.

## OPEN ACCESS

### Edited by:

Paolo Tosi,  
University of Trento, Italy

### Reviewed by:

Nikolai V. Kryzhevoi,  
Universitt Heidelberg, Germany  
Luca Evangelisti,  
University of Bologna, Italy

### \*Correspondence:

Paola Bolognesi  
paola.bolognesi@cnr.it

### Specialty section:

This article was submitted to  
Physical Chemistry and Chemical  
Physics,  
a section of the journal  
Frontiers in Chemistry

Received: 04 January 2019

Accepted: 28 February 2019

Published: 02 April 2019

### Citation:

Bolognesi P, Carravetta V, Sementa L, Barcaro G, Monti S, Manjari Mishra P, Cartoni A, Castrovilli MC, Chiarinelli J, Tosic S, Marinkovic BP, Richter R and Avaldi L (2019) Core Shell Investigation of 2-nitroimidazole. *Front. Chem.* 7:151. doi: 10.3389/fchem.2019.00151

**Keywords:** XPS, NEXAFS, mass spectrometry, 2-nitroimidazole, DFT, MCFCS calculations

## 1. INTRODUCTION

Inner shell electrons are localized on specific molecular sites, due to their “atomic-like” nature, and, because they are affected by the chemical environment, can provide details on specific molecular bonds. By means of the tunable and monochromatic X-ray synchrotron radiation, it is possible to deposit well-defined quanta of energy in selected molecular sites and to probe specific electronic configurations through core shell excitation and ionization. The question that arises then, is whether the molecular fragmentation induced by inner shell processes is also site-selective, i.e., affected by the “localization” of the core hole, as well as, in the case of photoabsorption, by the localization and character of the excited orbital. For more than three decades (Eberhardt et al., 1983; Hanson, 1990), this question has been addressed by using different experimental techniques, which combined ion, electron, and electron-ion coincidence spectroscopies to study both core ionization (Rühl et al., 1993; Nagaoka et al., 2011) and excitation (Rühl et al., 1993; Okada et al., 2003; Tanaka et al., 2006; Céolin et al., 2008; Bernini et al., 2012; Lin et al., 2014, 2015; Salén et al., 2014). The features in the absorption spectra are used to “localize” the electron vacancy, through a suitable choice of the photon energy, without detecting the photoelectron as in the case of core ionization. It has been argued that a localized core excitation could be used as a sort of “molecular knife” (Tanaka et al., 2001) to induce controlled bond breakings near the atom of the primary excitation. It is usually observed that the molecular fragmentation following core excitation is strongly influenced by both the molecular site of the initial excitation and the character of the excited molecular orbital. In fact, significant variations in the fragment branching ratios have been observed across different excitation thresholds. In some cases, (Ueda et al., 1999; Liu et al., 2005), an ultrafast molecular fragmentation takes place on a time scale comparable to the electronic decay time of the core hole. In such cases, the process being driven by the elongation of specific bonds adjacent to the core excited atom will be dominated by the formation of specific fragments “cut” around the atomic site



of excitation. However, in most cases the “molecular knife” interpretation of the site-selective bond scission is questionable, due to the existence of many fast electronic relaxation channels ending with the removal of one or more electrons from the valence shell and subsequent delocalization of the excess energy. Therefore, the “degree of localization” of the primary excitation is rapidly lost. Indeed, some authors suggested that the site-specific fragmentation patterns could be explained as a “memory effect” (Larkins, 1990; Habenicht et al., 1991), where the electronic relaxation is driven by the overlap between the core-hole and the valence orbitals in the final state and depends on the electron density of the valence orbitals near the excitation site. This was confirmed by electron-ion coincidence experiments on 2Br-pyrimidine (Bolognesi et al., 2015), where the preferential formation of certain fragments observed at selected resonant core excitation energies was found to depend on the overlap between inner shell excited and the valence ion states, while a direct correlation between a site-selected excitation and a bond breakage could not be established. Within this scenario, site-selective fragmentation patterns are mainly due to selective electronic relaxation mechanisms, which lead to the population of dissociative single and doubly ionized valence states, that are fragmented following their own peculiar pattern. The goal of the present study is to explore the electronic structure of 2-nitroimidazole (2NIM) in the core excitation and ionization regions at the C, N, and O K edges by experiments and quantum mechanics calculations and to investigate the possible correlations between these core excited electronic states and the following molecular fragmentation.

The nitroimidazole molecule ( $C_3H_3N_3O_2$ ) is made of an imidazole ring, ( $C_3H_4N_2$ ), where a hydrogen atom is replaced by the nitrogen dioxide ( $NO_2$ ) group bound to a carbon atom. For the X-ray photoelectron spectra (XPS) a qualitative approach, based on the known properties of the building blocks of nitroimidazoles, provides an excellent guideline for the interpretation of the spectrum, confirmed by the differential Density Functional Theory ( $\Delta$ DFT) calculations. The 2NIM core levels can be related to those of the two building blocks by a predictable chemical shift due to the higher electronegativity of the nitro group. The near-edge X-ray absorption fine spectra (NEXAFS) accurately assigned by quantum mechanics calculations, provide a description of the electronic structure of the main core excited states. Finally, the mass spectrometry experiments allow to follow the fate of the dissociative core excited/ionised states by evolution of the partial ion yields across the different thresholds.

The photoionization and photofragmentation properties of nitroimidazole isomers, including 2NIM, have already been investigated in the valence region for the neutral (Bolognesi et al., 2016; Cartoni et al., 2018) and protonated (Feketeová et al., 2015b) molecule. The 4(5)NIM isomers have also been studied by XPS and NEXAFS (Feketeová et al., 2015a) as well as by ion-ion coincidence experiments (PIPICO) (Itälä et al., 2017). Sections 2 and 3 describe the experimental and theoretical methods, while section 4 is devoted to the description and discussion of the XPS, NEXAFS, and mass spectrometry measurements. Section 5 contains summary and conclusions.

## 2. EXPERIMENTAL

The experiments were performed at the Gas Phase photoemission beamline (Blyth et al., 1999) of the Elettra synchrotron (Trieste, Italy) using the end station, already described in previous studies, for photoemission and mass spectrometry measurements (Bolognesi et al., 2015). Briefly, the radiation source of the Gas Phase beamline is an undulator (Diviacco et al., 1992) that provides fully linearly polarized radiation in the energy range from 13.5 to about 900 eV. Monochromatization of the radiation is provided by five interchangeable gratings and the energy selected photon beam reaches the interaction region in a spot size of a diameter of about 300  $\mu m$ . The experimental apparatus is a high vacuum chamber hosting a hemispherical analyzer (VG 220i) and a custom made Wiley McLaren (Wiley and McLaren, 1955) time-of-flight (TOF) spectrometer mounted opposite to each other at the magic angle with respect to the polarization axis of the photon beam. The hemispherical analyzer, which mounts six channeltron detectors for parallel acquisition, was used to measure the XPS spectra of the C, N, and O (1s) orbitals of 2NIM at about 90 eV above their respective ionization thresholds, with an overall energy resolution of 0.3 eV. Each XPS spectrum required an acquisition time of about 10 h, with a typical counting rate of the order of 10 counts/s. The chosen photon energies are sufficiently far from the ionization thresholds so that post-collision interaction effects can be neglected. The TOF spectrometer was operated with an extraction field of 700  $Vcm^{-1}$  and antisymmetric polarization of the repeller/extractor electrodes (Directed Energy Inc. model PVM4210). The operation mode can be either a continuous extraction, for the measurement of the total ion yield in the NEXAFS spectra, or a pulsed extraction for mass spectrometry, using a pulse generator (Stanford Research DG535) at 1 kHz frequency. In the NEXAFS spectra the photon energy resolution was 20 and 50 meV at the C, N, and O K-edges, respectively. The measured yields were normalized to the photon beam intensity variation read by a photodiode placed at the end of the beamline. The mass spectra were measured at several photon energies in the C, N, and O K near-edge regions, with a step size of 0.25 eV and a typical acquisition time of 800 s per point. In the data analysis, the background was subtracted to each raw mass spectrum and then the intensity of each  $m/z$  fragment was evaluated as the sum of yields within the time-of-flight range of interest (corresponding to about  $m/z \pm 0.5$ ). Then, the branching ratio of each fragment was obtained by normalization to the total ion yield.

Both the XPS and NEXAFS spectra were calibrated according to the well-known references of  $CO_2$  (Wight and Brion, 1974; Tronc et al., 1979, 1980; Hatamoto et al., 2007) ( $C(1s)^{-1}$  at 297.6 eV,  $O(1s)^{-1}$  at 541.3 eV,  $C(1s) \rightarrow \pi^*$  at 290.77 eV and  $O(1s) \rightarrow \pi^*$  at 535.4 eV) and  $N_2$  (Thomas and Shaw Jr, 1974; Sodhi and Brion, 1984) ( $N(1s)^{-1}$  at 409.9 eV and  $N(1s) \rightarrow \pi^*$  at 400.87 eV), inserted as diffuse gases in the vacuum chamber. The 2NIM sample (molar mass 113 Da and 98% purity) was purchased from Sigma Aldrich. The powder was introduced into the vacuum chamber in a crucible and heated to about 80°C to be sublimated for gas phase analysis. The background pressure was  $2 \times 10^{-8}$

mbar and a cold finger was used to reduce contamination from background residual water.

### 3. THEORY

Calculations were carried out for both ionization (XPS) and excitation (NEXAFS) of the core shells of the three C, three N, and two O atoms of 2NIM. The photoemission spectra were modeled by all-electron differential methods fully including electronic relaxation ( $\Delta$ HF) and partially including electronic correlation ( $\Delta$ DFT) by using the DALTON code (Angeli et al., 2013). With the same code, we carried out accurate multiconfigurational self-consistent field (MCSCF) calculations to assign a peculiar feature appearing in the oxygen K-edge XPS spectrum due to a shake-up process. The Restricted Active Shell (RAS) approximation, describing the electron correlation in the highest 12 valence levels, and the medium size Ahlrichs-VTZ basis set (Schäfer et al., 1992) were adopted. A valence electron method introduced recently (Iannuzzi and Hutter, 2007), with the use of a potential to describe the relaxation of the core hole, was employed for the simulation of the NEXAFS spectra. These calculations were performed with cp2k (Lippert et al., 1999) within the all-electron implementation of the Gaussian Augmented Plane Wave (GAPW) (Krack and Parrinello, 2000) method. The Kohn-Sham (KS) wave-functions were projected on a set of Gaussian contracted functions. We employed two different atomic basis sets: aug-cc-pVTZ (Dunning Jr, 1989) for the molecular structure optimization and aug-cc-pVQZ to improve the accuracy of the higher excited states of NEXAFS spectra.

The computational efficiency of the GAPW method relies on an auxiliary electronic density that is partitioned in an electronic part, smoothly varying between atoms and in an electronic part, rapidly varying close to the nuclei. For a fast evaluation of the Coulomb and Exchange potentials, a plane-wave expansion is adopted to project the former, whereas combinations of localized atomic functions describe the latter. Thus, beyond Gaussian basis sets, we used plane waves with an energy cut-off of 300Ry to expand the smooth part of the auxiliary electronic density. The BLYP (Becke, 1988; Lee et al., 1988) density functional was chosen for the exchange and correlation part of the KS hamiltonian. We calculated the NEXAFS spectra by following the protocol described by Iannuzzi and Hutter (2007) which is based on the direct calculation of both the excitation energy and the dipole transition element between the selected core orbitals and a certain number of virtual orbitals obtained through a full-core-hole transition potential (Jayawardane et al., 2001; Hetényi et al., 2004) on the adsorbing atoms. This method predicts accurate relative positions of the main NEXAFS features. In order to get the absolute energy scale for the full set of excitations at a given K-edge, we performed DFT calculations to estimate the energy difference between the ground state and the first core-excited state. The Stieltjes Imaging method (Langhoff, 1980; Cacelli et al., 1991) was applied to the discretized excitation spectrum, followed by

a convolution with a Gaussian (FWHM = 0.2 eV) to mimic both the finite lifetime of the excited states and the limited experimental resolution.

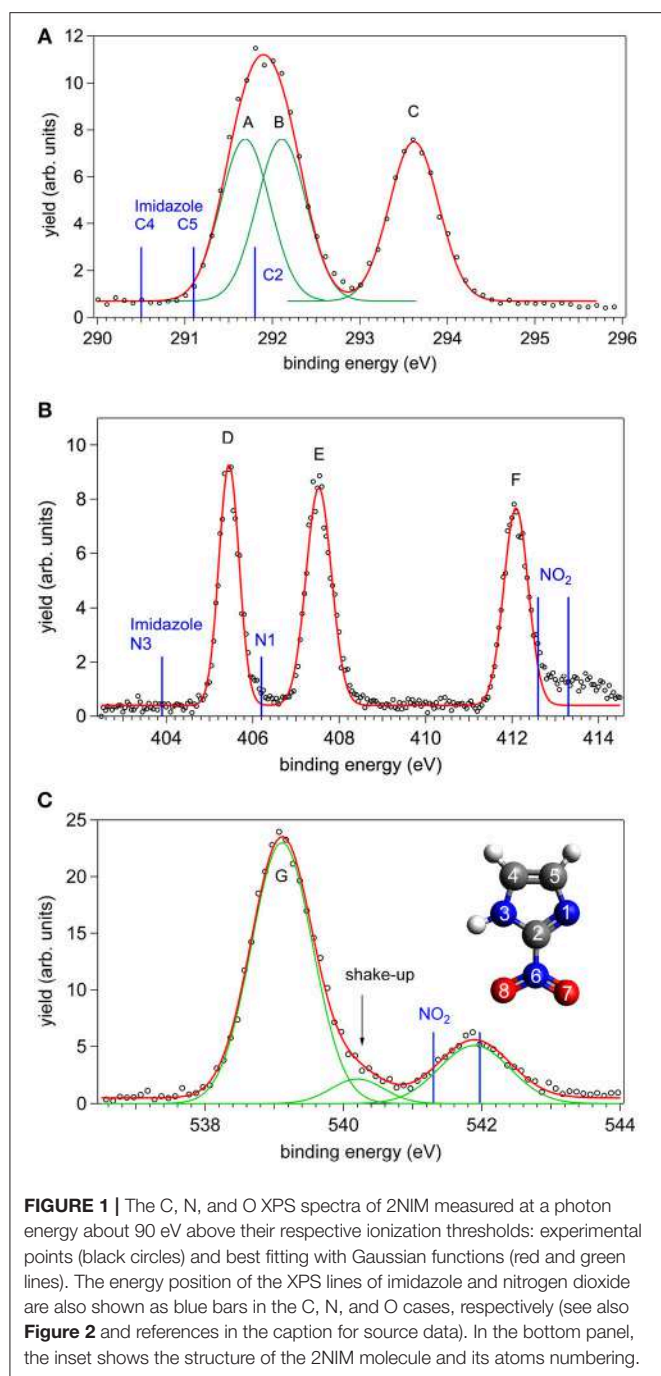
### 4. RESULTS AND DISCUSSION

The presentation of the results is organized in three subsections, devoted to the XPS, NEXAFS, and mass spectrometric experiments, respectively. For the XPS and NEXAFS experiments, a qualitative approach, based on the spectroscopy of imidazole and nitrogen dioxide molecules, guided a first assignment of the different features of the spectra. This was then fully validated by the  $\Delta$ HF,  $\Delta$ DFT,  $\Delta$ MCSCF, and TDDFT calculations: the discussion of the observed chemical shifts unravels the role played by the nitro group in the stabilization of the imidazole ring atoms. The theoretical prediction of the NEXAFS spectra allows to disentangle the contribution of the different non-equivalent atoms in each absorption spectrum and to analyze the charge distribution in the lowest unoccupied molecular orbitals, LUMO, and LUMO+1. The last subsection reports the results of the time of flight mass spectra measured at several photon energies in the C, N, and O near K-edge regions and the discussion of the site-selective molecular fragmentation.

#### 4.1. The XPS Spectra

The XPS spectra of 2NIM at the C, N, and O K edges are shown in **Figure 1**. The main C and N spectral features were tentatively fitted with three Gaussian functions with the same area, corresponding to the number of non-equivalent atoms of the same species. The results are indicated as peaks A to C for carbon, and D to F for nitrogen. In the O case, the two non-equivalent atoms O7 and O8 are expected to be non-degenerate. However, the calculated splitting of about 100 meV (see **Table 1**) combined with the vibrational broadening makes the two peaks unresolvable in the XPS measurement within the present experimental resolution. Therefore, only the average position of the two contributions is reported in the experimental data and the O (1s) peak is labeled G.

A first qualitative assignment of these XPS spectra is suggested by the energy positions of the main XPS bands for imidazole (Apen et al., 1993; Thomason et al., 2015) and nitrogen dioxide (Davis et al., 1973; Jolly et al., 1984), i.e., the building blocks of the nitroimidazole molecule. The core binding energies (BE) of these building blocks are represented by the vertical bars in **Figure 1**, and the corresponding values are reported in **Table 1**, together with the binding energies of 4- and 5-NIM isomers from Feketeová et al. (2015a). An overview of the 2NIM, imidazole and nitrogen dioxide XPS binding energies is also displayed in the diagram of **Figure 2**. Based on the qualitative analogies among the nitroimidazole isomers and their building block molecules, we assign the 2NIM XPS peaks A to G for increasing binding energies to the C4, C5, C2, N3, N1, N6, O7/8 atoms, respectively. This qualitative assignment is fully validated by our  $\Delta$ DFT calculations, also reported in **Table 1**. Apart from an average shift of about 1.1 eV for the C and N spectra and -0.42 eV for O, there is good agreement between the theoretical predictions and both



the experimental observations, and the qualitative assignment provided by the “building block approach.”

The three C(1s) XPS peaks in all nitroimidazoles show a clear influence of the presence and specific location of the NO<sub>2</sub> group on the imidazole ring. In fact, all C(1s) binding energies (black levels in **Figure 2**) are chemically shifted toward higher values with respect to those of the corresponding atoms in the imidazole molecule. These positive shifts are due to the electron withdrawing of the NO<sub>2</sub> group, producing a charge transfer from the imidazole ring to the nitro group, which reduces the

electronic relaxation around a core hole on the ring atoms, increasing their binding energies. In 2NIM, this effect is more pronounced on the C2 atom, which is directly involved in the C2-NO<sub>2</sub> bonding. The experimental data provided 1.82 eV for the C2 chemical shift, to be compared with an average shift of 1.1 eV for C4 and C5 with respect to imidazole. It should be noted that according to the Koopmans theorem (KT), ground state HF calculations predict chemical shifts of 2.5, 1.3, and 1.6 eV for the C2, C4, and C5 atoms, respectively, going from imidazole to 2NIM.  $\Delta$ SCF calculations, fully including electron relaxation around a specific core hole, predict instead 2.2, 1.7, and 0.7 eV respectively, to be compared to experimental values of 1.8, 1.2, and 1.0 eV (see **Figure 1**). It is clear, from this comparison, that an interpretation of the chemical shift as due to an “initial state effect” (KT) is only a rough approximation and can be erroneous in the prediction of the relative size of the chemical shift for non-equivalent atoms in the molecule. The inclusion of electronic relaxation around the core hole (final state effect) can instead provide a reliable estimation of the chemical shift.

For the N(1s) XPS spectrum, the comparison between 2NIM and its building blocks is more complex; in fact, it is necessary to distinguish the case of the ring atoms N1 and N3 of the imidazole and the N6 atom of the NO<sub>2</sub> molecule. The building block values are significantly separated in energy (around 7 eV), clearly manifesting the influence of the chemical environment on the core binding energy, with the nitrogen atoms surrounded by the two strongly electronegative oxygen atoms in NO<sub>2</sub>, or by carbon atoms, when embedded in the imidazole ring. In 2NIM, the N3 and N1(1s) electron binding energies, similar to the C case, present a positive shift with respect to imidazole, while N6 presents a negative shift with respect to nitrogen dioxide, i.e., shifting toward smaller binding energies. This can be explained by considering the same effect already discussed in the C case where, in the C2-NO<sub>2</sub> bond, the nitro group withdraws electron charge mostly from the C2 atom, but also, by inductive effect, from the entire imidazole ring. Therefore, the reduced screening on the N3 and N1 ring atoms increases their (1s) electron binding energies while on the N6 atom of the nitro group this has the opposite effect, increasing the shielding and therefore decreasing the N6(1s) binding energy with respect to the NO<sub>2</sub> isolated molecule.

In the binding energy of the O(1s) electrons, similarly to the N6 case, there is a significant negative shift of about -2.5 eV in 2NIM with respect to NO<sub>2</sub>. The break of symmetry with respect to the isolated NO<sub>2</sub> molecule is likely to introduce a chemical shift between the O7/O8 atoms. Theoretically, this has been estimated to be of 0.1 eV. In the experimental XPS spectrum at the O K-edge a small band at about 540.2 eV is clearly visible. To assign this particular feature, accurate MCSCF calculations were performed to include in the theoretical model both the electron relaxation described by the HF method and electron correlation. This was explicitly done for all the outer 12 valence electrons and the energy of the 2NIM ground state, the O(1s) core hole state and the lowest energy shake-up state are reported in the second column of **Table 2**. The MCSCF calculations predict an energy for the lowest shake-up state (HOMO-LUMO excitation) that is 1.6 eV above that of the core hole state, in excellent



**TABLE 1** | Comparison of present experimental and theoretical core ionization potentials of 2NIM with equivalent experimental and theoretical data for the 4- and 5NIM isomers (Feketeová et al., 2015a), imidazole (Becke, 1988), and nitric dioxide (Jayawardane et al., 2001).

Site	2NIM Expt(eV)	2NIM Th (eV)	4(5)NIM Expt (eV)	4NIM Th (eV)	5NIM Th (eV)	Imidazole	NO <sub>2</sub> *
C4	A, 291.69(2)	292.59	292.6	292.41	291.83	290.5	–
C5	B, 292.11(2)	293.14	293.1	292.16	292.89	291.1	–
C2	C, 293.62(2)	294.97	293.4	292.71	292.77	291.8	–
N3	D, 405.45(2)	406.37	406.37	405.40	405.31	403.9	–
N1	E, 407.53(2)	408.27	408.27	407.67	407.67	406.2	–
N6	F, 412.09(2)	413.66	413.66	411.28	411.73	–	412.6(5) 413.3(5)
O7	G, 539.10(2)	538.63	538.5	538.09	538.50	–	541.3(5)
O8		538.74		538.19	538.47	–	542.0(5)

The latter two molecules can be considered as building blocks of the nitroimidazole family of molecules (see text). Numbers in parenthesis represent the uncertainty of the present fitting procedure. \*NO<sub>2</sub> being an open shell molecule, the core ionization leads to two (<sup>3</sup>A<sub>1</sub> and <sup>1</sup>A<sub>1</sub>) states due to spin coupling.

agreement with the energy position of the peculiar band observed around 540.2 eV that therefore can be ascribed to a shake-up process. This is a clear example that the HOMO-LUMO energy difference predicted by a calculation for the initial ground state (estimated as large as about 10 eV at the HF level) should be considered only as a very rough approximation for the prediction of the energy level of the lowest shake-up state. In the present case the unusually low energy of the shake-up state derives from the electron distribution of the LUMO orbital in the final state which is mostly located close to the core hole (see next section). Similarly to the 4(5)NIM and related compounds, the O(1s) XPS spectrum shows a broad maximum at about 542 eV. This feature could not be ascribed to the presence of any possible residual gas or fragment from the decomposition of the 2NIM molecule. In the present work we do not have definite assignment for this feature, but in the work of (Feketeová et al., 2015a) it was assigned as a  $\pi - \pi^*$  shake-up.

## 4.2. The NEXAFS Spectra

The comparison between the experimental and theoretical NEXAFS spectra of 2NIM at the C, N, and O K-edges is reported in **Figures 3A–C**. All the computed spectra were convoluted with a Gaussian function (width = 0.2 eV) to mimic both the experimental response function and the vibrational broadening, and shifted by arbitrary amounts, reported in their respective figures, to obtain a good matching with the low energy bands of the experimental spectra. The calculated spectra neglect the vibrational distribution of the electronic states. This may change the position of the centroid, the shape and the relative intensity of the bands. Nevertheless, there is a very good agreement between theoretical predictions and experimental data in the low energy part of the spectra, i.e., in the region of the excitations involving the LUMO and LUMO+1. Some discrepancies are observed in the region approaching the continuum, due to the poor reproduction of the region of the Rydberg excitation by the adopted theoretical methods. The different colors in **Figures 3A–C** represent the individual contributions from the non-equivalent atoms and allow identifying the role played by each one in the different energy regions of the spectra, in particular on the discrete

features at the low energy side corresponding to excitations to the lowest virtual orbitals. The charge distribution of the LUMO and LUMO+1 orbitals are reported in **Figures 3D–F**, showing that these orbitals are all of  $\pi$  and antibonding nature. Above the ionization thresholds, broad features usually assigned to transitions to  $\sigma^*$  shape resonances are also observed. This kind of excited state involves antibonding  $\sigma$  orbitals quite localized in the core hole region and, as a consequence, the transition dipole moment can be large. However, their usually strong dissociative character, leads to a spreading of such intensity on a large band by a coupling, which depends on the atomic site and the bond environment. In all cases, the excitation energies of the non-equivalent atoms follow the same ordering as in the XPS spectra (see **Table 1**), even though the charge distribution of the different excited orbitals may produce a different core hole screening for each site and therefore modify the values of the chemical shift with respect to the ones measured in XPS. Concerning the comparison of 2NIM to imidazole, an opposite behavior can be observed in the binding energy shifts of the XPS and NEXAFS spectra. Indeed, while ionization energies of 2NIM shift to larger values with respect to imidazole, the excitation energies shift to a lower one, indicating a stabilization of the LUMO orbitals. This is clearly illustrated in **Figure 2**, where the binding energies of the LUMO (red bars, assigned according to the theoretical calculation) and of the ionization (black bars) at the C, N, and O K edges are reported for nitrogen dioxide, 2NIM and imidazole. Although in the core excitation the molecule is neutral, the LUMO is embedded in the field of an ion with a localized charge. This leads to a lowering of the LUMO energy with respect to the ground state of the molecule. This stabilization strongly depends on the charge of the core hole and its screening. In the case of 2NIM, the NO<sub>2</sub> group removes the charge to screen the core hole and the binding energy as well as the attractive force of the partially screened core hole on the LUMO electron increases, thus the LUMO in 2NIM is stabilized with respect to imidazole. This shows that the effect of the substituent group is opposite on the binding energy of the core orbitals and on the excitation energy of the LUMO. Another contribution to the lowering of the LUMO energy in the 2NIM is likely due to the hyperconjugation of the

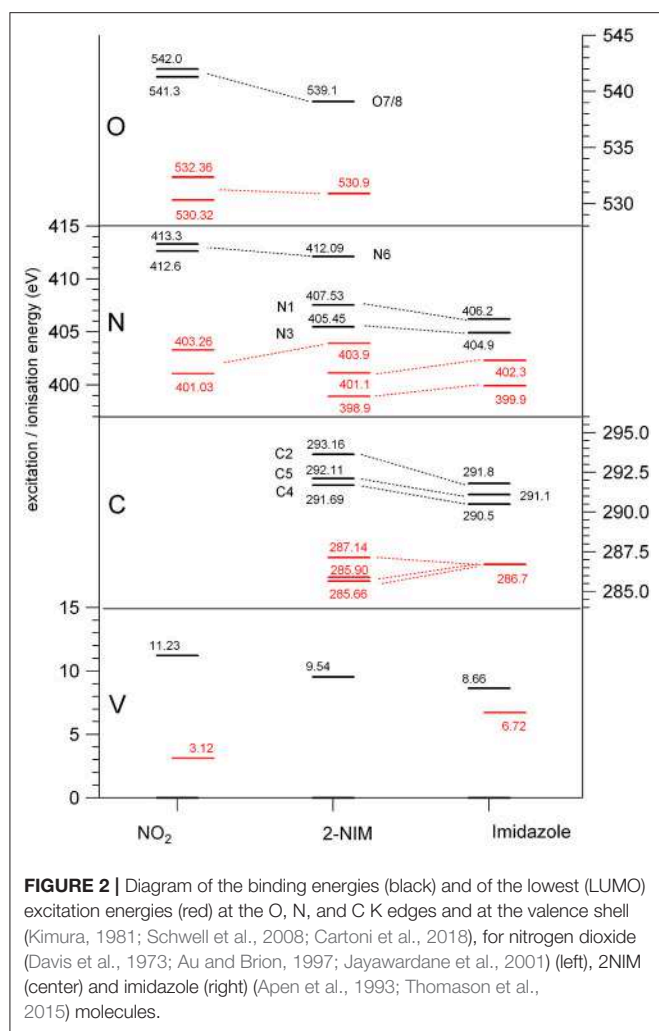


**TABLE 2** | Results of MCSCF calculations for: ground state, O core hole state and lowest energy O shake-up state of 2NIM; total energy in second column and relative energy (binding energy) in third column.

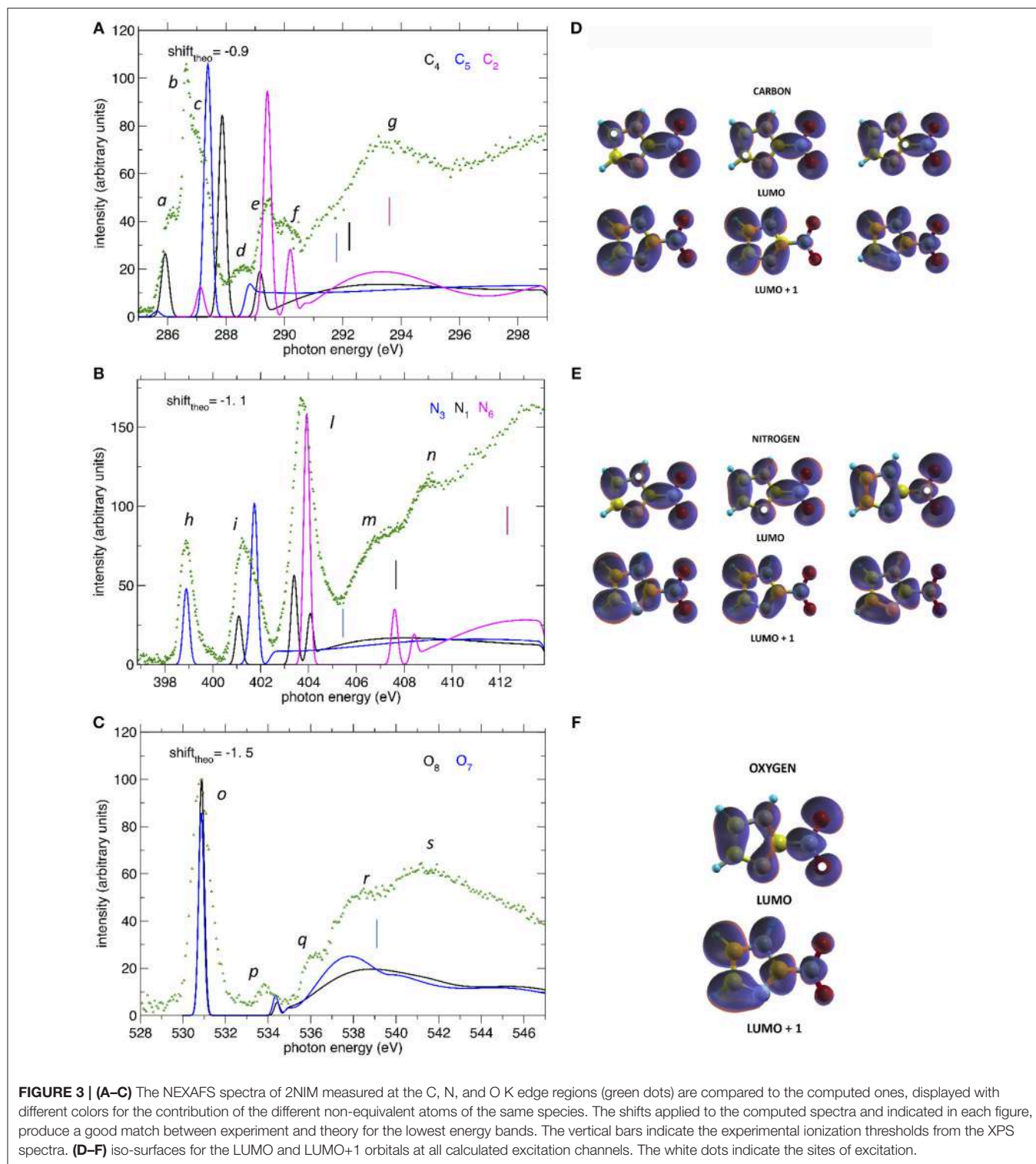
State	E(MCSCF)(au)	$\Delta E$ (eV)
GS	-428.41814	0.0
O1 corehole	-408.6122987	538.9
O1 shake-up	-408.553992	540.5

$\text{NO}_2$   $\pi$  orbitals with the aromatic orbitals of the imidazole ring. It is not straightforward to evaluate the amount of these two contributions in the observed lowering of the LUMO, but it is realistic to consider that both of them are present.

In the C NEXAFS spectrum (**Figure 3A**) we observed several structures, labeled *a* to *g*, organized in four main groups. The first group contains the partially resolved features *a* to *c* at 286, 286.6, and 287 eV, respectively. Previously published NEXAFS measurements of 4(5)NIM have empirically assigned this group of peaks (energy region 285.3–287.0 eV), to a series of C(1s)  $\rightarrow$   $\pi^*$  transitions (Feketeová et al., 2015a). In the present work,

supported by the theoretical predictions, we assigned the feature *a* mainly to a C5(1s)-LUMO transition with a minor contribution from the C4-LUMO, feature *b* to the C4(1s)-LUMO+1 transition with a minor contribution from the C2(1s)-LUMO and then feature *c* to C5(1s)-LUMO+1 transition. The tiny feature *d* at 288.6 eV is dominated by the C4 contribution while *e* and *f*, at 289.4 and 290.3 eV, respectively, are dominated by core excitations from C2, approaching the C4 and C5(1s) ionization continua. The broad feature *g* at 292–295 eV can be attributed, by present calculations, to  $\sigma^*$  resonances, with the strongest contributions due to excitations from the C2 core orbital to antibonding orbitals along C2-N6 and C2-N1 and, to a minor extent, from the C5 core orbital to antibonding orbitals along C5-N1. In the C NEXAFS like in the XPS there was a positive shift, i.e., toward higher excitation energies, of the C2(1s) excitation spectrum with respect to the C4 and C5 contributions, which are very close in energy. The gas phase electron energy loss (EEL) measurement of imidazole (Apen et al., 1993) assigned the overlapping contribution of the LUMO excitations from the three C atoms to a large, unresolved feature at 286.7 eV.

In the N NEXAFS spectrum, three distinct features labeled *h*, *i*, and *l* at 398.9, 401.1, and 403.9 eV were observed experimentally and were very well reproduced in both position and relative intensities by the theoretical predictions. According to the present calculations, their assignment follows the same ordering as in the XPS spectrum. The first feature, *h*, is attributed entirely to the N3(1s) excitation to the LUMO orbital, the second one, *i*, to the overlapping of the (1s) excitation from N1 to LUMO and from N3 to LUMO+1, while the third and strongest feature, *l*, has a mixed contribution from all three N sites, but is dominated by the N6(1s) to LUMO. The position and assignment of these three features are very close to the ones reported for the 4(5)NIM, i.e., about 400.55, 401.7, and 403.9 eV, respectively (Feketeová et al., 2015a), indicating that the N core excitation is not a sensitive fingerprint to distinguish the nitroimidazole isomers. Similar to the C case, an opposite trend was observed in the core ionization and excitation at the N K-edge. Indeed, the N3 and N1(1s) excitations of imidazole are located at 399.9 and 402.3 eV, respectively (Apen et al., 1993) (i.e., at higher excitation energy with respect to 2NIM) and the N(1s) excitation in  $\text{NO}_2$  is located at an average value of 402.34 eV (Zang et al., 1990; Gejo et al., 2003) (i.e., at lower energy compared to 2NIM). This is the opposite behavior with respect to the XPS, where N3 and N1 (1s) BE were shifted at higher binding energies compared to imidazole, while N6 was shifted toward lower binding energies compared to nitric dioxide. The increased electronic density with respect to  $\text{NO}_2$  results in a decreased binding energy of N6 while, as discussed above, the attraction of the screened hole on the electron of the LUMO destabilizes the LUMO itself. Considering that the hyperconjugation should always have a stabilizing effect on the LUMO, this result indicates that the most relevant effect in determining the stabilization/destabilization of the LUMO is the variation of the hole screening. The *m* and *n* features at around 407 and 409 eV, respectively, can be attributed, using present calculations, to a partial contribution of  $\pi^*$  transitions to LUMO+1 and LUMO+2 orbitals from the N6 core orbital as well as to  $\sigma^*$  transitions from N1 core orbital to antibonding



orbitals along N1-H and N1-C2. Similar broad features were also observed in both imidazole (at 411.4 and 415 eV), where they are attributed to C-N\* transitions, and in NO<sub>2</sub>, at 416.16 eV.

At the O K-edge, the NEXAFS spectrum below the ionization continuum is dominated by the intense peak *o* at 530.85 eV,

containing the overlapping contribution of the core excitations to the LUMO at atoms O7 and O8. Similarly to the XPS spectrum, the chemical shift between O7 and O8 does not give rise to a measurable shift in the observed peaks, as confirmed by the theoretical prediction of a chemical shift of 0.1 eV (see **Table 1**).



The position of the O(1s) LUMO+1, peak *p* at about 534 eV, is also quite well predicted by the theoretical model. Considering the shift of the O(1s) edge in the theoretical NEXAFS spectra, features *r* and *s*, at around 538 and 541 eV, respectively, can be attributed, by the present calculations, to transitions to  $\sigma^*$  orbitals along N6-O.

Concerning the charge distributions reported in **Figures 3D–F**, the most evident difference between the LUMO and LUMO+1 orbitals can be observed along the C2-N6 bond, which has a bonding/antibonding character in case of excitation to the LUMO/LUMO+1 states, respectively. More subtle differences are present among the different sites of excitation but, since the charge is quite delocalized, no evident correlation between the localization of the core hole and the charge distribution could be made.

### 4.3. Mass Spectra and Partial Ion Yield

The molecular fragmentation of 2NIM following the C, N, and O core excitation/ionization has been investigated by measuring time-of-flight (TOF) mass spectra at several photon energies across their respective near-edge regions. The mass spectra measured in the energy regions of the transitions from the C, N and O(1s) to the LUMO orbital are reported in **Figures 4A–C**, respectively, and compared with the ones obtained in the region just below their respective resonance regions. The assignment of the main fragments of interest in the present work is reported in **Figure 4** and the list of all fragments is collected in **Table S1**. In general, the enhanced photoabsorption cross section at the core excitation energies affects the intensity of all fragments, thus the partial ion yields vs. photon energy, mimics the overall shape of the NEXAFS spectrum. However, the fragmentation pattern itself, and therefore the molecular branching ratio, depend on the location of the inner hole (Okada et al., 2003; Tanaka et al., 2006; Céolin et al., 2008; Bernini et al., 2012; Lin et al., 2014, 2015; Salén et al., 2014). To prove this, **Figure 4** shows the superposition of the fragmentation mass spectra measured “on” and “off” resonance and the quantity  $(\text{Yield}_{\text{on}} - \text{Yield}_{\text{off}}) / \text{Yield}_{\text{off}}$  for the major fragments as vertical bars at the bottom of each panel. This quantity allows the variation of the yield “on” resonance, with respect to the “off” resonance one, to be evaluated for each fragment. A value of 1, for example, means that the yield on resonance has doubled, i.e., suffered 100% variation.

Beginning with the 2NIM parent ion ( $m/z$  113) one sees that its contribution to the mass spectra at the three edges is negligible, showing only a minor resonant enhancement in the case of C(1s)  $\rightarrow \pi^*$  excitation (**Figure 4A**). The fragments at  $m/z$  97 (2NIM-O)<sup>+</sup>, 83 (2NIM-NO)<sup>+</sup>, and 67 (2NIM-NO<sub>2</sub>)<sup>+</sup> involve the nitro group and share the property of leaving the imidazole moiety unfragmented, even though we cannot infer about its structure as a ring or an open/rearranged feature. Their contribution to the mass spectra is small, however these fragments show significant resonant behavior. At the C(1s)  $\rightarrow \pi^*$  resonance the (2NIM-NO<sub>2</sub>)<sup>+</sup> displays a noticeable decrease, while the 66<sup>+</sup> fragment, which corresponds to a further loss of a H atom from (2NIM-NO<sub>2</sub>)<sup>+</sup>, shows a smaller decrease (**Figure 4A**). The variation of fragment 83<sup>+</sup> is significant. According to a mass spectrometric and PEPICO study in the

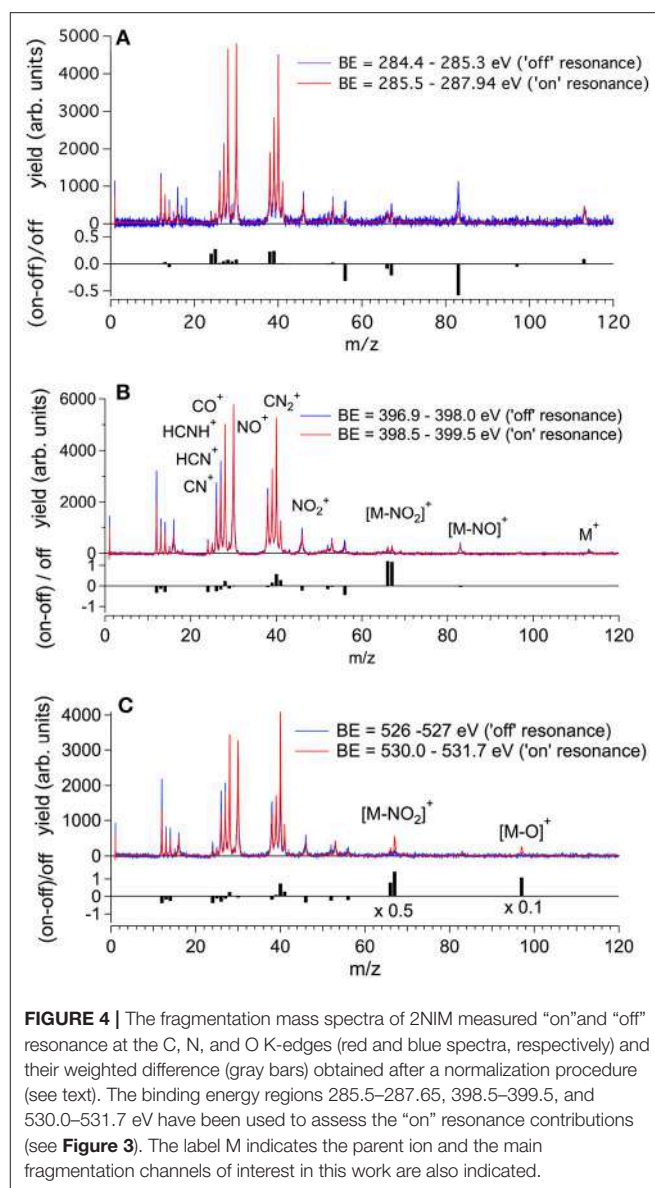


**FIGURE 4** | The fragmentation mass spectra of 2NIM measured “on” and “off” resonance at the C, N, and O K-edges (red and blue spectra, respectively) and their weighted difference (gray bars) obtained after a normalization procedure (see text). The binding energy regions 285.5–287.65, 398.5–399.5, and 530.0–531.7 eV have been used to assess the “on” resonance contributions (see **Figure 3**). The label M indicates the parent ion and the main fragmentation channels of interest in this work are also indicated.

valence region (Bolognesi et al., 2016), fragment 83<sup>+</sup> originates from a (slow) molecular rearrangement of the nitro group, with a swap in position between the O and N atoms, losing the NO group. The reduction of the intensity of this fragment suggests that C(1s) core excitation triggers “faster” fragmentation or decay processes with respect to this “slow” molecular rearrangement, which is therefore hampered. At the N(1s)  $\rightarrow \pi^*$  resonance (**Figure 4B**), the NO<sub>2</sub> loss channel does resonate, doubling the intensity of the fragments at  $m/z$  66 and 67, while at the O(1s)  $\rightarrow \pi^*$  resonance (see **Figure 4C**) both fragments display a very large increase, more than doubling their intensity. At this resonant excitation energy, an even larger increase is observed in fragment  $m/z$  97 due to the O loss. This fragment is barely present in the “off” resonance as well as in the mass spectra at the C and N continua and  $\pi^*$  resonances. The complementary fragments NO<sub>2</sub><sup>+</sup> ( $m/z$  46), NO<sup>+</sup> ( $m/z$  30),

and  $O^+$  ( $m/z$  16) do not display appreciable relative variations in the “on” resonance, a part of the  $NO_2^+$  fragment which suffers a small decrease at the N and  $O(1s) \rightarrow \pi^*$  resonances. This may indicate that (i) the observed  $NO^+$  and  $NO_2^+$  ions are mostly produced by direct photoionization and/or (ii) the complementary NO and  $NO_2$  molecules or their fragments are lost as neutral species. These interpretations may be confirmed by a quantitative comparison of the absolute variation of the intensity of the complementary fragments. However, such an estimate based on the present data is unreliable, because it would be affected by the kinetic energy distribution of the involved fragments, which in turn affects the detection efficiency. photoion-photoion coincidence (PEPIPICO) experiments (Itälä et al., 2017) reported that the dominant contribution in the fragmentation of doubly/multiply charged 4(5)NIM ions just above the C K-edge corresponds to the release of  $NO^+$ , while  $NO_2^+$  is either hardly produced or has a large probability to fragment, consistent with our observations.

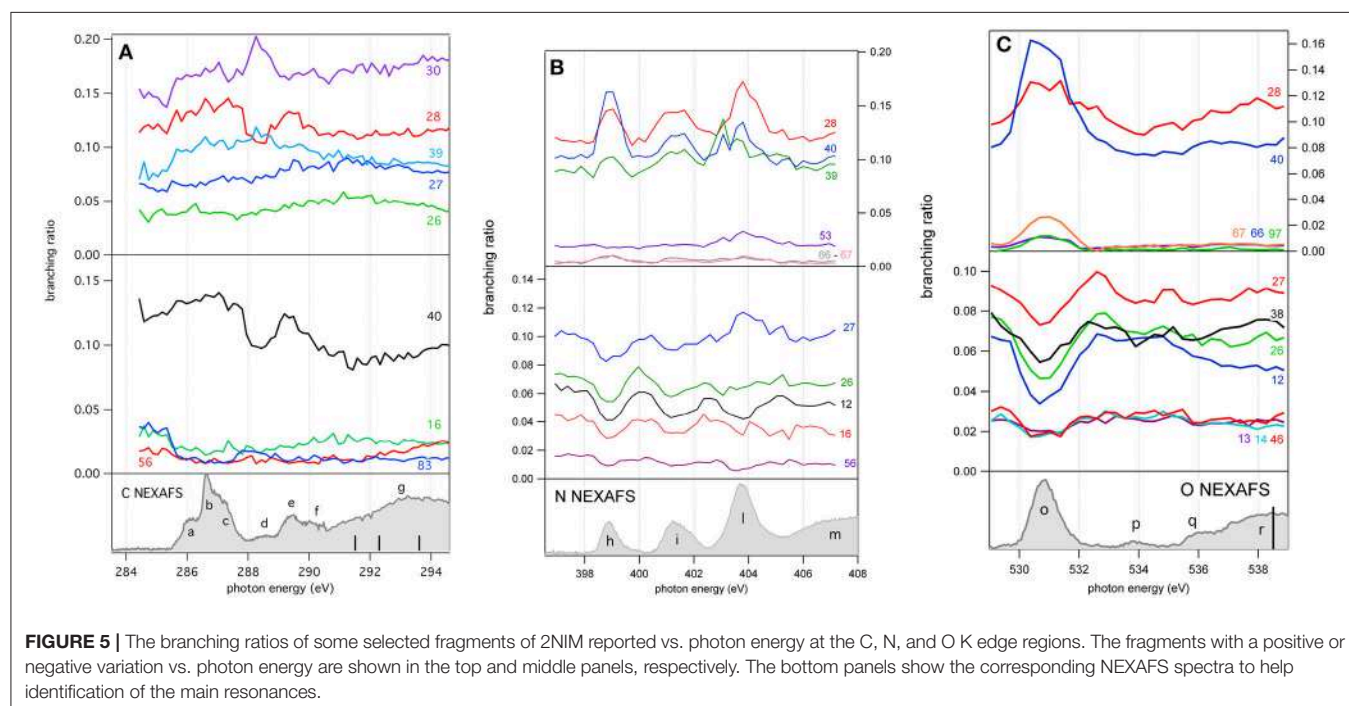
The  $m/z$  56, assigned to the  $HNCHCO^+$  fragment, is a peculiar fingerprint of 2NIM, not present in 4(5)NIM at least up to 60 eV photon energy (Bolognesi et al., 2016). Similar to  $30^+$  and  $28^+$ , its formation in the VUV energy range is related to the loss of NO and the subsequent fragmentation of the residual  $83^+$  fragment. It provides a minor contribution to the mass spectra, with a decrease of intensity at the core excitation, in particular in the C case, **Figure 4A**. Its branching ratio does not display peculiar resonance effects (see **Figures 5A,B**). Passing through core excitations and ionizations the fragmentation mechanisms could be different from the ones identified in the valence region, mainly due to the possibility for multiply-charged ion formations. However, the PEPIPICO experiments of (Itälä et al., 2017) in 4(5)NIM at 317 eV photon energy (i.e., still well below

the N K edge) do not display any significant signal for ion pairs including  $m/z$  fragments heavier than 46. Therefore, we deduced that double ionization events are not the major channels for the production of heavier fragments in 2NIM too.

The largest contribution to the 2NIM mass spectrum was provided by fragments in the  $m/z$  regions 38–42 and 24–30. The first region was dominated by the  $m/z$  40 fragment due to  $C_2H_2N^+$  and its correlated species  $C_2HN^+$  and  $C_2N^+$ , while the other region was populated by light species like  $NO^+$  ( $m/z$  30),  $CO^+ /HCNH^+$  ( $m/z$  28) and its correlated species  $HCN^+$  and  $CN^+$  due to fragmentation of both the imidazole or the nitro group. All the fragments in the  $m/z$  region 38–42 displayed a resonance effect with an increase of their intensity at the three  $\pi^*$  excitations, while in the region  $m/z$  24–30 the  $HCN^+$  and  $CN^+$  fragments displayed an opposite behavior and decreased their relative intensity at the N and  $O(1s) \rightarrow \pi^*$  resonances, showing how the “localization” of the core hole produces large effects on these fragmentation patterns.

A more complete view of the effect of the excitation of the inner-shell resonances is provided by the branching ratios variation of selected fragments reported vs. photon energy in **Figures 5A–C** for the C, N, and O K edge regions, respectively, while their values at selected photon energies spanning from 60 (Bolognesi et al., 2016) to 538 eV are reported in **Table S1** and displayed in **Figure S1**.

As already mentioned in the discussion of **Figure 4**, the 2NIM parent ion ( $m/z$  113) branching ratio decreased significantly with increased photon energy up to the oxygen K edge where its branching ratio vanishes (**Figure S1**). This trend is very common in molecular species, due to the large amount of energy delivered by inner shell excitation/ionization and to the many active fragmentation channels. Indeed, PEPIPICO experiments on



2NIM in the VUV energy range, clearly demonstrated that the molecular fragmentation is state-selective; just after the opening of the first fragmentation channel (the NO loss, at around 10.6 eV), the branching ratio of the parent ion drops to zero (Bolognesi et al., 2015, 2016; Cartoni et al., 2018) indicating that the lowest lying molecular orbital is the only one that allows preservation of the parent ion as an intact unit in the photoionization event, at least within a microsecond time scale. Therefore, with increased photon energy the cross section and, as a consequence, the contribution of the electronic ground state to the fragmentation mass spectrum, becomes less and less relevant and eventually negligible. Furthermore, the parent ion does not show any resonant behavior, as discussed above, indicating that the coupling of these core excited states to the cation electronic ground state is very poor. This was confirmed by the photoelectron spectra taken at the three main resonances at the N edge, which showed that the Resonant Auger process does not lead to an appreciable population of the cation HOMO state. Among the three regions shown in **Figure 5**, the carbon region (**Figure 5A**) is the one that displays the smallest variations. Weak resonance effects are observed in the region of the *a-c* resonances (see **Figure 3A** for the labeling), while some effects on *m/z* 30, 28, and 40 are observed in correspondence of the *d-f* resonances, with an enhancement of the *m/z* 30 branching ratio and a depletion on the other two.

In this region, according to the calculations, the main process is due to the population of the LUMO involved in the excitation of the C2 atom, the one directly bound to NO<sub>2</sub>. In the region of the nitrogen inner shell resonances (**Figure 5B**), the branching ratios of most of the fragments display resonance effects, attenuated in the case of *m/z* 53, 66, and 67. It is interesting to observe that at the *h* resonance, attributed to the population of the LUMO by the promotion of an electron from the N3(1s) orbital, the effects are opposite for the *m/z* 28, 39, and 40 and the *m/z* 12, 16, 26, 27, and 56. This opposite behavior is also observed in the region of the *i* resonance, but seems to disappear at the *l* resonance, where mainly the excitation of the LUMO with the core hole in the N6 site occurs. The observations in the oxygen region (**Figure 5C**) are similar, with large effects in the region of the *o* resonance. The branching ratios of fragments *m/z* 40 and 28 display a clear decrease for increasing photon energy (**Figure S1**) with an interesting enhancement on-resonance (**Figure 5**). These observations may suggest the important role of valence/inner valence fragmentation processes in the production of these fragments. The cross section of valence/inner valence states decreases at larger photon energies and in the core ionization continua, but shows significant enhancements at the core resonant excitations, where the valence shell states can be efficiently populated via Resonant Auger emission as shown in the N case, for example (**Figure 6**).

The resonant photoemission leads to a preferential population of the inner valence states (via spectator Resonant Auger decay) as compared to the direct photoemission measured just below the first resonance. In the binding energy region 13–18 eV, the PEPICO experiments (Bolognesi et al., 2016; Cartoni et al., 2018) have shown that the fragmentation is dominated by the release of fragments 28<sup>+</sup>, 40<sup>+</sup>. In the valence single ion states, fragment 40<sup>+</sup> originates by a chain of events where, following

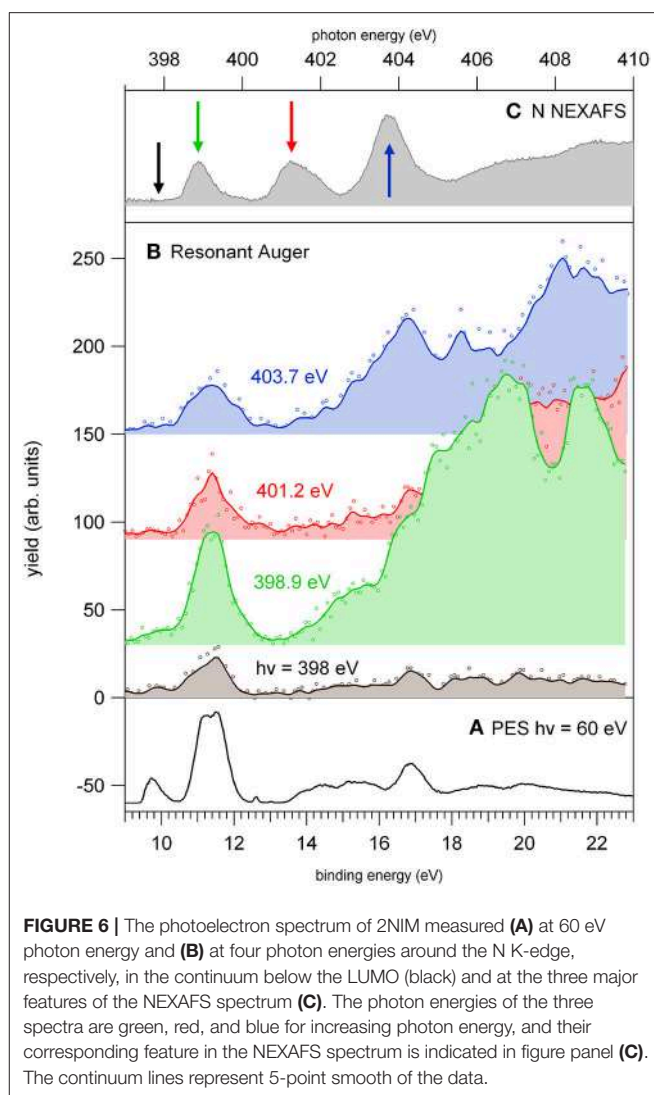


**FIGURE 6** | The photoelectron spectrum of 2NIM measured **(A)** at 60 eV photon energy and **(B)** at four photon energies around the N K-edge, respectively, in the continuum below the LUMO (black) and at the three major features of the NEXAFS spectrum **(C)**. The photon energies of the three spectra are green, red, and blue for increasing photon energy, and their corresponding feature in the NEXAFS spectrum is indicated in figure panel **(C)**. The continuum lines represent 5-point smooth of the data.

the NO<sub>2</sub> loss, the subsequent fragmentation of fragment 67<sup>+</sup> by HCN loss, leads to the HNCCH<sup>+</sup> fragment, that can exist both in its linear or ring structure (Bolognesi et al., 2016; Cartoni et al., 2018). Formation of fragment 28<sup>+</sup>, instead, is triggered by the NO loss, leading to fragment 83<sup>+</sup> that, after several molecular rearrangements and the release of HCN and CO neutral species, ends up in the HCNH<sup>+</sup> fragment at *m/z* 28. Moreover, at these core excitation energies, additional mechanisms of formation involving the fragmentation double and multiply charged ions, may also become active. A general trend is that for increasing photon energy the branching ratios of “small” fragments (*m/z* ≤ 30, with the exception of *m/z* 28) increases in comparison to the larger ones (see *m/z* 12 and 30 in **Figure S1**). Their branching ratios increase as new core ionization thresholds are crossed, while they decrease at resonant excitation energies. Considering the many pathways that could produce these fragments, their detailed discussion would be uncertain. However, they likely result from a stepwise fragmentation process, involving highly excited singly or multiply-charge ions. Thus, the observed difference can be



explained by the formation of excited dications via Auger decay when the excitation occurs above the K-edge, while on resonance, the Resonant Auger Electron processes populate cation states, hampering fragmentation patterns that require larger amount of energy.

## 5. CONCLUSIONS

The core excitation and ionization of 2NIM has been investigated by a set of complementary experimental techniques, which span from electron spectroscopies to mass spectrometry and by accurate computational methods for the prediction of photoemission and photoabsorption spectra. The XPS spectra can be interpreted at a qualitative level, by a building block approach with imidazole and nitrogen dioxide as constituents of nitroimidazoles; this assignment has been confirmed by theoretical simulations of the spectra. The electronegativity of the NO<sub>2</sub> ligand withdraws charge from the imidazole ring affecting its stability. We observed, in fact, that an initial state picture, corresponding to the KT approximation, may provide a rough, sometimes misleading, prediction of the chemical shifts in NIM. A reasonable prediction can only be obtained considering final state effects (polarization and screening due to the increased/decreased number of electrons around the ionization site). Moreover, the building block approach must be considered with caution when one of the constituents of the larger molecule, such as the NO<sub>2</sub> ligand in 2NIM, may change geometry (NO<sub>2</sub><sup>+</sup> is straight in gas phase and bent in 2NIM) and electronic structure (NO<sub>2</sub> is a radical, while 2NIM is not). While the core levels can be qualitatively related to the two different components, chemically shifted from the imidazole and NO<sub>2</sub> value by the predictable effect of the nitro group electronegativity, only  $\Delta$ DFT calculations could confirm the qualitative assignment and the relative values of the chemical shifts. This can be related to the recent observation in the photofragmentation spectra of 2NIM where, at least in the VUV energy region, the NO-loss was the most favorable fragmentation channel, from which all others followed. An intense “shoulder” observed on the high energy side of the main peak in the O(1s) photoemission spectrum, was assigned, by accurate MCSCF calculations, to the lowest shake-up state (HOMO-LUMO excitation) that is predicted to be located at an energy 1.6 eV above that of the core hole state. The unusually low energy of the shake-up state derives from the electron distribution of the LUMO orbital in the final state, which is mostly located close to the core hole.

In the NEXAFS spectra, the combined experimental and theoretical study provided the observation and assignment of the major features due to core electron excitation from the different, and well identifiable, atomic sites in the molecule as well as a description of the corresponding charge distribution in the LUMO and LUMO +1 orbitals. A stabilization of the LUMO

has been observed in 2NIM with respect to imidazole. In the mass spectrometry experiments, the tunability of the photon energy has been used to follow the evolution of the partial ion yields across the different core excited/ionized states of the molecule. Significant effects, especially for channels involving the release of the nitro group, were observed in terms of a variation of the branching ratios in the investigated regions. The cases of the NO<sub>2</sub>, NO, and O losses provide clear evidence of a correlation between the localization of the vacancy and the fragmentation mechanism. This may be considered as possible evidence of a “molecular knife” picture. On the other hand, for the smaller fragments, the observed effects could be rationalized considering that the preferential decay of core excited states is the Resonant Auger decay, which populates the cation states in the valence/inner valence region. The leading mechanism is therefore more of a “memory effect,” ruled by the coupling of the inner shell electronically excited state to the valence/inner valence states, and their following fragmentation.

## DATA AVAILABILITY

All datasets generated for this study are included in the manuscript and/or the **Supplementary Files**.

## AUTHOR CONTRIBUTIONS

PB, PM, ST, BM, RR, and LA performed the experiment. VC, LS, GB, and SM performed the theoretical calculations. AC, MC, and JC participated in the data analysis and interpretation. PB and LA planned the experiment and prepared the manuscript. All authors contributed to the interpretation of the results and the revision of the manuscript.

## FUNDING

We gratefully acknowledge support from the Progetto di Grande Rilevanza of the Italian Ministero degli Affari Esteri e della Cooperazione Internazionale (MAECI) Italia-Serbia A nanoview of radiation-biomatter interaction. ST and BM acknowledge the support from MESTD project #OI 171020.

## ACKNOWLEDGMENTS

The authors thank K.C. Prince for useful discussions.

## SUPPLEMENTARY MATERIAL

The Supplementary Material for this article can be found online at: <https://www.frontiersin.org/articles/10.3389/fchem.2019.00151/full#supplementary-material>

## REFERENCES

Aidas, K., Angeli, C., Bak, K. L., Bakken, V., Bast, R., Boman, L., et al. (2013). The dalton quantum chemistry program system. *WIREs Comput. Mol. Sci.* 4, 269–284. doi: 10.1002/wcms.1172

Apen, E., Hitchcock, A. P., and Gland, J. L. (1993). Experimental studies of the core excitation of imidazole, 4, 5-dicyanoimidazole, and s-triazine. *J. Phys. Chem.* 97, 6859–6866. doi: 10.1021/j100128a019

Au, J. W., and Brion, C. (1997). Absolute oscillator strengths for the valence-shell photoabsorption (2–200 eV) and the molecular and dissociative

- photoionization (11–80 eV) of nitrogen dioxide. *Chem. Phys.* 218, 109–126. doi: 10.1016/S0301-0104(97)00065-7
- Becke, A. D. (1988). Density-functional exchange-energy approximation with correct asymptotic behavior. *Phys. Rev. A* 38:3098. doi: 10.1103/PhysRevA.38.3098
- Bernini, R., Da Silva, L., Rodrigues, F., Coutinho, L., Rocha, A., and de Souza, G. (2012). Core level (S 2p) excitation and fragmentation of the dimethyl sulfide and dimethyldisulfide molecules. *J. Chem. Phys.* 136:144307. doi: 10.1063/1.3701567
- Blyth, R., Delaunay, R., Zitnik, M., Krempasky, J., Krempaska, R., Slezak, J., et al. (1999). The high resolution Gas Phase photoemission beamline, Elettra. *J. Electron. Spectrosc. Relat. Phenom.* 101, 959–964. doi: 10.1016/S0368-2048(98)00381-8
- Bolognesi, P., Casavola, A., Cartoni, A., Richter, R., Markus, P., Borocci, S., et al. (2016). Communication: Position does matter: The photofragmentation of the nitroimidazole isomers. *J. Chem. Phys.* 145:191102. doi: 10.1063/1.4967770
- Bolognesi, P., Kettunen, J., Cartoni, A., Richter, R., Tomic, S., Maclot, S., et al. (2015). Site- and state-selected photofragmentation of 2Br-pyrimidine. *Phys. Chem. Chem. Phys.* 17, 24063–24069. doi: 10.1039/C5CP02601F
- Cacelli, I., Carravetta, V., Rizzo, A., and Moccia, R. (1991). The calculation of photoionisation cross sections of simple polyatomic molecules by L2 methods. *Phys. Rep.* 205, 283–351. doi: 10.1016/0370-1573(91)90041-J
- Cartoni, A., Casavola, A., Bolognesi, P., Castrovilli, M., Catone, D., Chiarinelli, J., et al. (2018). Insights into 2- and 4 (5)-Nitroimidazole decomposition into relevant ions and molecules induced by VUV ionization. *J. Phys. Chem. A* 122, 4031–4041. doi: 10.1021/acs.jpca.8b01144
- Céolin, D., Travnikova, O., Bao, Z., Piancastelli, M., Tanaka, T., Hoshino, M., et al. (2008). Study of the dissociation of nitrous oxide following resonant excitation of the nitrogen and oxygen K-shells. *J. Chem. Phys.* 128:024306. doi: 10.1063/1.2812926
- Davis, D., Martin, R., Banna, M., and Shirley, D. (1973). Multiplet splitting in 1 s hole states of molecules. *J. Chem. Phys.* 59, 4235–4245. doi: 10.1063/1.1680617
- Diviacco, B., Bracco, R., Poloni, C., Walker, R., and Zangrando, D. (1992). Status of the development of insertion devices for ELETTRA. *Rev. Sci. Instrum.* 63, 388–391. doi: 10.1063/1.1142765
- Dunning, T. H. Jr. (1989). Gaussian basis sets for use in correlated molecular calculations. I. the atoms boron through neon and hydrogen. *J. Chem. Phys.* 90, 1007–1023. doi: 10.1063/1.456153
- Eberhardt, W., Sham, T., Carr, R., Krummacher, S., Strongin, M., Weng, S., and Wesner, D. (1983). Site-specific fragmentation of small molecules following soft-X-ray excitation. *Phys. Rev. Lett.* 50:1038. doi: 10.1073/1.1078920
- Feketeová, L., Plekan, O., Goonewardane, M., Ahmed, M., Albright, A. L., White, J., et al. (2015a). Photoelectron spectra and electronic structures of the radiosensitizer nimorazole and related compounds. *J. Phys. Chem. A* 119, 9986–9995. doi: 10.1021/acs.jpca.5b05950
- Feketeová, L., Postler, J., Zavras, A., Scheier, P., Denifl, S., and Richard, A. (2015b). Decomposition of nitroimidazole ions: experiment and theory. *Phys. Chem. Chem. Phys.* 17, 12598–12607. doi: 10.1039/C5CP01014D
- Gejo, T., Takata, Y., Hatsui, T., Nagasono, M., Oji, H., Kosugi, N., et al. (2003). Angle-resolved photoion spectroscopy of NO<sub>2</sub> and SO<sub>2</sub>. *Chem. Phys.* 289, 15–29. doi: 10.1016/S0301-0104(02)00724-3
- Habenicht, W., Baiter, H., Mueller-Dethlefs, K., and Schlag, E. W. (1991). Memory effects in molecular fragmentation induced by site-specific core excitation using a reflection time-of-flight mass spectrometer. *J. Phys. Chem.* 95, 6774–6780. doi: 10.1021/j100171a008
- Hanson, D. M. (1990). Chemistry induced by core electron excitation. *Adv. Chem. Phys.* 77, 1–38. doi: 10.1002/9780470141267.ch1
- Hatamoto, T., Matsumoto, M., Liu, X.-J., Ueda, K., Hoshino, M., Nakagawa, K., et al. (2007). Vibrationally resolved C and O 1s photoelectron spectra of carbon dioxide. *J. Electron. Spectrosc. Relat. Phenom.* 155, 54–57. doi: 10.1016/j.elspec.2006.10.002
- Hetényi, B., De Angelis, F., Giannozzi, P., and Car, R. (2004). Calculation of near-edge X-ray-absorption fine structure at finite temperatures: Spectral signatures of hydrogen bond breaking in liquid water. *J. Chem. Phys.* 120, 8632–8637. doi: 10.1063/1.1703526
- Iannuzzi, M., and Hutter, J. (2007). Inner-shell spectroscopy by the Gaussian and augmented plane wave method. *Phys. Chem. Chem. Phys.* 9, 1599–1610. doi: 10.1039/b615522g
- Itälä, E., Tanzer, K., Granroth, S., Kooser, K., Denifl, S., and Kukuk, E. (2017). Fragmentation patterns of 4 (5)-nitroimidazole and 1-methyl-5-nitroimidazole : the effect of the methylation. *J. Mass Spectrom.* 52, 770–776. doi: 10.1002/jms.3979
- Jayawardane, D., Pickard, C. J., Brown, L., and Payne, M. (2001). Cubic boron nitride: experimental and theoretical energy-loss near-edge structure. *Phys. Rev. B* 64:115107. doi: 10.1103/PhysRevB.64.115107
- Jolly, W., Bomben, K., and Eyermann, C. (1984). Core-electron binding energies for gaseous atoms and molecules. *At. Data Nucl. Data Tables* 31, 433–493. doi: 10.1016/0092-640X(84)90011-1
- Kimura, K. (1981). *Handbook of HeI Photoelectron Spectra of Fundamental Organic Molecules*. New York, NY: Halsted Press.
- Krack, M., and Parrinello, M. (2000). All-electron ab-initio molecular dynamics. *Phys. Chem. Chem. Phys.* 2, 2105–2112. doi: 10.1039/b001167n
- Langhoff, P. (1980). “Stieltjes-Tchebycheff moment-theory approach to photoeffect studies in Hilbert space,” in *Theory and Applications of Moment Methods in Many-Fermion Systems*, eds B. J. Dalton, S. M. Grimes, J. P. Vary, and S. A. Williams (Boston, MA: Springer), 191–212. doi: 10.1007/978-1-4613-3120-9
- Larkins, F. (1990). Theoretical interpretation of molecular Auger spectra. *J. Electron. Spectrosc. Relat. Phenom.* 51, 115–147. doi: 10.1016/0368-2048(90)80146-2
- Lee, C., Yang, W., and Parr, R. G. (1988). Development of the Colle-Salvetti correlation-energy formula into a functional of the electron density. *Phys. Rev. B* 37:785. doi: 10.1103/PhysRevB.37.785
- Lin, Y.-S., Lin, H.-R., Liu, W.-L., Lee, Y. T., Tseng, C.-M., Ni, C.-K., et al. (2015). Measurement and prediction of the NEXAFS spectra of pyrimidine and purine and the dissociation following the core excitation. *Chem. Phys. Lett.* 636, 146–153. doi: 10.1016/j.cplett.2015.07.033
- Lin, Y.-S., Lu, K.-T., Lee, Y. T., Tseng, C.-M., Ni, C.-K., and Liu, C.-L. (2014). Near-edge X-ray absorption fine structure spectra and site-selective dissociation of phenol. *J. Phys. Chem. A* 118, 1601–1609. doi: 10.1021/jp500284r
- Lippert, G., Hutter, J., and Parrinello, M. (1999). The Gaussian and augmented-plane-wave density functional method for ab initio molecular dynamics simulations. *Theor. Chem. Acc.* 103, 124–140. doi: 10.1007/s002140050523
- Liu, X., Prümper, G., Kukuk, E., Sankari, R., Hoshino, M., Makochekanwa, C., et al. (2005). Site-selective ion production of the core-excited CH<sub>3</sub>F molecule probed by auger-electron-ion coincidence measurements. *Phys. Rev. A* 72:042704. doi: 10.1103/PhysRevA.72.042704
- Nagaoka, S.-I., Fukuzawa, H., Prümper, G., Takemoto, M., Takahashi, O., Yamaguchi, K., et al. (2011). A study to control chemical reactions using Si: 2p core ionization: site-specific fragmentation. *J. Chem. Phys. A* 115, 8822–8831. doi: 10.1021/jp203664r
- Okada, K., Tanimoto, S., Morita, T., Saito, K., Ibuki, T., and Gejo, T. (2003). Molecular size effect on the site dependent photofragmentation of N and O k-shell excited CH<sub>3</sub>CO (CH<sub>2</sub>)<sub>n</sub> CN (n = 0–3). *J. Phys. Chem. A* 107, 8444–8448. doi: 10.1021/jp030172t
- Rühl, E., Heinzl, C., Baumgärtel, H., and Hitchcock, A. (1993). Ionic fragmentation of carbon 1s excited metallocenes. *Chem. Phys.* 169, 243–257. doi: 10.1016/0301-0104(93)80081-J
- Salén, P., Kamińska, M., Squibb, R. J., Richter, R., Alagia, M., Stranges, S., et al. (2014). Selectivity in fragmentation of N-methylacetamide after resonant K-shell excitation. *Phys. Chem. Chem. Phys.* 16, 15231–15240. doi: 10.1039/c4cp01067a
- Schäfer, A., Horn, H., and Ahlrichs, R. (1992). Fully optimized contracted Gaussian basis sets for atoms Li to Kr. *J. Chem. Phys.* 97, 2571–2577. doi: 10.1063/1.463096
- Schwell, M., Jochims, H.-W., Baumgärtel, H., and Leach, S. (2008). VUV photophysics and dissociative photoionization of pyrimidine, purine, imidazole and benzimidazole in the 7–18 eV photon energy range. *Chem. Phys.* 353, 145–162. doi: 10.1016/j.chemphys.2008.08.009
- Sodhi, R. N., and Brion, C. (1984). Reference energies for inner shell electron energy-loss spectroscopy. *J. Electron. Spectrosc. Relat. Phenom.* 34, 363–372. doi: 10.1016/0368-2048(84)80050-X
- Tanaka, K., Kizaki, H., Sumii, R., Matsumoto, Y., and Wada, S. (2006). Atomic position dependence of the primary core electron excitation on site-specific chemical bond scission. *Radiat. Phys. Chem.* 75, 2076–2079. doi: 10.1016/j.radphyschem.2005.11.026



- Tanaka, K., Sako, E. O., Ikenaga, E., Isari, K., Sardar, S. A., Wada, S.-I., et al. (2001). Control of chemical reactions by core excitations. *J. Electron. Spectrosc. Relat. Phenom.* 119, 255–266. doi: 10.1016/S0368-2048(01)00301-2
- Thomas, T. D., and Shaw, R. W. Jr. (1974). Accurate core ionization potentials and photoelectron kinetic energies for light elements. *J. Electron. Spectrosc. Relat. Phenom.* 5, 1081–1094. doi: 10.1016/0368-2048(74)85066-8
- Thomason, M. J., Seabourne, C., Sattelle, B., Hembury, G., Stevens, J., Scott, A., et al. (2015). Self-association of organic solutes in solution: a NEXAFS study of aqueous imidazole. *Faraday Discuss.* 179, 269–289. doi: 10.1039/C5FD00005J
- Tronc, M., King, G. C., and Read, F. (1979). Carbon K-shell excitation in small molecules by high-resolution electron impact. *J. Phys. B* 12:137. doi: 10.1088/0022-3700/12/1/020
- Tronc, M., King, G. C., and Read, F. H. (1980). Nitrogen K-shell excitation in N<sub>2</sub>, NO and N<sub>2</sub>O by high-resolution electron energy-loss spectroscopy. *J. Phys. B* 13:999. doi: 10.1088/0022-3700/13/5/025
- Ueda, K., Simon, M., Miron, C., Leclercq, N., Guillemin, R., Morin, P., et al. (1999). Correlation between nuclear motion in the core-excited CF<sub>4</sub> molecule and molecular dissociation after Resonant Auger decay. *Phys. Rev. Lett.* 83:3800. doi: 10.1103/PhysRevLett.83.3800
- Wight, G., and Brion, C. (1974). K-shell energy loss spectra of 2.5 keV electrons in CO<sub>2</sub> and N<sub>2</sub>O. *J. Electron Spectrosc. Relat. Phenom.* 3, 191–205. doi: 10.1016/0368-2048(74)80010-1
- Wiley, W., and McLaren, I. H. (1955). Time-of-flight mass spectrometer with improved resolution. *Rev. Sci. Instrum.* 26, 1150–1157. doi: 10.1063/1.1715212
- Zang, W., Sze, K., Brion, C., Tong, X., and Li, J. (1990). Inner-shell electron energy loss spectra of NO<sub>2</sub> at high resolution: Comparison with multichannel quantum defect calculations of dipole oscillator strengths and transition energies. *Chem. Phys.* 140:265. doi: 10.1016/0301-0104(90)87008-Y

**Conflict of Interest Statement:** The authors declare that the research was conducted in the absence of any commercial or financial relationships that could be construed as a potential conflict of interest.

The reviewer LE declared a past co-authorship with one of the authors VC to the handling editor.

Copyright © 2019 Bolognesi, Carravetta, Sementa, Barcaro, Monti, Manjari Mishra, Cartoni, Castrovilli, Chiarinelli, Tosic, Marinkovic, Richter and Avaldi. This is an open-access article distributed under the terms of the Creative Commons Attribution License (CC BY). The use, distribution or reproduction in other forums is permitted, provided the original author(s) and the copyright owner(s) are credited and that the original publication in this journal is cited, in accordance with accepted academic practice. No use, distribution or reproduction is permitted which does not comply with these terms.

# Communication: “Position” does matter: The photofragmentation of the nitroimidazole isomers

Cite as: J. Chem. Phys. **145**, 191102 (2016); <https://doi.org/10.1063/1.4967770>

Submitted: 28 September 2016 • Accepted: 01 November 2016 • Published Online: 21 November 2016

 P. Bolognesi, A. R. Casavola,  A. Cartoni, et al.



View Online



Export Citation



CrossMark

## ARTICLES YOU MAY BE INTERESTED IN

[Time-of-Flight Mass Spectrometer with Improved Resolution](#)

Review of Scientific Instruments **26**, 1150 (1955); <https://doi.org/10.1063/1.1715212>

[Experimental and theoretical studies of the decomposition of new imidazole based energetic materials: Model systems](#)

The Journal of Chemical Physics **137**, 114303 (2012); <https://doi.org/10.1063/1.4752654>

[Dissociation kinetics of excited ions: PEPICO measurements of  \$\text{Os}\_3\(\text{CO}\)\_{12}\$  – The 7–35 eV single ionization binding energy region](#)

The Journal of Chemical Physics **148**, 084301 (2018); <https://doi.org/10.1063/1.5018719>

The Journal  
of Chemical Physics

**SPECIAL TOPIC:** Low-Dimensional  
Materials for Quantum Information Science

Submit Today!



## Communication: “Position” does matter: The photofragmentation of the nitroimidazole isomers

P. Bolognesi,<sup>1,a)</sup> A. R. Casavola,<sup>1,a)</sup> A. Cartoni,<sup>1,2</sup> R. Richter,<sup>3</sup> P. Markus,<sup>1</sup> S. Borocci,<sup>4</sup> J. Chiarinelli,<sup>1</sup> S. Tošić,<sup>5</sup> H. Sa'adeh,<sup>6</sup> M. Masić,<sup>7</sup> B. P. Marinković,<sup>5</sup> K. C. Prince,<sup>3</sup> and L. Avaldi<sup>1</sup>

<sup>1</sup>*CNR-Istituto di Struttura della Materia, Area della Ricerca di Roma1, Monterotondo, Italy*

<sup>2</sup>*Dipartimento di Chimica, Sapienza Università di Roma, Roma, Italy*

<sup>3</sup>*Elettra-Sincrotrone Trieste, Basovizza, Italy*

<sup>4</sup>*Dipartimento per l'Innovazione nei Sistemi Biologici, Agroalimentari e Forestali (DIBAF), Università della Tuscia, Viterbo, Italy*

<sup>5</sup>*Institute of Physics Belgrade, University of Belgrade, Belgrade, Serbia*

<sup>6</sup>*Department of Physics, The University of Jordan, Amman, Jordan*

<sup>7</sup>*School of Chemistry, Cardiff University, Cardiff, United Kingdom*

(Received 28 September 2016; accepted 1 November 2016; published online 15 November 2016)

A combined experimental and theoretical approach has been used to disentangle the fundamental mechanisms of the fragmentation of the three isomers of nitroimidazole induced by vacuum ultra-violet (VUV) radiation, namely, 4-, 5-, and 2-nitroimidazole. The results of mass spectrometry as well as photoelectron–photoion coincidence spectroscopy display striking differences in the radiation-induced decomposition of the different nitroimidazole radical cations. Based on density functional theory (DFT) calculations, a model is proposed which fully explains such differences, and reveals the subtle fragmentation mechanisms leading to the release of neutral species like NO, CO, and HCN. Such species have a profound impact in biological media and may play a fundamental role in radiosensitising mechanisms during radiotherapy. *Published by AIP Publishing.* [<http://dx.doi.org/10.1063/1.4967770>]

Radiotherapy using different radiation sources like photons, electrons, and ion beams, has represented a major improvement in cancer treatment. Nevertheless, its lack of selectivity in the induced damage is still a serious drawback. Thus, a major issue in oncology therapy<sup>1</sup> is to devise tools to enhance the effects of radiation on tumour cells while minimising the damage to adjacent healthy tissues. An enhancement of the radiation damage<sup>2</sup> can be triggered directly in the DNA of tumour cells by selective incorporation of DNA base analogues,<sup>3</sup> for example, or indirectly, via radiation induced secondary processes leading to the release of free electrons<sup>4</sup> and reactive species, as well as oxygen and “oxygen mimetic” compounds.<sup>5</sup> Indeed hypoxia, which is a consequence of the inefficient vascularisation of some tumours, favours the metabolism and growth of tumour cells and makes them more resistant to radiotherapy<sup>6</sup> than the ones in a normally oxygenated environment. In this respect oxygen is a potent radiosensitiser.<sup>5</sup> Nitric oxide has long been recognized for its effects in tumour reoxygenation<sup>7–9</sup> and has been considered an even more efficient radiosensitiser than oxygen itself [see, for example, Ref. 10 and references therein]. The understanding of these radiosensitising mechanisms is of fundamental importance in the design and characterisation of novel drugs, reducing the risk of negative trials.<sup>11,12</sup>

2- and 5-nitroimidazole (C<sub>3</sub>H<sub>3</sub>N<sub>3</sub>O<sub>2</sub>, m = 113 amu) isomers, i.e., derivatives of imidazole containing one nitro group

are, respectively, the building blocks of misonidazole and nimorazole radiosensitisers used in clinical trials as “oxygen mimetic” compounds.<sup>5,13</sup> They increase the effectiveness of a given dose of radiation by reacting with radiation induced DNA radicals and reducing the DNA repairing capabilities<sup>9</sup> in otherwise resistant hypoxic tumour cells. In clinical trials, the 2-nitroimidazole drug appeared to be more effective than the 5-nitroimidazole one.<sup>2,12</sup> The fundamental reasons for such different behaviour are not yet understood and even though these drugs have a certain level of toxicity, there are still ongoing clinical trials aiming to refine the use of nimorazole.<sup>12</sup> In this work we present a joint experimental and theoretical study of the radiation induced fragmentation of 4-, 5-, and 2-nitroimidazole isomers, providing clear evidence of their different fragmentation patterns. The results suggest that particular products of their decomposition may influence the effectiveness of the radiosensitising action of their derivatives.

The experiments are based on the photofragmentation of isolated 4(5)- and 2-nitroimidazole molecules by the tunable synchrotron radiation of the GasPhase photoemission beamline<sup>14–16</sup> at Elettra (Trieste, Italy) and the vacuum ultra-violet (VUV) radiation of a rare gas discharge lamp.<sup>17</sup> The setups have been described elsewhere<sup>14,17</sup> and more details are reported in the [supplementary material](#). Briefly, the end station at Elettra consists of a 150 mm mean radius hemispherical electron energy analyzer (VG 220i) mounted opposite to a time of flight (TOF) spectrometer, operated in pulsed extraction mode. The electron and ion mass analysers can be operated independently, for photoelectron and mass spectroscopy

<sup>a)</sup>Authors to whom correspondence should be addressed. Electronic addresses: [paola.bolognesi@cnr.it](mailto:paola.bolognesi@cnr.it) and [annarita.casavola@cnr.it](mailto:annarita.casavola@cnr.it)

measurements, or simultaneously in photoelectron–photoion coincidence (PEPICO) experiments. In this PEPICO mode, ion-state selected mass spectra can be measured, where the fragmentation pattern following the ionization from a specific molecular orbital is directly accessed. In the experiments with the discharge lamp, the TOF spectrometer is operated with continuous extraction. The target molecules, 4- and 2-nitroimidazole, were purchased from Sigma Aldrich, with a specified purity of 97% and 98%, respectively. They are in the form of powders at ambient temperature and atmospheric pressure. Therefore they were introduced into the vacuum chamber in a crucible and heated to about 80 °C to be sublimated for gas phase analysis. The 4-nitroimidazole (4NI) and 5-nitroimidazole (5NI) are regioisomers that differ in the position of the H atom on either of the two N atoms within the imidazole ring (see inset in Figure 1) and are almost degenerate in energy. The 4NI isomer was found to be more stable than 5NI in water<sup>18</sup> and in the crystalline state,<sup>19</sup> while in the gas phase they coexist in a tautomeric equilibrium.<sup>18</sup> XPS measurements together with density functional theory (DFT) based theoretical calculations by Feketeová *et al.*<sup>20</sup> found a relative population of 1:0.7 for the 4NI:5NI molecules at 117 °C. Therefore, in the following, we will refer to the 4(5)NI sample assuming that both isomers coexist in gas phase experiments. The fragmentation mass spectra of the 4(5)NI and 2NI molecules measured at 60 eV photon energy and the assignment of the main fragmentation channels are shown in Figure 1.

The two samples display many similar features and relative intensities, but also a few intriguing peculiarities. The most striking differences are observed in the fragments at  $m/z$  55<sup>+</sup> and 56<sup>+</sup>, present exclusively in 4(5)NI and 2NI, respectively, and the fragment at  $m/z$  83<sup>+</sup>, which is one of the leading fragmentation channels in 2NI, but is almost absent in the 4(5)NI sample. Such differences were also observed in electron impact experiments.<sup>21</sup> The peaks at  $m/z$  55<sup>+</sup> and 56<sup>+</sup>

can be attributed to the loss of CNO<sub>2</sub> and HCN<sub>2</sub>O, respectively, while the  $m/z$  83<sup>+</sup> fragment can be unambiguously attributed to the loss of nitric oxide. The latter is particularly relevant for its potential implications in the biological context because of the well proven and recognised action of NO as radiosensitiser and vasodilator.<sup>9</sup>

Further support for these observations is provided by the PEPICO measurements. In Figure 2, the yield of each fragment is reported versus the binding energy of the valence orbital ionised. The corresponding photoelectron spectrum, also reported in Figure 2, is composed of two broad features resulting from the ionisation of the lower binding energy orbitals.<sup>20</sup> Apart from the parent ion observed at the ionization threshold and over the first band, the PEPICO spectra show that, within the experimental energy resolution of the coincidence measurements, several fragmentation channels open up almost simultaneously at a binding energy of about 10.7 eV, i.e., in the second band of the photoelectron spectrum, and display similar trends versus binding energy. At variance with the previously studied six membered ring molecules,<sup>15,22</sup> the nitroimidazoles display little state-selectivity in the fragmentation of these low-energy molecular orbitals. The main observation in Figure 2 is that fragments at  $m/z$  83<sup>+</sup> and 30<sup>+</sup> dominate in 2NI, while  $m/z$  28<sup>+</sup> and 55<sup>+</sup> fragments dominate in 4(5)NI. These observations are completely consistent with those of the mass spectra of Figure 1.

At first glance, the experimental spectra in Figures 1 and 2 may lead to the conclusion that 2NI releases a significant amount of NO, while 4(5)NI does not, explaining the enhanced performance of 2NI as a radiosensitiser. However, previous theoretical calculations<sup>20</sup> revealed very similar energetics for the NO-loss channel in the three isomers, suggesting that a more complex description is needed to explain the results. Thus, in order to explain these differences in the photofragmentation of nitroimidazole isomer radical cations, we have performed new theoretical calculations on the three

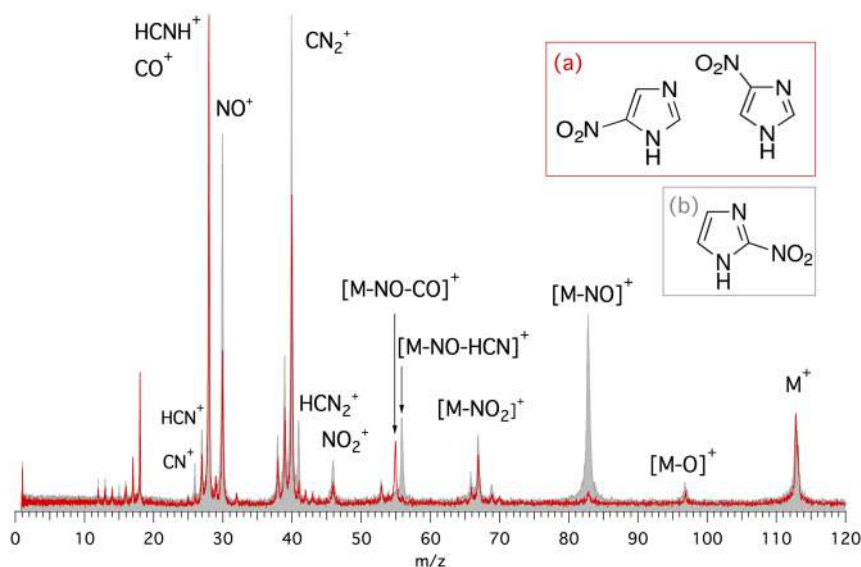


FIG. 1. Mass spectra of 4(5)-nitroimidazole (red line and inset (a)) and 2-nitroimidazole molecules (gray, full, area and inset (b)) measured at 60 eV photon energy. The assignment of the main fragments is reported. Clear differences can be observed in the intensity of fragments  $m/z$  83<sup>+</sup>, 56<sup>+</sup>, and 55<sup>+</sup>, as well as  $m/z$  30<sup>+</sup> and 28<sup>+</sup>. These specific fragmentation channels are discussed in the text. All masses are in amu.

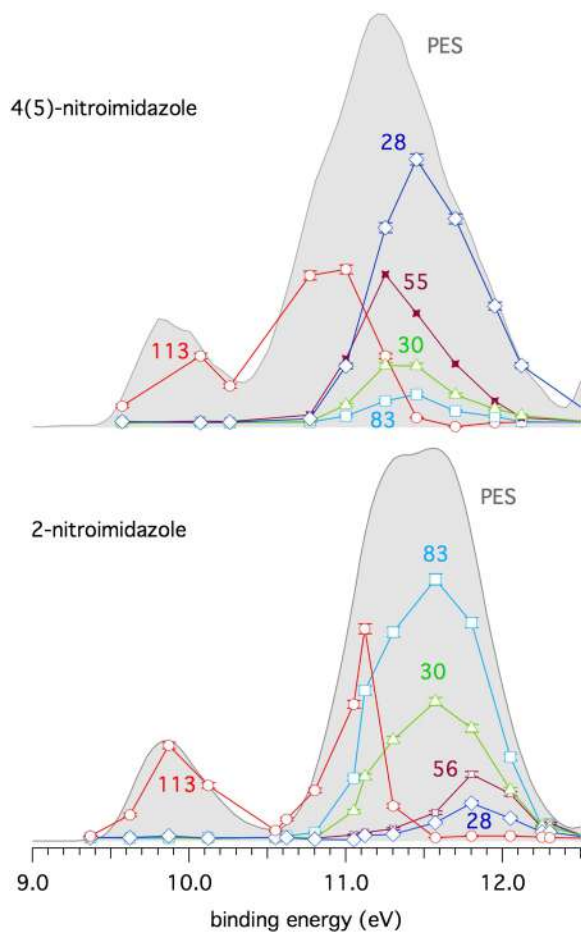


FIG. 2. PES (grey full area) and PEPICO spectra (coloured lines) of selected fragments of 4(5)- and 2-nitroimidazole measured at 60 eV photon energy. In these measurements, the kinetic energy of the photoelectron identifies the binding energy of a specific molecular orbital so that the mass spectrum measured in coincidence corresponds to the fragmentation of that specific electronic state. Here the intensities of all the fragments present in the measured PEPICO spectra are reported versus binding energy.

molecules, focusing on the NO and CO-loss pathways. A more extensive study, including other fragmentation channels and photoelectron spectroscopy, will be presented in a further publication.

All calculations were performed using Gaussian 09.<sup>23</sup> The geometries were optimized at the level of Density Functional Theory (DFT). In particular, the Becke, three-parameter, Lee-Yang-Parr (B3LYP) functional and the 6-311++G\*\* basis set were used. The frequency analysis was based on the normal mode harmonic approximation.<sup>24</sup> Accurate total energies were obtained by single-point coupled cluster calculations, CCSD,<sup>25</sup> using the same basis sets for the B3LYP calculations. The CCSD T1 diagnostic is within the recommended threshold of 0.02,<sup>26</sup> suggesting that these species are correctly described by a single-reference method. All critical points were characterized as energy minima or transition structures (TS) by calculating the corresponding B3LYP harmonic frequencies, also used to evaluate the zero-point energy correction. The TS were unambiguously related to their interconnected energy minima by intrinsic reaction coordinates (IRC) calculations (see the [supplementary material](#)).<sup>27,28</sup>

The resulting potential energy surfaces for the fragmentation of the 4NI, 5NI, and 2NI radical cation isomers are reported in Figures 3(a)–3(c). In all isomers the most stable structure of the radical cation corresponds to a quasi-planar arrangement with the nitro group out of the plane with respect to the neutral molecule (see the [supplementary material](#)). This structure allows the easy NO-loss following an intramolecular rearrangement in the nitro group, with energy barriers of 1.35,

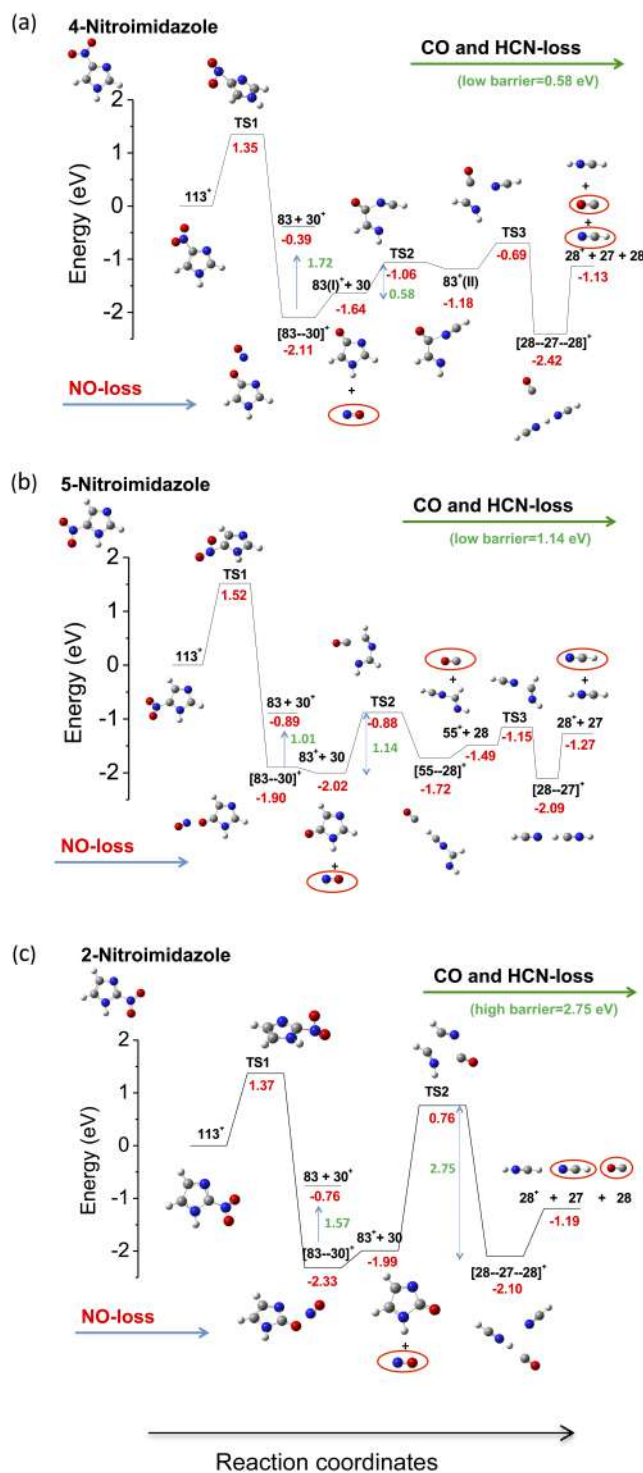


FIG. 3. Potential energy profiles for 4-, 5-, and 2-nitroimidazole (with zero point energy, ZPE) calculated at the CCSD//B3LYP level for the fragmentation of their corresponding molecular ions  $[M]^+$  ( $m$  113 amu). The energy is the sum of the energies of the products relative to that of the radical cation  $[M]^+$ .



1.52, and 1.37 eV for 4NI, 5NI, and 2NI, respectively. The second oxygen atom remains bound to the corresponding C atom in the ring. In all isomers, the NO-loss from the  $[83-30]^+$  adduct can produce the  $C_3H_3N_2O^+$  ion at  $m/z$  83<sup>+</sup>, which preserves the ring structure, or the  $NO^+$  ion at  $m/z$  30<sup>+</sup>. From the energetic point of view, the three isomers show a very similar behaviour in the formation of the 83<sup>+</sup> fragment, while the subsequent fate of the  $m/z$  83<sup>+</sup> ions is profoundly different. In 4NI (Figure 3(a)), the intermediate 83<sup>+</sup> fragment is unstable and, by overcoming an energy barrier of only 0.58 eV (TS2), it undergoes a ring opening, first rearranging into isomer 83<sup>+</sup> (II) and then fragmenting (TS3) into the ion  $HCNH^+$  ( $m/z$  28<sup>+</sup>) with the release of CO and HCN. In 5NI (Figure 3(b)), the 83<sup>+</sup> ion also fragments by overcoming an energy barrier of only 1.14 eV (TS2), into CO and  $HCNCHNH^+$  at  $m/z$  55<sup>+</sup> and then subsequently into the HCN molecule and the  $HCNH^+$  ion at  $m/z$  28<sup>+</sup> via TS3. The analysis of the potential energy surfaces of 2NI (Figure 3(c)) shows a different scenario. In this case, the 83<sup>+</sup> ion has to overcome a very large barrier of 2.75 eV (TS2) before the final fragmentation into HCN and CO molecules and the  $HCNH^+$  ion can take place. This shows that, from the energetic point of view, the fragmentation of the 83<sup>+</sup> intermediate is less favourable in 2NI than in the other isomers because the ring has a higher kinetic stability. Moreover, as can be observed in the mass spectra (Figure 1), the  $m/z$  30<sup>+</sup> peak is more intense in the 2NI isomer than in the 4NI and 5NI cases. This is because in 2NI the energy of 1.57 eV for the separation of  $NO^+$  is lower than the barrier for the following fragmentation of  $m/z$  83<sup>+</sup>, as shown in Figure 3. In the 4NI and 5NI isomers, the energy requirements are reversed, explaining the less intense  $m/z$  30<sup>+</sup> peak in their mass spectrum.

Additional support for these theoretical predictions is provided by the mass spectra measured at the photon energy of 16.67 eV (Ne I) of a rare gas discharge lamp (see the [supplementary material](#)).

These spectra show very asymmetric lineshapes for several features, giving clear evidence of metastable processes<sup>29</sup> leading to the formation of the  $m/z$  83<sup>+</sup> and 30<sup>+</sup> fragments in 2NI as well as 28<sup>+</sup> and 55<sup>+</sup> in 4(5)NI, with a time scale in the order of several tens to hundred ns. This suggests, in agreement with the theoretical description, that molecular rearrangements and two-step fragmentation mechanisms are at the origin of those fragments. Such asymmetric lineshapes could not be observed in the experiments at Elettra due to the pulsed operation of the experimental setup, with the extraction of the ions switching on about 500 ns after the ionisation event (see the [supplementary material](#)).

In summary, the calculations show that all of the nitroimidazole isomers are likely to release NO with similar probability. However, in 4(5)NI the subsequent fragmentation of the residual  $m/z$  83<sup>+</sup> intermediate destroys the imidazole ring releasing HCN and CO molecules, while in 2NI the higher stability of the ring leaves the intermediate intact. These results explain the different intensity of the fragments at  $m/z$  83<sup>+</sup>, 55<sup>+</sup>, 30<sup>+</sup>, and 28<sup>+</sup> observed in both the mass spectra and PEPICO measurements.

In conclusion, the possible implications of our results in the context of radiosensitising mechanisms suggest that

the products of decomposition of the different nitroimidazole isomers might play a role in determining their distinctive degrees of effectiveness in radiotherapy. Nitric oxide, NO, which can be released by all nitroimidazole isomers with about equal probability, is a very reactive radical with a short lifetime and the possibility to diffuse freely across membranes that make it a powerful signalling molecule for vasodilation.<sup>9,10</sup> Being released and active for a short while after irradiation and decomposition of the radiosensitisers, NO could have two actions, saturating dangling bonds in damaged DNA, making the damage permanent, and “favouring either drug delivery or the therapeutic efficacy of irradiation through transient tumour reoxygenation,” as suggested in Ref. 9. These effects, in addition to the redox mechanism, may provide the explanation of the potential of all nitroimidazoles as radiosensitisers active on hypoxic tumours.<sup>12</sup> On the other hand, the release of carbon monoxide, CO, and hydrogen cyanide, HCN, more pronounced in 4(5)NI isomers, may induce an opposite effect by efficiently attaching to haemoglobin<sup>30</sup> and inhibiting the cytochrome c oxidase<sup>31</sup> in mitochondria, respectively, therefore effectively reducing the needed oxygenation and the overall radiosensitising effect. The importance of these processes when nitroimidazole derivate radiosensitizers operate in real biological media depends on how the bio-environment influences their energetics. However the understanding of the very basic chemical and physical mechanisms that determine the molecular response of cells and their building blocks to radiosensitising drugs is of fundamental importance to increase the potential of radiotherapy. Moreover, despite the fact that the typical energies used in radiotherapy are in the keV to MeV range, i.e., far above the VUV range explored in this work, the present results do not lose their potential impact in the context of radiotherapy because it is well documented<sup>4,32</sup> that a large fraction of the radiation damage on biological systems is due to secondary processes releasing particles (electrons, ions, radicals) with a broad energy distribution, which can subsequently trigger the damaging of DNA and its surrounding environment.

See the [supplementary material](#) for detailed description of the experimental apparatuses and procedures, optimised geometries of parent ion and transition states, table of Electronic Energy ( $E_e$ ) and Zero Point Energy (ZPE) of all the stationary points investigated, and intrinsic reaction coordinate calculations for the transition state TS1.

This work is partially supported by the XLIC COST Action CM1204 via the STSM program, the Serbia–Italy Joint Research Project “Nanoscale Insight in the Radiation Damage,” the MIUR FIRB RBFR10SQZI project 2010. H.S. acknowledges the receipt of a fellowship from the ICTP Programme for Training and Research in Italian Laboratories, Trieste, Italy. S.T. and B.P.M. acknowledge partial support of MESTD Project No. OI171020. M.M. acknowledges the Erasmus + EU program for support during her stay at the GasPhase beamline of Elettra-Sincrotrone Trieste.

We are very grateful to Mr. A. Morabito and Mr. S. Rinaldi for their excellent technical support with the experiments.

- <sup>1</sup>A. C. Begg, F. A. Stewart, and C. Vens, *Nat. Rev. Cancer* **11**, 239–253 (2011).
- <sup>2</sup>M. M. Poggi, C. N. Coleman, and J. B. Mitchell, *Curr. Probl. Cancer* **25**, 334–411 (2001).
- <sup>3</sup>P. Wardman, *Clin. Oncol.* **19**, 397–417 (2007).
- <sup>4</sup>B. Boudaiffa, P. Cloutier, D. Hunting, M. A. Huels, and L. Sanche, *Science* **287**, 1658–1660 (2000).
- <sup>5</sup>S. Rockwell, I. T. Dobrucki, E. Y. Kim, S. T. Marrison, and V. T. Vu, *Curr. Mol. Med.* **9**, 442–458 (2009).
- <sup>6</sup>L. B. Harrison, M. Chadha, R. J. Hill, K. Hu, and D. Shasha, *Oncologist* **7**, 492–508 (2001).
- <sup>7</sup>P. Howard-Flanders, *Nature* **180**, 1191–1192 (1957).
- <sup>8</sup>L. H. Gray, F. O. Green, and C. A. Hawes, *Nature* **182**, 952–953 (1958).
- <sup>9</sup>P. Sonveaux, B. F. Jordan, B. Gallez, and O. Feron, *Eur. J. Cancer* **45**, 1352–1369 (2009).
- <sup>10</sup>P. Wardman, K. Rothkamm, L. K. Folkes, M. Woodcock, and P. J. Johnston, *Radiat. Res.* **167**, 475–484 (2007).
- <sup>11</sup>G. D. Wilson, S. M. Bentzen, and P. M. Harari, *Semin. Radiat. Oncol.* **16**, 2–9 (2006).
- <sup>12</sup>G. S. Higgins, S. M. O’Cathail, R. J. Muschel, and W. G. McKenna, *Cancer Treat. Rev.* **41**, 105–113 (2015).
- <sup>13</sup>W. R. Wilson and M. P. Hay, *Nat. Rev. Cancer* **11**, 393–410 (2011).
- <sup>14</sup>R. R. Blyth, R. Delaunay, M. Zitnik, J. Krempasky, J. Slezak, K. C. Prince, R. Richter, M. Vondracek, R. Camilloni, L. Avaldi, M. Coreno, G. Stefani, C. Furlani, M. De Simone, S. Stranges, and M.-Y. Adam, *J. Electron Spectrosc. Relat. Phenom.* **101–103**, 959–964 (1999).
- <sup>15</sup>P. Bolognesi, J. A. Kettunen, A. Cartoni, R. Richter, S. Tosic, S. Maclot, P. Rousseau, R. Delaunay, and L. Avaldi, *Phys. Chem. Chem. Phys.* **17**, 24063–24069 (2015).
- <sup>16</sup>O. Plekan, M. Coreno, V. Feyer, A. Moise, R. Richter, M. De Simone, R. Sankari, and K. C. Prince, *Phys. Scr.* **78**, 058105 (2008).
- <sup>17</sup>A. Cartoni, P. Bolognesi, E. Fainelli, and L. Avaldi, *J. Chem. Phys.* **140**, 184307 (2014).
- <sup>18</sup>P. Jimenez, J. Laynez, R. M. Claramunt, D. Sanz, J. P. Fayet, M. C. Vertut, J. Catalàn, J. L. G. de Paz, G. Pfister-Guillouzo, C. Guimon, R. Flammang, A. Maquestiau, and J. Elguero, “The problem of the tautomerism of 4 (5)-nitroimidazole: A theoretical and experimental study,” *New J. Chem.* **13**, 151–156 (1989).
- <sup>19</sup>A. I. Vokin, L. V. Sherstyannikova, I. G. Krivoruchka, T. N. Aksamentova, O. V. Krylova, and V. K. Turchaninov, *Russ. J. Gen. Chem.* **73**, 973–984 (2003).
- <sup>20</sup>L. Feketeová, O. Plekan, M. Goonewardane, M. Ahmed, A. L. Albright, J. White, R. A. J. O’Hair, M. R. Horsman, F. Wang, and K. C. Prince, *J. Phys. Chem. A* **119**, 9986–9995 (2015).
- <sup>21</sup>See <http://www.nist.gov> for Data from NIST Standard Reference Database 69: NIST Chemistry WebBook; NIST MS number 235477.
- <sup>22</sup>P. Bolognesi, P. O’Keeffe, and L. Avaldi, “Soft x-ray interaction with organic molecules of biological interest,” in *Radiation Damage in Biomolecular Systems, Biological and Medical Physics, Biomedical Engineering*, edited by G. G. Gomez-Tejedor and M. C. Fuss (Springer Science+Business Media B.V., 2012).
- <sup>23</sup>M. J. Frisch, G. W. Trucks, H. B. Schlegel, G. E. Scuseria, M. A. Robb, J. R. Cheeseman, G. Scalmani, V. Barone, B. Mennucci, G. A. Petersson *et al.*, GAUSSIAN 09, Revision A.02, Gaussian, Inc., Wallingford, CT, 2009.
- <sup>24</sup>M. W. Wong, *Chem. Phys. Lett.* **256**, 391–399 (1996).
- <sup>25</sup>K. Raghavachary, G. W. Trucks, J. A. Pople, and M. A. Head-Gordon, *Chem. Phys. Lett.* **157**, 479–483 (1989).
- <sup>26</sup>T. J. Lee and P. R. Taylor, *Int. J. Quantum Chem.* **36**, 199–207 (1989).
- <sup>27</sup>C. Gonzalez and H. B. Schlegel, *J. Chem. Phys.* **90**, 2154–2161 (1989).
- <sup>28</sup>C. Gonzalez and H. B. Schlegel, *J. Phys. Chem.* **94**, 5523–5527 (1990).
- <sup>29</sup>D. Proch, D. M. Rider, and R. N. Zare, *Chem. Phys. Lett.* **81**, 430–434 (1981).
- <sup>30</sup>J. M. Berg, J. L. Tymoczko, and L. Stryer, *Biochemistry*, 7th ed. (W. H. Freeman and Company, 2012), ISBN 13: 9781429229364.
- <sup>31</sup>S. Yoshikawa and W. S. Caughey, *J. Biol. Chem.* **265**, 7945–7958 (1990).
- <sup>32</sup>B. D. Michael and P. A. O’Neill, *Science* **287**, 1603–1604 (2000).



Cite this: *Phys. Chem. Chem. Phys.*,  
2015, **17**, 24063

## Site- and state-selected photofragmentation of 2Br-pyrimidine

P. Bolognesi,<sup>\*a</sup> J. A. Kettunen,<sup>b</sup> A. Cartoni,<sup>c</sup> R. Richter,<sup>d</sup> S. Tosic,<sup>e</sup> S. Maclot,<sup>fg</sup>  
P. Rousseau,<sup>fg</sup> R. Delaunay<sup>fg</sup> and L. Avaldi<sup>a</sup>

The fragmentation of the 2Br-pyrimidine molecule following direct valence photoionization or inner shell excitation has been studied by electron–ion coincidence experiments. 2Br-pyrimidine has been chosen as a model for the class of pyrimidinic building blocks of three nucleic acids and several radiosensitizers. It is known that the site- and state-localization of energy deposition, typical of inner shell excitation, results in the enhancement of the total ion yield as well as in changes in the relative intensity of the different fragmentation channels. Here we address the question of the origin of this selective fragmentation by using electron–ion coincidence techniques. The results show that the fragmentation is strongly selective in the final singly charged ion state, independently of the process that leads to the population of that state, and the dominant fragmentation patterns correlate with the nearest appearance potential.

Received 5th May 2015,  
Accepted 14th August 2015

DOI: 10.1039/c5cp02601f

www.rsc.org/pccp

## 1 Introduction

The ability to manipulate selective bond cleavage in target molecules offers unique chances to manage the local site physics and chemistry. Therefore the search for “molecular knife/scissors”<sup>1</sup> is attracting<sup>2</sup> a lot of interest. Inner shell photo-excitation/ionization is considered a suitable candidate for selective bond cleavage because core electrons are localized very close to the nucleus of one particular atom. Thus inner shell spectroscopies have been proposed and used<sup>3,4</sup> to explore site selectivity. Since these first experiments many studies have been performed in the gas-phase on molecular targets of increasing complexity<sup>5–16</sup> and also on surfaces.<sup>17–19</sup>

Nowadays, tunable soft X-ray sources can be combined with coincidence techniques, where the final products of a specific photoexcitation event are correlated with time, to provide unprecedented information on the photofragmentation of many particle systems. In this way detailed information not only on the electronic structure of the target, but also on its dissociation can be obtained. This is particularly relevant in the study of chemical processes (catalysis, environmental reactions, and biological systems) where decomposition provides information on the functioning of molecules. In this work the fragmentation of

the 2Br-pyrimidine molecule (C<sub>4</sub>H<sub>3</sub>BrN<sub>2</sub>) following direct valence photoionization or inner shell photoexcitation has been studied by electron–ion coincidence experiments. 2Br-pyrimidine is used as a model of halopyrimidine compounds, which represent a class of sensitizers used in radiotherapy.<sup>20</sup>

## 2 Experimental

The experiments have been performed at the gas phase photo-emission beamline<sup>21</sup> of the Elettra synchrotron radiation source (Trieste, Italy). The light source is an undulator of period 12.5 cm, 4.5 m long. The 100% linearly polarised radiation from the undulator is deflected to the variable angle-spherical grating monochromator using a pre-focusing mirror. The monochromator consists of entrance/exit slits and two optical elements: a plane mirror and a spherical grating. Five interchangeable gratings cover the energy region 13–1000 eV, with a typical resolving power of 10 000. Two refocusing mirrors after the exit slit provide a nearly circular focus (radius of about 300 μm) in the interaction region of the experimental chamber. In the present experiments, a fixed photon energy of 100 eV, with an energy resolution of about 20 meV was used for the measurements in the valence shell, and photon energies resonant with the strong π\* transitions from the C(1s), N(1s) and Br(3d) orbitals in the inner shell excitations.

The experimental chamber is maintained at a background pressure below 1 × 10<sup>−7</sup> mbar. The target molecules, which are in the form of a powder at standard ambient temperature and pressure, are kept in a test tube outside the vacuum chamber and admitted into the interaction region *via* a leak valve and a gas line that can be heated up to 60–70 °C on both the vacuum

<sup>a</sup> CNR-Istituto di Struttura della Materia, Area della Ricerca di Roma1, Monterotondo Scalo, Italy. E-mail: paola.bolognesi@cnr.it

<sup>b</sup> Department of Physics, University of Oulu, Finland

<sup>c</sup> Dipartimento di Chimica, Sapienza Università di Roma, Roma, Italy

<sup>d</sup> Elettra – Sincrotrone Trieste, Area Science Park, I-34012 Basovizza, Trieste, Italy

<sup>e</sup> Institute of Physics, University of Belgrade, Belgrade, Serbia

<sup>f</sup> CIMAP, UMR6252 CEA/CNRS/ENSICAEN/Unicaen, Caen, France

<sup>g</sup> Université de Caen Basse-Normandie, Caen, France



and air sides. The vapor pressure in the experimental chamber is in the order of a few  $10^{-6}$  mbar, sufficient to perform the experiments. The sample was purchased from Sigma-Aldrich, with purity higher than 99% and used without further purification. The effusive beam of the target molecules is admitted into the interaction region through a 0.7 mm stainless steel needle that is placed in between the repeller and extractor electrodes of the time-of-flight (TOF) spectrometer, about 2 mm away from the photon beam.

The end station is equipped with a commercial 150 mm mean radius hemispherical electron energy analyzer (VG 220i), with six channel electron multiplier detectors that allow for multidetection. The VG analyzer is mounted behind the repeller electrode of the TOF spectrometer, and the electrons pass through a 90% transmission gold mesh. A home-made Wiley–McLaren TOF mass spectrometer is mounted opposite to the VG electron analyzer. The TOF spectrometer, working in conjunction with the ‘virtually’ continuous ionization source provided by the multibunch operation mode of the synchrotron radiation, is operated in pulsed extraction mode. The repeller and extractor electrodes are polarised with antisymmetric voltages (manufacturer Directed Energy Inc., model PVM4210) driven by an external trigger and providing a typical extraction field of  $700 \text{ V cm}^{-1}$ . The electron and ion mass analyzers can be operated independently, for PES and mass spectroscopy measurements, respectively. In these operation modes (i) the hemispherical analyzer is normally operated with a pass energy of 5 eV, corresponding to a kinetic energy resolution of about 150 meV and (ii) the TOF spectrometer extraction field is triggered using a 1 kHz pulse generator (Stanford Research DG535) to extract the ions.

The two analyzers can be operated simultaneously for coincidence measurements. In this mode a residual penetration field from the drift tube of the TOF produces a kinetic energy shift of the photoelectron spectrum (easily taken into account by the calibration procedure) and a degradation of the energy resolution of the electron analyzer. Therefore in the coincidence mode the electron energy analyzer has been operated at a pass energy of 20 eV, with a gain in efficiency, but no further loss of resolution. The final energy resolution is estimated to be around 0.5 eV.

In order to perform electron–ion coincidence measurements, the electronic chain schematically reported in Fig. 1 of ref. 22, has been used. The amplified and discriminated signals from the channeltrons of the electron analyzer provide the start signals for six independent channels of a time-to-digital converter (TDC, model AM-GPX, ACAM Messelectronic) as well as the trigger for the extraction of the ions from the interaction region, after being combined in a ‘OR’ logic unit. The signal of the extracted ions provides the stop signal to all the TDC channels. Random coincidences are estimated by randomly pulsing at 100 Hz, *i.e.* a frequency comparable to the photoelectron count rate, and counted in a separate channel of the TDC. The PEPICO data have been analyzed using custom macros<sup>23</sup> developed for Igor Pro software. The measured mass spectra are normalized to the number of starts provided by photoelectrons, and the random coincidences to the number of random starts. The normalized spectra are then subtracted to produce the PEPICO spectra.

### 3 Results and discussion

Site- and state-selectivity implies the possibility to distinguish between the different chemical elements (Br, C, and N) in the molecule as well as atoms of the same element, in this case the C atoms in sites with different chemical environments. Inner shell ionization potentials of the different atoms (Br, C and N) are separated by more than 100 eV<sup>24</sup> and recent NEXAFS<sup>25</sup> experiments have shown significant chemical shifts among the three non-equivalent carbon atoms,  $C_5$ ,  $C_{4/6}$  and  $C_2$  (see the inset in Fig. 1 for the numbering of atoms). The mass spectra were measured at several photon energies, corresponding to the black dots in Fig. 1, in the region of the C(1s) excitations as well as just below the lowest inner-shell excitation (280 eV) and above the highest C(1s) ionization threshold (300 eV) for about 10–20 minutes per point. The total ion yield *versus* photon energy gives a ‘low’ resolution NEXAFS spectrum, as shown in Fig. 1. The  $C_2(1s \rightarrow \pi^*)$  excitation at 287.20 eV,<sup>25</sup> well separated from the  $\pi^*$  excitations of the  $C_5$  (284.84 eV) and  $C_{4/6}$  (285.49 eV) non-equivalent C sites is clearly identified. However, two mass spectra are displayed in Fig. 2a to show the effect of the resonant excitation on the different fragmentation channels. The ‘below resonance’ spectrum has been measured at a photon energy of 280 eV, where only the direct ionization of the valence/inner valence and Br states up to the 3d orbital is possible, while the ‘ $C_2\pi^*$ ’ spectrum has been measured at the photon energy of the  $C_2(1s \rightarrow \pi^*)$  excitation. The direct ionization contributes to this spectrum, most likely with a similar ionization cross-section and fragmentation pattern as observed in the spectrum measured at 280 eV. Clearly, the total ionization cross-section is enhanced by the strong resonant absorption (see the total ion yield spectrum in Fig. 1). In order to demonstrate that the fragmentation that follows the resonant excitation is qualitatively different from the one due to the direct ionization we have compared the two cases in Fig. 2a. The spectra have been normalized to the same total ion yield after background subtraction, and the ‘below resonance’ spectrum

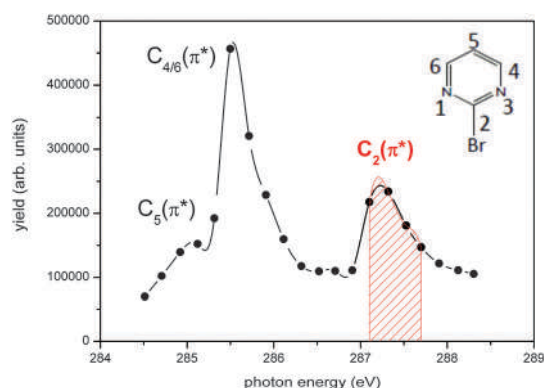
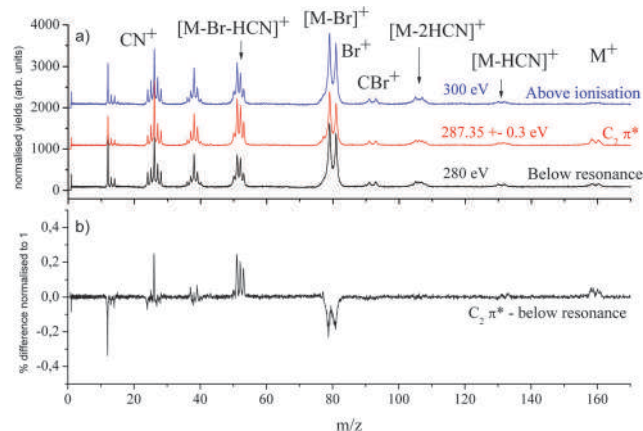


Fig. 1 A low resolution NEXAFS spectrum of 2Br-pyrimidine in the region of the C(1s  $\rightarrow \pi^*$ ) excitations. The black line is a cubic spline representation of the data to guide the eye while the red dashed area represents the integrated region where the  $C_2\pi^*$  spectrum reported in Fig. 2 has been measured. The inset at the top of the figure shows the schematic representation of the 2Br-pyrimidine molecule, with the corresponding numbering of atoms.



**Fig. 2** (a) The fragmentation mass spectra of 2Br-pyrimidine in the region of the  $C(1s \rightarrow \pi^*)$  excitation/ionization thresholds, measured at the  $C_2(1s \rightarrow \pi^*)$  excitation (region marked in red in Fig. 1) and in the ionization continuum below the inner shell resonances, at 280 eV. The three spectra have been shifted on the yield axis in order to allow for a better comparison with the 'below resonance' spectrum. (b) The difference spectrum obtained by subtracting the direct ionization contribution from the resonance one, after normalization to the same total area in the two spectra. This spectrum has been normalized to the maximum yield in the resonance spectrum in order to give a quantitative estimate of the effect.

has been then subtracted from the ' $C_2\pi^*$ ' resonance one. In this way the relative contributions of the different fragmentation patterns, due to resonant excitation, are highlighted. In the 'difference' spectrum reported in Fig. 2b the fragmentation channels that are enhanced, reduced or unaffected by the localization of the energy deposition on the  $C_2$  site will have a positive, negative or 'zero' signal, respectively. The most striking differences between the on- and off-resonance spectra correspond to the reduced formation of  $Br^+$  with respect to a slightly increased amount of parent ion and a much increased intensity in  $[M-Br-H_nCN]^+$ , with  $n = 0, 1, 2$ , and  $CN^+$  in the spectrum measured on-resonance. These observations show that also in this 6-membered ring molecule inner shell, *i.e.* localized, excitations result in an enhancement of the total ion yield and in rapid changes of the relative intensity of the different fragments, providing evidence of site-selective molecular fragmentation. The present work aims to explain the origin of this selectivity.

The inner shell excited states decay mainly *via* non-radiative, resonant Auger electron (RAE) emission to singly charged ion states, whose binding energies are  $BE = h\nu - KE_{RAE}$ , where  $BE$  is the binding energy,  $h\nu$  the photon energy and  $KE_{RAE}$  the kinetic energy of the resonant Auger electron. The type of resonant Auger decay can in principle be distinguished as "participator" or "spectator" transitions depending on whether the core-excited electron does take part in the decay or not. In the former case, the final state has a single hole,  $1h$  configuration, in the valence shell, while in the latter case it has two holes in the valence shell and an electron in the excited state,  $2h1p$  configuration. The same singly charged ion state can be populated by direct photoionization. In this process a photoelectron-photoion coincidence experiment allows the correlation of the fragmentation pattern with a particular

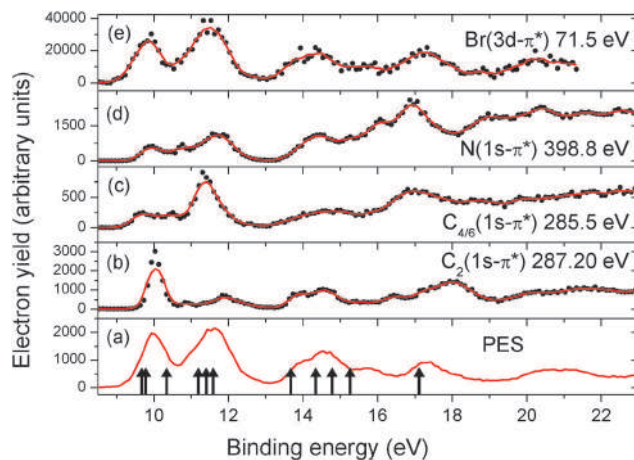


**Fig. 3** The photoelectron spectrum of the 2Br-pyrimidine molecule measured at 100 eV incident photon energy (a) and the resonant Auger electron spectra taken at the different inner shell excitations (b–e) are shown. The energy resolution is 150 meV at full width half maximum (FWHM). The red line is the three point smoothing of the raw data. The arrows in figure (a) indicate the position of the ion states calculated by O'Keeffe *et al.*<sup>26</sup> (see also Table 1).

singly charged ion state, providing state-selected information while the site specificity is lost, because of the delocalised nature of the valence orbitals. In Fig. 3 the four RAE spectra of the decay of the  $C_2$ ,  $C_{4/6}$  and  $N(1s \rightarrow \pi^*)$  and  $Br(3d \rightarrow \pi^*)$  excited states are reported over the binding energy range 8–22 eV of the final state and compared to the photoelectron spectrum obtained at 100 eV. O'Keeffe *et al.*<sup>26</sup> have made an experimental and computational study of the PES spectra of halogenated pyrimidines. Their study was limited to ion states with  $BE \leq 18$  eV because a He lamp was used as the excitation source. The SCF molecular orbital energies of the Kohn–Sham orbitals calculated in that work<sup>26</sup> at the B3LYP/6-311++G(d,p) level of theory are shown in Fig. 3a and collected in Table 1. Each of the two first features in the PES spectrum results from a manifold with a contribution by three different  $1h$  states. The p orbitals of the halogen introduce two orbitals whose orientation is parallel,  $n_{||}$ , or perpendicular,  $n_{\perp}$ , to the ring. In the next part of the spectrum at least four bands can be identified. Ionization of inner  $\sigma$  as well as  $\pi_1$  orbitals is predicted to contribute to the bands up to 16 eV. By analogy to the discussion of the PES spectrum of pyrimidine<sup>27,28</sup> one can expect that an increasing number of overlapping states, consisting of a mixture of  $1h$  and  $2h1p$  configurations, populates the region above 15 eV making a detailed assignment cumbersome.

Although the final electronic states reached in the resonant decay are the same as in the direct photoemission, the intensity distribution as shown in Fig. 3 is different. Indeed the intensities of the RAE spectra depend on the overlap of the wavefunctions of the intermediate and final states. The RAE spectrum at the  $Br(3d)$  excitation mimics very well the PES spectrum. This is explained by the large contribution of the Br p orbitals to the first two features in the PES spectrum and the close excitation energies where the  $Br(3d \rightarrow \pi^*)$  RAE ( $h\nu = 71.5$  eV) and PES (100 eV) spectra have been taken. A similar enhancement of the

**Table 1** Experimental and calculated band energies of 2Br-pyrimidine.<sup>26</sup> The Mulliken population analysis of the molecular orbitals (MOs) of 2Br-pyrimidine, the sum of the contributions of all atomic orbitals (AOs) belonging to the same atom to the electron density of a given MO expressed as a percentage of the total electron density on that MO, is also reported. Only contributions  $\geq 10\%$  are explicitly indicated. The correspondence with the PEPICO measurement in Fig. 4 is reported in the column 'Label'

Orbital	MO	Mulliken population <sup>26</sup>	Exp <sup>26</sup> (eV)	B3LYP <sup>26</sup> (eV)	Label
5b <sub>2</sub>	n <sub>N-</sub>	N <sub>1,3</sub> (27.6%); Br(14.1%)	9.93	9.67	1
3b <sub>1</sub>	$\pi_3$	C <sub>5</sub> (21.0%); Br(50.1%)		9.78	
6b <sub>2</sub>	n <sub>  </sub>	N <sub>1,3</sub> (10.8%); Br(64.6%)	10.83	10.34	
8a <sub>1</sub>	n <sub>N+</sub>	N <sub>1,3</sub> (20.7%); C <sub>2</sub> (14.7%); C <sub>5</sub> (12.3%)	11.24	11.19	
2b <sub>1</sub>	n <sub>⊥</sub>	C <sub>5</sub> (12.6%); Br(70.6%)	11.63	11.40	2
1a <sub>2</sub>	$\pi_2$	N <sub>1,3</sub> (33.7%); C <sub>4,6</sub> (16.0%)	11.89	11.59	
7a <sub>1</sub>	$\sigma$		13.73	13.67	
4b <sub>2</sub>	$\sigma$		14.48	14.34	3
1b <sub>1</sub>	$\pi_1$			14.78	
6a <sub>1</sub>	$\sigma$		15.58	15.26	
3b <sub>2</sub>	$\sigma$		17.08	17.11	4
5a <sub>1</sub>	$\sigma$			17.12	

first feature in the RAE spectrum at the C<sub>2</sub>(1s →  $\pi^*$ ) excitation is consistent with the observations in pyrimidine.<sup>27</sup> In the analysis of the C(1s →  $\pi^*$ ) excitations in pyrimidine by DFT calculations<sup>25</sup> it has been established that the C<sub>2v</sub> symmetry of the molecule is maintained in the C<sub>2</sub> and C<sub>5</sub> core excitations and that the lowest unoccupied orbital is of b<sub>1</sub> symmetry. Moreover, these results suggested that the C<sub>2</sub> and C<sub>5</sub>(1s →  $\pi^*$ ) excitations may strongly interact with each other altering the intensities predicted in the independent particle approximation. This may explain the large intensity of the first feature in the C<sub>2</sub> RAE spectrum, where the Mulliken population analysis shows that there is some contribution from the C<sub>5</sub> atom to the 3b<sub>1</sub> orbital. *Vice versa* in the case of the C<sub>4/6</sub> RAE spectrum, it is the second feature that is enhanced. The 1a<sub>2</sub> orbital is the one with the largest Mulliken population on C<sub>4/6</sub>. In the case of the RAE N spectrum, the first two features have a similar relative intensity to the PES spectrum, with a slight increase in the second one. This again can be explained by

the Mulliken population of the different orbitals involved. In the C and N(1s →  $\pi^*$ ) RAE spectra the bands above 14 eV are clearly enhanced. In this region a band of mixed  $\sigma$  and  $\pi$  symmetry and at higher energy other bands all of  $\sigma$  symmetry are located. In terms of participator transitions these features can be assigned to the 7a<sub>1</sub>, 4b<sub>2</sub>, 1b<sub>1</sub>, 6a<sub>1</sub>, 3b<sub>2</sub> and 5a<sub>1</sub> orbitals. While the enhancement below 16 eV is similar in the three RAE spectra, different intensities are observed above 16 eV. Whether these are the same bands of the PES spectrum, shifted due to a different overlap between the inner-shell excited and final ion states, or correspond to 'new' bands not accessed by direct excitation, cannot be established without proper calculations.

By selecting a resonant photon energy,  $h\nu$ , and detecting a resonant Auger electron with a specific kinetic energy, KE<sub>RAE</sub>, in coincidence with the parent or fragment ions a site- and state-selected study of the fragmentation of the molecule can be done. In Fig. 4 the coincidence mass spectra taken at a few binding energies in the case of the resonant Auger decay following C<sub>2</sub>(1s →  $\pi^*$ ) excitation (panels a and b) and the direct photoionization (panels c and d) are compared. The spectra are normalized to the number of starts provided by the photoelectrons. The feature at the highest  $m/z$  value corresponds to the parent ion with its relative isotopic splitting (50.8% and 49.2% abundance for the <sup>79</sup>Br and <sup>81</sup>Br isotopes, respectively). In a previous VUV study of the fragmentation of halopyrimidines<sup>29</sup> it was observed that the leading fragmentation channels are the HCN loss ( $m/z = 131/133$ ), the Br loss ( $m/z = 79$ ), the BrCN loss ( $m/z = 53$ ) and then the sequential or concerted loss of the HCN group and the Br atom or of the BrCN group and the H atom ( $m/z = 52$ ). In principle  $m/z = 79$  might be assigned to the <sup>79</sup>Br<sup>+</sup> fragment, corresponding to the breaking of the C–Br bond with the positive charge left on the Br atom. However, the absence of the twin peak due to the <sup>81</sup>Br isotope clearly indicates that this channel can be excluded at least in this energy regime. As for  $m/z = 52$  the same work<sup>29</sup> has shown that the BrHCN fragment is not formed due to energy considerations, whereas the two separated neutral fragments

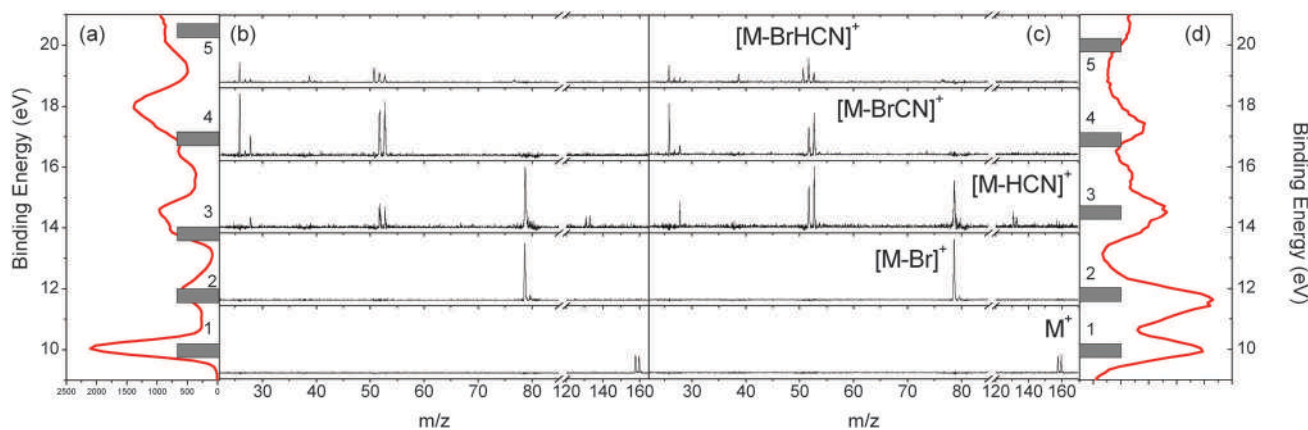


**Fig. 4** The energy selected mass spectra at a few binding energies for the case of the C<sub>2</sub>(1s →  $\pi^*$ ) excitation and (b) valence photoionization at 100 eV photon energy (c). In panels (a) and (d) the C<sub>2</sub>(1s →  $\pi^*$ ) RAE and PES spectra, respectively, are shown. The bars labeled 1 to 5 in panels (a) and (d) represent the selected energies for the PEPICO measurements and their width of about 500 meV at FWHM is the corresponding energy resolution. The correspondence with the different orbitals is reported in Table 1.



(BrCN + H or HCN + Br) have a more stable configuration. It has also been shown<sup>29</sup> that, at variance with the other halopyrimidines, the two fragmentation patterns proposed for the formation of  $m/z = 52$  are competitive in 2Br-pyrimidine, due to the electronegativity of the Br atom, which makes the rupture of the Br–C bond possible at lower energy. Finally the main features at  $m/z < 40$  are assigned to  $C_3H_2^+$ ,  $HCN^+$  and  $CN^+$  at  $m/z = 38$ , 27 and 26, respectively.

These results clearly show that (i) each energy selected mass spectrum is characterized by only a few fragments as compared to the unselected mass spectrum (see Fig. 2); (ii) it strongly depends on the singly charge electronic state populated by either the RAE decay or direct photoionization and that (iii) only a few fragmentation channels at a time are associated with a selected electronic state although lower energy fragmentation channels are already energetically open. So, for example, the appearance of the fragment at  $m/z = 79$  corresponds to the disappearance of the parent ion, and a similar situation occurs to  $m/z = 79$  when the fragments at  $m/z = 53$  and 52 appear. Regardless of the initial photoexcitation/ionization process the two coincidence mass spectra show a very similar behavior as long as the same final ionic state is selected. To prove that this observation is not accidental, a systematic investigation has been performed. The coincidence yields of seven fragments (from  $m/z = 158/160$  down to  $m/z = 26$ ) produced at photon energies corresponding to the excitation from the C(1s), N(1s) and Br(3d) to the LUMO state as well as for direct photoionization have been measured as a function of the binding energy of the singly charged final state. These results are reported in Fig. 5, showing that, independently of the excitation channel, the parent ion is only formed in correspondence with the three lower ion states, while the channel of the loss of the Br atom opens close to 11 eV and involves the  $n_{N+}$ ,  $n_{\perp}$  and  $\pi_2$  states. The HCN loss channel is mainly active for the states between 13 and 16 eV and results to be a minor channel. At about 14 eV also the (BrCN + H) loss as well as the  $HCN^+$  channels open up. The present observations are completely consistent with the measured values of the appearance energies of ref. 29.

The similar behavior of the fragmentation following valence photoionization and inner shell excitation can be explained by the fact that the fragmentation occurs on a timescale longer than the non-radiative relaxation of the inner shell vacancy. Thus, it is the charge distribution of the final singly charged ion that controls the fragmentation. The results in Fig. 5 also indicate that the geometrical structures of the inner shell excited states do not differ too much from that of the ground state. Indeed a different geometrical structure would allow one to access a different region of the potential energy surface of the singly charged ion state, with the possibility that highly excited vibrational states lead to a different fragmentation pattern. Moreover it is clear that a certain ionic state preferentially correlates with the nearest fragmentation threshold, even though other fragmentation channels are energetically open. A qualitative explanation of this latter observation, for the parent ion and the HCN and Br loss channels can be given considering the Hartree–Fock molecular orbitals of the 2Br-pyrimidine molecule

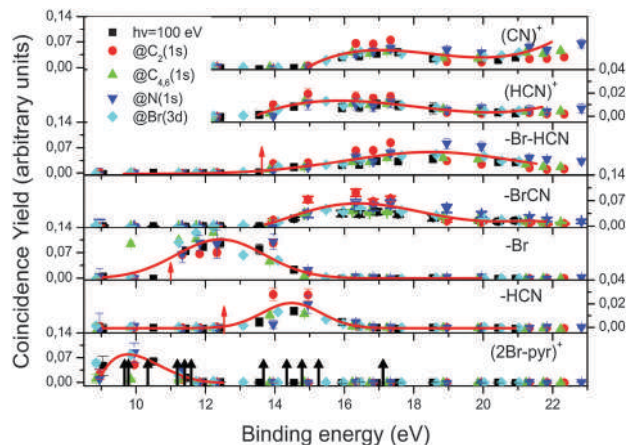


Fig. 5 The energy selected coincidence yield for several 2Br-pyrimidine fragments as a function of the binding energy of the singly charged ion state. The black arrows in the bottom panel indicate the position of the ion states calculated by O'Keeffe *et al.*<sup>26</sup> (see Table 1), while the red ones indicate the appearance energy of the fragments measured by Castrovilli *et al.*<sup>29</sup>

shown in Fig. 6. The first three orbitals are characterized by large Mulliken populations on the Br atom (see Table 1) and are antibonding. Thus the ionization of these orbitals reinforces the C–Br bond and the molecule does not fragment. In the  $n_{\perp}$

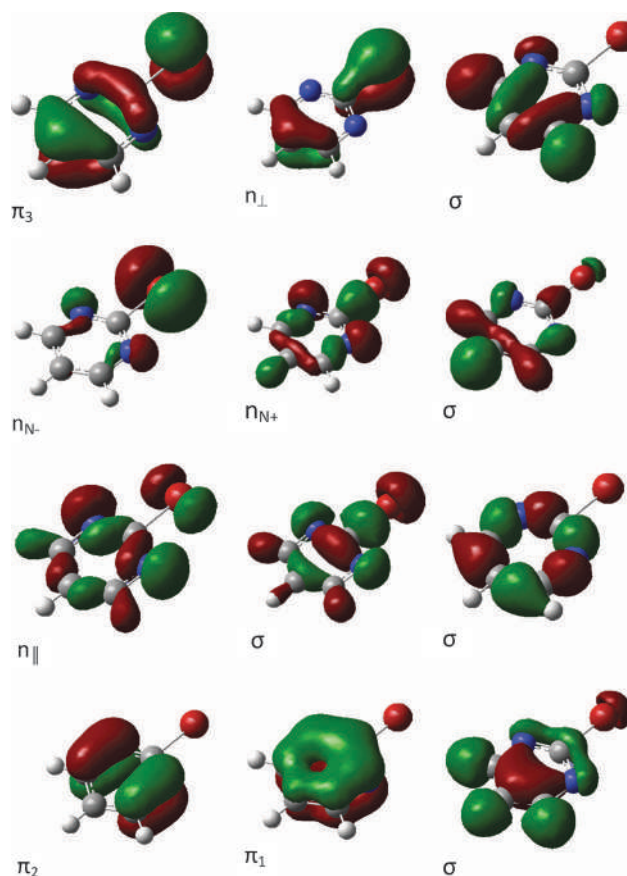


Fig. 6 Representation of the HF molecular orbitals of 2Br-pyrimidine (courtesy of P. O'Keeffe *et al.*<sup>26</sup>).

orbital the lone pair of the halogen atom is a bonding orbital. The ionization process involving this orbital weakens the C–Br bond leading to the Br loss (Fig. 5). Finally the HCN loss corresponds to the binding energy region of the  $\pi_1$  orbital that, being delocalized above and below the ring, once ionized may favor the breaking of the N3–C2 and C4–C5 bonds.

Thus combining the information of the RAE spectra and of the energy selected coincidence yield one can interpret the observation of the variation of the mass spectrum across inner shell excitation. Using Fig. 2b as an example, we see that the C<sub>2</sub> RAE decay, Fig. 3b, favors the population of the first band where the antibonding n orbital of the halogen atom is located, and this hampers the loss of the Br atom/ion resulting in a negative difference in Fig. 2b. *Vice versa*, the enhancement of the RAE spectrum above 14 eV, *i.e.* where the  $\pi_1$  orbital favors HCN loss, results in the positive signal in Fig. 2b.

## 4 Conclusions

In conclusion these results prove that in this six ring molecule the selectivity observed after inner shell excitation, in terms of the preferential production of certain fragments, depends on the different population of the singly charged valence or inner-valence electronic states in the resonant Auger decay. The site selectivity of the inner shell excitation appears to affect the yield of the fragments. Indeed depending on the overlap between the neutral inner shell excited states and the final singly charged ion states, the population of the singly charge ion states varies and therefore the fragmentation channels associated preferentially with those states vary consequently. Thus in the present measurements a direct correlation between a site-selected excitation and a bond breakage cannot be established. This is at variance, for example, with the observations of a recent experiment on *N*-methylacetamide,<sup>16</sup> a small peptide, where this correlation has been observed. Therefore the direct correlation between a site selective inner-shell excitation and the breaking of a bond, the concept behind the search for molecular ‘knife/scissors’, needs to be investigated case by case for different types of molecules. This conclusion is in agreement with the results of a previous study<sup>2</sup> on the fragmentation of X<sub>3</sub>SiC<sub>*n*</sub>–H<sub>*m*</sub>Si(CH<sub>3</sub>)<sub>3</sub> molecules, where *n* = 0–2, *m* = 0–4, and X = F or Cl, following Si2p photoionization. The conclusion of that work was that site-specific fragmentation is strongly molecule dependent, and it is favoured when inter-site electron migration cannot take place efficiently and the chemical environment of the atomic sites are very different.

The present data however confirm that the combination of selective soft X-ray excitation together with a change of the local chemistry can enhance the production of certain fragments. Considering that pyrimidine is the building block of some of the letters of the DNA/RNA alphabet and halopyrimidines are the basic constituents of an important class of radiosensitizers, such as bromo- and iodo-deoxyuridine (UdR) or the 5-fluorouracil (5-FU),<sup>30</sup> in the radiation damage language this finding translates the damaging/destruction of certain molecules or the selective production of reactive radicals (Br and/or H atom) and shed

further light on the nanoscopic effects of radiation damage and radiotherapeutic applications.

## Acknowledgements

This work is partially supported by the Serbia – Italy Joint Research Project “Nanoscale Insight in the Radiation Damage”. The support by the GALILEO G12-44 project ‘New light on radiosensitisers’ and the COST Actions nano-IBCT and XLIC *via* the STSM scheme and MIUR FIRB RBF10SQZI is acknowledged. J.A.K. acknowledges The Finnish Academy of Science and Letters and the Vilho, Yrjö and Kalle Väisälä Foundation.

## References

- 1 K. Tanaka, H. Kizaki, R. Sumii, Y. Matsumoto and S. Wada, *Radiat. Phys. Chem.*, 2006, **75**, 2076–2079.
- 2 S. Nagaoka, H. Fukuzawa, G. Prümper, M. Takemoto, O. Takahashi, K. Yamaguchi, T. Kakiuchi, K. Tabayashi, H. Suzuki, J. R. Harries, Y. Tamenori and K. Ueda, *J. Phys. Chem. A*, 2011, **115**, 8822–8831.
- 3 W. Eberhardt, T. K. Sham, R. Carr, S. Krummacher, M. Strongin, S. L. Weng and D. Wesner, *Phys. Rev. Lett.*, 1983, **50**, 1038.
- 4 W. Eberhardt, E. W. Plummer, I.-W. Lyo, R. Carr and W. K. Ford, *Phys. Rev. Lett.*, 1987, **58**, 207–210.
- 5 M. C. Nelson, J. Murakami, S. L. Anderson and D. M. Hanson, *J. Chem. Phys.*, 1987, **86**, 4442–4445.
- 6 C. Miron, M. Simon, N. Leclercq, D. L. Hansen and P. Morin, *Phys. Rev. Lett.*, 1998, **81**, 4104–4107.
- 7 K. Ueda, M. Simon, C. Miron, N. Leclercq, R. Guillemin, P. Morin and S. Tanaka, *Phys. Rev. Lett.*, 1999, **83**, 3800–3803.
- 8 A. Naves de Brito, R. Feifel, A. Mocellin, A. B. Machado, S. Sundin, I. Hjelte, S. L. Sorensen and O. Björneholm, *Chem. Phys. Lett.*, 1999, **309**, 377–385.
- 9 P. Morin, M. Simon, C. Miron, N. Leclercq, E. Kukk, J. D. Bozek and N. Berrah, *Phys. Rev. A: At., Mol., Opt. Phys.*, 2000, **61**, 050701.
- 10 K. Le Guen, M. Ahmad, D. Colin, P. Lablanquie, C. Miron, F. Penent, P. Morin and M. Simon, *J. Chem. Phys.*, 2005, **123**, 084302.
- 11 X. J. Liu, G. Prümper, E. Kukk, R. Sankari, M. Hoshino, C. Makochekanwa, M. Kitajima, H. Tanaka, H. Yoshida, Y. Tamenori and K. Ueda, *Phys. Rev. A: At., Mol., Opt. Phys.*, 2005, **72**, 042704.
- 12 H. Fukuzawa, G. Prümper, X.-J. Liu, E. Kukk, R. Sankari, M. Hoshino, H. Tanaka, Y. Tamenori and K. Ueda, *Chem. Phys. Lett.*, 2007, **436**, 51–56.
- 13 A. Mocellin, K. Wiesner, S. L. Sorensen, C. Miron, K. Le Guen, D. Céolin, M. Simon, P. Morin, A. B. Machado, O. Björneholm and A. Naves de Brito, *Chem. Phys. Lett.*, 2007, **435**, 214–218.
- 14 E. Itälä, D. T. Ha, K. Kooser, M. A. Huels, E. Rachlew, E. Nommiste, U. Joost and E. Kukk, *J. Electron. Spectrosc. Relat. Phenom.*, 2011, **184**, 119–124.
- 15 J. H. D. Eland, P. Linusson, M. Mucke and R. Feifel, *Chem. Phys. Lett.*, 2012, **548**, 90–94.

- 16 P. Salén, M. Kamińska, R. J. Squibb, R. Richter, M. Alagia, S. Stranges, P. van der Meulen, J. H. D. Eland, R. Feifel and V. Zhaunerchyk, *Phys. Chem. Chem. Phys.*, 2014, **16**, 15231.
- 17 M. C. K. Tinone, K. Tanaka, J. Maruyama, N. Ueno, M. Imamura and N. Matsubayashi, *J. Chem. Phys.*, 1994, **100**, 5988–5995.
- 18 E. O. Sako, Y. Kanameda, E. Ikenaga, M. Mitani, O. Takahashi, K. Saito, S. Iwata, S. Wada, T. Sekitani and K. Tanaka, *J. Electron Spectrosc. Relat. Phenom.*, 2001, **114–116**, 591–596.
- 19 S. Wada, H. Kizaki, Y. Matsumoto, R. Sumii and K. Tanaka, *J. Phys.: Condens. Matter*, 2006, **18**, S1629–S1653.
- 20 M. M. Poggi, C. N. Coleman and J. B. Mitchell, *Curr. Probl. Cancer*, 2001, **25**, 331.
- 21 R. R. Blyth, R. Delaunay, M. Zitnik, J. Krempasky, J. Slezak, K. C. Prince, R. Richter, M. Vondracek, R. Camilloni, L. Avaldi, M. Coreno, G. Stefani, C. Furlani, M. De Simone, S. Stranges and M. Y. Adam, *J. Electron Spectrosc. Relat. Phenom.*, 1999, **101–103**, 959–964.
- 22 O. Plekan, M. Coreno, V. Feyer, A. Moise, R. Richter, M. De Simone, R. Sankari and K. C. Prince, *Phys. Scr.*, 2008, **78**, 058105.
- 23 E. Kukk, R. Sankari, M. Huttula, A. Sankari, H. Aksela and S. Aksela, *J. Electron Spectrosc. Relat. Phenom.*, 2007, **155**, 141–147.
- 24 P. Bolognesi, G. Mattioli, P. O’Keeffe, V. Feyer, O. Plekan, Y. Ovcharenko, K. C. Prince, M. Coreno, A. Amore Bonapasta and L. Avaldi, *J. Phys. Chem. A*, 2009, **113**, 13593.
- 25 P. Bolognesi, P. O’Keeffe, Y. Ovcharenko, M. Coreno, L. Avaldi, V. Feyer, O. Plekan, K. C. Prince, W. Zhang and V. Carravetta, *J. Chem. Phys.*, 2010, **133**, 034302.
- 26 P. O’Keeffe, P. Bolognesi, A. Casavola, D. Catone, N. Zema, S. Turchini and L. Avaldi, *Mol. Phys.*, 2009, **107**, 2025–2037.
- 27 P. Bolognesi, P. O’Keeffe, Y. Ovcharenko, L. Avaldi and V. Carravetta, *J. Chem. Phys.*, 2012, **136**, 154308.
- 28 A. W. Potts, D. M. P. Holland, A. B. Trofimov, J. Schirmer, L. Karlsson and K. Siegbahn, *J. Phys. B: At., Mol. Opt. Phys.*, 2003, **36**, 3129.
- 29 M. C. Castrovilli, P. Bolognesi, A. Cartoni, D. Catone, P. O’Keeffe, A. Casavola, S. Turchini, N. Zema and L. Avaldi, *J. Am. Soc. Mass Spectrom.*, 2014, **25**, 351–367.
- 30 R. Watanabe and H. Nikjoo, *Int. J. Radiat. Biol.*, 2002, **78**, 953–966.

**Electron-impact excitation of silver**S. D. Tošić,<sup>1</sup> V. Pejčev,<sup>1</sup> D. Šević,<sup>1</sup> R. P. McEachran,<sup>2</sup> A. D. Stauffer,<sup>3</sup> and B. P. Marinković<sup>1</sup><sup>1</sup>*Institute of Physics, University of Belgrade, Pregrevica 118, 11080 Belgrade, Serbia*<sup>2</sup>*Research School of Physical Sciences and Engineering, Australian National University, Canberra, Australian Capital Territory 0200, Australia*<sup>3</sup>*Department of Physics and Astronomy, York University, Toronto, Ontario, Canada M3J 1P3*

(Received 23 March 2015; published 11 May 2015)

We measure the differential cross sections (DCSs) for the electron-impact excitation of the combined (two fine-structure levels) resonant  $4d^{10}5p\ ^2P_{1/2,3/2}$  and  $4d^95s^2\ ^2D_{5/2}$  states in silver from the  $4d^{10}5s\ ^2S_{1/2}$  ground state. A comparison with the predictions of the relativistic distorted-wave (RDW) approximation model is carried out. Relativistic distorted-wave calculations are performed for each level separately and are combined to compare with the measurements. Both the experimental and theoretical results are obtained at incident electron energies  $E_0$  of 10, 20, 40, 60, 80, and 100 eV and scattering angles  $\theta$  from  $10^\circ$  up to  $150^\circ$  (experiment) and from  $0^\circ$  to  $180^\circ$  (calculations). Absolute values for the experimental DCSs are obtained by normalizing relative DCSs to theoretical RDW results at  $40^\circ$  at all energies except at 10 eV, where we performed the normalization of the relative DCSs at  $10^\circ$  to our previous small-angle experimental DCS values [S. D. Tošić *et al.*, *Nucl. Instrum. Methods Phys. Res. Sect. B* **279**, 53 (2012)]. The integrated cross sections, which include integral  $Q_I$ , momentum transfer  $Q_M$ , and viscosity  $Q_V$  cross sections, are determined by numerical integration of the absolute DCSs.

DOI: [10.1103/PhysRevA.91.052703](https://doi.org/10.1103/PhysRevA.91.052703)

PACS number(s): 34.80.Dp

**I. INTRODUCTION**

This work is part of our project on electron-impact excitation of silver atoms in the medium- and low-energy regimes. Recently, we published the results of a combined experimental and theoretical study for the electron-impact excitation of the resonant  $4d^{10}5s \rightarrow 4d^{10}5p$  transition in the silver atom in the intermediate electron energy range from 10 to 100 eV at small scattering angles [1]. The comparison with the relativistic distorted-wave (RDW) calculations shows good agreement between experiment and theory especially at higher energies and smaller scattering angles. We are not aware of previous experiments on the angle dependences of the DCSs in the energy range considered here that we can compare to the present work. Even if we include theoretical investigations, there are limited results reported of this scattering process (see [1] and references therein).

The purpose of the present study is to provide reliable electron scattering data that are crucial for a better understanding of electron interactions with silver atoms as well as for many scientific and practical applications [1]. The silver atom is important in the field of laser cooling and trapping techniques and therefore it is an interesting candidate for a neutral-atom-based optical frequency standard. The resonant  $4d^{10}5p\ ^2P_{1/2,3/2}$  state, which is the main goal of the present investigation, is a fine-structure doublet with total angular momenta of  $J = 1/2$  and  $3/2$  and energies of 3.664 and 3.778 eV, respectively, and it is well suited for laser spectroscopic studies. Carlsson *et al.* [2] have measured the lifetimes of these states with high accuracy by time-resolved laser spectroscopy using the delayed coincidence technique, while Uhlenberg *et al.* [3] have performed high-resolution spectroscopic measurements of the  $4d^{10}5s\ ^2S_{1/2} \rightarrow 4d^{10}5p\ ^2P_{3/2}$  cooling transition. Generally, the lifetimes of the  $5p\ ^2P_{1/2}$  and  $5p\ ^2P_{3/2}$  states in silver are among the most accurately known of all atomic lifetimes. Comparing other possible systems such as Ca, Rb, Sr, Yb, and Cs used as optical frequency standards that are based on optically probed electronic transition, usually a forbidden

transition, with narrow bandwidth, there has been some interest in silver using a transition between the  $4d^{10}5s\ ^2S_{1/2}$  ground state and the metastable  $4d^95s^2\ ^2D_{5/2}$  level, which is an extremely narrow transition with a small natural linewidth ( $\approx 0.8$  Hz). Larkins and Hannaford [4] have determined the energy of the  $4d^95s^2\ ^2D_{5/2}$  metastable level and the frequency of the transition. Badr *et al.* [5] presented a detailed description of this optical two-photon excitation process and determined the frequency, hyperfine coupling constants, and isotope shift of this transition. This metastable state is important in terms of our present investigation since its energy of 3.749 eV lies between the combined resonant  $4d^{10}5p\ ^2P_{1/2,3/2}$  states and its contribution to the DCS could not be distinguished in experimental energy-loss spectra at the present energy resolution. Theoretically, each of these lines can be calculated separately and combined as required.

Here we present experimental and theoretical investigations of electron excitation of the silver atom from the ground state to the resonant line  $4d^{10}5p$  at impact energies from 10 to 100 eV. The present investigations are now extended over a wide range of scattering angles up to  $150^\circ$  for experiment and up to  $180^\circ$  for theory. The normalized experimental DCS values were extrapolated to  $0^\circ$  and  $180^\circ$  following the guidance of calculations and were numerically integrated in order to obtain the integral  $Q_I$ , momentum transfer  $Q_M$ , and viscosity  $Q_V$  cross sections. Relativistic distorted-wave calculations were performed for both fine-structure levels and combined to compare with the measurements.

This paper is organized as follows. The experimental technique and procedure are described in Sec. II. In Sec. III the RDW method is outlined. The results are shown and discussed in Sec. IV. A summary is given in Sec. V.

**II. EXPERIMENTAL TECHNIQUES AND PROCEDURES**

The apparatus used in this experiment is a conventional crossed-beam electron spectrometer especially designed for



electron–metal-atom investigations that has been described in detail earlier [1,6–11]. In this crossed-beam arrangement binary collisions are favored, the density of target particles is small enough to ensure that an incident electron interacts with only one target particle, and the density of the electron beam is low enough to ensure that the electrons do not interact with each other. Briefly, the experimental apparatus consists of a hemispherical electron energy selector with a hairpin thermoelectron source in order to provide a monoenergetic electron beam and an energy analyzer of the same type (two hemispheres of identical dimensions to the monochromator) equipped with a channel electron multiplier as a detector in order to analyze and detect the inelastically scattered electrons. The analyzer can be positioned from  $-30^\circ$  up to  $150^\circ$  with respect to the zero angle defined by the axis of the electron beam.

The vacuum chamber also contains an oven as a source of the atomic beam. A silver vapor beam was produced by heating a Knudsen-type crucible by two separate coaxial heaters. In this way the top and the bottom of the crucible can be independently heated and temperature gradients of approximately 100 K needed to avoid clogging were achieved (the top of the system was maintained at a higher temperature than the bottom). The stability of the oven's temperature was controlled and monitored by two thermocouples, one installed at the top of the crucible and the second at the bottom. The measurements were performed at a working temperature of about 1300 K. Water cooling, additional shields, and a liquid-nitrogen cold trap located above the oven and interaction region prevented contamination of the vacuum chamber from the Ag vapor and overheating of surrounding components. In order to achieve better compensation for the earth's magnetic

field, the vacuum chamber was shielded by a double  $\mu$ -metal shield and the measured magnetic field at the position of the interaction volume was below  $2 \times 10^{-7}$  T. The vacuum inside the chamber was provided by two diffusion pumps and a background pressure of the order of  $10^{-5}$  Pa was maintained.

The overall energy resolution (full width at half maximum) of the energy-loss spectra was typically 160 meV, while the angular resolution was  $1.5^\circ$ . The position of the true zero scattering angle was determined before each angular distribution measurement by checking the symmetry of the scattered electrons at negative and positive scattering angles (from  $-10^\circ$  to  $+10^\circ$ ). The scattered electron intensities were recorded in the accessible angular range at the fixed energy loss that corresponds to the excitation energy of the resonance transition. Due to the change of effective interaction volume versus scattering angle, the effective path length correction factors  $V_{\text{eff}}$  [12] determined for the present experimental conditions were applied and the corrections of measured scattered intensities were made. Before each measurement the energy-loss spectrum was accumulated in order to check the stability of the target beam and to verify the absence of double scattering. No structures that correspond to the residual background gas were observed. The relative DCSs obtained at 20, 40, 60, 80, and 100 eV were put on an absolute scale by normalization to the RDW values calculated at  $40^\circ$ . This scattering angle of  $40^\circ$  was chosen for normalization since the signal intensities at this angle are relatively large compared to those at larger scattering angles, while the influence of the effective path length correction factor is relatively small at small angles. Absolute DCSs at 10 eV were obtained by normalization to the absolute DCSs for the same excitation

TABLE I. Differential cross sections, in units of  $10^{-20} \text{ m}^2 \text{ sr}^{-1}$ , for electron excitation of the  $4d^{10}5p \ ^2P_{1/2,3/2}$  levels of silver. The numbers in parentheses are absolute uncertainties. The extrapolated values are given in square brackets. The last three lines are integral  $Q_I$ , momentum transfer  $Q_M$ , and viscosity  $Q_V$  cross sections obtained by integrating our measured DCS in units of  $10^{-20} \text{ m}^2$ .

Angle (deg)	Energy (eV)					
	10	20	40	60	80	100
10	30.9(3.2)	27.4(2.8)	14.3(2.5)	7.3(1.5)	4.8(1.2)	1.95(59)
20	10.2(3.0)	5.7(1.7)	1.85(55)	0.47(14)	0.35(11)	0.168(34)
30	1.89(57)	1.54(46)	0.222(66)	0.114(34)	0.155(46)	0.097(19)
40	0.39(12)	0.59(18)	0.073(22)	0.048(14)	0.071(21)	0.065(13)
50	0.130(39)	0.159(48)	0.051(15)	0.0222(66)	0.0277(83)	0.0293(59)
60	0.096(29)	0.047(19)	0.039(12)	0.0085(34)	0.0083(25)	0.0111(22)
70	0.055(16)	0.0189(75)	0.047(14)	0.0050(20)	0.0144(43)	0.0129(26)
80	0.0290(87)	0.0216(86)	0.026(11)	0.0052(21)	0.0155(46)	0.0148(45)
90	0.0190(57)	0.049(19)	0.0211(95)	0.0061(18)	0.0194(58)	0.0133(40)
100	0.0149(45)	0.0235(70)	0.045(13)	0.0120(36)	0.0066(33)	0.0072(21)
110	0.0033(16)	0.0194(58)	0.074(22)	0.0161(48)	0.0039(19)	0.0033(13)
120	0.0043(21)	0.037(11)	0.122(37)	0.0205(61)	0.00277(97)	0.0053(21)
130	0.0053(19)	0.044(13)	0.058(17)	0.0149(45)	0.00277(97)	0.0061(24)
140	0.0071(25)	0.047(14)	0.103(31)	0.0040(12)	0.00195(68)	0.00297(89)
150	0.040(14)	0.220(66)	0.144(43)	0.0041(12)	0.0033(12)	0.0075(22)
160	[0.03998]	[0.33047]	[0.46313]	[0.02323]	[0.01333]	[0.02668]
170	[0.04014]	[0.42993]	[0.80877]	[0.04753]	[0.02552]	[0.04923]
180	[0.04026]	[0.471]	[0.95841]	[0.05863]	[0.03104]	[0.05941]
$Q_I$	12.4(4.7)	11.2(3.8)	6.8(2.8)	4.5(2.0)	3.3(1.8)	3.0(1.9)
$Q_M$	3.3(1.4)	2.4(1.1)	1.81(96)	0.35(18)	0.23(13)	0.22(12)
$Q_V$	5.4(2.2)	3.1(1.2)	1.25(62)	0.46(23)	0.33(19)	0.26(15)

process at  $10^\circ$  [1]. Then the absolute DCSs were extrapolated to  $0^\circ$  and  $180^\circ$  and numerically integrated to yield integral  $Q_I$ , momentum transfer  $Q_M$ , and viscosity  $Q_V$  cross sections [Eqs. (1)–(3) in [7]]. Extrapolation of the DCS to  $0^\circ$  was made using the measured results at small scattering angles [1]. For extrapolation to  $180^\circ$  we used the RDW calculations for the given energy.

### III. THEORY

Electron-impact excitation of the silver atom is expected to show relativistic effects. In heavy and moderately heavy atoms such as silver ( $Z = 47$ ), these effects are manifested in the fine-structure splitting of the excited states. The RDW method formulated by Zuo *et al.* [13] includes both the fine structure of the atom and the spin-orbit coupling of the scattered electrons and was used for the calculation of the excitation processes in many electron-atom systems [7,14–17] including the electron-silver excitation [1,18]. In the present study we extend the RDW method to the electron excitation of the  $4d^{10}5p$  states of silver (a fine-structure doublet with the lower level having  $J = 1/2$  and the upper level  $J = 3/2$  with an energy splitting of 0.114 eV). Since we have already used this method for the same process at small scattering angles, the details of the calculation method are given in [1] and references therein. We calculated differential cross sections for each level separately and the combined results were compared with the measurements.

### IV. RESULTS AND DISCUSSION

Differential cross sections for the electron excitation of the  $4d^{10}5p \ ^2P_{1/2,3/2}$  states of silver were measured for scattering angles ranging from  $10^\circ$  to  $150^\circ$  and at intermediate electron-impact energies of 10, 20, 40, 60, 80, and 100 eV. Relativistic distorted-wave calculations were performed at the same energies and scattering angles up to  $180^\circ$ . The DCSs were also integrated over all angles and thus integrated cross

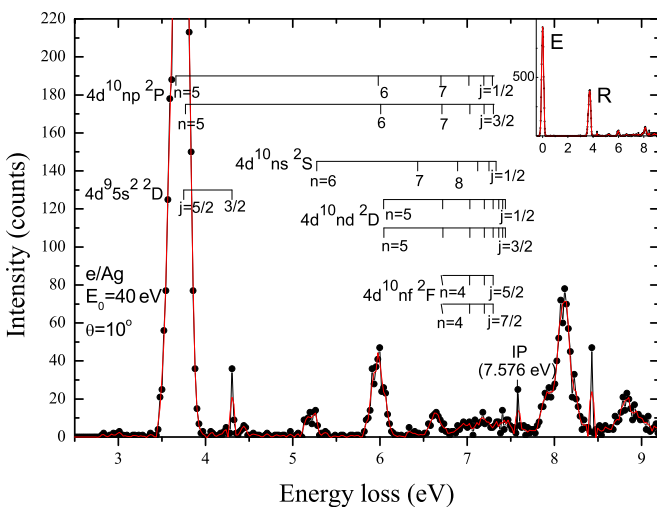


FIG. 1. (Color online) Energy-loss spectrum of silver at 40 eV electron-impact energy and  $10^\circ$  scattering angle. The energy-loss spectrum with features that correspond to the elastic scattering  $E$  and to the resonant excitation  $R$  is shown in the inset. Closed circles denote the measured intensity and the solid line shows the best fit.

sections were obtained. All results are presented in Table I and summarized in Figs. 1–5. The extrapolated experimental values obtained by using the normalized shape of the RDW cross sections are also given in Table I. See Supplemental Material in [19] for the numerical data from the RDW calculations.

The electron excitation of the silver atom is presented in an electron-energy-loss (EEL) spectrum at 40 eV impact energy and at a scattering angle of  $10^\circ$  as shown in Fig. 1. The energy range covered by this spectrum was adjusted to include the region below the first ionization limit of 7.576 eV [20] and the autoionization region up to 9.2 eV. The assignment of atomic energy states is given by using the results on the NIST website [21]. The low-energy region of this spectrum is dominated by an intense feature at about 3.7 eV that is due to the electron excitation of the  $4d^{10}5p \ ^2P_{1/2,3/2}$  fine-structure levels (our energy resolution was not high enough to resolve these two states). It is also evident that this structure is

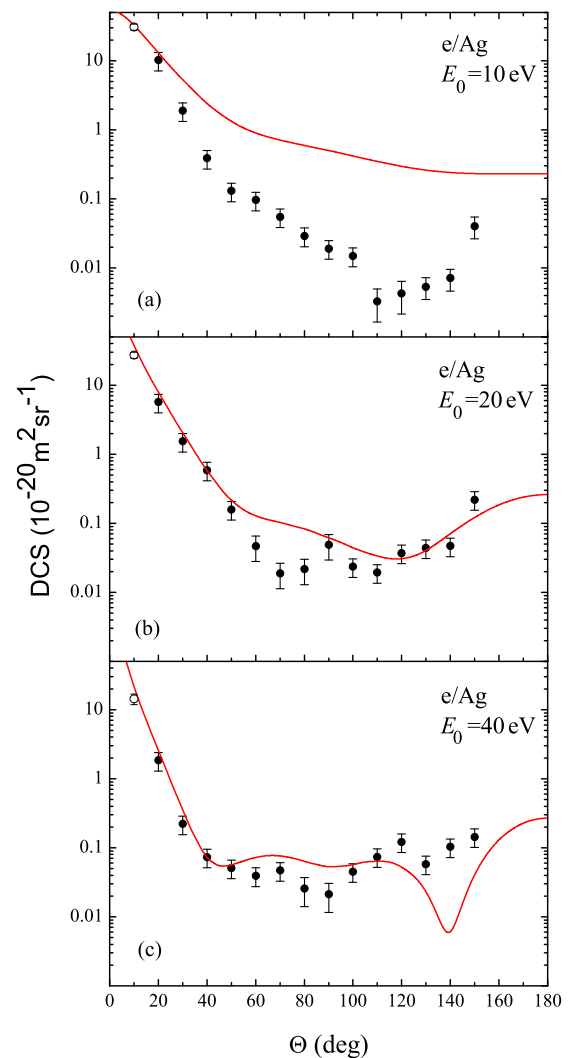


FIG. 2. (Color online) Differential cross sections for the  $4d^{10}5p \ ^2P_{1/2,3/2}$  excitation of silver at (a) 10 eV, (b) 20 eV, and (c) 40 eV electron-impact energies. Closed circles denote the present experimental results with uncertainties. The solid line shows the DCSs calculated by the RDW method for the combined levels.

clearly resolved from the other ones in the EEL spectrum including the feature that corresponds to elastic scattering (see the inset in Fig. 1). Also, the intensities of other peaks (each characteristic of a particular allowed or forbidden transition) are significantly smaller than that of the unresolved silver resonant line. The position of the  $4d^9 5s^2 \ ^2D_{5/2}$  metastable state with an energy of 3.749 eV lies between the  $4d^{10} 5p \ ^2P_{1/2}$  state at 3.664 eV and the  $4d^{10} 5p \ ^2P_{3/2}$  state at 3.778 eV. However, since the excitation from the  $\ ^2S$  ground state to the  $\ ^2D_{5/2}$  level is not a dipole-allowed transition (it decays by electron quadrupole radiation), we assume that its contribution to the measured excitation cross sections of the resonance  $\ ^2P$  states is negligible.

Figure 2 presents both the measured and calculated DCSs at electron-impact energies of 10, 20, and 40 eV. All DCSs are strongly forward peaked as is typical of a dipole-allowed transition. The experimental 10-eV data [Fig. 2(a)] exhibits a structure at  $50^\circ$  (inflection point) and one relatively deep minimum at  $110^\circ$ . There is an abrupt decrease in the cross section between  $100^\circ$  and  $110^\circ$  as well as a jump between  $140^\circ$  and  $150^\circ$ . This behavior was consistent in all data sets obtained at this particular impact energy. The data at 20 eV [Fig. 2(b)] exhibit the presence of two minima, one at  $70^\circ$  and the other at the same angle of  $110^\circ$  as at 10 eV, while the local maximum is at  $90^\circ$ . Again, the cross section increases significantly between  $140^\circ$  and  $150^\circ$ . The DCS at an electron energy of 40 eV [Fig. 2(c)] decreases markedly up to  $40^\circ$ , the

minimum is located at  $90^\circ$ , and then the DCS values increase as the scattering angle increases.

At 10 eV, the incident electron energy is too low for the RDW method to produce reliable results and there is agreement with the measurements only at angles below  $20^\circ$  (which is due to the normalization of the small scattering angle DCS to the RDW data at  $5^\circ$  [1]). At higher angles the experiment gives significantly smaller DCS values but with more structures in the shape. At 20 eV the RDW calculations are in better agreement but do not show the minimum around  $70^\circ$  seen in our measurements. At larger scattering angles they exhibit a shallow minimum near  $120^\circ$ , while the experiment has a deeper minimum around  $110^\circ$ . For 40 eV we observe good agreement in shape between the present experimental and the RDW results at angles up to  $110^\circ$ , though the values obtained from the measurements are lower than from  $60^\circ$ – $90^\circ$ , while at higher scattering angles the calculated DCSs show a deep minimum at  $140^\circ$  in contrast to the shallow experimental one observed at  $130^\circ$ .

The calculated DCSs for the excitation of the  $4d^{10} 5p \ ^2P_{1/2}$  and  $4d^{10} 5p \ ^2P_{3/2}$  states of Ag, as well as the differential

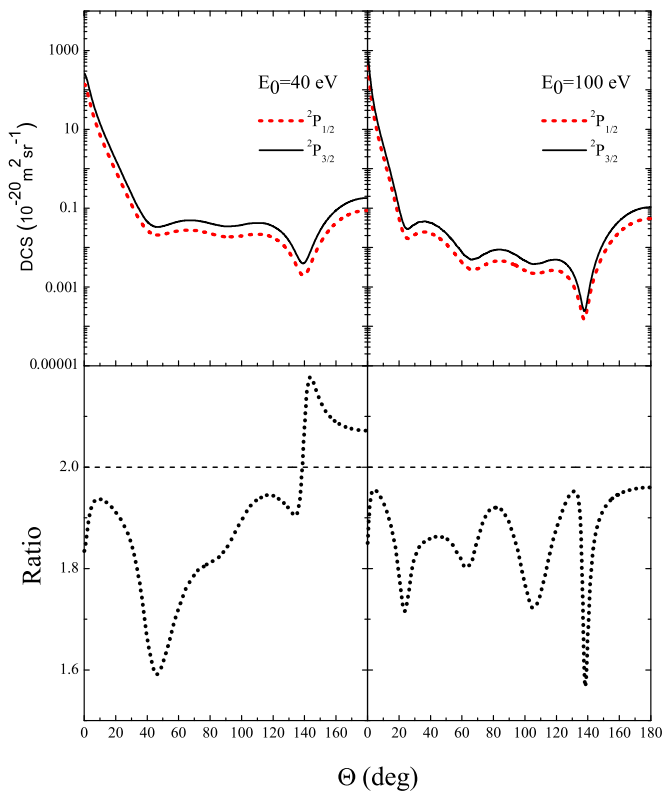


FIG. 3. (Color online) (a) Calculated differential cross sections for the  $4d^{10} 5p \ ^2P_{1/2}$  (dashed line) and  $4d^{10} 5p \ ^2P_{3/2}$  (solid line) excitations of silver and (b) differential branching ratios of the  $4d^{10} 5p \ ^2P_{1/2,3/2}$  states of Ag at 40 and 100 eV.

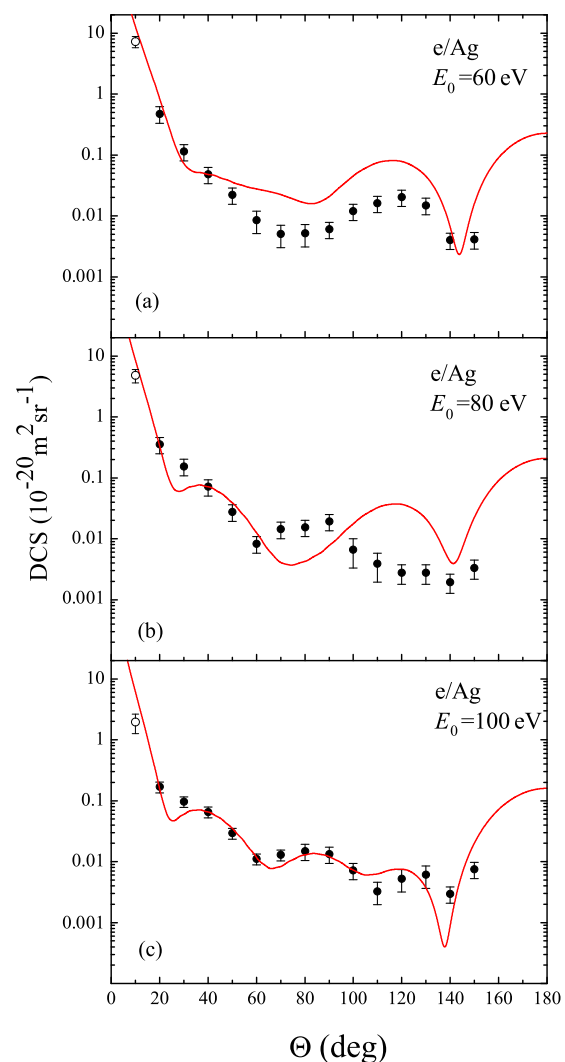


FIG. 4. (Color online) Same as for Fig. 2 except for (a) 60 eV, (b) 80 eV, and (c) 100 eV electron-impact energies.

branching ratios  $DCS_{3/2}/DCS_{1/2}$  at 40 and 100 eV electron-impact energies, are shown in Fig. 3. The results show that there are no noticeable differences in the shape of the cross-section data for  $^2P_{1/2}$  and  $^2P_{3/2}$  states, but the differential branching ratios show deviations from the fine-structure approximation value of 2 (Eq. 4 in [18]). Zeman *et al.* [18] have also found that this branching ratio deviates significantly from 2 at 30, 50, and 100 eV electron-impact energies, which indicates the existence of relativistic effects in silver atoms. These ratios show significant deviations from 2, ranging from 1.6 to 2.2 at 40 eV, and are primarily associated with the fact that the extrema occur at slightly different angles for the two fine-structure levels. This is particularly apparent at 100 eV, where there are several extrema in the calculated cross sections.

Differential cross-section results at 60, 80, and 100 eV are presented in Fig. 4. At an electron energy of 60 eV [Fig. 4(a)], both the measured and calculated curves have similar shapes over the whole angular range, though the theoretical results

are somewhat larger at angles greater than  $50^\circ$  except in the vicinity of a deep minimum at  $144^\circ$ . At 80 eV [Fig. 4(b)] the agreement between experiment and the RDW calculations is quite good at angles below  $60^\circ$ . However, above this angle the measurements show a broad maximum followed by a minimum, whereas the calculated DCSs have the opposite behavior except for the pronounced minimum at  $143^\circ$ , which approaches the measured value. The RDW calculations at 100 eV [Fig. 4(c)] agree quite well with the shape and absolute values of the experimental DCSs. However, there is some difference in magnitude in the region of the two higher minima.

The three-dimensional (3D) profile of the differential cross sections as a function of electron-impact energy and scattering angle is shown in Fig. 5. The figure clearly shows the position of the measured DCSs with respect to the calculated values. Strong forward peaked behavior at small scattering angles

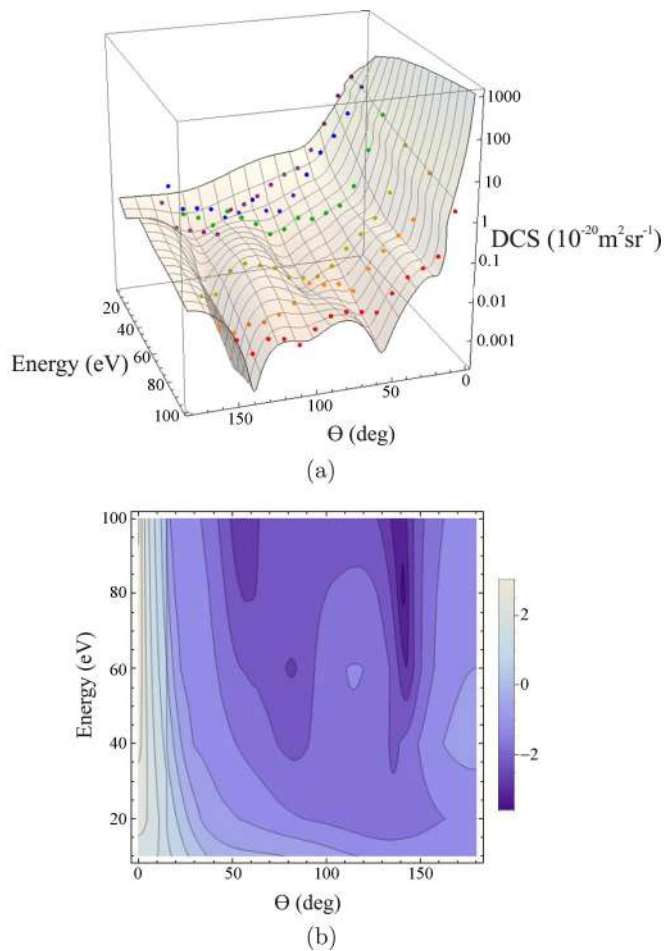


FIG. 5. (Color online) (a) The 3D profile of the differential cross sections as a function of electron-impact energy and scattering angle. Closed circles denote the present experimental results. The surface is made using the RDW data. (b) Contour plot of the RDW data. The vertical axis represents the electron-impact energy (in eV), while the horizontal axis represents the scattering angle (in degrees). The contour lines for the DCS are incremented in powers of 10 according to the legend on the right-hand side of the plot in units of  $10^{-20} \text{ m}^2 \text{ sr}^{-1}$ .

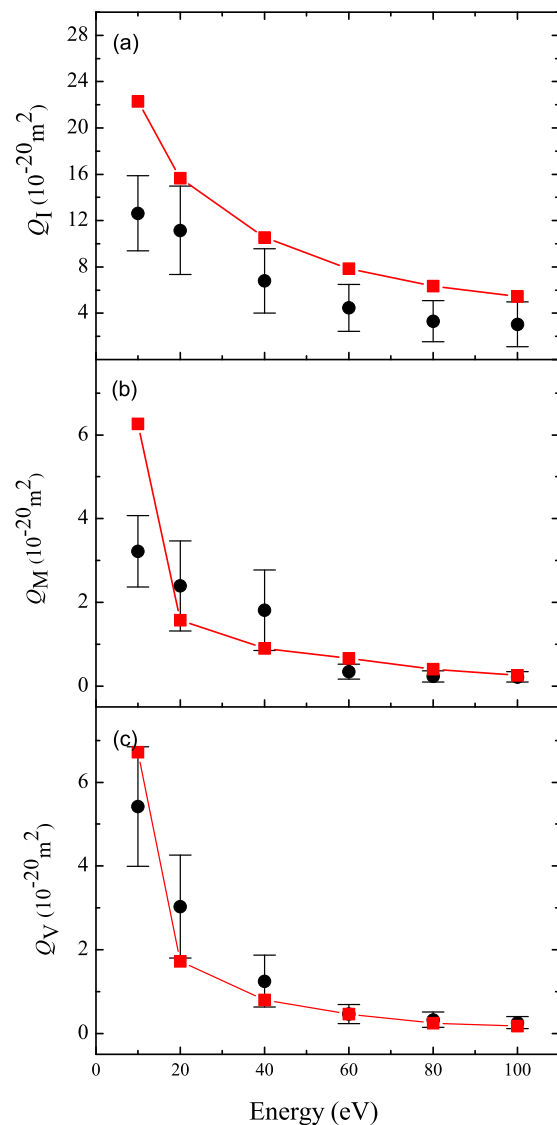


FIG. 6. (Color online) (a) Integral, (b) momentum transfer, and (c) viscosity cross sections for electron-impact excitation of the  $4d^{10}5p \ ^2P_{1/2,3/2}$  state of silver. The experimental points are the same as for Figs. 2 and 4. The solid lines with squares show the ICSs calculated by the RDW method for the combined levels.

characterizes the cross sections of the present transitions. The 3D surface shows a prominent valley near  $140^\circ$ , though the other structures are not as well defined.

In Fig. 6 we present the results for the integral  $Q_I$  [Fig. 6(a)], momentum transfer  $Q_M$  [Fig. 6(b)], and viscosity  $Q_V$  [Fig. 6(c)] cross sections for electron excitation of the combined  $4d^{10}5p^2P_{1/2,3/2}$  levels of silver. The formulas for these were given in [7]. At all electron energies, extrapolation of the experimental DCSs to  $0^\circ$  was based on the small-angle measurements [1], while extrapolation to  $180^\circ$  was made using the RDW calculated DCS profiles. The measurements confirm a monotonic decrease of  $Q_I$ ,  $Q_M$ , and  $Q_V$  with increasing incident electron energy as is also predicted by theory. Reasonably good agreement was achieved between experiment and theory concerning the shape of the energy dependences of all integrated cross sections, but theory gives slightly larger values of the integral cross sections at all electron energies. The main reason for this behavior is the fact that the present calculated DCSs are higher than the normalized measured ones over the whole angular range. For the momentum transfer and viscosity cross sections the calculated cross sections lie at the lower limits of the measured uncertainties at 20 and 30 eV, while there is closer agreement with the measurements at higher energies, especially for the viscosity cross sections.

It is assumed that the contribution of the  $4d^95s^2\ ^2D_{5/2}$  excitation to the measured scattered electron intensities can be neglected. Although the excitation of the optically forbidden states by electron impact will occur, the DCS for these excitations is small compared with the DCS for the resonant excitation. This is illustrated in Fig. 1, where the signal from the  $J = 3/2$  state is much smaller than that for the resonant excitation. Since the DCS for excitation of the  $J = 5/2$  state will have the same magnitude, it can be ignored in the

present measurements. Calculations are needed to provide a quantitative value for these DCSs. Also, as we already reported in our previous paper [1], the DCS for the combined levels can be represented as a sum of the DCSs for the excitation of the individual fine-structure levels.

## V. CONCLUSION

This paper has reported the results of experimental and theoretical studies of the electron-impact excitation of the  $4d^{10}5p$  state of silver at intermediate energies and for the full range of scattering angles. Experimental methods based on a crossed-beam technique as well as the apparatus employed were described. Calculations were carried out using the relativistic distorted-wave method. Differential and integrated cross sections were obtained at electron energies of 10, 20, 40, 60, 80, and 100 eV and scattering angles from  $10^\circ$  to  $150^\circ$  in the experiment, while the calculations cover the full angular range. Reasonable agreement was achieved between the present two sets of data at energies of 20 eV and above.

We are not aware of experimental data that we can compare to the present work. It would be interesting and important to continue investigations on this excitation process in order to obtain a more profound knowledge of electron excitation processes in silver atoms and to obtain more complete sets of scattering data that could be used in further modeling.

## ACKNOWLEDGMENTS

This work was supported by the Ministry of Education, Science and Technological Development of Republic of Serbia (Project No. OI 171020) and was conducted within the framework of the COST Action CM1301 (CELINA). We are grateful to A. Bunjac for technical support.

- 
- [1] S. D. Tošić, V. Pejčev, D. Šević, R. P. McEachran, A. D. Stauffer, and B. P. Marinković, Absolute differential cross sections for electron excitation of silver at small scattering angles, *Nucl. Instrum. Methods Phys. Res. Sect. B* **279**, 53 (2012).
- [2] J. Carlsson, P. Jonsson, and L. Stuesson, Accurate time-resolved laser spectroscopy on silver atoms, *Z. Phys. D* **16**, 87 (1990).
- [3] G. Uhlenberg, J. Dirscherl, and H. Walther, Magneto-optical trapping of silver atoms, *Phys. Rev. A* **62**, 063404 (2000).
- [4] P. L. Larkins and P. Hannaford, Precision measurement of the energy of the  $4d^95s^2\ ^2D_{5/2}$  metastable level in Ag I, *Z. Phys. D* **32**, 167 (1994).
- [5] T. Badr, M. D. Plimmer, P. Juncar, M. E. Himbert, Y. Louyer, and D. J. E. Knight, Observation by two-photon laser spectroscopy of the  $4d^{10}5s\ ^2S_{1/2} \rightarrow 4d^95s^2\ ^2D_{5/2}$  clock transition in atomic silver, *Phys. Rev. A* **74**, 062509 (2006).
- [6] S. Milisavljević, M. S. Rabasović, D. Šević, V. Pejčev, D. M. Filipović, L. Sharma, R. Srivastava, A. D. Stauffer, and B. P. Marinković, Electron-impact excitation of the  $6p7s\ ^3P_1$  state of Pb atom at small scattering angles, *Phys. Rev. A* **75**, 052713 (2007).
- [7] S. Milisavljević, M. S. Rabasović, D. Šević, V. Pejčev, D. M. Filipović, L. Sharma, R. Srivastava, A. D. Stauffer, and B. P. Marinković, Excitation of the  $6p7s\ ^3P_{0,1}$  states of Pb atoms by electron impact: Differential and integrated cross sections, *Phys. Rev. A* **76**, 022714 (2007).
- [8] S. D. Tošić, M. S. Rabasović, D. Šević, V. Pejčev, D. M. Filipović, L. Sharma, A. N. Tripathi, R. Srivastava, and B. P. Marinković, Elastic electron scattering by a Pb atom, *Phys. Rev. A* **77**, 012725 (2008).
- [9] M. S. Rabasović, V. I. Kelemen, S. D. Tošić, D. Šević, M. M. Dovahnych, V. Pejčev, D. M. Filipović, E. Yu. Remeta, and B. P. Marinković, Experimental and theoretical study of the elastic-electron-indium-atom scattering in the intermediate energy range, *Phys. Rev. A* **77**, 062713 (2008).
- [10] B. P. Marinković, V. Pejčev, D. M. Filipović, D. Šević, S. Milisavljević, and B. Predojević, Electron collisions by metal atom vapours, *Rad. Phys. Chem.* **76**, 455 (2007).
- [11] S. D. Tošić, V. I. Kelemen, D. Šević, V. Pejčev, D. M. Filipović, E. Y. Remeta, and B. P. Marinković, Elastic electron scattering by silver atom, *Nucl. Instrum. Methods Phys. Res. Sect. B* **267**, 283 (2009).



- [12] R. T. Brinkman and S. Trajmar, Effective path length corrections in beam-beam scattering experiments, *J. Phys. E* **14**, 245 (1981).
- [13] T. Zuo, R. P. McEachran, and A. D. Stauffer, Relativistic distorted-wave calculation of electron impact excitation of xenon, *J. Phys. B* **24**, 2853 (1991).
- [14] R. Srivastava, T. Zuo, R. P. McEachran, and A. D. Stauffer, Excitation of the  $^{1,3}P_1$  states of calcium, strontium and barium in the relativistic distorted-wave approximation, *J. Phys. B* **25**, 3709 (1992).
- [15] V. Zeman, R. P. McEachran, and A. D. Stauffer, Relativistic distorted-wave calculation of electron impact excitation of caesium, *J. Phys. B* **27**, 3175 (1994).
- [16] R. Srivastava, V. Zeman, R. P. McEachran, and A. D. Stauffer, Excitation of copper by electron impact in the relativistic distorted-wave approximation, *J. Phys. B* **28**, 1059 (1995).
- [17] S. Kaur, R. Srivastava, R. P. McEachran, and A. D. Stauffer, Excitation of thallium and lead atoms by electrons in the relativistic distorted-wave approximation, *J. Phys. B* **33**, 2539 (2000).
- [18] V. Zeman, R. P. McEachran, and A. D. Stauffer, Relativistic distorted-wave approximation of electron impact excitation of silver and gold, *Can. J. Phys.* **74**, 889 (1996).
- [19] See Supplemental Material at <http://link.aps.org/supplemental/10.1103/PhysRevA.91.052703> for the numerical data from the RDW calculations.
- [20] J. E. Sansonetti and W. C. Martin, Handbook of basic atomic spectroscopic data, *J. Phys. Chem. Ref. Data* **34**, 1559 (2005).
- [21] A. Kramida, Yu. Ralchenko, J. Reader, and NIST ASD Team, NIST Atomic Spectra Database, version 5.2, available at <http://physics.nist.gov/asd> (National Institute of Standards and Technology, Gaithersburg, 2014).

PAPER

## Inner shell photofragmentation of 2Cl-pyrimidine studied by mass spectrometry and electron–ion coincidence experiments

To cite this article: Paola Bolognesi *et al* 2020 *J. Phys. B: At. Mol. Opt. Phys.* **53** 244004

View the [article online](#) for updates and enhancements.







**IOP | ebooks™**

Bringing together innovative digital publishing with leading authors from the global scientific community.

Start exploring the collection—download the first chapter of every title for free.



# Inner shell photofragmentation of 2Cl-pyrimidine studied by mass spectrometry and electron–ion coincidence experiments

Paola Bolognesi<sup>1,\*</sup> , Antti Kettunen<sup>2</sup>, Patrick O’Keeffe<sup>1</sup> , Robert Richter<sup>3</sup>, Antonella Cartoni<sup>4,1</sup>, Anna Rita Casavola<sup>1</sup>, Mattea C Castrovilli<sup>1</sup>, Sanja Tosic<sup>5</sup>, Bratislav P Marinkovic<sup>5</sup>  and Lorenzo Avaldi<sup>1</sup> 

<sup>1</sup> CNR-Istituto di Struttura della Materia, Area Della Ricerca Roma 1, Roma, Italy

<sup>2</sup> Department of Physics, University of Oulu, Finland

<sup>3</sup> Elettra–Sincrotrone Trieste, Basovizza (Trieste), Italy

<sup>4</sup> Chemistry Department, Sapienza Università di Roma, Roma, Italy

<sup>5</sup> Institute of Physics Belgrade, University of Belgrade, Belgrade, Serbia

E-mail: [paola.bolognesi@cnr.it](mailto:paola.bolognesi@cnr.it)

Received 10 June 2020, revised 18 September 2020

Accepted for publication 14 October 2020

Published 19 November 2020



## Abstract

Photoelectron spectroscopy, mass spectrometry and electron–ion coincidence experiments combined with tunable synchrotron radiation have been used to study the decay and fragmentation of 2Cl-pyrimidine after Cl(2p), C(1s) and N(1s) excitations. The goal is to investigate how the state- and site-selected excitation and the chemical environment affect the fragmentation paths of the molecule and to make a comparison with fragmentation induced by direct valence ionization. It has been found that the site-selective inner shell excitation affects the branching ratio of the fragments, while the particular fragmentation channels of the cation are determined by the final state populated in the resonant decay of the core excited states. Effects of nuclear motion in the core excited states and the possible ultrafast molecular dissociation following the Cl(2p →  $\sigma^*$ ) core excitation are discussed.

Keywords: resonant Auger, PEPICO, mass spectrometry, 2Cl-pyrimidine

(Some figures may appear in colour only in the online journal)

## 1. Introduction

Due to their strong interaction with the nucleus, core electrons are ‘localized’ on a specific atom in the molecule and weakly affected by the surrounding environment. As such, their binding energy (BE) falls into a relatively narrow range that is characteristic of each atom/orbital combination, but the specific value within that range is a fingerprint of the surrounding environment, providing information on specific molecular bonds [1]. On the basis of this principle, core ionization is widely

used for qualitative and quantitative analysis of the elemental composition of molecules in the gas phase as well as of materials.

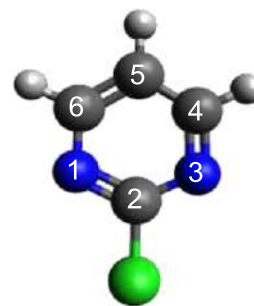
Going beyond its use as an analytical tool, it has been long investigated whether the selective removal of a core electron from a specific molecular site/orbital could also be used to control the molecular fragmentation inducing specific bond breakages [2–4]. Similarly to core ionization, the core electron excitation is characterized by the same atomic-like nature, meaning that even though the core electron is promoted to an empty orbital and not ejected into the continuum, the core vacancy is still localized on a specific atom (molecular site)

\* Author to whom any correspondence should be addressed.

and orbital (molecular state). Therefore, the core electron excitation provides a unique means to specifically target a particular molecular site and molecular orbital by tuning the photon energy to a specific resonant excitation energy.

It is commonly observed that the molecular fragmentation following core excitation is strongly influenced by both the molecular site of the initial excitation and the character of the excited molecular orbital [3, 5–14]. Indeed, significant variations in the fragment branching ratios have been observed across different excitation thresholds, leading to the proposed use of core excitation as a sort of ‘molecular knife’ [15] to induce specific molecular bond breakings. However, the ‘molecular knife’ interpretation of the site/state-selective bond scission is strongly molecule dependent. While it is favoured when inter-site electron migration cannot occur efficiently and the chemical environment of the atomic site is very different [3], it becomes questionable in the case where fast electronic relaxation channels efficiently redistribute the initially-localized core hole among singly and multiply ionized states before the molecular fragmentation occurs. In these cases the localization of the primary excitation is rapidly lost and the molecular fragmentation follows the fate of the single/multiple ionic state populated by the electronic relaxation, driven by a sort of ‘memory effect’ [16, 17] determined by the overlap between the initial and final electronic states. This scenario was clearly demonstrated in 2Br-pyrimidine [13], where significant differences in the molecular fragmentation measured at the C(1s), N(1s) and Br(3d) excitation energies were cancelled out when the final single ion states reached by the electron decay were singled out by the detection of the resonant Auger electron in coincidence with the fragment ions. In that case, a direct correlation between a site-selected excitation and a bond breakage could not be established, and the entire process was found to be governed by the specific coupling of the intermediate (neutral) and final (ionic) states.

In contrast, Ueda *et al* [18, 19] proved that the nuclear motion in the core excited state can affect the dissociation, thus preserving some selectivity. This occurs when the core hole lifetime is long, on the order of 10 fs, and a strong coupling between the electron and the nuclear motion exists, like in some  $\sigma^*$  resonances. In such cases, the population of the vibrational distribution of the final cation state may lead to a specific molecular dissociation channel. The limit of this process is represented by the ultrafast dissociation occurring directly in the core-excited state, like in HBr [20], where a clear Br atomic decay has been observed following Br(3d  $\rightarrow$   $\sigma^*$ ) excitation. Schematically, the ultra fast dissociation (UFD) process following a soft x-ray absorption can be described as the population of a repulsive inner shell excited state that continuously undergoes Auger decay. The electronic relaxations occurring at early times, i.e. at small internuclear distances, involve the undissociated molecule, while the ones occurring at later times, i.e. at larger internuclear distances, will eventually involve electronically-excited fragments. The latter case will produce sharp lines at specific kinetic energies (KE) in the electron spectrum, corresponding to the non-radiative decay of the fragment (Br atomic lines in reference [20]). On the other hand, the decay in the undissociated system will produce broad



**Scheme 1.** 2Cl-pyrimidine molecule with the atom labelling used in the text. The molecular mass is  $m = 114/116$  Da; throughout the article the notation ‘ $m/(m + 2)$ ’ will indicate the most abundant isotopic contribution of ions containing the  $^{35}\text{Cl}$  (75.8%) and  $^{37}\text{Cl}$  (24.2%) isotopes.

molecular features in the electron spectrum. From the experimental point of view, the features due to UFD can be identified in the spectra because they do not suffer energy dispersion with photon energy. A full quantum mechanical description of UFD in terms of wave packet dynamics based on the theory of resonant x-ray scattering [21] has been developed and showed that the dissociation and electronic relaxation should be treated as a one-step process. After the prototypical diatomic molecules, HBr and HCl, a series of studies investigated the process in more complex molecules, SiH<sub>4</sub> [22], CH<sub>3</sub>Cl [23] and other chlorinated methanes [24], H<sub>2</sub>O [25], O<sub>2</sub> [26], SF<sub>6</sub> [27] up to organic compounds [28]. These works showed that the competition between molecular dissociation and electron decay following inner shell excitation is quite common, even though the ideal situation, where the electron decay after a full dissociation of the two moieties is the dominant process, is a rare case.

In this work, we report the study of the electron decay and molecular fragmentation of 2Cl-pyrimidine in the Cl(2p), C(1s) and N(1s) near-edge regions by photoelectron spectroscopy, mass spectrometry and electron-ion coincidence experiments, in order to investigate possible correlations between core excitation, which involves core hole localization, and molecular fragmentation. To this end we exploited the photon energy tunability available at synchrotron radiation facilities to perform mass spectrometry across inner shell excitation/ionization regions, to measure the resonant Auger electron spectra at selected inner shell excitations and to perform photoelectron-ion coincidence measurements in both direct and resonant valence shell ionization. The latter experiments, which are characterized by a high selectivity in both the energy deposition and final state of the singly charged ion, enable to disentangle the role of the initially localized inner shell excitation and that of the final singly charged ion in specific fragmentation paths.

2Cl-pyrimidine (C<sub>4</sub>N<sub>2</sub>H<sub>3</sub>Cl, scheme 1) is a halogen substituted pyrimidine molecule, where the Cl atom is bound to the C2 site in between the two N atoms. Being the building block and model system for a class of radiosensitizers, the halosubstituted DNA bases have been investigated and their mechanisms of fragmentation discussed. In particular for the 2Cl-pyrimidine case, the core ionization [29] and excitation [30],

as well as the valence shell ionization [31] and fragmentation [32, 33] have been studied from both the theoretical and experimental point of view, providing the essential spectroscopic information for the present work devoted to the site-selective fragmentation.

## 2. Experimental and data analysis

The experiments were performed at the Gas Phase photoemission beamline [34] of the Elettra synchrotron radiation facility (Trieste, Italy) using the VG-TOF end-station already described in similar photoemission [29, 35], mass spectrometry [12, 30] and electron-ion coincidence experiments [13, 36].

At the Gas Phase beamline, the 100% linearly polarized radiation from the undulator (period 12.5 cm, length 4.5 m) is deflected to the variable angle spherical grating monochromator, which covers the energy region 13–1000 eV with five interchangeable gratings.

The experimental chamber is maintained at a background pressure of low  $10^{-8}$  mbar. The target molecules, which are in the form of a powder at standard ambient temperature and pressure, are kept in a test tube outside the vacuum chamber and admitted into the interaction region via a leak valve, in order to have a residual gas pressure of 2Cl-pyrimidine in the vacuum chamber of about  $2.5 \times 10^{-6}$  mbar. A 150 mm hemispherical electron energy (VG 220i) analyzer is mounted opposite to a Wiley–McLaren [37] time-of-flight (TOF) mass spectrometer, at the magic angle with respect to the polarization axis of the photon beam. A grounded needle mounted on a xyz-manipulator for precise alignment, enters the region between the repeller and extractor electrodes of the TOF and brings the effusive beam of 2Cl-pyrimidine into the interaction region, just few mm below the photon beam.

The ionization event takes place in a field free region: photoelectrons (PE) and resonant Auger electrons (RAE) ejected into the geometrical acceptance angle of the electron analyser located behind a mesh in the repeller electrode of the TOF are selected in kinetic energy by the hemispherical analyzer and detected by 6 independent channeltrons located along the dispersive plane of the analyzer. Extraction and TOF analysis of the ions produced by the ionization and fragmentation of the molecular species is triggered by a pulsed extraction field of  $700 \text{ V cm}^{-1}$  applied between the repeller/extraction electrodes of the TOF polarized with antisymmetric voltages (manufacturer Directed Energy Inc., model PVM4210). The electron and ion mass analyzers can be operated independently, for PE/RAE spectroscopy and mass spectroscopy (MS) measurements, respectively.

In the electron spectroscopy mode the hemispherical electron analyzer is operated with the TOF spectrometer switched off to prevent residual penetration fields from the drift tube of the TOF into the interaction region, that would degrade the electron energy resolution. A pass energy of 20 and 50 eV, corresponding to a kinetic energy resolution of about 0.5 and 1.2 eV, has been used for the PE and RAE measurements, respectively (see figure 1). The valence electron spectra were measured at 60 eV photon energy while the RAE spectra

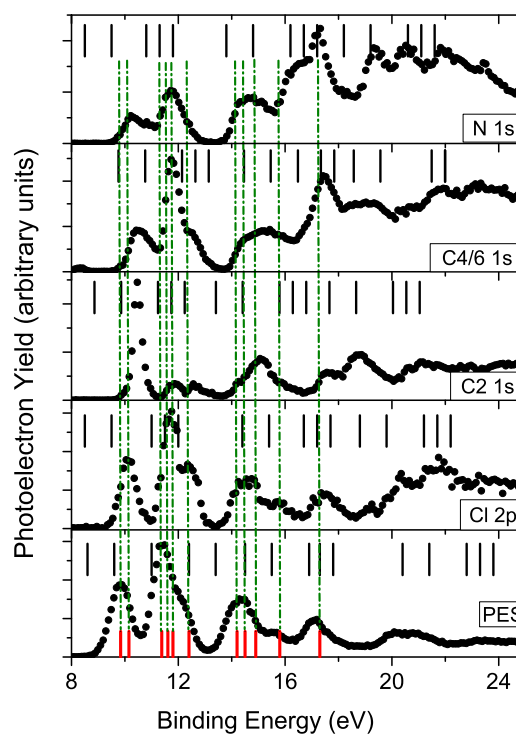


**Figure 1.** The resonant Auger spectra of 2Cl-pyrimidine recorded at the Cl( $2p_{3/2}^{-1} \rightarrow \sigma^*$ ), C4/6( $1s^{-1} \rightarrow \pi^*$ ), C2( $1s^{-1} \rightarrow \pi^*$ ) and N( $1s^{-1} \rightarrow \pi^*$ ) resonant excitations compared to the PES measured at 60 eV (bottom panel). All spectra have been reported on BE scale by subtracting the kinetic energy of the measured electron from the photon energy. The red bars in the bottom panel report the position of the ionic states [31], while the black bars in each spectrum indicate the BE where the electron-ion coincidence measurements have been performed.

where measured at the photon energies corresponding the Cl( $2p \rightarrow \sigma^*$ ), C4/6( $1s \rightarrow \pi^*$ ), C2( $1s \rightarrow \pi^*$ ) and N( $1s \rightarrow \pi^*$ ) transitions to the lowest unoccupied molecular orbitals, at photon energies 200.4, 285.53, 287.40, 398.7 eV, respectively. The photon energy and kinetic energy scales have been calibrated against the known spectroscopic information of 2Cl-pyrimidine [30].

In the mass spectrometry mode (see figures 2–4), the TOF spectrometer can be operated either in ‘total ion yield’ (TIY) mode for the measurement of the near edge x-ray fine structure (NEXAFS) spectra, or in MS mode, for the measurement of the mass-over-charge ( $m/z$ ) resolved fragmentation spectrum. In the TIY mode the TOF spectrometer is operated by a continuous dc voltage in the extraction region for the detection of the extracted ions by the TOF detector. The TIY reported versus the scanning photon energy and normalized to the photon intensity variation along the scan, provides the NEXAFS spectrum. For MS measurements, the extraction field has been operated in pulsed mode, triggered by a 1 kHz random pulse generator (Stanford Research DG535) to extract the ions and provide the time-zero for the measurement of the time of flight via a time-to-digital analyser (TDC model AM-GPX, ACAM Messelectronic). In the inner shell region, MS have been acquired at several photon energies scanning the Cl( $2p$ ), C( $1s$ ) and N( $1s$ ) near-edge regions. The acquisition time of each mass spectrum is of about 15 min/point and the photon

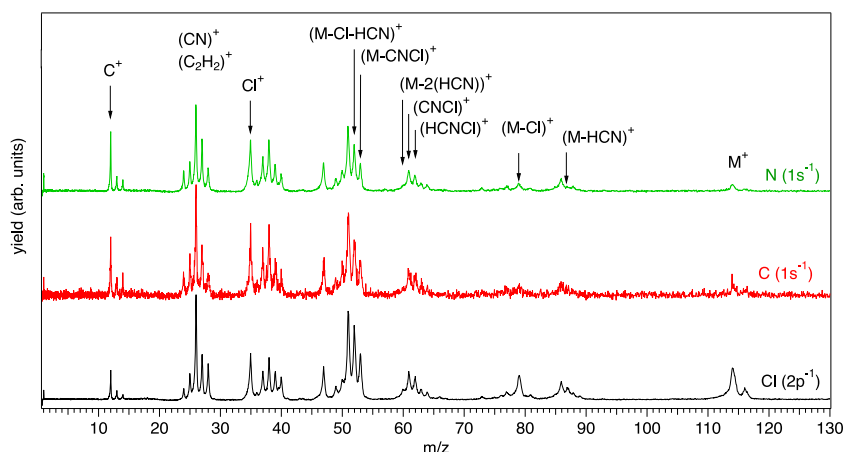


**Figure 2.** The mass spectra of 2Cl-pyrimidine measured at photon energies 207 eV (black), 292.6 eV (red) and 411.6 eV (green), i.e. above the Cl(2p), C4/6(1s) and N(1s) ionization thresholds. The three MS spectra have been displaced on the vertical axes to facilitate qualitative comparison. The main fragments discussed in the text are indicated.

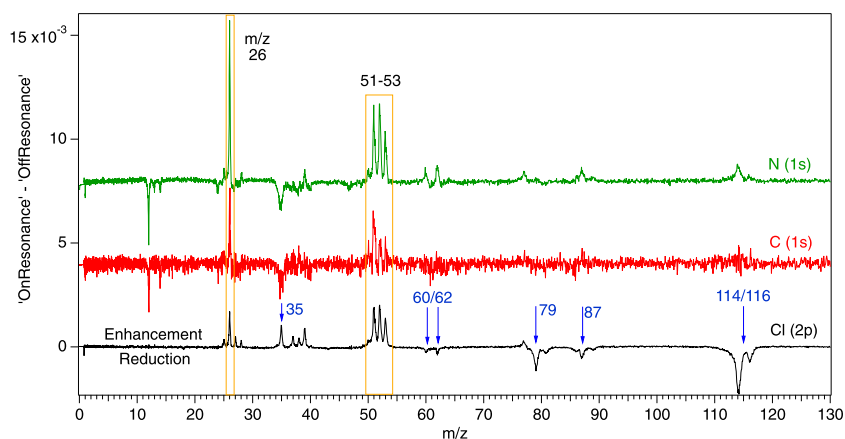


**Figure 3.** The ‘on resonance–off resonance’ spectra at the Cl(2p  $\rightarrow$   $\sigma^*$ ), C(1s  $\rightarrow$   $\pi^*$ ) and N(1s  $\rightarrow$   $\pi^*$ ) resonances. The ‘off resonance’ spectra are measured below the lowest resonance, i.e. at 196.2, 284.2 and 397.6 eV, respectively. The ‘on resonance’ spectra are integrated in the regions 199.4–203.0 and 284.6–288 eV for the Cl and C cases, respectively, and measured at 398.8 eV for the N case. In each case, areas of the resulting on- and off-resonance spectra are normalized to unity before the subtraction. The noisy difference spectrum in the C case is due to the low statistics of the ‘off resonance’ measurement performed at a photon energy where the beamline transmission is strongly reduced by C contaminations of the optical elements. The yellow boxes highlight the main regions which show similar behaviour for the three cases, while the blue arrows indicate the main differences between the Cl(2p) and the C, N(1s) cases.

energy steps is 0.4 eV. At each resonant photon energy, both resonant and direct ionization of valence states occur and the two contributions are indistinguishable. In order to highlight the relative changes in the fragmentation pattern due to core hole localization, in the data analysis: (i) each TOF mass spectrum has been background subtracted, using the representation of the background provided by the fitting of the mass spectrum where all peaks are removed; (ii) from the background subtracted spectrum the area of each peak has been calculated by adding up the yields in the  $m/z \pm 0.5$  region of interest; (iii) then these calculated areas have been normalized to the sum of the areas of all fragments in order to extract the branching ratio of each fragment at each photon energy. In order to provide an overview of the resonance behaviour, the difference between the ‘on resonance’ and ‘off resonance’ spectra normalized to equal total area are reported in figure 3. This procedure allows us identify at first sight the role that core hole localization can

play at the different molecular sites. Figure 3 refers to the  $\sigma^*$  and  $\pi^*$  transitions in the case of the Cl(2p), C(1s) and N(1s) respectively, while the branching ratios as function of photon energy reported in figure 4 allow the evolution of the branching ratio of each fragment versus photon energy to be followed.

The electron and ion analyzers can also be operated simultaneously for photoelectron–photoion coincidence (PEPICO) measurements, figures 5–7. The electronic chain schematically reported in figure 1 of reference [38] has been replicated for five channeltrons. The amplified and discriminated electron signals from the 5 channeltrons provide the ‘start’ for five independent channels of the TDC, as well as the trigger for the extraction of the ions from the interaction region, after being combined in an ‘OR’ logic unit. The signal of the extracted ions is fed as ‘stop’ into the five TDC channels. Random coincidences are estimated by randomly pulsing the ions extraction at 100 Hz, i.e. a frequency comparable to the

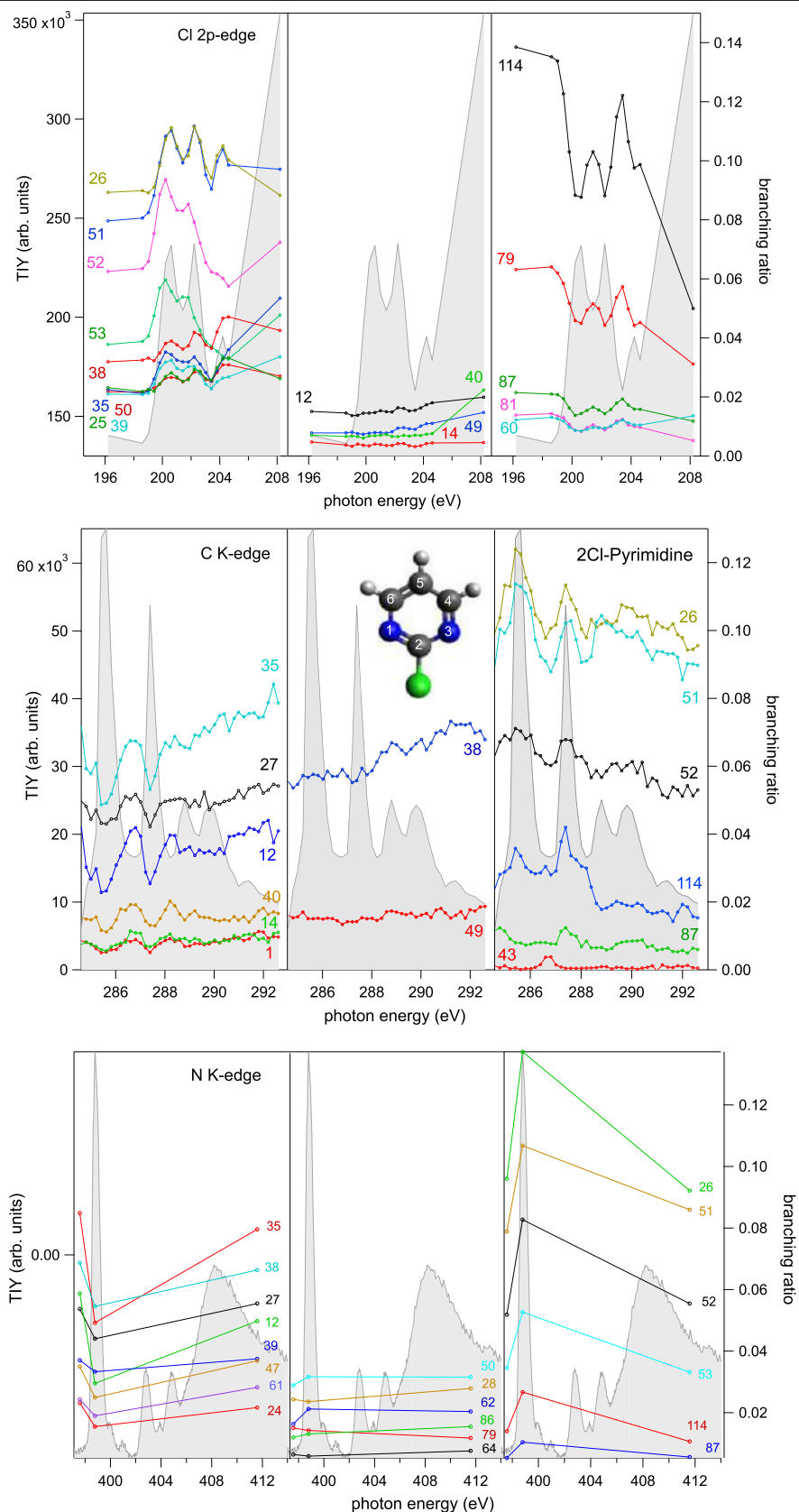


**Figure 4.** NEXAFS spectra (grey full area) and branching ratio of the most representative fragments at the Cl(2p) (top), C(1s) (middle) and N(1s) (bottom) excitation/ionization regions. The three panels of each figure arbitrarily regroup smaller (left panel) and larger (right panel) fragments, as well as fragments that do not show any significant resonant effect (central panel), see text.







**Table 1.** Experimental energies and B3LYP (6-311 ++ g(2df,2p)) calculations together with the assignment of the 2Cl-pyrimidine valence band and their respective Mulliken populations taken from reference [31]. Only Mulliken populations larger than 10% have been reported.

Molecular orbital	MO	Mulliken population (%)	Exp PES (eV)	B3LYP (eV)
6b <sub>2</sub>	$n_{N-}$	N1 29.0 N2 29.0	9.84	10.11
3b <sub>1</sub>	$\pi_3$	C2 14.0 C5 28.9 Cl 31.9	10.15	10.40
5b <sub>2</sub>	$n_{  }$	N1 11.4 C2 10.6 N3 11.4 Cl 58.7	11.38	11.30
8a <sub>1</sub>	$n_{N+}$	N1 24.0 C2 11.6 N3 24.0 C5 15.4 Cl 11.0	11.61	11.69
1a <sub>2</sub>	$\pi_2$	N1 33.8 N3 33.8 C4 15.9 C6 15.9	11.80	11.90
2b <sub>1</sub>	$n_{\perp}$	Cl 82.9	12.40	12.21
7a <sub>1</sub>	$\sigma_{C-Cl}$		14.2	14.40
4b <sub>2</sub>	$\sigma$		14.5	14.66
1b <sub>1</sub>	$\pi_1$		14.9	15.20
6a <sub>1</sub>	$\sigma$		15.8	15.74
3b <sub>2</sub>	$\sigma$		17.3	17.47

electronic decay of the core-excited states via their coupling to the outer (participator decay) and inner valence (spectator decay) states.

The mass spectra and fragments branching ratio measured versus the scanning photon energy in the near-edge regions are reported in section 3.2.

Finally, section 3.3 is devoted to the electron-ion coincidence experiments at the  $\sigma^*$  excitation of the Cl(2p) and at the  $\pi^*$  excitation of the C4/6(1s), C2(1s) and N(1s) core electrons.

### 3.1. The resonant Auger electron spectra

The resonant Auger electron spectra measured at the Cl( $2p_{3/2}^{-1} \rightarrow \sigma^*$ ), C4/6( $1s^{-1} \rightarrow \pi^*$ ), C2( $1s^{-1} \rightarrow \pi^*$ ) and N( $1s^{-1} \rightarrow \pi^*$ ) excited states are reported in figure 1, where they are compared with the PES measured at 60 eV photon energy. The low count rate that characterizes the resonance Auger spectra has hampered the investigation at the C5( $1s^{-1} \rightarrow \pi^*$ ) excitation, which has been observed to generate a small and partially unresolved feature in the NEXAFS spectrum [30].

The PES of 2Cl-pyrimidine has been previously studied by a combined experimental and theoretical approach, and in the present discussion (see table 1) we refer to that work [30]. Most of the orbitals of 2Cl-pyrimidine are analogous to those of pyrimidine, with its six member ring structure. The  $a_2$  and  $b_1$  symmetries characterize the out-of-plane,  $\pi$ -type orbitals while the  $a_1$  and  $b_2$  symmetries characterize the in-plane,

$\sigma$ -type orbitals. Among the six lowest molecular orbitals, the 6b<sub>2</sub> and 8a<sub>1</sub>  $\sigma$ -type orbitals are assigned as nitrogen lone pairs,  $n_{N-}$  and  $n_{N+}$ , respectively, while the 3b<sub>1</sub> and 1a<sub>2</sub> are assigned as  $\pi_3$  and  $\pi_2$ , distributed above and below the ring. The Cl atom adds two new orbitals to the outer valence manifold, related to the p orbitals of the halogen atom. The orientation of these orbitals can be parallel,  $n_{||}$ , or perpendicular,  $n_{\perp}$ , to the ring. In addition, the electronegative Cl substituent in position C2 perturbs the orbitals in the ring as compared to the pyrimidine case, by both inductive and resonant effects.

The non-radiative RAE decay of the excited inner shell populates the same outer and inner valence cationic states. However, due to the natural width of the core-excited states and the possible non parallel potential energy surfaces of the core excited and final ionic states, the features in the RAE spectra can be broader or shifted with respect to the ones appearing in the PES spectrum, as for example observed in the N<sub>2</sub>O case [7].

An intuitive guide to the interpretation of the RAE spectra of figure 1 is provided by the calculated Mulliken populations [31] reported in table 1. The low energy region, that extends from the ionization threshold up to BE  $\approx$  13 eV, contains clearly identifiable 1-hole states and is dominated by the participator decay. Consistently with the Mulliken population distributions (table 1), the Cl RAE spectrum displays noticeable contribution in the region of the  $\pi_3$ ,  $n_{||}$ ,  $n_{N+}$  and  $n_{\perp}$  orbitals, while the two features in the N( $1s^{-1} \rightarrow \pi^*$ ) RAE spectrum well align with the  $n_{N-}$  and  $n_{N+}$  orbitals (nitrogen lone pairs), and with the  $\pi_2$  orbital, which again sees the largest Mulliken population on the two nitrogen atoms. As for the carbon atoms, the C2 RAE in this region displays a dominant feature in correspondence of the  $\pi_3$  orbital, while the main peak of the C4/6 spectrum is in correspondence of the  $\pi_2$  orbital, in very good qualitative agreement with the distribution of the Mulliken population.

In the region 13 eV < BE < 20 eV, the PES spectrum shows a band at about 14.4 eV with the mixed  $\pi$  and  $\sigma$  contributions of the 7a<sub>1</sub>, 4b<sub>2</sub> and 1b<sub>1</sub> orbitals and then other bands at about 15.8 and 17.3 eV, all of  $\sigma$  symmetry. In terms of participator states these features can be associated with the 6a<sub>1</sub> and 3b<sub>2</sub> orbitals. It is interesting to observe that in both the Cl and C2 RAE spectra, a well-defined feature is clearly visible at the 7a<sub>1</sub> state (14.2 eV), which is assigned to a  $\sigma_{(C-Cl)}$  molecular orbital. At increasing binding energies, the breakdown of the single electron picture of the ionization increases the complexity of the photoelectron spectrum. This region is expected to be dominated by 2-hole-1-particle final states, with 2-hole configurations similar to those of doubly charged states, but with a ‘spectator’ electron screening the double hole. The bands at 16 and 17.3 eV are clearly enhanced in all the C and N RAE spectra, indicating that their  $\sigma$  nature couples well with the intermediate states. In a previous work [35] this region has been qualitatively interpreted by shifting the KVV Auger spectrum in energy due to the screening effect of the spectator electron. Being the main goal of the present work to investigate energy selected fragmentation of 2Cl-pyrimidine, we do not enter in the assignment and discussion of the RAE spectra in this high BE region.

### 3.2. The mass spectra and the partial ion yield in the Cl(2p), C(1s) and N(1s) near-edge regions

The background-subtracted mass spectra measured just above the Cl(2p), C4/6(1s) and N(1s) ionization thresholds are reported in figure 2, providing a broad overview of the fragmentation mass spectra in the different core ionization regions. The details of the effects of resonant core excitation and ionization can be seen in figures 3 and 4, and will be discussed later in this section.

All peaks in the MS appear to be broadened beyond the experimental resolution of the TOF spectrometer, due to the high kinetic energy released in fragmentation of double/multiply charged ions. Indeed, the observed mass spectra extend from the atomic fragments ( $H^+$ ,  $C^+$ ,  $N^+$ ,  $Cl^+$ ) up to the parent ion ( $m/z$  114/116), displaying a richer variety of fragments than previously reported in valence shell studies [32, 33]. Some of these fragments can be easily associated to the complementary moieties of a direct two-body fragmentation of the parent dication. This is the case, for example, of the ions at: (i)  $m/z$  87/89 ( $M-HCN^+$  and 27 ( $HCN^+$ ); (ii)  $m/z$  53 ( $M-CNCl^+$  and 61/63 ( $CNCl^+$ ); (iii)  $m/z$  52 ( $M-HCNCl^+$  and 62/64 ( $HCNCl^+$ ), and (iv)  $m/z$  79 ( $M-Cl^+$  and 35/37 ( $Cl^+$ ).

Even though the same fragments populate the MS in the different photon energy regions, the relative contribution of the various fragments changes as function of the photon energy. For example, the relative contribution to the mass spectrum of the parent ion,  $M^+$ , and larger fragments around the ( $M-HCN^+$  and ( $M-Cl^+$ ) regions is significantly reduced as the photon energy increases from the Cl(2p) to the C(1s) and N(1s) regions, while the relative contribution of smaller fragments ( $m/z < 50$  and atomic species in particular) becomes more relevant.

Further than the variation as function of the increasing photon energy, quantitative information on the effect of the resonance excitation can be deduced from the ‘on resonance –off resonance’ spectra in figure 3 and the branching ratio variation of the main fragments across the different core excitation resonances in figure 4.

Figure 3 shows how the resonant excitation in the three cases leads to many differences (see  $m/z$  35, 60/62, 79, 87/89 and 114/116) and some similarities (see  $m/z$  26 and the group  $m/z$  51–53) in the fragmentation paths. At the Cl(2p  $\rightarrow \sigma^*$ ) resonance, the branching ratios of the larger fragments ( $m/z > 70$ ) show a significant reduction, while the opposite is observed in the N(1s  $\rightarrow \pi^*$ ) case, and no resonant effect in the C(1s  $\rightarrow \pi^*$ ) case (see also figure 4). The decrease of the branching ratio of the larger fragments is counterbalanced by the increase of  $m/z$  35, 51–53 and 26 fragments at Cl(2p  $\rightarrow \sigma^*$ ) resonance. On the other hand, the branching ratio of the  $m/z$  12, 27 and 35 fragments display an enhancement at the C(1s  $\rightarrow \pi^*$ ) resonances.

In the C NEXAFS spectrum of 2Cl-pyrimidine (figure 4), there is a clear chemical shift among the three non-equivalent C atoms, with increasing excitation energy from the weak and partially unresolved C5, to C4/6 and finally C2, the highest in energy due to the highly electronegative neighbour Cl and N

atoms. However, in the fragments branching ratios there are no significant differences among the three C atoms, apart for the  $m/z$  87/89 ( $M-HCN^+$ ), with a selective enhancement at the C2 core hole localization (fragment 89 not shown).

In general, the core hole localization on the three non-equivalent C atoms shows the least effects compared to the localization at the Cl and N atoms, but it is qualitatively closer to the N than to the Cl case. This is not surprising, considering that both the C and N atoms build up the ring structure, with the Cl atom bound off-ring by the C2 atom.

In the N core-hole localization the observed picture of an enhanced branching ratio of large fragments ( $m/z > 55$ ) complemented by a reduction of atomic ionic species ( $C^+$ ,  $N^+$ ,  $Cl^+$ ) supports the scheme of a dominant single electron, resonant Auger, decay to the valence region.

### 3.3. The resonant Auger electron-ion coincidence experiments

The sum of all PEPICO mass spectra measured at a photon energy of 60 eV (figure 5) shows all the fragmentation channels opened up to BE 23 eV. Compared to the MS measured in the inner shell regions, the PEPICO spectra are better resolved in  $m/z$ , because their formation in single ionization events, which involve less kinetic energy released in the fragmentation compared to double/multiple ionizations active in inner shell ionization, limits the time spread in the time of flight of the ions.

A quick comparison between figure 5 (PEPICO valence shell ionization) and figure 2 (MS inner shell ionization) clearly shows how several fragmentation channels, like all the atomic ionic species ( $C^+$ ,  $N^+$ ,  $Cl^+$ ),  $m/z$  24–25 (possibly attributable to  $C_2^+$  and  $C_2H^+$ ),  $m/z$  47/49 ( $CCl^+$ ) and most of the fragments in the group 36–40 (likely related to the  $C_3H_3^+/HC_2N^+$  fragment at  $m/z$  39) are not observed in the direct valence shell ionization, at least up to BE 23 eV, or are below the sensitivity of the present PEPICO measurements. This indicates that these channels are not yet energetically open or/and not significantly populated by single ionization processes.

Among all fragments from the PEPICO measurements the branching ratio for parent ion and seven of the main fragments produced by direct valence ionization (60 eV photon energy) and by Cl(2p  $\rightarrow \sigma^*$ ), C4/6(1s  $\rightarrow \pi^*$ ), C2(1s  $\rightarrow \pi^*$ ) and N(1s  $\rightarrow \pi^*$ ) resonant Auger decay are reported in figure 6. The first onset on the breakdown curve of each respective case is reported in table 2, together with previously measured and calculated values of appearance energy [32]. When different values could be inferred depending on the resonant/non-resonant case considered, the values extracted from the resonant cases have been indicated by a ‘†’ symbol in table 2. At first sight, there are no major differences in the fragmentation following direct valence ionization or ionization via the intermediate inner shell excitations.

In all cases, the parent ion,  $M^+$ , is observed only over the two lower bands of the PES spectrum (BE 8–13 eV), which include the six lower MO, from the  $n_{N-}$  to the  $n_{\perp}$ . However, while in the valence ionization the  $M^+$  ion remains the only species for the entire range 8–13 eV, in all other cases where

**Table 2.** First onset of formation for the main 2Cl-pyrimidine fragments extracted from the PEPICO breakdown curves (figure 6) compared to the appearance energy literature data. The ‘†’ symbol indicates values from the resonant ionization case, when different from the non-resonant case.

	Appearance energy (eV)			
	<i>m/z</i>	This work	Exp. [33]	Th. [33]
M <sup>+</sup>	114/116	9.1(0.50)	9.54(0.05)	9.61
C <sub>4</sub> H <sub>3</sub> N <sub>2</sub> Cl <sup>+</sup>				
C <sub>3</sub> H <sub>2</sub> NCl <sup>+</sup>	87/ 89	13.40(0.55)	12.40(0.05)	12.35
(M–HCN) <sup>+</sup>		12.50(0.25) <sup>†</sup>		
C <sub>4</sub> H <sub>3</sub> N <sub>2</sub> <sup>+</sup>	79	12.40(0.60)	11.84(0.05)	11.92
(M–Cl) <sup>+</sup>		11.43(0.25) <sup>†</sup>		
C <sub>2</sub> HCl <sup>+</sup>	60/62	13.61(0.33)		
(M–2HCN) <sup>+</sup>				
C <sub>3</sub> H <sub>3</sub> N <sup>+</sup>	53	13.26(0.40)		
(M–Cl–CN) <sup>+</sup>				
C <sub>3</sub> H <sub>2</sub> N <sup>+</sup>	52	13.61(0.33)	13.92(0.1)	13.68
(M–Cl–HCN) <sup>+</sup>				
HCN <sup>+</sup>	27	14.90(0.5)		
CN <sup>+</sup>	26	14.85(0.3)		

the ionization proceeds via the resonant core excitation/decay, the M<sup>+</sup> branching ratio decreases already on the shoulder of the second band, in correspondence to the  $n_{\perp}$  orbital at 12.4 eV. In these cases, the lost intensity from M<sup>+</sup> at 12.4 eV is entirely drawn by the (M–Cl)<sup>+</sup> channel, which displays in this region its maximum intensity. Consistently, the Cl-loss mechanism appears to be significantly ‘delayed in energy’ in the direct valence ionization (see table 2). For this reason, the first onset of *m/z* 79 assigned as (M–Cl)<sup>+</sup> is registered at 11.2 eV in the resonant ionization cases, while at 12 eV in the direct ionization.

Both the (M–Cl)<sup>+</sup> and (M–HCN)<sup>+</sup> fragments are exclusively related to the BE region 12–16 eV. Even though shifted by about 1 eV and of lower intensity, the (M–HCN)<sup>+</sup> fragment, similarly to (M–Cl)<sup>+</sup>, appears to open at lower BE for the resonant with respect to the non-resonant valence ionization. Despite the small branching ratio, a similar mismatch in the take-off of the breakdown curves of the (M–Cl–HCN)<sup>+</sup>, (M–2HCN)<sup>+</sup> and (M–Cl–HCN)<sup>+</sup> fragments may also be proposed, with a ‘delayed onset’ in the Cl(2p) resonant ionization case.

For the (M–2HCN)<sup>+</sup>, (M–Cl–CN)<sup>+</sup> and (M–Cl–HCN)<sup>+</sup> fragments, the take-off of the break down curves is at about 13 eV, with a dominant contribution at 15–16 eV for (M–2HCN)<sup>+</sup>, or at about 18–20 eV for (M–Cl–HCN)<sup>+</sup> and (M–Cl–CN)<sup>+</sup>. The HCN<sup>+</sup> is a minor fragment in all cases, lacking any selectivity with respect to the molecular orbital.

#### 4. Discussion

The molecular fragmentations measured at the different core electron excitation/ionization regions (figure 2) show a general trend where increasing photon energy favours formation of smaller species and reduction of large ones. As already observed in other molecules [12, 13, 41–43, and references therein], this is an indication that more

substantial fragmentation takes place at higher photon energies, and can be easily explained by the dominant role played by the opening of new core ionization thresholds leading to a preferential decay via Auger and multiple Auger emission to doubly/multiply charged ions. The instability of double/multiple ions results in fast molecular fragmentations, as no evidence of a stable dication (*m/z* 57/58) appears in any of the spectra. Multiple ionizations are also most likely responsible for the several fragments not observed (at least within the present statistical accuracy) in the mass spectrum collected adding the PEPICO measurements for direct valence shell ionization up BE 23 eV shown in figure 5.

Figures 3 and 4 show that the primary hole localization on the Cl atom leads to a larger degree of molecular fragmentation (strong reduction in parent ion branching ratio) and an increased amount of smaller fragments. Previous observations via electron–ion coincidence measurements in different molecules reported that the participator resonant Auger decay towards the lowest singly charged ion states results in enhanced stability of the parent ion and large fragments [12, 14]. In order to explain the experimental observation in the Cl case, a few possibilities have been considered. The first one is that the Cl(2p →  $\sigma^*$ ) RAE decay occurs preferentially via spectator processes populating the inner valence region of the singly charged ion, subject to a strong fragmentation compared to the outer valence, see section 3.3. This hypothesis can be ruled out by the RAE spectrum in figure 1, which displays a noticeable contribution of participator processes leading to the population of the HOMO, HOMO-1 and HOMO-2 states. A second possible scenario may involve the decay of the inner shell excited state via the direct emission of two electrons towards a dication, which then fragments leading to the formation of two singly charged ions. The double Auger emission has been well studied in atoms, where it has been shown that the probability for such process increases as the energy distance between the inner shell excitation energy and



the double ionization potential decreases [44]. Thus it should not be unlikely that the process is observed after Cl(2p) excitation more than for C and N(1s). To support this possibility, we searched for traces of Cl<sup>+</sup> in the electron–ion coincidence spectra measured at the three inner excited states. Figure 7(b), that is the equivalent of figure 6 but for the case of the Cl(2p →  $\sigma^*$ ), shows how the Cl<sup>+</sup> fragment is clearly observed at BE > 19 eV. However, considering that the double ionization potential of 2Cl-pyrimidine as derived by Auger spectroscopy experiments [35] is at about 25 eV, also this second scenario has to be ruled out. A third possibility is that the core hole localization on the Cl atom of 2Cl-pyrimidine triggers an ultrafast molecular dissociation that may result in the emission of atomic autoionizing electrons when the non-radiative decay occurs at large distances, where the C<sub>4</sub>H<sub>3</sub>N<sub>2</sub> and Cl\* fragments are already apart.

The ultrafast dissociation mechanism, firstly observed in HBr [20] and then in other molecular systems [45], relies on the fact that in light molecules the reduced masses allow the fragments to move apart and reach a complete breakage of a chemical bond during the core-hole lifetime. This might appear unlikely in a heavier molecule like 2Cl-pyrimidine. However, as clearly shown in figure 7, we observe the formation of Cl<sup>+</sup> ions only in the PEPICO spectra measured at the Cl(2p<sub>3/2</sub> →  $\sigma^*$ ) excitation energy (figure 7(a)) and the breakdown curve of the Cl<sup>+</sup> ion (figure 7(b)) takes off in the region where the resonant Auger spectrum (figure 7(c)) measured at the Cl(2p<sub>3/2</sub> →  $\sigma^*$ ) excitation displays features that can be attributed to the decay to the Cl<sup>+</sup> 3s<sup>2</sup>3p<sup>4</sup> (<sup>3</sup>P, <sup>1</sup>D and <sup>1</sup>S) states.

These observations would support the scenario of a C2–Cl\* bond breaking and atomic autoionization of the core excited Cl atom, i.e. Cl\* → Cl<sup>+</sup> + e<sub>RAE</sub>. The observation of increased branching ratio of Cl<sup>+</sup> consistently supports the reduction in its counterpart (M–Cl)<sup>+</sup> at *m/z* 79, observed in figure 3.

As a rule of thumb, to prove this scenario one can use the classical motion model proposed in reference [20]. Using a Cl 2p lifetime  $\tau$  of about 10 fs [47], a C2–Cl dissociation limit in the ground state of 4.31 eV [48], the Cl ionization potential [49] and our measured Auger lines we get that in the course of the Cl 2p lifetime the C2–Cl bond stretches to about 1.4 $R_e$  ( $R_e = 1.73$  Å in the ground state, [48]). Considering the simplicity of the model this value can be considered consistent with the 2 $R_e$  value used as atomic limit in the literature for these processes. In their recent study of the ultrafast dissociation of chlorinate methanes, Kokkonen *et al* [24] observed Cl atomic lines in the Auger spectrum and Cl<sup>+</sup> ions even in the case where the classical motion along the potential energy surface indicates definitely smaller bond elongation than in the present case. Furthermore, Travnikova *et al* [50] showed that ultrafast dissociation in polyatomic molecules may also occur via a complex multimode dynamics and proposed it as a ‘*general process in complex core-excited systems with many degree of freedom*’. Even though the complexity of the multidimensional potential energy surface in the present case has hampered a theoretical proof the study of the fragmentation of 2Cl-pyrimidine in the VUV region [32] has shown that a few eV of internal energy are enough to trigger a complex rearrangement of the molecular structure, which lead to the opening of the ring and

to several fragmentation channels with Cl loss. Thus, *a priori* we cannot exclude that one of these rearrangements in the core excited state might drive a Cl\* loss with an atomic non radiative decay.

A common feature among the three cases in figure 3 is the strong ‘on resonance’ enhancement of the fragments at *m/z* 26, attributable to CN<sup>+</sup> and/or C<sub>2</sub>H<sub>2</sub><sup>+</sup>, and of the fragments in the region *m/z* 51–53, attributed to the H<sub>*n*</sub>NC<sub>3</sub><sup>+</sup>, with *n* = 1–3. These fragments are the main species also in the valence shell fragmentation [32]. The dominance of the *m/z* 26 could be explained by the high stability of the CN<sup>+</sup> and/or C<sub>2</sub>H<sub>2</sub><sup>+</sup> fragments as well as by the fact that many different fragmentation paths, both sequential or concerted, can be envisioned as leading to such final fragment. Similarly, in the valence shell fragmentation *m/z* 52 can be produced by several paths as shown in scheme 1 of reference [32], i.e. by the concerted losses of (H + ClCN) or (HCN + Cl\*), or by the loss of the HCICN group, or by the sequential loss of HCN followed by the Cl\* loss. All of these paths, even though leading to the same experimental observable, i.e. formation of the *m/z* 52 fragment, are characterized by different energetics as the result of different transition states and molecular rearrangements from the ground electronic structure of the ion, as well as different geometrical structures of both the charged and neutral fragments involved in the fragmentation. In the case of fragmentation following inner shell excitation the nuclear motion in the core-excited state can lead to the population of the potential energy surface of the singly charged ion states in different regions with respect to the direct valence photoionization. This is supported by PEPICO experiments showing the ‘delayed energy onset’ in the valence ionization breakdown curves of the (M–Cl)<sup>+</sup>, (M–HNC)<sup>+</sup> fragments with respect to all the resonant cases, as well as of the delayed onset in the Cl(2p) resonant ionization breakdown curves of the (M–CN)<sup>+</sup>, (M–2HNC)<sup>+</sup> and (M–Cl–CN)<sup>+</sup> fragments with respect to all other cases, see (figure 6). This may allow different pathways for the formation of fragment *m/z* 52 and its neighbouring fragments in the range 51–53, that differ by the loss/catch of an additional H atom, and therefore, the enhancement of these fragment in all cases of figure 3.

Despite the fact that, following core hole excitation and decay, all fragment yields are enhanced and approximately follow the shape of the NEXAFS spectrum measured by TIY, at the different resonant excitation photon energies (i.e. at the different molecular sites for core hole localization) the fragments branching ratios show significant sensitivity to the specific core hole localization, with variations of branching ratios on resonance of 20% or more (see figures 3 and 4). Thus one can certainly state that, as far as the intensity of the different channels is concerned, molecular fragmentation is significantly site- and state-selective. However the results of the PEPICO experiments, summarised in figure 6, show that the breakdown curves of the main fragments produced by the direct and resonant ionization of the valence shell display a very similar behaviour versus the BE of the final ion, regardless of the ionization occurring via the direct or resonant path. As already observed in the 2Br-pyrimidine case [13], this indicates that the selection of the fragmentation channel

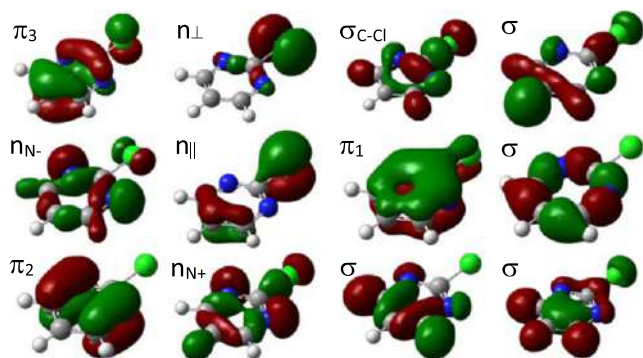


**Figure 8.** Representation of the HF molecular orbitals of 2Cl-pyrimidine [31].

is ruled mainly by the final ion state, regardless the direct or resonant ionization path. This points at a fast electron decay delocalizing the core vacancy from a specific atomic site to valence molecular orbitals. Despite this dominant behaviour, some hints of the role of the inner shell excitation can be observed in figure 6. The observation that (i) the  $M^+$  branching ratio decreases already on the shoulder of the second PES band in the case of resonant ionization and (ii) the first onset of some breakdown curves, for example of the Cl loss and HCN loss channels, are shifted in energy between the resonant and direct ionization stresses the role of the nuclear motion in the core-excited states. If the resonant Auger electron is emitted at a time scale comparable to the typical time of nuclear motion in the excited state, then part of the electronic excitation is converted in vibrational kinetic energy [18], affecting the vibrational distribution of the final cation state which can favour/hamper a specific molecular dissociation.

A qualitative interpretation for the parent ion, HCN and Cl loss channels can be given by considering the Hartree–Fock (HF) molecular orbitals of 2Cl-pyrimidine shown in figure 8. The first two orbitals are characterized by large Mulliken populations either on the N atoms ( $n_{N-}$  orbital) or on the C5, Cl and C2 atoms ( $\pi_3$  orbital) and are antibonding as far as the C2–Cl bond is concerned. Thus the ionization of these orbitals may be expected to reinforce the C2–Cl bond.

On the other hand, the  $n_{||}$  lone pair of the halogen atom (BE  $\sim 12$  eV) is a bonding orbital, and its ionization maybe expected to weaken the C2–Cl bond, leading to the Cl loss. These considerations are consistent with the observation of the parent ion up to about 13 eV and then the opening of the Cl loss channel (figure 6) in this region.

Finally, the HCN loss becomes relevant in the BE region of the  $\pi_1$  orbital, around 14 eV. Being the  $\pi_1$  a delocalized ring orbital, its ionization may be expected to favour ring breaking, and HCN loss. It is also interesting to observe that the channels for the Cl–CN and Cl–HCN loss open in the proximity of the BE of  $\sigma_{C-Cl}$  and  $\pi_1$  orbitals, which involve the C2–Cl bond and a delocalized charge distribution over the ring. The inner valence states present more delocalized orbitals, and attempts to identify qualitative correspondences between charge distribution of the molecular orbitals and related fragmentation becomes too uncertain. Furthermore, this qualitative correspondence should be taken with care, considering that the

nuclear motion occurring in the core-excited state during the Auger decay can lead to a charge distribution of the final ion state different from the one represented by the HF molecular orbitals.

## 5. Conclusions

The combination of tunable synchrotron radiation, direct and resonant photoemission, mass spectrometry and electron–ion coincidence spectroscopy has allowed to achieve a comprehensive view of the 2Cl-pyrimidine fragmentation in the region of the core shell excitations. The tunability of synchrotron radiation has been instrumental to excite selectively the core shell of the different atoms (C, N and Cl) and therefore to localize the initial hole in a specific site either in the ring or in the external Cl atom. The mass spectra in the near-edge region together with the electron–ion coincidence measurements at specific inner shell excitations revealed the different facets of the fragmentation following inner shell excitation in 2Cl-pyrimidine.

The mass spectra measured in the Cl(2p), C(1s) and N(1s) near-edge regions indicate how the fragmentation paths strongly depend on the site- and state-excitation, so that the combination of the state selectivity and local chemistry can enhance/deplete the production of certain fragments. The electron–ion coincidence measurements indicate the leading role of the final cation state in the determination of particular fragmentation channels. However, they also suggest that, due to the lifetime of the core-hole, the nuclear motion in the core excited states may affect the measured first onset of certain fragments in comparison to the appearance energy measured by direct photoionisation and that an ultrafast molecular dissociation in the case of the Cl(2p  $\rightarrow \sigma^*$ ) excitation may be responsible for the release of an inner shell excited Cl atom, followed by atomic autoionization. More specific experiments and calculations should be performed to fully confirm this observation.

Finally, considering that halopyrimidines are the basic constituents of an important class of radiosensitizers, in the radiation damage context the findings of the present work can contribute to understand the nanoscopic effects of radiation damage in terms of the damaging/destruction of certain molecules or the selective production of reactive radicals (Cl and/or H) and ions (Cl<sup>+</sup>).

## Acknowledgments

We would like to thank the authors of reference [31] for providing HF molecular orbitals of 2Cl-pyrimidine as displayed in figure 8. Work partially supported by the Italy-Sweden MAECI project ‘Novel molecular tools for the exploration of the nanoworld’; Progetto Grande Rilevanza Italy-Serbia ‘A nanoview of radiation-biomatter interaction’; COST Action CA18212-Molecular Dynamics in the GAS phase (MD-GAS); PRIN 20173B72NB Predicting and controlling the fate of biomolecules driven by extreme-ultraviolet radiation. The authors thank G Mattioli for providing the potential energy surface for the 2Cl-pyrimidine ground state.

## ORCID iDs

Paola Bolognesi  <https://orcid.org/0000-0002-6543-6628>  
 Patrick O’Keeffe  <https://orcid.org/0000-0002-8676-4436>  
 Bratislav P Marinkovic  <https://orcid.org/0000-0002-6904-6360>  
 Lorenzo Avaldi  <https://orcid.org/0000-0002-2990-7330>





## References

- [1] Siegbahn K 1982 *Science* **217** 111
- [2] Eberhardt W, Sham T K, Carr R, Krummacher S, Strongin M, Weng S L and Wesner D 1983 *Phys. Rev. Lett.* **50** 1038
- [3] Rühl E, Heinzl C, Baumgärtel H and Hitchcock A 1993 *Chem. Phys.* **169** 243
- [4] Nagaoka S-I et al 2011 *J. Phys. Chem. A* **115** 8822
- [5] Okada K, Tanimoto S, Morita T, Saito K, Ibuki T and Gejo T 2003 *J. Phys. Chem. A* **107** 8444
- [6] Tanaka K, Kizaki H, Sumii R, Matsumoto Y and Wada S 2006 *Radiat. Phys. Chem.* **75** 2076
- [7] Céolin D et al 2008 *J. Chem. Phys.* **128** 024306
- [8] Bernini R B, Da Silva L B G, Rodrigues F N, Coutinho L H, Rocha A B and de Souza G G B 2012 *J. Chem. Phys.* **136** 144307
- [9] Lin T-C, Liu Y-Y, Li M-H, Liu C-Y, Tseng S-Y, Wang Y-T, Chu H-H and Luo C-W 2014 *Chem.: Asian J.* **9** 1601
- [10] Tseng Y-S et al 2015 *Chem. Phys. Lett.* **636** 146
- [11] Salén P et al 2014 *Phys. Chem. Chem. Phys.* **16** 15231
- [12] Bolognesi P et al 2019 *Front. Chem.* **7** 151
- [13] Bolognesi P, Castrovilli M C, O’Keeffe P, Casavola A R, Catone D, Turchini S and Avaldi L 2012 *Nucl. Instrum. Methods Phys. Res. B* **279** 118
- [14] Bolognesi P, Kettunen J A, Cartoni A, Richter R, Tosic S, Maclot S, Rousseau P, Delaunay R and Avaldi L 2015 *Phys. Chem. Chem. Phys.* **17** 24063
- [15] Tanaka K, Sako E O, Ikenaga E, Isari K, Sardar S A, Wada S-I, Sekitani T, Mase K and Ueno N 2001 *J. Electron Spectrosc. Relat. Phenom.* **119** 255
- [16] Larkins F P 1990 *J. Electron Spectrosc. Relat. Phenom.* **51** 115
- [17] Habenicht W, Baiter H, Mueller-Dethlefs K and Schlag E W 1991 *J. Phys. Chem.* **95** 6774
- [18] Ueda K, Simon M, Miron C, Leclercq N, Guillemin R, Morin P and Tanaka S 1999 *Phys. Rev. Lett.* **83** 3800
- [19] Liu X et al 2005 *Phys. Rev. A* **72** 042704
- [20] Morin P and Nenner I 1986 *Phys. Rev. Lett.* **56** 1913
- [21] Salek P, Gel’mukhanov F and Agren H 1999 *Phys. Rev. A* **59** 1147
- [22] de Souza G G B, Morin P and Nenner I 1986 *Phys. Rev. A* **34** 4770
- [23] Thissen R, Simon M and Hubin-Franskin M J 1994 *J. Chem. Phys.* **101** 7548
- [24] Kokkonen E K, Patanen M, Cao W, Hrast M, Bučar K, Žitnik M and Huttula M 2018 *J. Chem. Phys.* **148** 174301
- [25] Jänkälä M N, Hempelmann A, Heiser F, Gessner O, Rüdell A and Becker U 1999 *Phys. Rev. A* **59** 300
- [26] Björneholm O et al 2000 *Phys. Rev. Lett.* **84** 2826
- [27] Sorensen M et al 2003 *Phys. Rev. Lett.* **91** 213003
- [28] Altarelli M et al 2004 *Elettra Highlights 2003–04* [www.elettra.trieste.it/images/Documents/SCIENCE/elettra\\_highlights\\_2003-2004.pdf](http://www.elettra.trieste.it/images/Documents/SCIENCE/elettra_highlights_2003-2004.pdf)
- [29] Bolognesi P et al 2009 *J. Phys. Chem. A* **113** 13593
- [30] Bolognesi P et al 2010 *J. Chem. Phys.* **133** 034302
- [31] O’Keeffe P, Bolognesi P, Casavola A, Catone D, Zema N, Turchini S and Avaldi L 2009 *Mol. Phys.* **107** 2025
- [32] Castrovilli M C, Bolognesi P, Cartoni A, Catone D, O’Keeffe P, Casavola A R, Turchini S, Zema N and Avaldi L 2014 *J. Am. Soc. Mass Spectrom.* **25** 351
- [33] Castrovilli M C, Bolognesi P, Casavola A R, Cartoni A, Catone D, O’Keeffe P and Avaldi L 2014 *Eur. Phys. J. D* **68** 253
- [34] Blyth R R et al 1999 *J. Electron Spectrosc. Relat. Phenom.* **101–103** 959
- [35] Bolognesi P, O’Keeffe P, Ovcharenko Y, Avaldi L and Carravetta V 2012 *J. Chem. Phys.* **136** 154308
- [36] Bolognesi P et al 2010 *J. Phys.: Conf. Ser.* **212** 012002
- [37] Wiley W C and McLaren I H 1955 *Rev. Sci. Instrum.* **26** 1150
- [38] Plekan O, Coreno M, Feyer V, Moise A, Richter R, Simone M D, Sankari R and Prince K C 2008 *Phys. Scr.* **78** 058105
- [39] Kukk E, Sankari R, Huttula M, Sankari A, Aksela H and Aksela S 2007 *J. Electron Spectrosc. Relat. Phenom.* **155** 141–7
- [40] Kukk E et al 2015 *Phys. Rev. A* **91** 043417
- [41] Yi-Shiue L, Kun-Ta L, Yuan T L, Chien-Ming T, Chi-Kung N and Chen-Lin L J 2014 *Phys. Chem. A* **118** 1601–9
- [42] Chiang Y-J, Lin Y-S, Lin H-R and Liu C-L 2018 *Chem. Phys. Lett.* **706** 215–22
- [43] Lin Y-S et al 2015 *Chem. Phys. Lett.* **636** 146–53
- [44] Heimann P A et al 1987 *J. Phys. B: At. Mol. Phys.* **20** 5005
- [45] Morin P and Miron C 2012 *J. Electron Spectrosc. Relat. Phenom.* **185** 259
- [46] Kivimäki A, Kukk E, Karvonen J, Mursu J, Nömmiste E, Aksela H and Aksela S 1998 *Phys. Rev. A* **57** 2724
- [47] Menzel A, Langer B, Viefhaus J, Whitfield S B and Becker U 1996 *Chem. Phys. Lett.* **258** 265
- [48] Mattioli G 2020 private communication
- [49] Wills A A, Cubric D, Ukai M, Currell F, Goodwin B J, Reddish T and Comer J 1993 *J. Phys. B: At. Mol. Opt. Phys.* **26** 2610
- [50] Travnikova O, Kimberg V, Flammini R, Liu X-J, Patanen M, Nicolas C, Svensson S and Miron C 2013 *J. Phys. Chem. Lett.* **4** 2361





# Roadmap on dynamics of molecules and clusters in the gas phase

Henning Zettergren<sup>1,a</sup>, Alicja Domaracka<sup>2</sup>, Thomas Schlathöler<sup>3</sup>, Paola Bolognesi<sup>4</sup>, Sergio Díaz-Tendero<sup>5,6,7</sup>, Marta Labuda<sup>8</sup>, Sanja Tosić<sup>9</sup>, Sylvain Maclot<sup>10,11</sup>, Per Johnsson<sup>10</sup>, Amanda Steber<sup>12,13</sup>, Denis Tikhonov<sup>12,13</sup>, Mattea Carmen Castrovilli<sup>4</sup>, Lorenzo Avaldi<sup>4</sup>, Sadia Bari<sup>12</sup> , Aleksandar R. Milosavljević<sup>14</sup> , Alicia Palacios<sup>5,7</sup>, Shirin Faraji<sup>3</sup>, Dariusz G. Piekarski<sup>15</sup>, Patrick Rousseau<sup>2</sup>, Daniela Ascenzi<sup>16</sup>, Claire Romanzin<sup>17</sup>, Ewa Erdmann<sup>8,5</sup>, Manuel Alcami<sup>5,7,18</sup>, Janina Kopyra<sup>19</sup>, Paulo Limão-Vieira<sup>20</sup>, Jaroslav Kočišek<sup>21</sup>, Juraĳ Fedor<sup>21</sup>, Simon Albertini<sup>22</sup>, Michael Gatchell<sup>22,1</sup>, Henrik Cederquist<sup>1</sup>, Henning T. Schmidt<sup>1</sup>, Elisabeth Gruber<sup>23</sup>, Lars H. Andersen<sup>23</sup>, Oded Heber<sup>24</sup>, Yoni Toker<sup>25</sup>, Klavs Hansen<sup>26</sup>, Jennifer A. Noble<sup>27</sup>, Christophe Jouvét<sup>27</sup>, Christina Kjær<sup>23</sup>, Steen Brøndsted Nielsen<sup>23</sup>, Eduardo Carrascosa<sup>28</sup>, James Bull<sup>29</sup>, Alessandra Candian<sup>30</sup> , and Annemieke Petrigani<sup>30</sup> 

- <sup>1</sup> Department of Physics, Stockholm University, 106 91 Stockholm, Sweden
- <sup>2</sup> Normandie Univ, ENSICAEN, UNICAEN, CEA, CNRS, CIMAP, 14000 Caen, France
- <sup>3</sup> Zernike Institute for Advanced Materials, University of Groningen, Nijenborgh 4, 9747 AG Groningen, The Netherlands
- <sup>4</sup> CNR-ISM, Area della Ricerca Roma1, Monterotondo Scalo, Italy
- <sup>5</sup> Departamento de Química, Facultad de Ciencias, Módulo 13, Universidad Autónoma de Madrid, 28049 Madrid, Spain
- <sup>6</sup> Condensed Matter Physics Center (IFIMAC), Universidad Autónoma de Madrid, 28049 Madrid, Spain
- <sup>7</sup> Institute for Advanced Research in Chemical Sciences (IAdChem), Universidad Autónoma de Madrid, 28049 Madrid, Spain
- <sup>8</sup> Department of Theoretical Physics and Quantum Information, Gdańsk University of Technology, Narutowicza 11/12, 80-233 Gdańsk, Poland
- <sup>9</sup> Institute of Physics, University of Belgrade, Belgrade, Serbia
- <sup>10</sup> Department of Physics, Lund University, P.O. Box 118, 22100 Lund, Sweden
- <sup>11</sup> *Present address:* Department of Physics, University of Gothenburg, Origovägen 6B, 41296 Gothenburg, Sweden
- <sup>12</sup> Deutsches Elektronen-Synchrotron DESY, Notkestr. 85, 22607 Hamburg, Germany
- <sup>13</sup> Institute of Physical Chemistry, Christian-Albrechts-Universität zu Kiel, Max-Eyth-Straße 1, 24118 Kiel, Germany
- <sup>14</sup> SOLEIL, l'Orme des Merisiers, St Aubin, BP 48, 91192 Gif-sur-Yvette Cedex, France
- <sup>15</sup> Institute of Physical Chemistry, Polish Academy of Sciences, Kasprzaka 44/52, 01-224 Warsaw, Poland
- <sup>16</sup> Department of Physics, University of Trento, Via Sommarive 14, 38123 Trento, Italy
- <sup>17</sup> Institut de Chimie Physique, UMR 8000 CNRS, Université Paris-Saclay, Orsay, France
- <sup>18</sup> Instituto Madrileño de Estudios Avanzados en Nanociencias (IMDEA-Nanociencia), 28049 Madrid, Spain
- <sup>19</sup> Faculty of Exact and Natural Sciences, Siedlce University of Natural Sciences and Humanities, 08-110 Siedlce, Poland
- <sup>20</sup> Atomic and Molecular Collisions Laboratory, CEFITEC, Department of Physics, Universidade NOVA de Lisboa, 2829-516 Caparica, Portugal
- <sup>21</sup> J. Heyrovský Institute of Physical Chemistry, The Czech Academy of Sciences, Dolejškova 3, 18223 Prague, Czech Republic
- <sup>22</sup> Institute for Ion Physics and Applied Physics, University of Innsbruck, Technikerstraße 25/3, 6020 Innsbruck, Austria
- <sup>23</sup> Department of Physics and Astronomy, Aarhus University, Ny Munkegade 120, 8000 Aarhus C, Denmark
- <sup>24</sup> Department of Particle Physics and Astrophysics, Weizmann Institute of Science, Rehovot 7610001, Israel
- <sup>25</sup> Department of Physics and Institute for Nanotechnology and Advanced Materials, Bar-Ilan University, Ramat-Gan 5290002, Israel
- <sup>26</sup> Center for Joint Quantum Studies and Department of Physics, School of Science, Tianjin University, 92 Weijin Road, Tianjin 300072, China
- <sup>27</sup> CNRS, Aix Marseille Univ., PIIM, Physique des Interactions Ioniques et Moléculaires, UMR 7345, 13397 Marseille, France
- <sup>28</sup> Laboratoire de Chimie Physique Moléculaire, École Polytechnique Fédérale de Lausanne, EPFL SB ISIC LCPM, Station 6, 1015 Lausanne, Switzerland
- <sup>29</sup> School of Chemistry, Norwich Research Park, University of East Anglia, Norwich NR4 7TJ, UK
- <sup>30</sup> Van 't Hoff Institute for Molecular Sciences, University of Amsterdam, Science Park 904, 1098 XH Amsterdam, The Netherlands

Received 5 September 2020 / Accepted 14 April 2021  
© The Author(s) 2021

**Abstract.** This roadmap article highlights recent advances, challenges and future prospects in studies of the dynamics of molecules and clusters in the gas phase. It comprises nineteen contributions by scientists with leading expertise in complementary experimental and theoretical techniques to probe the dynamics on timescales spanning twenty order of magnitudes, from attoseconds to minutes and beyond, and for systems ranging in complexity from the smallest (diatomic) molecules to clusters and nanoparticles. Combining some of these techniques opens up new avenues to unravel hitherto unexplored reaction pathways and mechanisms, and to establish their significance in, e.g. radiotherapy and radiation damage on the nanoscale, astrophysics, astrochemistry and atmospheric science.

## Contents

1	Introduction . . . . .	
2	Probing the molecular response to ultrashort XUV pulses produced by high-order harmonic generation . . . . .	
2.1	Status: description of the state of the art . . . . .	
2.2	Challenges and new directions . . . . .	
2.3	Concluding remarks . . . . .	
3	Paving the road toward understanding molecular processes with free electron lasers . . . . .	
3.1	Status: description of the state of the art . . . . .	
3.2	Challenges and new directions . . . . .	
3.3	Concluding remarks . . . . .	
4	Biomolecules interacting with synchrotron light . . . . .	
4.1	Status: description of the state of the art . . . . .	
4.2	Challenges and new directions . . . . .	
4.3	Concluding remarks . . . . .	
5	Using electrospray ionization to study structure and dynamics of large biomolecules at advanced light sources . . . . .	
5.1	Status: description of the state of the art . . . . .	
5.2	Challenges and new directions . . . . .	
5.3	Concluding remarks . . . . .	
6	Simulating light-induced molecular dynamics in 2020: from the picosecond to the attosecond scale . . . . .	
6.1	Status: description of the state of the art . . . . .	
6.2	Challenges and new directions . . . . .	
6.3	Concluding remarks . . . . .	
7	Experimental techniques for low-energy reactions of charged species . . . . .	
7.1	Status: description of the state of the art . . . . .	
7.2	Challenges and new directions . . . . .	
7.3	Concluding remarks . . . . .	
8	Interaction of keV ions with complex molecules and their clusters . . . . .	
8.1	Status: description of the state of the art . . . . .	
8.2	Challenges and new directions . . . . .	
8.3	Concluding remarks . . . . .	
9	Modeling molecular fragmentation . . . . .	
9.1	Status: description of the state of the art . . . . .	
9.2	Challenges and new directions . . . . .	
9.3	Concluding remarks . . . . .	
10	Electron interactions with gas-phase molecules . . . . .	
10.1	Status: description of the state of the art . . . . .	
10.2	Challenges and new directions . . . . .	
10.3	Concluding remarks . . . . .	
11	Interactions of low-energy electrons with clusters . . . . .	
11.1	Status: description of the state of the art . . . . .	
		11.2 Challenges and new directions . . . . .
		11.3 Concluding remarks . . . . .
12	Helium nanodroplets: a versatile medium for producing cold ions . . . . .	
12.1	Status: description of the state of the art . . . . .	
12.2	Challenges and new directions . . . . .	
12.3	Concluding remarks . . . . .	
13	Electrostatic ion-beam storage rings . . . . .	
13.1	Status: description of the state of the art . . . . .	
13.2	Challenges and new directions . . . . .	
13.3	Concluding remarks . . . . .	
14	Studies of photo-induced dynamics in biochromophores using electrostatic ion-storage rings . . . . .	
14.1	Status: description of the state of the art . . . . .	
14.2	Challenges and new directions . . . . .	
14.3	Concluding remarks . . . . .	
15	Electrostatic ion-beam traps . . . . .	
15.1	Status: description of the state of the art . . . . .	
15.2	Challenges and new directions . . . . .	
15.3	Concluding remarks . . . . .	
16	Cooling dynamics of molecules and clusters . . . . .	
16.1	Status: description of the state of the art . . . . .	
16.2	Challenges and new directions . . . . .	
16.3	Concluding remarks . . . . .	
17	Photo-fragment and photo-detachment spectroscopy in cryogenically cooled ion traps . . . . .	
17.1	Status: description of the state of the art . . . . .	
17.2	Challenges and new directions . . . . .	
17.3	Concluding remarks . . . . .	
18	Gas-phase fluorescence spectroscopy of complex molecular ions . . . . .	
18.1	Status: description of the state of the art . . . . .	
18.2	Challenges and new directions . . . . .	
18.3	Concluding remarks . . . . .	
19	Action spectroscopy of isomer-selected molecules . . . . .	
19.1	Status: description of the state of the art . . . . .	
19.2	Challenges and new directions . . . . .	
19.3	Concluding remarks . . . . .	
20	Deciphering the lifecycle of carbon macromolecules in space . . . . .	
20.1	Status: description of the state of the art . . . . .	
20.2	Challenges and new directions . . . . .	
20.3	Concluding remarks . . . . .	
	Author contributions . . . . .	
	References . . . . .	

<sup>a</sup> e-mail: [henning@fysik.su.se](mailto:henning@fysik.su.se) (corresponding author)

## 1 Introduction

Henning Zettergren, Alicja Domaracka, Thomas Schlathöler, Paola Bolognesi, Sergio Díaz-Tendero, Marta Labuda, and Sanja Tosic.

Core group of the MD-GAS COST Action CA18212.

Recent experimental and theoretical advances offer unique possibilities to study the electronic and structural dynamics of molecules interacting with different forms of radiation such as photons, electrons or heavier particles (ions, atoms, molecules). These advances include: (i) preparations of neutral and charged molecules and clusters in well-defined quantum states and structures (isomers); (ii) cryogenic storage of ions in new time domains; (iii) pump–probe schemes using advanced light sources and table-top laser systems; (iv) new spectroscopic techniques and methods to monitor emission of fragments, electrons and photons; and (v) theoretical and computational tools to treat the dynamics from ultrafast to ultraslow timescales (attoseconds to minutes and beyond). In this roadmap article, we present nineteen contributions where a combination of early career and more experienced researchers shares their views on the advances and future challenges within their areas of expertise.

Maclot and Johnsson open up the roadmap describing how table-top high-order harmonic generation (HHG) techniques may be used to produce attosecond extreme ultraviolet (XUV) pulses with the aim to unravel ultrafast electron and nuclear dynamics in molecules and clusters in unprecedented detail. Future challenges involve, e.g. implementing pump–probe schemes with two attosecond pulses for high temporal resolution and improved control, and to combine such ultrafast techniques with cryogenic storage devices and isomer selection methods.

Steber and Tikhonov describe the development of large-scale free electron laser (FEL) facilities for production of extremely intense, ultrashort, coherent pulses, and how they, combined with theoretical advances, have revolutionized the understanding of the dynamics of molecules in the gas phase over the last decade and a half. Upgrades to existing facilities and commissioning of new ones promise improved time resolution down to the attosecond regime and higher repetition rates. This will provide access to yet unexplored details on the very first steps in molecular reactions and its consequences for applications in, e.g. astrochemical and atmospheric sciences.

Castrovilli and Avaldi show that synchrotron radiation is a versatile tool for determining inherent spectroscopic properties of (bio)molecular systems and for studying the dynamics of molecules following absorption of photons spanning from the vacuum ultraviolet (VUV) to the hard X-ray regime. Here, key challenges for future studies are to develop methods to produce biomolecular targets with sufficient densities using, e.g. electrospray ionization (ESI) techniques or cluster aggregation sources, and to improve multi-coincidence

detection techniques to provide structural information (e.g. chirality).

Bari and Milosavljević focus their contribution on how ESI techniques may be used to study the structure and dynamics of complex molecular systems at advanced light sources such as synchrotrons and FELs. To exploit the full capabilities of spectroscopic techniques available at such facilities, state-of-the-art techniques need to be combined in novel ways. This involves, e.g. crossed-beam experimental setups combining high-flux ESI with isomer selection techniques under ultrahigh vacuum conditions.

Palacios and Faraji describe theoretical advances in simulating light-induced dynamics in molecules on ultrafast timescales, which are essential to interpret results and guide experiments at, e.g. advanced light sources. A particular theoretical challenge is to develop accurate methods for large molecules that include the initial electronic excitation and ionization on attosecond timescales, and the subsequent electronic-nuclear coupling occurring on femtosecond timescales and beyond. Quantum computers and computational statistical methods (e.g. machine learning) are promising tools to meet this challenge.

Ascenzi and Romanzin review important contributions and highlight recent advances in the field of low-energy ion–molecule reactions. Here, the key to a more fundamental understanding is to develop and combine state-of-the-art techniques in new ways. Future challenges involve, e.g. studies of reactions with metastable neutrals that are common in naturally occurring processes but remain largely unexplored in the laboratory, to prepare the reactants in well-defined quantum states and isomeric forms, and to study reactions under true interstellar conditions at low temperature environments.

Piekarski and Rousseau discuss collisions between keV ions and isolated complex molecules or weakly bound clusters of such molecules and show how the projectile charge, mass and velocity may be tuned to influence the ionization and fragmentation of isolated molecules or molecules in weakly bound clusters. New methods to bring fragile molecules and clusters into the gas phase, improved control of target masses, as well as pump–probe schemes combining ion and light pulses are keys to the understanding of such fundamental processes.

Erdmann and Alcamí focus on computational methods describing fragmentation dynamics on picosecond timescales. They point out that there is a need for new approaches to model delayed fragmentation processes, large molecules for which quantum chemical calculation tools are computationally too demanding and charged systems where density functional theory (DFT)-based approaches are not reliable. Another key challenge is to efficiently combine methods designed to follow the dynamics on different timescales.

Kopyra and Limão-Vieira discuss the developments of techniques to study electron interactions with gas-phase neutral molecules. These have been instrumental to advance the understanding of, e.g. radiation dam-

age mechanisms at the single molecule level and may provide key data of targeted compounds of importance for the development of environmental (green) technologies. Future challenges involve developing new tools to monitor neutral fragments, prepare targets of increasing complexity and follow electron dynamics on ultrafast times scales.

Kočišek and Fedor present experimental techniques to produce neutral clusters for studies of interactions with low-energy electrons and highlight results showing how the dynamics induced in molecules in such interactions is affected by the cluster environment. Improved characterization of the cluster target and the reaction products will be essential to provide benchmark data for accurate theoretical descriptions and a more fundamental understanding, and to gauge the significance of such processes in nature and in man-made technical applications.

Albertini and Gatchell demonstrate that superfluid He-nanodroplets are a powerful tool for producing cold ions and clusters. The development of a new generation He-droplet devices where the droplets are highly charged promises a more efficient production and better control over the initial cluster size distributions. This has the potential to open up new avenues for, e.g. gas-phase action spectroscopy using messenger techniques.

Cederquist and Schmidt present the developments of electrostatic ion-beam storage rings. Three cryogenically cooled ion-beam storage rings have recently been commissioned and are designed for unique studies and improved control of merged beams interactions involving ions and free electrons, ions and neutrals or two different ion species in opposite charge states. A particular challenge for future studies is preparation of intense beams of isomer selected ions in single or narrow ranges of quantum states. This is key to advance the understanding of, e.g. the origin and evolution of complex molecules in space.

Gruber and Andersen focus their contribution on studies of photo-initiated dynamics of isolated molecules combining ultrafast pump-probe schemes with electrostatic ion-beam storage. Pioneering studies demonstrate the capabilities of probing the excited state decay and ground state recovery of bio-chromophores. Future challenges involve, e.g. pre-cooling the ions in cryogenic traps/rings or in superfluid He-droplets to reveal the role of excited state energy barriers, and to study the electronic couplings in chromophore complexes.

Heber and Toker discuss the advantages of using electrostatic ion beam traps (EIBTs) for studying gas-phase dynamics of molecules and outline the prospects for future studies. Combined with ingenious detection schemes, EIBTs have the potential to act as a full reaction microscope where molecular cooling processes may be followed as a function of storage time. Applying ion mobility spectroscopy techniques opens up the study of the dynamics for specific isomers. The latest addition to the EIBT family is a hybrid two-trap system allowing for low-energy merged beams interactions with stored molecular ions having the same or opposite

charge states. Such studies are currently only possible at the electrostatic storage-ring facilities.

Hansen briefly reviews statistical models that have been developed to describe different types of molecular cooling processes. These models have been instrumental to successfully interpret results from studies at, e.g. electrostatic rings and traps where the dynamics is followed on microseconds timescales and beyond. Combined with the rapidly emerging development of such devices, these models are expected to significantly advance the understanding of highly excited molecules and clusters and how they cool. Of particular interest are more detailed studies of thermal emission of high-energy photons (recurrent fluorescence), which is believed to be important for the survival of, e.g. interstellar molecules.

Noble and Juvet describe recent advances in photo-fragment and photo-detachment spectroscopy using cryogenically cooled ion traps. The most advanced techniques offer a wide range of opportunities including, e.g. high spectroscopic resolution, high mass resolution, hole-burning spectroscopies, high-resolution photoelectron spectroscopy, and studying isomer-specific dynamics and size-selected clusters. Future challenges involve unravelling the mechanisms behind (non-statistical) selective fragmentation, generation and characterization of radical species, combining different techniques to fully characterize the molecule and its fragment and study selectively excited molecules.

Kjær and Brøndsted Nielsen briefly review the new emerging field of gas-phase fluorescence spectroscopy of (complex) molecular ions. This nondestructive technique provides direct measurements of the emitted photon spectra as well as information on excited state dynamics, and it has the potential to become an important standard spectroscopic tool. Here, challenges and future prospects aim to learn how to control fluorescence by, e.g. preparing the ions cold to increase the fluorescence yield and to develop new and efficient methods to study ion-molecule complexes. Such fundamental knowledge may, for instance, aid in engineering new fluorophores.

Carrascosa and Bull present isomer-selected action spectroscopy techniques and highlight their key properties and distinct advantages. The most recent developments are based on compact designs using printed circuit boards as ion-mobility spectrometers. Major challenges involve developing techniques that are cost effective and easy to integrate into new or existing instruments, and novel approaches to improve the performance of such techniques. Examples include improved resolving power using cyclic devices with cryogenically cooled buffer gases and multiple light and/or ion mobility stages.

Candian and Petrigiani describe how the synergy between astronomical observations, laboratory experiments and theoretical efforts have and will advance the understanding of the lifecycle of carbonaceous molecules in space such as, e.g. polycyclic aromatic hydrocarbons (PAHs) and fullerenes ( $C_{60}$  and  $C_{70}$ ). Recent advances open up the possibility to study, e.g.



excited state dynamics, anharmonic effects, isomerization and fragmentation processes of systems that are expected to be key players in astrophysical environments but so far remain largely unexplored in the laboratory and by theory. Such fundamental studies combined with the high spectral sensitivity and resolution of the James Webb Space Telescope are expected to revolutionize the way we understand the molecular universe

Covering all intriguing research activities dealing with dynamics of molecules and clusters in the gas phase is unfortunately out of the scope of this roadmap. Nevertheless, we believe that the present selection shows a rapidly moving field where new techniques and methods are constantly developed, and where future directions share common overarching challenges. These challenges include advancing:

- Methods to fully characterize molecules and clusters with increasing complexity in terms of their internal energy states and structures before interactions with photons, electrons or heavy particles. The combination of novel approaches highlighted in this roadmap is key to successfully implement such approaches and include, e.g. coupling soft ionization techniques (e.g. ESI) with isomer selection methods, cryogenic cooling and pre-trapping of ions, and state-selective photodissociation and photo-detachment techniques.
- Experimental techniques to monitor electronic and nuclear dynamics with improved temporal resolution and control and to follow the dynamics in unprecedented detail across ultrafast to ultra-slow timescales where the final state products are fully characterized and different competing relaxation pathways are disentangled (e.g. electron emission, isomerization, fragmentation, and radiative cooling). Examples include advanced pump–probe schemes using, e.g. attosecond- (HHG and FELs), femtosecond- and ion pulses, action- and fluorescence spectroscopy techniques with internally cold ions, improving long-time storage capabilities of ions, and multi-coincidence detection schemes for use under the most demanding vacuum conditions. Combining these tools in novel ways, for instance, advanced light sources or ion-accelerator facilities with cryogenically cooled ion-beam storage devices, is fundamental to further advance the understanding of the dynamics.
- Theoretical and computational tools treating the dynamics of molecules and clusters with increasing complexity and where the dynamics may be followed on timescales where different relaxation processes come into play. These include, e.g. coupled electron–nuclear dynamics on ultrafast timescales, delayed electron emission and fragmentation dynamics on timescales exceeding picoseconds, and radiative cooling occurring on milliseconds and beyond. Here, methods based on, e.g. machine learning and artificial intelligence are in their infancy and may play

important roles to address these challenges in the future.

The combination of these new and refined approaches in the laboratory and for computations is fundamental to further advance the understanding of the dynamics of molecules and clusters in the gas phase and thus also of its consequences for a broad range of astrophysics/chemistry, astronomy, atmospheric science and radiation science. The MD-GAS COST Action CA18212 ([www.mdgas.eu](http://www.mdgas.eu)) acts as an interdisciplinary platform for close collaborations and knowledge exchange between researchers performing fundamental studies of the dynamics of molecules and clusters in the gas phase (experiment and theory), and with key stakeholders from applied fields of sciences and industry. Such a concerted effort is key to tackle the current and future challenges outlined in this roadmap.

**Acknowledgements** This article is based upon work from COST Action CA18212—Molecular Dynamics in the GAS phase (MD-GAS), supported by COST (European Cooperation in Science and Technology).

## 2 Probing the molecular response to ultrashort XUV pulses produced by high-order harmonic generation

Sylvain Maclot and Per Johnsson, Department of Physics, Lund University, Sweden

### 2.1 Status: description of the state of the art

Fundamental chemical and physical processes in molecules are governed by electron and nuclear dynamics typically occurring at a timescale from atto- to picoseconds ( $10^{-18}$ – $10^{-12}$  s). The time-dependent electronic density is responsible for the subsequent nuclear motion taking place on a longer temporal scale. Its apprehension is thus crucial for inferring the mechanism of processes such as bond formation and bond breaking.

The emergence of coherent light pulses with femtosecond and attosecond duration provided the necessary temporal resolution to study ultrafast processes in atoms and molecules. Such pulses can be produced by high-order harmonic generation (HHG) techniques [1] and have their spectral range from the extreme ultraviolet (XUV) to the soft X-ray region. This type of source can be realized as a tabletop setup which is an advantage compared to free-electron lasers, which are costly large-scale facilities with highly competitive proposal-based access. Another asset of HHG sources lies in the availability of very high pulse repetition rates (MHz).

Since the first use of ultrashort light pulses to study atoms, the progress in fundamental understandings, the emergence of new technologies as well as the support offered by theoretical quantum chemistry enabled the study of more and more complex systems, such

as molecular hydrogen, molecular nitrogen, methane, acetylene, methanol, amino acids, polycyclic aromatic hydrocarbons (PAHs) and fullerenes just to name a few (see review [2] and Sect. 3 for some examples). For instance, understanding electron dynamics has been demonstrated to be key to unraveling the relaxation dynamics of ionized molecules [3]. Indeed, upon ionization, the charge/hole density evolves by moving across the different sites within the molecule on the femtosecond timescale [4].

The simplest type of photoionization experiment is done using single ultrashort XUV pulses. Fundamental insight into the dynamics of complex molecular systems is available indirectly with the help of theoretical quantum chemistry calculations [5]. As an example, a result from one of our recent studies performed at the Lund Attosecond Science Center (LASC) on the diamondoid adamantane (carbon cage— $C_{10}H_{16}$ ) using an intense XUV source is summarized in Fig. 1. Combining multi-particle detection (double velocity map imaging spectrometer), covariance analysis and quantum chemistry calculations allowed us to show that the doubly charged adamantane molecule is metastable and will spontaneously dissociate [6]. Thanks to the measured ion and electron kinematics combined with theoret-

cal calculations, we were able to discuss the internal energy distribution of the system and assess the energetic picture of the dication processes. As a result, we were able to demonstrate that, prior to dissociation, the cage structure of the dication will open and hydrogen migration(s) will occur (see Fig. 1).

A direct experimental way to precisely follow the ultrafast dynamics of complex molecular systems with temporal resolution lies in the use of pump-probe methods [7]. Within this approach, the system is ionized/excited from its initial state by an ultrashort light pulse (pump) and then probed by a second pulse arriving at a variable delay. Either of these interactions can result in photoionization/photo-excitation of molecules enabling diagnostics by time-resolved photoion-photoelectron spectroscopy.

Concerning experimental methods, the increase in complexity of systems of interest, i.e. number of degrees of freedom, number of electronic states, requires the use of multi-particle detection in coincidence (collection of all particles, ions and electrons, coming from the same molecule) coupled with high repetition rate laser sources in order to disentangle without ambiguity the dynamics of complex molecular systems. So far, the most powerful instrumental tool to tackle this chal-

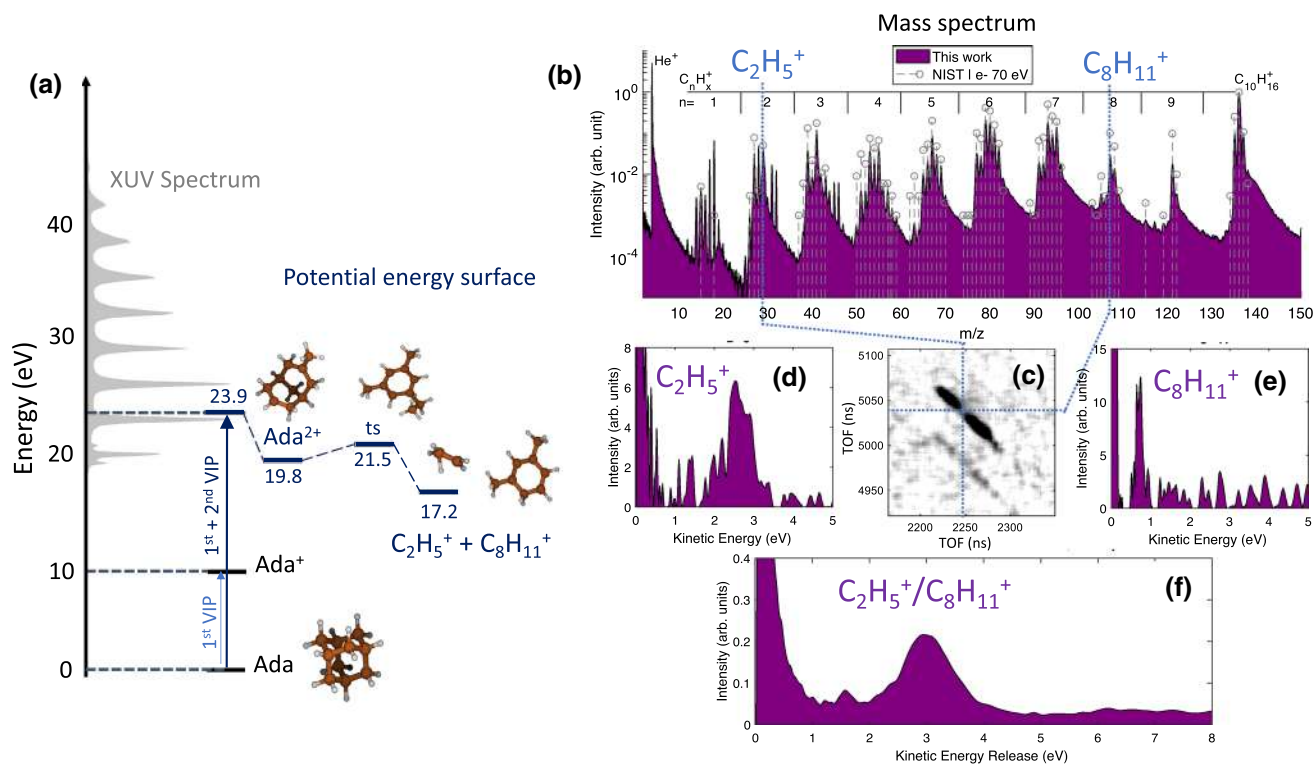


**Fig. 1** **a** Selected points of the calculated potential energy surface (PES) of adamantane (DFT level) overlapped by the experimental XUV spectrum (gray). The selected points correspond to the minima of the PES encountered during the fragmentation of the dication leading to the production of the photoion pair  $C_2H_5^+ / C_8H_{11}^+$ . **b** Mass spectrum, exhibiting a multitude of fragmentation channels with single hydrogen resolution. The correlation between the produced photo-fragments is examined through extracted TOF-TOF (time-of-flight) covariance maps, with a zoom-in around the studied photoion pair in panel (c). **d**, **e** Ion kinetic energy distributions of the two studied photoions extracted from TOF-VMI (velocity map imaging) covariance images. **f** Kinetic energy release distribution for the photoion pair that helped us confirming that the two-body Coulomb explosion resulted from an open cage geometry



lenge is the so-called reaction microscope device (ReMi or COLTRIMS [8]), which provides full kinematics of the interaction process.

It is worth mentioning that complementary spectroscopy techniques, such as high harmonic generation spectroscopy (HHGS) [9] and attosecond transient absorption spectroscopy [10], exist and largely contribute to the quest of understanding the dynamics of molecules.

## 2.2 Challenges and new directions

In spite of the improved understanding of the HHG process and the vast developments of related experimental technology over the last decades, the use of such sources faces various challenges in pursuit of unraveling ultrafast dynamics in molecules. For instance, the shortest available light pulses, i.e. single attosecond pulses (<100 as), have XUV spectra which span several tens of eV. When these are used for excitation, they populate a large number of excited states, which might result in complicated fragmentation dynamics. Another problem is that the most common “probe” pulses come from the laser driving the HHG process which has its spectral domain in the infrared or visual region. This poses a limitation to the temporal resolution (for example, the optical cycle of 800 nm radiation is 2.6 fs), as well as electric field strength that can be used without disturbing the studied dynamics (see pioneer work of F. Calegari for an example of XUV-IR pump–probe experiment [11]).

The latter issue can be tackled by using two XUV attosecond pulses to perform pump–probe measurements with a high temporal resolution and a weak electric field. This requires high-flux XUV sources, generally provided by very intense lasers, in order to enable sufficient signal from 2-photon absorption (one from each pulse). Some facilities, such as FORTH-IESL (Heraklion, Greece), RIKEN (Wako, Japan) and LASC (Lund, Sweden), have demonstrated the possibility to perform such experiments on atoms, but further progress needs to be made for these experiments to be fully adapted for investigations of molecular species. The challenges lie mainly in the stabilization of the HHG source, as well as in the low repetition rates characteristic of high-flux lasers (a few tens of Hz). New OPCPA-based laser technologies will be able to provide higher repetition rates alongside high pulse energies for future beamlines. An example of a very promising facility equipped with this type of source is the newly built ELI-ALPS [12] (Szeged, Hungary).

As an outlook, an interesting path beyond the state of the art would be to couple the above-mentioned ultrafast techniques with new sample environments, such as cryogenic rings (see Sect. 13). This would enable the selection of specific molecular conformations prior to interaction, helping both experimental interpretation and theoretical calculations.

## 2.3 Concluding remarks

The proliferation of HHG beamlines in the world and the strong interest in progressively larger polyatomic systems along with the continuous progress in theoretical quantum chemistry (see Sects. 6 and 9) foretell a bright and rich future for studies of ultrafast dynamics of molecules for the next decades. Furthermore, the technological and theoretical advances should be able to give access to the essentially unexplored dynamics occurring in molecular clusters.

## 3 Paving the road toward understanding molecular processes with free electron lasers

Amanda Steber and Denis Tikhonov, DESY, Germany

### 3.1 Status: description of the state of the art

For more than a decade, free electron lasers (FELs) have greatly advanced scientific endeavors in fields such as astrochemistry, atmospheric science, biology and energy transportation. They are intense radiation sources ranging from the THz to the hard X-ray regimes. This allows researchers to investigate the structure of systems, from atoms up to biomolecules and crystals, and their dynamics on timescales down to femto- (and recently atto-) seconds (fs). FELs, especially those operating between the vacuum ultraviolet (VUV) and hard X-ray regime, have proven to be instrumental in the field of molecular physics due to their unprecedented extremely intense (pulse energies as high as 4 mJ), ultrashort (sub-fs [13]), coherent pulses. The VUV Free-Electron Laser at Hamburg (FLASH) came online in 2005, and since then, more facilities, such as the LINAC Coherent Light Source (LCLS) in Stanford, the Japanese Spring-8 Angstrom Compact Free-Electron Laser (SACLA), the Free Electron laser Radiation for Multidisciplinary Investigations (FERMI) in Trieste, Italy and the European X-Ray Free-Electron Laser Facility (XFEL) in Hamburg, have come online operating up into the hard X-ray regime. They operate over a wide range of wavelengths and peak brilliance, as shown in Fig. 2.

These FELs have facilitated the study of phenomena such as the behavior of cold atomic and molecular systems—in particular the dynamics of excited states—and bond formation/destruction on the femto- and attosecond timescale. One glean information on the molecular structure, chirality, isomerization effects, charge transfer, non-Born Oppenheimer effects and photo-fragmentation pathways [14–16]. In order to look at these phenomena induced by radiation, the FELs many times have stationary beamlines that are equipped with ion time-of-flight (TOF) mass spectrometers, velocity map imaging (VMI) spectrometers, electron spectrometers, absorption or fluorescence exper-

iments, cold target recoil ion momentum spectrometers (COLTRIMS) and split-and-delay arrangements [14, 15].

A method used to monitor the dynamics of the molecules, which employs some of the above-mentioned techniques, is the pump-probe approach. This works in much the same way as described in Sect. 2, where two lasers, in this case the FEL and a table top laser or two FEL “beams,” can be used, or multi-photon absorption can induce indirect pump-probe effects. In these experiments, measurements are taken as the delay between the pump and probe is changed, where the pump initiates a chemical process and the probe changes the dynamical behavior of the system, allowing for new signal features from a transient species to be measured. In many cases, information from different measurements is merged together to provide details about the dynamics of the molecules. For instance, combining ionic mass spectra with electronic VMI measurements allows for the disentanglement of ionization/fragmentation channels. A very powerful set of tools in FEL-based ultrafast sciences are the covariance techniques [17]. Just recently, VMI 3D covariance imaging has progressed toward revealing information about the molecular structure and the dynamics happening through the course of the chemical reaction [18]. Direct imaging of the molecular motions by FELs is also available with more conventional diffraction techniques. They allow for the investigation of gas-phase dynamics using X-ray diffraction (XRD) due to their unprecedented intensity in the X-ray regime compared to other sources, such as X-ray tubes or synchrotrons [19]. Also, in comparison with time-resolved electron diffraction (TRED), FEL-based XRD shows better time resolution (due to the absence of electron-electron repulsion) and better shot-to-shot signal stability [20].

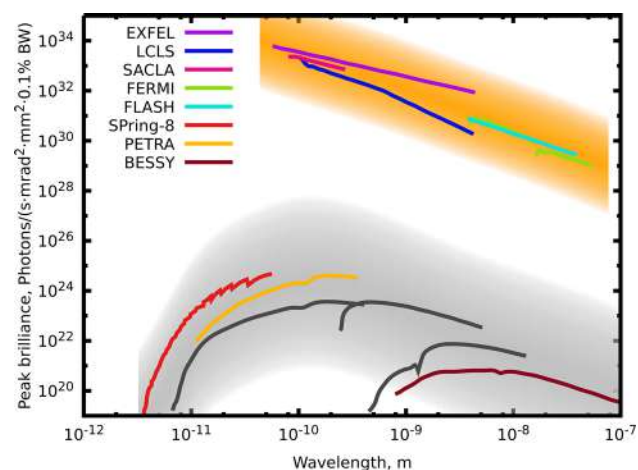
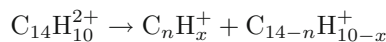


**Fig. 2** Peak brilliance vs wavelength of high photon energy FELs and at a few synchrotron facilities around the world. The curves in the orange region indicate FEL facility parameters, while the curves in the gray region represent synchrotron facilities

Theoretical work is being undertaken to investigate the dynamics of these pump-probe experiments that many times go beyond the Born-Oppenheimer approximation. The most popular methods which focus on chemical responses at the fs timescale include trajectory surface hopping molecular dynamics (TSH MD), ab initio multiple spawning (AIMS) and multi-configurational time-dependent Hartree (MCTDH) (see citations in Ref. [21]). They provide a treatment of the nuclear motions within several electronic states, but calculations of this nature are very computationally demanding (see Sect. 6 for more details).

All of these experimental and theoretical methods have culminated in state-of-the-art international collaborations aimed at carrying out investigations of the dynamics of gas-phase molecules. While many important studies have been done through these collaborations, we briefly outline just a few. One such study has been carried out on one of the most complex molecular systems studied in the gas phases with FELs thus far, the buckminsterfullerene ( $C_{60}$ ). In a series of works [22, 23] performed at the LCLS (Stanford) and the EXFEL (Hamburg), the authors found that upon interaction with X-ray radiation produced from FELs,  $C_{60}$  simultaneously undergoes a multitude of physical and chemical processes that are governed by the chemical bonding in this molecule [22, 23]. Upon core ionization, the Auger process was induced, which eventually led to the molecule being charged up to  $C_{60}^{8+}$  and breaking into molecular and atomic ion charge states through Coulomb explosions. They were able to accurately model this behavior through molecular dynamics simulations.

Another collaborative effort has focused on the study of polycyclic aromatic hydrocarbons (PAHs). In the group of Prof. Melanie Schnell, efforts have been made to understand how harsh VUV radiation impacts the hydrogenation state, fragmentation and isomerization of PAHs with experiments done at CFEL-ASG Multi-Purpose (CAMP) end-station [24] of FLASH. Successful interpretation of the interplay between ionization and fragmentation channels in these complex system relies on the simultaneous analysis of multiple data sets, including TOF-MS and electronic and ionic VMI images. The analysis was supported by theoretical modeling [21], and it was found that phenanthrene ( $C_{14}H_{10}$ ) undergoes several ionization steps as well as fragmentation. Based on covariance analysis, Coulomb explosion leads to the fragmentation of



with  $n = 2, 3, 4$  [21]. Figure 3 shows the experimental and theoretical ion yields for the dication and  $C_2H_x^+$  fragment. At  $t > t_0$ , the IR pulse destroys the dications formed by the XUV. This is reflected by the change of behavior in the ion yield. The transient peaks at  $t \sim t_0$  are a signatures of short-lived intermediates. By modeling and experimental analysis, we attribute these intermediates to the PAH molecular/ionic excited states [21].

Molecular chirality has also been a target of study in FELs, in particular with its ultrafast manifestation, such as the work performed in Ref. [25]. The authors used photoelectron circular dichroism (PECD), which relies on forward–backward asymmetry in electron emission upon ionization with circularly polarized pulses [26]. These studies have proved challenging not only because of need in circularly polarized light from FELs, but also because of the high event statistics needed for such studies. In order to achieve the required statistics, either long beam times or high repetition rates are needed for the experiments.

### 3.2 Challenges and new directions

While the current state-of-the-art facilities have allowed for interesting chemical and physical processes happening in molecular systems to be scrutinized, scientists in this area are forever pushing the boundaries forward in an attempt to understand the very first steps in molecular reactions. In order to do so, it is imperative that FEL sources are able to routinely provide  $\leq 10$  fs of time resolution, even as short as attoseconds, with faster repetition rates, and sequences of FEL pulses. This would at the same time require that detectors and measurement devices are able to keep up with the upgrades to efficiently collect shot-to-shot data and analysis techniques evolved to disentangle these complicated datasets. In order to provide a full picture, the new experimental

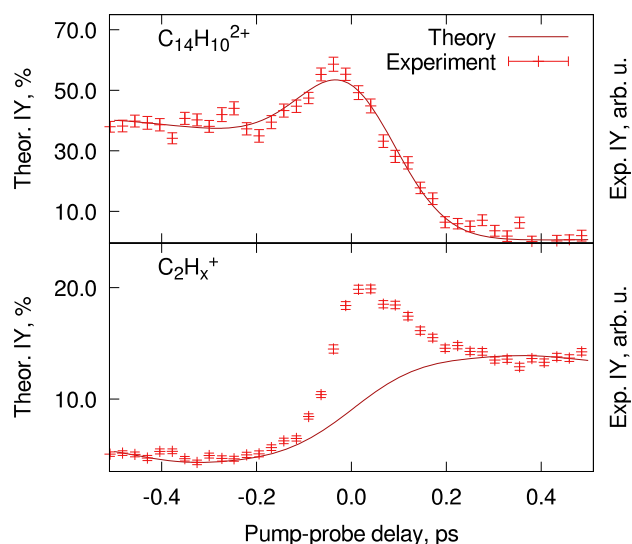


**Fig. 3** The relative ion yields of phenanthrene<sup>2+</sup> ( $C_{14}H_{10}^{2+}$ ) and the  $C_2H_x^+$  fragment after several time delays in the pump–probe experiments. The negative delays indicate that the IR pulse (810 nm) is the first pulse followed by the FEL pulse (30.3 nm), and for positive delays, the FEL pulse acts as the pump pulse. As can be seen, there is a slight increase in the ion yield of the dication around  $t_0$  which then depletes over time, whereas the reverse is true for the  $C_2H_x^+$  fragment. The step size between each point is  $\sim 25$  fs, and each point consists of approximately 1400 acquisitions. The data and theoretical treatment were first presented in Ref. [21]

setups are becoming more and more keen on combining multiple techniques for providing full insight into the systems of study. Parallel to these efforts, theoretical methods should become less computationally expensive and more accurate to provide a valid explanation of the processes observed in experiments.

Over the coming years, new FEL facilities will be coming online, and many of the older FELs will be upgraded. The European XFEL, with its superconducting linear particle accelerators, has achieved repetition rates of  $\sim 27,000$  Hz and pulse durations of  $\leq 100$  fs, while FERMI has shown how using a seeded FEL in the high-gain harmonic generation configuration can improve shot-to-shot wavelength stability, transverse coherence and low-intensity fluctuations among others [27]. The LCLS-II facility is currently under construction. This instrument will implement seeding technology and superconducting linear particle accelerators, achieving repetition rates of  $\sim 1$  MHz and sub-fs pulse durations. The FLASH facility will undergo several upgrades during the FLASH2020+ project, which will see FLASH1 become a seeded FEL, pump–probe laser upgrades, and an eventual repetition rate of 1 MHz. These facilities along with the SwissFEL and the Shanghai High Repetition Rate XFEL and Extreme Light Facility (SHINE) will allow for further experimentation unraveling dynamics of the molecules in the gas phase.

### 3.3 Concluding remarks

The study of molecular processes in the gas phase with FELs has come a long way since FLASH first came online in 2005. With the existing facilities and their slated upgrades, as well as new facilities, this field will continue to grow and techniques will be honed to gain insight into bond formation/destruction and the interplay between electronic and nuclear motion. The increase in repetition rate will allow for the investigation of weak effects that require numerous data acquisitions that otherwise could not be studied. This will spur new understanding of elementary chemical processes in the fields of atmospheric sciences, astrochemistry, biological systems and energy transportation.

## 4 Biomolecules interacting with synchrotron light

Mattea Carmen Castrovilli and Lorenzo Avaldi, CNR-ISM, Monterotondo Scalo, Italy

### 4.1 Status: description of the state of the art

Synchrotron radiation with its tunability from the VUV to the hard X-ray regions, high flux and polarization control represents a highly valuable tool for a spectroscopic characterization of molecules of biological interest as well as to investigate the dynamical processes induced by the absorption of the radiation. The most

straightforward approach to investigate the interaction of radiation with bio-matter using a tunable source is to vary the photon energy and to study photo-absorption. Below the ionization threshold, where outer electrons are promoted to empty states, direct light absorption or optical emission techniques are adopted, while above it photoionization mass spectrometry (PIMS) becomes the most suitable approach. The measurements of ionization energies and appearance energy (AE) of parent and fragment ions lead to the determination of key thermochemical quantities such as enthalpy of formation and bond dissociation energies. For example, the combined theoretical and experimental investigation of the AE of halopyrimidines and nitroimidazoles [28], with their derived compounds metronidazole and misonidazole, shed light on the radiosensitizing function of these classes of molecules, while PIMS on collagen peptides [29], the most abundant protein in the human body, showed that at low photon energy (14–20 eV), neutral molecules are lost from the amino-acid residue side-chains of both the precursor peptide and the photoionized peptide radical cation in a radical-induced process that mainly targets the Asp side-chain leading to abundant  $\text{CO}_2$  loss. This channel then is quenched in unfolded peptide due to the decrease in radical migration.

Photoemission and X-ray photoemission spectroscopies (PES and XPS), where the kinetic energy (KE) of the photoionized electron is measured at a fixed photon energy ( $h\nu$ ), allow the reconstruction of the electronic distribution of the molecular orbitals of binding energy  $\text{BE} = h\nu - \text{KE}$ . In the valence shell, the comparison of theoretical predictions and experimental photoelectron spectra in the case of antibiotics, radiosensitizers and their building blocks, but also sugars and lipids, has provided useful information on the electronic charge distribution of the outer orbitals and other properties useful to model the chemical behavior of these compounds. In the inner shell, the localized nature of the core electrons implies that each atom is affected by its surrounding chemical environment and site-selective information can be obtained. Differences among families of similar molecules (e.g. isomers, or analogues) or the effect of functionalization can be identified, assessed and discussed in terms of the measured and calculated inner-shell chemical shifts. The measurements of the N 1s spectrum of proline amino acid that allow to identify different conformers [30] can be taken as an example of the potentiality of the technique. Then, electron energy distributions measured over a broad range of kinetic energies up to several hundreds eV (including the Auger decay of core ionic states or autoionization of excited states) can be used to characterize the complete electron emission spectrum. These emission spectra at different photon energies represent the benchmark data for the Monte Carlo and Ion Tracking simulation codes [31], used to evaluate the direct and indirect radiation damage within the biological medium.

The simultaneous detection of electrons and ions in time coincidence, i.e. from the same ionization event in the photoelectron-photoion (PEPICO, Fig.

4) and photoelectron-photoion-photoion coincidence (PEPIPI-CO) experiments [32], allows for a better control over the many variables in the physical process, adding further insights into molecular fragmentation. In a series of PEPICO experiments on the building blocks of radiosensitizer compounds, it has been shown that molecular fragmentation following core excitation is strongly influenced by both the molecular site of the initial excitation and the character of the excited molecular orbital. While site/state-selective bond scission is favored when inter-site electron migration cannot occur efficiently and the chemical environment of the atomic site is very different, it becomes questionable in the case where fast electronic relaxation channels efficiently redistribute the initially localized core hole toward singly and multiply ionized states before fragmentation occurs (see Sect. 9). The selectivity and efficiency of the PEPICO technique have also allowed to find traces of minor processes like the isomerization with H transfer and dehydration of the parent ion in amino acids [33], which are relevant processes in the biological environment.

Molecular chirality is widely recognized for its relevance to the building blocks of life and its vital role for medicine and health. The advantage of synchrotron radiation, over the Xe-arc lamps of laboratory circular dichroism (CD) instruments, is the high intensity, in the VUV region below 200 nm and the broad energy range covered. Synchrotron radiation circular dichroism (SRCD) spectroscopy has been exploited to study base-base interactions in DNA/RNA, as the difference in the CD spectrum of a mononucleotide and strands of nucleotides provides evidence of interactions between neighboring bases in the electronically excited state [34] or in some cases of photo-lesion occurred on single strand. The low value ( $10^{-3}$ – $10^{-4}$ ) of the asymmetry in CD, due to the second-order perturbation level in the electric dipole/magnetic dipole and electric dipole/electric quadrupole interference terms, hampers its use for isolated molecules in the gas phase. Con-

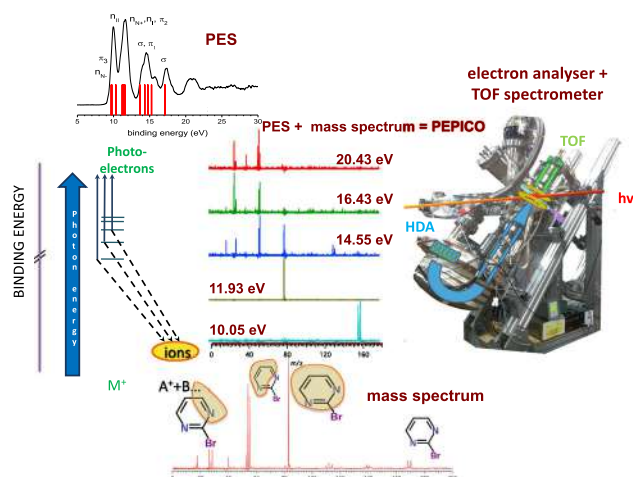


**Fig. 4** Scheme and setup of a PEPICO experiment



versely, photoelectron circular dichroism (PECD) [35], which appears already in the electron dipole term of the transition matrix element, is characterized by asymmetries in the range of  $10^{-1}$ – $10^{-2}$ . Thus, in the last years PECD has been exploited to study the conformational effects from isomerism and group substitution, conformer populations and clustering.

## 4.2 Challenges and new directions

The main challenge in studying bio-systems is their intrinsic fragility that hampers the production of beams of isolated biomolecules via thermal evaporation, which, however, has the advantage to produce beam of neutral molecules. The electrospray ionization (ESI) technique (see Sect. 5) represents the most suited tool to bring nucleotides, proteins or peptides from solution into the gaseous phase. The coupling of this versatile ion source with spectroscopic techniques implies that the mass selected ions generated in the gas phase by an ESI source are collected in an ion trap and then excited with the radiation. The combination of ESI sources with tandem mass spectrometers and ion traps has been successfully used to measure partial ion yield NEXAFS spectra of systems with sizes up to a few thousands of amu and to address, for example, photo-induced processes in molecular recognition [36]. An improvement of the throughput of the sources is the challenge to be faced to perform electron spectroscopies on these systems.

H-bonds and van der Waals interactions are ubiquitous in nature and influence the structure, stability, dynamics and function of molecules and materials and therefore play a crucial role in bio-systems. The study of these interactions in gas-phase homogeneous or hydrated clusters of increasing size (see Sect. 8) can give information on structures and mechanisms at work in both the liquid and condensed phases. Also, in this case the main challenge is the production of a controlled cluster beam with enough density. First attempts in this direction combining a gas aggregation source to produce neutral uracil clusters and XPS, where the weak, non-covalent interactions modulate the chemical shift, have been reported [37].

Metal nanoparticles are increasingly used in the biological field, due to the wide spectrum of potential applications, which include both diagnostic and therapeutic or their combination (theranostic) [38,39]. While the possibility to exploit a wide range of materials, the established methods for the synthesis in different sizes, the easy functionalization of their surface to control the interaction with the bio-environment are making nanoparticles more and more popular, there is still a lack of understanding of the many processes that occur upon their irradiation and can explain their behavior, for example, as radiosensitizer. Synchrotron radiation with its broad tunability and fluxes and inner shell spectroscopies with their chemical selectivity can contribute to understand the electronic structure and emission spectra of metal nanoparticles and the chem-

istry induced by the functionalization of such complex aggregates. Studies of isolated nanoparticles are still rare. Some XPS experiments have been performed on 4-nitrothiophenolon gold nanoparticles [40], and recently, a valence study using angle resolved photoemission has been reported [41].

As for the investigation of chirality, the use of multi-coincidence technique, where up to five correlated fragment ions have been detected simultaneously [42], may pave the way to the determination of absolute configuration on the single-molecule level in the gas phase. Moreover, the recently introduced time resolved transient circular dichroism in the VUV region, which exploits the synchrotron natural polarization, allows to access timescales down to ns like in the isomer concentration changes during/after photo-isomerization [43].

## 4.3 Concluding remarks

The electronic structure and geometrical arrangement (conformation, isomerization, tautomerization) of molecules determine the functioning of bio-systems at the macroscale. For example, the functionality of complex molecules, like enzymes and proteins, is closely related to the details of their conformation and the macroscopic effects of radiation damage in living cells strongly depend on processes initiated at the atomic and molecular level of their constituents. Synchrotron radiation and all the armory of synchrotron-based spectroscopic tools, from the many particle coincidence experiments to the imaging techniques, represent a unique combination to unveil the radiation-induced processes in bio-systems of increasing complexity in gas phase.

**Acknowledgements** Work partially supported Italy–Sweden MAECI project “Novel molecular tools for the exploration of the nanoworld.”

## 5 Using electrospray ionization to study structure and dynamics of large biomolecules at advanced light sources

Sadia Bari, Deutsches Elektronen-Synchrotron DESY, Hamburg, Germany

Aleksandar R. Milosavljević, Synchrotron SOLEIL, Gif-sur-Yvette Cedex, France

### 5.1 Status: description of the state of the art

Investigating the interaction of light with biologically relevant molecules has gained interest for a wide variety of research fields including photochemical reactions such as light harvesting as well as radiation damage in proteins and DNA related to cutting-edge cancer treatment techniques. However, in the condensed and liquid phases, disentangling direct and indirect radia-



tion effects is often impossible. Although the investigated systems are certainly not in their natural environment, gas-phase experiments offer several advantages: The incoming projectile (photon, electron, ion) is well defined (energy, direction, charge, etc.), the target is well defined (chemical formula, structure, quantum state, temperature, mass, charge, etc.), and the interaction products are well defined (photoelectrons, ionic fragments, scattered electrons, emitted photons, etc.) and can be efficiently analyzed. In the beginning, studies on isolated biomolecules in the gas phase were limited to small molecules that are stable against thermal decomposition, because there were typically brought to the gas phase using ovens [44].

Electrospray ionization (ESI) [45] is a gentle, state-of-the-art technique to introduce intact, complex biomolecular ions from solution into the gas phase and into vacuum. The first photo-activations of electrosprayed biomolecules were performed as early as the 1980s [46], and a good overview of laser-based experiments can be found in a review by Brodbelt [47]. The advanced light sources such as synchrotrons (see Sect. 4) and free-electron lasers (FELs, see Sect. 3) have the great advantage of superior photon brilliance, a wide photon energy range (from infrared, through visible, vacuum ultra violet (VUV) up to X-rays) and, in the case of FELs, short intense pulses. More than a decade ago, the coupling of ESI tandem mass spectrometers at such light sources was introduced for a novel and unique way to investigate structure and dynamics of complex gas-phase biomolecules [29,36,48–51]. In all the applied setups, the light interaction with a selected ion precursor takes place in ion traps to account for the low target density due to the space charge (see also Sect. 8, 13, 14 and 17). Using ion traps, the high-resolution tandem mass spectrometry allowed the study of photon-induced fragmentation in a wide photon energy domain. Moreover, from partial and total ions yields one could determine excitation and ionization energies of the investigated systems (so-called action spectroscopy). In the soft X-ray regime, near-edge X-ray absorption fine structure (NEXAFS) spectroscopy or near-edge X ray absorption mass spectrometry (NEXAMS) probes transition between atomic core levels and orbitals of the molecular bonding states. Therefore, this action spectroscopy is a powerful site-selective, structural tool that provides information on the electronic structure, chemical environment as well as the 3D structure of the molecules. More recently, the site selectivity of this method has shown the dependence of backbone fragmentation on hydration upon X-ray absorption of water, representing a great potential for studying relaxation mechanisms in radiation damage to hydrated biomolecules in a bottom-up approach [52]. Furthermore site-selective dissociation on resonant excitation of sulfur electrons in sulfur-containing peptides was proven and paves the way for pump-probe studies of biomolecules at FELs [53].

## 5.2 Challenges and new directions

Although recent years have seen great progress in gas-phase investigation of complex electrosprayed systems at advanced light sources, the exploited techniques were always based solely on mass spectrometry. Therefore, the existing experimental setups do not allow exploiting a full potential of very powerful spectroscopic techniques presently accessible at advanced light sources, such as photoelectron spectroscopy (PES), including X-ray photoelectron spectroscopy (XPS), photoelectron photoion coincident (PEPICO) spectroscopy (see Sect. 4), velocity map imaging (VMI), etc. Indeed, the photoelectrons cannot be extracted from the ion traps and be analyzed in kinetic energy, both due to specific trap geometries and strong trapping fields that would significantly disturb kinetic energies of ejected electrons. Even if one overcomes later limitations (for example, by a novel trap design and short pre-detection shutdown of the trapping fields), additional difficulties arise from low-vacuum conditions in the interaction region due to the cooling gas used in the ion traps to increase their efficiency (typically He at a pressure of  $\approx 10^{-3}$  mbar). Moreover, there is a growing interest to study even more complex systems that can be produced by ESI, such as clusters, hydrated biomolecules, specific ligand complexes and functionalized nanoparticles, as well as conformer-selected biopolymers. The latter studies cannot be performed efficiently by using only RF ion traps. Technical developments toward a crossed-beams experiment, in which a focused target ion beam produced by an ESI source would be crossed by a focused photon beam inside a well-defined interaction region under high-vacuum, could allow efficient extraction and analyses of produced photoelectrons and photoions [16]. Developing such an experimental technique is rather challenging, however, as briefly elaborated below.

The essential challenge is to achieve an acceptable signal-to-noise level in the measurement, which is directly proportional to the photoionization cross section of the target and the target density in the interaction region. Whereas a high ionization cross section is expected for relatively large systems under investigation, it is experimentally non-trivial to achieve a high target density. ESI is an atmospheric pressure ionization source, and therefore, one should transfer with a minimum loss a high ion current produced by ESI to a high vacuum conditions ( $\approx 10^{-9}$ – $10^{-10}$  mbar). The high vacuum is needed both to efficiently extract photoelectrons and to decrease the background contribution. To achieve such a high-current ion beam under high vacuum, one needs a complex system where the ESI source is followed by multiple differentially pumped stages, a system of ion funnels and ion guides to collect and preserve the ions and a lens system to focus the ion beam in the interaction region. A basic principle for such a source has been laid out a few years ago for ion soft-landing applications [54]. Furthermore, in the case of a crossed-beams experiment, there should be a compromise between a well-defined small focal point

and the ion acceleration that decreases both the effective ion density and the detection efficiency. Finally, due to low expected photoelectron signals a PEPICO detection scheme should be the most effective, allowing to filter out the background contribution. However, this might be an additional experimental challenge since the primary target beam is also made of charged particles that must be filtered out.

We have recently performed a proof-of-principle experiment in a collaborative project between DESY and SOLEIL synchrotron, using a high-flux ESI source developed at DESY, coupled to the MAIA branch of the PLEIADES beamline at SOLEIL (Fig. 5). The ESI source included an ion funnel stage, an ion guide stage and a quadrupole  $m/z$  filter. The target was the ubiquitin protein ( $10^+$  charge state), and the photoelectrons were acquired in coincidence with the ionized precursor detected downstream the interaction region. The measurements showed that besides a high-flux ESI source, highly focused photon and ion beams, ultrahigh vacuum conditions in the interaction region and an efficient PEPICO detection scheme are necessary to perform such studies.

### 5.3 Concluding remarks

In conclusion, the ESI technique combined with the last generation synchrotron light sources and FELs offers great potential to study a plethora of complex systems therefore bridging the gap between condensed/liquid phase studies and gas-phase studies of well-defined small isolated targets. So far, such studies have been performed using ion traps and newly developed state-of-the-art experiments based on tandem mass spectrometry and action spectroscopy techniques. However, further progress is necessary to exploit the full potential of both the spectroscopic methods available presently at the synchrotron and FEL sources, and variety of target systems that can be produced by ESI. One possible direction is the development of a crossed-beam experimental setup, with a high-flux ESI source, alternatively coupled to pickup gas cells,  $m/z$  and ion mobility filters [55] (see Sects. 15, 19), delivering an intensive and well-focused target ion beam into ultrahigh vacuum conditions and coupled to state-of-the-art photoelectron and coincident analyzers.

**Acknowledgements** The authors would like to thank all colleagues and collaborators who, in the last decade, have made it possible to study complex gas-phase biomolecules during many beam times. S.B. acknowledges funding from the Initiative and Networking Fund of the Helmholtz Association through the Young Investigators Group program. A.R.M. acknowledges support by SOLEIL synchrotron.

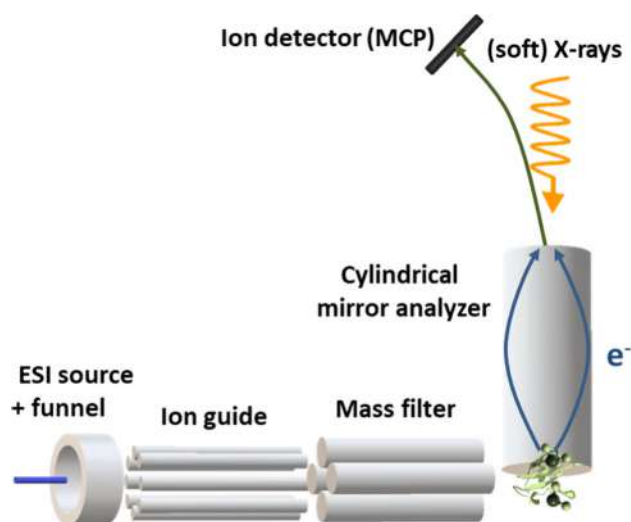


**Fig. 5** Simplified schematic figure of the ubiquitin protein photoelectron spectroscopy experiment performed at PLEIADES beamline, SOLEIL [56]

## 6 Simulating light-induced molecular dynamics in 2020: from the picosecond to the attosecond scale

Alicia Palacios, Departamento de Química, Universidad Autónoma de Madrid, Spain

Shirin Faraji, Theoretical Chemistry, University of Groningen, Netherlands

### 6.1 Status: description of the state of the art

Photo-induced processes lie at the heart of numerous natural phenomena, such as photosynthesis, human vitamin D production, circadian rhythm and visual response. In life sciences, optical technologies use light to visualize, detect and control biological processes in living tissues. These techniques include genetically encoded fluorescent proteins, biosensors and optogenetics. Furthermore, the world faces a rapidly increasing demand for sustainable energy, and thus, there is an enormous interest in understanding the mechanistic principles of photochemical reactions that convert sunlight into fuel. The interest in the mechanistic details of these phenomena motivated the development of sophisticated time-resolved spectroscopies, pushing further impressive advances in laser technology in the last half a century, which have enabled the real-time observation of such light-triggered processes. These techniques have rapidly evolved from the first picosecond pulse radiolysis system built in the late sixties to detect transient species in a chemical reaction, to the most recent attosecond pump-probe experiments that are able to measure time delays of a few attoseconds in the photoelectron emission from two different atomic shells [2, 3].

Time-resolved spectroscopic techniques have already given access to trace and manipulate a wide range of

physical processes at different timescales. For example, the light promoted isomerization and intramolecular proton transfer between amino acids in the retinal chromophore of rhodopsin have been identified and measured in femtosecond time-resolved fluorescence experiments, while conformational changes in the chromophore environment were found to proceed in the millisecond to the picosecond timescales [57]. The most recent experiments, combining isolated attosecond and femtosecond pulses, have demonstrated the existence charge migration in amino acids in the sub-femtosecond range, indicating how preceding light-induced electron dynamics dictates the nuclear rearrangements and eventual fragmentation paths [5, 11, 58]. Even in the simplest molecular targets, the complexity of the resulting spectra can only be unraveled by means of solid theoretical input. Primary photo-induced processes occurring in both nature or clean energy devices, in general, involve inherently quantum processes such as photovoltaics effect, electron-hole migration or electron transfer phenomena [59], which need to be treated in a full-quantum mechanical manner, which is still a demanding task. Theoretical methods are thus nowadays facing new challenges that can be encompassed in the investigation of the coupled effect between electronic and nuclear motions and in the need of high-level electronic structure calculations, in particular, when higher energy photons are involved and ionization is possible. The significance of these effects or the accuracy of the methodology required strongly depends on the light frequency, timescale (as illustrated in Fig. 6) and specific phenomena under inspection.

## 6.2 Challenges and new directions

Photo-induced molecular dynamics at room temperature has been widely described using ground state chemistry methods, where an independent and classical picture of nuclear motion in the fundamental state already provides an accurate description of the process. However, this ultrafast dynamics often involves multiple electronic states that come into play as nuclear motion proceed, through non-adiabatic couplings between electronic and nuclear degrees of freedom (DOFs) [60, 61]. More interestingly, the advent of optical pulses in the subfemtosecond time domain opens the door to the unexplored scenario of attochemistry, where the broadband of the pulse can already create coherently an initial wave packet built of sev-

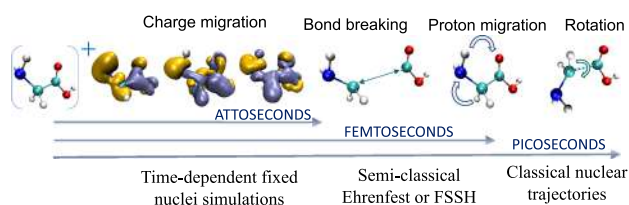


**Fig. 6** Illustration of different timescales for ultrafast processes occurring upon photoionization of glycine amino acid, and the theoretical methods employed to simulate them

eral electronic states. The theoretical strategies to time-resolve electron–nuclear dynamics then rely on two approaches, namely full-dimensional semiclassical molecular dynamics calculations and quantum wave packet propagation.

The most popular versions of the semiclassical approaches are the Ehrenfest formalism [62], where the forces felt by the nuclei are gradients of an average electronic surface, and the more accurate Tully’s fewest switches surface hopping (FSSH) [63], where transitions between electronic states are described by a stochastic algorithm. These methods have been successfully applied to retrieve dynamical information on relatively large systems; however, they fail to represent nuclear quantum effects such as tunneling, zero point energy and quantum decoherence. While zero point energy leaking and tunneling are important issues in ground-state dynamics, the geometric phase (a consequence of the existence of a conical intersection) is a multi-state quantum effect that is not taken into account in independent trajectory simulations [64]. Extended versions of FSSH pursue to overcome other important methodological limitations as describing superexchange population transfer [65], where two electronic states are coupled indirectly through an intermediate state with higher energy. FSSH also lacks the representation of transitions to high-lying states due to the missing classically forbidden transitions. This is relevant, for example, in describing electron-transfer mechanism, since electron transfer can proceed via the intermediate virtual state, which is hardly populated. Several extensions have been introduced to account for missing quantum effects in trajectory-based methods, as for the development of *ab initio* multiple spawning methods using Gaussian moving basis sets [66, 67], which are very promising approaches although the computational burden is considerably increased [64].

The second approach, a full quantum mechanical description of the molecular wave packet propagation, does not suffer from these drawbacks; however, it is limited by the exponential growth of computational resources as the number of DOFs increases [68]. With the current computational capabilities, a full-dimensional method that accounts for electrons and nuclei at equal footing is only possible for hydrogenic molecules [5]. A reliable alternative is the multi-configuration time-dependent Hartree method (MCTDH) method which solves the TDSE by a variational method and has been successfully applied for targets up to few tens of degrees of freedom [58, 68, 69]. In particular, its multilayer variant which enables the treatments of larger systems [70]. Although it still scales exponentially, the computational effort is greatly reduced by using time-adaptable single particle functions to construct a set of Hartree product configurations. By increasing the number of configurations, the MCTDH method converges to the numerically exact solution, while keeping the computational effort closer to a semiclassical picture. Additionally, to break the exponential scaling further and to remove the restrictions of the grid, the wave packet can be expanded

over localized traveling basis functions of Gaussian shape that are variationally optimized and do not follow classical trajectories, known as variational multi-configuration Gaussian (vMCG) approach [71].

However, as for the mean-field and surface-hopping methods, its accuracy and computational efficiency remain bounded to the model potentials or the quantum chemistry method employed to describe the electronic structure. Since the introduction of Hartree–Fock theory almost a century ago, wave function-based *ab initio* methods have greatly evolved and a large manifold of post-Hartree–Fock methods accounting for electron correlation terms (Configuration Interaction, Coupled Cluster, Moller–Plesset perturbation theory or MCTDH) are available in most commercial (e.g., Q-Chem, Gaussian, MOLCAS, MOLPRO) and open-access (e.g., OpenMOLCAS, GAMESS, NWChem) software packages for chemistry simulations. When the exponential wall makes wave function methods impracticable, density-based methods are the only available choice. Density functional theory (DFT) methods include electron correlation through exchange-correlation functionals, still by means of a single Slater determinant that, in practice, limits its applications to describe singly excited electronic states. Even though DFT methods are known to underestimate barriers of chemical reactions, dissociation energies in ions or charge transfer excitation energies, and overestimate binding energies, they have shown to work remarkably well for structural and thermodynamics properties.

Despite the manifold of quantum chemistry packages currently available for electronic structure calculations of complex molecules isolated in the gas phase, further theoretical efforts are still required to account for photo-induced phenomena where electron correlation plays a critical role, such as core-hole states leading to Auger decay or multiple excited bound states leading to autoionization [58]. Moreover, deep insights on molecular photoionization problems can only be achieved by properly describing the electron in the continua coupled to the remaining ion, for which a scattering formalism is required [5]. These phenomena arise when molecules are exposed to highly intense field or to frequencies in the extreme ultraviolet (XUV) and X-ray range as produced in by high-order harmonic generation set ups [3, 12] and free electron lasers (FEL)[13, 24, 27], i.e., sources that are able to produce coherent light pulses with durations in the attosecond scale and wavelengths in the atomic size. The newest FEL facilities have been built with the promise of using this highly coherent ultrashort and intense light to probe matter in an unprecedented and unique way, for instance, measuring structural changes in proteins and enzymes before radiation damage occurs or resolving the structure of single biological particles prior crystallization [72]. More importantly, these sources can access fundamental processes that are still to be understood even in the simplest molecules. From the theoretical side, time-dependent scattering methods that provide an explicit evaluation of the electronic continuum wave function are nowadays under development. Above-mentioned

bound-state methods have been employed the definition of the Dyson norm, resulting from a direct projection of states from the neutral molecule to the cation [73], as a very approximated value to the ionization yield. More elaborated approaches describe the continuum electron using Coulomb functions, thus accounting for the long-range part of the potential, although still are unable to reproduce the multicenter character of a molecular potential. The most sophisticated methods are based on Schwinger or complex Kohn variational principles or on close-coupling approaches as those implemented in Lippmann–Schwinger, R-matrix, Galerkin, ePolyScat, XCHEM or the most recently developed algebraic diagrammatic construction (ADC) scheme ([5, 58, 60] and references there in). These methods commonly incorporate discrete variable representation (DVR) or B-spline functions to properly represent the long-range part, combined with a representation using Gaussian or Slater-type orbitals implemented in standard quantum chemistry packages for a more efficient representation of the bound part of the wave function. These methodologies have been first applied to atoms with great success. The complexity introduced by the nuclear motion DOFs limits most of the existing applications in large molecules to calculations within the fixed nuclei approximation, although first attempts to include nuclear motion are under progress [60].

The ongoing developments of theoretical tools employed in gas-phase photochemistry come together with novel implementations to treat biological systems in their natural environment, i.e., in a solvent. These same tools can be employed to simplify the description of large-size targets as DNA or proteins, where one can concentrate on an active molecular site of the system and treat the remaining part as a solvating environment. This is the essence of the multi-scaling approaches such as hybrid quantum mechanics/molecular mechanics (QM/MM) [74]. The outcomes of QM/MM simulations depend crucially on the choice of the QM region, and one needs to carefully investigate convergence of the results with regard to the size of a QM region. Additionally, the short timescales accessible for QM/MM molecular dynamics (MD) simulations generally do not allow to investigate processes that occur on longer timescales (e.g., nanoseconds). Thus, one is restricted to performing transient dynamics along previously chosen reaction coordinates that requires some system-specific information on describing the underlying process. The identification of the relevant coordinates is not straightforward since there are many nuclear DOFs in large systems. These ambiguities may well be the origin of the many different conflicting theoretical hypotheses proposed for a given process [75].

### 6.3 Concluding remarks

*Ab initio* theoretical methods enable a rational design of novel molecules and materials. Moreover, ongoing and forthcoming applications using the newest



laser technologies to explore gas-phase molecules are strongly pushing theory toward the development of full-dimensional quantum wave packet time-dependent approaches. In pursuing this goal, trajectory-based ground- and bound excited-state chemistry simulations move forward to incorporate a quantum description of the coupled electron–nuclear dynamics in processes occurring in the femtosecond to picosecond timescales, where the nuclei move significantly upon excitation involving several electronic states. On the other hand, sophisticated quantum chemistry packages using multi-reference approaches are being implemented in scattering-based approaches born in the area of atomic physics to describe XUV and X-ray-induced excitation and ionization of large molecules. These methods are only available within the fixed nuclei approximation, which can already account for the ultrafast electronic processes accessible in state-of-the-art attosecond experiments. However, the proper description of the subsequent nuclear arrangements and fragmentation paths requires of further developments.

The scalability of these methods to larger molecules, e.g. a typical chromophore has around 30 heavy atoms, is, however, limited to the current computational capabilities. New directions are being taken to overcome this limitation. Among those, it is worth to mention the long awaited availability of quantum computers, for which quantum algorithms, with scalabilities that can reach up to hundreds of DOFs, are under development for the simulation of structural and dynamical properties of molecules [76]. Alternative strategies to efficiently compute electronic structure in large molecules are based on machine learning [77] and artificial intelligence (neuromorphic computing and robotic technologies) [78]. In recent years, computational statistical learning methods (machine learning, neural networks, deep learning, unsupervised clustering, etc.) have found to provide very promising approaches to construct potential energy surfaces and have been successfully applied for both ground-state molecular dynamics simulations and (non-adiabatic) excited-state simulations [79]. Although by using those fitted potentials, the computational time for molecular dynamic simulations can be substantially reduced, the generation of the training data, which samples the important regions of the conformational space [80], still remains a big bottleneck.

**Acknowledgements** Shirin Faraji is thankful to Innovational Research Incentives Scheme Vidi 2017 (016.Vidi.189.044) financed by the Dutch Research Council (NWO). AP acknowledges support from the *Ministerio de Ciencia e Innovación* in Spain through Project PID2019-105458RB-I00 and a *Ramón y Cajal* contract.

## 7 Experimental techniques for low-energy reactions of charged species

Daniela Ascenzi, Department of Physics, University of Trento, Italy

Claire Romanzin, Institut de Chimie Physique, Université Paris-Saclay, France

### 7.1 Status: description of the state of the art

Low-energy ion–molecule reactions root from the very origins of mass spectrometry and positive rays’ studies, in the first years of twentieth century. It has developed in a strong field of research through the century, building from the development of advanced instrumental techniques for ion production, transport and energy definition, specific neutral sample production, optimization of their interaction region and quantitative detection methodologies, including the determination of the internal state distribution of products. The variety of ion–molecule reactive systems studied so far is vast, ranging from organic to organometallic species and biomolecular systems, but also from singly and multiply charged positive and negative ions to ionic clusters. Unravelling the role of reactions involving charged species permits to tackle fundamental questions in astrochemistry, organic and inorganic reaction mechanisms, biochemistry and catalysis. Beyond the fundamental interest on reaction dynamics, the quantitative outputs from these experiments, namely branching ratios, kinematic constants or cross sections and thermochemical information (tabulated in the form of extensive databases) are beneficial to models describing the behavior and evolution of plasmas of all sorts, from astrophysical media (e.g., [81] and refs therein), to flames or laboratory and industrial plasmas.

It is beyond the scope of this short section to provide an exhaustive review of the field, but we wish to mention here the main tools that have been developed to study the so-called low energy ion–neutral reactions, i.e., reactive collisions where collision energies range from fractions of meV to about 100 eV (for interactions at higher collision energies see Sect. 8). Indeed, it is nowadays possible to reach collision energies in the mK regime! We will describe here after aspects related to ion generation and selection, interaction region with the neutral partner, products detection and correlation.

Everything starts with the ion generation. If electron impact is a longstanding and universal ionization method, other methods are widely used for their remarkable specificities. Photoionization, via lasers or synchrotron radiation, is particularly adapted to control the energy deposition within the reactant ion, thus paving the way for state-specific reactivity. Soft ionization techniques based on chemical ionization (i.e., ion–molecule reaction) have also emerged and are now standard analytical tools. This is, for instance, the case of proton transfer reaction mass spectrometry (PTR-MS), a technique that was introduced and optimized for



quantitative trace gas analysis and which is now daily used by thousands of users, with special reference to atmospheric sciences ([82], and refs therein). Yet, when one thinks about “soft ionization,” electrospray ionization (ESI) technique comes first and it is the method of choice to deliver in the gas-phase large (positively and negatively) charged molecules such as biomolecules, as detailed in Sect. 5.

Considering the interaction region between the ion and the neutral partner, the panel of experimental arrangements is large. One of the most popular and versatile is the selected ion flow tube (SIFT) technique, in which a flow of mass selected ions driven by a carrier gas reacts with a neutral target added downstream. The density of carrier gas guarantees thermal equilibrium of the target ion, thanks to multiple collisions with the non-reacting buffer gas, while the kinetic behavior of the flux allows for distance/time extraction of reaction rate coefficients and product branching ratios. The possibility to cool or heat up the buffer permits to measure rates as a function of temperature. This is illustrated in a recent work [83] where a laser vaporization ion source is coupled to a variable temperature (in the range 300–600 K) SIFT setup to generate  $\text{MgO}^+$  ions and study their reactivity with  $\text{CH}_4$ , a system of potential interest in the catalytic activation of methane. The experimental results show counterintuitive behavior of reduced yield for the most exoergic channel, underlying the importance of reaction dynamics and theoretical calculations to interpret the reactivity of such “simple” systems.

A revolution in the field came with the ability to handle slow charged ions by confining them via fast oscillatory electric fields. The development of radiofrequency (RF) multipolar ion guides has led to guided ion-beam (GIB) setups where collisions with neutral targets take place in a scattering cell. This experimental arrangement permits to measure cross sections that are more informative on the reactive process than measurements of thermally averaged rate coefficients [84]. It should be noted at this point that an alternative way to trap ions for gas-phase molecular dynamics study is by electrostatic ion-beam traps, as detailed in Sect. 15.

GIB is a natural 2D ion trap, but going 3D leads to great benefits. Paul traps (such as those described in Sect. 18) or Fourier-transform ion cyclotron resonance (FT-ICR) is conventional tools to evaluate ion–molecule reactivity. Multipolar ion traps such as the 22-pole trap have become, in its cryogenically cooled version, a standard tool for the measurement of rate constants of low-temperature astrochemically relevant reactions of cations and anions [85, 86]. The quest to gain insights into fundamental aspects of chemical reactions has stimulated the development of molecular beam-based devices: Crossed-beams apparatuses remain forefront techniques to measure product differential scattering cross sections at variable collision energies that can be reduced by adopting lower crossing angles or merging supersonic beams onto a single axis (merged beams, see below). Coupling crossed-beam experiments with velocity map ion imaging techniques

reveals correlation between products, thus allowing a detailed reconstruction of the reaction dynamics [87].

While this short review focuses on experiments, one should not forget that a close interplay with theory is essential. Theoretical methods can fill the gaps when experimental limitations preclude laboratory studies, and conversely, the production of high-quality experimental data is fundamental to benchmark theoretical studies and guide their development. Due to computational limitations, the vast majority of ion–neutral reaction systems comprising more than three atoms are treated by combining full quantum ab initio calculations of the potential energy hypersurface with quasi-classical trajectory methods (see, for instance, [88, 89]), while collisions involving biomolecular ions require classical trajectories and molecular mechanics [90, 91].

## 7.2 Challenges and new directions

In spite of the large amount of experimental technologies available to investigate low-energy ion–molecule reactions, there are three main aspects that are facing various challenges and on which researchers are concentrating their efforts: (i) extending the studies to reactions between ions and unstable neutrals (excited atoms, molecules or radicals); (ii) reaching an extreme control in quantum state selectivity of the reagents; and (iii) reaching low and ultralow collision energies and/or temperatures.

*Reactions with unstable neutrals* While reactivity between charged species and stable neutrals has been widely addressed, the reaction with atoms/molecules in excited states as well as with radicals is still largely unexplored, despite their relevance in natural plasmas and biological environments (free radicals and ions are highly reactive intermediates formed upon interaction of ionizing radiation with living cells). A way to prevent recombination/decay of the short lived species prior to reaction is to inject them in the buffer gas of a SIFT instrument. In this way, reactions of H, N and O atoms,  $\text{O}_2(^1\Delta_g)$ , organic radicals (e.g.,  $\text{CH}_3$ ,  $\text{C}_2\text{H}_5$ ) have been studied with several cations and anions, including species of biological relevance such as deprotonated nucleobases, amino acid anions, sulfur containing anions, heterocyclic and aromatic anions (see, for instance, Ref. [92]).

*Quantum state selection* How chemical reactions are influenced by the electronic, vibrational and rotational excitation of the reactants is a long-standing issue in chemical reaction dynamics. Understanding how the initial quantum states of the reactants or their structures (i.e., isomers) drive the reactivity is also relevant to correctly model complex media such as plasmas or planetary ionospheres in which excited species and isomers are present. Photo-excitation with lasers or synchrotron radiation associated with various experimental setups (crossed beam, GIB or 3D trap) and ion detection techniques is a method of choice to induce specific population of reactants and to control the internal energy of either the neutral (see, for instance, [87] where

vibrational excitation of the neutral partner is achieved using IR laser) or the charged species [93–97]. Quantum state selectivity of atomic and molecular cations can be obtained using threshold photoelectron–photoion coincidence (PEPICO) techniques, in which the time coincidence of ions with electrons having near zero kinetic energy allows to prepare vibrationally and electronically state-selected ions. Such techniques exploit the high tunability of synchrotron radiation (see Sects. 4 and 5 for synchrotron radiation tools for spectroscopic and dynamical processes) and are used, for instance, at the VUV beamline of SOLEIL synchrotron facility, to study state-selected reactivity in a GIB apparatus on which absolute reaction cross sections are measured, as a function of both the ion excitation and the collision energy [93]. Recent developments also allow to generate state selected molecular ions from beams of clusters or radicals [94], thus widening the range of possible studies, in particular to characterize the role of micro-solvation and isomer-specific reactivity [95].

Alternatively, a double quadrupole–double octopole ion–molecule reaction apparatus has been coupled with high-resolution visible–ultraviolet laser pulsed field ionization–photoion methods to study the reactivity of molecular ions (e.g.,  $\text{N}_2^+$ ,  $\text{O}_2^+$ ,  $\text{H}_2^+$  and  $\text{H}_2\text{O}^+$ ) in selected electronic, spin–orbit and ro–vibronic states; more recently the addition of a pulsed laser ablation ion source has extended the studies to spin–orbit state selected transition metal cations (see [96] for the vanadium case). Even more challenging than studies on the role of excited states in cation–neutral reactions are those dealing with excitation of anions, since very rarely atomic anions have bound excited state. A very recent advance is represented by a photoelectron energy spectrometer equipped with a cold octopole RF ion trap to study the reactivity of ground and excited state palladium anions with  $\text{H}_2$  [97].

*Low and ultralow collision energies/reaction temperatures* One of the main experimental challenges in ion–molecule studies is the possibility to reproduce in the laboratory the low temperatures (down to few tens of Kelvins) of naturally occurring cold environments such as the interstellar medium. Recently, noticeable works were presented, developing a SIFT-like injection system for a supersonic flow setup (CRESU) [98], reaching temperature as low as 49 K and opening a new field of applications of CRESU-type instruments for ion–molecule reactions. Similarly, the use of cryogenic 22-pole trap setups with buffer gas cooling has proved effective to study reactions of both cations (e.g.  $\text{H}_3^+$ ,  $\text{O}^+$ ,  $\text{OH}^+$ ,  $\text{CH}^+$ , etc.) and anions (e.g.,  $\text{H}^-/\text{D}^-$ ,  $\text{O}^-$ ,  $\text{OH}^-$ ,  $\text{NH}_2^-$ , etc.) with simple molecules (e.g., ortho and para  $\text{H}_2$ ) as well as H/D atoms from room temperature down to about 10 K (for a recent example, see [85]). By coupling 22-pole traps with IR lasers, the effect of vibrational excitation of the molecular ion on reactivity at low temperatures is possible, revealing unexpected behaviors such as the decrease in the reaction rate due to ro–vibrational excitation [86].

An emerging frontier is represented by collisions at temperatures  $< 10$  K. Reaching such ultralow collision energies/temperatures with ions is particularly challenging, primarily because ions can be “heated up” by stray electric fields, thus reducing the collision energy resolution. New methodologies are in their development phase, and the interested reader is referred to two recent reviews on the chemistry at ultralow temperatures that include sections dedicated to charged systems [99,100]. Alternative novel techniques using electrostatic ion-beam storage rings to measure reaction rates at low temperatures are discussed in Sect. 13. Two of the most promising developments employ an improved version of the merged beam technique and the phenomenon of coulomb crystallization of ions in a trap. In the first case, ultralow collision energies in the range between 0 and  $30 \text{ K} \cdot k_B$  have been obtained using highly excited Rydberg atoms or molecules in place of the ions. (The Rydberg electron shields the ionic core from stray field, but it acts as a spectator and does not affect the reactivity.) The ultralow energies are reached by merging a supersonic beam of the neutral in its ground state with a second supersonic beam of the Rydberg atom or molecule translationally cooled using a surface-electrode Rydberg–Stark decelerator and deflector. The technique has been used so far to investigate the reaction of  $\text{He}^+$  with  $\text{CH}_3\text{F}$  and, more recently, of  $\text{H}_2^+$  with HD [101].

The second breakthrough is the possibility to generate cold molecular ions by sympathetic cooling of charged species with laser-cooled atomic ions in Coulomb crystals. These are formed when laser-cooled, trapped atomic cations reach low enough temperatures to produce ordered structures. Studies of ion–atom interactions over a temperature range that can extend down to tens of  $\mu\text{K}$  have become feasible thanks to the development of hybrid trapping techniques, i.e., the combination of traps for ions (such as linear Paul traps) and atoms (magneto-optical traps). The co-trapping of molecular ions within the Coulomb crystal cools the ions to translational temperatures similar to the laser-cooled atomic ions [102]. Coupling cooled molecular ions with cold neutral sources (e.g. supersonically cooled molecular beams slowed down using Stark decelerators) will extend the study of state-to-state chemical reactions to more chemically complex systems, with control over all reaction parameters.

### 7.3 Concluding remarks

The future will see an increase in the molecular complexity of the ion–neutral reaction systems probed under controlled conditions, by developing spectroscopic methods to sensitively detect the internal energy content of product ions and by finding new ways to overcome some of the limitations with the current techniques. The big challenge will be to combine existing tools in new ways to study systems of increased complexity and broad chemical interest. Moreover, as the understanding of reaction dynamics goes together

with a close interplay between theory and experiments, advanced theoretical methodologies will be essential to guide the interpretation and rationalize the experimental results.

**Acknowledgements** We thank Roland Thissen and Christian Alcaraz (Institut de Chimie Physique, Université Paris-Saclay) for their help during manuscript elaboration.

## 8 Interaction of keV ions with complex molecules and their clusters

Dariusz G. Piekarski, Institute of Physical Chemistry, Polish Academy of Sciences, Warsaw, Poland

Patrick Rousseau, Normandie Université, CIMAP, Caen, France

### 8.1 Status: description of the state of the art

*Fundamental processes* During the interaction, the projectile charge and energy determine the final charge and energy states of the molecular target (see Fig. 7a). An ion projectile with keV kinetic energy is considered as slow with respect to the velocity of the electrons in the target. Thus, the electron capture is the dominant charge transfer process in which one electron of the molecule is captured by the incoming ion after lowering of the Coulombic barrier by the projectile charge [103]. This resonant charge transfer can occur at large distance in the case of multiply charged ion collisions, and therefore, multiple electron captures are usually observed leading to the formation of “cold” multiply charged molecular cations [104]. Thus varying the charge state of the projectile, the excitation energy associated with keV ion collisions ranges from few eV [105] to few 10s of eV [106]. When the ion trajectory is penetrating the molecular system and as the projectile is a massive particle, energy can be deposited both on the electrons by friction with the electronic cloud, the so-called electronic energy loss, and on the nuclei in binary collisions, the so-called nuclear energy loss. In the latter case, the energy transfer is localized on specific bonds of the molecule and can lead to prompt and specific non-statistical fragmentation schemes [107].

*Ion–molecule collisions* In ion–molecule collision due to charge exchange and energy deposition from the projectile to the target, the latter undergoes ionization, excitation and eventually fragmentation processes (see Fig. 7). The *quasi*-symmetric fission for doubly charged species is typically known as Coulomb explosion (CE). Detailed studies of isolated positively charged biomolecules like amino acids, nucleobases and their derivatives have been recently investigated by collaborative theoretical and experimental works by means of molecular dynamics (MD), potential energy surface (PES) and coincidence mass spectrometry techniques

(see Fig. 7b, c). Further details on calculations are given in Sect. 9.

Another approach that implements classical molecular dynamics simulations to study irradiation processes in particular applied to focused electron beam deposition of tungsten hexacarbonyl  $W(CO)_6$  precursor molecules on a hydroxylated  $SiO_2$  surface has also been proposed [108]. The combination of parameterized interatomic potentials with MD and reactive force fields allowed to study the dissociation processes at timescales up to hundreds of nanoseconds for few hundreds of  $W(CO)_6$  molecules. For the same system, very good agreement with the experiments was achieved by including the Monte Carlo (MC)-type simulations for the electron transport in these materials [109]. It was possible to unambiguously identify unexpected mechanisms behind the fragmentation patterns observed experimentally. Such unexpected reactivities initiated by the capture of two (or more) have been observed as a stabilization effect of the isomerization (H, OH migration and cyclization) leading to the metastable resistance against the expected CE. For instance, the ultrafast H migration competes with the CE within the first 40 femtoseconds leading to the stable dication of diol for glycine [110]. keV ion impacts on  $\alpha$ - and  $\beta$ -alanine led, respectively, to  $H_3^+$  emission [111] and hydroxyl group migration [112]. Metastable, long-lived dicationic species, including reactive nitrogen and oxygen species (RNS and ROS), were observed either due to the presence of the peptide bond for N-acetylglycine [113] or due to long chain in amino acids like  $\gamma$ -aminobutyric acid [114]. Proton transfer was also observed between sugar- and base-part of thymidine in competition with the expected glycosidic bond cleavage [105]. The above-mentioned unexpected dissociation pathways are expected to be found for many other systems, for which the reactivity is triggered by the keV ion impact [106].

Recently, Erdmann et al. [115] efficiently combined the PES, MD and MC for description of the irradiation driven chemistry. Chemical transformations induced by another sources such as (i) X-ray in the mixed water–ammonia clusters focusing on the microscopic observable [116] and (ii) electron impact showing H-migration in ethanol [117] were efficiently combined with PES and MD methodology. Interesting reactivity driven by low-energy atomic and molecular ions formed by galactic cosmic rays in the Earth’s atmosphere of highly oxygenated molecule has been studied focusing on both microscopic and molecular level understanding of nucleation, binding, evaporation, thermal effects, etc. of various clusters [118].

*Ion–cluster collisions* While gas-phase experiments on isolated molecules give access to the intrinsic properties of the molecular systems, weakly bound molecular clusters allow to study the effect of a simple chemical environment on those properties. On the one hand, the cluster can act as a buffer dissipating the excess of energy due to the collision by successive losses of monomer units, and thus, an overall reduced molecular dissociation is observed [104], and this reduction is

even larger in the case of hydrated clusters [119]. This is due to the fact that the weak intermolecular bonds between the cluster constituents break preferably to the intramolecular covalent molecular bonds. Interestingly, the weak interaction between cluster components could also lead to additional fragmentation channels involving atoms participating in the H-bonding [119]. In the case of multiply charged clusters, the Coulomb repulsion between fragments could also be partly converted into internal energy, and therefore, a more important molecular dissociation is observed [104]. On the second hand, beside being a buffer for energy, the cluster can also act as a reservoir of matter, and thus, a reactivity inside of the cluster can be observed when a reactive fragment is produced within the cluster. In H-bound clusters, after ionization, a proton transfer occurs in several 10s of femtosecond (fs) before the cluster dissociates and protonated clusters are observed [119]. In van der Waals cluster of carbonaceous molecules such as fullerenes and polycyclic aromatic hydrocarbons (PAHs), a rich molecular growth has been observed due to the massive aspect of the projectile. In binary collision, the incoming ion can kick out a single atom from a molecule leading to prompt (fs) non-statistical dissociation channels [107] and to highly reactive species. Since the latter are surrounded by other residues in the cluster, they can further react with neighboring molecules to produce new covalently bound species as observed in clusters of PAH [120], fullerene [121] or a mixture of PAH and fullerene [122]. The very good agreement between experimental mass spectra and classical molecular dynamics simulation validates the proposed scenario. Recently, the formation of polypeptides from amino acid clusters has been reported [123]. The formation mechanism has been explored by quantum chemistry calculations. There the initial step is the protonation of the clusters after ionization which stabilized the clusters and allows further reactivity leading to the formation of peptide bonds between the cluster constituents.

## 8.2 Challenges and new directions

Unexpected mechanisms appear when the complexity of the molecular systems increases such as in peptides or proteins. However, bringing into the gas phase such targets is not possible by thermal evaporation. Pioneering keV ion collisions experiments have been done using electrospray ion sources to produce gas-phase peptides [124] or proteins [125]. However, the target beams produced are not dense and an ion trap is required to enhanced the target density. A step further will be to perform the usual crossed-beams experiments with more intense target and projectile beams. Considering the effects of the environment in ion-cluster collisions, so far the experiments have been performed with a size distribution of clusters. In order to get better insight into the threshold sizes associated with different mechanisms such as the molecular growth, size-selected targets are necessary. Again low-density target beams are expected and such experiments are challenging. Finally, as shown in Fig. 7, according to the molecular dynamics different timescales are associated with the different mechanisms discussed above. Thus, time-resolved ion-molecule collision experiments are very interesting as keV ion beams are a very peculiar pump compared to photons. However, due to the low density of ion beams produced by conventional ion accelerators such pump-probe experiments at least on the shortest timescales are kind of Grail quest. Nevertheless, pump-probe experiments at longer timescale ( $\mu\text{s}$ ) may be considered coupling an ion accelerator with an electrostatic storage devices such as a linear trap or a storage ring (see Sects. 13, 14 and 15).

## 8.3 Concluding remarks

In the last decade, the numerous combined experimental and theoretical efforts showed the roadmap to

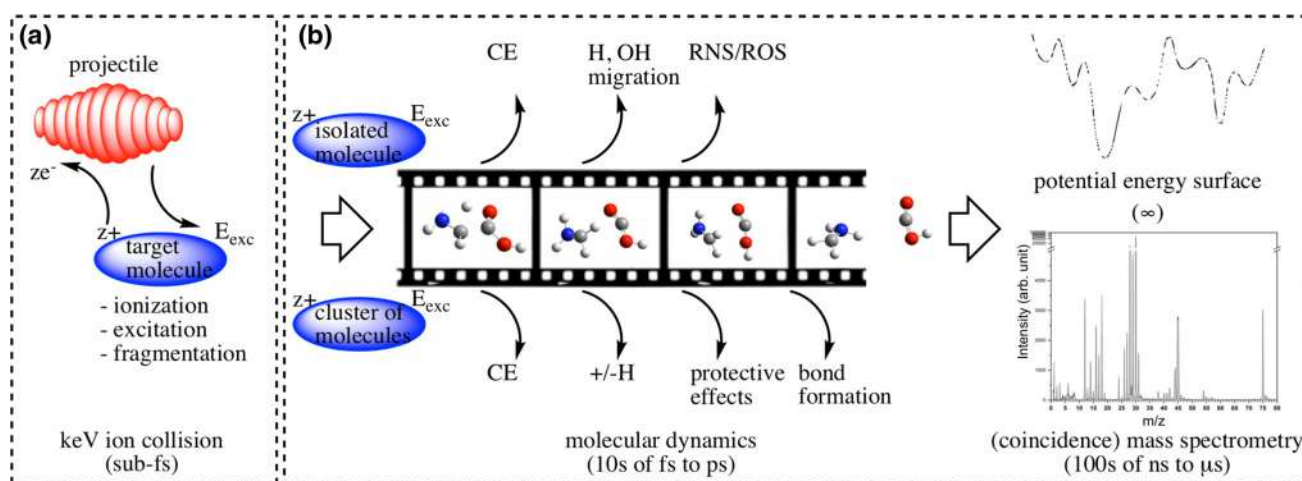


**Fig. 7** Scheme of physical processes observed for both isolated and cluster of molecules in keV ion-target collisions



unravel the processes driven by keV ion collisions on complex molecular systems. It was possible to divide the physical processes into accessible time domains (see (a) and (b) in Fig. 7) and to cross-validate the experimental and theoretical observable by mass spectrometry and MD/PES simulations, respectively. This allows unambiguously to identify and to explain in detail the extremely fast and very slow physical events (see Sects. 6, 9). In the near future, more complex systems can be studied by means of electrospray ion source techniques as well as more efficient methodologies and accurate electronic structure methods accounting for the highly charged, large and weakly bound systems.

## 9 Modeling molecular fragmentation

Ewa Erdmann, Faculty of Applied Physics and Mathematics, Gdańsk University of Technology, Gdańsk, Poland

Manuel Alcamí, Departamento de Química, Facultad de Ciencias, Universidad Autónoma de Madrid, Spain

### 9.1 Status: description of the state of the art

Ionizing radiation interacting with molecules in the gas phase can induce numerous processes, including electronic transitions (electronic excitation, charge transfer and ionization) and nuclear excitations (rotation, vibration and fragmentation of the molecule). Understanding the fragmentation processes induced by photons, electrons and ions is crucial to many disciplines such as radiation cancer therapy, astrophysics, astrochemistry, plasma physics and atmospheric science. In this section, we highlight theoretical approaches aimed to describe molecular fragmentation processes in the gas phase and present an outlook for future studies in this field. Theoretical approaches to modeling decay processes that take place in competition with fragmentation, such as radiative cooling and delayed electron emission, are reviewed in Sect. 16. The theoretical models used to describe light-induced intramolecular electronic processes that occur in a shorter scale prior to fragmentation are reviewed in Sect. 6.

The large number of electronic and nuclear degrees of freedom involved in the study of molecular fragmentation represents the main challenge to use fully quantum mechanical methods. One of the main approximations usually needed is to consider that all electronic processes involved in the excitation of the molecule are much faster than the fragmentation and therefore the latter is treated as a post-collisional process. Fragmentation is thus considered as a relatively slow process in which excess energy is transferred to dissociative nuclear degrees of freedom. Various methodologies for studying molecular fragmentation have emerged ranging from quantum chemical, semiempirical to statistical, their applicability strongly depends on the size of the system and the timescale needed for dissociation.

The most challenging situation is when after the excitation the system is located in a highly excited electronic state. For instance, after photoemission of a core electron, Auger decay can leave the system in a doubly charged state in which electrons have been removed from inner orbitals. In this case, fragmentation dynamics starts at the same time as electronic relaxation and movement of electrons and nuclei should be considered simultaneously. Non-adiabatic molecular dynamics (see [126] and references therein) simulations are used to describe molecular fragmentation of such systems. Particularly, time-dependent density functional theory (TDDFT) molecular dynamics in the Ehrenfest formalism allows to self-consistently model both electronic and vibronic excitations. In practice, such simulations are limited to simulation times of around few hundred fs mainly due to the very small time step necessary for correct propagation of the electron dynamics. Timescale of the fragmentation process usually falls in the range of ps. However, once the system has relaxed to the ground state, further evolution can be treated with Born–Oppenheimer molecular dynamics (BOMD). With this theoretical approach, López-Tarifa et al. [61] were able to determine the effect of ionization of different molecular orbitals on the fragmentation of doubly ionized uracil molecule produced in collisions with 100 keV protons. A good agreement with the 2D time-of-flight ion coincidence spectrum was obtained, reproducing the most intense coincidence islands and their shapes.

Another approach is to assume that fragmentation occurs in the ground electronic state and the system follows the lowest energy pathway. This has been adopted in many theoretical studies employing different methodologies. One successful theoretical approach relies on the combination of *ab initio* molecular dynamics (AIMD) simulations in the ground state and exploration of the potential energy surface (PES) with density functional theory (DFT). Such methodology works under the assumption of efficient redistribution of the excitation energy across all vibrational degrees of freedom, so that excess excitation energy can be introduced as internal vibrational temperature in a molecule in an electronic ground state. In order to mimic the sudden ionization, the simulations consider vertical transition. The computational cost of the simulations mainly depends on the particular AIMD methodology used. For instance, efficient implementations, as the atom-centered density matrix propagation method (ADMP), allow to run hundreds of trajectories with simulation times of the order of few hundred fs in systems of the order of a dozen atoms. These dynamics allow to evaluate, for different internal energies, the relative importance of different channels as Coulomb explosions, isomerization or combined isomerization + fragmentation, and to identify intermediates that many times would not be envisaged following chemical intuition. Once the most relevant intermediates have been identified, they can be studied in detail using DFT methods to obtain their energetics and structural properties. Also transition states connecting different intermediates can



be located, providing a general view of the PES, the lowest energy pathways and the corresponding energy barriers. All this information is extremely valuable for a correct interpretation of experiments. Combination of ADMP simulations and PES exploration has been successfully applied, e.g. to predict unusual hydroxyl migration induced by 48 keV  $O^{6+}$  collisions with  $\beta$ -alanine [112].

For larger systems and/or longer simulation times, AIMD can be replaced by the self-consistent charge density functional tight binding (SCC-DFTB) method [127]. As previously mentioned, maximum simulation times available for quantum chemistry molecular dynamics are of the order of few ps; however, those can be extended until a nanosecond with SCC-DFTB methodology and still provide reliable results [128]. Purely classical molecular dynamics simulations are suitable for modeling fragmentation of more complex molecular systems and at longer time scales (ns) if adequate many-body force fields are included. Investigation of chemical bonding without expensive quantum mechanical calculations is attainable, e.g., with the Adaptive Intermolecular Reactive Empirical Bond Order (AIREBO) potential [129] implemented in the LAMMPS software package [130]. In addition to LAMMPS, several molecular dynamics codes are available, one of them being NAMD [131]—an open-source software designed for high-performance simulations of large biomolecular systems.

It has been shown that under certain experimental conditions, ion impact can induce bottom-up processes of molecular growth by species produced in a cluster fragmentation covalently bonding with other molecular fragments or intact monomers. Such reactions are of great importance among others in the fields of astrophysics and the atmospheric sciences because they constitute possible ways of formation of PAHs and fullerenes in space or formation of aerosols in the atmosphere. From a theoretical point of view, ion-cluster collisions have been typically modeled with classical molecular dynamics simulations due to high complexity of those systems (as many as few hundred atoms). Importantly, such theoretical approaches are only able to model neutral systems. For large molecules with many delocalized electrons (e.g., fullerenes), exclusion of charges is thought to have minor effect on the MD results. However, for clusters of smaller molecules inclusion of charges, e.g., with SCC-DFTB method, might improve the predictions of molecular properties. In the case of 12 keV Ar collision with pyrene clusters [120], this method has been applied in a simplified manner (only for trajectories that resulted in molecular growth and included only the reacting fragments identified in the classical calculations). DFTB simulations reproduced the classical simulations results quite well, but at higher temperatures DFTB molecular dynamics simulations predicted easier bond cleavages than simulations of classical molecular dynamics.

One interesting modification of classical molecular dynamics simulations adequate to study complex

molecular systems over nanosecond timescales consists in the introduction of random and local modifications of the classical force fields to account for chemical transformations, i.e., bond cleavages/formations, dangling bonds and changes in molecular topology of the system. Such approach allows to study irradiation driven chemistry—a family of chemical modifications induced by irradiation with external fields. This methodology called Irradiated Driven Molecular Dynamics (IDMD) [108] has been implemented into the MBN Explorer software package [132] and applied to the study of focused electron beam deposition of tungsten hexacarbonyl  $W(CO)_6$  precursor molecules on a hydroxylated  $SiO_2$  surface demonstrating its potential to describe complex dynamics and nanostructure formation and growth [109].

Statistical methodologies such as Weisskopf theory, the RRKM Theory of Unimolecular Reactions and Microcanonical Metropolis Monte Carlo method also play a key role in the investigation of fragmentation processes due to significantly reduced computational cost with respect to molecular dynamics. In the study of  $C^{6+}$  collisions with  $C_{60}$  [133], the rate constants for  $C_2$  and  $C_2^+$  emission from the excited and charged fullerene were calculated within the Weisskopf formalism and subsequently used to evaluate the fragmentation dynamics. The fundamental RRKM theory is widely applied in photodissociation or thermal decomposition studies to predict molecular fragmentation rate constants. In order to produce a breakdown diagram, one needs to locate all rate-limiting transition states, which is generally a formidable task in systems with large number of nuclear degrees of freedom. However, a recently developed transition state search using chemical dynamics simulations (TSSCDS) methodology [134] shows promising results for global and automatic location of stationary points of a PES with semiempirical accelerated dynamics simulations and is now implemented in the AutoMeKin code [135]. Combination of TSSCDS with chemical dynamics simulations (implemented in the VENUS package) has recently allowed for correct prediction of fragmentation patterns involved in the Collision-Induced Dissociation of deprotonated cysteine-S-sulfate [90]. Another recent implementation, named  $M_3C$  [136], introduces entropy maximization as a procedure equivalent to an MD simulation in the infinite integration time limit. This approach has proven to be a successful tool for obtaining fragmentation breakdown curves of, e.g. adamantane dication [6].

Finally, different methodologies aim to compute mass spectra from first principles. Quantum chemical electron ionization mass spectrometry (QCEIMS) has been developed by combining elements of statistical theory (used for the assignment of a statistical charge to a fragment) with BOMD and has been shown to correctly reproduce experimental mass spectra of organic compounds [137]. Other approaches based in Chemical Dynamics Simulations have been recently reviewed [91].

## 9.2 Challenges and new directions

*Delayed fragmentation* Interaction of ionizing radiation with complex molecules may lead to time delayed processes due to their energy storing capabilities connected with large number of nuclear degrees of freedom. Such systems can remain internally “hot” and with that hinder the observation of fragmentation channels at threshold energies. Experimental observations have indicated production of metastable species surviving on the microsecond timescale before the fragmentation, e.g. in  $C^{6+}-C_{60}$  collisions [133]. Hence, from a theoretical perspective, there is a need of new, reliable statistical methodologies that could explain such processes on an appropriate timescale.

*Large molecules* The drawback of employing AIMD-based approaches for elucidation of fragmentation patterns is the need to run a large number of long calculations, which is unfeasible for larger systems. Depending on the underlying quantum chemical method, molecular dynamics simulations quickly become very expensive, so efficient code parallelization of AIMD approaches is crucial for the technical feasibility of such calculations.

*Charge distribution* Most of the previously discussed methodologies employ DFT as the underlying quantum chemical method. It is well known that this level of theory can lead to unphysical fractional charges; thus, DFT-calculated charge distributions must always be approached with caution. When obtained fractional charges are close to +0.5, dissociation on various PESs with charge asymmetrically and alternatively distributed might occur. Moreover, fractional charges are also expected within Ehrenfest–TDDFT as Ehrenfest dynamics evolves the electronic and nuclear degrees of freedom on an average potential. Explicitly considering the transitions between various electronic states would remove such discrepancies.

## 9.3 Concluding remarks

Studies of molecular fragmentation are essential to various branches of science. MD-based approaches described in the present review are able to explore energetically available regions of phase space in an automatic manner and thus identify fragmentation pathways that sometimes do not follow the “chemical intuition.” On the other hand, statistical methodologies proved to be powerful tools in extending the simulation times close to the experimental timescale. Efficient combination of these different techniques is necessary to explore fragmentation at long times. Proceeding beyond the state of the art will require accompanying experimental data that could aid with testing and benchmarking of the newly developed theoretical procedures.

**Acknowledgements** This work was supported by the MINECO project CTQ2016-76061-P and MICINN project PID2019-110091GB-I00.

## 10 Electron interactions with gas-phase molecules

Janina Kopyra, Faculty of Exact and Natural Sciences, Siedlce University of Natural Sciences and Humanities, Siedlce, Poland

Paulo Limão-Vieira, Atomic and Molecular Collisions Laboratory, CEFITEC, Department of Physics, Universidade NOVA de Lisboa, Portugal

### 10.1 Status: description of the state of the art

Electron scattering on atoms and/or neutral molecules is one of the most essential classes of chemical reactions and has been studied extensively in gas phase over a long period of time. These processes are of high importance for understanding and developing of many naturally and technologically occurring processes [138]. Among them, the attachment of low-energy electrons to molecules is an important process considering multiple perspectives, including atmospheric, environmental, (nano)technological (e.g., gaseous dielectrics, gas discharge lasers, plasma etching industry, electronic industry, nanofabrication, modification and functionalization of the surfaces) applications. In addition to the aforementioned, this process and its specificity are relevant for radiation chemistry. Therefore, a detailed knowledge of dissociative attachment is important for understanding and modeling electron driven processes.

Over the past decades, a vast time was dedicated to study interaction of low-energy electrons with biomolecules. Such interaction is considered to play a pivotal role in the description of radiation damage to living cells on a molecular level. This stems from the fact that high-energy radiation generates an exceeding amount of secondary electrons having initial energies in the range of a few tens of eV. Within picoseconds, these secondary electrons are slowed down; however, prior being solvated they may still induce reactions. Twenty years ago, it has been shown that single and double strand breaks can be caused by low-energy electron (LEE) impact to plasmid DNA [139]. As a result, strong activities emerged to understand the fundamental damage mechanisms. Initially, mainly small organic compounds, which represent the building blocks of biomacromolecules, have been studied. These included dissociative electron attachment (DEA) to the building blocks of DNA, namely the nucleobases, the phosphate and the sugar units. This stems from the fact that they are relatively easy to evaporate to be studied directly in the gas phase or deposited as thin films in the condensed phase [140]. In this way, interaction cross sections and fragmentation patterns are accessible. On this line of research activities, a peculiarity has been demonstrated namely site and bond selectivity in the loss of a neutral hydrogen atom from nucleobases at sub-excitation energies, < 3 eV [141]. More recently, DEA and electron transfer studies have been extended to nucleosides showing a particular fragility

of the glycosidic bond. Up to now, there is only one experimental gas-phase study on the entire nucleotide, 2'-deoxycytidine 5'-monophosphate (dCMP) [142]. The results indicated that in dCMP electron attachment can induce bond breakage between the phosphate group and the sugar not only by direct electron localization on the phosphate unit but also indirectly by initial electron localization on the nucleobase and subsequent transfer of the excess electron to the sugar-phosphate backbone. However, as was shown the majority of bond ruptures within dCMP nucleotide results from direct electron attachment to the sugar-phosphate backbone.

Recent advances in electron-molecule interactions and the associated instrumentation have led to the development of a softer method for bringing non-volatile/fragile samples into the gas phase. As such, LIAD (laser-induced acoustic desorption) is a promising technique not yet fully explored in the field of electron-induced damage to more complex molecules. The first results obtained from ribose-5'-phosphate unit [143] did demonstrate that it can be successfully used for the fragile systems which otherwise could be easily thermally destroyed. The challenges in studying complex biomolecules can also be overcome using a DNA origami technique [144]. This method is successfully applied to study electron-induced decomposition of biotinylated target sequences (oligonucleotides of specific sequence) attached to the DNA origami platforms that are immobilized on Si/SiO<sub>2</sub> substrates. After electron irradiation, the remaining intact oligonucleotides are visualized by atomic force microscopy with streptavidin, which allows a quantitative analysis of the electron-induced damage.

Given the growing application of radiotherapy employed in anticancer treatment, there is still a need to develop more effective methods of sensitizing cancer cells to radiation, thereby lowering the lethal dose of ionizing radiation. Most of the therapeutics used are derivatives of nucleosides substituted with electroaffinic substituents and are relatively easy incorporated into the DNA structure. These so-called radiosensitizers are promising chemical agents that modify radiation response of tumor tissue by increasing DNA damage and producing highly reactive species or by reduction of the targeted molecule (as the case of nimorazole [145]). These chemicals, as shown by recent studies, are prone to dissociative electron attachment that is at least in part responsible for the final biological effect. More recently, metal-based nanoparticles have been suggested as effective radiosensitizers. The possible mode of action of these metallic nanoparticles includes the radiation-induced release of an avalanche of low-energy secondary electrons that are responsible for further damage of DNA.

## 10.2 Challenges and new directions

Significant developments have been made during the last decades in exploring electron-induced processes in molecules as a function of phase and stage of aggrega-

tion. Such has been attained by combining high-resolution beams with state-of-the-art spectroscopic (and spectrometric) tools capable of unraveling key features relevant to assess the nature of transient molecular states. In most of the environments noted before, where electrons play relevant roles in the local chemistry, one key aspect is still related to neutral dissociation (ND) which is central to electronically excited precursors yielding neutral fragmentation, although the products of ND appear to be more difficult to monitor than charged products. Thus, detailed knowledge of the nature of the electronically excited states by experimental and theoretical methods is also demanded to assess the nature of the excited states from which estimates of ND cross sections can be obtained.

The international scientific community has long ago identified the need to increase the complexity of molecular targets in the gas phase, where different experimental techniques have been put forward to allow more complex molecular structures to be probed (e.g. electrospray—see Sect. 5, LIAD), not only at room temperatures but in the case of clusters and complexes (Sect. 11) at particular cold temperatures [146] (Sect. 12). The recent advances in the physical-chemistry of gas-liquid interface (e.g. atmospheric chemistry) are still in its early days as to the majority of different environments where they prevail, but still posing an enormous challenge from the experimental and theoretical point of views to larger macromolecular systems.

The reaction microscope developed to obtain relevant information on the vector momenta of several ions and electrons resulting from atomic or molecular fragmentation is still a powerful electron momentum spectroscopy technique, which has been evolving into different fields with special attention to the investigation of high-intensity short-pulse laser-induced fragmentation of atoms and molecules [8]. This technique coupled with state-of-the-art methodologies involving tunable high-intensity short-pulse VUV, or even X-ray self-amplifying (SASE) free-electron lasers (FELs, see Sect. 3), yields an important opportunity to explore and monitor the time evolution of correlated atomic and molecular electronic processes on attosecond timescales.

Finally, from the theoretical point of view, quantum chemical tools capable of providing fast and complex electron dynamics data on attosecond timescale processes (e.g., HHG, FEL and photo-induced dynamics of molecular systems, see Sects. 2, 3, 6) will demand a considerable joint effort seeking for efficient and reliable supercomputer facilities, notwithstanding the considerable challenge as to the breakdown in the Born-Oppenheimer approximation.

## 10.3 Concluding remarks

Electron interactions with gas-phase atoms and/or molecules are still necessary to provide important data to assess the role of such target compounds under isolated conditions where key spectroscopic features will be hidden or even quenched as a function of the envi-

ronment. Here, we have decided to focus on the current global political decisions regarding the long-term strategies under the Paris 2019 agreement. These are mainly related to the environmental impact and the urgent need to keep finding replacement feedstock gases for the semiconductor manufacturing industry, given that the majority of the traditionally used, and most efficient chemical compounds have been banned due to their strong contribution to global warming and ozone depletion. This is a result of an international effort that we have embraced as part of a larger programs aimed at understanding the underlying molecular mechanism of targeted compounds, and the role of these trace gases in the Earth's chemical and physical environments, and investigate alternative compounds for the development of a so-called green technology. The experimental techniques in electron and photon interactions with molecules allow a comprehensive and unique methodology to probe the role of such compounds in different environments where they determine the local chemistry, thus with considerable societal impacts. The current rising need for improved technologies capable of delivering faster and larger amounts of data, as well as a growing demand on efficient and reliable communications in the different sectors of the global economy, demands a rapid response from the micro- and nanotechnological industries exerting an enormous pressure on the processing capabilities of such semiconductor plants.

**Acknowledgements** JK acknowledges the support from a statutory activity subsidy (No. 25/20/B) from the Polish Ministry of Science and Higher Education. PLV acknowledges the Portuguese National Funding Agency FCT through Research Grants CEFITEC (UIDB/00068/2020) and PTDC/FIS-AQM/31281/2017.

## 11 Interactions of low-energy electrons with clusters

Jaroslav Kočíšek and Juraj Fedor, J. Heyrovský Institute of Physical Chemistry, Czech Republic

### 11.1 Status: description of the state of the art

In this section, low-energy electrons (LEE) are considered those having a kinetic energy below the ionization threshold. Their collisions with molecules can lead to the formation of transient anion states—resonances. This can be followed by dissociative electron attachment (DEA). DEA has several peculiarities, e.g., it is the only fragmentation process operative at sub-excitation energies, and the fragmentation pattern is often strongly dependent on the electron energy (bond selectivity). DEA often occurs in complex environments where LEE is formed as secondary species after passage of high-energy radiation through matter. Examples include radiation damage to living tissue, chemoradiation therapy of cancer, focused electron beam-induced

deposition (FEBID) and processes on atmospheric and astrophysical ices. In all these cases, the interaction of the target molecules with LEE will be influenced by the surrounding environment.

Experimental studies of environmental effects on DEA are complicated by the fact that the mean free path of LEE in a dense bulk environment is short, on the order of nm. Tracing the LEE before their solvation in liquids therefore requires ultrafast spectroscopy [147]. Another experimental approach, which is a subject of the present contribution, is to study interactions of free electrons with clusters—nm sized models of bulk. The correct modeling of the environmental conditions is then reduced to preparation of neutral cluster target of specific composition or thermodynamic state. Current state-of-the-art techniques used to prepare neutral clusters for LEE studies are outlined in Fig. 8.

The most important environmental effects on the interaction of LEE which were identified so far include:

(i) Suppression of molecular fragmentation induced by LEE [148, 149]. Several mechanisms were proposed for the stabilization of transient negative anions and closing of dissociation channels by the environment. These include caging of dissociation products, energy transfer to the solvent or changing the molecular dipole moment [150–153]. Recently, another mechanism was proposed, based on a strong coupling of the inter- and intra-molecular vibrational motion [154].

(ii) Molecules of the environment can allow for additional reaction pathways. A well-explored example is the mechanism of proton transfer after electron attachment, e.g., in the formic acid dimer [155]. This mechanism will be particularly important in complex molecules with several electron-affinic moieties. For example, in deoxycytidine monophosphate (dCMP), the electron attachment primary occurs on the cytidine base. In a water environment, the base is neutralized by proton transfer from the neighboring molecules and the electron is transferred to a sugar moiety [156]. As a result, the dissociation of a glycosidic bond is the primary fragmentation channel in water [157], in contrast to the dissociation of a sugar–phosphate bond in isolated dCMP [142].

(iii) An important process is self-scavenging (autoscavenging in heterogeneous clusters) caused by inelastic scattering of an electron on one molecule, which becomes electronically excited, and subsequent DEA of the decelerated electron to another molecule [158, 159]. Energy transfer to the solvent (i) causes stabilization of TNI up to high energies and enhancement of parent ion signal. Contrary to that, self-scavenging enhances dissociation at these energies. Simply, electronic excitation in one of the cluster molecules can result in dissociation of another cluster molecule. This means that with a rising number of different molecules in the local environment, DEA can occur in a wide interval of energies of the impinging electrons in contrast to narrow resonances typical for isolated molecules. The probability of LEE-induced dissociation in real environments may be therefore much higher



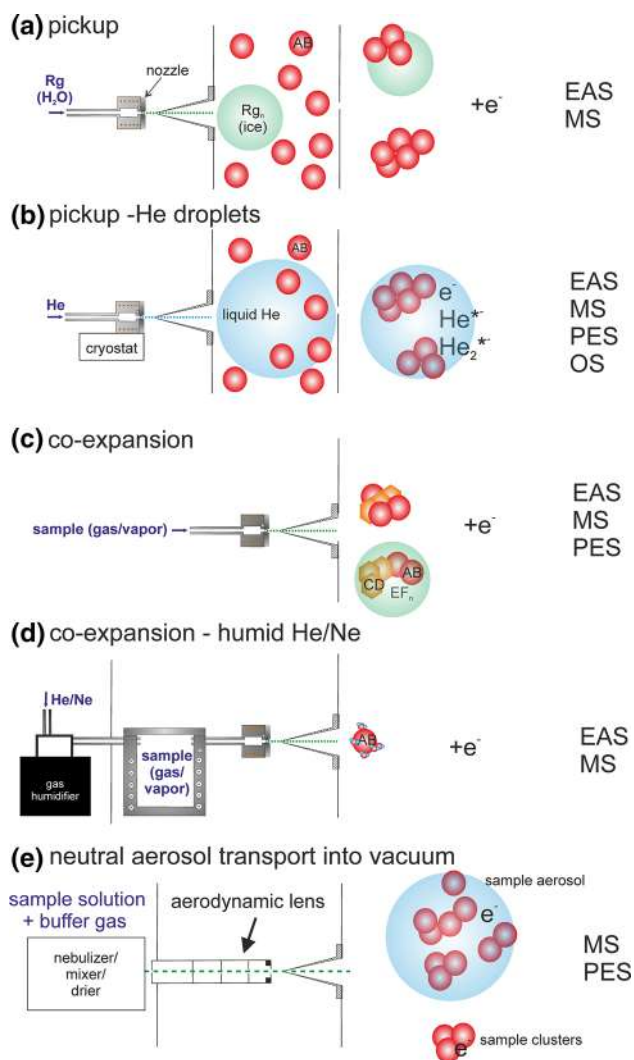


**Fig. 8** Various approaches to study interaction of free LEE with clusters such as electron attachment spectroscopy (EAS), mass spectrometry (MS), photoelectron spectroscopy (PES) or optical spectroscopy (OS) and methods to prepare molecular beams of neutral clusters: **a** clusters of rare gas or selected molecule such as water pick up sample molecules, which aggregate to form clusters; this method is useful for studies of processes on surfaces and interfaces. **b** He droplets reach sizes of micrometers; the size allows for pickup of molecules with very low vapor pressures and studies of interactions at liquid He temperature. **c** Co-expansion enables studies of heterogeneous clusters of many components. **d** Use of humidified gas as one of the components of the co-expansion enables studies of single hydrated molecules. **e** Aerosol transport into vacuum enables studies of fragile molecules that cannot be sublimed

than estimated from cross sections known for isolated molecules.

## 11.2 Challenges and new directions

One advantage of clusters is that they are sufficiently small to be described theoretically. For direct compar-

ison with experiment, however, it is important to work with well-defined and controlled target clusters. The main drawbacks of the present state-of-the-art experiments, as shown in Fig. 8, are that (i) all the techniques work with size distributions of clusters, (ii) we do not know the thermodynamic state of the clusters and (iii) often we cannot distinguish the pre- and post-interaction effects of the solvent.

Better defined clusters can be produced by improved control of expansion conditions (e.g. Fig. 8d) [160]. It may be also advantageous to use approaches toward controlled chemical dynamics such as electrostatic deflectors selecting the neutral cluster species according to their effective-dipole-moment-to-mass ratio [161]. Another approach to better define the target state is the technique of He droplets (Fig. 8b), where the clusters cool down to 0.37 K. However, at the same time here the He matrix prevents the direct interaction of LEE with embedded clusters [146].

The techniques used so far to prepare target clusters are based on expansion or pickup of the studied molecules in the form of gas or vapor. This limits the studies to thermally stable molecules, which can be evaporated or sublimed. A possible approach to study clusters of thermally sensitive molecules is by forming an aerosol of studied molecules and solvent (Fig. 8d). The aerosols can be transported into vacuum directly [162] or after drying the solvent [163]. Another possible approach may be to select neutral species from an electrospray ion source.

It is also challenging to detect neutral reaction by-products. Theoretical modeling often predicts complex rearrangement reactions in neutral dissociation products. While there have been initial attempts to characterize neutrals in electron interactions with isolated molecules in the gas phase [164], there are no such studies for clusters. The cross sections for interaction with LEE are generally small, and therefore, even the use of sensitive techniques of neutral detection such as laser-induced fluorescence, resonance-enhanced multi-photon ionization or single-photon ionization may be challenging.

Reaction of LEE in clusters may result in polymerization or isomerization, which cannot be experimentally proved in the current state-of-the-art experiments. Polymerization reactions may be traced by conceptually simple techniques such as collision-induced dissociation. Unambiguous identification of novel bonding motifs or isomerization reactions will then require the analysis of reaction products by advanced optical spectroscopy techniques.

As mentioned above, intermolecular charge transfer may play an important role after LEE interaction in complex environments, but their experimental studies are scarce. Theoretically proposed processes such as interatomic Coulombic electron capture have not been experimentally observed at all [165]. Identification of these processes will require a combination of cluster molecular beams with advanced coincidence techniques [8].



### 11.3 Concluding remarks

Electron collisions with free clusters represent a powerful tool for probing the environmental effects on reaction dynamics. It is worth noting that in cluster physics, the main focus has been historically on photo-induced processes. The apparent importance of LEE-induced reactions in natural and technological processes offers new directions which may be interesting to explore in the future.

**Acknowledgements** We acknowledge the support of the Czech Science Foundation via grants no 19-01159S and 20-11460S, and Czech Ministry of Youth, Education and Sports via grant no LTC20067.

## 12 Helium nanodroplets: a versatile medium for producing cold ions

Simon Albertini and Michael Gatchell, Institute for Ion Physics and Applied Physics, University of Innsbruck, Austria

### 12.1 Status: description of the state of the art

Droplets of helium ( $^4\text{He}$  specifically will be discussed here) have been used for decades to produce and study cold atoms, molecules and clusters—both as neutrals and ions [146,166]. Ranging in sizes from thousands to billions of atoms or more, He droplets are able to capture essentially any gas-phase atom or molecules they interact with. Due to the superfluid nature of the droplets, they possess an exceptionally high thermal conductivity and cooling power that allows captured dopants to rapidly cool to the 0.37 K equilibrium temperature of the droplets. This allows a wide range of clusters consisting of one or more species to be grown within the cold liquid that can be extracted to the gas phase for further studies [146,166]. In addition to producing cold clusters for experiments using mass spectrometry, the weak interactions between He atoms and the solvated species make helium nanodroplets an ideal matrix for spectroscopic studies of cold, complex molecules and ions [146,166,167].

The intrinsic properties of pristine helium clusters and droplets have been the focus of numerous studies over the years. These have revealed remarkable structures such as Atkins snowballs [146,168] and quantum vortices [146,169]. The term Atkins snowballs describes a class of cationic helium clusters for which electrostriction effects cause the surrounding atoms to bind strongly to the ionic core. The resulting clusters are essentially in a solid state, commonly referred to as snowballs, and have a density that surpasses that of solid He [168]. Similar snowballs have later been found when other ionic species are solvated in He and can often be identified from magic numbers (corresponding to solvation shells) in mass spectra [146,170,171].

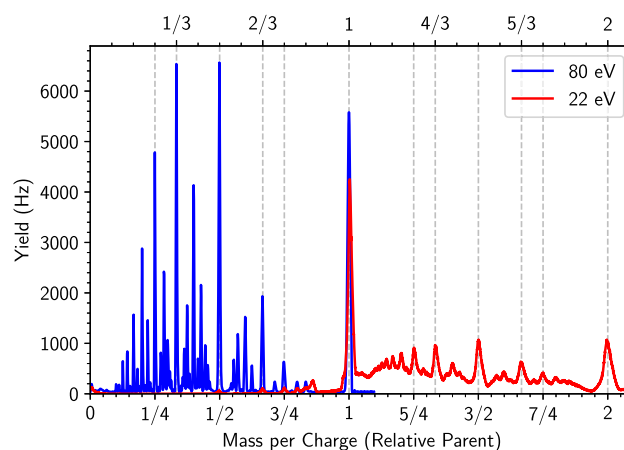


**Fig. 9** Mass-per-charge selected cationic helium droplets ( $3.8 \times 10^6$  He atoms per charge) have been impacted a second time with energetic electrons and measured using an electrostatic analyzer. Low-energy electrons (red) reduce the net charge of the precursor droplets, increasing their mass-per-charge ratio, and high energy electrons (blue) increase the net charge, decreasing the mass-per-charge ratios. Adapted from Laimer et al. [172]

Quantum vortices carry quantized angular momentum in quantum fluids, e.g. superfluid He, and were first identified in large ( $> 300$  nm diameter) helium droplets doped with Ag atoms where the vortices facilitated the growth of nanowires [169].

A recent development in our understanding of He nanodroplets and their potential applications was the discovery of stable, highly charged droplets [172]. The cohesive forces in liquid helium are extremely weak, only 0.6 meV per atom [146], and there was some uncertainty regarding the stability of multiple charge centers in a single droplet. Strongly ionizing helium droplets, e.g. with high currents of energetic electrons, will generally reduce the average mass-per-charge ratio of a population. Possible explanations were either fragmentation of droplets after accumulation of charges, e.g. by Coulomb explosions, or a charge buildup in the droplet.

Figure 9 shows results from measurements of cationic droplets with a selected size of 3.8 million He atoms per charge (produced by electron impact ionization on neutral droplets) that were impacted a second time with electrons at two different energies [172]. At 80 eV (in blue), above the 24.6 eV ionization energy of He, the net charges of the droplets are increased leading to a series of narrow peaks with mass-per-charge ratios lower than that of the size-selected precursors. The positions of the product peaks are exclusively at rational fractions of the precursors that are determined by the ratios between the precursor and product charge states. The evidence that these products are the result of charge buildup and not fragmentation comes from the red curve in Fig. 9. With electron energies below the ionization energy of He, here 22 eV, the net charge of the droplets is decreased, increasing their mass-per-charge ratios. Again, the positions of the product peaks

are at rational fractions of that of the precursors. Since the droplets cannot gain mass after they are formed, these peaks must arise from multiply charged droplets that are partially neutralized [172]. In this study, net charge states of up to 55+ were directly identified and their critical sizes were determined, with higher charge states being inferred indirectly.

## 12.2 Challenges and new directions

Even with the recent advances in our understanding of the characteristics of He droplets, our main motivation is still driven by their use in ion- and cluster physics. Helium nanodroplets are a versatile medium for producing cold ions and complexes of practically any atomic or molecular species. In light of this, we have begun developing a new generation of devices that utilize highly charged droplets of liquid He [173]. What sets this new type of setup apart from previous ones is that dopants are deposited into charged droplets instead of neutral ones. Dopants captured by neutral droplets tend to coalesce into a single cluster near the center of droplets, which are then ejected into the gas phase upon ionization of the droplets [146, 166]. In contrast, pickup into multiply charged droplets leads to multicenter growth of clusters where each charge center acts as an individual nucleation site. The simultaneous growth of many clusters in a single droplet leads to a higher number of smaller clusters with a narrower size distribution compared to clusters grown in neutral droplets [173].

One area of broad interest where these techniques are expected to play an important role is in spectroscopic studies of complex ions. For many complex molecular species, direct measurements of gas-phase spectra under optimal conditions, e.g. at low temperatures, present severe technical difficulties. A widely used alternative has long been matrix isolation spectroscopy, but even with cold rare gas matrices the spectra are often perturbed in a way that makes direct comparisons with, e.g., accurate astronomical data difficult. Another approach is messenger spectroscopy where the loss of loosely bound atomic or molecular tags from an ion complex is measured as a function of wavelength with a mass spectrometer [174]. If the tagged ion absorbs light, the excitation energy will cause the complex to fragment and the measured ion yield spectrum will thus be an approximation of its absorption spectrum.

In messenger spectroscopy, the chemical shift in the band positions induced by the messenger species can be minimized by using tags with as weak interactions as possible [175]. For this, He is ideal. However, the low binding energy of He to other species means that temperatures on the order of a few kelvin are required to form He-tagged ions. This has been achieved in, e.g., cryogenic ion traps, and the method was particularly well demonstrated when the  $C_{60}^+$  ion became the first identified carrier of diffuse interstellar bands [167, 176].

Helium-tagged ions are readily produced from doped He droplets, and this method was successfully used to confirm the spectrum of  $C_{60}^+$  [167, 177]. With He

droplets, it is possible to form ions solvated in essentially any number of He atoms, which allows the action spectrum of ions to be studied as a function of the degree of solvation (see Fig. 10) more efficiently than in traps. A benefit of this is that the gas-phase spectrum can be more accurately estimated from the action spectra and it also provides information on the structures of solvation layers, which in turn can be used to gain information of the structures of the ions themselves [178]. Here, a close cooperation between experimentalists and theorists is important for the interpretation of results and to identify details on the solvation structures. The theoretical studies of ions solvated in He present a number of technical challenges due to the low binding energies involved as well as the low mass of the He atoms. Because of this, quantum descriptions of nuclear motion are generally required to properly sample the dynamics of He solvation layers [170, 179]. The advancement of experimental methods using highly charged droplets has started to show improvements relevant to these types of studies as well, in particular with regard to controlling the number of tagged species formed and in forming more challenging complexes such as tagged anions.

## 12.3 Concluding remarks

Helium droplets have proven to be a very powerful tool for producing cold ions and clusters. The development of new techniques using charged droplets is enabling a new generation of experiments, the first of which having recently been commissioned. Other applications being investigated are the use of charged He droplets in pro-

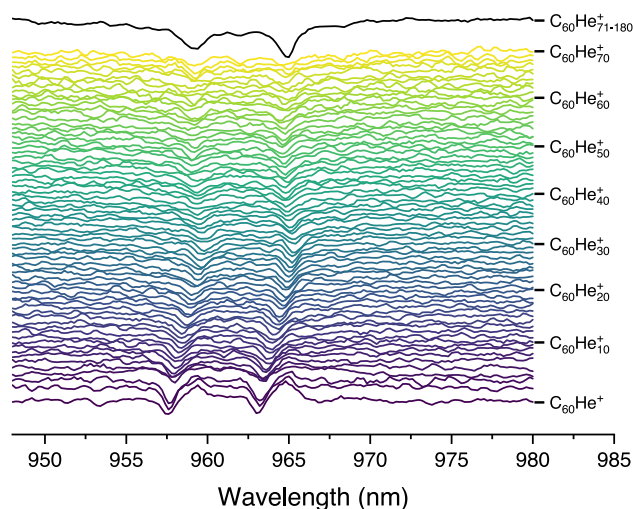


**Fig. 10** Measured yields of  $C_{60}^+$  ions solvated in different numbers of He atoms as a function of the wavelength of the probing laser [167, 177]. Absorption of photons by the fullerene ion triggers the loss of He, depleting the yield of clusters that are in resonance. Shifts in the band position are visible between different numbers of solvating He atoms

ducing well-defined beams of nanoparticles for technical applications such as surface deposition.

**Acknowledgements** We thank Paul Scheier for his invaluable support and input. This work was supported by the EU commission, EFRE K-Regio FAENOMENAL EFRE 2016-4, the Austrian Science Fund FWF (P31149 and I4130) and the Swedish Research Council (Contract No. 2016-06625).

## 13 Electrostatic ion-beam storage rings

Henrik Cederquist and Henning T. Schmidt, Department of Physics, Stockholm University, Sweden

### 13.1 Status: description of the state of the art

Worldwide, about ten electrostatic ion-beam storage rings are in operation [180]. At DESIREE, the Double ElectroStatic Ion Ring ExpERiment, at Stockholm university, it is possible to store two keV ion beams—one with negatively and one with positively charged ions—on 8.7 m circumference trajectories. These two beams may be merged for studies of charge-, mass- and energy-transfer processes down to sub-eV collision energies [181, 182]. The CSR, the Cryogenic Storage Ring, at the Max Planck Institute in Heidelberg is larger, has a circumference of 35 m, and is equipped with a free-electron target, a neutral-beam target and in the future it will be equipped with a gas-jet target for kinematically complete studies of ion–neutral reactions at keV–MeV energies [183]. By using the merged-beams technique, reactions between the stored ions and free electrons or neutral species can be studied down to micro- and millielectronvolts in CSR. RICE, RIKEN Cryogenic Electrostatic Ring, at the RIKEN laboratory in Japan [184], has, like the CSR, a beam target for merging the stored ion beam with neutral atoms or molecules. RICE is smaller with a circumference of 2.9 m. DESIREE, CSR and RICE are operated at cryogenic temperatures between about 5 K (RICE) and 13 K (DESIREE). Thus, most stored ions relax spontaneously toward thermal equilibrium at these low temperatures such that rotational, vibrational, and electronic excitations are strongly limited after some time. Ideally, and in practice for favorable cases, molecular-ion beams with all their molecules in a single rovibrational quantum state may thus be formed. The cryogenic cooling of DESIREE, CSR and RICE also leads to very low residual gas densities ( $10^2$ – $10^4$  H<sub>2</sub> molecules per cm<sup>3</sup>) and thus possibilities for very long ion-beam storage lifetimes. The very low temperatures and pressures are similar to those in interstellar space and action spectroscopy on internally cold ions is a common highly attractive option at these three storage rings. Furthermore, measurements of reaction rates at low temperatures can be directly related to astronomical observations of cold interstellar regions.

The era of electrostatic ion-beam storage rings began with the construction and commissioning of ELISA at

Aarhus University in the 1990s [185]. The development of electrostatic—rather than magnetic—devices was to a large extent motivated by the possibility to store beams of different types of heavy ions. This is a common advantage of all purely electrostatic ion-beam storage rings, and also of the conceptually related ion-beam traps [186, 187] (see Sect. 15). For all the electrostatic storage devices, the settings on beam deflectors and lenses for ion-beam storage only depend on the kinetic energy per charge of the ions and not on the mass. ELISA paved the way for other electrostatic ion-beam storage devices through a range of highly successful studies of properties of isolated biomolecules, biomolecules in solution, clusters, and other molecules and in particular fullerenes such as C<sub>60</sub>. In these studies, the action spectroscopy method, in which the photo-absorption spectrum is recorded by measuring the probability for photo-induced fragmentation or electron detachment as a function of the wavelength of the photon, was often used [188] (see Sect. 14). ELISA has a circumference of 7.1 m and is normally operated at room temperature, as is the smaller electrostatic ion-beam ring, SAPHIRA, which was commissioned at Aarhus University in 2015 [189]. SAPHIRA is used for photo-fragmentation studies by the action spectroscopy method and it has a square-shaped structure with a side length of 1.0 m. The World's second and third electrostatic ion-beam storage rings were, however, built much earlier in Japan at KEK, Tsukuba [190] and at the Tokyo Metropolitan University, TMU [191].

The TMU ring is similar to ELISA and mainly used for photo-fragmentation and photo-detachment studies. A prominent example is the direct observation of recurrent fluorescence [192], which is a very fast molecular relaxation process driven by couplings between vibrationally hot ions in the electronic ground state and electronically excited states with less vibrational excitations. This type of process has also been studied at Mini-ring, a 75 cm circumference ion-beam storage ring, at Université Lyon 1 in Lyon [193]. The Mini-ring has conical electrostatic ion-beam mirrors inspired by the ion-beam trap, CONEtrap in Stockholm [187], and its small size makes it easy to handle and operate at a reasonably low cost. At TMU in Tokyo, the  $\mu$ -ring with an 88 cm circumference was recently commissioned and its usefulness for measurements of absolute charge exchange cross sections was demonstrated [194]. The smaller rings, Mini- and  $\mu$ -ring, are well suited for studies of decay processes on  $\mu$ s and ms timescales whereas the larger rings are used for measurements of slower or much slower decay processes up to minutes or hours.

### 13.2 Challenges and new directions

Common challenges for the electrostatic ion-beam storage rings are the preparation and loading of positively and negatively charged ions for in-ring experiments. Here, the ongoing development aims for a broad selection of atomic, molecular, cluster, fullerene, and biomolecular ion-beams, as well as for meth-



ods to handle micro-solvated ions and ions in He-nanodroplets. A range of plasma-, sputter-, electron-cyclotron-resonance- (ECR), cluster-, electrospray- and nanodroplet sources are needed to fulfill these goals. In addition, ion-mass selection devices with sufficient resolution to separate ions, in particular heavy ions, of nearby masses should be combined with accumulation and pre-cooling traps in order to form ion bunches of sufficient intensities and suitable duration for cyclic injection in the storage rings. The latter is to be able to inject sufficiently intense ion bunches—ideally with all ions having the same mass, charge, internal energy, and conformation—and to store them long enough for further manipulation (e.g. with lasers) for experiments. The preparation of beams of small molecular ions with nearly all of them in a single ro-vibrational quantum state has been demonstrated for  $\text{OH}^-$  at both CSR and DESIREE [195, 196]. Diatomic molecules, such as  $\text{OH}^-$ , have only one possible conformation, while larger molecules may have many different forms. Ways to select specific molecular isomers for injection and in-ring storage have to be developed.

For the three cryogenic ion-beam storage rings [181–184], the key aim is to be able to prepare ions—in particular molecular ions—in a single well-defined quantum state. Having ions in well-defined states is a clear advantage as this strongly limits the number of calculations needed for comparisons with results of newly developed quantum-state-specific models. A very broad distribution of initial states in the experiment could conceal distinct state-sensitive phenomena through the need to average over many initial quantum states when evaluating the model. The importance of experiments on internally cold ions was recently demonstrated through measurements of dissociative-recombination rates as functions of the rotational state in  $\text{HeH}^+ + e^-$  reactions (all  $\text{HeH}^+$  ions in the vibrational ground state  $v=0$ ) at CSR [197]. It was then found that the rate is a strong function of the rotational excitation, which is in stark contrast to what has been assumed in earlier astrophysical models. At DESIREE, the branching fraction for the population of the Li (3s) state—important for gauging the Li abundance in stars—was measured in  $\text{Li}^+ + \text{D}^-$  mutual neutralization reactions [198] at meV energies. In the next step, reactions between small internally cold molecular anions and atomic cations present in the interstellar medium will be performed with improved methods to control the overlap between the merged beams in DESIREE. Additional trends in the field are studies of stabilities of astrophysical reaction products. It is of particular interest to study knockout fragments of polycyclic aromatic hydrocarbon (PAH) molecules and fullerenes, as these fragments of interstellar molecules are highly reactive. Likewise, stabilities of molecular fusion products, in particular fusions between fullerenes or between PAH molecules, will also be studied for comparisons with astronomical observations using the action spectroscopy method.

Further challenges include studies of inherent properties of multiply charged anions, where stability issues

are of large interest for, for example,  $\text{C}_{60}^{2-}$ . Inherent stabilities of metal clusters and reactions with biomolecular ions in vacuum will also be important fields of study. Recent experiments unexpectedly revealed that slow electron emission, rather than fragmentation, dominates the decay of  $\text{Ag}_2^-$  clusters of certain internal excitations [199]. Molecules and atoms in charged nanodroplets of helium will be used for highly sensitive action spectroscopy measurements using the so-called tagging technique.

### 13.3 Concluding remarks

A key feature of electrostatic ion-beam storage rings and traps is that ions of any mass can be conveniently stored. Further key features of *cryogenic*, electrostatic ion-beam rings are the possibilities to produce beams of (light or heavy) ions in narrow ranges of, or in single, quantum states. There are three cryogenic storage rings in operation where it is possible to merge stored ion beams with (i) stored beams of ions in the opposite charge state (DESIREE); (ii) free electrons (CSR); (iii) beams of neutral atoms or molecules (RICE and CSR); and (iv) laser beams (RICE, CSR and DESIREE). Major challenges involve beam preparation with isomer selection and in-ring separations of molecular and cluster reaction products with high mass resolution.

**Acknowledgements** We want to thank all colleagues of the electrostatic ion-storage ring community for many interesting and pioneering experiments of which only a small fraction are presented in this brief report. DESIREE is a Swedish National Infrastructure (Swedish Research Council contract No. 2017-00621). The authors further acknowledge individual Swedish Research Council grants (2019-04379 and 2018-04092) and the support from the Knut and Alice Wallenberg Foundation for the project “Probing charge- and mass-transfer reactions on the atomic level” (2018.0028).

## 14 Studies of photo-induced dynamics in bio-chromophores using electrostatic ion-storage rings

Elisabeth Gruber and Lars H. Andersen, Department of Physics and Astronomy, Aarhus University, Denmark

### 14.1 Status: description of the state of the art

Many important processes in nature and in man-made devices are light-driven and proceed with remarkably high efficiency upon molecular photo-excitation. In conventional spectroscopy, the absorption of light in a sample of molecules is normally determined from the intensity of incident and transmitted light according to the Lambert–Beer law. To study the photo-physics of (bio)molecules under vacuum conditions, free from perturbation by nearby molecules, or in a well-defined and controllable environment with known perturba-

tions, gas-phase action spectroscopy has been established as the first-choice method (see also Sects. 18, 19). Here, a detectable “action” induced by photo-absorption, i.e. dissociation, electron detachment or fluorescence, is used to register absorption events with high efficiency, hence determining absorption spectra, and provide benchmark data for quantum-chemical calculations.

In the last decades, several devices have been developed for action spectroscopy, including electrostatic ion-storage devices, accelerator mass spectrometers, reflectron time-of-flight mass spectrometers, ion traps and photoelectron spectrometers. Here, we focus on electrostatic ion storage rings [200]. The first electrostatic storage-ring ELISA was developed at Aarhus University in 1997 [185] and was initially used for lifetime studies, including research on thermalization of hot metal-cluster ions [201]. Later, other electrostatic rings were constructed to study processes induced by interactions with photons, ions or electrons [180]. The general advantage of these electrostatic storage devices is that they allow some relaxation of vibrationally excited states, which is particularly relevant when a hot ion source is used, as well as an efficient detection of reaction products. Moreover, they are, in principle, free from mass restrictions and therefore ideal tools for studies on dilute targets of heavy molecular systems.

By combining an electrospray-ionization source with an ion trap prior to ion injection into the ELISA storage ring, the electronic absorption spectra of closed-shell biomolecular ions were measured in groundbreaking experiments [188, 202]. The yield of neutral products following either photo-detachment or photo-fragmentation was taken to represent the gas-phase absorption spectrum.

Studies on molecular chromophores, the photo-active part of photo-active proteins, have attracted immense attention not only because of their crucial role for the functioning of living organisms and applications, but also because they are excellent systems for studying elementary processes, such as photo-isomerization, light-driven energy transfer and charge separation. These processes proceed typically on a femto-to-picosecond timescale, and hence ultrafast, optical techniques are required to follow such reactions together with detection schemes to reveal the status of the molecular system in real time.

## 14.2 Challenges and new directions

The development of laser pulses with short time duration has opened a new era of molecular research, primarily for probing the nuclear dynamics in the molecules. Zewail was awarded the Nobel prize for his contributions in this field [7]. This type of work has later been followed in many other groups, primarily working with negative ions, where photoelectrons conveniently may be detected [203–207].

The combination of ultrafast pump–probe schemes with an electrostatic ion-storage ring technique gives

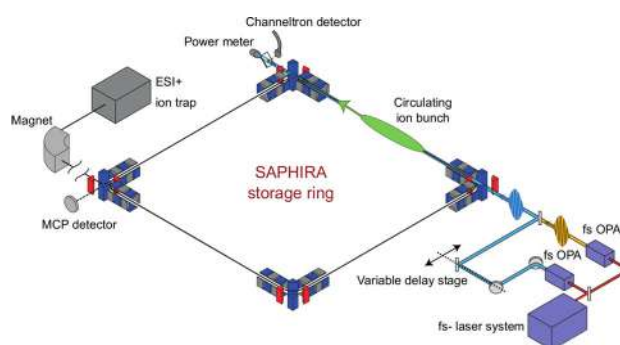


**Fig. 11** The SAPHIRA ion-storage ring, equipped with an ESI source and an ion trap that optionally may be cooled with liquid nitrogen. In the ring, stored ions may be studied by time-resolved action spectroscopy upon excitation by tunable fs laser pulses. Figure adapted from [210]

a new approach to resolve ultrafast photo-initiated dynamics of molecular ions in vacuum (see also contributions on other gas-phase techniques in Sects. 2 and 3). It was recently successfully engineered and implemented at the electrostatic ion-storage ring SAPHIRA at Aarhus University, for details see Ref. [189].

At SAPHIRA (Fig. 11), a tunable femtosecond laser system is used for fs-pump–probe spectroscopy on stored molecular ions. The method combines the pump–probe time delay with the action-response time registered in the ring, and is hence based on time in two dimensions. In short, we register when a given molecular system is capable of absorbing a (second) probe photon upon initial pump excitation, by registering the fast/prompt action in the ring, associated with the extra energy gain provided by the absorption of two photons (instead of one). The prompt molecular photo-response is typically on the sub  $\mu\text{s}$ –ms timescale and hence detected by a detector located immediately after the interaction region. The method is highly advantageous for mapping out the excited-state decay as well as the ground-state recovery, and is applicable for negative as well as positive ions. First results with this new technique have demonstrated the superiority of using fs-laser pulses [208] and the applicability to study dynamical processes of bio-chromophores [209, 210].

Measurements have been performed with molecules at room temperature or pre-cooled to 100 K in the present ion trap. A significant temperature dependence on the excited state lifetime reveals the role of energy barriers in the electronically excited states [209, 210]. It was shown that the isolated deprotonated GFP chromophore is trapped for 1.2 ns in the first excited state when cooled to 100 K, establishing conditions for fluorescence in the gas phase (see Fig. 12). Direct detection of fluorescence from the gas-phase chromophore is, however, still lacking. Our next step is to pre-cool the ions in a cryogenic multi-pole trap (liquid helium temperature) before injection into the storage ring to further investigate rate-limiting excited-state energy barriers and for improved spectroscopy (less in-homogeneous broaden-



ing). Other cooling schemes are discussed in Sects. 11 and 12.

Another approach to obtain cold molecular ions is to use cryogenically cooled storage rings. Recently, the facility at DESIREE at Stockholm University [182], at CSR at the Max-Planck Institute for Nuclear Physics in Heidelberg [183], and at RICE at RIKEN, Japan [184] have become operational (see also Sects. 13, 15). Here, the whole ring is cooled down to 10 K, which, in addition to cold ions, ensures very high vacuum conditions and long storage lifetimes (up to an hour) which also provides rotational cooling. Another exciting method is to embed chromophores into superfluid helium nanodroplets [211, 212]. With an equilibrium temperature of  $\sim 0.4$  K, superfluid helium droplets can serve as gentle matrices to provide an isothermal environment at cryogenic temperature. The low temperature reduces the number of populated quantum states and freezes out structural fluctuations. Further, liquid helium is optical transparent from the deep UV to the far IR.

Another challenge is to move from single isolated molecules to larger molecular complexes to study the electronic coupling between multiple chromophores, energy and charge transfer processes and the role of interactions with a host medium. Such experimental data provide benchmark values for quantum calculations, making theoretical progress possible and hopefully reliable for large-scale applications.

### 14.3 Concluding remarks

Action spectroscopy is a very powerful method to explore spectroscopy and dynamics of gas-phase

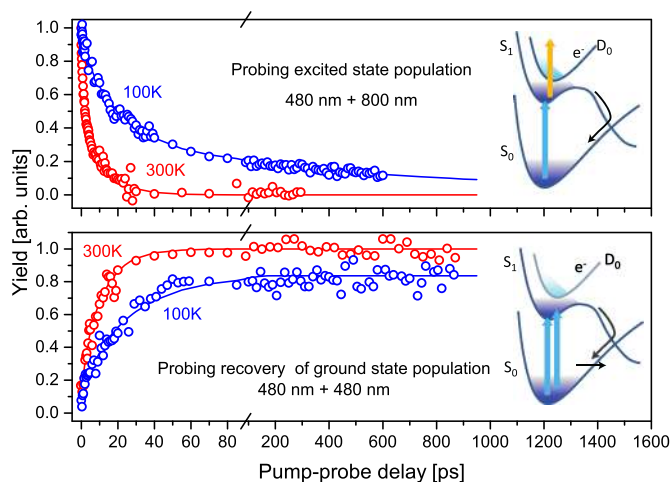


**Fig. 12** Excited-state decay (upper figure) and ground-state recovery (lower figure) of GFP chromophore anions, pumped at 480 nm, and probed at 800 nm (for the excited state lifetime) or 480 nm (for the ground state recovery). The data were recorded at 300 K (room temperature) and at 100 K by pre-cooling them in an ion trap. The cooled ions show a much longer decay due to trapping behind a potential energy barrier in the first excited state. Data are taken from [209]

molecules. We have demonstrated how pump-probe schemes may be combined with detection of time-resolved action in ion-storage rings to reveal internal dynamics of molecules. We have also shown that temperature matters for the dynamics, and we foresee that with new cooling schemes, exciting new photo-physics will be revealed at the many ion-storage rings.

## 15 Electrostatic ion-beam traps

Oded Heber, Department of Particle Physics and Astrophysics, Weizmann Institute of Science, Israel

Yoni Toker, Department of Physics and Institute for Nanotechnology and Advanced Materials, Bar-Ilan University, Israel

### 15.1 Status: description of the state of the art

Electrostatic ion-beam traps (EIBTs) have been used for studying the gas-phase internal dynamics of molecules for many years [200]. Many EIBTs exist worldwide for various usages including, for example, high-resolution charge detection mass spectroscopy of large molecules [213] and isotope separation [214]. EIBTs have an advantage as a tool for studying gas-phase internal dynamics of molecules due to their compact size which can fit into a university-size laboratory. EIBTs are efficient tools for studying photon absorption bands and photon emission of isolated ions as well as controlling the molecular environmental temperature. Also, as will be described below, they are efficient tools for studying collisions including intra-beam collision, collisions with electrons, gas targets and other beams.

The dynamics of molecules is strongly dependent on the internal energy distribution (IED) of the molecules. Therefore, control over the ions' IED is important. Generally there are two ways to control the IED: (1) Conditioning of the molecules before injection into the EIBT, e.g., by buffer-gas cooling; (2) Manipulation of the ions' IED inside the trap. For the former option care must be taken that following conditioning and prior to injection the ions' IED does not change, for example, due to collisional heating during acceleration. For the latter case, one process which occurs spontaneously is radiative cooling which eventually results in the equilibration of the ions with the EIBT's temperature. For this goal it is desirable to have the ability to control the EIBT's temperature and to be able to cool it down to cryogenic temperatures. Indeed, recent years have seen the advent of cryogenic electrostatic storage rings and EIBTs, with EIBTs being simpler to cool due to their compact size.

It is also desirable to be able to cool the kinetic degrees of freedom of the trapped ions. One promising avenue for achieving cooling is through autoresonance, where ions within the EIBT are accelerated by chirping a small oscillation frequency, which causes an enhancement of the coldest population by ion-ion interactions. Recently, the ability to cool the kinetic degrees of free-

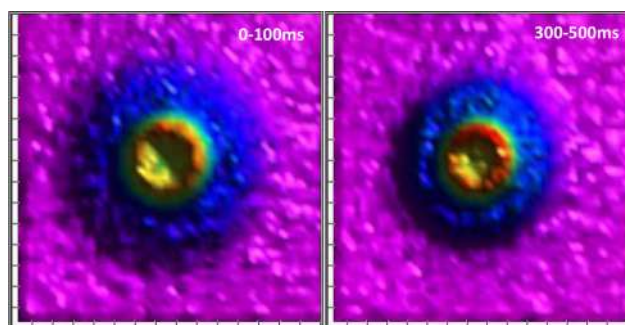


**Fig. 13** Photoelectron image of trapped  $\text{OH}^-$ . The inner circle (red–orange) is from Q transitions, while the outer disk (blue) is from P transitions. The left image is produced by electrons from molecules trapped for 0–100 ms, and the right is for 300–500 ms trapping time

dom using autoresonance was demonstrated [215]. It remains to be seen whether the external kinetic temperature and IED are coupled, and if autoresonance can also be used to cool the IED.

## 15.2 Challenges and new directions

One of the challenges in studying the internal dynamics of molecules is to characterize all the different reaction products following an excitation or collision and do so as a function of the ions internal energy distribution and as a function of time. The EIBT can potentially meet this challenge with a full reaction microscope: with simultaneous detection of photons, electrons, neutral and charged fragments. Detection of each of these products has been implemented separately in EIBTs. However, the full combination of all of them simultaneously is still a challenge. For example, in a few groups a velocity map imaging (VMI) electron spectrometer has been combined with an EIBT, such that upon photo-excitation one can detect the emitted electrons and deduce their kinetic energy, and simultaneously also measure the neutral products [216]. Figure 13 shows a VMI image of electrons from  $\text{OH}^-$ , measured in coincidence with the neutral OH after laser interaction for two different trapping time regimes [217]. The image clearly shows the rotational cooling of  $\text{OH}^-$ .

Following excitation by a short laser pulse or by collisions, ions often dissociate (by emitting an electron or fragmenting) on very long timescales ranging up to milliseconds. This fascinating phenomena has been the subject of a great deal of research in its own right, and is important to account for in deducing the correct shape of an absorption band due to kinetic shifts. Statistical dissociation has been used as a tool for studying statistical properties of ions, for example, for radiative cooling measurements [218], for calorimetry [219]. In a recent work, it was shown that one can describe simultaneously the isomerization, the delayed electron emission and internal cooling for  $\text{C}_{10}^-$  molecules [220]. Even though statistical dissociation has been known for over 30 years, the proper methodology for modeling it is still an ongoing research topic and currently depends on the

simultaneous deduction of many molecular parameters such as the ions activation energy, IED, polarizability, etc. We expect that the study of statistical dissociation of ions photoexcited from their vibrational ground state will provide a stringent test of theory and a significant step forward. Moreover, we expect this goal to be achieved in the near future thanks to cryogenically cooled electrostatic storage devices.

As EIBTs, are purely electrostatic devices, they can trap any molecular ion (positive, negative and multiply charged) using the same electrode settings, as long as the kinetic energy to charge ratio is the same. This allows to trap many different molecules simultaneously, and to study the interactions between them. For studying collision dynamics, it is essential to control the relative velocities of the different ions. Recently, an EIBT called hybrid EIBT (HEIBT) was designed with this goal in mind [221]. The device, shown in Fig. 14, is composed of two EIBTs: The inner EIBT traps ions with lower kinetic energy and the outer for higher kinetic energy ions. The relative energy can be tuned to match the velocities. Moreover the HEIBT can trap simultaneously two different species with the same charge or with opposite charges. It is expected that such a device will be a new compact tool for time dependent studies of molecular ion reactions at very low collision energies.

One complication that arises in studying molecules composed of more than three atoms is that they may have different stable conformations, different isomers, which may possess very different dynamical properties. For example, studies of the retinal protonated Schiff base (RPSB), have shown that even when sprayed from an *all-trans* solution the isomer distribution in the gas-phase consists of many isomers, which have different photon-absorption bands [222]. Notably, different isomers have the same charge over mass ratio and cannot be separated with conventional mass spectrometric techniques. It is therefore highly desirable to have an isomer selection stage prior to injection into the EIBT. The most promising approach for achieving this goal is through ion mobility spectroscopy (IMS). IMS enables separation of isomers according to the differences in their collisional cross section with a buffer gas. Conventional drift tube IMS relies on long drift tubes. However, novel developments such as trapped ion mobility spectroscopy (TIMS) and structures for lossless ion manipulation (SLIM) offer compact methods for achieving high-resolution IMS separation which potentially can be mounted on ion source platforms and combined with EIBTs. We expect in the coming years that the combination of EIBTs with IMS will permit isomer dependent studies of the dynamics in molecular systems.

## 15.3 Concluding remarks

EIBTs are a versatile tool for studying time dependent dynamics of molecules in the gas phase. New techniques such as cryogenically cooled EIBTs, combination of EIBTs with VMI photoelectron spectrometers, use of sophisticated ion sources which include IMS separa-

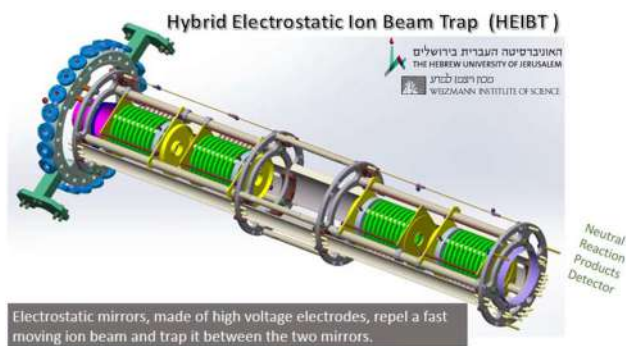


**Fig. 14** A drawing of the HEIBT located at the Hebrew University of Jerusalem, Israel. The four mirrors are in green, and each mirror can be slid longitudinally to permit different geometries

tion, sophisticated cooling techniques such as autoresonance cooling and the hybrid trap for ion–ion collisions promise to open new exciting new prospects and possibilities.

**Acknowledgements** We would like to thank Michael Rappaport for his help in writing this paper.

## 16 Cooling dynamics of molecules and clusters

Klavs Hansen, Center for Joint Quantum Studies, Tianjin University, Tianjin, P.R.China

### 16.1 Status: description of the state of the art

Molecules and clusters containing sufficient randomized (thermal) excitation energy can potentially decay through a number of channels. These can often be modeled in terms of an activation energy and a frequency factor which multiplies what can be imagined as an effective Boltzmann factor.

The most frequently encountered decays are the fragmentation processes that are known as unimolecular reactions. These include loss of a single atom or larger moieties. The most commonly used description is RRKM, which was suggested as a model for traversal of a saddle point in the potential energy curve in a one dimensional trajectory. This has been elaborated with the addition of angular momentum to the channel in the so-called phase space theory [223].

A third theory is based on detailed balance, originally derived to describe thermal decay in nuclei. It is particularly useful for clusters as these very rarely have any saddle point but absorb and emits monomers without any reverse process activation barrier. Saddle point transition states seem also to be much less frequent occurrences for molecules than a naive consideration of dynamics on Born–Oppenheimer surfaces would suggest, as judged by measured kinetic energy release distributions.

The kinetic energy resolved detailed balance rate constant for evaporation of a single atom is [224]

$$k(E, \varepsilon) = \frac{gm}{\pi^2 \hbar^3} \sigma(\varepsilon) \varepsilon \frac{\rho_p(E - E_a - \varepsilon)}{\rho_r(E)} \quad (1)$$

(ignoring angular momentum quantization and constraints imposed by its conservation).  $g$  is the atomic electronic degeneracy,  $m$  the reduced mass of the channel,  $\sigma$  the inverse reaction capture cross section,  $\varepsilon$  the kinetic energy release, the  $\rho$ 's the level densities of the species indicated by the subscripts ( $p$  for product,  $r$  for reactant), and  $E_a$  the evaporative activation energy.

Another potential channel is thermal electron emission, the molecular analogue of macroscopic thermionic emission. In neutral systems it tends to be present in clusters of highly refractory elements, because the activation energy for this channel is the ionization energy versus the competing unimolecular dissociation energy, and only for refractory elements will the difference in these two values be in favor of electron emission. The rate constant for this process is also derived by application of detailed balance, and Eq. (1) only needs to be modified for the mass, the level densities and the degeneracy  $g$  [225]. As the process depends on thermally excited electronic degrees of freedom, it may for consistency be relevant to include these degrees of freedom into the level densities.

The third channel, thermal radiation, can also be derived with detailed balance. It differs from the two other channels both by having a lower activation energy, which is simply the emitted photon energy, and by a much smaller frequency factor. The latter is related to the much smaller density of states of the emitted photons compared to that of free atoms or electrons. Combined, these two facts make the channel the dominant one at low energies, and it is therefore of special interest for experiments on long timescales, in particular but not restricted to storage-ring experiments [182, 183, 185, 192, 226]. In addition, the quantum nature of the photon modifies its emission rate constant with the contribution from stimulated emission. The resulting photon emission rate constant is [225]

$$k(E, \nu) d\nu = \frac{8\pi\nu^2}{c^2} \sigma(\nu) \frac{\frac{\rho(E-h\nu)}{\rho(E)}}{1 - \frac{\rho(E-2h\nu)}{\rho(E-h\nu)}} d\nu \quad (2)$$

Figure 15 illustrates the typical behavior of the observable emission rate constants for  $C_4^-$ .

This equation describes both the radiation from vibrational transitions and the radiation that originates in thermally excited electronic states, a phenomenon that has received some attention recently. The high oscillator strength of electronic transitions can more than compensate for the relatively low population of these states, and the time constants of these processes, for historical reasons called recurrent fluorescence, can have time constants on the order of  $\mu$ s, versus the typically ms values for vibrational transitions. The energy



of the excited state plays the role of activation energy for the process, and the emission rate constants can therefore vary dramatically between molecules of similar kind but with an even very small difference in chemical composition.

Decays of molecular beams come with a special feature when internal energy distributions have a width that exceeds the relatively small value  $\delta E$  determined by

$$\frac{\delta E}{E} \gtrsim \frac{1}{\ln(\omega t)}, \quad (3)$$

where  $\omega$  is the frequency factor of the dominant decay,  $t$  is the time after production of the beam in the source, and  $E$  is the energy of the decaying molecules. The right hand side is around 0.05 for the microsecond timescales of single pass devices and smaller for the long times realized in ion traps and storage rings [182–185, 189]. The range of rate constants across such distributions produces a decay rate,  $R$ , which varies with time as a power law [201]:

$$R \equiv \int_0^\infty k(E)e^{-k(E)t}dE \approx C/t, \quad (4)$$

where  $C$  is the heat capacity of the decaying system. The power of  $-1$  on time will acquire corrections from a finite heat capacity and the slow variation of the width of the distribution, and the experimentally observed power is often slightly below  $-1$ .

The power law decay can be derived independently of the precise dependence of the rate constants on the excitation energy. The only requirement is that it varies rapidly with energy. This is the case for both thermionic emission and the usual unimolecular decay rate constants, and both types of decays have a propensity to

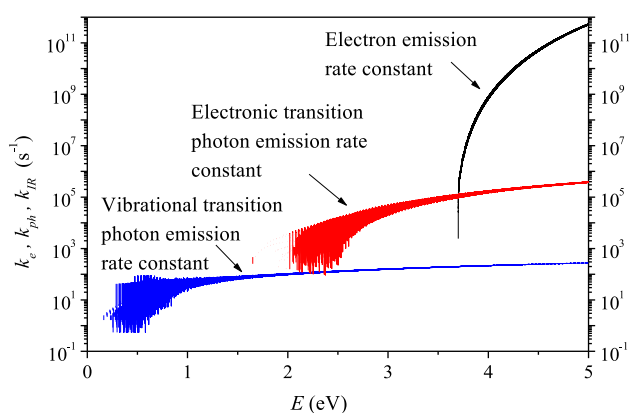


**Fig. 15** Calculated emission rate constants for  $C_4^-$  for the processes indicated in the frame, published in [226]. The rate constant for fragmentation has a form similar to that of electron emission. It is only appreciable at much higher energy due to its high activation energy and does not compete with electron emission for the anion. The slow variation of both photon rates with energy is a common feature for these channels

show power law decay rates. Photon emission rate constants, in contrast, usually have a much slower energy dependence and can in general not be expected to follow this simple behavior.

The power law decay also provides the expressions for the amount of the metastable decay that is often seen in time-of-flight mass spectrometers as a delayed decay between mass selection and detection. The relative amount of this component of the beam is simply the integrated and normalized decay rate. It contains information about the relative dissociation energies of the decaying cluster and its precursor, in addition to their heat capacities. Some results on this were derived by Klots [227], remarkably without the knowledge of the power law decay which simplifies derivations.

The power law decay has likewise been extremely useful as a tool to measure the presence and magnitude of dark channels. A dark (non-observed) channels can influence the power law decay in several different way, depending on its nature. The first observation of this kind was the thermionic emission rate of  $C_{60}$  which showed the expected power law nature, but with a power around 0.65 [228]. The explanation was found in the loss of  $C_2$  from the neutral molecule. The observed power provided a value for the activation energy of this channel, a value which is significant higher than the number commonly accepted at the time, but which is close to the currently accepted value.

Another channel for which the power law has provided a very powerful diagnostic tool is the thermal photon emission [229, 230]. Radiative cooling will modify the power law decay by suppressing it at long times with an exponential factor. The precise form of the factor depends on the magnitude of the emitted photons. In the small photon energy limit the emission will cause a practically continuous energy loss. The time constant for the exponential suppression in this limit involves several quantities, such as the emitted power, the molecular heat capacity, and the dissociation energy. It should be emphasized that the measured time constants for these cases are *not* the photon emission time constants. In the other limit, of large photon energies, emission of a single high-energy photon will quench any further unimolecular decay, and in this limit is the measured quenching time constant equal to the photon emission time constant. The quenched power law curves that result from these two limits are slightly different, but similar enough to prevent an experimental identification of the type of photon emission from the shape of the quenched curves alone.

Although the two types of quenching have very similar temporal behavior, the origins of the exponential suppression are different. Emission of large energy photons will deplete the decaying part of the energy distribution and is therefore similar to a normal exponential decay, e.g., a radioactive decay of a nucleus. The small photon energy cooling, in contrast, suppresses the decay by introducing an exponential decay of the value of the time constant.

## 16.2 Challenges and new directions

The phenomenon of thermal high-energy photon emission results from a finite thermal population of the emitting state, without any major restrictions on its presence. The only important requirement is that radiationless transitions after photo-excitation occur. This ensures that the inverse process can happen by time reversal. Radiationless transitions are indeed a very common phenomenon and the thermal emission of visible and near-IR photons is therefore much more common for highly excited species than apparent from the literature. At present the direct detection of photons emitted in such processes have only been accomplished for  $C_4^-$  and  $C_6^-$  [192]. In both cases an optical filter was used to select the emitted photon wavelength to correspond to the absorbing value. This background elimination greatly supported the identification of the measured photons, but is an unnecessary limitation once the assignment of the origin of the emitted photon has been established. Future measurements of emission spectra in the visible and near-infrared sectors will provide much more detailed information about the emitting molecules, as will time resolved measurements. This development will take place at traps and storage rings [185, 226, 231]. Although photon detection efficiencies will remain below those of massive particles for some time, the technique promises ultimately nondestructive information on a par with or surpassing the one obtained by measurements of unimolecular fragmentation.

In parallel with such experimental activity, developments of unimolecular reaction rate theories will be both necessary and fruitful. Although the subject is more than a century old, it still harbors open questions. Some of these are posed particularly acutely for decays of clusters. One question is the role of the traditional saddle point transition state which seems to be absent in clusters and certainly is so in the bulk limit for virtually all materials. (For the elements, only zinc is known to be an exception to this rule.) Another question is the role of angular momentum in the description of the particles. As a conserved quantity, angular momentum must obviously enter a description of thermal reactions in vacuum. Nevertheless, it is well known that vibrational motion can carry angular momentum, both on general grounds [232] and as described, e.g., for helium droplets [233]. Although rotational motion in the transition state has attracted attention in the past, this aspect of angular momentum in the description of reactivity is fairly unexplored.

Molecular beam studies share a good vacuum with the interstellar and star-forming regions of space, and the dynamics studied in the laboratory provides important information for the quantitative description of the interstellar molecular dynamics [234]. Molecules formed by collisions in space are guaranteed to be born with enough excess energy to fragment, and also to dissipate energy through emission of photons and potentially also electrons or atoms in channels that differ from that of the formation process. As a competing channel to frag-

mentation, radiative cooling therefore plays an essential role for the survival rate of the collision complexes. The possibility to form surviving larger molecules in a second collision step will then obviously also benefit from radiative stabilization. The formation of large molecules, including those of biological nature, will thus be characterized by survival of the fittest on the fundamental molecular level.

## 16.3 Concluding remarks

The development of ion traps and storage rings, in particular of the cryogenic variety, has greatly extended the time range for which it is possible to observe the decay dynamics of mass selected gas-phase molecules and clusters. In such studies, the non-exponential decays have appeared as an important diagnostic tool. Combined with the emerging field of spectroscopy of thermally emitted photons, it promises to open new venues for studies of highly excited molecules and clusters.

## 17 Photo-fragment and photo-detachment spectroscopy in cryogenically cooled ion traps

Jennifer A. Noble and Christophe Juvet, PIIM Laboratory, CNRS/Aix-Marseille Université, France

### 17.1 Status: description of the state of the art

The general principle of photo-fragment or photo-detachment spectroscopy is as follows: ions generated in different charge states (radical cation, protonated, deprotonated, etc.) and different structures (isomeric or tautomeric) using a source such as a discharge or an electrospray ionization (ESI) source are guided into a cryogenically cooled ion trap where they are cooled to temperatures of a few Kelvin by collisions with a buffer gas. Laser excitation induces fragmentation and/or photodissociation, and the products are extracted into a mass spectrometer for analysis. The photo-fragment or photo-detachment process is monitored as a function of the laser wavelength to generate the spectrum.

Major advances in the experimental technique have been made over the past 15 years, beginning with the cooling of ions via cryogenic technology [235]. Compared to room temperature, at a few tens of Kelvin, molecules present restricted isomers and discrete vibrational/rotational levels can be distinguished in their spectra. Contemporary cryogenic ion spectroscopic results are analogous to those achieved from around 40 years ago onwards for neutrals in supersonic jets, as is evident from the examples provided in multiple sections of this roadmap.

Advances in mass resolution—before and after trapping—have allowed more precise selection or measurement of individual masses. Ion mobility tech-



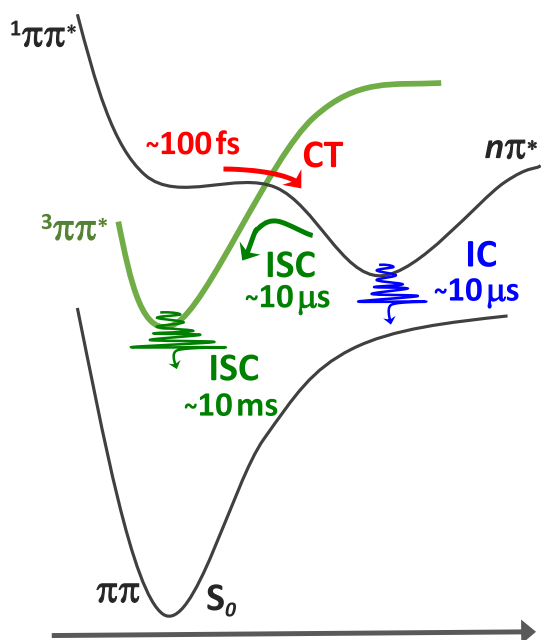


**Fig. 16** Using a cold ion trap, one can follow the molecular relaxation dynamics over more than 12 orders of magnitude: The ultrafast fs excited state lifetime prior to charge transfer (CT) is obtained from line broadening; the ps, ns and  $\mu$ s evolutions of CT, internal conversion (IC) and intersystem crossing (ISC) by pump-probe methods using ps and ns lasers; and the longer ms to s dynamics of ISC and ground state ( $S_0$ )/secondary fragmentation by delayed extraction of the fragment(s) from the trap. The schematic is inspired by the complicated time evolution of the dynamics of protonated cytosine, adapted from Ref. [242]

niques (see Sect. 19) allow the selection of a single isomer or tautomer of a given mass, and thus the study, for example, of its specific dynamics [236]. Most recently, the coupling of a cold trap with orbitrap technology has allowed the development of a combination of high spectroscopic resolution with a high resolution in mass [237].

Throughout the community, a multitude of photo-fragment and photo-detachment spectroscopies are applied to cold, trapped ions, from single laser UV-visible photo-fragmentation to pump-probe depletion/gain spectroscopies. The coupling of ESI with advanced light sources for the study of biomolecules over a wide photon energy domain is reviewed in Sect. 5. Of particular note has been the development of hole-burning spectroscopies, which allow the differentiation of bands

belonging to different species by comparing the spectral response of different channels to bleaching of a selected transition. The latest variant to be adopted was UV/UV hole-burning spectroscopy, due to the complications arising from the pump and probe pulses both generating the same product [238]. In this section we concentrate on action spectroscopy methods, but the nondestructive technique of fluorescence spectroscopy can also provide complementary information on excited state dynamics for certain (fluorescent!) ions, as discussed in the following section (Sect. 18).

In the case of negative ions, the cooling of the parent coupled with the development of the high-resolution photoelectron spectrometer has shed new light on the photo-detachment process as well as allowing the characterization of deprotonated ions and their photo-detachment products—i.e. dehydrogenated radicals—which are often the intermediates in reactions [239]. Following photo-detachment of the deprotonated ion, the resulting dehydrogenated radical is not necessarily stable. If the photo-detachment is performed after the extraction of the deprotonated ion from the cold trap, the detection of the fast neutrals formed upon fragmentation of the dehydrogenated radical allows measurement of the kinetic energy released by the fragmentation process [240].

The generation of size-selected clusters or larger aggregates can be achieved by the addition of a second cold trap between the ion source and the photo-fragmentation trap. The systematic study of size-selected clusters consisting of an ion surrounded by increasing numbers of solvent molecules allows the investigation of the influence of the solvent molecule on the dynamics of the system [241]. This approach can, to a first order, be considered analogous to a study of the first solvation shell of the ion in a liquid solvent, allowing parallels to be drawn between gas-phase and solution-phase experiments.

One of the most remarkable outcomes of the work produced by the community in recent years is the revelation that the temporal range over which dynamics in molecular ions and their clusters can be experimentally observed extends more than 15 orders of magnitude. Indeed, it has been observed that the dynamics of photo-fragmentation extend over this entire temporal range—even for a molecule of a well-defined energy—with excited state relaxation occurring on the femtosecond timescale, ground state fragmentation of the parent ions in the nanosecond to millisecond range, and secondary fragmentation occurring over seconds, as illustrated in Fig. 16.

## 17.2 Challenges and new directions

The wealth of spectroscopic studies performed to date using cryogenic ion traps have revealed and characterized photon-driven processes in molecular systems of varying charge states. The interpretation of these data represents a major challenge for *ab initio* calculation methods. Consider, for example, the experimen-

tal evidence that different, highly selective, fragmentation channels can be accessed upon the excitation of extremely closely-spaced excited states, with selective fragmentation being observed not only between two electronic states, but even between vibrational levels within the same electronic excited state differing in energy by less than 1 %. The assumption made in the statistical fragmentation argument is that once in the ground state, the whole potential surface can be explored by the molecule. In this case, the selective fragmentation cannot be attributed to overcoming certain barriers to fragmentation routes. Can the on-the-fly method be applied to these molecular systems in order to pinpoint the origin of the new fragmentation channels opened up by the tiny change in energy? While excited states of closed-shell molecules are typically very well simulated in calculations, open-shell structures still offer an interesting conundrum. The development of additional, more specialized, experimental setups dedicated to the generation and characterization of charged and/or neutral radical species is required to provide a thorough benchmark for theoretical efforts in this area.

Other experimental developments which promise to revolutionize the field include the new analytical methods of mass spectrometry which combine mass with the spectral fingerprint for a full diagnostic of the molecule and its fragments. It has previously been demonstrated that the development of a multi-step (UV/ms)<sup>n</sup> process, where the parent ion and fragment(s) are successively excited then mass characterized, could go a long way to resolving some of the outstanding issues of molecular characterization in pharmaceutical research and development [243]. Finally, the laser-induced inhibition of complex growth (LIICG) method [244], in which the internal energy introduced into the molecule by the laser prevents it forming clusters with atoms such as helium in the trap, is a technique which is potentially universally-available but has not yet been extensively applied. It is a very promising method for the study of selectively excited molecules, although the distribution of the injected energy across a large number of states means that, for certain larger molecular systems, the experiment requires careful calibration in order to extract an exploitable signal.

### 17.3 Concluding remarks

Since the pioneering work of the EPLF team [235], photo-fragment and photo-detachment spectroscopy in cryogenically cooled ion traps has flourished [175, 245]. This method has opened the door to the high precision study of very big and “floppy” molecular systems; the characterization, for example, of decapeptide [246]—a polypeptide consisting of a chain of ten amino acids—would previously have been inconceivable. The technique has also allowed the study of molecular species in different charge states which were hitherto totally unexplored (protonated, deprotonated, dehydrogenated, etc.), providing information on ions

and radicals which represent reaction intermediates in domains as diverse as biology and astrophysics.

**Acknowledgements** We thank Claude Dedonder for her invaluable input.

## 18 Gas-phase fluorescence spectroscopy of complex molecular ions

Christina Kjær and Steen Brøndsted Nielsen, Department of Physics and Astronomy, Aarhus University, Denmark

### 18.1 Status: description of the state of the art

Action spectroscopy has for many years provided significant information on electronic transition energies of isolated molecular ions in vacuo. It is an indirect technique based on either photodissociation, electron detachment, or photoisomerization (see Sects. 14.1, 17.1, 19.1) to identify photon absorption, which is necessary as the ion density is too low for traditional light-transmission experiments. However, the requirement of “action” is an inherent problem, in particular, in the case of complex ions with many degrees of freedom or strongly bound ones as there is limited dissociation within the time frame of the mass spectrometer, typical a few microseconds to tens of milliseconds dependent on the setup [247]. The result is no “action” or spectra skewed toward the blue. A nondestructive technique is therefore advantageous such as fluorescence spectroscopy where emitted photons are detected.

While there is no molecular size limitation in fluorescence spectroscopy, it is still challenging to measure fluorescence from a thin cloud of ions, say 1 million ions in a volume of 1 mm<sup>3</sup>. To put things in perspective, compare with the  $6 \times 10^{13}$  ions in the same volume of a 0.1-mM solution, a difference of seven orders of magnitude! Clearly, the background counts of scattered photons and the noise level have to be kept as low as possible in the gas-phase experiment. Nevertheless, beautiful work has been done by several groups to establish the intrinsic photophysics of many fluorescent molecular ions and the impact of a microenvironment, including transition energies determined from dispersed fluorescence spectra and excited-state lifetimes (see, e.g. [248] and PIs listed in Table 1). Also gas-phase Förster resonance energy transfer (FRET) experiments on macromolecular ions labeled with two fluorescent dyes have revealed important information on folding motifs of peptides, proteins, and nucleic acids [249, 250], information that traditionally is established in ion-mobility experiments.

One large advantage of the gas-phase experiment is that the impact of individual perturbations can be disentangled one at a time, e.g., how much a nearby charge affects the spectroscopic properties as previously done for rhodamine dyes [251]. Also noteworthy, even though the ion density is much lower than in solution, the gas-phase experiment is in itself much cleaner as only mass-

**Table 1** Summary of fluorescence setups for ions produced by ESI or MALDI and timeline

Year	PI	Trap	Location
2002	J. H. Parks [255]	Paul	The Rowland Institute at Harvard
2004	A. G. Marshall [256]	LQT	Florida State University
2005	R. Zenobi [257]	Penning	ETH Zürich
2009	J. I. Cline/K. M. Ervin [258]	Paul	University of Nevada
2009	R. A. Jockusch [250]	Paul	University of Toronto
2010	M. M. Kappes/D. Schooss [252]	Paul	KIT
2016	S. Brøndsted Nielsen [231]	Paul	Aarhus University
2018	A. Ferzoco [253]	LQT	The Rowland Institute at Harvard
2018	K. Honma [259]	Paul	University of Hyogo
2020	R. Zenobi [260]	Paul	ETH Zürich

selected ions contribute to the fluorescence; there are no impurities.

In a typical experiment, complex ions are formed in the gas phase by electrospray ionization (ESI) and transferred to an ion trap where they are stored, and those of interest are mass selected. Often a Paul trap is used as here the ions are located in the center after collisional cooling and act as a point source for light emission. Still, it is non-trivial to extract the emitted photons after photo-excitation, and collection efficiencies are often less than half a percent. In our luminescence setup (denoted LUNA [231]) we use a cylindrical Paul trap where the exit electrode is a mesh grid to allow as many photons as possible to exit the “fluorescence cell.” This approach increases the collection efficiency to about 5%.

A summary of laboratories that have reported fluorescence from ions produced by ESI or MALDI (matrix-assisted laser desorption/ionization) is given in Table 1 including the year of the first publication and the type of trap (Paul, linear quadrupole trap (LQT), or Penning). Different lasers have been used in combination with the mass spectrometers, both CW and pulsed ones with low repetition rates (10–20 Hz) and very high rates (80 MHz). A high repetition rate has obvious advantages but does not allow for mass selection in between each laser irradiation event, and collisional cooling can also be an issue when the time between two laser pulses is only 12.5 ns (cf., 80 MHz).

Most experiments are done at room temperature but it is worth to mention two unique setups built by Kappes, Schooss and their co-workers [252] and Ferzoco and co-workers [253] where ions are cooled to low temperatures. The former operates close to 77 K (liquid nitrogen temperature) while in the latter, ions are stored in a LQT at ambient to cryogenic temperatures. Indeed, the almost open geometry of the linear ion trap and the collection optics gives an excellent signal; about  $10^7$  photons per second are collected from between the trapping rods.

## 18.2 Challenges and new directions

A fluorescence experiment obviously only makes sense if the ions are fluorescent! This is an obstacle in many

cases, in particular as it is hard to detect fluorescence if the quantum yield is too low (lower limit is about 0.1% in our experiments). Fluorescence can be quenched because of out-of-plane deformations of the chromophore or twist motions, and freezing out this motion as much as possible often increases the fluorescence. One prime example is the green fluorescent protein (GFP) chromophore anion that is non-fluorescent in solution and in vacuo while fluorescence in solutions is established at liquid nitrogen temperatures (see discussion in [254] with references). According to pump-probe experiments, the excited-state lifetime of the isolated chromophore anion is long (about 1 ns) at 100 K [209], and a relevant experiment would be to establish if the isolated anion is fluorescent at low temperatures. It is in this regard important to reduce RF heating in the trap, which is most easily done by mass selection at a prior stage and not in the trap itself. Oxyluciferin is another non-fluorescent ion at room temperature that may become fluorescent upon cooling; this ion accounts for the bioluminescence seen from many light-emitting insects such as fireflies.

Another interesting aspect is how a single solvent molecule (e.g., water) or a molecular dipole (e.g., betaine that has a dipole moment of 12 D) affects the fluorescence, both the quantum yield and the spectrum itself. Clearly, amino acid residues in a protein cavity are crucial to suppress the intramolecular twist motions that quickly brings the chromophore from the excited state back to the ground state, either due to space restrictions inside the cavity (steric crowding) or by providing high local electric fields at relevant chromophore sites (for example, a protonated arginine residue close to the phenolate oxygen in case of the GFP chromophore anion). Experiments on ion-molecule complexes are, however, non-trivial as unwanted reactions such as photodissociation would quickly reduce the number of ions in the trap to zero. One way could be to seed the helium buffer gas with water vapor to constantly reform the complexes. These experiments would require a low frequency laser (e.g., 20 Hz) to have enough time to remove bare ions between irradiation events.

Finally, it is worth to emphasize that fluorescence experiments can provide significant information on the

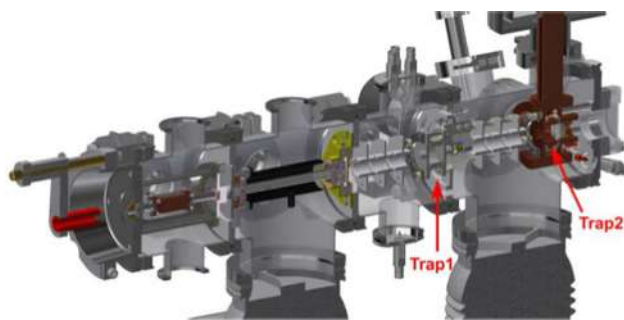


**Fig. 17** LUNA2 is a new setup to measure luminescence from cold, photoexcited molecular ions that is under construction in our laboratory. It contains two traps: Trap1 is used as a pretrap and to filter off unwanted ions. Ions of interest are transferred to Trap2, placed in a copper block cooled to 1q-N<sub>2</sub> temperature. In Trap2, photo-excitation is done, and emitted photons are collected and detected

excited-state dynamics as structural changes are evidenced from large Stokes shifts, one example being the fluorescein anion. Indeed, being able to measure dispersed fluorescence spectra on a picosecond timescale would provide unprecedented information on the dynamics and associated microenvironmental changes.

### 18.3 Concluding remarks

How to turn on fluorescence (or how to slow down excited-state dynamics) is in our view an interesting prospect for the future. Such fundamental understanding is to be obtained from experiments done at low temperatures and on cleverly designed ion–molecule complexes and could be beneficial for the engineering of new fluorophores, in particular in the red region of the visible spectrum where light penetration through tissue is high. In our laboratory, we are currently developing LUNA2 that operates at 77-K temperature, and where mass selection is done before the ions enter the cold Paul trap (Fig. 17).

Gas-phase fluorescence spectroscopy of complex ions is still in its infancy, involving a limited number of groups worldwide. However, new instrumental developments could very well boost this area of research, and in a few years, fluorescence detection may become a standard method in the ever increasing toolkit of mass spectrometry. We believe the future is bright.

## 19 Action spectroscopy of isomer-selected molecules

Eduardo Carrascosa, Laboratoire de Chimie Physique Moléculaire, École Polytechnique Fédérale de Lausanne, Switzerland

James Bull, School of Chemistry, University of East Anglia, United Kingdom

### 19.1 Status: description of the state of the art

Many gas-phase ions can exist in more than one isomeric form, each of which may have distinct absorption properties and excited-state dynamics. Examples include carbon clusters, which have 1D linear chains, 2D rings, and 3D structures, polycyclic aromatic hydrocarbons (Sect. 20) with structural isomers, and photoactive protein chromophores or biomolecules (Sects. 4, 5, 14, 17), which often have several geometric isomers, tautomeric and (de)protomeric forms. Biomolecular ions typically have a high degree of conformational fluxionality, ideally requiring action spectroscopy techniques to sample this complexity in a sensitive manner. However, the gas-phase abundance of each isomer usually depends on many factors including the precursor form and any solvation environment, the ion source (e.g. electrospray ionization (Sects. 5, 14, 17, 18), laser ablation, thermal evaporation), and the collisional treatment of the ions as they are introduced into vacuum. For example, energetic collisions between the target ions and background gas by extraction, acceleration or RF fields before spectroscopic investigation can increase the target ion's internal vibrational energy (temperature), inducing interconversion between the isomers. On the other hand, if there are substantial isomerization barriers, an ion source may generate kinetically-trapped species. Although many implementations of gas-phase action spectroscopy select target ions based on their mass-to-charge ( $m/z$ ) ratio, e.g. time-of-flight, quadrupole, or sector mass spectrometers, these approaches are unable to distinguish isomers.

The most common strategy for separating isomers in the gas-phase is through ion mobility spectrometry (IMS) [261]. In IMS, charged isomers propelled through a buffer gas (e.g. He, N<sub>2</sub> or CO<sub>2</sub>) under the influence of an electric field are separated according to their collision cross sections ( $\Omega$ ).  $\Omega$ , which represents the effective collisional surface area presented by an ion, typically has two contributions: a small impact parameter (hard-sphere collision) component, and a large impact parameter (glancing collision) component. Whereas He buffer gas is best suited for distinguishing isomers with substantially different shapes defined by the first contribution, buffer gases such as N<sub>2</sub>, CO<sub>2</sub>, or those seeded with organic dopants are suited for distinguishing isomers with differing long-range intermolecular interactions, including dipole-quadrupole and hydrogen bonding.

There are four primary IMS techniques: drift-time (or drift-tube) ion mobility spectrometry (DTIMS), traveling-wave ion mobility spectrometry (TWIMS), field-asymmetric ion mobility spectrometry (FAIMS), and trapped ion mobility spectrometry (TIMS), with each having certain advantages [261–263]. Selected key properties are summarized in Table 2. SLIM-IMS (structures for lossless ion manipulations ion mobility spectrometry) is a promising development, which involves isomer separation using printed circuit boards [264].



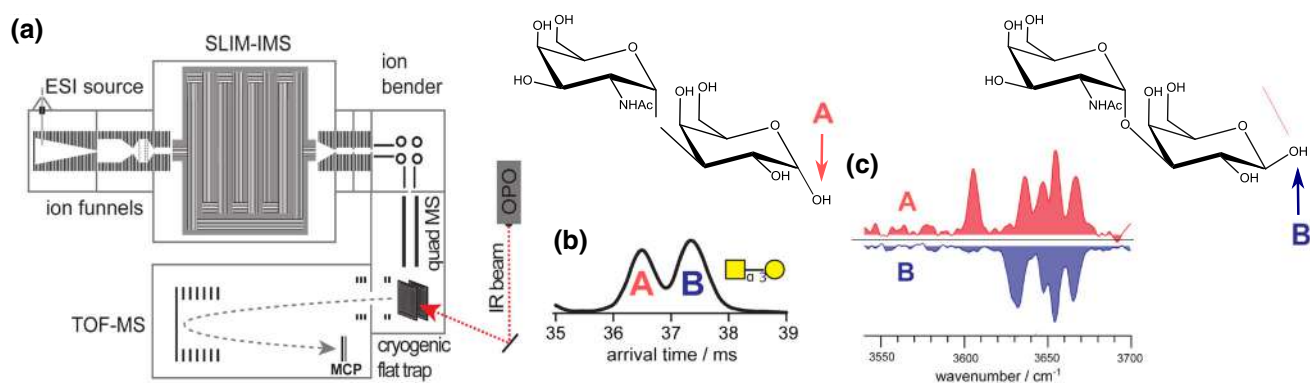


**Fig. 18** Action spectroscopy with SLIM-IMS and cryogenic ion trapping: **a** schematic illustration of the instrumentation, **b** arrival time distribution of two electrosprayed anomers (A and B), **c** IR spectra of mobility-selected and cryocooled anomer ions A and B. Molecular structures of A and B are shown with the arrows indicating the important equatorial (red) and axial (blue) hydroxide groups. Key: ESI—electrospray ionization, TOF-MS—time-of-flight mass spectrometry, quad MS—quadrupole mass filter, MCP—multi-channel plate detector, OPO—optical parametric oscillator. Figure adapted from Ref. [274]

Several research groups have coupled IMS techniques with tunable light sources to enable isomer-selected action spectroscopy. Implementations include IMS coupled with photoelectron spectroscopy [265,266], photodissociation spectroscopy [267–272], and photoisomerization spectroscopy [273]. A recent example of isomer-specific IR action spectroscopy is shown in Fig. 18 [274]. In this example, a SLIM-IMS device has been coupled with a quadrupole mass filter, cryogenic ion trap and time-of-flight (reflectron) mass spectrometer. The study was able to separate and identify two glycan anomers from the ion's arrival time distribution (ATD, Fig. 18b). Glycan anomers are difficult to distinguish using other ion mobility techniques because  $\Omega$  values for different anomers usually differ by less than 1%. Cryogenic cooling of each isomer in the trap and messenger tagging allowed acquisition of distinct isomer-specific IR spectra in the hydroxide stretching region (Fig. 18c). Supporting experiments on labelled

and methylated analogues gave unambiguous assignment of each ATD peak to an anomer structure.

## 19.2 Challenges and new directions

Current challenges in this field can be divided into two categories: (1) development of universal and cost effective isomer-selection instrumentation that can be easily coupled with existing action spectroscopy experiments, (2) new strategies for improving information content during spectral acquisition.

Currently, isomer-specific action spectroscopy instrumentation is either built by specialist research groups [265,266,273], or is based on modified commercial mass spectrometers [268,271,272]. General availability of a well-characterized IMS device, such as SLIM-IMS with ion trapping capacity, which could be easily integrated into new or existing instrument, would be a decisive step in setting isomer-selected action spectroscopy as the standard. Cryocooling potential is highly desirable.

The second major challenge is improving the key performance characteristics of IMS techniques (Table 2) and the development of methodology to provide enhanced information content. In the first instance, this

**Table 2** Key properties of the main IMS techniques.  $\Omega$  is the collision cross section and  $\frac{\Omega}{\Delta\Omega}$  is the resolving power.  $T_{\text{eff}}$  is the ion effective temperature and  $T$  is the buffer gas temperature. Note, FAIMS separates isomers based on their difference in mobility in high and low electric field

	DTIMS	TWIMS	FAIMS	TIMS	SLIM-IMS
Resolving power	> 100	< 300	< 100	< 500	< 650
Measure $\Omega$	Yes	Partially	No	Partially	Partially
$T_{\text{eff}}$	$\approx T$	$> T$	$\gg T$	$> T$	$> T$
Portability	Low	Low	Medium	Medium	High
Dynamic range	Low	Low	High	Medium	Low
Sensitivity	Low	Medium	High	High	Medium
Cryopotential	Medium	Low	Very low	Medium	High



could be through improving resolving power (e.g. cyclic devices) combined with cryocooled buffer gas. While a lower temperature of buffer gas improves isomer separation, it also allows separation and isolation of isomers with low barriers to interconversion (e.g. rotamers), which rapidly interconvert at elevated temperatures. This can be particularly important for resolving specific biomolecule interactions and photochemistry, for example, open versus  $\pi$ -stacked structures of DNA polynucleotides [275]. Enhancing information content might involve the use of several light sources to photogenerate and probe isomeric intermediates, or incorporation of additional orthogonal analysis techniques (e.g. multi-dimensional action spectroscopy). A significant development by the Bieske group involved coupling of two ion mobility stages with laser spectroscopy, allowing isomer-selection of a target ion [273]. This strategy has enabled simultaneous monitoring of photoisomerization, photodissociation, and photo-detachment (for anions). Furthermore, the methodology can be adapted to numerous IMS and photo stages, allowing the study of multi-step photoreactions in the gas phase.

### 19.3 Concluding remarks

Isomer-resolved action spectroscopy is a rapidly evolving field, offering the capacity to study the photochemistry and photophysics of individual isomers. The possibility that an ion source could generate more than one gas-phase isomer is an important, possibly crucial, factor to consider for gas-phase systems such as biomolecules due to the range of potential isomers. There is an increasing expectation that robust action spectroscopy investigations should include some degree of isomer selectivity.

## 20 Deciphering the lifecycle of carbon macromolecules in space

Alessandra Candian and Annemieke Petrigiani, van 't Hoff Institute for Molecular Sciences, University of Amsterdam, The Netherlands

### 20.1 Status: description of the state of the art

Carbon is one of the most abundant elements in the Universe, produced by nucleosynthesis in dying low-mass stars; this together with its unique ability to form multiple stable bonds with itself and other elements, makes carbon one of the building blocks of life. Understanding carbon chemistry, i.e., the path of carbon species from their synthesis to their transformation and destruction down to their delivery in exosolar system is of paramount importance. Key organic species are polycyclic aromatic hydrocarbon (PAH) molecules, in which 10% of all cosmic carbon could be locked. PAHs are detected in space through the aromatic infrared bands (AIBs), a family of emission features in the mid-

infrared (3–20  $\mu\text{m}$  or 3100 to 500  $\text{cm}^{-1}$ ) seen toward different astronomical environments in our Galaxy and beyond (see [276] for a recent review). Since their discovery in the previous century, much effort had gone into their spectroscopy and the development of astronomical PAH models. As our understanding advances, the importance of the underlying mechanisms driving and affecting the spectral signatures, evolution, and the role these large hydrocarbons play in the production of other (organic) species, has become increasingly apparent.

PAHs are efficient energy converters that absorb UV/Vis photons coming from young stars and re-emit them in the infrared, producing the AIBs. The high spectral resolution achieved by past space observatories (ISO and Spitzer) has allowed astronomers to have a better grasp of the composition of the astronomical PAH population. Astro-PAHs have a size between roughly 40 and 120 carbon atoms [277] and their charge varies from  $-1$  to  $+2$  depending on a fine-tuned balance between the hardness of the radiation impinging on PAHs and the density of the gas where they reside. There is evidence that in astronomical environments PAHs can have heteroatom substitutions and side groups [276]. The variations in the appearance of the astronomical spectra hint to an active chemistry molding the populations of astro-PAH (Fig. 19), originating from the photoevaporation of very small (nanometer size) carbonaceous grains. The state-of-the-art model of the photophysical evolution of astro-PAHs (e.g. [278]) considers mostly charge and H-coverage. The latter has implications for the formation of  $\text{H}_2$ , the most abundant molecule in space. PAHs can also act as source of smaller hydrocarbons, which importance has recently also been assessed [279]. Not included in astronomical modeling (yet), is the role of isomerization, which has now also been shown to play a role in the dynamics of photodissociation of astro-PAHs [280–282].

In 2010, the Buckminsterfullerene  $\text{C}_{60}$  was detected through its vibrational modes in the planetary nebula TC 1 [283]; since then  $\text{C}_{60}$  have been discovered in many other environments, including the diffuse interstellar medium. Indeed, thanks to a state-of-the-art experiment, the electronic transitions of the radical cation of fullerene,  $\text{C}_{60}^+$ , have been matched to four diffuse interstellar bands (or DIBs) [176] a set of more than 200 unidentified absorption bands in the UV–visible that have been named “the longest standing puzzle in astronomical spectroscopy.” The discovery of  $\text{C}_{60}$  in regions where also PAHs are present has pushed forward the idea that the lifecycle of these carbon macromolecules is intertwined; the top-down formation of  $\text{C}_{60}$  from the photoprocessing of large PAHs has been proved experimentally [284] but the details of the process and the intermediates have yet to be characterized.

## 20.2 Challenges and new directions

To model the processes driving PAHs evolution requires detailed studies of these processes and corresponding spectral behavior of the species involved. This includes studies of vibrational normal modes, UV photo-absorption cross sections and ionization yields, electron attachment, recombination, reactivity to atomic hydrogen, and photodissociation rates [279], to name a few. In many cases, these processes have been necessarily studied for only a handful of relatively small PAHs, either neutral or positively charged, sometimes with additional hydrogen atoms or substitutions, and the results are applied to larger PAHs without further adjustment. For fullerenes and carbon cages experimental studies are limited to  $C_{60}$  and  $C_{70}$ . Theoretical chemistry methods can be used to study molecular systems of astrochemical interest with less limits in shape and charge. Statistical rate theory applications are often used in kinetic studies for small molecules. Such studies typically employ Density Functional Theory (DFT) for most properties (geometries, vibrational frequencies) and, when the size of the system allows, higher accuracy calculations, such as ab-initio or composite methods, for, e.g., relative energies [286,287]. For large carbonaceous molecules, thorough investigation of dissociation channels using static DFT quickly becomes unfeasible. In this situation, molecular dynamics (MD) simulations provide a powerful tool, not only to complement statistical theories, but also to tackle other questions, for example, overlooked reactions pathways. The accuracy of MD simulations in predicting the dynamics of a system depends on the method used to compute the force. The reactive empirical bond order (REBO) models and the adaptive interatomic

reactive empirical bond order (AIREBO) are natural choices when studying clustering and dimerization of large carbon and hydrocarbon structures, because these models enable bond formation or bond breaking at relatively small computational cost [288]. Molecular dynamics (MD) based on density functional tight binding (DFTB) (see Sect. 9) provides a computationally-efficient tool to investigate photo-induced fragmentation and isomerization; not only does it compare successfully with experimental results, it also gives energetics comparable to standard DFT [280]. Alternatively, isomerization pathways and equilibrium properties at fixed total energy in the canonical or microcanonical ensembles can be described using biased Monte-Carlo methods [289]. Potential energy of specific molecular configurations are determined using a reactive force field, such as AIREBO, which includes also the effects of anharmonicity, and the thermodynamical properties are evaluated through the Wang-Landau approach; this approach consists in random walk around the configurations that is quickly able to visit all the available states and build an estimate of the density of configurational states.

To avoid the limitation of remaining trapped into local free-energy-minimum conformations when exploring the energy surface—a realistic problem for large hydrocarbons—replica exchange MD simulations or metadynamics should be considered [290]. MD calculations create a large amount of data that need to be analyzed and processed in order to obtain results such as reaction barriers that are ingredients for photo-physical models. Automated software that uses graph theory to extract reactive pathways from MD simulations and then simulates the fragmentation dynamics through kinetic approaches can thus be used to great advantage.

Experiments on the fragmentation of large, non-standard PAHs with different charge states and break-fullerenes are fundamental to benchmark the results of the simulations. Advances in experimental technique have opened up new possibilities to study these species and learn more about their isomerization and radiative lifetimes. Ion mobility spectrometry (IMS) has undergone major developments (see Sect. 19) that allow for increasingly improved separation and identification of isomeric species. Combining IMS with the current state-of-the-art mass spectrometric and spectroscopic techniques offers much potential to study photo-induced isomerization and fragmentation.

The anharmonic behavior of molecules strongly affect the reaction rates through density of states and energy barriers. Understanding the anharmonic behavior of PAHs, which is now possible at least for small sizes [291] thanks to synergy between state-of-the-art calculations and experiments, will allow an accurate modeling of reaction rates with the exciting possibility to implement machine learning techniques to extended the knowledge to larger molecules [292] such as fullerene. IR inactive normal modes are essential in the calculations of density of states. Here, techniques such as zero-electron kinetic energy (ZEKE) spectroscopy could

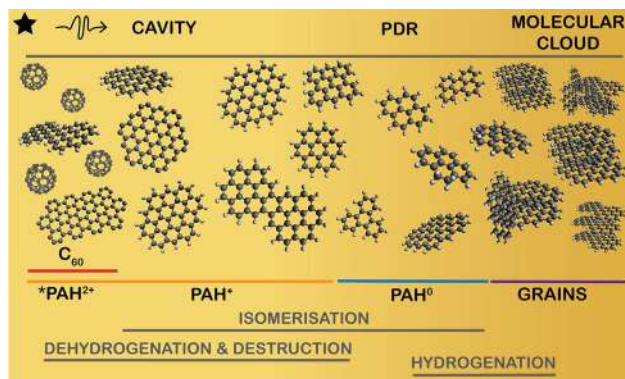


**Fig. 19** Evolution of carbonaceous material across a star forming region, adapted from Ref. [285]. The dominant charge/type of material and the processes at play are indicated in the bottom of the figure. Carbonaceous very small grains, residing in the dense molecular cloud, are converted to free flying PAHs in the photodissociation region (PDR) that is created by photons below 13.6 eV illuminating the outer layers of the cloud. Closer to star, in the so-called cavity, the density and strength of photons change the PAH populations and led to the formation of  $C_{60}$

provide important information on not only IR-, but also Raman-active modes.

Finally, a deeper understanding of the ultrafast radiative and non-radiative processes occurring after photo-excitation is fundamental to assess the stability of molecules and correctly model their behavior. With the emergence of electrostatic storage rings (see Sect. 13) that allow for long storage times under ultrahigh vacuum conditions, experimental investigations on radiative cooling of increasingly larger species are becoming possible. At the same time, the field of excited state quantum dynamics is rapidly evolving with the promise of being applied to carbon macromolecules in the very near future.

### 20.3 Concluding remarks

The James Webb Space Telescope (JWST), the next infrared space telescope a joint European-Northern American venture, is now scheduled to be launched in Fall 2021. Thanks to its superior spectral sensitivity and resolution, JWST is expected to deliver incredible spectra, opening up a new window on the evolution of carbonaceous material in space. A timely and concerted effort on both experimental and theoretical sides is fundamental to exploit JWST capabilities and its promise to revolutionize our view of the carbonaceous universe.

**Acknowledgements** The authors are supported by a VIDI grant (723.014.007) of A.P. from The Netherlands Organisation for Scientific Research (NWO).

### Author contributions

All authors contributed equally through the writing of the individual sections in the manuscript. All authors have read and approved the final manuscript.

**Funding Information** Open access funding provided by Stockholm University.

**Data Availability Statement** This manuscript has no associated data or the data will not be deposited. [Authors' comment: No new data is being presented in this review article.]

**Open Access** This article is licensed under a Creative Commons Attribution 4.0 International License, which permits use, sharing, adaptation, distribution and reproduction in any medium or format, as long as you give appropriate credit to the original author(s) and the source, provide a link to the Creative Commons licence, and indicate if changes were made. The images or other third party material in this article are included in the article's Creative Commons licence, unless indicated otherwise in a credit line to the material. If material is not included in the article's Creative Commons licence and your intended use is not permitted by statutory regulation or exceeds the permitted use, you will need

to obtain permission directly from the copyright holder. To view a copy of this licence, visit <http://creativecommons.org/licenses/by/4.0/>.

### References

1. M. Ferray, A. L'Huillier, X.F. Li, L.A. Lompre, G. Mainfray, C. Manus, *J. Phys. B: At. Mol. Opt. Phys.* **21**(3), L31 (1988). <https://doi.org/10.1088/0953-4075/21/3/001>
2. F. Lépine, M.Y. Ivanov, M.J.J. Vrakking, *Nat. Photonics* **8**(3), 195 (2014). <https://doi.org/10.1038/nphoton.2014.25>
3. M. Nisoli, P. Decleva, F. Calegari, A. Palacios, F. Martín, *Chem. Rev.* **117**(16), 10760 (2017). <https://doi.org/10.1021/acs.chemrev.6b00453>
4. H.J. Wörner, C.A. Arrell, N. Banerji, A. Cannizzo, M. Chergui, A.K. Das, P. Hamm, U. Keller, P.M. Kraus, E. Liberatore, P. Lopez-Tarifa, M. Lucchini, M. Meuwly, C. Milne, J.E. Moser, U. Rothlisberger, G. Smolentsev, J. Teuscher, J.A. van Bokhoven, O. Wenger, *Struct. Dyn.* **4**(6), 061508 (2017). <https://doi.org/10.1063/1.4996505>
5. A. Palacios, F. Martín, *WIREs Comput. Mol. Sci.* **10**(1), 1 (2020). <https://doi.org/10.1002/wcms.1430>
6. S. Maclot, J. Lahl, J. Peschel, H. Wikmark, P. Rudawski, F. Brunner, H. Coudert-Alteirac, S. Indrajith, B.A. Huber, S. Díaz-Tendero, N.F. Aguirre, P. Rousseau, P. Johnsson, *Sci. Rep.* **10**, 2884 (2020). <https://doi.org/10.1038/s41598-020-59649-1>
7. A.H. Zewail, *J. Phys. Chem. A* **104**(24), 5660 (2000). <https://doi.org/10.1021/jp001460h>
8. J. Ullrich, R. Moshhammer, A. Dorn, R. Dörner, L.P.H. Schmidt, H. Schmidt-Böcking, *Rep. Prog. Phys.* **66**(9), 1463 (2003). <https://doi.org/10.1088/0034-4885/66/9/203>
9. J.P. Marangos, *J. Phys. B: At. Mol. Opt. Phys.* **49**(13), 132001 (2016). <https://doi.org/10.1088/0953-4075/49/13/132001>
10. R. Geneaux, H.J.B. Marroux, A. Guggenmos, D.M. Neumark, S.R. Leone, *Philos. Trans. R. Soc. A: Math. Phys. Eng. Sci.* **377**(2145), 20170463 (2019). <https://doi.org/10.1098/rsta.2017.0463>
11. F. Calegari, D. Ayuso, A. Trabattoni, L. Belshaw, S. De Camillis, S. Anumula, F. Frassetto, L. Poletto, A. Palacios, P. Decleva, J.B. Greenwood, F. Martín, M. Nisoli, *Science* **346**(6207), 336 (2014). <https://doi.org/10.1126/science.1254061>
12. S. Kühn, M. Dumergue, S. Kahaly, S. Mondal, M. Füle, T. Csizmadia, B. Farkas, B. Major, Z. Várallyay, E. Cormier, M. Kalashnikov, F. Calegari, M. Devetta, F. Frassetto, E. Månsson, L. Poletto, S. Stagira, C. Vozzi, M. Nisoli, P. Rudawski, S. Maclot, F. Campi, H. Wikmark, C.L. Arnold, C.M. Heyl, P. Johnsson, A. L'Huillier, R. Lopez-Martens, S. Haessler, M. Bocoum, F. Boehle, A. Vernier, G. Iaquaniello, E. Skantzakis, N. Papadakis, C. Kalpouzos, P. Tzallas, F. Lépine, D. Charalambidis, K. Varjú, K. Osvay, G. Sansone, J. Phys. B: At. Mol. Opt. Phys. **50**(13), 132002 (2017). <https://doi.org/10.1088/1361-6455/aa6ee8>
13. J. Duris, S. Li, T. Driver, E.G. Champenois, J.P. MacArthur, A.A. Lutman, Z. Zhang, P. Rosenberger,



- J.W. Aldrich, R. Coffee, G. Coslovich, F.J. Decker, J.M. Glowina, G. Hartmann, W. Helml, A. Kamalov, J. Knurr, J. Krzywinski, M.F. Lin, J.P. Marangos, M. Nantel, A. Natan, J.T. O'Neal, N. Shivaram, P. Walter, A.L. Wang, J.J. Welch, T.J.A. Wolf, J.Z. Xu, M.F. Kling, P.H. Bucksbaum, A. Zholents, Z. Huang, J.P. Cryan, A. Marinelli, *Nat. Photonics* **14**(1), 30 (2020). <https://doi.org/10.1038/s41566-019-0549-5>
14. J. Ullrich, A. Rudenko, R. Moshhammer, *Annu. Rev. Phys. Chem.* **63**(1), 635 (2012). <https://doi.org/10.1146/annurev-physchem-032511-143720>
  15. R. Moshhammer, K. Schnorr, in *Synchrotron Light Sources and Free-Electron Lasers: Accelerator Physics, Instrumentation and Science Applications*, ed. by E.J. Jaeschke, S. Khan, J.R. Schneider, J.B. Hastings (Springer International Publishing, Cham, 2020), pp. 1493–1524. [https://doi.org/10.1007/978-3-030-23201-6\\_26](https://doi.org/10.1007/978-3-030-23201-6_26)
  16. K. Ueda, E. Sokell, S. Schippers, F. Aumayr, H. Sadeghpour, J. Burgdörfer, C. Lemell, X.M. Tong, T. Pfeifer, F. Calegari, A. Palacios, F. Martin, P. Corkum, G. Sansone, E.V. Gryzlova, A.N. Grum-Grzhimailo, M.N. Piancastelli, P.M. Weber, T. Steinle, K. Amini, J. Biegert, N. Berrah, E. Kukk, R. Santra, A. Müller, D. Dowek, R.R. Lucchese, C.W. McCurdy, P. Bolognesi, L. Avaldi, T. Jahnke, M.S. Schöffler, R. Dörner, Y. Mairesse, L. Nahon, O. Smirnova, T. Schlathölter, E.E.B. Campbell, J.M. Rost, M. Meyer, K.A. Tanaka, *J. Phys. B: At. Mol. Opt. Phys.* **52**(17), 171001 (2019). <https://doi.org/10.1088/1361-6455/ab26d7>
  17. L.J. Frasinski, *J. Phys. B: At. Mol. Opt. Phys.* **49**(15), 152004 (2016). <https://doi.org/10.1088/0953-4075/49/15/152004>
  18. J.W.L. Lee, H. Köckert, D. Heathcote, D. Papat, R.T. Chapman, G. Karras, P. Majchrzak, E. Springate, C. Vallance, *Commun. Chem.* **3**(1), 72 (2020). <https://doi.org/10.1038/s42004-020-0320-3>
  19. M.P. Minitti, J.M. Budarz, A. Kirrander, J.S. Robinson, D. Ratner, T.J. Lane, D. Zhu, J.M. Glowina, M. Kozina, H.T. Lemke, M. Sikorski, Y. Feng, S. Nelson, K. Saita, B. Stankus, T. Northey, J.B. Hastings, P.M. Weber, *Phys. Rev. Lett.* **114**, 255501 (2015). <https://doi.org/10.1103/PhysRevLett.114.255501>
  20. L. Ma, H. Yong, J.D. Geiser, A. Moreno Carrascosa, N. Goff, P.M. Weber, *Struct. Dyn.* **7**(3), 034102 (2020). <https://doi.org/10.1063/4.0000010>
  21. D.S. Tikhonov, A. Datta, P. Chopra, A.L. Steber, B. Manschwetus, M. Schnell, *Z. Phys. Chem.* **234**(7–9), 1507 (2020). <https://doi.org/10.1515/zpch-2020-0009>
  22. B.F. Murphy, T. Osipov, Z. Jurek, L. Fang, S.K. Son, M. Mucke, J.H.D. Eland, V. Zhaunerchyk, R. Feifel, L. Avaldi, P. Bolognesi, C. Bostedt, J.D. Bozek, J. Grilj, M. Guehr, L.J. Frasinski, J. Glowina, D.T. Ha, K. Hoffmann, E. Kukk, B.K. McFarland, C. Miron, E. Sistrunk, R.J. Squibb, K. Ueda, R. Santra, N. Berrah, *Nat. Commun.* **5**(1), 4281 (2014). <https://doi.org/10.1038/ncomms5281>
  23. N. Berrah, A. Sanchez-Gonzalez, Z. Jurek, R. Obaid, H. Xiong, R.J. Squibb, T. Osipov, A. Lutman, L. Fang, T. Barillot, J.D. Bozek, J. Cryan, T.J.A. Wolf, D. Rolles, R. Coffee, K. Schnorr, S. Augustin, H. Fukuzawa, K. Motomura, N. Niebuhr, L.J. Frasinski, R. Feifel, C.P. Schulz, K. Toyota, S.K. Son, K. Ueda, T. Pfeifer, J.P. Marangos, R. Santra, *Nat. Phys.* **15**(12), 1279 (2019). <https://doi.org/10.1038/s41567-019-0665-7>
  24. B. Erk, J.P. Müller, C. Bomme, R. Boll, G. Brenner, H.N. Chapman, J. Correa, S. Düsterer, S. Dziarzhytski, S. Eisebitt, H. Graafsma, S. Grunewald, L. Gumprecht, R. Hartmann, G. Hauser, B. Keitel, C. von Korff Schmising, M. Kuhlmann, B. Manschwetus, L. Mercadier, E. Müller, C. Passow, E. Plönjes, D. Ramm, D. Rompotis, A. Rudenko, D. Rupp, M. Sauppe, F. Siewert, D. Schlosser, L. Strüder, A. Swiderski, S. Techert, K. Tiedtke, T. Tilp, R. Treusch, I. Schlichting, J. Ullrich, R. Moshhammer, T. Möller, D. Rolles, *J. Synchrotron Radiat.* **25**(5), 1529 (2018). <https://doi.org/10.1107/S1600577518008585>
  25. P. Schmidt, V. Music, G. Hartmann, R. Boll, B. Erk, S. Bari, F. Allum, T.M. Baumann, G. Brenner, M. Brouard, M. Burt, R. Coffee, S. Dörner, A. Galler, P. Grychtol, D. Heathcote, L. Inhester, M. Kazemi, M. Larsson, J. Lee, Z. Li, A. Lutmann, B. Manschwetus, L. Marder, R. Mason, S. Moeller, T. Osipov, H. Otto, C. Passow, D. Rolles, P. Rupprecht, K. Schubert, L. Schwob, R. Thomas, C. Vallance, C. von Korff Schmising, R. Wagner, P. Walter, T.J.A. Wolf, V. Zhaunerchyk, M. Meyer, A. Ehresmann, A. Knie, P.V. Demekhin, M. Ilchen, *J. Phys: Conf. Ser.* **1412**, 112009 (2020). <https://doi.org/10.1088/1742-6596/1412/11/112009>
  26. M.H.M. Janssen, I. Powis, *Phys. Chem. Chem. Phys.* **16**, 856 (2014). <https://doi.org/10.1039/C3CP53741B>
  27. E. Allaria, R. Appio, L. Badano, W.A. Barletta, S. Bassanese, S.G. Biedron, A. Borgia, E. Busetto, D. Castonovo, P. Cinquegrana, S. Cleva, D. Cocco, M. Cornacchia, P. Craievich, I. Cudin, G. D'Auria, M. Dal Forno, M.B. Danailov, R. De Monte, G. De Ninno, P. Delgiusto, A. Demidovich, S. Di Mitri, B. Diviacco, A. Fabris, R. Fabris, W. Fawley, M. Ferianis, E. Ferrari, S. Ferry, L. Froehlich, P. Furlan, G. Gaio, F. Gelmetti, L. Giannessi, M. Giannini, R. Gobessi, R. Ivanov, E. Karantzoulis, M. Lonza, A. Lutman, B. Mahieu, M. Molloch, S.V. Milton, M. Musardo, I. Nikolov, S. Noe, F. Parmigiani, G. Penco, M. Petronio, L. Pivetta, M. Predonzani, F. Rossi, L. Rumiz, A. Salom, C. Scafuri, C. Serpico, P. Sigalotti, S. Spampinati, C. Spezzani, M. Svandrlík, C. Svetina, S. Tazzari, M. Trovo, R. Umer, A. Vascotto, M. Veronese, R. Visintini, M. Zaccaria, D. Zangrando, M. Zangrando, *Nat. Photonics* **6**(10), 699 (2012). <https://doi.org/10.1038/nphoton.2012.233>
  28. A. Cartoni, A.R. Casavola, P. Bolognesi, M.C. Castrovilli, D. Catone, J. Chiarinelli, R. Richter, L. Avaldi, *J. Phys. Chem. A* **122**(16), 4031 (2018). <https://doi.org/10.1021/acs.jpca.8b01144>
  29. L. Schwob, M. Lalonde, D. Egorov, J. Rangama, R. Hoekstra, V. Vizcaino, T. Schlathölter, J.C. Pouilly, *Phys. Chem. Chem. Phys.* **19**, 22895 (2017). <https://doi.org/10.1039/C7CP03376A>
  30. O. Plekan, V. Feyer, R. Richter, M. Coreno, M. de Simone, K.C. Prince, V. Carravetta, *Chem. Phys. Lett.* **442**(4), 429 (2007). <https://doi.org/10.1016/j.cplett.2007.05.110>
  31. A. Verkhovtsev, A. Traore, A. Muñoz, F. Blanco, G. García, *Radiat. Phys. Chem.* **130**, 371 (2017). <https://doi.org/10.1016/j.radphyschem.2016.09.021>

32. T. Arion, U. Hergenahhn, J. Electron Spectrosc. Relat. Phenom. **200**, 222 (2015). <https://doi.org/10.1016/j.elspec.2015.06.004>
33. J. Chiarinelli, P. Bolognesi, A. Domaracka, P. Rousseau, M.C. Castrovilli, R. Richter, S. Chatterjee, F. Wang, L. Avaldi, Phys. Chem. Chem. Phys. **20**, 22841 (2018). <https://doi.org/10.1039/C8CP03473G>
34. N.C. Jones, S.B. Nielsen, S.V. Hoffmann, Phys. Chem. Chem. Phys. **22**, 2188 (2020). <https://doi.org/10.1039/C9CP05292E>
35. I. Powis, in *Advances in Chemical Physics*, ed. by S.A. Rice (John Wiley & Sons, Ltd. 2008), chap. 5, pp. 267–329. <https://doi.org/10.1002/9780470259474.ch5>
36. M. Abdelmouleh, M. Lalande, V. Vizcaino, T. Schlathöler, J.C. Pouilly, Chem. A Eur. J. **26**(10), 2243 (2020). <https://doi.org/10.1002/chem.201904786>
37. G. Mattioli, L. Avaldi, P. Bolognesi, J.D. Bozek, M.C. Castrovilli, J. Chiarinelli, A. Domaracka, S. Indrajith, S. Maclot, A.R. Milosavljević, C. Nicolafrancesco, C. Nicolas, P. Rousseau, Sci. Rep. **10**, 10381 (2020). <https://doi.org/10.1038/s41598-020-69947-3>
38. J. Schuermann, A.F. Bagley, R. Berbeco, K. Bromma, K.T. Butterworth, H.L. Byrne, B.D. Chithrani, S.H. Cho, J.R. Cook, V. Favaudon, Y.H. Gholami, E. Gargioni, J.F. Hainfeld, F. Hespeels, A.C. Heuskin, U.M. Ibeh, Z. Kuncic, S. Kunjachan, S. Lacombe, S. Lucas, F. Lux, S. McMahon, D. Nevozhay, W. Ngwa, J.D. Payne, S. Penninckx, E. Porcel, K.M. Prise, H. Rabus, S.M. Ridwan, B. Rudek, L. Sanche, B. Singh, H.M. Smilowitz, K.V. Sokolov, S. Sridhar, Y. Stanishevskiy, W. Sung, O. Tillement, N. Virani, W. Yantasee, S. Krishnan, Phys. Med. Biol. **65**(21), 21RM02 (2020). <https://doi.org/10.1088/1361-6560/ab9159>
39. M. Yamada, M. Foote, T.W. Prow, WIREs Nanomed. Nanobiotechnol. **7**(3), 428 (2015). <https://doi.org/10.1002/wnan.1322>
40. R. Schürmann, K. Ebel, C. Nicolas, A.R. Milosavljević, I. Bald, J. Phys. Chem. Lett. **10**(11), 3153 (2019). <https://doi.org/10.1021/acs.jpcllett.9b00848>
41. D.K. Božanić, G.A. Garcia, O. Sublemontier, J. Pajović, V. Djoković, L. Nahon, J. Phys. Chem. C **124**(44), 24500 (2020). <https://doi.org/10.1021/acs.jpcc.0c08152>
42. M. Pitzer, M. Kunitski, A.S. Johnson, T. Jahnke, H. Sann, F. Sturm, L.P.H. Schmidt, H. Schmidt-Böcking, R. Dörner, J. Stohner, J. Kiedrowski, M. Reggelin, S. Marquardt, A. Schießer, R. Berger, M.S. Schöffler, Science **341**(6150), 1096 (2013). <https://doi.org/10.1126/science.1240362>
43. F. Auvray, D. Denetiere, A. Giuliani, F. Jamme, F. Wien, B. Nay, S. Zirah, F. Polack, C. Meneglier, B. Lagarde, J.D. Hirst, M. Réfrégiers, Struct. Dyn. **6**(5), 054307 (2019). <https://doi.org/10.1063/1.5120346>
44. A.R. Milosavljević, A. Giuliani, C. Nicolas, in *X-ray and Neutron Techniques for Nanomaterials Characterization*, ed. by C.S.S.R. Kumar (Springer, Berlin, 2016), pp. 451–505. [https://doi.org/10.1007/978-3-662-48606-1\\_8](https://doi.org/10.1007/978-3-662-48606-1_8)
45. J.B. Fenn, Angew. Chem. Int. Ed. **42**(33), 3871 (2003). <https://doi.org/10.1002/anie.200300605>
46. W.D. Bowers, S.S. Delbert, R.L. Hunter, R.T. McIver, J. Am. Chem. Soc. **106**(23), 7288 (1984). <https://doi.org/10.1021/ja00335a094>
47. J.S. Brodbelt, Chem. Soc. Rev. **43**(8), 2757 (2014). <https://doi.org/10.1039/C3CS60444F>
48. N.C. Polfer, J. Oomens, Mass Spectrom. Rev. **28**(3), 468 (2009). <https://doi.org/10.1002/mas.20215>
49. S. Bari, O. Gonzalez-Magaña, G. Reitsma, J. Werner, S. Schippers, R. Hoekstra, T. Schlathöler, J. Chem. Phys. **134**(2), 024314 (2011). <https://doi.org/10.1063/1.3515301>
50. A.R. Milosavljević, C. Nicolas, J. Lemaire, C. Dehon, R. Thissen, J.M. Bizau, M. Réfrégiers, L. Nahon, A. Giuliani, Phys. Chem. Chem. Phys. **13**, 15432 (2011). <https://doi.org/10.1039/C1CP21211G>
51. T. Schlathöler, G. Reitsma, D. Egorov, O. Gonzalez-Magaña, S. Bari, L. Boschman, E. Bodewits, K. Schnorr, G. Schmid, C.D. Schröter, R. Moshhammer, R. Hoekstra, Angew. Chem. Int. Ed. **55**(36), 10741 (2016). <https://doi.org/10.1002/anie.201605335>
52. A.R. Milosavljević, K. Jänkälä, M.L. Ranković, F. Canon, J. Bozek, C. Nicolas, A. Giuliani, Phys. Chem. Chem. Phys. **22**, 12909 (2020). <https://doi.org/10.1039/D0CP00994F>
53. L. Schwob, S. Dörner, K. Atak, K. Schubert, M. Timm, C. Bülow, V. Zamudio-Bayer, B. von Issendorff, J.T. Lau, S. Techert, S. Bari, J. Phys. Chem. Lett. **11**(4), 1215 (2020). <https://doi.org/10.1021/acs.jpcllett.0c00041>
54. K.D.D. Gunaratne, V. Prabhakaran, Y.M. Ibrahim, R.V. Norheim, G.E. Johnson, J. Laskin, Analyst **140**, 2957 (2015). <https://doi.org/10.1039/C5AN00220F>
55. I. Aloui, V. Legros, A. Giuliani, W. Buchmann, Rapid Commun. Mass Spectrom. **34**(S2), e8773 (2020). <https://doi.org/10.1002/rcm.8773>
56. S. Bari, J.M. Bizau, K. Schubert, L. Schwob, S. Dörner, J. Bozek, C. Nicolas, D. Cubaynes, A. Milosavljević, (2021). In preparation
57. J.M. Sullivan, P. Shukla, Biophys. J. **77**(3), 1333 (1999). [https://doi.org/10.1016/S0006-3495\(99\)76983-3](https://doi.org/10.1016/S0006-3495(99)76983-3)
58. A.I. Kuleff, L.S. Cederbaum, J. Phys. B: At. Mol. Opt. Phys. **47**(12), 124002 (2014). <https://doi.org/10.1088/0953-4075/47/12/124002>
59. S. Faraji, D. Zhong, A. Dreuw, Angew. Chem. Int. Ed. **55**(17), 5175 (2016). <https://doi.org/10.1002/anie.201511950>
60. F. Agostini, B.F.E. Curchod, Wiley Interdiscipl. Rev. Comput. Mol. Sci. **9**, e1417 (2019). <https://doi.org/10.1002/wcms.1417>
61. P. López-Tarifa, M.A. Hervé du Penhoat, R. Vuilleumier, M.P. Gaigeot, I. Tavernelli, A. Le Padellec, J.P. Champeaux, M. Alcamí, P. Moretto-Capelle, F. Martín, M.F. Politis, Phys. Rev. Lett. **107**, 023202 (2011). <https://doi.org/10.1103/PhysRevLett.107.023202>
62. C.A. Rozzi, F. Troiani, I. Tavernelli, J. Phys.: Condens. Matter **30**(1), 013002 (2018). <https://doi.org/10.1088/1361-648X/aa948a>
63. J.C. Tully, J. Chem. Phys. **93**(2), 1061 (1990). <https://doi.org/10.1063/1.459170>
64. M. Persico, G. Granucci, Theoret. Chem. Acc. **133**(9), 1526 (2014). <https://doi.org/10.1007/s00214-014-1526-1>



65. L. Wang, D. Trivedi, O.V. Prezhdo, J. Chem. Theory Comput. **10**(9), 3598 (2014). <https://doi.org/10.1021/ct5003835>
66. D.V. Makhov, W.J. Glover, T.J. Martinez, D.V. Shalashilin, J. Chem. Phys. **141**(5), 054110 (2014). <https://doi.org/10.1063/1.4891530>
67. M. Ben-Nun, J. Quenneville, T.J. Martínez, J. Phys. Chem. A **104**(22), 5161 (2000). <https://doi.org/10.1021/jp994174i>
68. M.H. Beck, A. Jäckle, G.A. Worth, H.D. Meyer, Phys. Rep. **324**(1), 1 (2000). [https://doi.org/10.1016/S0370-1573\(99\)00047-2](https://doi.org/10.1016/S0370-1573(99)00047-2)
69. S. Faraji, S. Gomez-Carrasco, H. Köppel, *Conical Intersection: Theory, Computation and Experiment* (World Scientific, Singapore, 2011)
70. U. Manthe, J. Chem. Phys. **128**(16), 164116 (2008). <https://doi.org/10.1063/1.2902982>
71. G. Richings, I. Polyak, K. Spinlove, G. Worth, I. Burghardt, B. Lasorne, Int. Rev. Phys. Chem. **34**(2), 269 (2015). <https://doi.org/10.1080/0144235X.2015.1051354>
72. G. Geloni, Z. Huang, C. Pellegrini, in *X-Ray Free Electron Lasers: Applications in Materials, Chemistry and Biology*, ed. by U. Bergmann, V. Yachandra, J. Yano (The Royal Society of Chemistry, 2017), chap. 1, pp. 1–44. <https://doi.org/10.1039/9781782624097-00001>
73. Y. Öhrn, G. Born, P.O. Löwdin, in *Advances in Quantum Chemistry*, vol. 13 (Academic Press, 1981), pp. 1–88. [https://doi.org/10.1016/S0065-3276\(08\)60291-9](https://doi.org/10.1016/S0065-3276(08)60291-9)
74. H. Martin Senn, W. Thiel, Angew. Chem. Int. Ed. **48**, 1198 (2009). <https://doi.org/10.1002/anie.200802019>
75. S. Faraji, A. Dreuw, Photochem. Photobiol. **93**(1), 37 (2017). <https://doi.org/10.1111/php.12679>
76. Y. Cao, J. Romero, J.P. Olson, M. Degroote, P.D. Johnson, M. Kieferová, I.D. Kivlichan, T. Menke, B. Peropadre, N.P.D. Sawaya, S. Sim, L. Veis, A. Aspuru-Guzik, Chem. Rev. **119**(19), 10856 (2019). <https://doi.org/10.1021/acs.chemrev.8b00803>
77. M. Gastegger, J. Behler, P. Marquetand, Chem. Sci. **8**, 6924 (2017). <https://doi.org/10.1039/C7SC02267K>
78. J. Hermann, Z. Schätzle, F. Noé, Nat. Chem. **12**(10), 891 (2020). <https://doi.org/10.1038/s41557-020-0544-y>
79. J. Westermayr, P. Marquetand, Mach. Learn. Sci. Technol. **1**(4), 043001 (2020). <https://doi.org/10.1088/2632-2153/ab9c3e>
80. J. Westermayr, M. Gastegger, M.F.S.J. Menger, S. Mai, L. González, P. Marquetand, Chem. Sci. **10**(35), 8100 (2019). <https://doi.org/10.1039/C9SC01742A>
81. V. Vuitton, R.V. Yelle, S.J. Klippenstein, S.M. Hörst, P. Lavvas, Icarus **324**, 120 (2019). <https://doi.org/10.1016/j.icarus.2018.06.013>
82. B. Yuan, A.R. Koss, C. Warneke, M. Coggon, K. Sekimoto, J.A. de Gouw, Chem. Rev. **117**(21), 13187 (2017). <https://doi.org/10.1021/acs.chemrev.7b00325>
83. B.C. Sweeny, H. Pan, A. Kassem, J.C. Sawyer, S.G. Ard, N.S. Shuman, A.A. Viggiano, S. Brickel, O.T. Unke, M. Upadhyay, M. Meuwly, Phys. Chem. Chem. Phys. **22**, 8913 (2020). <https://doi.org/10.1039/D0CP00668H>
84. I. Savic, S. Schlemmer, D. Gerlich, ChemPhysChem. **21**(13), 1429 (2020). <https://doi.org/10.1002/cphc.202000258>
85. Š. Roučka, S. Rednyk, A. Kovalenko, T.D. Tran, R. Plašil, Á. Kálosi, P. Dohnal, D. Gerlich, J. Glosík, Astron. Astrophys. **615**, L6 (2018). <https://doi.org/10.1051/0004-6361/201833264>
86. C.R. Markus, O. Asvany, T. Salomon, P.C. Schmid, S. Brünken, F. Lipparini, J. Gauss, S. Schlemmer, Phys. Rev. Lett. **124**, 233401 (2020). <https://doi.org/10.1103/PhysRevLett.124.233401>
87. T. Michaelsen, B. Bastian, A. Ayasli, P. Strübin, J. Meyer, R. Wester, J. Phys. Chem. Lett. **11**(11), 4331 (2020). <https://doi.org/10.1021/acs.jpcllett.0c01095>
88. G. Czakó, T. Györi, B. Olasz, D. Papp, I. Szabó, V. Tajti, D.A. Tasi, Phys. Chem. Chem. Phys. **22**, 4298 (2020). <https://doi.org/10.1039/C9CP04944D>
89. N. Bulut, A. Aguado, C. Sanz-Sanz, O. Roncero, J. Phys. Chem. A **123**(41), 8766 (2019). <https://doi.org/10.1021/acs.jpca.9b06081>
90. V. Macaluso, D. Scuderi, M.E. Crestoni, S. Fornarini, D. Corinti, E. Dalloz, E. Martínez-Núñez, W.L. Hase, R. Spezia, J. Phys. Chem. A **123**(17), 3685 (2019). <https://doi.org/10.1021/acs.jpca.9b01779>
91. A. Martin Somer, V. Macaluso, G.L. Barnes, L. Yang, S. Pratihari, K. Song, W.L. Hase, R. Spezia, J. Am. Soc. Mass Spectrometry **31**(1), 2 (2020). <https://doi.org/10.1021/jasms.9b00062>
92. C.M. Nichols, Z.C. Wang, W.C. Lineberger, V.M. Bierbaum, J. Phys. Chem. Lett. **10**(17), 4863 (2019). <https://doi.org/10.1021/acs.jpcllett.9b01997>
93. B. Cunha de Miranda, C. Romanzin, S. Chefdeville, V. Vuitton, J. Žabka, M. Polášek, C. Alcaraz, J. Phys. Chem. A **119**(23), 6082 (2015). <https://doi.org/10.1021/jp512846v>
94. A. Cernuto, A. Lopes, C. Romanzin, B. Cunha de Miranda, D. Ascenzi, P. Tosi, G. Tonachini, A. Maranzana, M. Polášek, J. Žabka, C. Alcaraz, J. Chem. Phys. **147**(15), 154302 (2017). <https://doi.org/10.1063/1.4990514>
95. M. Polášek, E.L. Zins, C. Alcaraz, J. Žabka, V. Křížová, L. Giacomozzi, P. Tosi, D. Ascenzi, J. Phys. Chem. A **120**(27), 5041 (2016). <https://doi.org/10.1021/acs.jpca.5b12757>
96. C.Y. Ng, Y. Xu, Y.C. Chang, A. Wannenmacher, M. Parziale, P.B. Armentrout, Phys. Chem. Chem. Phys. **23**, 273 (2021). <https://doi.org/10.1039/D0CP04333H>
97. R. Tang, X. Fu, Y. Lu, C. Ning, J. Phys. Chem. Lett. **10**(4), 702 (2019). <https://doi.org/10.1021/acs.jpcllett.8b03859>
98. B. Joalland, N. Jamal-Eddine, D. Papanastasiou, A. Lekkas, S. Carles, L. Biennier, J. Chem. Phys. **150**(16), 164201 (2019). <https://doi.org/10.1063/1.5086386>
99. J. Toscano, H.J. Lewandowski, B.R. Heazlewood, Phys. Chem. Chem. Phys. **22**, 9180 (2020). <https://doi.org/10.1039/D0CP00931H>
100. B.R. Heazlewood, T.P. Softley, Nat. Rev. Chem. **5**(2), 125 (2021). <https://doi.org/10.1038/s41570-020-00239-0>
101. K. Höveler, J. Deiglmayr, J.A. Agner, H. Schmutz, F. Merkt, Phys. Chem. Chem. Phys. **23**, 2676 (2021). <https://doi.org/10.1039/D0CP06107G>
102. A.D. Dörfler, P. Eberle, D. Koner, M. Tomza, M. Meuwly, S. Willitsch, Nat. Commun. **10**(1), 5429 (2019). <https://doi.org/10.1038/s41467-019-13218-x>

103. P. Rousseau, B.A. Huber, in *Nanoscale Insights into Ion-Beam Cancer Therapy*, ed. by A.V. Solov'yov (Springer International Publishing, 2017), chap. 4, pp. 121–157
104. P. Rousseau, A. Lawicki, A. Holm, M. Capron, R. Maisonnay, S. Maclot, E. Lattouf, H. Johansson, F. Seitz, A. Méry, J. Rangama, H. Zettergren, S. Rosén, H. Schmidt, J.Y. Chesnel, A. Domaracka, B. Manil, L. Adoui, H. Cederquist, B. Huber, *Nucl. Instrum. Methods Phys. Res. Sect. B* **279**, 140 (2012). <https://doi.org/10.1016/j.nimb.2011.10.050>
105. S. Maclot, R. Delaunay, D.G. Piekarski, A. Domaracka, B.A. Huber, L. Adoui, F. Martín, M. Alcamí, L. Avaldi, P. Bolognesi, S. Díaz-Tendero, P. Rousseau, *Phys. Rev. Lett.* **117**, 073201 (2016). <https://doi.org/10.1103/PhysRevLett.117.073201>
106. B. Li, A.R. Allouche, J. Bernard, R. Brédy, D.B. Qian, X. Ma, S. Martin, L. Chen, *J. Chem. Phys.* **146**(12), 124302 (2017). <https://doi.org/10.1063/1.4978626>
107. M.H. Stockett, H. Zettergren, L. Adoui, J.D. Alexander, U. Bērziņš, T. Chen, M. Gatchell, N. Haag, B.A. Huber, P. Hvelplund, A. Johansson, H.A.B. Johansson, K. Kulyk, S. Rosén, P. Rousseau, K. Stöckel, H.T. Schmidt, H. Cederquist, *Phys. Rev. A* **89**, 032701 (2014). <https://doi.org/10.1103/PhysRevA.89.032701>
108. G.B. Sushko, I.A. Solov'yov, A.V. Solov'yov, *Eur. Phys. J. D* **70**, 217 (2016). <https://doi.org/10.1140/epjd/e2016-70283-5>
109. P. de Vera, M. Azzolini, G. Sushko, I. Abril, R. Garcia-Molina, M. Dapor, I.A. Solov'yov, A.V. Solov'yov, *Sci. Rep.* **10**(1), 20827 (2020). <https://doi.org/10.1038/s41598-020-77120-z>
110. S. Maclot, D.G. Piekarski, A. Domaracka, A. Méry, V. Vizcaino, L. Adoui, F. Martín, M. Alcamí, B.A. Huber, P. Rousseau, S. Díaz-Tendero, *J. Phys. Chem. Lett.* **4**(22), 3903 (2013). <https://doi.org/10.1021/jz4020234>
111. S. Bari, P. Sobocinski, J. Postma, F. Alvarado, R. Hoekstra, V. Bernigaud, B. Manil, J. Rangama, B. Huber, T. Schlathölder, *J. Chem. Phys.* **128**(7), 074306 (2008). <https://doi.org/10.1063/1.2830032>
112. D.G. Piekarski, R. Delaunay, S. Maclot, L. Adoui, F. Martín, M. Alcamí, B.A. Huber, P. Rousseau, A. Domaracka, S. Díaz-Tendero, *Phys. Chem. Chem. Phys.* **17**, 16767 (2015). <https://doi.org/10.1039/C5CP01628B>
113. J. Kocisek, D.G. Piekarski, R. Delaunay, B.A. Huber, L. Adoui, F. Martín, M. Alcamí, P. Rousseau, A. Domaracka, J. Kopyra, S. Díaz-Tendero, *J. Phys. Chem. A* **119**(37), 9581 (2015). <https://doi.org/10.1021/acs.jpca.5b06009>
114. D.G. Piekarski, R. Delaunay, A. Mika, S. Maclot, L. Adoui, F. Martín, M. Alcamí, B.A. Huber, P. Rousseau, S. Díaz-Tendero, A. Domaracka, *Phys. Chem. Chem. Phys.* **19**, 19609 (2017). <https://doi.org/10.1039/C7CP00903H>
115. E. Erdmann, N.F. Aguirre, S. Indrajith, J. Chiarinelli, A. Domaracka, P. Rousseau, B.A. Huber, P. Bolognesi, R. Richter, L. Avaldi, S. Díaz-Tendero, M. Alcamí, M. Labuda, *Phys. Chem. Chem. Phys.* **23**, 1859 (2021). <https://doi.org/10.1039/D0CP04890A>
116. B. Oostenrijk, D. Barreiro, N. Walsh, A. Sankari, E.P. Månsson, S. Maclot, S.L. Sorensen, S. Díaz-Tendero, M. Gisselbrecht, *Phys. Chem. Chem. Phys.* **21**, 25749 (2019). <https://doi.org/10.1039/C9CP04221K>
117. E. Wang, X. Shan, L. Chen, T. Pfeifer, X. Chen, X. Ren, A. Dorn, *J. Phys. Chem. A* **124**(14), 2785 (2020). <https://doi.org/10.1021/acs.jpca.0c02074>
118. C. Frege, I.K. Ortega, M.P. Rissanen, A.P. Praplan, G. Steiner, M. Heinritzi, L. Ahonen, A. Amorim, A.K. Bernhammer, F. Bianchi, S. Brilke, M. Breitenlechner, L. Dada, A. Dias, J. Duplissy, S. Ehrhart, I. El-Haddad, L. Fischer, C. Fuchs, O. Garmash, M. Gonin, A. Hansel, C.R. Hoyle, T. Jokinen, H. Junninen, J. Kirkby, A. Kürten, K. Lehtipalo, M. Leiminger, R.L. Mauldin, U. Molteni, L. Nichman, T. Petäjä, N. Sarnela, S. Schobesberger, M. Simon, M. Sipilä, D. Stolzenburg, A. Tomé, A.L. Vogel, A.C. Wagner, R. Wagner, M. Xiao, C. Yan, P. Ye, J. Curtius, N.M. Donahue, R.C. Flagan, M. Kulmala, D.R. Worsnop, P.M. Winkler, J. Dommen, U. Baltensperger, *Atmos. Chem. Phys.* **18**, 65 (2018). <https://doi.org/10.5194/acp-18-65-2018>
119. P. Markush, P. Bolognesi, A. Cartoni, P. Rousseau, S. Maclot, R. Delaunay, A. Domaracka, J. Kocisek, M.C. Castrovilli, B.A. Huber, L. Avaldi, *Phys. Chem. Chem. Phys.* **18**, 16721 (2016). <https://doi.org/10.1039/C6CP01940D>
120. R. Delaunay, M. Gatchell, P. Rousseau, A. Domaracka, S. Maclot, Y. Wang, M.H. Stockett, T. Chen, L. Adoui, M. Alcamí, F. Martín, H. Zettergren, H. Cederquist, B.A. Huber, *J. Phys. Chem. Lett.* **6**(9), 1536 (2015). <https://doi.org/10.1021/acs.jpclett.5b00405>
121. R. Delaunay, M. Gatchell, A. Mika, A. Domaracka, L. Adoui, H. Zettergren, H. Cederquist, P. Rousseau, B. Huber, *Carbon* **129**, 766 (2018). <https://doi.org/10.1016/j.carbon.2017.12.079>
122. A. Domaracka, R. Delaunay, A. Mika, M. Gatchell, H. Zettergren, H. Cederquist, P. Rousseau, B.A. Huber, *Phys. Chem. Chem. Phys.* **20**, 15052 (2018). <https://doi.org/10.1039/C8CP01179F>
123. P. Rousseau, D.G. Piekarski, M. Capron, A. Domaracka, L. Adoui, F. Martín, M. Alcamí, S. Díaz-Tendero, B.A. Huber, *Nat. Commun.* **11**, 3818 (2020). <https://doi.org/10.1038/s41467-020-17653-z>
124. S. Bari, R. Hoekstra, T. Schlathölder, *Phys. Chem. Chem. Phys.* **12**, 3376 (2010). <https://doi.org/10.1039/B924145K>
125. A.R. Milosavljević, P. Rousseau, A. Domaracka, B.A. Huber, A. Giuliani, *Phys. Chem. Chem. Phys.* **19**, 19691 (2017). <https://doi.org/10.1039/C7CP02075A>
126. I. Tavernelli, *Acc. Chem. Res.* **48**, 792 (2015). <https://doi.org/10.1021/ar500357y>
127. F. Spiegelmann, N. Tarrat, J. Cuny, L. Dontot, E. Posenitskiy, C. Martí, A. Simon, M. Rapacioli, *Adv. Phys. X* **5**(1), 1710252 (2019). <https://doi.org/10.1080/23746149.2019.1710252>
128. M. Gatchell, M.H. Stockett, N. de Ruelle, T. Chen, L. Giacomozzi, R.F. Nascimento, M. Wolf, E.K. Anderson, R. Delaunay, V. Vizcaino, P. Rousseau, L. Adoui, B.A. Huber, H.T. Schmidt, H. Zettergren, H. Cederquist, *Phys. Rev. A* **92**, 050702 (2015). <https://doi.org/10.1103/PhysRevA.92.050702>
129. S.J. Stuart, A.B. Tutein, J.A. Harrison, *J. Chem. Phys.* **112**(14), 6472 (2000). <https://doi.org/10.1063/1.481208>

130. S. Plimpton, J. Comput. Phys. **117**(1), 1 (1995). <https://doi.org/10.1006/jcph.1995.1039>
131. J.C. Phillips, R. Braun, W. Wang, J. Gumbart, E. Tajkhorshid, E. Villa, C. Chipot, R.D. Skeel, L. Kalé, K. Schulten, J. Comput. Chem. **26**(16), 1781 (2005). <https://doi.org/10.1002/jcc.20289>
132. I.A. Solov'yov, A.V. Yakubovich, P.V. Nikolaev, I. Volkovets, A.V. Solov'yov, J. Comput. Chem. **33**(30), 2412 (2012). <https://doi.org/10.1002/jcc.23086>
133. H. da Silva, J. Oller, M. Gatchell, M.H. Stockett, P.A. Hervieux, L. Adoui, M. Alcamí, B.A. Huber, F. Martín, H. Cederquist, H. Zettergren, P. Rousseau, S. Díaz-Tendero, Phys. Rev. A **90**, 032701 (2014). <https://doi.org/10.1103/PhysRevA.90.032701>
134. E. Martínez-Núñez, Phys. Chem. Chem. Phys. **17**, 14912 (2015). <https://doi.org/10.1039/C5CP02175H>
135. A. Rodríguez, R. Rodríguez-Fernández, S.A. Vázquez, G.L. Barnes, J.J.P. Stewart, E. Martínez-Núñez, J. Comput. Chem. **39**(23), 1922 (2018). <https://doi.org/10.1002/jcc.25370>
136. N.F. Aguirre, S. Díaz-Tendero, P.A. Hervieux, M. Alcamí, F. Martín, J. Chem. Theory Comput. **13**, 992 (2017). <https://doi.org/10.1021/acs.jctc.6b00984>
137. C.A. Bauer, S. Grimme, J. Phys. Chem. A **120**(21), 3755 (2016). <https://doi.org/10.1021/acs.jpca.6b02907>
138. L.G. Christophorou, D.L. McCorkle, A.A. Christodoulides, *Electron Molecule Interactions and their Applications*, vol. 1 & 2 (Academic Press, New York, 1984)
139. B. Boudaïffa, P. Cloutier, D. Hunting, M.A. Huels, L. Sanche, Science **287**(5458), 1658 (2000). <https://doi.org/10.1126/science.287.5458.1658>
140. I. Baccarelli, I. Bald, F.A. Gianturco, E. Illenberger, J. Kopyra, Phys. Rep. **508**(1), 1 (2011). <https://doi.org/10.1016/j.physrep.2011.06.004>
141. S. Ptasinska, S. Denifl, P. Scheier, E. Illenberger, T.D. Märk, Angew. Chem. Int. Ed. **44**(42), 6941 (2005). <https://doi.org/10.1002/anie.200502040>
142. J. Kopyra, Phys. Chem. Chem. Phys. **14**, 8287 (2012). <https://doi.org/10.1039/C2CP40847C>
143. I. Bald, I. Dąbkowska, E. Illenberger, Angew. Chem. Int. Ed. **47**(44), 8518 (2008). <https://doi.org/10.1002/anie.200803382>
144. A. Keller, I. Bald, A. Rotaru, E. Cauët, K.V. Gothelf, F. Besenbacher, ACS Nano **6**(5), 4392 (2012). <https://doi.org/10.1021/nm3010747>
145. R. Meißner, J. Kočíšek, L. Feketeová, J. Fedor, M. Fárnik, P. Limão-Vieira, E. Illenberger, S. Denifl, Nat. Commun. **10**(1), 2388 (2019). <https://doi.org/10.1038/s41467-019-10340-8>
146. A. Mauracher, O. Echt, A.M. Ellis, S. Yang, D.K. Bohme, J. Postler, A. Kaiser, S. Denifl, P. Scheier, Phys. Rep. **751**, 1 (2018). <https://doi.org/10.1016/j.physrep.2018.05.001>
147. J. Ma, F. Wang, S.A. Denisov, A. Adhikary, M. Mostafavi, Sci. Adv. **3**, 12 (2017). <https://doi.org/10.1126/sciadv.1701669>
148. M. Neustetter, J. Aysina, F.F. da Silva, S. Denifl, Angew. Chem. Int. Ed. **54**(31), 9124 (2015). <https://doi.org/10.1002/anie.201503733>
149. J. Kočíšek, A. Pysanenko, M. Fárnik, J. Fedor, J. Phys. Chem. Lett. **7**(17), 3401 (2016). <https://doi.org/10.1021/acs.jpcllett.6b01601>
150. H. Hotop, M.W. Ruf, M. Allan, I.I. Fabrikant, B. Bederson, H. Walther, in *Advances In Atomic, Molecular, and Optical Physics*, vol. 49 (Academic Press, 2003), pp. 85–216. [https://doi.org/10.1016/S1049-250X\(03\)80004-6](https://doi.org/10.1016/S1049-250X(03)80004-6)
151. J.D. Gorfinkiel, Eur. Phys. J. D **74**(3), 51 (2020). <https://doi.org/10.1140/epjd/e2020-100550-7>
152. R.F. da Costa, M.T.d.N. Varella, M.H.F. Bettega, M.A.P. Lima, Eur. Phys. J. D **69**(6), 159 (2015). <https://doi.org/10.1140/epjd/e2015-60192-6>
153. I.I. Fabrikant, Eur. Phys. J. D **72**(6), 96 (2018). <https://doi.org/10.1140/epjd/e2018-90082-2>
154. J. Med, Š. Sršen, P. Slavíček, A. Domaracka, S. Indrajith, P. Rousseau, M. Fárnik, J. Fedor, J. Kočíšek, J. Phys. Chem. Lett. **11**(7), 2482 (2020). <https://doi.org/10.1021/acs.jpcllett.0c00278>
155. M. Allan, Phys. Rev. Lett. **98**, 123201 (2007). <https://doi.org/10.1103/PhysRevLett.98.123201>
156. M. McAllister, M. Smyth, B. Gu, G.A. Tribello, J. Kohanoff, J. Phys. Chem. Lett. **6**(15), 3091 (2015). <https://doi.org/10.1021/acs.jpcllett.5b01011>
157. J. Kočíšek, B. Sedmidubská, S. Indrajith, M. Fárnik, J. Fedor, J. Phys. Chem. B **122**(20), 5212 (2018). <https://doi.org/10.1021/acs.jpcc.8b03033>
158. O. Ingólfsson, F. Weik, E. Illenberger, Int. J. Mass Spectrom. Ion Process. **155**(1), 1 (1996). [https://doi.org/10.1016/S0168-1176\(96\)04392-3](https://doi.org/10.1016/S0168-1176(96)04392-3)
159. J. Lengyel, J. Kočíšek, M. Fárnik, J. Fedor, J. Phys. Chem. C **120**(13), 7397 (2016). <https://doi.org/10.1021/acs.jpcc.6b00901>
160. J. Poštulka, P. Slavíček, J. Fedor, M. Fárnik, J. Kočíšek, J. Phys. Chem. B **121**(38), 8965 (2017). <https://doi.org/10.1021/acs.jpcc.7b07390>
161. M. Johny, J. Onvlee, T. Kierspel, H. Bieker, S. Trippel, J. Küpper, Chem. Phys. Lett. **721**, 149 (2019). <https://doi.org/10.1016/j.cplett.2019.01.052>
162. K. Kitajima, H. Tsuchida, T. Majima, M. Saito, J. Chem. Phys. **150**(9), 095102 (2019). <https://doi.org/10.1063/1.5081883>
163. B.W. LaFranchi, G.A. Petrucci, Int. J. Mass Spectrom. **258**(1), 120 (2006). <https://doi.org/10.1016/j.ijms.2006.06.013>
164. Z. Li, A.R. Milosavljević, I. Carmichael, S. Ptasinska, Phys. Rev. Lett. **119**, 053402 (2017). <https://doi.org/10.1103/PhysRevLett.119.053402>
165. T. Jahnke, U. Hergenbahn, B. Winter, R. Dörner, U. Frühling, P.V. Demekhin, K. Gokhberg, L.S. Cederbaum, A. Ehresmann, A. Knie, A. Dreuw, Chem. Rev. **120**(20), 11295 (2020). <https://doi.org/10.1021/acs.chemrev.0c00106>
166. J.P. Toennies, A.F. Vilesov, Angew. Chem. Int. Ed. **43**(20), 2622 (2004). <https://doi.org/10.1002/anie.200300611>
167. H. Linnartz, J. Cami, M. Cordiner, N.L.J. Cox, P. Ehrenfreund, B. Foing, M. Gatchell, P. Scheier, J. Mol. Spectrosc. **367**, 111243 (2020). <https://doi.org/10.1016/j.jms.2019.111243>
168. K.R. Atkins, Phys. Rev. **116**, 1339 (1959). <https://doi.org/10.1103/PhysRev.116.1339>
169. L.F. Gomez, E. Loginov, A.F. Vilesov, Phys. Rev. Lett. **108**, 155302 (2012). <https://doi.org/10.1103/PhysRevLett.108.155302>



170. R. Rodríguez-Cantano, T. González-Lezana, P. Villarreal, *Int. Rev. Phys. Chem.* **35**(1), 37 (2016). <https://doi.org/10.1080/0144235X.2015.1132595>
171. F. Calvo, *J. Phys. Chem. A* **119**(23), 5959 (2015). <https://doi.org/10.1021/jp510799h>
172. F. Laimer, L. Kranabetter, L. Tiefenthaler, S. Albertini, F. Zappa, A.M. Ellis, M. Gatchell, P. Scheier, *Phys. Rev. Lett.* **123**(16), 165301 (2019). <https://doi.org/10.1103/PhysRevLett.123.165301>
173. L. Tiefenthaler, J. Ameixa, P. Martini, S. Albertini, L. Ballauf, M. Zankl, M. Goulart, F. Laimer, K. von Haefen, F. Zappa, P. Scheier, *Rev. Sci. Instrum.* **91**(3), 033315 (2020). <https://doi.org/10.1063/1.5133112>
174. M. Okumura, L.I. Yeh, Y.T. Lee, *J. Chem. Phys.* **83**(7), 3705 (1985). <https://doi.org/10.1063/1.449127>
175. H.J. Zeng, N. Yang, M.A. Johnson, *Faraday Discuss.* **217**, 8 (2019). <https://doi.org/10.1039/C9FD00030E>
176. E.K. Campbell, M. Holz, D. Gerlich, J.P. Maier, *Nature* **523**(7560), 322 (2015). <https://doi.org/10.1038/nature14566>
177. M. Kuhn, M. Renzler, J. Postler, S. Ralser, S. Spieler, M. Simpson, H. Linnartz, A.G.G.M. Tielens, J. Cami, A. Mauracher, Y. Wang, M. Alcamí, F. Martín, M.K. Beyer, R. Wester, A. Lindinger, P. Scheier, *Nat. Commun.* **7**, 13550 (2016). <https://doi.org/10.1038/ncomms13550>
178. M. Gatchell, P. Martini, F. Laimer, M. Goulart, F. Calvo, P. Scheier, *Faraday Discuss.* **217**, 276 (2019). <https://doi.org/10.1039/C8FD00178B>
179. T. González-Lezana, O. Echt, M. Gatchell, M. Bartolomei, J. Campos-Martínez, P. Scheier, *Int. Rev. Phys. Chem.* **39**(4), 465 (2020). <https://doi.org/10.1080/0144235X.2020.1794585>
180. H.T. Schmidt, *Phys. Scr.* **T166**, 014063 (2015). <https://doi.org/10.1088/0031-8949/2015/t166/014063>
181. R.D. Thomas, H.T. Schmidt, G. Andler, M. Björkhage, M. Blom, L. Brännholm, E. Bäckström, H. Danared, S. Das, N. Haag, P. Halldén, F. Hellberg, A.I.S. Holm, H.A.B. Johansson, A. Källberg, G. Källersjö, M. Larsson, S. Leontein, L. Liljeby, P. Löfgren, B. Malm, S. Mannervik, M. Masuda, D. Misra, A. Orbán, A. Paál, P. Reinhed, K.G. Rensfelt, S. Rosén, K. Schmidt, F. Seitz, A. Simonsson, J. Weimer, H. Zettergren, H. Cederquist, *Rev. Sci. Instrum.* **82**(6), 065112 (2011). <https://doi.org/10.1063/1.3602928>
182. H.T. Schmidt, R.D. Thomas, M. Gatchell, S. Rosén, P. Reinhed, P. Löfgren, L. Brännholm, M. Blom, M. Björkhage, E. Bäckström, J.D. Alexander, S. Leontein, D. Hanstorp, H. Zettergren, L. Liljeby, A. Källberg, A. Simonsson, F. Hellberg, S. Mannervik, M. Larsson, W.D. Geppert, K.G. Rensfelt, H. Danared, A. Paál, M. Masuda, P. Halldén, G. Andler, M.H. Stockett, T. Chen, G. Källersjö, J. Weimer, K. Hansen, H. Hartman, H. Cederquist, *Rev. Sci. Instrum.* **84**(5), 055115 (2013). <https://doi.org/10.1063/1.4807702>
183. R. von Hahn, A. Becker, F. Berg, K. Blaum, C. Breitenfeldt, H. Fadil, F. Fellenberger, M. Froese, S. George, J. Göck, M. Grieser, F. Grussie, E.A. Guerin, O. Heber, P. Herwig, J. Kartheim, C. Krantz, H. Kreckel, M. Lange, F. Laux, S. Lohmann, S. Menk, C. Meyer, P.M. Mishra, O. Novotný, A.P. O'Connor, D.A. Orlov, M.L. Rappaport, R. Repnow, S. Saurabh, S. Schippers, C.D. Schröter, D. Schwalm, L. Schweikhard, T. Sieber, A. Shornikov, K. Spruck, S. Sunil Kumar, J. Ullrich, X. Urbain, S. Vogel, P. Wilhelm, A. Wolf, D. Zajfman, *Review of Scientific Instruments* **87**(6), 063115 (2016). <https://doi.org/10.1063/1.4953888>
184. Y. Nakano, Y. Enomoto, T. Masunaga, S. Menk, P. Bertier, T. Azuma, *Rev. Sci. Instrum.* **88**(3), 033110 (2017). <https://doi.org/10.1063/1.4978454>
185. S.P. Møller, *Nucl. Instrum. Methods Phys. Res. Sect. A* **394**(3), 281 (1997). [https://doi.org/10.1016/S0168-9002\(97\)00673-6](https://doi.org/10.1016/S0168-9002(97)00673-6)
186. D. Zajfman, O. Heber, L. Vejby-Christensen, I. Ben-Itzhak, M. Rappaport, R. Fishman, M. Dahan, *Phys. Rev. A* **55**, R1577 (1997). <https://doi.org/10.1103/PhysRevA.55.R1577>
187. H.T. Schmidt, H. Cederquist, J. Jensen, A. Fardi, *Nucl. Instrum. Methods Phys. Res. Sect. B* **173**(4), 523 (2001). [https://doi.org/10.1016/S0168-583X\(00\)00415-8](https://doi.org/10.1016/S0168-583X(00)00415-8)
188. S.B. Nielsen, A. Lapierre, J.U. Andersen, U.V. Pedersen, S. Tomita, L.H. Andersen, *Phys. Rev. Lett.* **87**, 228102 (2001). <https://doi.org/10.1103/PhysRevLett.87.228102>
189. H.B. Pedersen, A. Svendsen, L.S. Harbo, H.V. Kiefer, H. Kjeldsen, L. Lammich, Y. Toker, L.H. Andersen, *Rev. Sci. Instrum.* **86**(6), 063107 (2015). <https://doi.org/10.1063/1.4922826>
190. T. Tanabe, K. Noda, M. Saito, S. Lee, Y. Ito, H. Takagi, *Phys. Rev. Lett.* **90**, 193201 (2003). <https://doi.org/10.1103/PhysRevLett.90.193201>
191. S. Jinno, T. Takao, Y. Omata, A. Satou, H. Tanuma, T. Azuma, H. Shiromaru, K. Okuno, N. Kobayashi, I. Watanabe, *Nucl. Instrum. Methods Phys. Res. Sect. A* **532**(1), 477 (2004). <https://doi.org/10.1016/j.nima.2004.06.070>
192. Y. Ebara, T. Furukawa, J. Matsumoto, H. Tanuma, T. Azuma, H. Shiromaru, K. Hansen, *Phys. Rev. Lett.* **117**, 133004 (2016). <https://doi.org/10.1103/PhysRevLett.117.133004>
193. J. Bernard, G. Montagne, R. Brédy, B. Terpend-Ordacière, A. Bourgey, M. Kerleroux, L. Chen, H.T. Schmidt, H. Cederquist, S. Martin, *Rev. Sci. Instrum.* **79**(7), 075109 (2008). <https://doi.org/10.1063/1.2957609>
194. J. Matsumoto, R. Saiba, K. Gouda, E. Makino, K. Hashimoto, K. Fueta, N. Kondo, H. Shiromaru, *Nucl. Instrum. Methods Phys. Res. Sect. B* **454**, 23 (2019). <https://doi.org/10.1016/j.nimb.2019.05.002>
195. C. Meyer, A. Becker, K. Blaum, C. Breitenfeldt, S. George, J. Göck, M. Grieser, F. Grussie, E.A. Guerin, R. von Hahn, P. Herwig, C. Krantz, H. Kreckel, J. Lion, S. Lohmann, P.M. Mishra, O. Novotný, A.P. O'Connor, R. Repnow, S. Saurabh, D. Schwalm, L. Schweikhard, K. Spruck, S. Sunil Kumar, S. Vogel, A. Wolf, *Phys. Rev. Lett.* **119**, 023202 (2017). <https://doi.org/10.1103/PhysRevLett.119.023202>
196. H.T. Schmidt, G. Eklund, K.C. Chartkunchand, E.K. Anderson, M. Kamińska, N. de Ruelle, R.D. Thomas, M.K. Kristiansson, M. Gatchell, P. Reinhed, S. Rosén, A. Simonsson, A. Källberg, P. Löfgren, S. Mannervik, H. Zettergren, H. Cederquist, *Phys. Rev. Lett.* **119**, 073001 (2017). <https://doi.org/10.1103/PhysRevLett.119.073001>

197. O. Novotný, P. Wilhelm, D. Paul, Á. Kálosi, S. Saurabh, A. Becker, K. Blaum, S. George, J. Göck, M. Grieser, F. Grussie, R. von Hahn, C. Krantz, H. Kreckel, C. Meyer, P.M. Mishra, D. Muell, F. Nuesslein, D.A. Orlov, M. Rimmler, V.C. Schmidt, A. Shornikov, A.S. Terekhov, S. Vogel, D. Zajfman, A. Wolf, *Science* **365**(6454), 676 (2019). <https://doi.org/10.1126/science.aax5921>
198. G. Eklund, J. Grumer, S. Rosén, M. Ji, N. Punnakayathil, A. Källberg, A. Simonsson, R.D. Thomas, M.H. Stockett, P. Reinhed, P. Löfgren, M. Björkhage, M. Blom, P.S. Barklem, H. Cederquist, H. Zettergren, H.T. Schmidt, *Phys. Rev. A* **102**, 012823 (2020). <https://doi.org/10.1103/PhysRevA.102.012823>
199. E.K. Anderson, A.F. Schmidt-May, P.K. Najeeb, G. Eklund, K.C. Chartkunchand, S. Rosén, Å. Larson, K. Hansen, H. Cederquist, H. Zettergren, H.T. Schmidt, *Phys. Rev. Lett.* **124**, 173001 (2020). <https://doi.org/10.1103/PhysRevLett.124.173001>
200. L.H. Andersen, O. Heber, D. Zajfman, *J. Phys. B: At. Mol. Opt. Phys.* **37**(11), R57 (2004). <https://doi.org/10.1088/0953-4075/37/11/r01>
201. K. Hansen, J.U. Andersen, P. Hvelplund, S.P. Møller, U.V. Pedersen, V.V. Petrunin, *Phys. Rev. Lett.* **87**, 123401 (2001). <https://doi.org/10.1103/PhysRevLett.87.123401>
202. L.H. Andersen, I.B. Nielsen, M.B. Kristensen, M.O.A. El Ghazaly, S. Haacke, M.B. Nielsen, M.Å. Petersen, *J. Am. Chem. Soc.* **127**(35), 12347 (2005). <https://doi.org/10.1021/ja051638j>
203. D.W. Boo, Y. Ozaki, L.H. Andersen, W. Lineberger, *J. Phys. Chem. A* **101**(36), 6688 (1997). <https://doi.org/10.1021/jp9711353>
204. A. Stolow, *Annu. Rev. Phys. Chem.* **54**(1), 89 (2003). <https://doi.org/10.1146/annurev.physchem.54.011002.103809>
205. D.M. Neumark, *Annu. Rev. Phys. Chem.* **52**(1), 255 (2001). <https://doi.org/10.1146/annurev.physchem.52.1.255>
206. J.R. Verlet, *Chem. Soc. Rev.* **37**(3), 505 (2008). <https://doi.org/10.1039/B700528H>
207. D. Parker, R. Minns, T. Penfold, G. Worth, H. Fielding, *Chem. Phys. Lett.* **469**(1–3), 43 (2009). <https://doi.org/10.1016/j.cplett.2008.12.069>
208. H.V. Kiefer, H.B. Pedersen, A.V. Bochenkova, L.H. Andersen, *Phys. Rev. Lett.* **117**, 243004 (2016). <https://doi.org/10.1103/PhysRevLett.117.243004>
209. A. Svendsen, H.V. Kiefer, H.B. Pedersen, A.V. Bochenkova, L.H. Andersen, *J. Am. Chem. Soc.* **139**(25), 8766 (2017). <https://doi.org/10.1021/jacs.7b04987>
210. H.V. Kiefer, E. Gruber, J. Langeland, P.A. Kusocheck, A.V. Bochenkova, L.H. Andersen, *Nat. Commun.* **10**(1), 1210 (2019). <https://doi.org/10.1038/s41467-019-09225-7>
211. F. Bierau, P. Kupser, G. Meijer, G. von Helden, *Phys. Rev. Lett.* **105**(13), 133402 (2010). <https://doi.org/10.1103/PhysRevLett.105.133402>
212. M. Alghamdi, J. Zhang, A. Oswalt, J.J. Porter, R.A. Mehl, W. Kong, *J. Phys. Chem. A* **121**(36), 6671 (2017). <https://doi.org/10.1021/acs.jpca.7b05718>
213. J.A. Hogan, M.F. Jarrold, *J. Am. Soc. Mass Spectrom.* **29**(10), 2086 (2018). <https://doi.org/10.1021/jasms.8b05683>
214. R.N. Wolf, M. Eritt, G. Marx, L. Schweikhard, *Hyperfine Interact.* **199**(1), 115 (2011). <https://doi.org/10.1007/s10751-011-0306-8>
215. R.K. Gangwar, K. Saha, O. Heber, M.L. Rappaport, D. Zajfman, *Phys. Rev. Lett.* **119**, 103202 (2017). <https://doi.org/10.1103/PhysRevLett.119.103202>
216. K. Saha, A. Prabhakaran, V. Chandrasekaran, M.L. Rappaport, O. Heber, D. Zajfman, *Rev. Sci. Instrum.* **88**(5), 053101 (2017). <https://doi.org/10.1063/1.4982034>
217. C.J. Johnson, B.B. Shen, B.L.J. Poad, R.E. Continetti, *Rev. Sci. Instrum.* **82**(10), 105105 (2011). <https://doi.org/10.1063/1.3641875>
218. Y. Toker, O. Aviv, M. Eritt, M.L. Rappaport, O. Heber, D. Schwalm, D. Zajfman, *Phys. Rev. A* **76**, 053201 (2007). <https://doi.org/10.1103/PhysRevA.76.053201>
219. Y. Toker, A. Svendsen, A.V. Bochenkova, L.H. Andersen, *Angew. Chem. Int. Ed.* **51**(35), 8757 (2012). <https://doi.org/10.1002/anie.201203746>
220. K. Saha, V. Chandrasekaran, O. Heber, M.A. Iron, M.L. Rappaport, D. Zajfman, *Nat. Commun.* **9**(1), 912 (2018). <https://doi.org/10.1038/s41467-018-03197-w>
221. A. Shahi, R. Singh, Y. Ossia, D. Zajfman, O. Heber, D. Strasser, *Rev. Sci. Instrum.* **90**(11), 113308 (2019). <https://doi.org/10.1063/1.5114908>
222. N.J.A. Coughlan, B.D. Adamson, L. Gamon, K. Catani, E.J. Bieske, *Phys. Chem. Chem. Phys.* **17**, 22623 (2015). <https://doi.org/10.1039/C5CP03611A>
223. W. Forst, *Theory of unimolecular reactions* (Academic Press (New York and London), 1973)
224. P.A. Hervieux, D.H.E. Gross, *Z. Phys. D Atoms Mol. Clust.* **33**(4), 295 (1995). <https://doi.org/10.1007/BF01437510>
225. J.U. Andersen, E. Bonderup, K. Hansen, *J. Phys. B: At. Mol. Opt. Phys.* **35**(5), R1 (2002). <https://doi.org/10.1088/0953-4075/35/5/201>
226. N. Kono, T. Furukawa, H. Tanuma, J. Matsumoto, H. Shiromaru, T. Azuma, K. Najafian, M.S. Pettersson, B. Dynefors, K. Hansen, *Phys. Chem. Chem. Phys.* **17**, 24732 (2015). <https://doi.org/10.1039/C5CP02549D>
227. C.E. Klots, *Z. Phys. D* **21**, 335 (1991)
228. K. Hansen, O. Echt, *Phys. Rev. Lett.* **78**, 2337 (1997)
229. J.U. Andersen, C. Brink, P. Hvelplund, M.O. Larsson, B.B. Nielsen, H. Shen, *Phys. Rev. Lett.* **77**, 3991 (1996). <https://doi.org/10.1103/PhysRevLett.77.3991>
230. P. Ferrari, E. Janssens, P. Lievens, K. Hansen, *Int. Rev. Phys. Chem.* **38**(3–4), 405 (2019). <https://doi.org/10.1080/0144235X.2019.1678929>
231. M.H. Stockett, J. Houmøller, K. Støchkel, A. Svendsen, S. Brøndsted Nielsen, *Rev. Sci. Instrum.* **87**(5), 053103 (2016). <https://doi.org/10.1063/1.4948316>
232. L.D. Landau, E.M. Lifshitz, *Quantum Mechanics* (Pergamon Press, London, 1959)
233. D.M. Brink, S. Stringari, *Z. Phys. D* **15**, 257 (1990)
234. L. Bizzocchi, D. Prudenzeno, V.M. Rivilla, A. Pietropoli-Charmet, B.M. Giuliano, P. Caselli, J. Martín-Pintado, I. Jiménez-Serra, S. Martín, M.A. Requena-Torres, F. Rico-Villas, S. Zeng, J.C.



- Guillemin, A&A **640**, A98 (2020). <https://doi.org/10.1051/0004-6361/202038083>
235. J.A. Stearns, S. Mercier, C. Seaiby, M. Guidi, O.V. Boyarkin, T.R. Rizzo, *J. Am. Chem. Soc.* **129**(38), 11814 (2007). <https://doi.org/10.1021/ja0736010>
236. G. Papadopoulos, A. Svendsen, O.V. Boyarkin, T.R. Rizzo, *J. Am. Soc. Mass Spectrom.* **23**(7), 1173 (2012). <https://doi.org/10.1021/jasms.8b04319>
237. V. Kopysov, A. Makarov, O.V. Boyarkin, *Anal. Chem.* **87**(9), 4607 (2015). <https://doi.org/10.1021/acs.analchem.5b00822>
238. H. Kang, G. Féraud, C. Dedonder-Lardeux, C. Jouvét, *J. Phys. Chem. Lett.* **5**(15), 2760 (2014). <https://doi.org/10.1021/jz5012466>
239. L.S. Wang, *J. Chem. Phys.* **143**(4), 040901 (2015). <https://doi.org/10.1063/1.4927086>
240. J.A. Noble, J.P. Aranguren-Abate, C. Dedonder, C. Jouvét, G.A. Pino, *Phys. Chem. Chem. Phys.* **21**, 23346 (2019). <https://doi.org/10.1039/C9CP04302K>
241. B.M. Marsh, J.M. Voss, E. Garand, *J. Chem. Phys.* **143**(20), 204201 (2015). <https://doi.org/10.1063/1.4936360>
242. M. Broquier, S. Soorkia, G. Pino, C. Dedonder-Lardeux, C. Jouvét, G. Grégoire, *J. Phys. Chem. A* **121**(34), 6429 (2017). <https://doi.org/10.1021/acs.jpca.7b06423>
243. C. Dedonder, G. Féraud, C. Jouvét, *J. Chem. Phys.* **141**(13), 131101 (2014). <https://doi.org/10.1063/1.4896981>
244. S. Chakrabarty, M. Holz, E.K. Campbell, A. Banerjee, D. Gerlich, J.P. Maier, *J. Phys. Chem. Lett.* **4**(23), 4051 (2013). <https://doi.org/10.1021/jz402264n>
245. O.V. Boyarkin, *Int. Rev. Phys. Chem.* **37**(3–4), 559 (2018). <https://doi.org/10.1080/0144235X.2018.1547453>
246. N.S. Nagornova, T.R. Rizzo, O.V. Boyarkin, *Angew. Chem. Int. Ed.* **52**(23), 6002 (2013). <https://doi.org/10.1002/anie.201301656>
247. J.A. Wyer, (Springer Berlin Heidelberg, Berlin, Heidelberg, 2013), chap. 3, pp. 21–44. [https://doi.org/10.1007/978-3-642-40190-9\\_3](https://doi.org/10.1007/978-3-642-40190-9_3)
248. A.M. Nagy, F.O. Talbot, M.F. Czar, R.A. Jockusch, *J. Photochem. Photobiol. A* **244**, 47 (2012). <https://doi.org/10.1016/j.jphotochem.2012.06.017>
249. A.S. Danell, J.H. Parks, *Int. J. Mass Spectrom.* **229**(1), 35 (2003). [https://doi.org/10.1016/S1387-3806\(03\)00253-7](https://doi.org/10.1016/S1387-3806(03)00253-7)
250. F.O. Talbot, A. Rullo, H. Yao, R.A. Jockusch, *J. Am. Chem. Soc.* **132**(45), 16156 (2010). <https://doi.org/10.1021/ja1067405>
251. C. Kjær, H. Lissau, N.K. Gravesen Salinas, A. Østergaard Madsen, M.H. Stockett, F.E. Storm, T. Holm Hansen, J.U. Andersen, B.W. Laursen, K.V. Mikkelsen, M. Brøndsted Nielsen, S. Brøndsted Nielsen, *ChemPhysChem* **20**(4), 533 (2019). <https://doi.org/10.1002/cphc.201800933>
252. M. Kordel, D. Schooss, C. Neiss, L. Walter, M.M. Kappes, *J. Phys. Chem. A* **114**(17), 5509 (2010). <https://doi.org/10.1021/jp100636x>
253. V. Rajagopal, C. Stokes, A. Ferzoco, *J. Am. Soc. Mass Spectrom.* **29**(2), 260 (2018). <https://doi.org/10.1021/jasms.8b05741>
254. J. Langeland, C. Kjær, L.H. Andersen, S. Brøndsted Nielsen, *ChemPhysChem* **19**(14), 1686 (2018). <https://doi.org/10.1002/cphc.201800225>
255. J.T. Khoury, S.E. Rodriguez-Cruz, J.H. Parks, *J. Am. Soc. Mass Spectrom.* **13**(6), 696 (2002). <https://doi.org/10.1021/jasms.8b01800>
256. J. Friedrich, J. Fu, C.L. Hendrickson, A.G. Marshall, Y.S. Wang, *Rev. Sci. Instrum.* **75**(11), 4511 (2004). <https://doi.org/10.1063/1.1795111>
257. V. Frankevich, X. Guan, M. Dashtiev, R. Zenobi, *Eur. J. Mass Spectrom.* **11**(5), 475 (2005). <https://doi.org/10.1255/ejms.720>
258. N.A. Sassin, S.C. Everhart, B.B. Dangi, K.M. Ervin, J.I. Cline, *J. Am. Soc. Mass Spectrom.* **20**(1), 96 (2009). <https://doi.org/10.1021/jasms.8b03299>
259. K. Honma, *Phys. Chem. Chem. Phys.* **20**(42), 26859 (2018). <https://doi.org/10.1039/C8CP04067B>
260. P. Tiwari, J.B. Metternich, M.F. Czar, R. Zenobi, *J. Am. Soc. Mass Spectrom.* **32**(1), 187 (2021). <https://doi.org/10.1021/jasms.0c00264>
261. G.A. Eiceman, Z. Karpas, H.H. Hill Jr., *Ion Mobility Spectrometry*, 3rd edn. (CRC Press, London, 2013)
262. F. Lanucara, S.W. Holman, C.J. Gray, C.E. Eyers, *Nat. Chem.* **6**(4), 281 (2014). <https://doi.org/10.1038/nchem.1889>
263. M.E. Ridgeway, M. Lubeck, J. Jordens, M. Mann, M.A. Park, *Int. J. Mass Spectrom.* **425**, 22 (2018). <https://doi.org/10.1016/j.ijms.2018.01.006>
264. L. Deng, Y.M. Ibrahim, A.M. Hamid, S.V.B. Garimella, I.K. Webb, X. Zheng, S.A. Prost, J.A. Sandoval, R.V. Norheim, G.A. Anderson, A.V. Tolmachev, E.S. Baker, R.D. Smith, *Anal. Chem.* **88**(18), 8957 (2016). <https://doi.org/10.1021/acs.analchem.6b01915>
265. R. Fromherz, G. Ganteför, A.A. Shvartsburg, *Phys. Rev. Lett.* **89**, 083001 (2002). <https://doi.org/10.1103/PhysRevLett.89.083001>
266. M. Vonderach, O.T. Ehrler, P. Weis, M.M. Kappes, *Anal. Chem.* **83**(3), 1108 (2011). <https://doi.org/10.1021/ac1029677>
267. G. Papadopoulos, A. Svendsen, O.V. Boyarkin, T.R. Rizzo, *Faraday Discuss.* **150**, 243 (2011). <https://doi.org/10.1039/C0FD00004C>
268. B. Bellina, J.M. Brown, J. Ujma, P. Murray, K. Giles, M. Morris, I. Compagnon, P.E. Barran, *Analyst* **139**, 6348 (2014). <https://doi.org/10.1039/C4AN01656D>
269. A.L. Simon, F. Chiro, C.M. Choi, C. Clavier, M. Barbaire, J. Maurelli, X. Dagany, L. MacAleese, P. Dugourd, *Rev. Sci. Instrum.* **86**(9), 094101 (2015). <https://doi.org/10.1063/1.4930604>
270. O. Hernandez, S. Isenberg, V. Steinmetz, G.L. Glish, P. Maitre, *J. Phys. Chem. A* **119**(23), 6057 (2015). <https://doi.org/10.1021/jp511975f>
271. S.J.P. Marlton, B.I. McKinnon, B. Ucur, A.T. Maccarone, W.A. Donald, S.J. Blanksby, A.J. Trevitt, *Faraday Discuss.* **217**, 453 (2019). <https://doi.org/10.1039/C8FD00212F>
272. N.J.A. Coughlan, P.J.J. Carr, S.C. Walker, C. Zhou, M. Guna, J.L. Campbell, W.S. Hopkins, *J. Am. Soc. Mass Spectrom.* **31**(2), 405 (2020). <https://doi.org/10.1021/jasms.9b00039>
273. B.D. Adamson, N.J.A. Coughlan, P.B. Markworth, R.E. Continetti, E.J. Bieske, *Rev. Sci. Instrum.* **85**(12), 123109 (2014). <https://doi.org/10.1063/1.4903753>

274. S. Warnke, A. Ben Faleh, V. Scutelnic, T.R. Rizzo, J. Am. Soc. Mass Spectrom. **30**(11), 2204 (2019). <https://doi.org/10.1021/jasms.8b06266>
275. J. Gidden, M.T. Bowers, J. Am. Soc. Mass Spectrom. **14**, 161 (2003). <https://doi.org/10.1021/jasms.8b01923>
276. A.G.G.M. Tielens, Rev. Mod. Phys. **85**(3), 1021 (2013). <https://doi.org/10.1103/RevModPhys.85.1021>
277. B.A. Croiset, A. Candian, O. Berné, A.G.G.M. Tielens, Astron. Astrophys. **590**, A26 (2016). <https://doi.org/10.1051/0004-6361/201527714>
278. H. Andrews, A. Candian, A.G.G.M. Tielens, Astron. Astrophys. **595**, A23 (2016). <https://doi.org/10.1051/0004-6361/201628819>
279. M.S. Murga, M.S. Kirsanova, A.I. Vasyunin, Y.N. Pavlyuchenkov, Mon. Not. R. Astron. Soc. **497**(2), 2327 (2020). <https://doi.org/10.1093/mnras/staa2026>
280. A. Simon, M. Rapacioli, G. Rouaut, G. Trinquier, F.X. Gadea, Philos. Trans. R. Soc. A Math. Phys. Eng. Sci. **375**(2092), 20160195 (2017). <https://doi.org/10.1098/rsta.2016.0195>
281. P. Castellanos, A. Candian, J. Zhen, H. Linnartz, A.G.G.M. Tielens, Astron. Astrophys. **616**, A166 (2018). <https://doi.org/10.1051/0004-6361/201833220>
282. Wiersma, Sandra D., Candian, Alessandra, Bakker, Joost M., Martens, Jonathan, Berden, Giel, Oomens, Jos, Buma, Wybren Jan, Petrigani, Annemieke, A&A **635**, A9 (2020). <https://doi.org/10.1051/0004-6361/201936982>
283. J. Cami, J. Bernard-Salas, E. Peeters, S.E. Malek, Science **329**, 1180 (2010). <https://doi.org/10.1126/science.1192035>
284. J. Zhen, P. Castellanos, D.M. Paardekooper, H. Linnartz, A.G.G.M. Tielens, Astrophys. J. **797**(2), L30 (2014). <https://doi.org/10.1088/2041-8205/797/2/L30>
285. H. Andrews, C. Boersma, M.W. Werner, J. Livingston, L.J. Allamandola, A.G.G.M. Tielens, Astrophys. J. **807**(1), 99 (2015). <https://doi.org/10.1088/0004-637X/807/1/99>
286. Y.A. Dyakov, C.K. Ni, S.H. Lin, Y.T. Lee, A.M. Mebel, Phys. Chem. Chem. Phys. **8**, 1404 (2006). <https://doi.org/10.1039/B516437K>
287. E.A. Solano, P.M. Mayer, J. Chem. Phys. **143**(10), 104305 (2015). <https://doi.org/10.1063/1.4930000>
288. M. Hanine, Z. Meng, S. Lu, P. Xie, S. Picaud, M. Devel, Z. Wang, Astrophys. J. **900**(2), 188 (2020). <https://doi.org/10.3847/1538-4357/abab06>
289. P. Parneix, A. Gamboa, C. Falvo, M. Bonnin, T. Pino, F. Calvo, Mol. Astrophys. **7**, 9 (2017). <https://doi.org/10.1016/j.molap.2017.05.001>
290. M. Rapacioli, A. Simon, C.C.M. Marshall, J. Cuny, D. Kokkin, F. Spiegelman, C. Joblin, J. Phys. Chem. A **119**(51), 12845 (2015). <https://doi.org/10.1021/acs.jpca.5b09494>
291. C.J. Mackie, A. Candian, X. Huang, E. Maltseva, A. Petrigani, J. Oomens, W.J. Buma, T.J. Lee, A.G.G.M. Tielens, Phys. Chem. Chem. Phys. **20**, 1189 (2018). <https://doi.org/10.1039/C7CP06546A>
292. J. Lam, S. Abdul-Al, A.R. Allouche, J. Chem. Theory Comput. **16**(3), 1681 (2020). <https://doi.org/10.1021/acs.jctc.9b00964>

## Measurements of differential cross sections for elastic electron scattering and electronic excitation of silver and lead atoms

This content has been downloaded from IOPscience. Please scroll down to see the full text.

2012 J. Phys.: Conf. Ser. 399 012004

(<http://iopscience.iop.org/1742-6596/399/1/012004>)

View [the table of contents for this issue](#), or go to the [journal homepage](#) for more

Download details:

IP Address: 147.91.81.240

This content was downloaded on 30/09/2015 at 11:07

Please note that [terms and conditions apply](#).

## Measurements of differential cross sections for elastic electron scattering and electronic excitation of silver and lead atoms

**S. D. Tošić**

Laboratory for Atomic Collision Processes, Institute of Physics,  
University of Belgrade, Pregrevica 118, 11080 Belgrade, Serbia

E-mail: sanja.tosic@ipb.ac.rs

**Abstract.** This paper presents absolute differential cross sections (DCSs) and integrated cross sections (ICSs) for both elastic and inelastic electron scattering by lead and silver atoms in the energy range from 10 to 100 eV. The DCSs were measured as a function of scattering angle. Scattering angles are from  $1^\circ$  to  $150^\circ$  for the excitations of the unresolved  $4d^{10}5p\ ^2P_{1/2, 3/2}$  silver line and  $6p7s\ ^3P_{0,1}$  lead line, while for the elastic scattering they span from  $10^\circ$  to  $150^\circ$ . The measurements utilize crossed beam technique with effusive atomic beam being perpendicularly crossed by electron beam. Monoenergetic electron beam is obtained by means of hemispherical selector and it is focused by cylindrical electrostatic lenses while effusive atomic beam is formed by heating of Knudsen type oven. Absolute values for the resonance states are obtained by normalization of relative differential cross sections to the optical oscillator strengths, while the absolute values for the elastic scattering are obtained from the intensity ratios at particular scattering angles. Obtained absolute DCSs were extrapolated to  $0^\circ$  and  $180^\circ$  and numerically integrated to yield integral, momentum transfer and viscosity cross sections. The experimental results have been compared with the corresponding calculations.

### 1. Introduction

Electron interaction with metal atom vapours provides fundamental information on the structure and collisional dynamics of atomic system, as well as information on basic interaction between particles in scattering process. The main observable in these processes is differential cross section (DCS) which indicates the probability of specific interaction at certain electron energy and scattering angle and it is given by:

$$DCS = \frac{k_f}{k_i} |A_{fi}|^2 \quad (1)$$

where  $A_{fi}$  is a scattering amplitude and  $k_f$  and  $k_i$  are wave vectors of scattered and incident particles, respectively. Beside the general importance of both experimental and theoretical collisional electron cross section data for understanding and explanation of fundamental electron interaction with isolated metal atoms, there is also a particular relevance of these results for the biomedical radiation research as well as for many plasma diagnostic and modeling techniques which require electron impact cross sections as input data for the calculation of plasma parameters [1, 2]. Besides this, detailed electron-metal atom collision data are very important in astrophysics for spectra's analysis, for chemical composition determination of various astrophysical objects and also for its abundance analysis [3-12].



They are essential for determination of transport properties in astrophysical plasmas of some stellar atmospheres and also for modeling of some metal rich stellar atmospheres (atmospheres of some DZ white dwarfs) [13].

In metal atoms, DCS for resonant electron excitation is more pronounced than DCS for elastic scattering. To determine the absolute DCS experimentally, it is necessary to know several parameters [14]. Generally, experimental investigations are often limited by the high working temperature which is necessary to vaporize the metal sample in order to produce a well collimated effusive atomic beam. At the same time, at these temperatures, metal deposition can make contacts between electron lenses, which can induce difficulties during the measurements.

Here we present experimentally obtained absolute differential cross sections (DCSs) for both elastic and inelastic electron scattering by lead and silver atoms as well as corresponding integrated cross sections. The DCSs were measured at intermediate electron impact energies from 10 eV to 100 eV and scattering angles are from  $1^\circ$  to  $150^\circ$  for the combined excitations of the unresolved  $4d^{10}5p^2P_{1/2, 3/2}$  silver line and  $6p7s^3P_{0,1}$  lead line, while for the elastic scattering they span from  $10^\circ$  to  $150^\circ$ . The experimental results have been compared with the corresponding calculations.

## 2. Experimental technique and procedure

In the crossed beam arrangement where an electron beam has been perpendicularly crossed by the effusive atomic beam, the scattered electrons have been analyzed in the high resolution electron spectrometer ESMA which has been described in our previous papers dealing with electron scattering by other metal targets [15-20].

A hairpin thermoelectron source was used and electron beam was formed by the electron monochromator which consists of systems of cylindrical electrostatic lenses and hemispherical electrostatic energy selector. Scattered electrons were analyzed by the hemispherical electron energy analyzer which is of the same type as the monochromator. It can rotate around the atomic beam axis so we could analyze and detect scattered electrons in the scattering angle range from  $-30^\circ$  to  $150^\circ$ . A channel electron multiplier was used as a detector.

A metal vapor beam was produced by heating an oven crucible containing metal by two separate heaters. In this way we separately heated the top and bottom of the oven and provided a variable temperature difference at approximately 100 K. The working temperature was about 1170 K for Pb and 1300 K for Ag and background pressure was of the order of  $10^{-5}$  Pa. The overall energy resolution (FWHM) was typically 120 meV for Pb and 160 meV for Ag while the angular resolution was  $1.5^\circ$ . The position of true zero scattering angle was determined before each angular distribution measurement by checking the symmetry of the inelastically scattered electrons at negative and positive scattering angles (usually from  $-10^\circ$  to  $+10^\circ$ ). The measured angular distributions were converted into relative DCSs by using the appropriate effective length correction factors [21]. The absolute values of differential cross sections for excitation are obtained through the normalization procedure to the optical oscillator strengths (OOS) for the observed transition. Following the method described by Felfli and Msezane [22], we normalized the relative DCSs by using the forward scattering function (FSF) introduced by Avdonina *et al.* [23]. Due to this procedure which is based on Lassetre limiting theorem and the fact that GOS tends to OOS as momentum transfer squared ( $K^2$ ) tends to zero, relative DCSs were converted to the generalized oscillator strengths according to formula:

$$GOS(K, E) = \frac{\omega k_i}{2 k_f} K^2 DCS(K, \theta) \quad (2)$$

where  $\omega$  is the excitation energy,  $k_i$  and  $k_f$  are the electron momenta before and after the collision, respectively, and the momentum transfer  $K$  is defined by:

$$K^2 = 2E \left[ 2 - \frac{\omega}{E} - 2\sqrt{1 - \frac{\omega}{E} \cos \theta} \right] \quad (3)$$

where  $E$  is the impact energy. The obtained GOS values were fitted and extrapolated from the small values of  $K^2$  obtained from zero scattering angle at each electron impact energy (Eq. 3) and normalized to the FSF. These normalization factors were then used to obtain absolute DCS values. FSF procedure was applied at all energies except at 10 eV for electron silver excitation where the necessary condition  $E > 2.5\omega$  is not satisfied ( $\omega$  is the excitation energy of the transition). A more detailed description of the normalization procedure has been described in details in our previous papers [15, 24]. Briefly, in the case of lead we generate FSF using the OOS value of 0.21 for the  $6p7s\ ^3P_1$  state ( $6p7s\ ^3P_0$  is optically forbidden). In the case of silver, contrary to the case of lead, both unresolved states are optically allowed and have appropriate OOS values so we used the OOS values of 0.452 for the  $^2P_{3/2}$  level and 0.223 for the  $^2P_{1/2}$  level. The absolute values for the elastic scattering are obtained from the intensity ratios at particular scattering angles.

Obtained absolute DCSs were extrapolated to  $0^\circ$  and  $180^\circ$  using the measured values at small scattering angles and corresponding calculations, relativistic distorted wave calculations (RDW) for excitation processes [15, 16] and optical potential calculations for elastic electron scattering [17, 19]. After extrapolation, numerical integration was applied and integral, momentum transfer and viscosity cross sections were derived using formulas

$$Q_I = 2\pi \int_0^\pi \sigma(\theta) \sin \theta \, d\theta \quad (4)$$

$$Q_M = 2\pi \int_0^\pi \sigma(\theta) \left[ 1 - \left( 1 - \frac{\omega}{E_0} \right)^{1/2} \cos \theta \right] \sin \theta \, d\theta \quad (5)$$

$$Q_V = 2\pi \int_0^\pi \sigma(\theta) \left[ 1 - \left( 1 - \frac{\omega}{E_0} \right) \cos^2 \theta \right] \sin \theta \, d\theta \quad (6)$$

where  $\sigma$  is the differential cross section (DCS) and  $\omega$  is the excitation energy.

### 3. Results

#### 3.1 Electron scattering by lead atom

Both the elastic electron scattering and electron-impact excitation of the unresolved  $6p7s\ ^3P_{0,1}$  levels of Pb atom have been investigated. The measurements at small scattering angles for the resonant  $6p^2\ ^3P_0 \rightarrow 6p7s\ ^3P_1$  transition in Pb are shown in Figure 1. One can see the normalized generalized oscillator strengths (GOSs) determined through normalizations to the optical oscillator strength using the forward scattering function (FSF) method [24]. It is evident that absolute GOS values for zero scattering angles lie on the FSF curve and also that the normalized GOSs decrease with increasing momentum transfer. At 20 eV we have linear dependence of  $K^2$  but this linearity decreases at higher energies.

The absolute DCSs values for the  $6p7s\ ^3P_{0,1}$  excitation at 60, 80 and 100 eV electron impact energies are presented in Figure 2 and compared with the relativistic distorted-wave (RDW) calculations using multi-configuration (MCGS) and single-configuration (SCGS) wave functions for the atomic states [16]. The comparison between our experimental data and theoretical results shows that there is excellent agreement in both the shape and magnitude except at 100 eV and scattering angles between

70° and 120° where the experiment gives somewhat smaller values. The good agreement is also evident at small scattering angles (see inset in Figure 2).

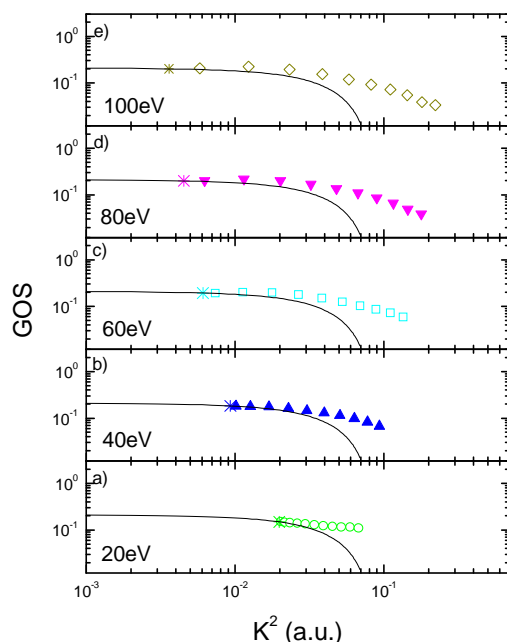


**Figure 1.** Generalized oscillator strengths (GOS) for the  $6p7s\ ^3P_1$  state of lead atoms versus momentum transfer squared ( $K^2$ ) at 20, 40, 60, 80 and 100 eV electron-impact energies. The stars show the appropriate minimal values of  $K^2$  for zero scattering angle and the solid line represents the forward scattering function (FSF) generated using the optical oscillator strength (OOS) value of 0.21 [24].

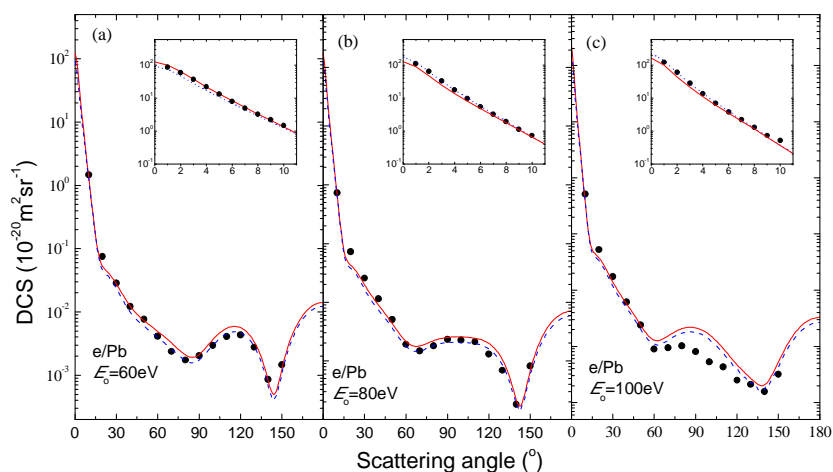


**Figure 2.** Differential cross sections for the  $6p7s\ ^3P_{0,1}$  excitation of lead at (a) 60 eV, (b) 80 eV and (c) 100 eV electron impact-energies. Filled circles with error bars denote the present experimental results. The solid line shows DCSs calculated by the MCGS approximation and the dashed line shows the results obtained using the SCGS approximation [16]. In the insets, the low angle parts of DCS are zoomed out.

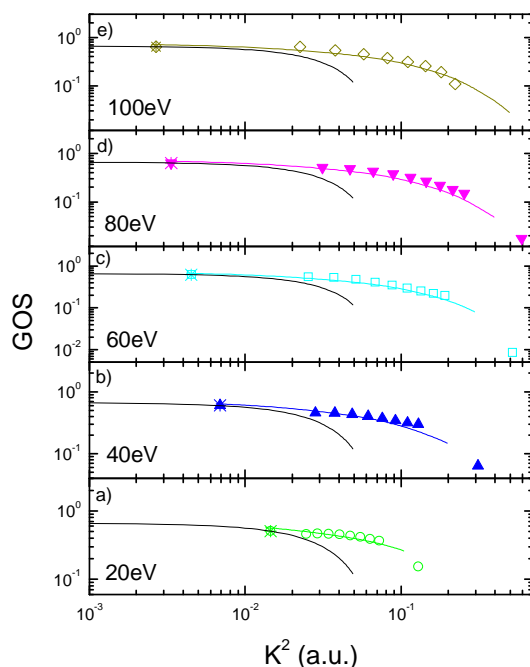


**Figure 3.** Generalized oscillator strengths (GOS) for the  $4d^{10}5p^2P_{1/2, 3/2}$  state of silver atoms versus momentum transfer squared ( $K^2$ ) at 20, 40, 60, 80 and 100 eV electron-impact energies. Labels are the same as for the Fig. 1. The colour solid lines represent corresponding RDW calculations [15].

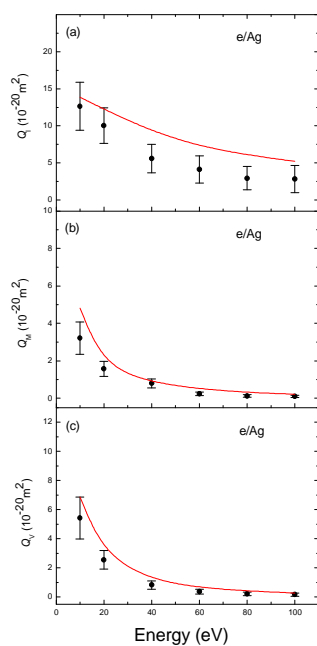


**Figure 4.** (a) Integral  $Q_I$ , (b) momentum transfer  $Q_M$ , and (c) viscosity cross sections  $Q_V$  for electron impact excitation of the  $4d^{10}5p^2P_{1/2,3/2}$  state of silver atom. Filled circles with error bars denote the present experimental results while the solid line shows the combined ICSs calculated by the RDW method.

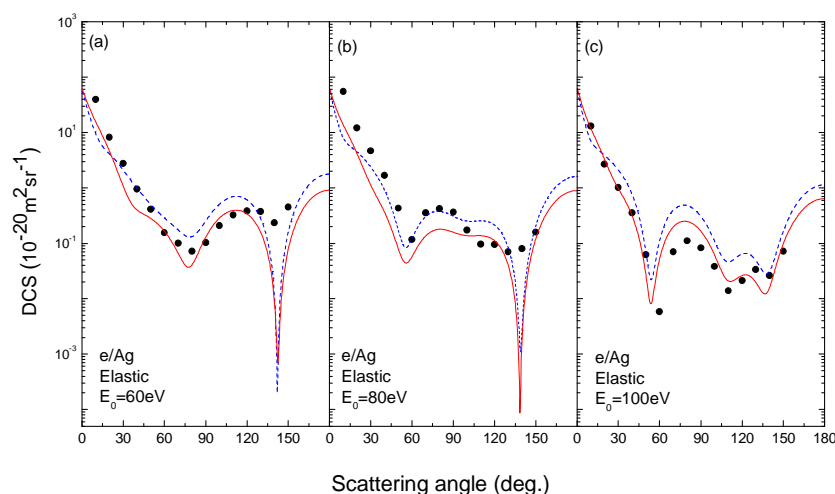


**Figure 5.** Differential cross sections for the elastic electron scattering by silver atoms at (a) 60 eV, (b) 80 eV and (c) 100 eV electron impact-energies. Filled circles with error bars denote the present experimental results. The dashed line shows the results obtained using the SEPSO calculation while solid line shows DCSs calculated by the SEPASO approximation [19].

### 3.2 Electron scattering by silver atom

We have also investigated the electron excitation of the first combined resonant  $4d^{10}5p$  state of silver atom as well as the elastic electron scattering by this target [15, 19]. The obtained results for generalized oscillator strengths (GOS) are presented in Figure 3 together with corresponding relativistic distorted wave (RDW) calculations [15] where the atomic orbitals and wave functions for both the ground and excited states (fine-structures levels) were calculated using the multiconfiguration Dirac–Fock (MCDHF) program [25]. Since both unresolved states of silver are optically allowed and therefore they both have the OOS values, we generated FSF using OOS value of 0.675 which was obtained as a sum of the OOS values of the  $^2P_{1/2}$  (0.223) and  $^2P_{3/2}$  (0.452) levels of silver [19]. As expected [22], the region of linearity of the GOS values decreases as  $E$  increases from threshold. Good agreement between experiment and theoretically obtained GOS results for combined the  $4d^{10}5p^2P_{1/2,3/2}$  excitation using RDW calculations verify that our normalization is reliable. At 10 eV electron impact energy where the necessary condition for normalization defined as  $E > 2.5\omega$  is not satisfied, we normalized our experimental results to the calculated RDW data.

In Figure 4 we present results for integrated cross sections. As one can see, both experiment and theory predict decreasing of  $Q_I$ ,  $Q_M$  and  $Q_V$  with increasing incident electron energy and there is a good agreement in shape of ICS curves. At 10 eV and 20 eV theory gives slightly higher ICS values but since the calculated DCSs are higher than the measured ones over the whole angular range this is not surprising.

Figure 5 shows present measured DCSs for elastic electron scattering by silver together with optical potential calculations [19]. There are two sets of calculated results, with (SEPASO) and without (SEPSO) taking into account absorption effects (potential). It is evident that experimental data exhibit the same shape as the theories and that both approximations give very similar results.




#### 4. Conclusion

The elastic and inelastic electron collisions with Pb and Ag atoms have been investigated. We have obtained absolute values for generalized oscillator strengths (GOS), differential cross sections (DCS) and integrated cross sections (ICS) for electron impact excitation of the  $4d^{10}5p^2P_{1/2, 3/2}$  silver line and the  $6p7s^3P_{0,1}$  lead line, as well as DCSs and ICSs for elastic electron scattering by these targets. Measurements were performed at electron energies of 10, 20, 40, 60, 80 and 100 eV and at scattering angles up to  $150^\circ$ . The measured results were put on the absolute scale using FSF method. Comparisons with corresponding relativistic distorted wave (RDW) calculations for excitation [15, 16, 24] and optical potential calculations for elastic scattering [17, 19] were made. We found reasonably good agreement between experiment and theory.

It is known that the data about electron metal atom cross sections are of particularly interest for different applications in many fields such as the astrophysics, biomedicine, plasma physics, surface and material science etc. In order to contribute to research in these areas by getting new reliable results, our future work will be concentrated to the electron interaction with other metal atoms.

#### 5. References

- 
- [1] Marinković B P, Pejčev V, Filipović D M, Šević D, Milosavljević A R, Milisavljević S, Rabasović M S, Pavlović D and Maljković J B 2007 *Journal of Physics: Conf. Ser.* **86** 012006
  - [2] Fortov V E, Iakubov I T and Khrapak A G 2007 Chapter Electrical conductivity of partially ionized plasma *Physics of Strongly Coupled Plasma* (Oxford University Press)
  - [3] Van Eck S, Goriely S, Jorissen A and Plez B 2001 *Nature* **412** 793
  - [4] Cowan J J, Sneden C, Truran J W and Burris D L 1996 *ApJ* **460** L115
  - [5] Goswami A, Aoki W, Beers T C, Christlieb N, Norris J E, Ryan S G and Tsangarides S 2006 *MNRAS* **372**, 343
  - [6] Cardelli J A 1994 *Science* **265**, 209
  - [7] Smith G 1988 *J. Phys. B: At. Mol. Opt. Phys.* **21** 2827
  - [8] Dimitrijević M S and Sahal-Brechot S 1999 *Astron. Astrophys. Suppl. Ser.* **140** 191
  - [9] Liang Gui-Yun, Bian Xia and Zhao Gang 2004 *Chinese Physics* **13** 0891
  - [10] Holweger H 1972 *Solar. Phys.* **25** 14
  - [11] Thoren P 2000 *Astron. Astrophys.* **358** L21
  - [12] Chmielewski Y 2000 *Astron. Astrophys.* **353** 666
  - [13] Sreckovic V A, Ignjatovic Lj M, Mihajlov A A and Dimitrijevic M S 2010 *Monthly Notices of the Royal Astronomical Society* **406** 590
  - [14] Rabasović M S, Tošić S D, Pejčev V, Šević D, Filipović D M and Marinković B P 2008 *Facta Universitatis, Series Phys. Chem. Technol.* **6** 119
  - [15] Tošić S D, Pejčev V, Šević D, McEachran R P, Stauffer A D and Marinković B P 2012 *Nucl. Instr. Meth. B*, **279** 53
  - [16] Milisavljević S, Rabasović M S, Šević D, Pejčev V, Filipović D M, Lalita Sharma, Rajesh Srivastava, Stauffer A D and Marinković B P 2008 *Phys. Rev. A*, **76** 022714
  - [17] Tošić S D, Rabasović M S, Šević D, Pejčev V, Filipović D M, Lalita Sharma, Triphati A N, Rajesh Srivastava and Marinković B P 2008 *Phys. Rev. A*, **77** 012725
  - [18] Rabasović M S, Tošić S D, Šević D, Pejčev V, Filipović D M and Marinković B P 2009 *Nucl. Instr. Meth. B*, **267** 279
  - [19] Tošić S D, Kelemen V I, Šević D, Pejčev V, Filipović D M, Remeta E Y and Marinković B P 2009 *Nucl. Instr. Meth. B*, **267** 283
  - [20] Predojević B 2006 CP876 *The Physics of Ionized Gases: 23<sup>rd</sup> Summer School and International Symposium* ed Lj Hadžijevski, B P Marinković and N Simonović (American Institute of Physics) p 88

- [21] Brinkman R T and Trajmar S 1981 *J. Phys. E*, **14** 245
- [22] Felfli Z and Msezane A Z 1998 *J. Phys. B: At. Mol. Opt. Phys.* **31** L165
- [23] Avdonina N B, Felfli Z and Msezane A Z 1997 *J. Phys. B: At. Mol. Opt. Phys.* **30** 2591
- [24] Milisavljević S, Rabasović M S, Šević D, Pejčev V, Filipović D M, Lalita Sharma, Rajesh Srivastava, Stauffer A D and Marinković B P 2008 *Phys. Rev. A*, **75** 052713
- [25] Grant I P, McKenzie B J, Norrington P B and Pyper N C 1980 *Comput. Phys. Commun.* **21** 207

### **Acknowledgments**

I am very grateful to Dr B P Marinković, Dr V Pejčev and other colleagues from the Laboratory of Atomic Collision Processes. I am also grateful to Dr R Srivastava, Dr A Stauffer, Dr R Mc Eachran, Dr V Kelemen and Dr E Yu Remeta for performing and sending calculated cross sections results. The work was supported by the Ministry of Education, Science and Technological Development of Republic of Serbia (Project No. 171020) and ESF/COST Action MP1002 Nano-scale insights in ion beam cancer therapy (Nano-IBCT).



# 28<sup>th</sup> Summer School and International Symposium on the Physics of Ionized Gases

Aug. 29 - Sep. 2, 2016, Belgrade, Serbia

## CONTRIBUTED PAPERS

&

ABSTRACTS OF INVITED LECTURES,  
TOPICAL INVITED LECTURES, PROGRESS REPORTS  
AND WORKSHOP LECTURES

Editors:

Dragana Marić, Aleksandar Milosavljević,  
Bratislav Obradović and Goran Poparić



University of Belgrade,  
Faculty of Physics



Serbian Academy  
of Sciences and Arts

## FRAGMENTATION OF HALOTHANE MOLECULE BY SYNCHROTRON RADIATION

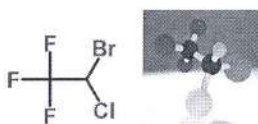
S. D. Tošić<sup>1</sup>, P. Bolognesi<sup>2</sup>, L. Avaldi<sup>2</sup>, R. Richter<sup>3</sup> and B. P. Marinković<sup>1</sup>

<sup>1</sup> *Institute of Physics Belgrade, University of Belgrade, Pregrevica 118, 11080 Belgrade, Serbia*

<sup>2</sup> *CNR-Istituto di Struttura della Materia, Area della Ricerca di Roma1, Monterotondo Scalo, Italy*

<sup>3</sup> *Elettra-Sincrotrone Trieste, Area Science Park, I-34012 Basovizza, Trieste, Italy*

Halothane (C<sub>2</sub>HBrClF<sub>3</sub>, 2-bromo-2-chloro-1,1,1-trifluoroethane) is one of the most extensively used halogenated anesthetics in medicine and the only one containing Br. It has a structure of a polyhalogenated organic molecule where the two carbon atoms experience very different chemical environments due to the bonding to different halogen atoms.



The fragmentation of C<sub>2</sub>HBrClF<sub>3</sub> by high energy photons and electron beams has been studied by De Souza et al. [1], while recently, Ferreira da Silva et al. [2] investigated theoretically and experimentally the VUV photoabsorption spectrum. Maljković et al. [3] reported the differential cross sections for elastic electron scattering by halothane at 100 eV in a combined experimental and theoretical work. Here we present the results of the photofragmentation study of the halothane molecule obtained at Gas phase beamline of Elettra. NEXAFS as well as mass spectra were measured at different photon energies across C 1s, Cl 2p, Cl 2s, Br 3d, Br 3p, Br 3s and F 1s ionization edges.

**Acknowledgements:** This work is supported by Ministry of Education, Science and Technological Development of Republic of Serbia (Project No. OI 171020) and by the Serbia – Italy Joint Research Project “A nanoview of radiation-biomatter interaction”.

### REFERENCES

- [1] G. G. B. de Souza et al. *Quim. Nova*, 24 (3), 311 (2001).
- [2] F. Ferreira da Silva et al. *J. Phys. Chem. A* 119, 8503 (2015).
- [3] J. Maljković et al. *Publ. Astron. Obs. Belgrade* No. 89, 33, (2010).



# 27<sup>th</sup> Summer School and International Symposium on the Physics of Ionized Gases

August 26-29, 2014, Belgrade, Serbia

## CONTRIBUTED PAPERS

&

**ABSTRACTS OF INVITED LECTURES,  
TOPICAL INVITED LECTURES, PROGRESS  
REPORTS AND WORKSHOP LECTURES**

Editors:

Dragana Marić

Aleksandar R. Milosavljević

Zoran Mijatović



Institute of Physics, Belgrade  
University of Belgrade



Serbian Academy  
of Sciences and Arts



**27<sup>th</sup> Summer School and International  
Symposium on the Physics of Ionized  
Gases**

**SPIG 2014**

**CONTRIBUTED PAPERS**

&

ABSTRACTS OF INVITED LECTURES,  
TOPICAL INVITED LECTURES, PROGRESS REPORTS  
AND WORKSHOP LECTURES

*Editors*

Dragana Marić, Aleksandar R. Milosavljević and  
Zoran Mijatović

Institute of Physics, Belgrade  
University of Belgrade

Serbian Academy  
of Sciences and Art

Belgrade, 2014

CONTRIBUTED PAPERS & ABSTRACTS OF INVITED  
LECTURES, TOPICAL INVITED LECTURES, PROGRESS  
REPORTS AND WORKSHOP LECTURES  
of the 27<sup>th</sup> Summer School and International Symposium on  
the Physics of Ionized Gases

August 26 – 29, 2014, Belgrade, Serbia

*Editors:*

Dragana Marić, Aleksandar R. Milosavljević and Zoran Mijatović

*Publishers:*

Institute of Physics, Belgrade  
Pregrevica 118, P. O. Box 68  
11080 Belgrade, Serbia

Klett izdavačka kuća d.o.o.  
Maršala Birjuzova 3-5, IV sprat  
11000 Belgrade

*Computer processing:*

Sanja D. Tošić, Nikola Škoro and Miloš Ranković

*Printed by*

**CICERO**  
Belgrade

*Number of copies*

300

ISBN 978-86-7762-600-6

©2014 by the Institute of Physics, Belgrade, Serbia and Klett izdavačka kuća d.o.o. All rights reserved. No part of this book may be reproduced, stored or transmitted in any manner without the written permission of the Publisher.

## INTEGRATED CROSS SECTIONS FOR ELECTRON EXCITATION OF THE $4d^{10}5p$ STATE OF THE Ag ATOM

S. D. Tošić<sup>1</sup>, V. Pejčev<sup>2</sup>, D. Šević<sup>1</sup>, R. P. McEachran<sup>3</sup>, A. D. Stauffer<sup>4</sup>  
and B. P. Marinković<sup>1</sup>

<sup>1</sup>*Institute of Physics, University of Belgrade, Pregrevica 118, 11080 Belgrade,  
Serbia*

<sup>2</sup>*Faculty of Natural Sciences, University of Kragujevac, Radoja Domanovića 12,  
34000 Kragujevac, Serbia*

<sup>3</sup>*ARC Centre for Antimatter-Matter Studies, Australian National University,  
Canberra, ACT 0200, Australia*

<sup>4</sup>*Department of Physics and Astronomy, York University, Toronto, ON M3J 1P3  
Canada*

**Abstract.** We have investigated the electron-impact excitation of the combined (two fine-structure levels) resonant  $4d^{10}5p^2P_{1/2,3/2}$  state in silver from the ground  $4d^{10}5s$  state both experimentally and theoretically. Measurements are presented for the combined level while the relativistic distorted wave (RDW) calculations were carried out for each level separately and for the combined level as well. Both the experimental and theoretical results were obtained in the incident electron energy ( $E_0$ ) range from 10 to 100 eV with experimental scattering angles ( $\theta$ ) from  $10^\circ$  up to  $150^\circ$ . Experimental absolute differential cross sections (DCSs) were determined through normalization of the relative DCSs at  $10^\circ$  to our previous small angle experimental DCS values. The integrated cross sections which include integral ( $Q_I$ ), momentum transfer ( $Q_M$ ), and viscosity ( $Q_V$ ) cross sections were determined by numerical integration of the absolute DCSs.

### 1. INTRODUCTION

In this paper, we continue our study of the combined resonant  $4d^{10}5p^2P_{1/2,3/2}$  state of the silver atom excited from the ground state by electron impact [1]. Those results at small scattering angles show that the measured differential cross sections were generally in quite good agreement with the relativistic distorted-wave (RDW) calculations especially at higher energies and smaller scattering angles. Thus, we established the experimental DCSs at  $10^\circ$  as a base for the normalization of our present relative measurements of the DCSs which are extended over a wide range of scattering angles up to  $150^\circ$  for experiment and up to  $180^\circ$  for theory. The energy range remains the same (from

10 to 100 eV). In this way, we obtained absolute DCS values which were extrapolated to  $0^\circ$  and  $180^\circ$  and numerically integrated to obtain the integral ( $Q_I$ ), momentum transfer ( $Q_M$ ) and viscosity ( $Q_V$ ) cross sections. Since the observed excited state has two fine-structure levels with total angular momentum  $J = 1/2$  and  $3/2$  which cannot be distinguished in the present experiment, measured results are presented for the excitation of the combined level. RDW calculations were performed for both fine-structure levels and for the combined excitation.

## 2. EXPERIMENT

The apparatus used is a conventional crossed-beam electron spectrometer described in more detail in our recent papers dealing with electron scattering by silver and lead atoms [1-3]. In the crossed beam arrangement the electron beam is formed in a system of cylindrical electrostatic lenses and hemispherical energy selectors. The scattered electrons are detected by a rotating analyzer that covers an angular range from  $-30^\circ$  to  $150^\circ$ , in the plane perpendicular to the atomic beam. The analyzer is of the same construction as the electron monochromator except that it has a channel electron multiplier as a single-electron detector at the end.

A silver vapour beam was produced by heating a Knudsen-type oven crucible containing silver metal by two separate coaxial heaters. The working temperature was about 1300 K, the background pressure was of the order of  $10^{-5}$  Pa, the overall energy resolution (FWHM) was typically 160 meV while the angular resolution was  $1.5^\circ$ . The position of the true zero scattering angle was determined before each angular distribution measurement by checking the symmetry of the scattered electrons at negative and positive scattering angles (usually from  $-10^\circ$  to  $+10^\circ$ ). Due to the change of effective interaction volume versus scattering angle, the effective path length correction factors  $V_{\text{eff}}$  [4] determined for the present experimental conditions were applied and corrections of the measured scattered intensities was made. The obtained relative DCSs were put on an absolute scale by normalization to the absolute DCSs for the same excitation process at  $10^\circ$  [1]. Our experimental integrated cross sections are obtained by the extrapolation of the absolute DCSs to  $0^\circ$  using our previously reported results at small angles and to  $180^\circ$  using the appropriate RDW calculation followed by numerical integration. Integral ( $Q_I$ ), momentum transfer ( $Q_M$ ) and viscosity ( $Q_V$ ) cross sections are defined as:

$$Q_I = 2\pi \int_0^\pi DCS(\theta) \sin \theta \, d\theta \quad (1)$$

$$Q_M = 2\pi \int_0^\pi DCS(\theta) \left[ 1 - \left( 1 - \frac{\omega}{E_0} \right)^{1/2} \cos \theta \right] \sin \theta \, d\theta \quad (2)$$

$$Q_V = 2\pi \int_0^\pi DCS(\theta) \left[ 1 - \left( 1 - \frac{\omega}{E_0} \right) \cos^2 \theta \right] \sin \theta d\theta \quad (3)$$

where  $DCS(q)$  is absolute differential cross section,  $\omega$  is excitation energy and  $E_0$  is electron impact energy. The details of the RDW method for calculating the DCSs were given in [1] and references therein.

### 3. RESULTS AND DISCUSSION

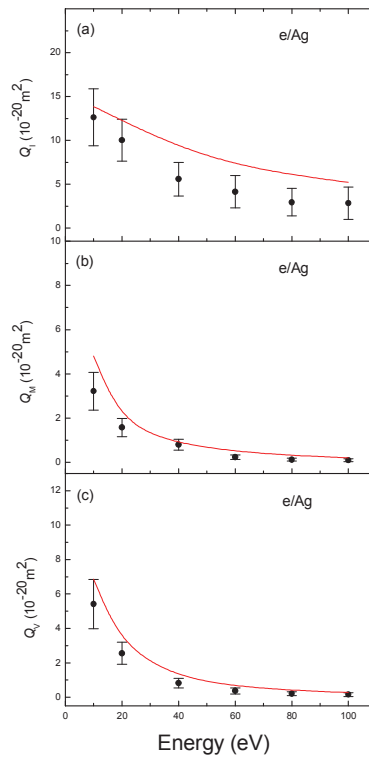


**Figure 1.** (a) Integral, (b) momentum transfer, and (c) viscosity cross sections for electron impact excitation of the  $4d^{10}5p^2P_{1/2,3/2}$  state of the silver atom. Filled circles with error bars denote the present experimental results. The solid line shows the combined DCSs calculated by the RDW method.

In Figure 1 we show the results for the integral ( $Q_I$ ) (a), momentum transfer ( $Q_M$ ) (b) and viscosity ( $Q_V$ ) (c) cross sections for electron excitation of the  $4d^{10}5p^2P_{1/2,3/2}$  state of silver. Experiment confirms a slow decrease of  $Q_I$ ,  $Q_M$  and  $Q_V$  with increasing incident electron energy as is also predicted by theory. One can see that reasonably good agreement was achieved between experiment and theory concerning the shape of the energy dependences of all integral cross



sections but theory gives slightly larger values of all integral cross sections at all electron energies though they lie within the limits of the error bars in several cases. The main reason for this behaviour is the fact that the present calculated DCSs are higher than the normalized measured ones over the whole angular range.

Considering excitation of the  $4d^{10}5p^2P_{1/2,3/2}$  fine structure levels, it should be mentioned that there is also the  $4d^95s^2D_{5/2}$  state with an energy of 3.749 eV which is intermediate to these fine-structure doublet (with energies of 3.664 eV and 3.778 eV, respectively). One should expect that there must be some contribution from the excitation of this level in our measurements. However, since this excitation from the  $^2S$  ground level to the  $^2D$  state belongs to the electric quadrupole transition, we suppose that its contribution to the excitation cross sections of the resonance  $^2P$  states is negligible. Also, as we already reported in our previous paper [1], the DCS for the combined levels can be represented as a sum of DCSs for excitation of the individual levels.

#### 4. CONCLUSION

Electron impact excitation from the ground state of silver has been studied both experimentally and theoretically. Measurements have been performed at 10, 20, 40, 60, 80 and 100 eV electron energies and scattering angles from  $10^\circ$  to  $150^\circ$ . Calculations were also carried out for the same energies and scattering angles up to  $180^\circ$ . We conclude that good agreement is achieved between the present two sets of data especially at higher energies.

#### Acknowledgements

This work is supported by RS MESTD under the grant OI 171020 and it was conducted within the framework of the COST Action CM1301 (CELINA).

#### REFERENCES

- [1] S. D. Tošić, V. Pejčev, D. Šević, R. P. McEachran, A. D. Stauffer and B. P. Marinković, Nucl. Instr. Meth. B, 279, 53 (2012).
- [2] S. Milisavljević, M. S. Rabasović, D. Šević, V. Pejčev, D. M. Filipović, Lalita Sharma, Rajesh Srivastava, A. D. Stauffer and B. P. Marinković, Phys. Rev. A, 76, 022714 (2008).
- [3] S. D. Tošić, M. S. Rabasović, D. Šević, V. Pejčev, D. M. Filipović, Lalita Sharma, A. N. Tripathi, Rajesh Srivastava and B. P. Marinković, Phys. Rev. A, 77, 012725 (2008).
- [4] R. T. Brinkman and S. Trajmar, J. Phys. E, 14, 245 (1981).



*Ambasciata d' Italia  
Belgrado*

## **Serbia - Italia**

Italian - Serbian Cooperation on  
Science, Technology and Humanities

(Edited by P. R. Andjus and P. Battinelli)

November 16, 2015, University of Belgrade

ASSOCIAZIONE ITALIANI E SERBI  
SCIENZIATI E STUDIOSI || BELGRADO  
АСОЦИЈАЦИЈА ИТАЛИЈАНСКИХ И СРПСКИХ  
НАУЧНИКА И ИСТРАЖИВАЧА || БЕОГРАД

**AI<sub>S</sub>3**

**Scientific Committee:**

- Pavle Andjus – *University of Belgrade*  
Paolo Battinelli – *Italian Embassy*  
Miroslav Dramićanin – *Vinča Institute of Nuclear Sciences*  
Gradimir Milanović – *Serbian Academy of Sciences and Arts*  
Viktor Nedović – *Ministry of Education, Science and  
Technological Development*  
Ivanka Popović – *University of Belgrade*  
Snežana Smederac – *University of Novi Sad*  
Sanja Vraneš – *Institute Mihajlo Pupin*

ISBN 978-86-7522-048-0

*Printed by:*  
SIGRa star, Belgrade  
sigra.star@gmail.com

## CONTENTS

<b>PREFACE</b> .....	7
<b>OPENING SPEECH</b> .....	9
<b>H.E. Giuseppe Manzo, Ambassador of the Italian Republic</b> .....	9
<b>Section I</b>	
<b>Research Projects of Particular Relevance 2013 – 2015</b> .....	13
<i><b>Towards molecular and genomic markers in Amyotrophic Lateral Sclerosis</b></i> <i>Nadia D'Ambrosi, Camilla Bernardini, Mirko Baranzini, Claudia Donno, Stefan Stamenovic, Mina Peric, Danijela Bataveljic, Pavle Andjus, Fabrizio Michetti</i> .....	15
<i><b>FEEDNEEDS: trends in R&amp;D in the Italian and Serbian feed sectors</b></i> <i>Pinotti Luciano, Caprarulo Valentina, Ottoboni Matteo, Giromini Carlotta, Agazzi Alessandro, Rossi Luciana, Tretola Marco, Antonella Baldi, Giovanni Savoini, Čolović Radmilo, Đuragić Olivera, Vukmirović Đuro, Lević Jovanka</i> .....	21
<i><b>Heavy metals in soils and plants of Rome and Novi Sad urban areas</b></i> <i>Angelone M., Manojlovic M., Armiento G., Čabilovski R., Crovato C., De Cassan M., Massanisso P., Montereali M.R., Vidojević D.</i> .....	27
<i><b>A nanoscale insight in radiation damage</b></i> <i>Paola Bolognesi, Sanja Tosic, Bratislav Marinkovic, Lorenzo Avaldi</i> .....	33
<i><b>Liquid-crystal-tunable subwavelength optical resonators</b></i> <i>Dimitrios C. Zografopoulos, Goran Isić, Borislav Vasić, Radoš Gajić, Romeo Beccherelli</i> .....	39
<i><b>ROBust Decentralised Estimation fOr large-scale systems (RODEO)</b></i> <i>Gianluca Fadda, Mauro Franceschelli, Alessandro Pilloni, Alessandro Pisano, Elio Usai, Željko Đurovic, Aleksandra Marjanović, Veljko Papić, Predrag Tadić, Sanja Vujnović</i> .....	45
<i><b>Development and implementation of two novel portable instruments for the analyses of Cultural Heritage: portable scanner XRF and portable XRD</b></i> <i>Stefano Ridolfi, Maja Gajic Kvascev, Velibor Andric, Daniela Korolija Crkvenjakov, Milica Maric Stojanovic, Susanna Crescenzi, Ilaria Carocci, Fabio De Chirico, Giovanni Ettore Gigante</i> .....	51
<b>Section II</b>	
<b>Research Projects for Exchange of Researchers 2013 – 2015</b> .....	59
<i><b>Cell cycle aberrations and oxidative stress in age related neurodegenerative diseases: The role of food antioxidants</b></i> <i>Francesca Giampieri, Luca Mazzoni, Massimiliano Gasparrini, Tamara-Yuliett Forbes-Hernandez, Sadia Afrin, Andrea Cabarkapa, Lada Zivkovic, Vladan Bajic, Dragana Dekanski, Biljana Spremo-Potparevic, Maurizio Battino</i> .....	61

## A nanoscale insight in radiation damage

Paola Bolognesi<sup>1</sup>, Sanja Tosic<sup>2</sup>, Bratislav Marinkovic<sup>2</sup> and Lorenzo Avaldi<sup>1</sup>

<sup>1</sup> CNR-Istituto di Struttura della Materia, Area della Ricerca di Roma 1, Italia,  
paola.bolognesi@cnr.it & lorenzo.avaldi@ism.cnr.it

<sup>2</sup> Institute of Physics, Belgrade, Serbia, seka@ipb.ac.rs & bratislav.marinkovic@ipb.ac.rs

### INTRODUCTION

The understanding that the macroscopic damage can be tracked down to a microscopic scale, where the initial processes involving the elementary constituents are the same as those studied in molecular physics and photochemistry, has been a key development in the study of radiation damage (Garcia and Fuss 2012). The advent of new radiation sources and novel instrumentation with the capability of imaging atoms and molecules disclose the possibility to determine how matter functions during chemical reactions and physical and biological processes.

One of the aims of the major importance project Italy-Serbia “Nanoscale insights in radiation damage” is to study basic processes in benchmark molecules of biological interest exploiting the potentiality of new instrumentation. In this paper the study of two test cases are reported. In the first one the tunability and intensity of the synchrotron radiation of Elettra (Trieste) in combination with high selective electron-ion coincidence techniques has been used to study the fragmentation of 2Br-pyrimidine, while in the second one angular resolved electron scattering experiments on alanine are reported. Pyrimidine is one of the building blocks of DNA bases and its halogenated derivatives represent prototype molecules of radiosensitizing compounds, given to patients who undergo radiotherapy treatments. Alanine is one of twenty standard aminoacids encoded by the human genetic code. The investigation of electron interaction with the main constituents of proteins, like the aminoacids, provide valuable information on the processes leading to radiation damage of a living cell.

### 2Br-PYRIMIDINE FRAGMENTATION

The experiments have been performed at the GasPhase photoemission beamline of the Elettra synchrotron radiation facility, Trieste (Italy), which provides radiation from 13.6 to above 1000 eV (Blyth et al. 1999). The end station is equipped with a hemispherical electron energy analyzer (VG 220i) and a Wiley-McLaren Time of Flight (TOF) mass spectrometer mounted opposite to each other. The electron and ion mass analysers can be operated independently, for photoemission (PES) and mass spectroscopy measurements, respectively, as well as simultaneously for electron-ion coincidence experiments.

We have studied the fragmentation of 2Br- pyrimidine following direct valence shell photoionization as well as C and N 1s inner shell excitations (Bolognesi et al. 2015).



The C and N atoms in the 2Br- pyrimidine ring structure are chemically different and the Br atom, with its strong electronegativity, affects the electron cloud distribution. In the case of valence ionization the detection of the fragment ions in coincidence with energy selected photoelectrons, i.e. photoelectron-photoion coincidence experiments (PEPICO), allows a state selected study on the fragmentation of different cation states. In the case of inner shell excitation the fragment ions are detected in coincidence with the resonant Auger electrons, the non-radiative decay that populates the same final cation states as in direct valence photoionization. The advantage of these latter experiments is that due to the inner shell absorption the selectivity on the atomic site of the initial energy deposition is added, too.

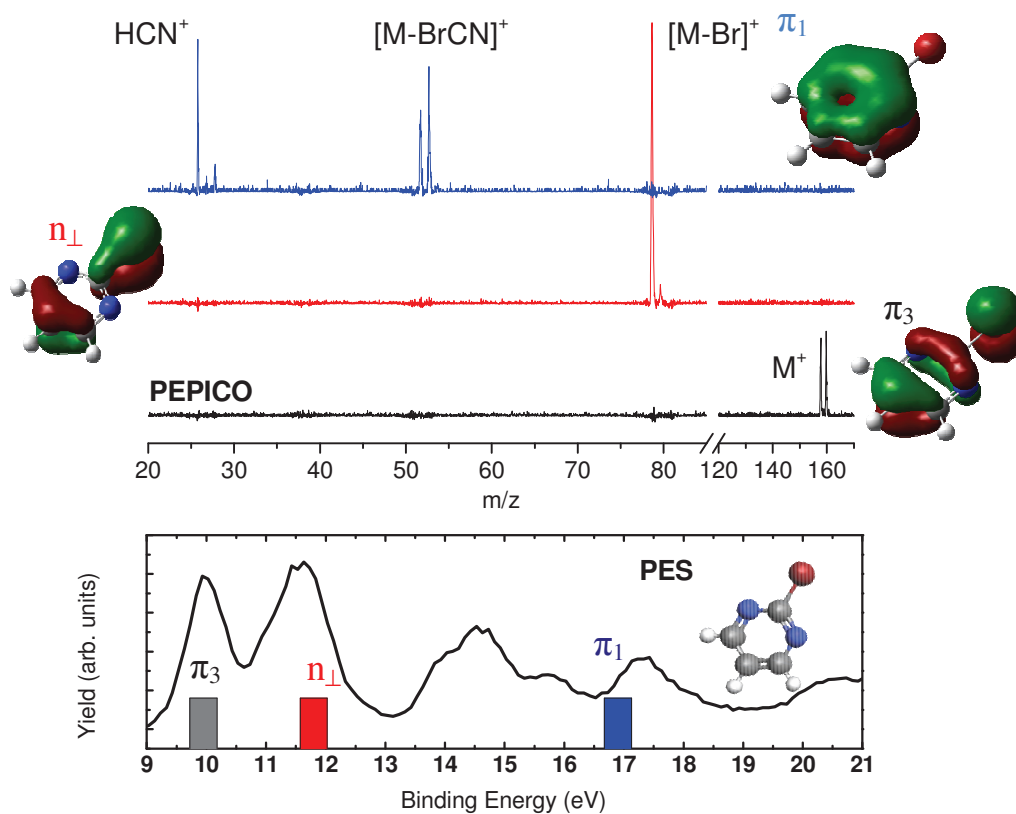


Fig.1 PES spectrum of 2Br-pyrimidine at  $h\nu=100$  eV (bottom panel). PEPICO spectra, i.e. mass spectra where the photoelectron kinetic energy selects the ionization of the  $\pi_3$ ,  $n_{\perp}$  and  $\pi_1$  valence orbitals (top panel).

Fig.1 clearly shows that the type of fragmentation is strongly dependent on the ionic state populated. For example, the loss of the Br atom occurs preferentially after the ionization of the  $n_{\perp}$  orbital, while the break of the ring is favoured by the ionization of the  $\pi_1$  orbital. This means that a preferential bond breaking and the production of a certain fragment is ruled by the charge distribution and nuclear rearrangement of a particular cation state. Similar results are observed (Bolognesi et al. 2015) when the same cation state is populated via inner shell excitation and the following resonant Auger process. This can be rationalized by the fact that the Auger decay occurs on a time scale much faster than nuclear rearrangement. In summary these results show that, similar to the pyrimidine case (Bolognesi et al. 2012) the fragmentation patterns of the 2Br-pyrimidine display a strong selectivity on the final ion states populated by direct valence ionization or inner shell excitation/decay. The chemical and site sensitivity in the initial energy deposition affects only the relative intensity of the different fragmentation channels.

## ELECTRON SCATTERING ON ALANINE

The electron scattering experiments have been performed with the modified electron spectrometer previously used for metal vapours (ESMA – Electron Spectrometer for Metal Atoms) (Marinković et al 2008) at the Institute of Physics in Belgrade. The apparatus consists of a fixed hemispherical monochromator and a rotatable analyzer of the same size, electrostatic lenses, a single electron channeltron as a detector. An oven is used as a source of an effusive beam of sublimated alanine molecules. The powder sample of 99% purity of DL-Alanine was heated to 460 K, a temperature where no decomposition was observed. The molecular beam was crossed perpendicularly by the mono-energetic electron beam and the scattered electrons were detected in the angular range from 0° to 150°.

In the experiments both electron energy loss spectra and electron elastic scattering differential cross sections (DCS) of alanine at incident energies from 20 to 80 eV have been measured. In the case of the differential cross sections the measurements extended from 10° to 150°. In Fig.2 the energy loss spectrum measured at 80 eV incident energy and 2° scattering angle is reported. The spectrum in the region below the ionization threshold of the molecule at about 9.6 eV, shows some features which correspond to the excitation of a bound electron to  $\pi^*$  or  $\sigma^*$  empty orbitals which involve the CO bond in the carboxylic group or the CH bonds, respectively. The DCSs for elastic scattering have been measured on the absolute scale and span from two decades at 20 eV to three decades at 80 eV. All of them are peaked in the forward direction and display a minimum at approximately 100° scattering angle. The full set of recorded data have been deposited within the BEAMDB (Belgrade Electron Atom/Molecule DataBase (Marinković et al 2015). The BEAMDB is a part of the RADAM (Radiation Damage) portal that contains several data bases covering specific interactions of photons, electron/positrons and ions with biomolecules as well as multiscale and radiobiological phenomena (Denifl et al, 2013).

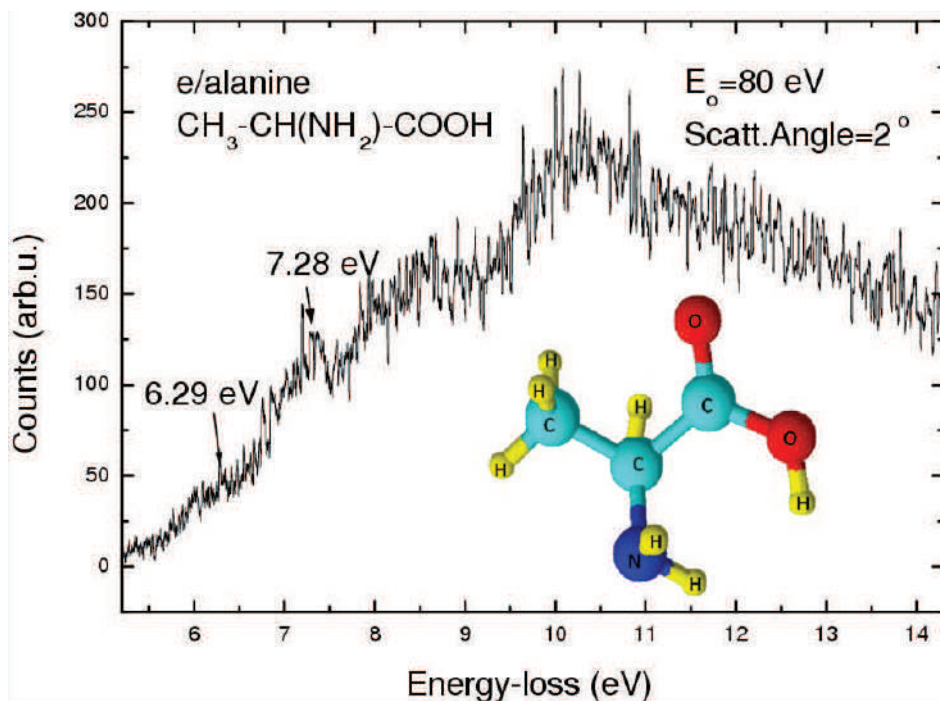


Fig. 2. An energy loss spectrum of 80 eV electrons scattered at the angle of  $2^\circ$  from alanine,  $\text{CH}_3\text{-CH(NH}_2\text{)-COOH}$ , molecule.

## CONCLUSIONS

As far as the relative biological effectiveness of soft X-ray absorption in cells is concerned, the results in 2Br-pyrimidine indicate that depending on the ionized orbital the radiation can induce a direct damage (break of the ring) or an indirect one releasing a radical (e.g. Br atom) that then can generate secondary damage.

In the interaction of photons or hadrons with cells electrons with a large spread of energies are produced as the result of the ionization of the medium. These secondary electrons are the key agents in any therapeutic process. The knowledge of their scattering cross section and how they deposit energy in the basic constituents of the cells is fundamental to develop proper Monte Carlo simulations aiming to determine necessary doses in radiation treatments. The measurements in alanine shown here as well in the other *molecules of life* contribute to the development of reliable database for these simulations.

## Acknowledgements

Work partially supported by the Serbia – Italy Joint Research Project “Nanoscale Insight in the Radiation Damage” and MESTD project OI#171020. The support of the COST Actions nano-IBCT and XLIC via the STSM scheme is acknowledged.

## Reference

- Blyth R. R. et al. (1999) The high resolution Gas Phase Photoemission Beamline at Elettra, *J. Electron Spect. Rel. Phenom.*, 101-103, 959-964
- Bolognesi P., Kettunen A., Cartoni A., Richter R., Tosic S., Maclot., Rousseau P., Delaunay R. and Avaldi L. (2015) Site- and state- selected photofragmentation of 2Br-pyrimidine. *Phys. Chem. Chem. Phys.*, 17 (37), 24063-9
- Bolognesi P., O’Keffee P. and Avaldi L., Chapter X in Garcia Gomez-Tejedor G. and Fuss M.C. (2012). Radiation Damage in Biomolecular Systems”, Springer, 2012
- S Denifl, G Garcia, B A Huber, B P Marinković, N Mason, J Postler, H Rabus, G Rixon, A V Solov’ov, E Surraud, and A V Yakubovich, (2013) Radiation damage of biomolecules (RADAM) database development: current status, *J. Phys. Conf. Ser.* **438** 012016
- Garcia Gomez-Tejedor G. and Fuss M.C. (2012). Radiation Damage in Biomolecular Systems”, Springer, 2012
- Marinković B. P., Blanco F., Šević D., Pejčev V., García G., Filipović D. M., Pavlović D., and Mason N. J., (2008) Elastic scattering of electrons from alanine, *Int. J. Mass Spectrom.* **277** 300 – 304.
- Marinković B. P., Vujčić V., Sushko G., Vudragović D., Marinković D. B., Đorđević S., Ivanović S., Nešić M., Jevremović D., V Solov’ov A. and Mason N. J., (2015) Development of Collisional Data Base for Elementary Processes of Electron Scattering by Atoms and Molecules, *Nucl.Instrum. Meth. B* **354**, 90-95.

# **III Meeting on Astrophysical Spectroscopy - A&M DATA**

December 6 to 9, 2021, Palić, Serbia

## **BOOK OF ABSTRACTS AND CONTRIBUTED PAPERS**

**Edited by Vladimir A. Srećković, Milan S. Dimitrijević and  
Nikola Cvetanović**

# **A&M DATA**



UNIVERSITY OF BELGRADE | BELGRADE  
INSTITUTE OF PHYSICS | BELGRADE  
NATIONAL INSTITUTE OF  
THE REPUBLIC OF SERBIA

Belgrade 2021



## **Scientific Committee**

Milan S. Dimitrijević, **Co-Chairman**  
Vladimir A. Srećković, **Co-Chairman**

Nebil Ben Nessib, Saudi Arabia  
Nikolai N. Bezuglov, Russia  
Vesna Borka Jovanović, Serbia  
Magdalena Christova, Bulgaria  
Nikola Cvetanović, Serbia  
Rafik Hamdi, Tunisia  
Dragana Ilić, Serbia  
Darko Jevremović, Serbia  
Predrag Jovanović, Serbia  
Andjelka Kovačević, Serbia  
Jelena Kovačević, Serbia  
Evaggelia Lyratzi, Greece  
Bratislav Marinković, Serbia  
Zoran Mijić, Serbia  
Luka Č. Popović, Serbia  
Branko Predojević, Republic of Srpska  
Sylvie Sahal Bréchet, France  
Saša Simić, Serbia

## **Local Organizing Committee**

Vladimir A. Srećković, Institute of Physics, Belgrade, **Chairman**  
Jovan Aleksić, Astronomical Observatory, Belgrade  
Nikola Cvetanović, Faculty of Transport and Traffic Engineering, Belgrade  
Milan S. Dimitrijević, Astronomical Observatory, Belgrade  
Aleksandra Kolarski, Institute of Physics, Belgrade  
Aleksandra Nina, Institute of Physics, Belgrade  
Nikola Veselinović, Institute of Physics, Belgrade  
Veljko Vujčić, Astronomical Observatory, Belgrade

## **Organizers:**

Institute of Physics Belgrade, Serbia and  
Astronomical Observatory Belgrade, Serbia

Text arrangement by computer: Tanja Milovanov

ISBN 978-86-82441-54-0

Published and copyright © by Institute of Physics Belgrade, Pregrevica 118,  
11080 Belgrade Serbia

Financially supported by the Ministry of Education, Science and Technological  
Development of Serbia

---

Production: Skripta Internacional, Mike Alasa 54, Beograd in 50 copies

## Electron-metal atom vapor cross sections maintained within BEAM database

**B. P. Marinković<sup>1\*</sup>, D. Šević<sup>1</sup>, S. Ivanović<sup>1</sup>, N. Uskoković<sup>1</sup>, S. D. Tošić<sup>1</sup>,  
M. S. Rabasović<sup>1</sup> and B. Predojević<sup>2</sup>**

<sup>1</sup>*Institute of Physics Belgrade, University of Belgrade, Pregrevica 118,  
11080 Belgrade, Serbia*

<sup>\*</sup>*E-mail: bratislav.marinkovic@ipb.ac.rs*

<sup>2</sup>*Faculty of Science, University of Banja Luka, Mladena Stojanovića 2,  
78000 Banja Luka, Republic of Srpska, Bosnia and Herzegovina*

Belgrade Electron-Atom/Molecule (BEAM) database [<http://servo.aob.rs/emol>] has been created in order to curate cross sections for electron interactions with atomic and molecular particles and with the aim to be a part (node) of other portals, as well as to fulfil a broader task of maintaining A/M data in a comprehensive way. It became an integral part of two portals: RADAM (Radiation Damage) database [1] and VAMDC (Virtual Atomic and Molecular data Centre) [2,3]. A significant number of entries within BEAM belongs to electron cross sections for metal vapor atoms. Elastic cross sections (Mg, Hg, Ag, Yt, Bi, Rb, Pb, Sb, Cd) and excitation cross sections (Mg, Hg, Ag, Yt, Na, Ca, Bi) have been compiled from the published refereed sources. Data entries within BEAM follow IAEA classification scheme for processes [4] and use their standards for labelling of atomic states according Pyvalem as a Python package [5].

### References

- [1] S. Denifl, *et al.*, J. Phys. Conf. Ser. 438 012016 (2013).
- [2] M. L. Dubernet, *et al.*, J. Phys. B 49, 074003 (2016).
- [3] D. Albert, *et al.*, Atoms 8(4), 76 (2020).
- [4] C. Hill, *et al.*, INDC(NDS) Publication 0812, (IAEA- International Atomic Energy Agency - Nuclear Data Section, Vienna International Centre, 2020) <https://nds.iaea.org/publications/indc/indc-nds-0812/>
- [5] <https://pypi.org/project/pyvalem/> (accessed on 25.11.2021).

## Excitation of silver atoms from the ground S state to the first excited P state by electron impact

S. D. Tošić\*, D. Šević and B. P. Marinković

*Institute of Physics Belgrade, University of Belgrade, Pregrevica 118, 11080  
Belgrade, Serbia*

*\*E-mail: seka@ipb.ac.rs*

Silver is extensively employed in various scientific, technological and practical applications [1-3]. In our previous papers we reported results (differential DCSs and integrated ICSs cross sections) of combined experimental and theoretical study of excitation of the silver atom from the ground  $4d^{10}5s^2S$  state to the first combined resonant  $4d^{10}5p^2P_{1/2,3/2}$  state (fine-structure doublet with total angular momenta of  $J = 1/2$  and  $3/2$  and energies of 3.664 and 3.778 eV, respectively) [4, 5]. Recently, we published results for electron impact excitation of the  $4d^95s^2D_{3/2}$  (4.304 eV) and  $4d^{10}6s^2S_{1/2}$  (5.276 eV) states [6]. Since McNamara *et al.* in their relativistic convergent close coupling (RCCC) computation [7] raised queries about the validity of our DCSs for resonant excitation, we have reanalyzed the earlier experimental DCS data. We have found that DCSs at 20 and 40 eV need to be renormalized due to incorrectly splicing our very forward-angular distributions onto our middle and backward-angular distributions. The new appropriate renormalization factor were applied and here we present new experimental DCSs results and the comparison with calculated relativistic distorted wave (RDW) and nonrelativistic atomic optical potential model data.

### References

- [1] V. A. Dzuba, S. O. Allehabi, V. V. Flambaum, J. Li and S. Schiller, *Phys. Rev. A* 103, 022822 (2021).
- [2] T. Badr, M. D. Plimmer, P. Juncar, M. E. Himbert, Y. Louyer and D. J. E. Knight, *Phys. Rev. A* 74, 062509 (2006).
- [3] D. Kasen, B. Metzger, J. Barnes, E. Quataert and E. Ramirez-Ruiz, *Nature (London)* 551, 80 (2017).
- [4] S. D. Tošić, V. Pejčev, D. Šević, R.P. McEachran, A.D. Stauffer and B.P. Marinković, *Nucl. Instrum. Methods B* 279, 53 (2012).
- [5] S. D. Tošić, V. Pejčev, D. Šević, R. P. McEachran, A. D. Stauffer and B. P. Marinković, *Phys. Rev. A* 91, 052703 (2015).
- [6] , B. P. Marinković, S. D. Tošić, D. Šević, R. P. McEachran, F. Blanco, G. García and M. J. Brunger, *Phys. Rev. A* 104, 022808 (2021).
- [7] K. McNamara, D. V. Fursa and I. Bray, *J. Phys. B* 51, 085203 (2018).

## Integrated cross sections for electron impact excitation of atomic silver

S. D. Tošić\*, D. Šević and B. P. Marinković

Institute of Physics Belgrade, University of Belgrade, Pregrevica 118, 11080  
Belgrade, Serbia

\*E-mail: seka@ipb.ac.rs

Here we present integrated (integral  $Q_i$ , momentum transfer  $Q_M$ , and viscosity  $Q_V$ ) cross sections (ICSs) for electron-impact excitation of the  $(4d^{10}5s) \ ^2S_{1/2} \rightarrow (4d^{10}5p) \ ^2P_{1/2,3/2}$ ,  $(4d^{10}5s) \ ^2S_{1/2} \rightarrow (4d^95s^2) \ ^2D_{3/2}$  and  $(4d^{10}5s) \ ^2S_{1/2} \rightarrow (4d^{10}6s) \ ^2S_{1/2}$  transitions in atomic silver at impact energies  $E_0$  from 10 to 100 eV.

ICSs for all states were derived from the corresponding differential cross sections DCSs at each  $E_0$ . We extrapolated our experimental DCSs to  $0^\circ$  (using the measured results at small scattering angles for resonant transition [1] and corresponding theory for other two states [2]) and  $180^\circ$  (using the RDW calculations for the given energy [2,3]), performed an interpolation, and then undertake the appropriate integration. The new renormalized experimental DCSs for resonant excitation at 20eV and 40 eV were used (see abstract Excitation of silver atoms from the ground S state to the first excited P state by electron impact by S. D. Tošić *et al.*).

### References

- [1] S. D. Tošić, V. Pejčev, D. Šević, R.P. McEachran, A.D. Stauffer and B.P. Marinković, Nucl. Instrum. Methods B 279, 53 (2012).
- [2] B. P. Marinković, S. D. Tošić, D. Šević, R. P. McEachran, F. Blanco, G. García and M. J. Brunger, Phys. Rev. A 104, 022808 (2021).
- [3] S. D. Tošić, V. Pejčev, D. Šević, R. P. McEachran, A. D. Stauffer and B. P. Marinković, Phys. Rev. A 91, 052703 (2015).

## **Investigation and modeling of the free-electron density and temperature during the formation of laser-induced breakdown of plasma in air at various laser parameters**

**H. Delibašić Marković<sup>1</sup>, V. Petrović<sup>1</sup>, I. Petrović<sup>2</sup> and S. Tošić<sup>3</sup>**

*<sup>1</sup>Faculty of Science, University of Kragujevac, Serbia*

*<sup>2</sup>Academy of Professional Studies Šumadija, Department in Kragujevac, Serbia*

*<sup>3</sup>Institute of Physics Belgrade, University of Belgrade, Belgrade, Serbia*

The free-electron density equation and two temperature coupled equations during laser-induced ablation of air at atmospheric pressure are solved. In doing so, calculations were carried out to determine the comparative contribution of the mechanisms responsible for electron gain and losses in LIB of air. The solutions are initially obtained for the energy sources with a Gaussian distribution to describe the contribution of different pulse-width regimes. More general results provided in this study maintain the appealing aspects of other approximate solutions and reduce them under the respective conditions. Obtained results agree well with the numerical and experimental observations reported in the literature.



**TWENTY-FIRST INTERNATIONAL SUMMER SCHOOL ON  
VACUUM, ELECTRON AND ION TECHNOLOGIES**

**VEIT 2019**

**23 - 27 September 2019  
SOZOPOL, BULGARIA**

**PROGRAM  
ABSTRACTS**

**Editors: M. Dimitrova, Ch. Ghelev and E. Vasileva**

ORGANIZED BY

**INSTITUTE OF ELECTRONICS**  
BULGARIAN ACADEMY OF SCIENCES, SOFIA, BULGARIA

**DUTCH INSTITUTE FOR FUNDAMENTAL ENERGY RESEARCH**  
EINDHOVEN, THE NETHERLANDS

CO-FINANCED by the  
MINISTRY OF EDUCATION AND SCIENCE, BULGARIAN  
SCIENCE FUND, Project № KP-06-MNF/21/16.07.2019



**CHAIRS OF THE SCHOOL**

**M. Dimitrova,**

Institute of Electronics, Bulgarian Academy of Sciences, Sofia, Bulgaria

**M.C.M. van de Sanden,**

Dutch Institute for Fundamental Energy Research, Eindhoven, The Netherlands

**INTERNATIONAL ADVISORY COMMITTEE**

<b>N. Guerassimov</b>	Bulgarian Academy of Sciences, Sofia, Bulgaria
<b>M. Dimitrova</b>	Czech Academy of Sciences, Prague, Czech Republic
<b>R. Panek</b>	Czech Academy of Sciences, Prague, Czech Republic
<b>Th. Czerwiec</b>	Institut Jean Lamour (IJL), Ecole des Mines de Nancy, Nancy, France
<b>W. Möller</b>	Forschungszentrum Dresden-Rossendorf, Dresden, Germany
<b>B. Rauschenbach</b>	IOM and Leipzig University, Leipzig, Germany
<b>H. Kersten</b>	IEAP University of Kiel, Kiel, Germany
<b>D. Mataras</b>	University of Patras, Patras, Greece
<b>V. Guerra</b>	Instituto Superior Técnico, Lisboa, Portugal
<b>G. Dinescu</b>	National Institute for Laser, Plasma and Radiation Physics, Magurele Bucharest, Romania
<b>Z. Petrovic</b>	Institute of Physics, Belgrade, Serbia
<b>M. Mozetic</b>	"Jozef Stefan" Institute, Ljubljana, Slovenia
<b>K. Larsson</b>	Uppsala University, Uppsala, Sweden
<b>I. Katardjiev</b>	Uppsala University, Uppsala, Sweden
<b>M.C.M. (Richard) van de Sanden</b>	Dutch Institute for Fundamental Energy Research (DIFFER), Eindhoven, The Netherlands
<b>M. Ürgen</b>	Istanbul Technical University, Istanbul, Turkey
<b>A. Ehiasarian</b>	Sheffield Hallam University, Sheffield, UK
<b>I. Petrov</b>	University of Illinois, Urbana, IL, USA

**LOCAL ORGANIZING COMMITTEE**

**Ch. Angelov, M. Dimitrova (Chair), Ch. Ghelev, P. Ivanova, E. Taskova, E. Vasileva**

**MAIN SCIENTIFIC TOPICS:**

- **THIN FILMS DEPOSITION**
- **SURFACES AND THIN FILMS PROCESSING AND ANALYSIS**
- **COATINGS FOR ADVANCED APPLICATIONS**
- **PLASMA-SURFACE INTERACTION AND PLASMA DIAGNOSTICS**
- **MODELING AND COMPUTER SIMULATION**

**PLENARY AND POSTER SESSIONS:**

**A: PLASMA-SURFACE INTERACTION AND PLASMA DIAGNOSTICS.  
MODELING AND COMPUTER SIMULATION**

**B: THIN FILMS DEPOSITION.  
COATINGS FOR ADVANCED APPLICATIONS**

**C: SURFACES AND THIN FILMS PROCESSING AND ANALYSIS**

**ABBREVIATIONS:**

**TL – TOPIC LECTURE  
PR – PROGRESS REPORT  
OP – ORAL PRESENTATION  
PA – POSTER SESSION A  
PB – POSTER SESSION B  
PC – POSTER SESSION C**

**PC-14****PHOTO-INDUCED FRAGMENTATION OF THE TITANIUM (IV) ISO-PROPOXIDE MOLECULE**

S.D. Tošić<sup>1</sup>, M. Radibratović<sup>2</sup>, J. Chiarinelli<sup>3, 4</sup>, M. Milčić<sup>5</sup>, P. Bolognesi<sup>4</sup>, L. Avaldi<sup>4</sup>,  
R. Richter<sup>6</sup>, M. Coreno<sup>4,6</sup> and B.P. Marinković<sup>1</sup>

<sup>1</sup>Institute of Physics Belgrade, University of Belgrade, Pregrevica 118, 11080 Belgrade, Serbia

<sup>2</sup>Institute of Chemistry, Technology and Metallurgy – Center for Chemistry,  
University of Belgrade, Njegoševa 12, 11000 Belgrade, Serbia

<sup>3</sup>Dipartimento di Scienze, Università di Roma Tre, Rome, Italy

<sup>4</sup>Istituto di Struttura della Materia (CNR-ISM), Area della Ricerca di Roma 1,  
Monterotondo Scalo, Italy

<sup>5</sup>Faculty of Chemistry, University of Belgrade, Studentski trg 16, Belgrade, Serbia

<sup>6</sup>Elettra-Sincrotrone Trieste, Area Science Park, I-34012 Basovizza, Trieste, Italy

Emerging techniques in nanoscience and nanotechnologies have become an essential tool in various disciplines. As a result, major improvements in the production new nanomaterials with specific physical and chemical properties have been achieved using different physical and chemical methods. Many of these methods lead to the deposition of arbitrarily shaped metallic, semiconducting or insulating nano-structures. It is known that the TiO<sub>2</sub> nanoparticles have good electrical, optical and magnetic properties and have found applications in optoelectronic devices, sensors, alloy materials, solar cells, and self-cleaning surfaces [1]. We present both experimental and theoretical results related to the photo-induced fragmentation of the core-excited titanium (IV) iso-propoxide Ti[OCH(CH<sub>3</sub>)<sub>2</sub>]<sub>4</sub> molecule, which is an organometallic precursor used for deposition of nano-sized TiO<sub>2</sub> films [2, 3]. The experiments were performed at the gas-phase photoemission beamline of the Elettra synchrotron radiation source (Trieste, Italy) [4-7]. Computational spectroscopy and extensive molecular dynamics (MD) simulations were used to investigate and characterize the main fragmentation channels observed in the mass spectra measured.

**Acknowledgments:** The work was partially supported by the MAECI Serbia–Italy Joint Research Project “A nanoview of radiation-biomatter interaction” and the MESTDRS (OI 171020, OI 172065).

[1] J. Bogdan *et al.* *Nanoscale Research Letters* (2015) 10:57, DOI 10.1186/s11671-015-0753-2.

[2] A. Sandell *et al.* *J. Appl. Phys.*, **92** 3381 (2002).

[3] A. Čenovar *et al.* *Advances in Natural Science: Theory & Applications*, **1** 133 (2012).

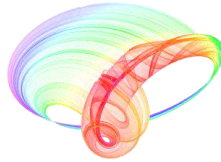
[4] J. Chiarinelli *et al.* *Frontiers in Chemistry*, **7** 329 (2019).

[5] P. Bolognesi *et al.* *Frontiers in Chemistry*, **7** 151 (2019).

[6] P. Bolognesi *et al.* *J. Chem. Phys.*, **145** 191102 (2016).

[7] P. Bolognesi *et al.* *Phys. Chem. Chem. Phys.*, **17** 24063 (2015).

# Book of abstracts



## PHOTONICA2019

The Seventh International School and Conference on  
Photonics, 26 August – 30 August 2019, Belgrade, Serbia

& Machine Learning with Photonics Symposium  
(ML-Photonica 2019)



& ESUO Regional Workshop



& COST action CA16221



Editors: Milica Matijević, Marko Krstić and Petra Beličev

Belgrade, 2019



ABSTRACTS OF TUTORIAL, KEYNOTE, INVITED LECTURES,  
PROGRESS REPORTS AND CONTRIBUTED PAPERS

of

The Seventh International School and Conference on Photonics  
PHOTONICA2019, 26 August – 30 August 2019, Belgrade, Serbia

and

Machine Learning with Photonics Symposium

and

ESUO Regional Workshop

Editors

Milica Matijević, Marko Krstić and Petra Beličev

Technical Assistance

Danka Stojanović and Goran Gligorić

Publisher

Vinča Institute of Nuclear Sciences

Mike Petrovića Alasa 12-14, P.O. Box 522

11000 Belgrade, Serbia

Printed by

Serbian Academy of Sciences and Arts

Number of copies

300

ISBN 978-86-7306-153-5

## Inner-shell spectroscopy of titanium (IV) iso-propoxide

S. D. Tošić<sup>1</sup>, M. Radibratović<sup>2</sup>, J. Chiarinelli<sup>3, 4</sup>, M. Milčić<sup>5</sup>, P. Bolognesi<sup>4</sup>, L. Avaldi<sup>4</sup>,  
R. Richter<sup>6</sup>, M. Coreno<sup>4, 6</sup> and B. P. Marinković<sup>1</sup>

<sup>1</sup> *Institute of Physics Belgrade, University of Belgrade, Pregrevica 118, 11080 Belgrade, Serbia*

<sup>2</sup> *Institute of Chemistry, Technology and Metallurgy – Center for Chemistry,  
University of Belgrade, Njegoševa 12, 11000 Belgrade, Serbia*

<sup>3</sup> *Dipartimento di Scienze, Università di Roma Tre, Rome, Italy*

<sup>4</sup> *Istituto di Struttura della Materia (CNR-ISM), Area della Ricerca di Roma 1, Monterotondo Scalo, Italy*

<sup>5</sup> *University of Belgrade, Faculty of Chemistry, Studentski trg 16, Belgrade, Serbia*

<sup>6</sup> *Elettra-Sincrotrone Trieste, Area Science Park, I-34012 Basovizza, Trieste*

e-mail: marinkov@ipb.ac.rs

The quality and properties of synthesized nano structure strongly depend on several factors, like the choice of substrate and the appropriate precursors as well as the optimal conditions for substrate-precursor reaction. For deposits such as TiO<sub>2</sub> these factors become particularly important because directly affect properties such as magnetism and conductivity [1].

In the view of the intense activity related to synthesis of nanomaterials based on TiO<sub>2</sub>, we investigated inner-shell ionization and excitation in the titanium (IV) iso-propoxide Ti[OCH(CH<sub>3</sub>)<sub>2</sub>]<sub>4</sub> molecule, which, due to its structure and chemical characteristics is considered as an efficient precursor for deposition of TiO<sub>2</sub> thin films. Complementary experimental techniques (XPS, NEXAFS, mass spectrometry) as well as extensive molecular dynamics (MD) simulations have been used to investigate the photo induced fragmentation of Ti[OCH(CH<sub>3</sub>)<sub>2</sub>]<sub>4</sub>. The experiments have been performed at the Gas Phase photoemission beamline of the Elettra synchrotron radiation source (Trieste, Italy) [2, 3].

ACKNOWLEDGMENT: Work partially supported by the MAECI Serbia–Italy Joint Research Project “A nanoview of radiation-biomatter interaction” and the MESTDRS (OI 171020, OI 172065).

### REFERENCES

- [1] A. Botman et al., *Nanotechnology* 20, 372001 (2009).
- [2] J. Chiarinelli et al., *Frontiers in Chemistry* 7, 329 (2019).
- [3] P. Bolognesi et al., *Frontiers in Chemistry* 7, 151 (2019).



# 29<sup>th</sup> Summer School and International Symposium on the Physics of Ionized Gases

Aug. 28 - Sep. 1, 2018, Belgrade, Serbia

## CONTRIBUTED PAPERS &

ABSTRACTS OF INVITED LECTURES,  
TOPICAL INVITED LECTURES, PROGRESS REPORTS  
AND WORKSHOP LECTURES

Editors:

Goran Poparić, Bratislav Obradović,  
Duško Borka and Milan Rajković



Vinča Institute of  
Nuclear Sciences



Serbian Academy  
of Sciences and Arts

**29<sup>th</sup> Summer School and International  
Symposium on the Physics of Ionized  
Gases**

**S P I G 2018**

**CONTRIBUTED PAPERS**

**&**

**ABSTRACTS OF INVITED LECTURES,  
TOPICAL INVITED LECTURES, PROGRESS REPORTS  
AND WORKSHOP LECTURES**

*Editors*

**Goran Poparić, Bratislav Obradović,  
Duško Borka and Milan Rajković**

**Vinča Institute of  
Nuclear Sciences**

**Serbian Academy  
of Sciences and Arts**

**Belgrade, 2018**

CONTRIBUTED PAPERS & ABSTRACTS OF INVITED  
LECTURES, TOPICAL INVITED LECTURES, PROGRESS  
REPORTS AND WORKSHOP LECTURES

of the 29<sup>th</sup> Summer School and International Symposium on  
the Physics of Ionized Gases

August 28 – September 1, 2018, Belgrade, Serbia

*Editors:*

Goran Poparić, Bratislav Obradović,  
Duško Borka and Milan Rajković

*Publisher:*

Vinča Institute of Nuclear Sciences,  
University of Belgrade,  
P.O. Box 522,  
11001 Belgrade, Serbia

*Computer processing:*

Tatjana Milovanov

*Printed by*

Skripta Internacional, Mike Alasa 54, Beograd

***Number of copies***

200

ISBN 978-86-7306-146-7

© 2018 by Vinča Institute of Nuclear Sciences, University of Belgrade  
All rights reserved. No part of this book may be reproduced, stored or  
transmitted in any manner without the written permission of the Publisher.



# COMPUTATIONAL TOOLS FOR STUDYING X-RAY – MOLECULE INTERACTIONS: PHOTOFRAGMENTATION OF HALOTHANE

M. Radibratović<sup>1</sup>, S. D. Tošić<sup>2</sup>, M.C. Castrovilli<sup>3</sup>, J. Chiarinelli<sup>3,6</sup>, P. Bolognesi<sup>3</sup>,  
L. Avaldi<sup>3</sup>, R. Richter<sup>4</sup>, M. Coreno<sup>3,4</sup>, B. P. Marinković<sup>2</sup> and M. K. Milčić<sup>5</sup>

<sup>1</sup>*ICTM – Center for Chemistry, UB, Njegoševa 12, 11000 Belgrade, Serbia*

<sup>2</sup>*Institute of Physics Belgrade, UB, Pregrevica 118, 11080 Belgrade, Serbia*

<sup>3</sup>*Istituto di Struttura della Materia-CNR (ISM-CNR), Area della Ricerca  
di Roma 1, Monterotondo Scalo, Italy*

<sup>4</sup>*Elettra-Sincrotrone Trieste, Area Science Park, Basovizza, Trieste, Italy*

<sup>5</sup>*UB, Faculty of Chemistry, Studentski trg 12-16, Belgrade, Serbia*

<sup>6</sup>*Università degli Studi RomaTre, Roma, Italy*

Halothane (C<sub>2</sub>HBrClF<sub>3</sub>), one of the most commonly used halogenated anesthetics, play a significant role in the destruction of the earth's ozone layer [1]. Photofragmentation experiments in the VUV and soft X-ray energy regions performed at Elettra synchrotron have shown that the mass spectra of halothane is dominated by lighter mass fragments. To explain the experimental findings extensive computational studies were conducted. Low level, but fast and accurate self-consistent charge density-functional tight-binding (SCC-DFTB) theoretical method was employed to simulate the fragmentation of singly and doubly charged halothane ions from their ground state electron configurations at different temperatures. A number of fragmentation paths were simulated producing almost all fragments found in the mass spectra. For the main fragmentation pathways, the minima and the transition states on the potential energy surface were described with more accurate computational methods.

In order to obtain a better insight in the photofragmentation pathways nonadiabatic dynamics simulations were conducted using trajectory surface hopping method (Newton-X program), combined with TD-DFT (Gaussian09) and MCSCF (Columbus) electronic structure methods. The results have shown the relevance of the cation excited states in the photofragmentation processes.

**Acknowledgements:** Work partially supported by the MESTDRS (Grant Numbers 172065, 171020) and MAECI Serbia–Italy Joint Research Project “A nanoview of radiation-biomatter interaction”.

## REFERENCES

[1] A. C. Brown et al., Nature 341 (1989) 635.

PAPER • OPEN ACCESS

## “Position” does matter : the photofragmentation of the nitroimidazole isomers

To cite this article: J. Chiarinelli *et al* 2017 *J. Phys.: Conf. Ser.* **875** 032007

View the [article online](#) for updates and enhancements.

You may also like

- [Growth mechanisms for doped clusters](#)  
Ewald Janssens and Peter Lievens

- [Photofragmentation of ionic carbon monoxide](#)  
G Hinojosa, M M Sant'Anna, A M Covington *et al.*

- [New insight on the photofragmentation of CH<sub>2</sub>I<sub>2</sub>](#)  
A R Casavola, A Cartoni, P Bolognesi *et al.*



The Electrochemical Society  
Advancing solid state & electrochemical science & technology

242nd ECS Meeting

Oct 9 – 13, 2022 • Atlanta, GA, US

Abstract submission deadline: **April 8, 2022**

Connect. Engage. Champion. Empower. Accelerate.

**MOVE SCIENCE FORWARD**



Submit your abstract



## “Position” does matter : the photofragmentation of the nitroimidazole isomers

J. Chiarinelli<sup>\*§1</sup>, P. Bolognesi<sup>\*2</sup>, A. Casavola<sup>\*</sup>, A. Cartoni<sup>o\*</sup>, M.C. Castrovilli<sup>\*</sup>, D. Catone<sup>\*</sup>, R. Richter<sup>†</sup>, S. Borocci<sup>‡</sup>, S. Tosic<sup>#</sup>, H. Sa’adeh<sup>&</sup>, M. Masic<sup>§</sup>, B.P. Marinkovic<sup>#</sup>, K.C. Prince<sup>†</sup> and L. Avaldi<sup>\*</sup>

<sup>\*</sup> CNR-Istituto di Struttura della Materia, Area della Ricerca di Roma 1, 00016 Monterotondo Scalo, Italy

<sup>§</sup> Dipartimento di Scienze, Università di Roma Tre, Via della Vasca Navale 84, 00146 Roma

<sup>‡</sup> Dipartimento per l’Innovazione nei Sistemi Biologici, Agroalimentari e Forestali (DIBAF),  
Università della Tuscia, Viterbo, Italy

<sup>†</sup> Elettra Sincrotrone Trieste, Area Science Park, Basovizza, Trieste, Italy

<sup>#</sup> Institute of Physics Belgrade, University of Belgrade, Belgrade, Serbia

<sup>&</sup> Department of Physics, The University of Jordan, Amman, Jordan

<sup>o</sup> Dipartimento di Chimica, Sapienza Università di Roma, Roma, Italy

<sup>§</sup> School of Chemistry, Cardiff University, Cardiff, United Kingdom

**Synopsis** Experimental and theoretical spectroscopic methods have been combined to disentangle the fundamental mechanism of VUV induced fragmentation of the three isomers of nitroimidazole radiosensitisers.

Radiotherapy is one of main techniques used in cancer treatment and radiosensitizers are drugs used to selectively improve its effectiveness against tumour cells. Misonidazole and Nimorazole are two radiosensitizers with similar chemical structure. However clinical trials have shown that they have different efficiency in the tumor treatment. In order to understand why this happens we have studied the photofragmentation of 2-nitroimidazole and 4(5)-nitroimidazole, which are the “building blocks” of Misonidazole and Nimorazole, respectively. To the purpose time of flight mass spectrometry has been used to investigate the fragmentation of these molecules. These measurements have been then extended via the determination of the Appearance Energies (AE) of the different fragments and by Photoelectrons-Photoions Coincidences (PEPICO) experiments using synchrotron radiation [1]. To interpret the results DFT calculations [1] have been also performed.

The mass spectra of the two molecules display many similar features and relative intensities, but also a few intriguing peculiarities. The most striking differences are the fragments at  $m/z$  55<sup>+</sup> and 56<sup>+</sup>, present exclusively in 4(5)NI and 2NI, respectively, and the fragment at  $m/z$  83<sup>+</sup>, which is one of the leading fragmentation channels in 2NI, but is almost absent in the 4(5)NI sample. The results of mass spectrometry are confirmed by the photoelectron-photoion coincidence measurements.

Based on DFT calculations, a model is proposed which fully explains such differences, and reveals the subtle fragmentation mechanisms leading to the release of neutral species like NO, CO and HCN. The present results

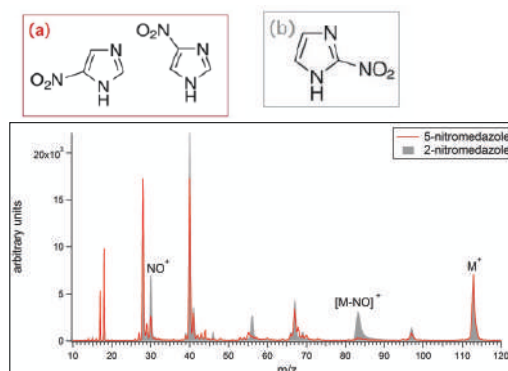


**Figure 1.** Mass Spectra of 4(5)-nitroimidazole (red line and scheme a) and 2-nitroimidazole (grey area and scheme b) molecules measured with a He lamp.

suggest that the products of decomposition of the different nitroimidazole isomers might play a role in determining their distinctive degrees of effectiveness in radiotherapy.

**Acknowledgments:** Work partially supported by the Serbia–Italy Joint Research Project “Nanoscale Insight in the Radiation Damage”.

### References

- [1] P. Bolognesi et al. J Chem Phys Comm. 145, 191102 (2016)

<sup>1</sup>E-mail: [jacopochiarinelli@gmail.com](mailto:jacopochiarinelli@gmail.com)

<sup>2</sup>E-mail: [paola.bolognesi@cnr.it](mailto:paola.bolognesi@cnr.it)



# CEPAS 2017

**7<sup>th</sup> Conference on Elementary Processes  
in Atomic Systems**



**3<sup>rd</sup> – 6<sup>th</sup> September 2017**

**Průhonice, Czech Republic**





## The photofragmentation of the core excited halothane molecule

S.D. Tošić<sup>1</sup>, M. Radibratović<sup>2</sup>, M. Milčić<sup>3</sup>, P. Bolognesi<sup>4</sup>, L. Avaldi<sup>4</sup>, R. Richter<sup>5</sup>, M. Coreno<sup>4,5</sup>, B.P. Marinković<sup>1</sup>

<sup>1</sup>Institute of Physics Belgrade, University of Belgrade, Pregrevica 118, 11080 Belgrade, Serbia

<sup>2</sup>Institute of Chemistry, Technology and Metallurgy – Center for Chemistry, University of Belgrade, Njegoševa 12, 11000 Belgrade, Serbia

<sup>3</sup>University of Belgrade, Faculty of Chemistry, Studentski trg 16, Belgrade, Serbia

<sup>4</sup>Istituto di Struttura della Materia-CNR (ISM-CNR), Area della Ricerca di Roma 1, Monterotondo Scalo, Italy

<sup>5</sup>Elettra-Sincrotrone Trieste, Area Science Park, I-34012 Basovizza, Trieste, Italy

In recent years, great attention has been paid to halogenated anesthetics and their role in the destruction of the earth's ozone layer [1]. One of the most commonly used is halothane (C<sub>2</sub>HBrClF<sub>3</sub>). Compared to the other volatile anesthetics from the same group (halogenated chlorofluorocarbons) this bromide-containing agent is the most destructive against ozone.

We present both experimental and theoretical results related to the photofragmentation of the core-excited halothane molecule. The experiments have been performed at the Gas Phase photoemission beamline of the Elettra synchrotron radiation source (Trieste, Italy) using photons near the C 1s ionization edge (~ 300 eV). The mass spectrum [as shown in Fig.1] is dominated by lighter mass fragments.

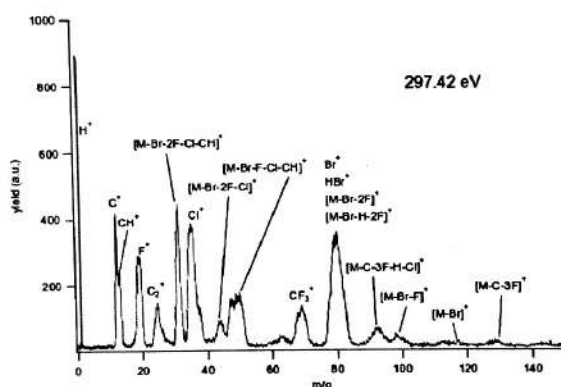


Figure 1: The fragmentation mass spectra of halothane.

To explain the observed large number of lighter mass fragments extensive molecular dynamics (MD) simulations of C<sub>2</sub>HBrClF<sub>3</sub><sup>2+</sup> ion at different temperatures were performed. All MD simulations were carried out in the microcanonical (NVE) ensemble using Verlet algorithm for time integration. At each step of the simulation the potential energy was calculated by minimizing the electronic energy with self-consistent charge-density-functional tight-binding (SCC-DFTB) method as implemented in the DFTB+ code [2]. The results of MD simulations have confirmed the experimental findings: there are fragmentation paths producing almost all fragments found in the mass spectra. For the main fragmentation pathways the minima and the transition states on the potential energy surface were calculated with more accurate quantum chemical methods.

Work partially supported by the MAECI Serbia-Italy Joint Research Project "A nanoview of radiation-biomatter interaction" and the MESTDRS (OI 171020, OI 172065).

[1] A.C. Brown *et al.*, Nature **341** (1989) 635.

[2] B. Aradi *et al.*, J. Phys. Chem. A **111** (2007) 5678.



$$\frac{f(x)}{g(x)} = \frac{f'(x) \cdot g(x) - f(x) \cdot g'(x)}{g^2(x)}$$

$$\operatorname{tg}(\alpha + \beta) = \frac{\operatorname{tg} \alpha + \operatorname{tg} \beta}{1 - \operatorname{tg} \alpha \operatorname{tg} \beta}$$

3<sup>rd</sup>  
**XLIC**  
XUV/X-ray light and fast  
ions for ultrafast chemistry

# GENERAL MEETING

**COST**  
EUROPEAN COOPERATION  
IN SCIENCE AND TECHNOLOGY

(COST ACTION CM 1204)

**2-4 NOVEMBER 2015  
DEBRECEN, HUNGARY**



# PROGRAMME AND BOOK OF ABSTRACTS



**3<sup>rd</sup> XLIC GENERAL MEETING**  
**2-4 NOVEMBER, 2015**

Organised by: *ATOMKI / DE / ELFT*

**Venue**

Centrum Hotel, Debrecen, Hungary

The conference will be hosted at Centrum Hotel, Debrecen, Hungary. The hotel is located in the very heart of the city, at 4-8 Kalvin square, next to the Reformed Great Church. All lectures, the poster sessions and the management committee meeting will be held here.

**Book of Abstracts**

*This book contains the camera-ready copies of the abstracts as sent by the authors. In few cases only minor corrections were made.*

*Publisher:* ATOMKI / DE / ELFT, Dr. Károly Tökési

*Editor:* Péter Badankó

*Printed by:* REXPO Kft., Manager: János Rácz

*ISBN:* 978-963-8321-51-0

## WELCOME

Welcome to the 3<sup>rd</sup> XLIC General Meeting XUV/X-ray light and fast ions for ultrafast chemistry (XLIC), organized in Debrecen (Hungary).

The workshop is an annual meeting of CM1204 action, which deals with physical and chemical phenomena induced by electromagnetic fields and charged particles. The meeting is planned for 2<sup>nd</sup> - 4<sup>th</sup> November, 2015. It will take place at Centrum Hotel, Debrecen, Hungary. There will be 24 talks given by invited speakers, 12 oral presentations by early stage scientists and 2 poster sessions.

The organization of this meeting and its funding with COST CM1204 budget was approved in the 3<sup>rd</sup> MC meeting, held in Gdansk (Poland) on October 10<sup>th</sup>, 2014.

The objectives of the workshop are to assess the state of the art in the current understanding of a variety of basic phenomena in the electron and atom dynamics such as charge-exchange processes collective as well as single-particle excitation and ionization, energy loss, and photon emission processes, collision induced physical, chemical and biological reactions radiation damage and materials modification.

The XLIC conference is held for the 3<sup>rd</sup> time. Previous conferences were organized in Madrid (Spain, 2013), Gdansk (Poland, 2014). It is a great honour for Debrecen to be the host of this prestigious event in 2015.

Debrecen is the second largest city of Hungary, one of the most important educational, research and cultural centres in Middle-Europe. Stadiums of Debrecen have given place to great sport events (like European Championship of Swimming, 2012) and the Carnival of Flowers attracts thousands of visitors from all over Europe every year. In addition, there are a lot of sights that must be seen, for instance the Great Church at the beautiful main square, Déri Museum, Reformed College and its unique library, the Great Forest and the main building of the University of Debrecen, but we could continue this list.

The 3<sup>rd</sup> XLIC conference is held at the Centrum Hotel. The hotel is located in the historic city centre of Debrecen, only 50 meters from the Great Reformed Church and the main square, the venue of many cultural events, in the close vicinity of the most important attractions, office buildings and institutions. It is one of the hotels of Eastern Hungary that provides ideal conditions for the work and recreation of business travellers, while also satisfying the needs of tourists in search of a lively atmosphere and vibrant experiences.

We hope that all participants will have a lively and successful meeting while enjoying the attractive surroundings in this beautiful region of Hungary. We hope, furthermore, we may offer exciting scientific programs in addition to various social and cultural programs, where you can enjoy the famous Hungarian dishes and wine, too. Organizers have been doing their best to guarantee pleasant experiences for everyone.

Károly Tökési  
*Chair*  
3<sup>rd</sup> XLIC General Meeting

András Csehi  
*Co-Chair*  
3<sup>rd</sup> XLIC General Meeting

## Search for the ‘molecular scissor’ via site- and state-selected molecular fragmentation studies

P. Bolognesi<sup>1\*</sup>, A. Kettunen<sup>2</sup>, A. Cartoni<sup>3,1</sup>, R. Richter<sup>4</sup>, S. Tosic<sup>5</sup>, S. Maclot<sup>6</sup>, P. Rousseau<sup>6</sup>, R. Delaunay<sup>6</sup>, P. Markus<sup>1</sup>, H. Sa’adeh<sup>7</sup>, Maša Masić<sup>8</sup>, B. Marinkovic<sup>5</sup>, K. Prince<sup>4</sup>, L. Avaldi<sup>1</sup>

<sup>1</sup>CNR-Istituto di Struttura della Materia, Area della Ricerca di Roma1, Monterotondo Scalo, Italy

<sup>2</sup>Department of Physics, University of Oulu, Finland

<sup>3</sup>Dipartimento di Chimica, Sapienza Università di Roma, Roma, Italy

<sup>4</sup>Elettra-Sincrotrone Trieste, Basovizza, Italy

<sup>5</sup>Institute of Physics, University of Belgrade, Belgrade, Serbia

<sup>6</sup>CIMAP, CEA/CNRS/ENSICAEN, Université de Caen Basse-Normandie, Caen, France

<sup>7</sup>Department of Physics, The University of Jordan, Amman, Jordan

<sup>8</sup>Cardiff University, School of Chemistry, Cardiff, United Kingdom

\*Corresponding author: paola.bolognesi@cnr.it

The search for ‘molecular knife/scissors’ i.e. the ability to selectively control molecular fragmentation, is attracting a lot of interest [1,2]. This idea implies the possibility that the localization of the energy deposition into specific atomic sites and/or molecular orbitals could be used to control and address the fate of the molecule following photon absorption, i.e. the molecular fragmentation. Indeed, mass spectra measured at photon energies across inner shell excitation thresholds display marked differences (see Figure 1), suggesting a site-selected fragmentation. In this work we consider the cases of halopyrimidines [3] and nitroimidazoles, two classes of radiosensitisers, to investigate and explain the mechanisms of site- and state-selective fragmentation via a combination of spectroscopic techniques (mass spectrometry, photoelectron, resonant Auger electron as well as electron-ion coincidence spectroscopy) and tunable synchrotron radiation from the Gas Phase beamline of Elettra.

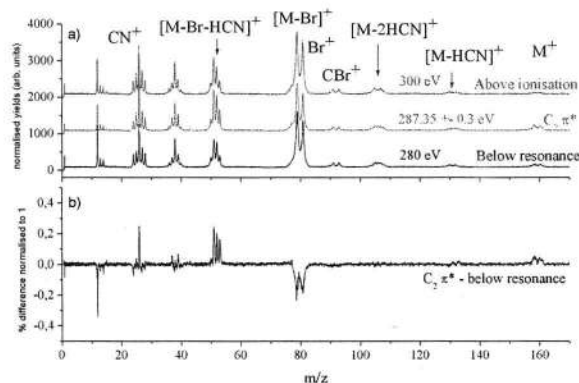


Figure 1: a) The fragmentation mass spectra of 2Br-pyrimidine measured at the  $C_2(1s \rightarrow \pi^*)$  excitation (red spectrum) and in the ionization continuum below/above the inner shell resonances. b) The difference spectrum obtained by subtracting the direct ionization contribution from the resonance one.

**Acknowledgments:** Work partially supported by the XLIC COST Action, the Serbia – Italy Joint Research Project “Nanoscale Insight in the Radiation Damage”, the MIUR FIRB RBF10SQZI project 2010, the ICTP TRIL Programme and project OII71020.

### References

- [1] K. Tanaka *et al*, *Radiat. Phys. Chem.*, **75**, 2076-2079, (2006)
- [2] S. Nagaoka *et al*, *J Phys. Chem A*, **115**, 8822-8831, (2011)
- [3] P. Bolognesi *et al*, *Phys. Chem. Chem. Phys.*, DOI: 10.1039/C5CP02601F, (2015)



	MONDAY		TUESDAY	WEDNESDAY
8:00-9:00				
9:00-10:00	<b>Registration</b>		<b>Invited 8</b> Thomas Baumert	<b>Invited 12</b> Piero Decleva
10:00-11:00			<b>Invited 9</b> Luca Argenti	<b>Invited 13</b> Daniela Ascenzi
11:00-12:00			<b>Invited 10</b> Rebeca de Nalda	<b>Invited 14</b> Daniel Dundas
12:00-13:00			<b>Invited 11</b> Morten Forre	<b>Invited 15</b> Ronnie Hoekstra
13:00-14:00	<b>Lunch Opening (13:20)</b>		<b>Coffee break</b>	<b>Coffee break</b>
14:00-15:00	<b>Lunch</b>		<b>Young Scientist Forum I</b> Sandra Gomez Mark Stockett Helena Levola András Csehi Aleksander Simonsen Morgane Vacher	<b>Invited 16</b> Leticia Gonzalez
15:00-16:00			<b>Invited 17</b> Nadja Doslic	
16:00-17:00			<b>Invited 18</b> Matjaz Zitnik	
17:00-18:00	<b>Lunch</b>		<b>Lunch</b>	<b>Lunch</b>
18:00-19:00	<b>Invited 1</b> Thomas Weinacht	<b>Conference Photo (14:20)</b>	<b>Young Scientist Forum II</b> Rudy Delaunay Katrin Tanzer Michael Gatchell Vera Krizova Dmitrii Egorov Thomas Kierspel	<b>Invited 19</b> Eva Lindroth
19:00-20:00	<b>Invited 2</b> Franck Lepine			<b>Invited 20</b> Jimena Gorfinkiel
20:00-	<b>Invited 3</b> Alicia Palacios	<b>Young Scientist Forum II</b>		<b>Invited 21</b> Sándor Borbély
	<b>Coffee break</b>			<b>Coffee break</b>
	<b>Invited 4</b> Benjamin Lasorne			<b>Invited 22</b> Jan Petter Hansen
	<b>Invited 5</b> Alexander Kuleff	<b>Coffee break</b>		<b>Invited 23</b> Marta Labuda
	<b>Invited 6</b> Attila G. Császár			<b>Invited 24</b> Nikolay Shvetsov-Shilovskiy
	<b>Invited 7</b> Alejandro Saenz	<b>Poster Session II</b>		<b>Dinner</b>
	<b>Poster Session I</b>	<b>XLIC MC meeting</b>		
	<b>Welcome dinner</b>	<b>Conference dinner</b>		



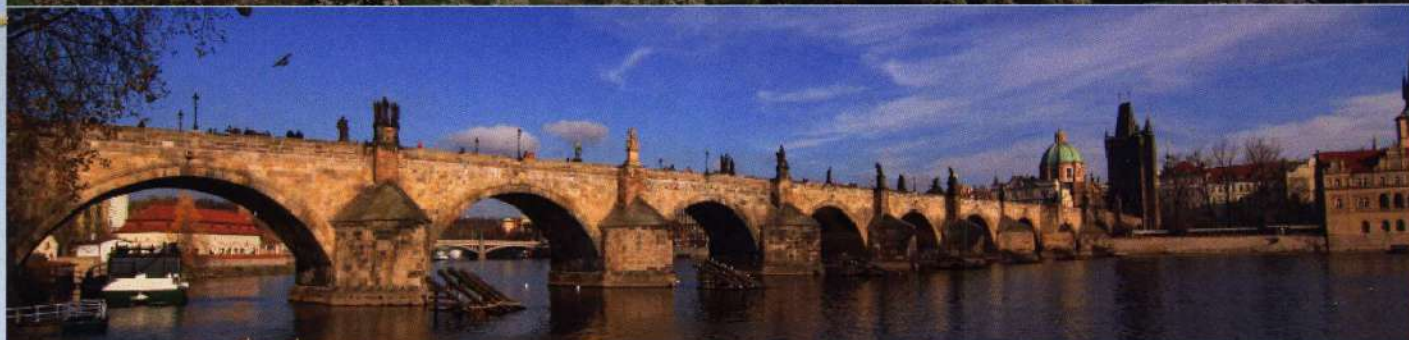


COST is supported by the  
EU Framework Programme  
Horizon 2020

# 4<sup>th</sup> XLIC General Meeting COST Action CM1204

14 - 16 March 2017

Prague, Czech Republic



**BOOK OF ABSTRACTS**





# “Position” does matter: The photofragmentation of the nitroimidazole isomers

P. Bolognesi,<sup>1\*</sup> A. R. Casavola,<sup>1\*</sup> A. Cartoni,<sup>1,2</sup> R. Richter,<sup>3</sup> P. Markus,<sup>1</sup> S. Borocci,<sup>4</sup> J. Chiarinelli,<sup>1,8</sup> S. Tošić,<sup>5</sup> H. Sa'adeh,<sup>6</sup> M. Masič,<sup>7</sup> B. P. Marinković,<sup>5</sup> K. C. Prince,<sup>3</sup> and L. Avaldi<sup>1</sup>

<sup>1</sup>CNR-Istituto di Struttura della Materia, Area della Ricerca di Roma1, Monterotondo, Italy

<sup>2</sup>Dipartimento di Chimica, Sapienza Università di Roma, Roma, Italy

<sup>3</sup>Elettra-Sincrotrone Trieste, Basovizza, Italy

<sup>4</sup>Dipartimento per l'Innovazione nei Sistemi Biologici, Agroalimentari e Forestali (DIBAF), Università della Tuscia, Viterbo, Italy

<sup>5</sup>Institute of Physics Belgrade, University of Belgrade, Belgrade, Serbia

<sup>6</sup>Department of Physics, The University of Jordan, Amman, Jordan

<sup>7</sup>School of Chemistry, Cardiff University, Cardiff, United Kingdom

<sup>8</sup>Dipartimento di Scienze, Università di Roma Tre, Roma, Italy

\*Corresponding author: paola.bolognesi@cnr.it and annarita.casavola@cnr.it

Radiotherapy is one of main techniques used in cancer treatment and radiosensitizers are drugs used to selectively improve its effectiveness against tumor cells. Misonidazole and Nimorazole are two radiosensitizers with similar chemical structure. However clinical trials have shown that they have different efficiency in the tumor treatment. In order to understand why this happens we have studied the photo-fragmentation of 2-nitroimidazole and 4(5)-nitroimidazole, which are the “building blocks” of Misonidazole and Nimorazole, respectively. Time of Flight Mass spectrometry (fig 1) shows important differences in their fragmentation, which can be linked with medical applications. To have a better knowledge of these processes we have also measured Appearance Energy (AE) and Photoelectron-Photoion Coincidences (PEPICO) with Synchrotron Light (Elettra, Trieste), and performed theoretical calculations Ref. 1.

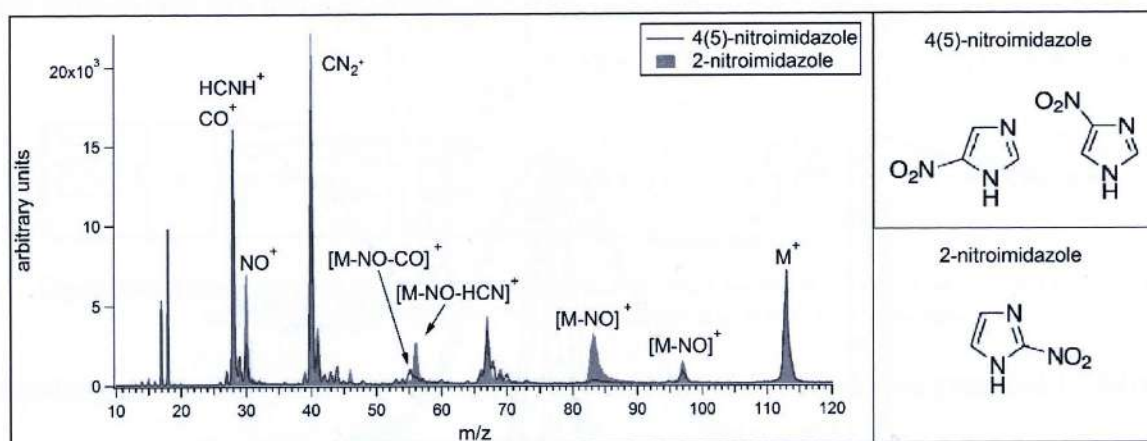


Figure 1: Time of Flight Mass Spectrum (TOF-MS).

**Acknowledgments:** This work is partially supported by the XLIC COST Action M1204 via the STSM program and the Serbia–Italy Joint Research Project “Nanoscale Insight in the Radiation Damage”.

## References

[1] P. Bolognesi et al. J Chem Phys Comm. 145, 191102 (2016)



**Meeting of the XLIC Working Group 2**

**WG2 Expert Meeting on Biomolecules**

**27-30 April 2015, Fruška gora, Serbia**



Institute of Physics Belgrade  
University of Belgrade

This Book of Abstracts is supported by COST CM 1204 (XLIC) Action

This Book of Abstracts may be cited as:  
COST Action Cm1204 - Book of Abstract - WG2 Expert Meeting on Biomolecules,  
April, 2015

© COST Office, 2015

No permission to reproduce or utilise the contents of this Book of Abstracts by any means is necessary, other than in the case of images, diagrams or other material from other copyright holders. In such cases, permission of the copyright holders is required.

Neither the COST Office nor any person acting on its behalf is responsible for the use which might be made of the information contained in this publication. The COST Office is not responsible for the external websites referred to in this publication.

## Fragmentation of halopyrimidines and halouraciles by photoionization and ion impact

P. Bolognesi<sup>1</sup>, M.C. Castrovilli<sup>1</sup>, A. Kettunen<sup>2</sup>, A. Cartoni<sup>3</sup>, R. Richter<sup>4</sup>, S. Tomic<sup>5</sup>, S. Maclot<sup>6</sup>, P. Rousseau<sup>6</sup>, R. Delaunay<sup>6</sup>, A. Domaracka<sup>6</sup>, B. Huber<sup>6</sup> and L. Avaldi<sup>1</sup>

<sup>1</sup>CNR-Istituto di Struttura della Materia, Area della Ricerca di Roma1, Monterotondo Scalo, Italy

<sup>2</sup>Department of Physics, University of Oulu, Finland

<sup>3</sup>Dipartimento di Chimica, Sapienza Università di Roma, Roma, Italy

<sup>4</sup>Elettra-Sincrotrone Trieste, Basovizza, Italy

<sup>5</sup>Institute of Physics, University of Belgrade, Belgrade, Serbia

<sup>6</sup>CIMAP, CEA/CNRS/ENSICAEN, Université de Caen Basse-Normandie, Caen, France

In recent years we have focused our interest in processes induced in isolated molecules by soft X-ray and ion beams. By photon ionization the site and state of the energy deposition are well defined and the following chain of processes are characterized by coincidence techniques. In the fragmentation induced by low energy ions, the effects of the increasing complexity of the target and the role played by the ‘environment’ on the properties of the single molecule are addressed.

In the presentation two examples will be discussed. The first one is the photofragmentation of 2Cl-pyrimidine following inner shell excitation or direct valence ionization studied via electron-ion coincidence techniques. The experiments have been performed at the Gasphase photoemission beamline at Elettra, Trieste (Italy). The results show that the resonant Auger process following inner shell excitation selectively populates the final states of the singly charged ion and the site and state selected fragmentation patterns appear to depend only on the final state of the singly charged ion. The comparison with state selected photofragmentation after valence ionization confirms the role of the cationic state in the type of fragments produced.

In the second example the fragmentation of 5Br-uracil isolated molecules, homogeneous clusters and hydrated clusters by C<sup>4+</sup> ions has been studied. The experiments have been performed at the ARIBE beamline of the GANIL facility, Caen (France). The observation of series of hydrated fragments provides the experimental evidence that a few water molecules attached to the 5Br-uracil can induce a tautomerisation process. This process can lead to mutagenesis and therefore to a different pairing in the DNA bases and can explain the radiosensitizing effect of compounds bases on 5Br-uracil.

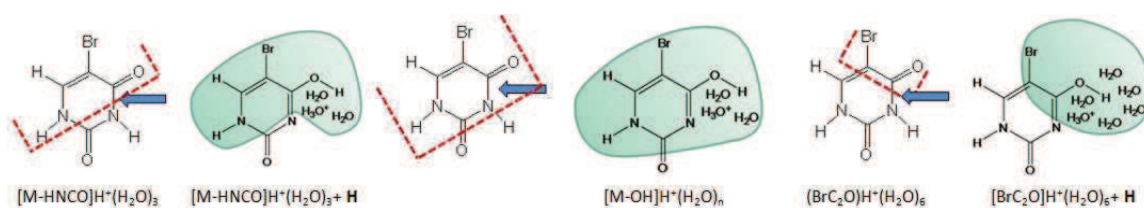


**Fig.1.** Schematic of the main fragments whose hydrated series are observed and assigned in the mass spectrum of hydrated clusters of 5Br-uracil. The blue arrows indicate the suggested site of hydration and the red dashed lines surround the charged (detected) fragment; M indicates the parent ion. The proposed tautomerisation processes mediated through the presence of a sufficient number of water molecules is also shown.



## Cross section set and transport properties of $\text{Ne}^+$ in $\text{CF}_4$

This content has been downloaded from IOPscience. Please scroll down to see the full text.

2015 J. Phys.: Conf. Ser. 635 022099

(<http://iopscience.iop.org/1742-6596/635/2/022099>)

View [the table of contents for this issue](#), or go to the [journal homepage](#) for more

Download details:

IP Address: 147.91.81.242

This content was downloaded on 09/02/2017 at 13:17

Please note that [terms and conditions apply](#).

You may also be interested in:

[Expression for momentum-transfer scattering in inelastic collisions in electron transport in a collisional plasma](#)

Toshiaki Makabe and Ronald White

[Electron transport analysis in water vapor](#)

Satoru Kawaguchi, Kazuhiro Takahashi, Kohki Satoh et al.

[The cross section set of perfluorocyclobutane](#)

Masahiro Yamaji and Yoshiharu Nakamura

[Updated compilation of electron-Cl<sub>2</sub> scattering cross sections](#)

J Gregório and L C Pitchford

[Resistive Plate Chambers: electron transport and modeling](#)

D Bošnjakovi, Z Lj Petrovi and S Dujko

[Electron transport coefficients in the mixtures of H<sub>2</sub>O with N<sub>2</sub>, O<sub>2</sub>, CO<sub>2</sub> and dry air for the optimization of non-thermal atmospheric pressure plasmas](#)

G Ruíz-Vargas, M Yousfi and J de Urquijo

## Cross section set and transport properties of $\text{Ne}^+$ in $\text{CF}_4$

Z. Raspopović\*, Ž. Nikitović\*, S. Tošić and V. Stojanović\*<sup>1</sup>

\*Institute of Physics Belgrade, University of Belgrade, P.O. Box 57, 11000 Zemun Serbia

**Synopsis** Cross section set for scattering  $\text{Ne}^+$  ions in  $\text{CF}_4$  is assessed by using available experimental data for charge transfer cross sections. Monte Carlo method is used to calculate transport properties of  $\text{Ne}^+$  ions in  $\text{CF}_4$ .

Charge transfer reactions of ions with molecules are unavoidable elementary processes in modeling kinetics in terrestrial, industrial, and astrophysical plasmas. In selected cases charge transfer reactions are known to represent the most significant part of a cross section set. Line spectra of excited atoms obtained in spectrometric measurements in  $\text{CF}_4$  indicate that the charge transfer reaction is dominant process in collisions with inert gas ions. Thus, in this work we assessed cross section set for  $\text{Ne}^+$  in  $\text{CF}_4$  by using existing experimental data [1] for charge transfer collisions producing radical ions of  $\text{CF}_4$ .

Since no direct information is found in the literature how mobility of high recombination energy ions such as  $\text{Ne}^+$  ions behaves in  $\text{CF}_4$  we also calculated transport parameters by using Monte Carlo simulation technique [2].

The cross sections presented by Fisher *et al* [1] were used to determine the elastic momentum transfer cross section (“elastic” in Fig. 1) assuming the total momentum transfer cross section  $\sigma_{\text{mt}}$  is known. At low energies we assumed that  $\sigma_{\text{mt}}$  is Langevin’s cross section and elastic momentum transfer cross section is determined by deducing all reactive cross sections.

Average polarizability of  $\text{CF}_4$  is not well established [1] and may produce discrepancy for calculated mobility of ions in  $\text{CF}_4$  [3] and thus affect plasma parameters prediction in modeling. We adopted value of  $3.86 \text{ \AA}^3$  used by Stojanović *et al* [3] who found excellent agreement between experimental and calculated mobility of  $\text{CF}_3^+$  ions in  $\text{CF}_4$ .

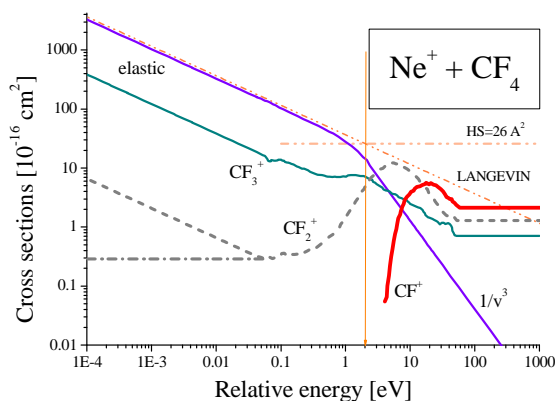


**Figure 1.** Cross section set for  $\text{Ne}^+ + \text{CF}_4$ .

Further, extrapolation of elastic momentum transfer cross section trend beyond crossing point of Langevin’s and hard sphere (HS) cross section [1] is done by smoothly connecting to  $1/v^3$  trend [4] where  $v$  is the center-of-mass velocity (see Fig. 1).

At all ion kinetic energies above 50 eV reactive cross sections are extrapolated by constant values.

Effect of various extrapolations (short dot-dashed or dashed line in Fig. 1) of unusual behavior at low energy, observed with measurements of the cross section leading to formation of  $\text{CF}_2^+$  (where irrespective of the  $\text{Ne}^+$  spin state exothermic behavior of reaction is expected) is found negligible on mobility. Reduced mobility for  $\text{Ne}^+$  ions as a function of  $E/N$  ( $E$ -electric field,  $N$ -gas density) compared with Langevin’s value is shown in Fig. 2.

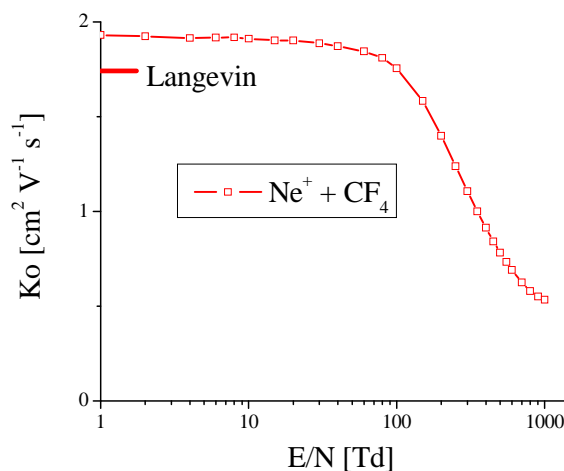


**Figure 2.** Reduced mobility for  $\text{Ne}^+$  in  $\text{CF}_4$  at 300 K.

### References

- [1] E R Fisher *et al.* 1990, *J.Chem.Phys.* **92** 2296
- [2] Z Lj. Petrović Z. Lj *et al.* 2009 *J. Phys. D: Appl. Phys.* **42** 194002.
- [3] V Stojanović *et al.* 2014 *J. Phys. Conf. Ser.* **514** 012059
- [4] P S Krstić and D R Schultz 2009 *J. Phys. B: At. Mol. Opt. Phys.* **42** 065207

<sup>1</sup>E-mail: stoyanov@ipb.ac.rs



Electron scattering by silver: excitation of the  $4d^9 5s^2 \ ^2D_{3/2}$  and  $4d^{10} 6s \ ^2S_{1/2}$  states

This content has been downloaded from IOPscience. Please scroll down to see the full text.

2015 J. Phys.: Conf. Ser. 635 052054

(<http://iopscience.iop.org/1742-6596/635/5/052054>)

View [the table of contents for this issue](#), or go to the [journal homepage](#) for more

Download details:

IP Address: 147.91.83.242

This content was downloaded on 14/09/2015 at 11:01

Please note that [terms and conditions apply](#).

## Electron scattering by silver: excitation of the $4d^9 5s^2 \ ^2D_{3/2}$ and $4d^{10} 6s \ ^2S_{1/2}$ states

S. D. Tošić<sup>1</sup>, V. Pejčev, D. Šević and B. P. Marinković

Institute of Physics, University of Belgrade, Pregrevica 118, Belgrade, Serbia

**Synopsis** Differential cross sections (DCSs) for electron impact excitation of the  $4d^9 5s^2 \ ^2D_{3/2}$  and  $4d^{10} 6s \ ^2S_{1/2}$  states of silver atom have been measured. Relative DCSs have been obtained by comparing intensities of these states relative to the resonant  $^2P$  state at scattering angles from  $10^\circ$  to  $150^\circ$  and at electron impact energies from 10 eV to 60 eV.

The aim of our study is to provide reliable electron scattering data which are of great importance for a better understanding of electron interactions with silver atoms as well as for many scientific and practical applications [1]. The silver atom is very important in the field of laser cooling and trapping techniques.

Here we present experimentally obtained relative differential cross sections (DCSs) for electron impact excitation of the  $4d^9 5s^2 \ ^2D_{3/2}$  (4.304 eV) and  $4d^{10} 6s \ ^2S_{1/2}$  (5.276 eV) states of silver atom from the ground  $4d^{10} 5s \ ^2S$  state. The DCSs have been determined by using inelastic ( $4d^9 5s^2 \ ^2D_{3/2}$ ,  $4d^{10} 6s \ ^2S_{1/2}$ )-to-inelastic ( $4d^{10} 5p \ ^2P_{1/2,3/2}$  resonance state) intensity ratios and relative DCSs for the resonance state. The results have been obtained at electron impact energies ( $E_0$ ) of 10, 20, 40 and 60 eV and at scattering angles from  $10^\circ$  to  $150^\circ$  in steps of  $10^\circ$ .

Our scattering experiment is performed in crossed electron-atom beam arrangement in which an atomic beam is perpendicularly crossed by monoenergetic electron beam. The electron spectrometer ESMA [1] consists of a hemispherical electron energy selector with a hair-pin thermo-electron source and an energy analyzer of the same type with a channel electron multiplier as a detector. The analyzer can rotate from  $-30^\circ$  up to  $150^\circ$  with respect to the zero angle defined by the axis of the electron beam.

The well collimated effusive Ag vapour beam has been produced by heating oven crucible containing silver atoms. All the elements of the system are placed inside a high vacuum chamber. The real zero position of the scattered signal has been determined from the symmetry at positive and negative scattering angles.

The inelastically scattered electron current intensities are detected as a function of scattering angle up to  $150^\circ$  and then converted to relative DCSs

using the effective path length correction factors [2] determined for the present experimental conditions. Obtained relative inelastic DCSs for electron impact excitation of the  $4d^9 5s^2 \ ^2D_{3/2}$  and  $4d^{10} 6s \ ^2S_{1/2}$  states of silver at 40 eV electron impact energy are presented in figure 1.

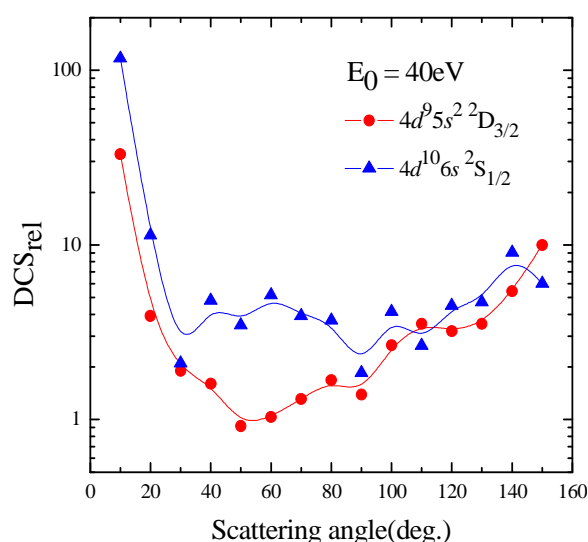


**Figure 1.** Relative differential cross sections for the excitation of the  $^2D_{3/2}$  and  $^2S_{1/2}$  states of silver atom at 40 eV electron impact energy as a function of scattering angle.

It is interesting and important to continue investigations of electron excitation processes in silver atoms in order to obtain a more profound knowledge and to obtain more complete sets of scattering data that could be used in theoretical modeling and numerical simulations.

### References

- [1] S. D. Tošić *et al* 2012 *NIMB* **279**, 53
- [2] R. T. Brinkman and S. Trajmar 1981 *J. Phys. E: Sci. Instrum.* **14**, 245

<sup>1</sup>E-mail: seka@ipb.ac.rs



## Selectivity in the photofragmentation of halo-pyrimidines

This content has been downloaded from IOPscience. Please scroll down to see the full text.

2015 J. Phys.: Conf. Ser. 635 112041

(<http://iopscience.iop.org/1742-6596/635/11/112041>)

View [the table of contents for this issue](#), or go to the [journal homepage](#) for more

Download details:

IP Address: 147.91.83.242

This content was downloaded on 14/09/2015 at 11:06

Please note that [terms and conditions apply](#).



## Selectivity in the photofragmentation of halo-pyrimidines

P. Bolognesi<sup>\*1</sup>, A. Kettunen<sup>†</sup>, A. Cartoni<sup>&</sup>, R. Richter<sup>#</sup>, S. Tosic<sup>§</sup>, S. Maclot<sup>§</sup>, P. Rousseau<sup>§</sup>,  
R. Delaunay<sup>§</sup>, A. Domaracka<sup>§</sup>, L. Avaldi<sup>\*</sup>

<sup>\*</sup> CNR-Istituto di Struttura della Materia, Area della Ricerca di Roma1, Monterotondo Scalo, Italy

<sup>†</sup> Department of Physics, University of Oulu, Finland

<sup>&</sup> Dipartimento di Chimica, Sapienza Università di Roma, Roma, Italy

<sup>#</sup> Elettra-Sincrotrone Trieste, Basovizza, Italy

<sup>§</sup> Institute of Physics, University of Belgrade, Belgrade, Serbia

<sup>§</sup> CIMAP, CEA/CNRS/ENSICAEN, Université de Caen Basse-Normandie, Caen, France

**Synopsis** The fragmentation of 2Br-, 2Cl- and 5Br-pyrimidine following direct valence photoionization or inner shell excitation and decay has been studied by electron-ion coincidence experiments. The results show that the fragmentation is strongly selective on the final singly charged ion state and the dominant fragmentation patterns correlate to the nearest appearance potential.

Pyrimidines are an important class of organic molecules because the pyrimidine ring forms the base structure of three nucleic acids (uracil, cytosine and thymine) and their halogenated substituted bases have found applications as radiosensitizers in radiotherapy.

In a previous work on pyrimidine [1] it has been observed that the resonant Auger spectrum shows a selective population of the final states of the cation and the site and state selected fragmentation patterns appear to depend only on these final states. In this work we have studied the fragmentation of 2Br-, 2Cl- and 5Br-pyrimidine following direct valence shell photoionization as well as inner shell excitations. In the case of valence ionization the detection of the fragment ions in coincidence with energy selected photoelectrons allows a state selected study on the different cation states involved in the process. In the case of inner shell excitation the fragment ions are detected in coincidence with the resonant Auger electrons. In this way the selectivity on the site of the initial energy deposition is added, too.

The experiments have been performed at the Gas Phase Beamline at the Elettra Synchrotron (Trieste).

In Figure 1 the electron-ion coincidence yield for several 2Br-pyrimidine fragments as a function of the binding energy of the cation state measured either in direct photoionization at 100 eV or following the inner shell excitation are shown. Regardless of the initial process the coincidence mass spectra show a very similar behavior as long as the same final ionic state is selected. This behavior of the fragmentation can

be explained by the fact that the fragmentation occurs on a time scale longer than the non-radiative relaxation of the inner shell vacancy. It is also clear that a certain ionic state preferentially correlates to the nearest fragmentation threshold, even though other fragmentation channels are energetically open.

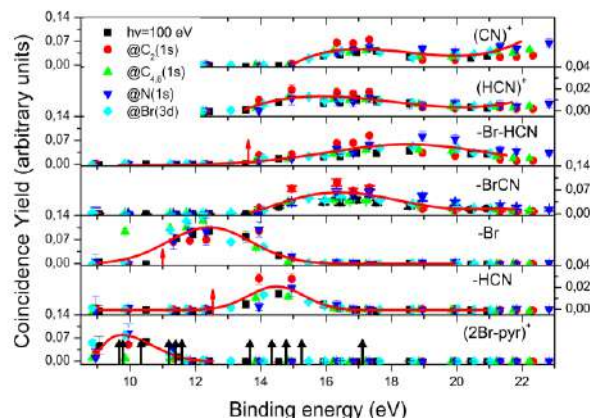


**Figure 1.** The PEPICO coincidence yields as a function of the binding energy of the cation state. The black arrows in the bottom panel indicate the position of the ion states, while the red ones the measured appearance energy of the fragments.

**Acknowledgments** Work partially supported by the Serbia – Italy Joint Research Project “Nanoscale Insight in the Radiation Damage”.

### References

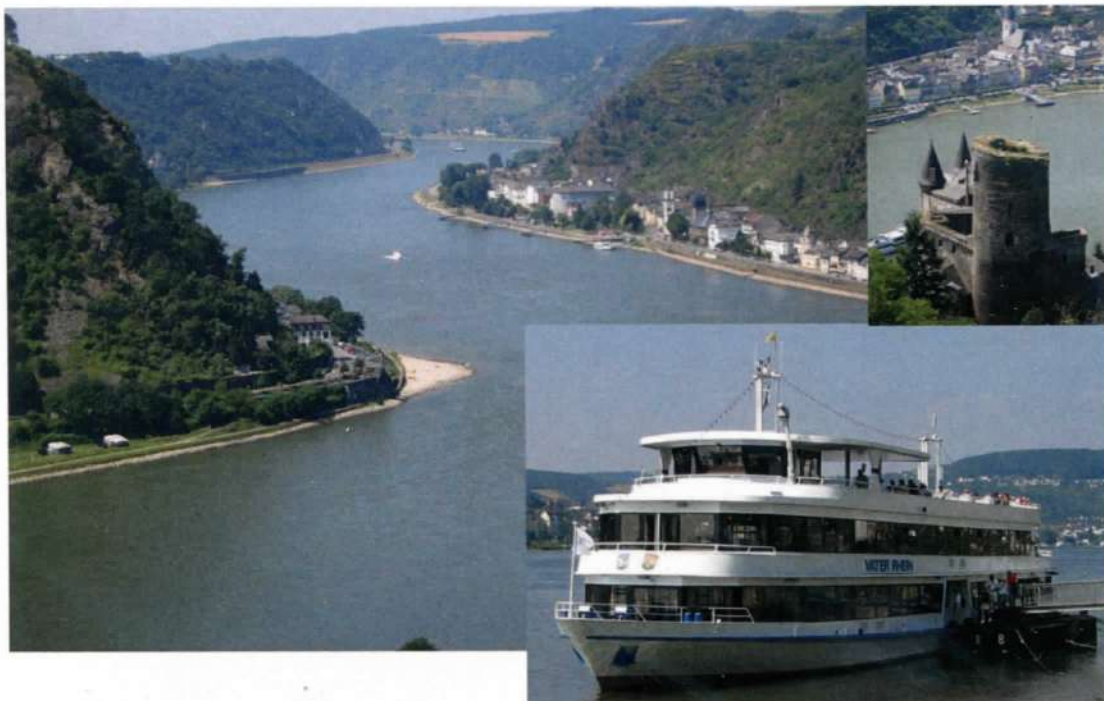
[1] P. Bolognesi *et al* 2012 in “Radiation Damage in Biomolecular Systems”, G. Garcia Gomez-Tejedor and M.C. Fuss eds., Springer, 165-176

<sup>1</sup>E-mail: [Paola.Bolognesi@cnr.it](mailto:Paola.Bolognesi@cnr.it)



**3<sup>rd</sup> International Conference**  
**"Radiation Damage in Biomolecular Systems:**  
***Nanoscale Insights into***  
***Ion-Beam Cancer Therapy***  
***(Nano-IBCT 2014)"***

Boppard am Rhein  
Germany  
October 27-31, 2014



**Book of Abstracts**



## SELECTIVITY IN THE PHOTOFRAGMENTATION OF HALO-PYRIMIDINES

P. Bolognesi<sup>1</sup>, A. Kettunen<sup>2</sup>, A. Cartoni<sup>3</sup>, R. Richter<sup>4</sup>, S. Tosic<sup>5</sup>, S. Maclot<sup>6</sup>, P. Rousseau<sup>6</sup>,  
R. Delaunay<sup>6</sup>, A. Domaracka<sup>6</sup>, L. Avaldi<sup>1</sup>

<sup>1</sup>CNR-Istituto di Struttura della Materia, Area della Ricerca di Roma1, Monterotondo Scalo, Italy

E-mail: paola.bolognesi@cnr.it

E-mail: lorenzo.avaldi@ism.cnr.it

<sup>2</sup>Department of Physics, University of Oulu, Finland

E-mail: ank@iki.fi

<sup>3</sup>Dipartimento di Chimica, Sapienza Università di Roma, Roma, Italy

E-mail: antonella.cartoni@uniroma1.it

<sup>4</sup>Elettra-Sincrotrone Trieste, Basovizza, Italy

E-mail: robert.richter@elettra.trieste.it

<sup>5</sup>Institute of Physics, University of Belgrade, Belgrade, Serbia

E-mail: seka@ipb.ac.rs

<sup>6</sup>CIMAP, CEA/CNRS/ENSICAEN, Université de Caen Basse-Normandie, Caen, France

E-mail: maclot@ganil.fr

E-mail: prousseau@ganil.fr

E-mail: delaunay@ganil.fr

E-mail: domaracka@ganil.fr

Pyrimidines are an important class of organic molecules because the pyrimidine ring forms the base structure of three nucleic acids (uracil, cytosine and thymine) and their halogenated substituted bases have found applications as radiosensitizers in radiotherapy. The observation of high relative biological effectiveness of soft X-ray in cells [1] has raised the question whether this is due to a specific physical/chemical effect or to the preferential localization of the ionizations in the DNA bases. In the former case this implies a fragmentation process induced by the radiation, while the latter implies that the bond breaks are due to the electron swarms produced following the absorption of the soft X-ray. To answer these questions we have undertaken an extensive study of the electron spectra from the inner shell ionized and excited molecules as well as their site selected fragmentation patterns.

In a series of works on pyrimidine [2] it has been observed that the resonant Auger spectrum shows a selective population of the final states of the singly charged ion and the site and state selected fragmentation patterns appear to depend only on the final state of the singly charged ion. Based on these previous results in this work we have studied the fragmentation of 2Br-, 2Cl- and 5Br-pyrimidine following direct valence shell photoionization as well as C and N 1s inner shell excitations. In the case of valence ionization the detection of the fragment ions in coincidence with energy selected photoelectrons allows a state selected study on the different cation states involved in the process. In the case of inner shell excitation the fragment ions are detected in coincidence with the resonant Auger electrons. In this way the selectivity on the site of the initial energy deposition is added, too.

In figure 1 an example of the fragmentation of the 2Cl-pyridime after valence photoionization is shown. The observation of the parent ion or its fragment ions strongly depends on the excited cationic state. The comparison with the fragmentation following the population of the same states via site-selective inner shell excitation indicates that the major role is played by the final

cationic state. Similarities and differences in the fragmentation as a function of the excitation site and halogenation will be presented in the poster.

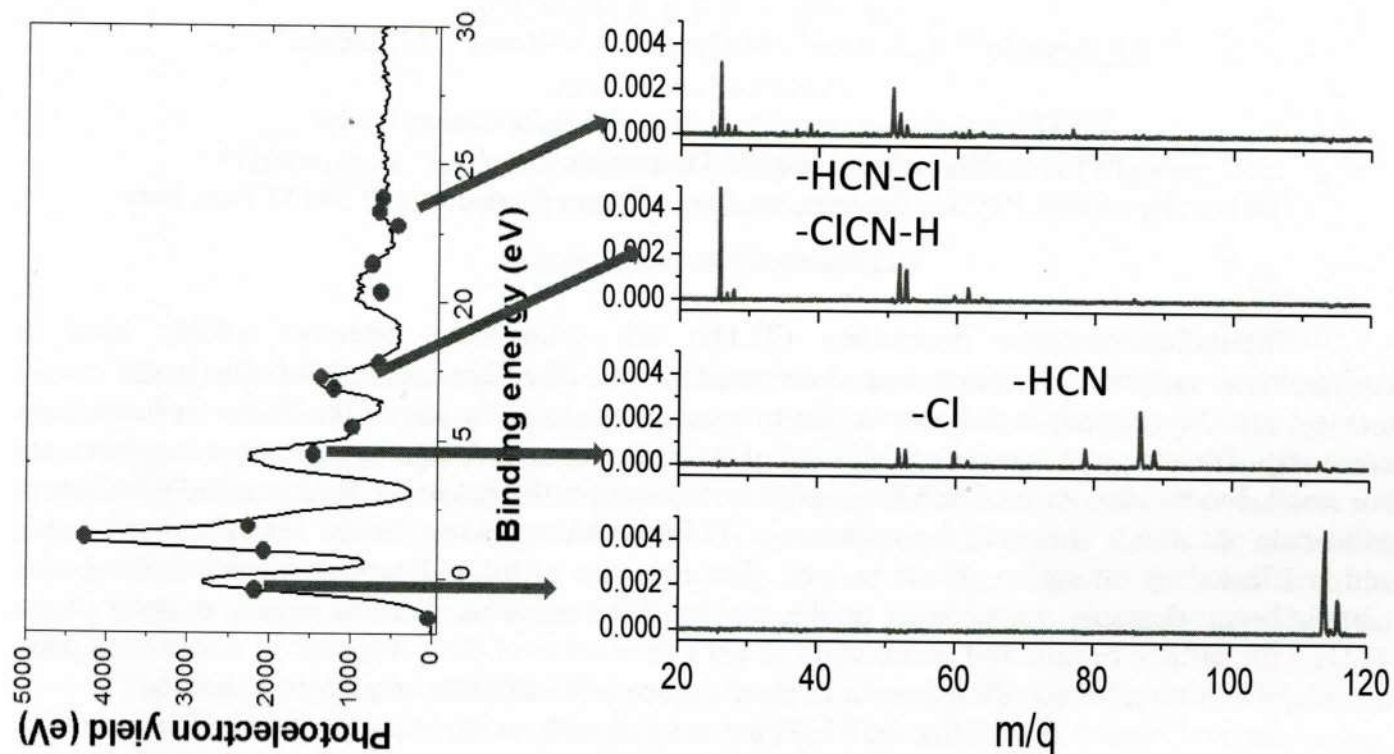


Figure 1: Photofragmentation of 2Cl-pyrimidine studied by a photoelectron-photoion coincidence experiment at 100 eV. On the left panel the photoelectron spectrum of the molecule is shown, while on the right panel some coincidence mass spectra at different binding energies are reported.

Acknowledgments: Work partially supported by the Serbia – Italy Joint Research Project “Nanoscale Insight in the Radiation Damage”. The support by the COST Action nano-IBCT via the STM scheme is acknowledged.

#### REFERENCES

- [1] B Fayard et al., *Radiat. Res.* **157**, 538 (2002)
- [2] P. Bolognesi et al., *J. Chem. Phys.* **136**, 154308 (2012); in “*Radiation Damage in Biomolecular Systems*”, G.Garcia Gomez-Tejedor and M.C. Fuss eds., Springer, 2012, p165-176 ; *J. Chem. Phys.* **133**, 034302 (2010); *J. Phys. Conf. Series* **212**, 012002 (2010); *J. Chem. Phys.* **133**, 034302 (2010); *J. Phys. Chem. A* **113**, 13593 (2009)



**FUNDAMENTALS**  
and **APPLICATIONS**

**LIGHT**  
**MATTER** for  
**INTERACTIONS**

*biophysics*  
*biomedicine*  
*communications*  
*sensors*  
*devices*

**WORKSHOP** on  
**PHOTONICS**

*Kopaonik*

**11.3-14.3.2018.**

*Organizers!*

*Sponsors*





UNIVERZITET U BEOGRADU  
Institut za fiziku



Konferencija  
**Jedanaesta radionica fotonike  
(2018)**

**Zbornik apstrakata**

Kopaonik, 11–14.3.2018.

# Photon interaction with (bio)molecules - Near-edge X-ray absorption fine-structure (NEXAFS) spectroscopy

Bratislav P. Marinković, Sanja D. Tošić

*Institute of Physics Belgrade, University of Belgrade, Pregrevica 118, 11080 Belgrade, Serbia*

**Contact:** B.P. Marinković ([bratislav.marinkovic@ipb.ac.rs](mailto:bratislav.marinkovic@ipb.ac.rs))

**Abstract.** Binary collisions of molecules with energy selected atomic particles (photons, electrons, ions) are an ideal tool for determining the structure of molecules and ascertaining their behaviour in the surrounding. Some of the experimental techniques that probe the inner shell molecular structure include Auger ejected electron spectroscopy [1] or Near-edge X-ray absorption fine-structure (NEXAFS) spectroscopy [2]. In NEXAFS an X-ray photon promotes an inner-shell electron to an unoccupied molecular orbital forming a core excited state. When the energy of photon equals to this difference the photoabsorption cross section (PAXC) is enhanced i.e. exhibits the resonant behaviour. In the case when a molecule comprises of atoms of the same kind but having different surrounding atoms, the chemical shift is introduced in the PAXC. Owing to this, the fundamental mechanisms of the fragmentation of different isomers could be elucidated [3].

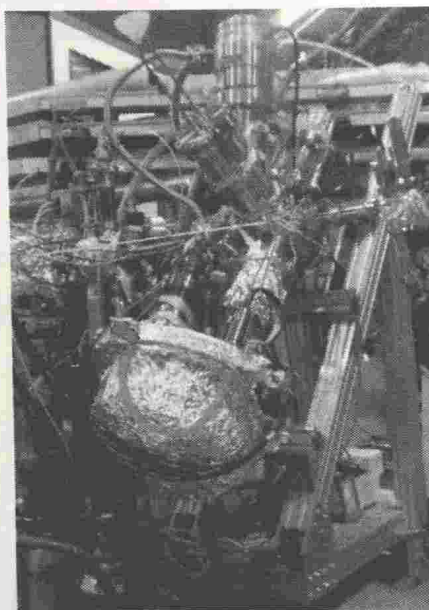


Figure 1. The photoelectron - photoion coincidence (PEPICO) spectrometer at the Gas Phase photoemission beamline of the Elettra synchrotron radiation facility. The electron energy hemispherical analyser (blue) and the time of flight mass spectrometer are mounted opposite to each other at the interaction region, where the vapor beam (light blue) and the photon beam (red) cross each other. [according to 3]

At the GasPhase beamline of the Elettra synchrotron facility in Trieste we have investigated several classes of molecules: halo-pyrimidines; nitroimidazoles, and halothane. The results of mass spectrometry as well as photoelectron-photoion and photoion-photoion coincidence spectroscopy display striking differences in the radiation-induced decomposition.

## REFERENCES

- [1] J. J. Jureta, B. P. Marinković, L. Avaldi, *Eur. Phys. J. D* **70** (2016) 199 [15pp].
- [2] A. R. Milosavljević, A. Giuliani, C. Nicaolas, *Gas-Phase Near-Edge X-ray Absorption Fine Structure (NEXAFS) Spectroscopy of Nanoparticles, Biopolymers and Ionic Species*, in *Nanoscience and Nanotechnology* Vol.5, Springer-Verlag, Berlin, Heidelberg (2016) pp.451-505.
- [3] P. Bolognesi, A. R. Casavola, A. Cartoni, R. Richter, P. Markus, S. Borocci, J. Chiarinelli, S. Tošić, H. Sa'adeh, M. Masič, B. P. Marinković, K. C. Prince and L. Avaldi, *J. Chem. Phys.* **145** (2016) 191102 [5pp].

[< BACK TO SEARCH RESULTS](#)

# Citation Report

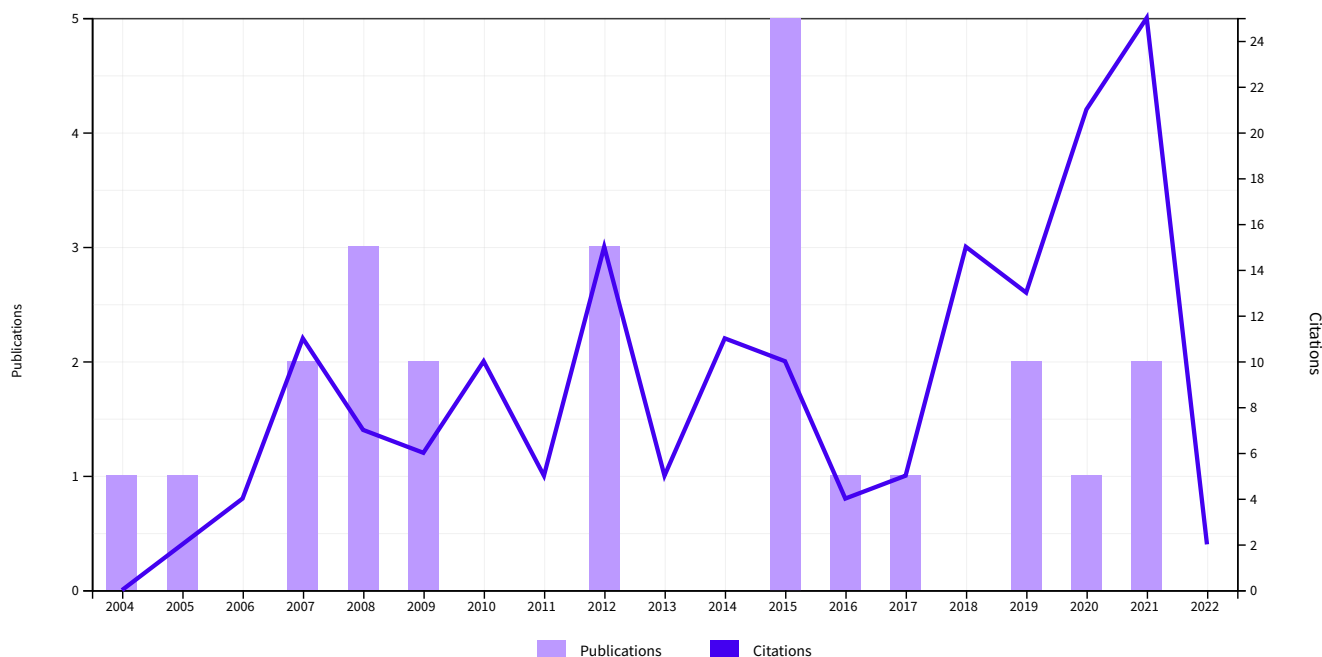
Analyze Results

[Export Full Report](#)

<p><b>Publications</b></p> <p><b>24</b></p> <p>Total</p> <p>From 1996 ▾ to 2022 ▾</p>	<p><b>Citing Articles</b></p> <p><b>115</b> <a href="#">Analyze</a></p> <p>Total</p> <p><b>99</b> <a href="#">Analyze</a></p> <p>Without self-citations</p>	<p><b>Times Cited</b></p> <p><b>171</b></p> <p>Total</p> <p><b>134</b></p> <p>Without self-citations</p>	<p><b>7.13</b></p> <p>Average per item</p>	<p><b>9</b></p> <p>H-Index</p>
---	---	--	--	--------------------------------


Times Cited and Publications Over Time

[DOWNLOAD ▾](#)



24 Publications	Citations							Average per year	Total
	Sort by: Citations: highest first ▾								
	< 1 of 1 >								
	2018	2019	2020	2021	2022				
<b>Total</b>	15	13	21	25	2			9.5	171
1 <a href="#">Site- and state-selected photofragmentation of 2Br-pyrimidine</a> <i>Bolognesi, P; Kettunen, JA; (...); Avaldi, L</i> 2015   <i>PHYSICAL CHEMISTRY CHEMICAL PHYSICS</i> 17 (37), pp.24063-24069	5	2	4	8	0			2.75	22
<a href="#">Elastic electron scattering by silver atom</a>	2	0	1	2	0			1.36	34

2	<a href="#">Tosic, SD; Kelemen, VI</a> ; (...); <a href="#">Marinkovic, BP</a> 4th Conference on Elementary Processes in Atomic Systems Jan 2009   <a href="#">NUCLEAR INSTRUMENTS &amp; METHODS IN PHYSICS RESEARCH SECTION B-BEAM INTERACTIONS WITH MATERIALS AND ATOMS</a> 267 (2) , pp.283-287							
3	Experimental and theoretical study of the elastic-electron-indium-atom scattering in the intermediate energy range <a href="#">Rabasovic, MS; Kelemen, VI</a> ; (...); <a href="#">Marinkovic, BP</a> Jun 2008   <a href="#">PHYSICAL REVIEW A</a> 77 (6)	0	0	2	1	0	1.13	17
4	Elastic electron scattering by a Pb atom <a href="#">Tosic, SD; Rabasovic, MS</a> ; (...); <a href="#">Marinkovic, BP</a> Jan 2008   <a href="#">PHYSICAL REVIEW A</a> 77 (1)	2	2	1	0	0	1.13	17
5	Communication: "Position" does matter: The photofragmentation of the nitroimidazole isomers <a href="#">Bolognesi, P; Casavola, AR</a> ; (...); <a href="#">Avaldi, L</a> Nov 21 2016   <a href="#">JOURNAL OF CHEMICAL PHYSICS</a> 145 (19)	2	5	4	2	0	2.14	15
6	Differential and integrated cross sections for the elastic electron scattering by calcium atom <a href="#">Milisavljevic, S; Sevic, D</a> ; (...); <a href="#">Marinkovic, BP</a> Jul 28 2005   <a href="#">JOURNAL OF PHYSICS B-ATOMIC MOLECULAR AND OPTICAL PHYSICS</a> 38 (14) , pp.2371-2384	0	3	2	0	0	0.83	15
7	Differential and integrated cross sections for the electron excitation of the 4 P-1(o) state of calcium atom <a href="#">Milisavljevic, S; Sevic, D</a> ; (...); <a href="#">Marinkovic, BP</a> Sep 28 2004   <a href="#">JOURNAL OF PHYSICS B-ATOMIC MOLECULAR AND OPTICAL PHYSICS</a> 37 (18) , pp.3571-3581	1	1	0	0	0	0.74	14
8	Electron collisions by metal atom vapours <a href="#">Marinkovic, BP; Pejcev, V</a> ; (...); <a href="#">Predojevic, B</a> 3rd Conference on Elementary Processes in Atomic Systems Mar 2007   <a href="#">RADIATION PHYSICS AND CHEMISTRY</a> 76 (3) , pp.455-460	1	0	1	2	0	0.69	11
9	Absolute differential cross sections for electron excitation of silver at small scattering angles <a href="#">Tosic, SD; Pejcev, V</a> ; (...); <a href="#">Marinkovic, BP</a> 5th International Conference on Elementary Processes in Atomic Systems (CEPAS) May 15 2012   <a href="#">NUCLEAR INSTRUMENTS &amp; METHODS IN PHYSICS RESEARCH SECTION B-BEAM INTERACTIONS WITH MATERIALS AND ATOMS</a> 279 , pp.53-57	1	0	0	2	0	0.82	9
10	Electron impact excitation of the 6s S-2(1/2) state of In atom at small scattering angles <a href="#">Rabasovic, MS; Tosic, SD</a> ; (...); <a href="#">Marinkovic, BP</a> 4th Conference on Elementary Processes in Atomic Systems Jan 2009   <a href="#">NUCLEAR INSTRUMENTS &amp; METHODS IN PHYSICS RESEARCH SECTION B-BEAM INTERACTIONS WITH MATERIALS AND ATOMS</a> 267 (2) , pp.279-282	0	0	1	0	0	0.57	8
11	Excitation of the 6p7s P-3(0.1) states of Pb atoms by electron impact: Differential and integrated cross sections <a href="#">Milisavljevic, S; Rabasovic, MS</a> ; (...); <a href="#">Marinkovic, BP</a> Aug 2007   <a href="#">PHYSICAL REVIEW A</a> 76 (2)	0	0	1	0	0	0.5	8
12	Roadmap on dynamics of molecules and clusters in the gas phase <a href="#">Zettergren, H; Domaracka, A</a> ; (...); <a href="#">Petrignani, A</a> May 2021   <a href="#">EUROPEAN PHYSICAL JOURNAL D</a> 75 (5)	0	0	0	2	2	2	4
13	Radiation Damage Mechanisms of Chemotherapeutically Active Nitroimidazole Derived Compounds <a href="#">Chlarinelli, J; Casavola, AR</a> ; (...); <a href="#">Avaldi, L</a> May 14 2019   <a href="#">FRONTIERS IN CHEMISTRY</a> 7	0	0	2	1	0	0.75	3

14	<p><a href="#">Core Shell Investigation of 2-nitroimidazole</a>  <a href="#">Bolognesi, P;</a> <a href="#">Carravetta, V;</a> (...); <a href="#">Avaldi, L</a>            Apr 2 2019   <a href="#">FRONTIERS IN CHEMISTRY</a> 7</p>	0	0	2	1	0	0.75	3
15	<p><a href="#">Electron-impact excitation of silver</a>  <a href="#">Tosic, SD;</a> <a href="#">Pejcev, V;</a> (...); <a href="#">Marinkovic, BP</a>            May 11 2015   <a href="#">PHYSICAL REVIEW A</a> 91 (5)</p>	1	0	0	1	0	0.25	2
16	<p><a href="#">Electron-impact excitation of the (4d(10)5s) S-2(1/2)-&gt; (4d(9)5s(2)) D-2(3/2) and (4d(10)6s) S-2(1/2) -&gt;(4d(10)6s) 2S(1/2) transitions in silver: Experiment and theory</a>  <a href="#">Marinkovic, BP;</a> <a href="#">Tosic, SD;</a> (...); <a href="#">Brunger, MJ</a>            Aug 10 2021   <a href="#">PHYSICAL REVIEW A</a> 104 (2)</p>	0	0	0	1	0	0.5	1
17	<p><a href="#">Inner shell photofragmentation of 2Cl-pyrimidine studied by mass spectrometry and electron-ion coincidence experiments</a>  <a href="#">Bolognesi, P;</a> <a href="#">Kettunen, A;</a> (...); <a href="#">Avaldi, L</a>            Dec 28 2020   <a href="#">JOURNAL OF PHYSICS B-ATOMIC MOLECULAR AND OPTICAL PHYSICS</a> 53 (24)</p> <p> Enriched Cited References</p>	0	0	0	1	0	0.33	1
18	<p><a href="#">Selectivity in the photofragmentation of halo-pyrimidines</a>  <a href="#">Bolognesi, P;</a> <a href="#">Kettunen, A;</a> (...); <a href="#">Avaldi, L</a>            29th International Conference on Photonic, Electronic, and Atomic Collisions (ICPEAC) 2015   XXIX INTERNATIONAL CONFERENCE ON PHOTONIC, ELECTRONIC, AND ATOMIC COLLISIONS (ICPEAC2015), PTS 1-12 635</p>	0	0	0	1	0	0.13	1
19	<p><a href="#">Measurements of differential cross sections for elastic electron scattering and electronic excitation of silver and lead atoms</a>  <a href="#">Tosic, SD</a>            26th Summer School and International Symposium on the Physics of Ionized Gases (SPIG) 2012   26TH SUMMER SCHOOL AND INTERNATIONAL SYMPOSIUM ON THE PHYSICS OF IONIZED GASES (SPIG 2012) 399</p>	0	0	0	0	0	0.09	1
20	<p><a href="#">"Position" does matter : the photofragmentation of the nitroimidazole isomers</a>  <a href="#">Chiarinelli, J;</a> <a href="#">Bolognesi, P;</a> (...); <a href="#">Avaldi, L</a>            30th International Conference on Photonic, Electronic, and Atomic Collisions (ICPEAC) 2017   XXX INTERNATIONAL CONFERENCE ON PHOTONIC, ELECTRONIC, AND ATOMIC COLLISIONS (ICPEAC2017) 875</p>	0	0	0	0	0	0	0
21	<p><a href="#">Cross section set and transport properties of Ne+ in CF4</a>  <a href="#">Raspopovic, Z;</a> <a href="#">Nikitovic, Z;</a> (...); <a href="#">Stojanovic, V</a>            29th International Conference on Photonic, Electronic, and Atomic Collisions (ICPEAC) 2015   XXIX INTERNATIONAL CONFERENCE ON PHOTONIC, ELECTRONIC, AND ATOMIC COLLISIONS (ICPEAC2015), PTS 1-12 635</p>	0	0	0	0	0	0	0
22	<p><a href="#">Electron scattering by silver: excitation of the 4d(9)5s(2) D-2(3/2) and 4d(10)6s S-2(1/2) states</a>  <a href="#">Tosic, SD;</a> <a href="#">Pejcev, V;</a> (...); <a href="#">Marinkovic, BP</a>            29th International Conference on Photonic, Electronic, and Atomic Collisions (ICPEAC) 2015   XXIX INTERNATIONAL CONFERENCE ON PHOTONIC, ELECTRONIC, AND ATOMIC COLLISIONS (ICPEAC2015), PTS 1-12 635</p>	0	0	0	0	0	0	0
23	<p><a href="#">Excitation of silver by electron impact</a>  <a href="#">Tosic, SD;</a> <a href="#">Pejcev, V;</a> (...); <a href="#">Stauffer, AD</a>            27th International Conference on Photonic, Electronic and Atomic Collisions (ICPEAC) 2012   XXVII INTERNATIONAL CONFERENCE ON PHOTONIC, ELECTRONIC AND ATOMIC COLLISIONS (ICPEAC 2011), PTS 1-15 388</p>	0	0	0	0	0	0	0
24	<p><a href="#">ELECTRON IMPACT EXCITATION OF Ag ATOM: ENERGY-LOSS SPECTROSCOPY</a>  <a href="#">Tosic, SD;</a> <a href="#">Sevic, D;</a> (...); <a href="#">Marinkovic, BP</a>            24th Summer School and International Symposium on Physics of Ionized Gases 2008   24TH SUMMER SCHOOL AND INTERNATIONAL SYMPOSIUM ON THE PHYSICS OF IONIZED GASES, CONTRIBUTED PAPERS (84) , pp.49-52</p>	0	0	0	0	0	0	0

Citation Report Publications Table



© 2021 Clarivate  
Training Portal  
Product  
Support

Data Correction  
Privacy  
Statement  
Newsletter

Copyright  
Notice  
Cookie Policy  
Terms of Use

Manage cookie  
preferences

Follow  
Us

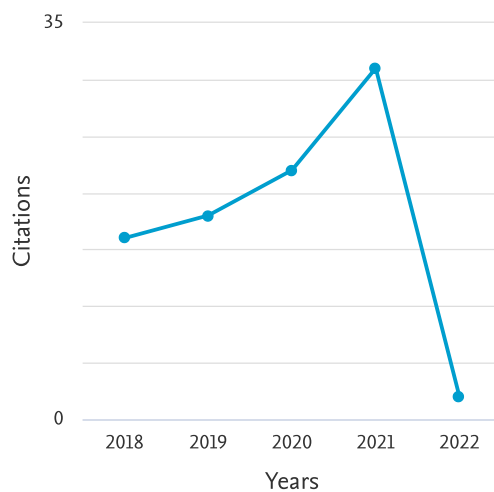




# Citation overview

[← Back to document results](#)[↗ Export](#) [Print](#)

This is an overview of citations for the documents you've selected.


Document *h*-index : 9 [View \*h\*-graph](#)24 cited documents [+ Add to list](#)Date range:  to   Exclude self citations of all authors  Exclude citations from books [Update](#)Sort on: [▼](#) Page [Remove](#)

Documents	Citations		<2018	2018	2019	2020	2021	2022	Subtotal	>2022	Total
<input type="checkbox"/> 1	Electron-impact excitation of the (4d105s) S1/2 2 →(4d95s2) ...	2021					1		1		1
<input type="checkbox"/> 2	Roadmap on dynamics of molecules and clusters in the gas pha...	2021					2	1	3		3
<input type="checkbox"/> 3	Inner shell photofragmentation of 2Cl-pyrimidine studied by ...	2020					1		1		1
<input type="checkbox"/> 4	Radiation damage mechanisms of chemotherapeutically active n...	2019				1	3		4		4
<input type="checkbox"/> 5	Core shell investigation of 2-nitroimidazole	2019				2	1		3		3
<input type="checkbox"/> 6	"position" does matter : the photofragmentation of the nitro...	2017							0		0
<input type="checkbox"/> 7	Communication: "Position" does matter: The photofragmentatio...	2016	2	2	7	3	3	1	16		18
<input type="checkbox"/> 8	Selectivity in the photofragmentation of halo-pyrimidines	2015					1		1		1
<input type="checkbox"/> 9	Electron scattering by silver: Excitation of the 4d <sup>9</sup>	2015							0		0
<input type="checkbox"/> 10	Site- and state-selected photofragmentation of 2Br-pyrimidin...	2015	4	5	2	4	8		19		23

			Total	121	16	18	22	31	2	89	0	210
<input type="checkbox"/>	11	Electron-impact excitation of silver	2015		1			1		2		2
<input type="checkbox"/>	12	Absolute differential cross sections for electron excitation...	2012	6	1			2		3		9
<input type="checkbox"/>	13	Measurements of differential cross sections for elastic elec...	2012	1		1				1		2
<input type="checkbox"/>	14	Excitation of silver by electron impact	2012							0		0
<input type="checkbox"/>	15	Electron impact excitation of the $6s\ ^2S_{1/2}$	2009	8			1			1		9
<input type="checkbox"/>	16	Elastic electron scattering by silver atom	2009	18	2		1	2		5		23
<input type="checkbox"/>	17	Experimental and theoretical study of the elastic-electron-i...	2008	15			2	1		3		18
<input type="checkbox"/>	18	Elastic electron scattering by a Pb atom	2008	12	2	3	1	1		7		19
<input type="checkbox"/>	19	Excitation of the $6p7s\ P\ 0,1\ 3$ states of Pb atoms by electro...	2007	7			1			1		8
<input type="checkbox"/>	20	Cross section data for electron collisions in plasma physics	2007	3	1		2	2		5		8
<input type="checkbox"/>	21	Electron-impact excitation of the $6p7s\ P13$ state of Pb atom ...	2007	9		1	1			2		11
<input type="checkbox"/>	22	Electron collisions by metal atom vapours	2007	7	1		1	2		4		11
<input type="checkbox"/>	23	Differential and integrated cross sections for the elastic e...	2005	12		3	2			5		17
<input type="checkbox"/>	24	Differential and integrated cross sections for the electron ...	2004	17	1	1				2		19

Display:   results per page

1

 Top of page

## About Scopus

[What is Scopus](#)

[Content coverage](#)

[Scopus blog](#)

[Scopus API](#)

[Privacy matters](#)

## Language

[日本語に切り替える](#)

[切换到简体中文](#)

[切换到繁體中文](#)

[Русский язык](#)

## Customer Service

[Help](#)

[Tutorials](#)

[Contact us](#)

---

## ELSEVIER

[Terms and conditions](#) ↗ [Privacy policy](#) ↗

Copyright © Elsevier B.V. ↗. All rights reserved. Scopus® is a registered trademark of Elsevier B.V.

We use cookies to help provide and enhance our service and tailor content. By continuing, you agree to the use of cookies.



Број: 660-01-00006/462  
27.04.2018. године  
Београд

ИНСТИТУТ ЗА ФИЗИКУ			
ПРИМЉЕНО: 11-06-2018			
Рад.јед.	б р о ј	Арх.шифра	Прилог
0801	845/1		

На основу члана 22. став 2. члана 70. став 4. и члана 86. ст. 1. и 2. Закона о научноистраживачкој делатности ("Службени гласник Републике Србије", број 110/05 и 50/06 – исправка, 18/10 и 112/15), члана 3. ст. 1. и 3., члана 32. став 1., члана 35. став 1. и члана 40. Правилника о поступку, начину вредновања и квантитативном исказивању научноистраживачких резултата истраживача ("Службени гласник Републике Србије", број 24/16, 21/17 и 38/17) и захтева који је поднео

*Инстџиуџ за физику у Београду*

Комисија за стицање научних звања на седници одржаној 26.04.2018. године, донела је

**ОДЛУКУ  
О СТИЦАЊУ НАУЧНОГ ЗВАЊА**

**Др Сања Тошић**  
стиче научно звање  
**Научни сарадник**  
Реизбор

у области природно-математичких наука - физика

**О Б Р А З Л О Ж Е Њ Е**

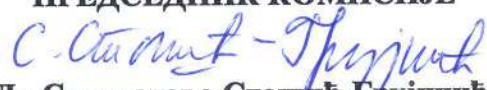
*Инстџиуџ за физику у Београду*

утврдио је предлог број 988/1 од 18.07.2017. године на седници Научног већа Института и поднео захтев Комисији за стицање научних звања број 1003/1 од 20.07.2017. године за доношење одлуке о испуњености услова за реизбор у научно звање **Научни сарадник**.

Комисија за стицање научних звања је по претходно прибављеном позитивном мишљењу Матичног научног одбора за физику на седници одржаној 26.04.2018. године разматрала захтев и утврдила да именована испуњава услове из члана 70. став 4. и члана 86. ст. 1. и 2. Закона о научноистраживачкој делатности ("Службени гласник Републике Србије", број 110/05 и 50/06 – исправка, 18/10 и 112/15), члана 3. ст. 1. и 3., члана 32. став 1., члана 35. став 1. и члана 40. Правилника о поступку, начину вредновања и квантитативном исказивању научноистраживачких резултата истраживача ("Службени гласник Републике Србије", број 24/16, 21/17 и 38/17) за реизбор у научно звање **Научни сарадник**, па је одлучила као у изреци ове одлуке.

Доношењем ове одлуке именована стиче сва права која јој на основу ње по закону припадају.

Одлуку доставити подносиоцу захтева, именованој и архиви Министарства просвете, науке и технолошког развоја у Београду.

**ПРЕДСЕДНИК КОМИСИЈЕ**  
  
Др Станислава Стојић-Грујић,  
научни саветник

**МИНИСТАР**  
  
Младен Шарчевић





*Ministero degli Affari Esteri  
e della Cooperazione Internazionale*

## Domanda di contributo (L. 401/90)

Identificativo	<b>PGR00220</b>
Anno	<b>2016</b>
Paese	<b>Serbia</b>

*Elementi generali*

Macrosettore	<b>Basic Sciences</b>
Titolo (in Italiano)	<b>Una visione nanoscopica dell'interazione di radiazione con sistemi biologici</b>
Titolo (in altra lingua)	<b>A nanoview of radiation-biomatter interaction</b>
Parola chiave #1	<b>Radiation damage on biomolecules/radiosensitisers</b>
Parola chiave #2	<b>Mass spectrometry of nano clusters</b>
Parola chiave #3	<b>ElectroSpray Ionisation source</b>

*Ente proponente italiano*

Struttura	<b>CNR</b>
Dp./Ist.	<b>Istituto di Struttura della Materia, Cds 087.001</b>
Indirizzo	<b>CNR-ISM, Area della Ricerca di Roma 1, Via Salaria, Km. 29,300</b>
C.A.P.	<b>00015</b>
Città	<b>Monterotondo Scalo (Roma)</b>
Telefono	<b>06-90672218</b>
Fax	<b>06-90672238</b>
Ente pubblico	<b>Sì</b>
Codice fiscale	<b>80054330586</b>
Partita IVA	<b>02118311006</b>
IBAN, PER I SOLI PROPONENTI SPROVVISTI DI UN CONTO DI TESORERIA	<b>IT12H0100003245348300167369</b>
Banca	<b>BANCA D'ITALIA - ROMA TESORERIA PROV.LE STATO VIA MILANO, 60G 00100 ROMA(RM)</b>
Conto Tesoreria	
Località	

*Responsabile scientifico italiano*

Titolo	<b>Dr.</b>
Cognome	<b>BOLOGNESI</b>
Nome	<b>PAOLA</b>
Qualifica	<b>Ricercatore</b>

Indirizzo	<b>CNR-ISM, Area della Ricerca di Roma 1, Via Salaria, Km. 29,300</b>
C.A.P.	<b>00015</b>
Città	<b>Monterotondo Scalo (Roma)</b>
Telefono	<b>06-90672218</b>
Fax	<b>06-90672238</b>
Cellulare	<b>3492582058</b>
Email principale	<b>paola.bolognesi@cnr.it</b>
Email secondaria	<b>paola.bolognesi@ism.cnr.it</b>

C.V.

Paola Bolognesi (PhD in Physics 1999, Manchester University, UK) is CNR Researcher, member of the Molecular Dynamics group (ISM,Rome), since 2001.

In her career she has been involved, initially as participant and then as PI, in many national (PRIN,FIRB) and international (FP7,Marie Curie grants,COST actions, Galileo program, Bilateral initiatives) projects and successful beamtime applications at Large Scale Infrastructures (Synchrotron, IonBeam and FEL sources). She has been visiting scientist in international labs (Daresbury,Paris, Caen,Sendai, Stanford). This has allowed developing her expertise in atomic and molecular spectroscopy and dynamics of photon/ion/electron interaction with species of increasing complexity. Her interests span from the characterization of electron correlations in atoms and molecules to the study of collective excitations in highly symmetric systems like fullerenes or the mass spectrometry of environmental species. Now she is leading the activity of the group for the study of the nanoscale processes in radiation damage and functioning of sensitizer molecules used in radiotherapy.

Her scientific activity is witnessed by more than 100 publications in int. journals of high IF, 17 oral presentations at Int. Conferences and many seminars. She is ViceChair of the XLIC COST and active participant of another COST in the field of radiation damage and nanoscopic approach to biology. She serves as referee for many journals of high IF,has been external evaluator of several PhD thesis, tutor of PhD students and postdocs and evaluator for international laboratories (Canadian Light Source) and funding agencies (FWO, Netherlands).

#### Publicazioni

[1] M.C. Castrovilli, P. Bolognesi, A. Cartoni, D. Catone, P. O'Keeffe, A.Casavola, S. Turchini, N. Zema, L. Avaldi  
Photofragmentation of halogenated pyrimidine molecules in the VUV range  
J. Am. Soc. Mass Spectrom. 25 (2014) 351

[2] Murphy et al 'Buckyball Explosion by Intense Femtosecond X-Ray Pulses: A Model System for Complex Molecules'  
Nature Communications 5 (2014) 4281

[3] E. Sokell, P. Bolognesi, A. Kheifets, I. Bray, S. Safgren and L. Avaldi  
Signature of two-electron interference in angular resolved double photoionization of Mg  
Phys. Rev. Lett. 110 (2013) 083001

[4] P. Bolognesi, P. O'Keeffe and L. Avaldi 'Soft X-ray interaction with organic molecules of biological interest', Chapter X in 'RadiationDamage In Biomolecular Systems', SpringerVerlag (2012), G. Garcia and M.C. Fuss, ed.

[5] P. Bolognesi, G. Mattioli, P. O'Keeffe, V. Feyer, O. Plekan, E. Ovcharenko, K. Prince, M. Coreno, A. Amore Bonapasta and L. Avaldi  
Investigation of halogenated pyrimidines by X-ray photoemission spectroscopy and theoretical DFT methods.  
J. Phys. Chem. A 113 (2009) 13593

#### *Ente proponente straniero*

Denominazione	<b>Institute of Physics, University of Belgrade (IPB)</b>
Indirizzo	<b>Pregrevica 118,11080 Belgrade</b>
Telefono	<b>+381 11 37 1 3007</b>
Fax	<b>+381 11 31 62 190</b>
Ente pubblico	<b>Sì</b>

#### *Responsabile scientifico straniero*

Cognome	<b>Tosic</b>
Nome	<b>Sanja</b>
Qualifica	<b>Research Assistant Professor</b>
Email	<b>seka@ipb.ac.rs</b>

C.V.

Sanja Tosic (PhD in Physics 2012, Faculty of Physics, University of Belgrade, Serbia) is experimental physicist working in the Laboratory for Atomic Collision Processes at the Institute of Physics Belgrade, Serbia. She has been involved in many national and international projects (COST MP1002 Nano-IBCT, COST CM1204 XLIC, bilateral research projects) and has a successful cooperation with several experimental and theoretical research groups (Roma, Canberra, Toronto, Uzhgorod, Roorkee). Her scientific activity was initially focused on the study of atomic collision processes technique of crossed beams, through the study of the scattering of electrons in complex atomic targets (Ca, Pb, In, Ag). Her present interests are in basic processes on molecules of biological interest (research based on electron -atom/molecule interactions, combined investigation on electron scattering and soft X-ray absorption by biomolecules etc). The obtained results she has

published in international journals of high IF, invited lectures and contributions at the international and national conferences and seminars. She was a member of the Organizing Committees of the several conferences (20th SPIG 2006, 1st CEAMPP 2008, 5th CEPAS 2011, 2nd CEAMPP 2011, 27thSPIG 2014, WG2 Expert meeting on biomolecules 2015). She has also worked as an author of problems for high school students contest at Serbian Physical Society.

---

## Publicazioni

1. S.D. Tošić, V. Pejčev, D. Šević, R.P. McEachran, A.D. Stauffer, B.P. Marinkovic  
Electron-impact excitation of silver  
Phys. Rev. A 91(2015)052703
2. P. Bolognesi, M.C. Castrovilli, A. Kettunen, A. Cartoni, R. Richter, S. Tosić, S. Maclot, P. Rousseau, R. Delaunay, A. Domaracka, B. Huber, L. Avaldi,  
Fragmentation of halopyrimidines and halouracils by photoionization and ion impact  
Proc. WG2 Expert Meeting on Biomolecules, COST CM1204, XLIC - XUV/X-ray Light and fast Ions for ultrafast Chemistry, April 27-30, 2015, Book of Abstracts, Eds. P. Bolognesi and A. Milosavljević, Invited Talk, p.41.
3. S.D. Tošić, V. Pejčev, D. Šević, R.P. McEachran, A.D. Stauffer, B.P. Marinkovic  
Integrated Cross Sections for Electron Excitation of the 4d105p State of the Ag Atom  
Proc. 27th Summer School and Int. Symp. on Physics of Ionized Gases – SPIG 2014, 26th - 29th August 2014, Belgrade, Serbia, Contributed Papers & Abstracts of Invited Lectures, Topical Invited Lectures, Progress Reports and Workshop Lectures, (IOP Belgrade and SASA, Belgrade, Serbia), pp.46-49.  
ISBN: 978-86-7762-600-6.
4. S.D. Tošić, V. Pejčev, D. Šević, R.P. McEachran, A.D. Stauffer, B.P. Marinkovic  
Absolute differential cross sections for electron excitation of silver at small scattering angles  
Nucl. Instrum. Meth. B. 279(2012)53
5. S.D. Tošić, V.I. Kelemen, D. Šević, V. Pejčev, D. M. Filipovic, E. Yu. Remeta, B.P. Marinkovic  
Elastic electron scattering by silver atom  
Nucl. Instrum. Meth. B 267(2009)28

---

## *Descrizione delle attività in programma*

### Sintesi del progetto

A key development in the study of radiation damage has been triggered by the understanding that macroscopic alterations are originated at the microscopic scale, where processes involving the elementary constituents are the same studied in molecular physics. The advent of new radiation sources and instrumentation that allow to 'image molecules at work', discloses the possibility to determine how matter functions during chemical reactions and biological processes. This, for example, has led to the establishment of the European Cost MP1002 'Nanoscale insights into Ion Beam Cancer Therapy', just concluded, which aimed "to combine, using a multiscale approach, the unique experimental and theoretical expertise available within Europe to acquire greater insight at the nanoscopic and molecular level into radiation damage induced by ion impact". The proponent groups represented their respective countries in the managing committee of the Action and via this proposal would like to reinforce their common interests. Both groups have established experience on the detection of charged particles produced by the interaction of radiation with building blocks of life molecules using laboratory sources and synchrotron radiation. The Italian team has the scientific responsibility of the atomic and molecular physics programs at the synchrotron Elettra since 1994 and the Serbian team has complementary expertise in electron collision experiments. Now they intend to exploit new opportunities to study the structure and dynamics of complex biomolecules isolated, embedded in homogeneous or hydrated clusters as well as in interaction with radiotherapy drugs. The project, which is organized in two parts, one devoted to the study basic processes in benchmark molecules using existing instrumentation and the other one to the development of new techniques to produce beams of nanoaggregates will be the seed of an Italian-Serbian scientific platform for nanoscale insight into radiation damage.

---

### Obiettivi fissati per l'anno 2016

The main objective of the project for the first year is to share the expertise of the two groups to study a) basic processes in benchmark molecules and in b) biomolecules of increasing complexity developing new instrumentation and methods.

a) Basic processes in benchmark molecules.

The basic mechanisms of radiation damage will be investigated using electrons (Belgrade), VUV (Rome) and soft-X ray (Trieste). Photoionisation and photofragmentation experiments of nitroimidazole radiosensitisers will be performed at Elettra to unravel basic mechanisms of functioning of this class of molecules and to explain the fundamental reasons of the diverse effectiveness of the different members of the family. Similar studies will be performed on halopyrimidines, another class of radiosensitiser. A VUV lab source will be equipped with an oven source, and used to perform off-line tests to characterize the evaporation conditions of the biomolecules.

b) New instrumentation and methods to study nanoaggregates of increasing complexity.

In the study of gas phase biomolecules as well as in their potential applications to nanomedicine and material science, the thermal evaporation to produce the target beam quickly reaches its limit of feasibility. This occurs already at the level of nucleosides and some amino acids, due to their thermal lability. To move forwards in the study of larger and more realistic systems, the goal is to consider biomolecules embedded in clusters as well as their selective deposition. The challenge is the construction of a multipurpose setup based on the use of an ElectronSprayIonization, ESI, source for the production of the species. During this first year, a non-commercial ESI will be set-up and characterized. This activity will benefit of the complementary expertise from the group of Belgrade, which has already experience in the handling of a similar source.

---

## Gruppo di ricerca e metodologia prevista

### a) Basic processes in benchmark molecules.

The experimental setups of the two teams are complementary. The Italian group has electro-electron and electron-ion coincidence spectrometers in the lab in Rome and at Elettra, the Serbian group operates low energy spectrometers with high energy/angular resolutions in the Belgrade lab. Together, they will tackle nanoscale investigations of radiation damage from different facets and with different ionizing sources.

Ionizing radiation damages a biological tissue mainly via secondary electrons produced by interaction of the radiation with the cells. Thus most of the attention is paid to investigate the electron interaction with basic components of a biological sample. The Serbian team will run electron impact experiments covering the range of low incident energies, where mainly electron capture in temporary negative ion resonances occurs. Angle resolved experiments, in addition, will provide a more complete data set to simulation codes of radiation damage used to determine dose delivery to biological tissues in radiotherapy. The ability to manipulate selective bond cleavage offers unique chances to manage the local physics and chemistry. Inner shell photo-excitation/ionization are suitable candidates for a selective bond cleavage because core electrons are localized near a particular atom. The two team jointly will exploit the properties of tunable synchrotron radiation in combination with techniques where ions and electrons are time correlated, to provide unprecedented information on the photofragmentation of biomolecules. This approach, supported by theoretical calculation performed by some members of the Italian team, will be applied to nitroimidazole, studying their site- and state-selected photon induced fragmentation as function of the position of the nitro substituent, NO<sub>2</sub>. The purpose is to characterise the radiation damage as well as the radiosensitising mechanisms of this class of radiosensitisers, and to compare them with the mechanisms already identified in halopyrimidines and halouracils. Recent collaborations with the group at Ganil (Caen) via the Italian-French program Galileo and the COST nanoIBCT has opened up the possibility to study radiation damage induced by ion impact. This allows on one hand to investigate different fragmentation mechanisms to be compared with the ones active in photon absorption, and on the other hand to simulate the conditions used in hadron therapy near the Bragg peak via proper choice of the incident ions and energy.

### b) New instrumentation and methods for the study of nanoaggregates of increasing complexity.

Biomolecular nanoaggregates and nanoparticles (NP) find more and more applications in future enabling technologies from medicine to bioelectronics. Among others, halosubstituted DNA bases and NP are very promising radiosensitisers, but their basic mechanisms of functioning at the nanoscale still await explanations. The study of these elementary processes suffers by the fact that even simple biomolecules are impossible to obtain in the gas phase by thermal evaporation. The combination of ESI and mass spectrometry will overcome this limit allowing also the investigation of the effects of nanohydration, disentangling the role of the environment on the radiosensitizing mechanisms. The Rome group is building a setup consisting of an ESI source, transport and focus system of the ion beam, a quadrupole filter to mass-select the produced species and a trap to store and ionize them. The products will be analyzed by an orthogonal TOF. Natural biomolecules of increasing complexity (nucleosides, nucleotides and oligonucleotide), isolated or nanosolvated as well as drugs used in radiotherapy (gemcitabine, cisplatin and Au/Ag NP) will be studied, individually or in interaction. The same set-up can also be used for ESI-MS studies of nanoclusters (NC), i.e. NP with a size <2nm, a metallic core with less than 100 atoms and amazing properties.

---

## Fonti del cofinanziamento

The estimated cost of the project for CNR-ISM in 2016 is 56 k€. This will be covered by a co-funding from a CNR Progetto Premiale (26 k€). The group at IPB in Belgrade will fund the activity in their lab with a budget of approximately 10 k€.

---

## Risultati attesi

The expected scientific results (2016) are:

Multi differential Electron impact cross section of biomolecules in different energy ranges. These will extend the database that has been built within the European Cost Action MP1002 'Nanoscale insights into Ion Beam Cancer Therapy (Nano-IBCT)'. Investigation of the radiation damage mechanisms of 2 and 4(5)-nitroimidazole by photoemission, mass spectrometry and site- and state-selected photon induced fragmentation studies, complemented by theoretical calculations.

The expected technological results (2016) are:

Implementation and characterization of a high throughput ESI source, that will be subsequently expanded into a versatile and multipurpose laboratory setup for mass spectrometry of biomolecules, nanoaggregates, nanoparticles and nanoclusters produced by the ESI. Development of a technology to deposit biomaterials on a substrate by soft landing.

Training and dissemination (2016).

The collaboration will allow the training of early stage researchers and PhD students in sophisticated spectroscopic and spectrometric techniques with laboratory sources as well as with synchrotron radiation and ion beams available at international facilities, providing them the opportunity to face an interdisciplinary activity with the challenge to develop new instrumentation and methodology. The results of the joint activities will be presented in international conferences ECAMPXII, SPIG 2016 and MPS2016 as well as COST meetings.

---

## Continuazione di progetto già esistente:

## PIANO ECONOMICO - FINANZIARIO

TABELLA 1: PREVENTIVO				
DESCRIZIONE	Numero	Importo unitario (€)	Totale (€)	
a. Viaggi e soggiorni ricercatori stranieri in Italia	2	1.000	2.000	
b. Viaggi e soggiorni ricercatori italiani all'estero	2	750	1.500	
c. Prestazioni professionali e/o di terzi	0	0	0	
d. Contratti per personale non strutturato	1	20.000	20.000	
e. Organizzazione di workshops			0	
f. Pubblicazioni o altre forme di disseminazione			1.000	
g. Materiale consumabile			25.000	
h. Materiale inventariabile (max10% di TOTALE COSTI)			0	0,00%
i. Altro			1.500	
<b>SUBTOTALE COSTI</b>			<b>51.000</b>	
j. Costi per personale strutturato (min 30% - max 45% di TOTALE COSTI)			25.000	30,86%
k. Costi di gestione (max10% della somma SUBTOTALE COSTI + voce j)			5.000	6,58%
<b>TOTALE COSTI</b>			<b>81.000</b>	

TABELLA 2: FONTI DI FINANZIAMENTO		
DESCRIZIONE	IMPORTO (€)	%
A. Cofinanziamento Ente Proponente	30.000	37,04%
B. Cofinanziamento richiesto al MAECI	25.000	30,86%
C. Cofinanziamento Ente estero	0	0,00%
D. Cofinanziamento altro	26.000	32,10%
<b>TOTALE FINANZIAMENTI</b>		<b>81.000</b>

Specificare su quali voci della Tabella 1 sarà attribuito il cofinanziamento alle voci C. e D. della Tabella 2

Consumable, dissemination, partial support for Contratti per personale non strutturato.

(1) Elenco materiale non inventariabile

Maintenance of instruments (vacuum pumps, gauges, power supplies), vacuum components (flanges, vacuum gauges), chemicals and solvents, electrical components, detectors.

(2) Elenco materiale inventariabile

(3) Elenco altre spese

Travelling and living expenses of the members of the italian team for common activities of the italian and Serbian groups at Elettra.





Subject	From	Date	Size
Elettra: Proposal Review Panel evaluation and Beamtime Allocation	useroffice@elettra.eu	2018-06-11 15:28	4 KB

Select: Threads: Messages 1 to 1 of 1

**Subject Elettra: Proposal Review Panel evaluation and Beamtime Allocation**  
From useroffice@elettra.eu  
To seka@ipb.ac.rs  
Cc kevin.prince@elettra.eu, luca.gregoratti@elettra.eu, marcello.coreno@elettra.eu, robert.richter@elettra.eu, silvano.lizzit@elettra.eu  
Date 2018-06-11 15:28

You will receive this message until you access the following information in the VUO.

Dear Dr. Sanja TOSIC,

the peer review of the proposal you have submitted to Elettra in response to our last call has now been completed, and we are glad to inform you that your proposal has been awarded 30 operational shifts on the GASPHASE beamline, together with the related technical and organizational support. However we regret to inform you that your proposal has not been awarded ICTP support.

Details on the proposal evaluation process and on beamtime allocation can be found at: <https://vuo.elettra.eu>

1. Enter the site with your ID and password;
2. Click on the link "Already submitted proposals";
3. Select the proposal 20180158 to check the evaluation;
4. Check your evaluation in the box "Review Process Information";
5. Check the allocation dates in the box "Proposal Schedule".

Before your arrival all participants will have to submit an access request.

Please check the website:

<https://vuo.elettra.eu>

in the section "Access requests to Elettra laboratory".

# ELETTRA PROPOSAL DESCRIPTION

**Proposal number: 20180158**

**Title: Investigation of the fragmentation mechanisms of halogenated anesthetics**

Proposer: Sanja TOSIC

Beamline(s): GASPHASE

Required shifts: 30

Objectives: The photon induced radiation damage mechanisms of halogenated inhalational anesthetics sevoflurane, enflurane and isoflurane will be investigated by mass spectrometry and compared to the results already obtained for the other volatile anesthetics. The effect of photon interactions on these molecule systems will be studied both experimentally and theoretically. In combination with DFT calculations we will explain the fragmentation mass spectra and completely describe main fragmentation pathways including reactants, products, transition states, activation energies etc.

do not change anything above this line

## 1. Background

There are lot of forcing agents that dictate the direction and magnitude of the climate change. First of all, human activities result in the release of a large amount of different chemical compounds into the atmosphere which impact the environment and human health. So, substantial effort has been dedicated to assessing the direct and indirect impacts of human activities on climate. Global climate change is caused primarily by the increased atmospheric concentrations of the major long-lived greenhouse gases  $\text{CO}_2$ ,  $\text{CH}_4$ ,  $\text{N}_2\text{O}$  and halogenated organic compounds. In recent years, the attention towards halogenated anesthetics and their overall contribution to global climate change and the environment has increased [1,2]. The major atmospheric effects that may arise from emission of volatile anesthetics are their contributions to ozone depletion in the stratosphere and to greenhouse warming in the troposphere [3]. The stratospheric ozone layer is now known to be damaged by long living chlorine- and bromine-containing compounds. The most commonly used inhaled anesthetics undergo very little *in vivo* metabolism in clinical use. More than 95% of these volatile anesthetics is not metabolized by the patient and these agents remain in a form that may pollute the environment. These pollutants will end up in the atmosphere whereas those species with long lifetime in the troposphere will reach stratosphere in significant quantities.

## 2. Motivation for the present proposal

The purpose of the present experimental proposal is to investigate photon induced fragmentation of volatile halogenated agents sevoflurane (halogenated with fluorine), enflurane and isoflurane (halogenated with fluorine and chlorine) molecules and to determine their fragmentation pattern. To the best of our knowledge, no results appear in the present scientific literature on gas phase photoionization of these molecules. Our proposed experimental work addresses their electronic structure, and it can offer important insight on photon-driven reactions. The proposed research program will be carried out at Elettra with the group from CNR-ISM, whom we already cooperated with in a recent series of measurements on halothane molecule ( $\text{C}_2\text{HBrClF}_3$ ) during a recent internal beam times obtained at the Gas Phase beamline (March 2016, September 2017). We have performed extensive and detailed studies of the fragmentation mechanisms of this molecule, one of the most commonly used halogenated anesthetics. Compared to the other volatile anesthetics from the same group (halogenated chlorofluorocarbons) this bromide-containing agent is the most destructive against ozone. Preliminary obtained results shows several different fragmentation pathways which contain fragments observed in the atmosphere. Also, the mass spectra show a strong contribution of lighter mass fragments [4, 5] (Figure 1 a).

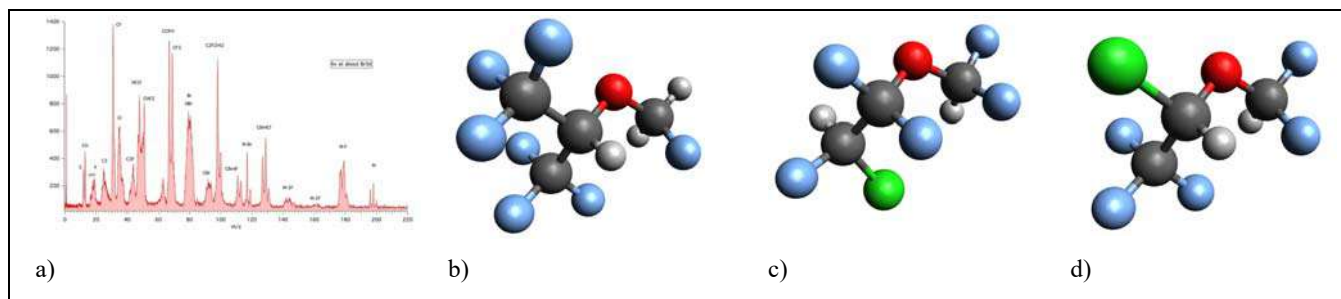


Figure 1: a) Mass spectrum of halothane; Structural formulas of b) sevoflurane; c) enflurane; d) isoflurane

Building on the successful results of the previous study of the halothane molecule we will now continue the study of the halogenated inhalational anesthetics sevoflurane ( $\text{C}_4\text{H}_3\text{F}_7\text{O}$ ), enflurane ( $\text{C}_3\text{H}_2\text{ClF}_5\text{O}$ ) and isoflurane ( $\text{C}_3\text{H}_2\text{ClF}_5\text{O}$ ) which is the structural isomer of enflurane. Our aim is to investigate the effects of the variations in the fragmentation patterns due to the substituent groups and their position in the molecule. The proposed targets are shown in Figure 1: (b) sevoflurane; c) enflurane and d) isoflurane. This complementary expertise will contribute to the successful realization of our project. More detailed insight in the ground state electronic structure and properties as well as fragmentation pathways of investigated molecules can be obtained by analyzing experimental results with state of the art quantum chemical methods [6, 7]. Members of our team at IPB are also experienced in computational chemistry [8-11]. Beyond ground state geometries and molecular electronic properties, calculations on transition state and intermediate species will provide potential energy profiles for most probable fragmentation pathways. Thus, based on mass spectrometry results, we plan to develop a model for photon induced fragmentation pathways for investigated molecule.

### 3. Experimental plan

The targets that we will use for this experiment belong to the halogenated volatile anesthetics. An experiment on halothane molecule has been recently performed at Gas Phase beam line using valence and inner shell photoionization. The experimental plan is to move forward in the identification and explanation of fragmentation patterns of sevoflurane, enflurane and isoflurane molecules using the same experimental approach. This proposal will focus on:

1. the measurements of the PES and NEXAFS of sevoflurane, enflurane and isoflurane molecules at several photon energies;
2. the study of the mass spectra via TOF mass spectrometry at several photon energies across the C(1s), F(1s), O(1s) and Cl(2s) thresholds and in the valence energy region;
3. the measurement of the photoelectron-ion coincidence (PEPICO) yield to investigate the state-selected fragmentation of valence shell orbitals.

For these experiments, we would like to use the Gas Phase beamline and the end-station equipped with the VG electron analyser and the ion TOF analyser mounted opposite to each other. A test tube mounted outside the vacuum chamber and connected to the gas line, with a needle valve regulating the gas flow will be used. The electronic for PEPICO experiments, with pulsed extraction of the ions to the TOF analyser triggered by the gas pulse generator or by the discriminated signals of the six channeltrons of the VG analyser will be needed.

### 4. Explain why this work calls for access to Elettra

The Gas Phase beamline at Elettra can provide both the high flux and good intensity for resolving the features in the recorded spectra. Together with photon energy tunability we can obtain suitable experimental set-up essential for characterization of our samples. Based on our previous experience with halogenated volatile anesthetics, for the present experiments we expect that we will need about 3 shifts for setting up of the experiment, 4 shifts/molecule to perform the PES characterization of valence and core hole ionic states and about 5 shifts/molecule to perform the proposed experiments of photoemission and photofragmentation.

### 5) References

- [1] A. C. Brown et al., Nature 341 635 (1989)
- [2] S. Yasny et al., Anesth. Prog. 59 154 (2012)
- [3] T. Langbein et al., Br J Anaesth. 82 66 (1999)
- [4] S. D. Tošić et al., Proc. The Workshop on X-ray Interaction with Biomolecules in Gas Phase (XiBiGP), August 29th 2016, Belgrade, Serbia, p.447.
- [5] S. D. Tošić et al., 7th Conference on Elementary Processes in Atomic Systems (CEPAS), 03-06 September 2017, Pruhonice, Czech Republic, Poster presentation, M-25.
- [6] M. Ahmed et al. The Journal of Physical Chemistry A, 118 645 (2014)
- [7] P. Bolognesi et al. The Journal of Chemical Physics 145 191102 (2016)
- [8] I. S. Antonijević et al. Crystal Growth and Design, 16 632 (2016)
- [9] M. P. Mitoraj et al. Journal of Computational Chemistry, 36 (3) 171 (2015)
- [10] A. Mitrović et al. RSC Advances, 5 107 88241 (2015)
- [11] M. Radibratovic et al. PLoS ONE, 11(12): e0167973 (2016)



Република Србија

Министарство просвете, науке и технолошког развоја

Годишњи извештај о раду на пројекту у 2019. години

ПРОГРАМ	ОСНОВНА ИСТРАЖИВАЊА
---------	---------------------

ОБЛАСТ	Физика
--------	--------

Назив пројекта	Физика судара и фотопроцеса у атомским, (био)молекулским и нанодимензионим системима
----------------	--

Евиденциони број	171020
------------------	--------

# Годишњи извештај о раду на пројекту у 2019. години

<b>Име:</b> Братислав
<b>Презиме:</b> Маринковић
<b>Број телефона:</b> 316-0882
<b>E-mail адреса:</b> bratislav.marinkovic@ipb.ac.rs
<b>Радна организација:</b> 200024-Универзитет у Београду, Институт за физику
<b>Град:</b> Belgrade
<b>Број поште:</b> 11080
<b>Страна 1 - Општи подаци</b>
<b>Програм</b> ОСНОВНА ИСТРАЖИВАЊА
<b>Област</b> Физика
<b>Број пројекта</b> 171020
<b>Назив Пројекта</b> Физика судара и фотопроеца у атомским, (био)молекулским и нанодимензионим системима
<b>Тип пројекта</b> Б-Експериментални
<b>Страна 2 - Опис истраживања</b>
<p><b>Циљеви истраживања (према достављеном плану истраживања) остварени у 2019. години имајући у виду значај, квалитет и ниво остварених резултата.</b> ТЕМА 1. ИНТЕРАКЦИЈЕ ЕЛЕКТРОНА, ЈОНА И ФОТОНА СА АТОМИМА И (БИО)МОЛЕКУЛИМА (КОНСТИТУЕНТИМА ИЛИ АНАЛОГНИМА ДНК МОЛЕКУЛА) РАДИ БОЉЕГ РАЗУМЕВАЊА ПРОЦЕСА РАДИЈАЦИОНОГ ОПШТЕЊЕЊА. Задатак 1.1 а) На апаратури ОНРНА (Omicron High Resolution Hemispherical Analyser) измерени су спектри избачених електрона аутојонизационих стања и Coster-Kronig прелаза у атому Ar, а публиковани у међународном часопису [P18. Energy analysis of ejected electrons in the region of the Ar L1–L2,3M Coster-Kronig transitions (25-56 eV) induced by electron impact, J. Electron Spectrosc. 237, 146898 (2019) 6pp]. б) На апаратури ESMA завршена су и публикована мерења диференцијалних пресека за еластично расејање електрона при упадним енергијама електрона од 10-100 eV на атому Zn [P12. Experimental and theoretical cross sections for elastic electron scattering from zin, Phys. Rev. A 99, 062702 (2019) 10pp]. Задатак 1.2 (руководилац задатка др Јелена Маљковић): а) Извршена су мерења еластичног расејања електрона на молекулу три-етил-фосфату. Резултати су обрађени и публиковани [P03. Elastic electron scattering cross sections for triethyl phosphate molecule at intermediate electron energies from 50 to 250 eV, Eur. Phys. J.D 73, 27 (2019) 5pp]. б) Прелиминарна мерења еластичног расејања електрона на молекулу метана су представљена на престижним међународним конференцијама ECAMP13 и XXXI ICPEAC [CI08. Integral cross sections for elastic electron scattering by methane molecule; CI01. Elastic electron scattering from methane molecule in the energy range from 50-300 eV] в) У оквиру пост доктората у сарадњи са колегама из Прага обављен је рад о дисоцијативној јонизацији молекула флуоронитрила [O02 Phys. Chem. Chem. Phys. 21(30) 16451-16458 (2019)]. Задатак 1.3 Изучавана је теорија судара тешких честица: а) Публикован је рад у коме је примењена динамичка адијабатска теорија судара у опису атома водоника у s-стању [P05. Classical representation for hydrogen atom in s-states, Quantum Stud.: Math. Found. 6(2) 225-233 (2019)]. б) (руководилац задатка др Ненад Милојевић): Истраживан је парцијални и укупни пресек за захват електрона из K-љуске вишеелектронских мета од стране потпуно огољених пројектила. Написан је и публикован прегледни рад на ову тему у репомираном часопису. [P15. State-selective and total cross sections for electron capture from the K-shell of multi-electron atoms by fully stripped projectiles. At. Data Nucl. Data Tables, (2019) 18pp]. ТЕМА 2. ИНТЕРАКЦИЈЕ СА ПОВРШИНАМА НА НАНОМЕТАРСКОЈ СКАЛИ (НАНОКАПИЛАРЕ, НАНОТАЧКЕ) КОЈЕ ВОДЕ ФУНКЦИОНАЛИЗАЦИЈИ МАТЕРИЈАЛА ИЛИ МОДИФИКАЦИЈИ НАНОФИЛМОВА. Задатак 2.1: (руководилац задатка др Милош Ранковић): Завршена тематика. Задатак 2.2 а) (руководилац задатка др Маја Рабасовић): Извршена су мерења оптичких особина прашкастих нано материјала (Sr2CeO4:Eu, GdVO4:Sm; Gd2Zr2O7:Eu, CaWO4:Nd), као и апконверзионог материјала (Gd2O3:Er, Yb). Могућности примене материјала YVO4:Eu3+ за мерења промене температуре су публиковани [P22. J. Phys. D: Appl. Phys. 53, 015106, 10pp, online 1st Oct. 2019]. Резултати анализе и карактеризације материјала CdSe/ZnS-PMMA публиковани су у раду [P17. Optical properties CaWO4:Nd3+/PMMA composite layered structures, Opt. Mater. 96, 109361 (2019) 8pp]. Оптичке особине материјала CaWO4:Nd су представљене у раду [P11. Optical properties and fluorescence of quantum dots CdSe/ZnS-PMMA composite films with interface modifications, Opt. Mater. 92, 405-410 (2019)]. б) Настављено је изучавање ласерски индукованог пробоја и посматрани различити временски размаци узорковања [P01. Laser-Induced Plasma Measurements Using Nd:YAG Laser and Streak Camera: Timing Considerations, Atoms, 7(1), 6 (2019) 12pp]. в) Испитивана је локализација електрона у двоелектронским квантним тачкама у зависности од јачине спољашњег магнетног поља и веза са квантном преплетеношћу најнижих стања и публикован је рад. [P19. Effect of the magnetic field on electron density distributions in two-electron quantum dots. J. Phys. A. Math. Theo. 52, 435303 (2019) 21pp]. 2.3 Настављена је обрада резултата TiO2 мемристора добијених FEBID техником. ТЕМА 3. ФОТОПРОЦЕСИ ВЕЗАНИ ЗА ИНТЕРАКЦИЈЕ ЛАСЕРСКОГ И СИНХРОТРОНСКОГ ЗРАЧЕЊА СА АТОМИМА, ЈОНИМА И (БИО)МОЛЕКУЛИМА. Задатак 3.1 а) Интеракција ласерског зрачења са биомолекулима (руководилац задатка др Маја Рабасовић): Настављено је изучавање временски разложених луминесцентних спектра алкалоида биљке руса [CI10. Nonlinear microscopy and time resolved fluorescence spectroscopy of Chelidonium majus L. Proc. PHOTONICA2019]. б) <b>Интеракција синхротронског зрачења са (био)молекулима (руководилац задатка др Сања Тошић):</b> Проучавани су могући механизми фрагментације молекула као директне последице апсорпције X зрачења помоћу подесивог синхротронског зрачења у комбинацији са различитим експерименталним техникама (PES, XPS, NEXAFS, PEPICO, PIPICO, масена спектрометрија) на различитим молекулима: i) нитроимдазолима [P10. Radiation Damage Mechanisms of Chemotherapeutically Active Nitroimidazole Derived Compounds, Front. Chem. 7, 329 (2019) 14pp; P06. Core shell investigation of 2-nitroimidazole, Front. Chem. 7, 151 (2019) 13pp]; ii) Титанијум-изо-пропоксид (органометалик, прекурсор за хемијску депозицију и ФЕБИД технику високе резолуције која омогућава стварање и уређивање наноструктурних материјала) [CI13. Photo-induced fragmentation of the titanium (IV) iso-propoxide molecule, VEIT 2019: CI12. Inner-shell spectroscopy of titanium (IV) iso-propoxide, PHOTONICA2019]. Ова истраживања су представљена и на уводном предавању у оквиру прве европске радионице корисника синхротрона одржане у Београду ESUO Organization [IT02. Core Shell Investigation and Radiation Damage Mechanisms of Nitroimidazole Compounds studies at the Gasphase Beamline @ Elettra, Photonica 2019 and 1st ESUO Regional Meeting, Belgrade, 28.08.2019] Задатак 3.2 (руководилац задатка др Предраг Коларж): Истражена ефективна доза озрачености појединих делова Балкана [O01. Effective Doses Estimated from the Results of Direct Radon and Thoron Progeny Sensors (DRPS/DTPS), Exposed in Selected Regions of Balkans, Radiation</p>



XX International Workshop on  
Low-Energy Positron and Positronium Physics

XXI International Symposium on  
Electron-Molecule Collisions and Swarms

V Workshop on Non-Equilibrium Processes

*18-21 July 2019, Belgrade, Serbia*



# POSMOL 2019

## BOOK OF ABSTRACTS

XX Међународна радионица о физици  
ниско енергијских позитрона и позитронијума

XXI Међународни симпозијум о  
електрон-молекулским сударима и ројевима

V Радионица о неравнотежним процесима



Serbian Academy of  
Sciences and Arts



UNIVERSITY OF BELGRADE |  
INSTITUTE OF PHYSICS | BELGRADE

Panacomp  
Wonderland Travel  
Lufthansa City Center

**XX International Workshop on  
Low-Energy Positron and Positronium Physics**

**XXI International Symposium on  
Electron-Molecule Collisions and Swarms**

**V Workshop on Non-Equilibrium Processes**

# **POSMOL 2019**

## **BOOK OF ABSTRACTS**

*Editors*

David Cassidy, Michael J. Brunger,  
Zoran Lj. Petrović, Saša Dujko, Bratislav P. Marinković,  
Dragana Marić and Sanja Tošić

Serbian Academy  
of Sciences and Arts

Institute of Physics Belgrade  
University of Belgrade

Belgrade, 2019

BOOK OF ABSTRACTS of the  
XX International Workshop on Low-Energy Positron and Positronium Physics  
XXI International Symposium on Electron-Molecule Collisions and Swarms  
V Workshop on Non-Equilibrium Processes

18-21 July 2019, Belgrade, Serbia

*Editors:*

David Cassidy, Michael J. Brunger,  
Zoran Lj. Petrović, Saša Dujko, Bratislav P. Marinković,  
Dragana Marić and Sanja Tošić

*Publishers:*

Serbian Academy of Sciences and Arts  
Kneza Mihaila 35  
11000 Belgrade, Serbia

Institute of Physics Belgrade  
Pregrevica 118, P. O. Box 68  
11080 Belgrade, Serbia

*Computer processing:*

Dragana Marić and Sanja Tošić

*Printed by*

**Serbian Academy of Sciences and Arts**  
Belgrade

*Number of copies*

250

ISBN 978-86-7025-819-8

©2019 by the Serbian Academy of Sciences and Arts and Institute of Physics Belgrade, Serbia. All rights reserved. No part of this book may be reproduced, stored or transmitted in any manner without the written permission of the Publisher.



**Dr Sanja Tošić**

Institute of Physics  
University of Belgrade  
Pregrevica 118  
11080 Belgrade  
Serbia

**26<sup>th</sup> Summer School and  
International Symposium on  
the Physics of Ionized Gases  
Zrenjanin, Serbia  
August, 27 – 31, 2012**

Novi Sad, 4<sup>th</sup> January 2012

Dear Dr Tošić,

We are writing to you on behalf of the Scientific and Organizing Committees of the 26<sup>th</sup> Summer School and International Symposium on the Physics of Ionized Gases (SPIG 2012), to be held from August, 27 to 31, 2012 in Zrenjanin, Serbia.

It is our pleasure to invite you to attend SPIG 2012 and present a **progress report** in Section 1 with a title "MEASUREMENTS OF DIFFERENTIAL CROSS SECTIONS FOR ELASTIC ELECTRON SCATTERING AND ELECTRONIC EXCITATION OF METAL ATOMS". The progress report (20 minutes, including questions and discussions) will be organized in the corresponding section.

Unfortunately, due to the limited conference budget, we can not exempt you from paying the conference fee and cover your accommodation and travel expenses.

Looking forward to see you in Zrenjanin.

Yours sincerely,

A handwritten signature in black ink, appearing to read "M. Kuraica".

Milorad M. Kuraica  
(Chairman of the Scientific Committee)

A handwritten signature in black ink, appearing to read "Zoran Mijatović".

Zoran Mijatović  
(Chairman of the Organizing Committee)



## 28<sup>th</sup> Summer School and International Symposium on the Physics of Ionized Gases

August 29 – September 2, 2016, Belgrade, Serbia

### X-ray Interaction with **B**iomolecules in **G**as **P**hase (XiBiGP) workshop

**Dr Sanja Tošić**

Institute of Physics Belgrade,  
University of Belgrade,  
Pregrevica 118,  
11080 Zemun,  
Serbia

Belgrade, 18<sup>th</sup> May 2016

Dear Dr Tošić,

On behalf of the Scientific and Organizing Committees, we have the pleasure to invite you to attend the 28<sup>th</sup> *Summer School and International Symposium on the Physics of Ionized Gases* (SPIG 2016) and present a **lecture** (30 min, including questions and discussions) at the *Workshop on X-ray Interaction with Biomolecules in Gas Phase (XiBiGP)*.

The SPIG 2016 will be held from 29<sup>th</sup> August to 2<sup>nd</sup> September in Belgrade, Serbia. The XiBiGP workshop is scheduled for 29<sup>th</sup> of August. The details of the conference are available at [www.spig2016.ipb.ac.rs](http://www.spig2016.ipb.ac.rs). Unfortunately, due to the limited conference budget, the organizers cannot commit to any financial support.

We hope that you will be able to accept our invitation. Please let us know by the 25<sup>th</sup> of May 2016 and, if possible, send us the title of your lecture.  
We look forward to welcoming you to Belgrade in 2016.

Yours sincerely,

**Dragana Marić**

(Co-Chair of the SPIG 2016 Scientific Committee)

**Aleksandar R. Milosavljević**

(Co-Chair of the SPIG 2016 Scientific Committee  
and Co-Chair of the **XiBiGP** Workshop)

**Paola Bolognesi**

(Co-Chair of the  
**XiBiGP** Workshop)

---

#### Local organizing Committee:

Faculty of Physics, University of Belgrade  
Studentski trg 12  
11000 Belgrade, Serbia

Tel: +381 11 715-8151  
Fax: +381 11 328-2619

E-mail: [spig2016@ff.bg.ac.rs](mailto:spig2016@ff.bg.ac.rs)  
Web: [www.spig2016.ipb.ac.rs](http://www.spig2016.ipb.ac.rs)



## ЗАПИСНИК

са редовне седнице Научног већа Института за физику одржане 15.11.2016. године

Присутни чланови:

Научни саветници: др Душан Арсеновић, др Антун Балаж, др Александар Богојевић, др Ненад Вукмировић, др Драгана Јовић Савић, др Драгана Марић, др Зоран Петровић, др Слободан Првановић, др Марија Радмиловић Рађеновић, др Љиљана Симић

Виши научни сарадници: др Мира Аничич Урошевић, др Магдалена Ђорђевић, др Миљивоје Ивковић, др Бојан Николић, др Душка Поповић, др Владимир Срећковић, др Дарко Танасковић, др Бранислав Цветковић

Научни сарадници: др Ивана Васић, др Дејан Јоковић, др Саша Лазовић, др Јелена Маљковић, др Зоран Мијић, др Марија Митровић Данкулов, др Марко Николић, др Никола Петровић, др Марко Спасеновић

Одсутни чланови:

Научни саветници: др Најдан Алексић, др Саша Дујко, др Радомир Жикић, др Лидија Живковић, др Бранислав Јеленковић, др Душан Јовановић, др Братислав Маринковић, др Милица Миловановић, др Александар Милосављевић, др Милан Петровић, др Зоран Поповић, др Небојша Ромчевић, др Душанка Стојановић, др Драгутин Шевић

Виши научни сарадници: др Предраг Коларж, др Зорица Лазаревић

Научни сарадници: др Борислав Васић, др Милан Радоњић

*Депоновали своје гласове “за” изборе у звања: др Најдан Алексић, др Саша Дујко, др Братислав Маринковић, др Милица Миловановић*

За рад на седници је усвојен следећи

## ДНЕВНИ РЕД

1. Усвајање записника са претходне редовне седнице Научног већа Института за физику која је одржана 13.09. 2016. године.

2. Утврђивање предлога за избор у научно звање и избор у истраживачко звање (извештај Комисије за вредновање научног рада):

- 2.1. др Марко Спасеновић - избор у звање виши научни сарадник (извештај, презентација);
- 2.2. др Татјана Агатоновић Јовин - избор у звање научни сарадник (извештај, презентација);
- 2.3. др Милош Ранковић - избор у звање научни сарадник (извештај, презентација);
- 2.4. др Мирјана Перишић - избор у звање научни сарадник (извештај, презентација);

- 2.5. др Бојана Вишић - избор у звање научни сарадник ([извештај,презентација](#));
- 2.6. др Маја Кузманоски - реизбор у звање научни сарадник ([извештај,презентација](#));
- 2.7. Марко Младеновић - реизбор у звање истраживач сарадник ([извештај,презентација](#)).

3. Покретање поступака за изборе у звања ([извештај](#) Комисије за вредновање научног рада о материјалима кандидата):

- 3.1. др Ненад Лазаревић - избор у звање виши научни сарадник ([материјал](#));
- 3.2. др Немања Лучић - избор у звање научни сарадник ([материјал](#));
- 3.3. др Данко Бошњаковић - избор у звање научни сарадник ([материјал](#));
- 3.4. др Бранка Хаџић - избор у звање научни сарадник ([материјал](#));
- 3.5. Илија Симоновић - избор у звање истраживач сарадник ([материјал](#));
- 3.6. др Дарко Васиљевић - реизбор у звање виши научни сарадник ([материјал](#));
- 3.7. др Ненад Сакан - реизбор у звање научни сарадник ([материјал](#));
- 3.8. Владимир Лончар - реизбор у звање истраживач сарадник ([материјал](#));
- 3.9. Војислав Милошевић -реизбор у звање истраживач сарадник ([материјал](#));
- 3.10. промена комисије за избор др Саше Лазовића у звање виши научни сарадник

4. Избор представника за веће научних области природно-математичких наука ([допис](#)). Кандидати:

- 4.1. др Гордана Маловић ([предлог](#));
- 4.2. др Жељка Никитовић ([предлог](#)).

5. Избор представника за различите одсеке Одељења НИВО ДФС ([списак одсека са досадашњим члановима](#)):

5.1. Одсек за астрономију и астрофизику  
- др Владимир Срећковић ([предлог](#));

5.2. Одсек за квантну и математичку физику  
- др Љубица Давидовић ([предлог](#));  
- др Игор Франовић;

5.3. Одсек за примењену и рачунарску физику  
- др Марко Николић ([предлог](#));  
- др Милош Радоњић ([предлог](#));

5.4. Одсек за физику кондензоване материје и статистичку физику  
- др Марија Митровић Данкулов ([предлог](#));  
- др Ивана Васић ([предлог](#));

5.5. Одсек за физику језгра, елементарних честица и основних интеракција  
- др Ненад Врањеш ([предлог](#));  
- др Марко Војиновић;

5.6. Одсек за оптику и фотонику  
- др Марина Лекић ([предлог](#));  
- др Александар Крмпот ([предлог](#));

5.7. Одсек за наставу, историју и филозофију физике  
- др Бојан Николић;

6. Обавештења, питања и предлози.

1. Записник са редовне седнице Научног већа Института за физику одржане 13.09.2016. године усвојен је једногласно.

2. Пре почетка гласања о утврђивању предлога за избор односно реизбор у научна звања Комисија за вредновање научног рада поднела је извештај о пристиглим извештајима Комисија за изборе у звања. Закључак Комисије је да сви извештаји садрже све неопходне квалитативне и квантитативне елементе прописане Правилником о изборима у звање.

Констатовано је да постоји кворум за пуноважно утврђивање предлога за избор у звање виши научни сарадник.

2.1 По усменом излагању *др Радоша Гајића*, референта, након краће дискусије, једногласно је утврђен предлог за избор у звање виши научни сарадник за **др Марка Спасеновића**.

Констатовано је да постоји кворум за пуноважно утврђивање предлога за избор/реизбор у звање научни сарадник.

2.2 По усменом излагању *др Јелене Крстић*, референта, након краће дискусије, једногласно је утврђен предлог за избор у звање научни сарадник за **др Татјану Агатоновић Јовин**.

2.3 По усменом излагању *др Ненада Симоновића*, референта, након краће дискусије, једногласно је утврђен предлог за избор у звање научни сарадник за **др Милоша Ранковића**.

2.4 По усменом излагању *др Андреје Стојића*, референта, након краће дискусије, једногласно је утврђен предлог за избор у звање научни сарадник за **др Мирјану Перишић**.

2.5 По усменом излагању *др Ненада Лазаревића*, референта након краће дискусије, једногласно је утврђен предлог за избор у звање научни сарадник за **др Бојану Вишић**.

2.6 По усменом излагању *др Зорана Мијића*, након краће дискусије, једногласно је утврђен предлог за реизбор у звање научни сарадник за **др Мају Кузманоски**.

Констатовано је да постоји кворум за пуноважно доношење одлуке за избор/ реизбор у звање истраживач сарадник.

2.7 По усменом излагању *др Ненада Вукмировића*, референта, након краће дискусије, једногласно је донета одлука о реизбору **Марка Младеновића** у звање истраживач сарадник.

3. Пре почетка гласања о покретањима поступака за изборе у звања, Комисија за вредновање научног рада поднела је извештај о пристиглим захтевима за покретање поступака. Извештај је прослеђен свим кандидатима који су поднели молбу за избор у звање.

3.1. Једногласно је покренут поступак за избор **др Ненада Лазаревића** у звање виши научни сарадник.

У Комисију за писање извештаја су именовани др Маја Шћепановић, научни саветник, Институт за физику, 1. референт, академик Зоран В. Поповић, научни саветник, Институт за физику, академик Милан Дамњановић, редовни професор Физичког факултета у Београду

3.2. Једногласно је покренут поступак за избор **др Немање Лучића** у звање научни сарадник.

У Комисију за писање извештаја су именовани: др Бранислав Јеленковић, научни саветник, Институт за физику, 1. референт, др Дејан Тимотијевић, научни саветник, Институт за физику, др Јасна Црњански, доцент Електротехничког факултета у Београду

3.3. Једногласно је покренут поступак за избор **др Данка Бошњакковића** у звање научни сарадник.

У Комисију за писање извештаја су именовани: др Саша Дујко, научни саветник, Институт за физику, 1. референт, академик Зоран Петровић, научни саветник, Институт за физику, др Јован Цветић, редовни професор Електротехничког факултета у Београду

3.4. Једногласно је покренут поступак за избор **др Бранке Хаџић** у звање научни сарадник.

У Комисију за писање извештаја су именовани: др Јелена Трајић, виши научни сарадник, Институт за физику, 1. референт, др Зорица Лазаревић, виши научни сарадник, Институт за физику, др Јаблан Дојчиловић, редовни професор Физичког факултета у Београду

3.5 Једногласно је покренут поступак за избор **Илије Симоновића** у звање истраживач сарадник.

У Комисију за писање извештаја су именовани: др Саша Дујко, научни саветник, Институт за физику, 1. референт, проф. др Срђан Буквић, редовни професор Физичког факултета у Београду, академик Зоран Петровић, научни саветник, Институт за физику

3.6 Једногласно је покренут поступак за реизбор **др Дарка Васиљевића** у звање виши научни сарадник.

У Комисију за писање извештаја су именовани: др Дејан Пантелић, научни саветник, Институт за физику, 1. референт, др Бранислав Јеленковић, научни саветник, Институт за физику, проф. др Бећко Касалица, ванредни професор Физичког факултета у Београду

3.7. Једногласно је покренут поступак за реизбор **др Ненада Сакана** у звање научни сарадник.

У Комисију за писање извештаја су именовани: др Владимир Срећковић, виши научни сарадник, Институт за физику, 1. референт, др Љубинко Игњатовић, научни саветник,

Институт за физику, проф. др Срђан Буквић, редовни професор Физичког факултета у Београду, др Зоран Симић, виши научни сарадник, Астрономска опсерваторија, Београд

3.8 Једногласно је покренут поступак за реизбор **Владимира Лончара** у звање истраживач сарадник.

У Комисију за писање извештаја су именовани: др Антун Балаж, научни саветник, Институт за физику, 1. референт, др Ненад Вукмировић, научни саветник, Институт за физику, проф. др Срђан Шкрбић, ванредни професор Природноматематичког факултета у Новом Саду

3.9 Једногласно је покренут поступак за реизбор **Војислава Милошевића** у звање истраживач сарадник.

У Комисију за писање извештаја су именовани: др Бранка Јокановић, научни саветник, Институт за физику, 1. референт, проф. др Слободан Вуковић, научни саветник у пензији, ИХТМ, Београд, др Горан Исић, научни сарадник, Институт за физику

3.10. Већином гласова за уз два гласа против и три уздржана изабрана је комисија за писање извештаја за избор **др Саше Лазовића** у звање виши научни сарадник.

У Комисију за писање извештаја су именовани: др Јозо Јурете, научни саветник, 1. референт, Институт за физику, др Бранислав Јеленковић, научни саветник, Институт за физику, проф. др Стеван Стојадиновић, ванредни професор Физичког факултета у Београду.

4. За представника за веће научних области природно-математичких наука изабрана је др Гордана Маловић

5. Др Ненад Вукмировић је изнео став да организација регистрована као Друштво физичара Србије није репрезентативна организација физичара. Та организација је регистрована 2012. године након што је 2011. године угашено друштво физичара које је радило годинама. У тренутној организацији двотрећинску већину у Скупштини чине наставници физике који су и изабрали председника Одељења НИВО, иако наставници физике не могу бити компетентни за питања високог образовања и истраживања. И остала тела те организације не репрезентују на прави начин физику у Србији. С обзиром на наведено, предложио је да Научно веће Института за физику не именује своје представнике за Одељење НИВО.

За различите одсеке Одељења НИВО ДФС изабрани су следећи сарадници:

Одсек за астрономију и астрофизику  
- др Владимир Срећковић;

Одсек за квантну и математичку физику  
- др Љубица Давидовић;  
- др Игор Франовић;



Одсек за примењену и рачунарску физику

- др Марко Николић
- др Милош Радоњић;

Одсек за физику кондензоване материје и статистичку физику

- др Марија Митровић Данкулов;
- др Ивана Васић;

Одсек за физику језгра, елементарних честица и основних интеракција

- др Ненад Врањеш ;
- др Марко Војиновић;

Одсек за оптику и фотонику

- др Марина Лекић;
- др Александар Крмпот;

Одсек за наставу, историју и филозофију физике

- др Бојан Николић;

Одсек за атомску и молекулску физику

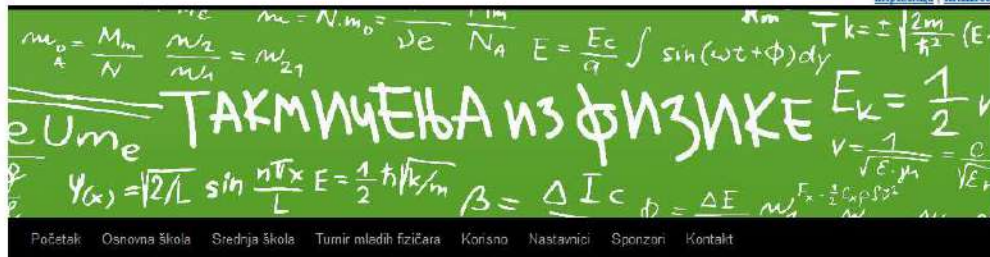
- др Јелена Маљковић;
- др Сања Тошић;

Одсек за физику плазме и јонизованих гасова

- др Никола Шкоро;
- Срђан Марјановић.

**Председник Научног већа**

**др Марија Радмиловић Рађеновић**



Klikova od 7.2.2012. je bilo:

Komisija za takmičenja srednjih škola je u školskoj 2012/2013. godini imala sledeći sastav:

5859917

Predsednik komisije:

dr Aleksandar Krmpot [aleksandar.krmpot@dfs.rs](mailto:aleksandar.krmpot@dfs.rs)

Sekretar komisije:

dr Milovan Šuvakov [milovan.suvakov@dfs.rs](mailto:milovan.suvakov@dfs.rs)

1. razred:

Autor: dr Zoran Mijić [zoran.mijic@dfs.rs](mailto:zoran.mijic@dfs.rs)

Autor: Zoran Popović [zoran.popovic@dfs.rs](mailto:zoran.popovic@dfs.rs)

Recenzent: dr Nevena Puač [nevena.puac@dfs.rs](mailto:nevena.puac@dfs.rs)

2. razred:

Autor: dr Sanja Tošić [sanja.tosic@dfs.rs](mailto:sanja.tosic@dfs.rs)

Autor: dr Bojan Nikolić [bojan.nikolic@dfs.rs](mailto:bojan.nikolic@dfs.rs)

Recenzent: dr Dragan Markušev [dragan.markusev@dfs.rs](mailto:dragan.markusev@dfs.rs)

3. razred:

Autor: dr Milan Radonjić [milan.radonjic@dfs.rs](mailto:milan.radonjic@dfs.rs)

Autor: Vladimir Veljić [vladimir.veljic@dfs.rs](mailto:vladimir.veljic@dfs.rs)

Recenzent: dr Antun Balaž [antun.balaz@dfs.rs](mailto:antun.balaz@dfs.rs)

4. razred:

Autor: dr Nenad Vukmirović [nenad.vukmirovic@dfs.rs](mailto:nenad.vukmirovic@dfs.rs)

Autor: Veljko Janković [veljko.jankovic@dfs.rs](mailto:veljko.jankovic@dfs.rs)

Recenzent: dr Darko Tanasković [darko.tanaskovic@dfs.rs](mailto:darko.tanaskovic@dfs.rs)

Komisija za takmičenja srednjih škola je u školskoj 2011/2012. godini imala sledeći sastav:

Predsednik komisije:

dr Aleksandar Krmpot [aleksandar.krmpot@dfs.rs](mailto:aleksandar.krmpot@dfs.rs)

Sekretar komisije:

dr Milovan Šuvakov [milovan.suvakov@dfs.rs](mailto:milovan.suvakov@dfs.rs)

1. razred:

Autor: dr Zoran Mijić [zoran.mijic@dfs.rs](mailto:zoran.mijic@dfs.rs)

Autor: Zoran Popović [zoran.popovic@dfs.rs](mailto:zoran.popovic@dfs.rs)

Recenzent: dr Nevena Puač [nevena.puac@dfs.rs](mailto:nevena.puac@dfs.rs)

2. razred:

Autor: dr Sanja Tošić [sanja.tosic@dfs.rs](mailto:sanja.tosic@dfs.rs)

Autor: dr Bojan Nikolić [bojan.nikolic@dfs.rs](mailto:bojan.nikolic@dfs.rs)

Recenzent: dr Dragan Markušev [dragan.markusev@dfs.rs](mailto:dragan.markusev@dfs.rs)

3. razred:

Autor: Milan Radonjić [milan.radonjic@dfs.rs](mailto:milan.radonjic@dfs.rs)

Autor: Milan Žeželj [milan.zezelj@dfs.rs](mailto:milan.zezelj@dfs.rs)

Recenzent: dr Antun Balaž [antun.balaz@dfs.rs](mailto:antun.balaz@dfs.rs)

4. razred:

Autor: dr Nenad Vukmirović [nenad.vukmirovic@dfs.rs](mailto:nenad.vukmirovic@dfs.rs)

Autor: dr Mihailo Rabasović [mihailo.rabasovic@dfs.rs](mailto:mihailo.rabasovic@dfs.rs)

Recenzent: dr Darko Tanasković [darko.tanaskovic@dfs.rs](mailto:darko.tanaskovic@dfs.rs)



# 29<sup>th</sup> Summer School and International Symposium on the Physics of Ionized Gases

August 28 – September 1, 2018, Belgrade, Serbia

- Home >
- About SPIG >
- Committees >
- News >
- Deadlines >
- Topics & Program >
- Invited Lectures >
- Workshops >
- Registration >
- Papers >
- Location >
- Travel Information >
- Accommodation >
- Links >
- Contact >
- First Announcement >
- Second Announcement >
- Conference Poster >

- SPIG 2016 Homepage >
- SPIG 2014 Homepage >
- SPIG 2012 Homepage >
- SPIG 2010 Homepage >
- SPIG 2008 Homepage >

Previous SPIG Lecturers >

## SPIG SCIENTIFIC COMMITTEE

- G. Poparić (Co-Chair), Serbia
- B. Obradović (Co-Chair), Serbia
- D. Borka, Serbia
- S. Buckman, Australia
- J. Burgdörfer, Austria
- J. Cvetić, Serbia
- M. Danezis, Greece
- Z. Donko, Hungary
- V. Guerra, Portugal
- D. Ilić, Serbia
- M. Ivković, Serbia
- I. Mančev, Serbia
- D. Marić, Serbia
- N. J. Mason, UK
- A. R. Milosavljević, France
- K. Mima, Japan
- Z. Mišković, Canada
- L. Nahon, France
- P. Roncin, France
- I. Savić, Serbia
- Y. Serruys, France
- N. Simonović, Serbia
- M. Škorić, Japan
- M. Trtica, Serbia
- S. Tošić, Serbia

## SPIG 2018 ORGANIZING COMMITTEE

Vinča Institute of nuclear sciences  
Serbian Academy of Sciences and Arts

- D. Borka (Co-chair)
- M. Rajković (Co-chair)
- V. Borka Jovanović (Co-Secretary)
- N. Potkonjak (Co-Secretary)
  
- N. Konjević
- N. Cvetanović
  
- J. Aleksić
- M. Nešić
- S. Živković
- J. Ciganović
- Biljana Grozdanić
- Aleksandra Hreljac

## SPIG ADVISORY COMMITTEE

- D. Belić
- N. Bibić
- M. S. Dimitrijević
- S. Đurović
- N. Konjević
- M. Kuraica
- J. Labat
- G. Malović
- B. P. Marinković
- Z. Mijatović
- M. Milosavljević
- Z. L.J. Petrović
- L. Popović
- J. Purić
- B. Stanić

## News

**Nov 25 2017**

[First Announcement](#)

**March 19 2018**

[Second  
Announcement](#)

**April 19 2018**

[Reduced fees for  
late registration](#)

**June 15 2018**

[Extended deadline  
for papers to 1.7.](#)



Vinča Institute of  
Nuclear Sciences



Serbian Academy of  
Sciences and Arts



# 30<sup>th</sup> Summer School and International Symposium on the Physics of Ionized Gases

August 24 - 28, 2020, Šabac, Serbia

- [Home >](#)
- [About SPIG >](#)
- [Committees >](#)
- [News >](#)
- [Deadlines >](#)
- [Topics & Program >](#)
- [Invited Lectures >](#)
- [Virtual Posters >](#)
- [Workshops:](#)
- [XIBIGP >](#)
- [BegFust >](#)
- [VAMDC >](#)
- [Registration >](#)
- [Financial Support >](#)
- [Abstracts & Papers >](#)
- [EPJD Topical Issue >](#)
  
- [Location >](#)
- [Travel Information >](#)
- [Accommodation >](#)
- [Sponsors >](#)
- [Links >](#)
  
- [Contact >](#)
  
- [First Announcement >](#)
- [Second Announcement >](#)
- [Final Announcement >](#)

- [SPIG 2018 Homepage >](#)
- [SPIG 2016 Homepage >](#)
- [SPIG 2014 Homepage >](#)
- [SPIG 2012 Homepage >](#)
- [SPIG 2010 Homepage >](#)
- [SPIG 2008 Homepage >](#)

- [Previous SPIG Lecturers >](#)

## SPIG SCIENTIFIC COMMITTEE

- D. Borka (Co-chair), Serbia
- L. Č. Popović (Co-chair), Serbia
  
- R. White, Australia
- J. Burgdörfer, Austria
- J. Cvetić, Serbia
- E. Danezis, Greece
- Z. Donko, Hungary
- V. Guerra, Portugal
- D. Ilić, Serbia
- M. Ivković, Serbia
- I. Mančev, Serbia
- D. Marić, Serbia
- N. J. Mason, UK
- A. Milosavljević, France
- K. Mima, Japan
- Z. Mišković, Canada
- L. Nahon, France
- B. Obradović, Serbia
- G. Poparić, Serbia
- P. Roncin, France
- I. Savić, Serbia
- Y. Serruys, France
- N. Simonović, Serbia
- M. Škorić, Japan
- M. Trtica, Serbia
- S. Tošić, Serbia

## SPIG 2020 ORGANIZING COMMITTEE

**Organizer:**  
University of Belgrade, Faculty of Mathematics  
Department of Astronomy

**Co-organizers:**  
University of Belgrade, Institute of Physics  
Astronomical Observatory of Belgrade

## Members:

- D. Ilić (Co-chair)
- V. Srećković (Co-chair)
  
- J. Kovačević-Dojčinović (Co-secretary)
- N. Cvetanović (Co-secretary)
  
- J. Aleksić
- A. Kovačević
- S. Marčeta-Mandić
- A. Nina
- D. Onić
- S. Simić
- V. Zeković

## SPIG ADVISORY COMMITTEE

- D. Belić
- N. Bibić
- M. S. Dimitrijević
- S. Đurović
- N. Konjević
- M.M. Kuraica
- J. Labat
- G. Malović
- B. P. Marinković
- Z. Mijatović
- M. Milosavljević
- Z. Lj. Petrović
- L. Č. Popović
- J. Purić
- B. Stanić

## News

**12.12.2020**  
[Extended deadline for EPJD till January 31](#)

**July 3 2020**  
[Final Announcement](#)

**July 2 2020**  
Spig shifted to full Virtual

**June 31 2020**  
[Virtual poster upload](#)

**June 4 2020**  
[2nd announcement & Important update](#)

**March 29 2020**  
[Upcoming deadlines extended](#)

**March 1 2020**  
[Special Session "Atomic Collisions ..."](#)  
[VAMDC Workshop](#)

**Jan 31 2020**  
[Prelim. list of lectures](#)

**Jan 26 2020**  
[Financial support](#)

**Dec 22 2019**  
[EPJ D Topical Issue](#)

**Oct 10 2019**  
[First Announcement](#)

Follow us!



Our Sponsors:



Telekom Srbija

Media Sponsors:



## 2nd general meeting of the COST Action CA18212

### Date:

4th to 8th of October 2021, in virtual format

### Deadlines:

25th August 2021	Registration open
5th September 2021	Abstract submission deadline for Early Career Investigator (ECI) forum speaker selection and poster presenters
12th September 2021	Abstract submission deadline for poster presenters
26th September 2021	Registration deadline

### Websites:

- [Registration website](#)
- [Speakers](#)
- [Programme](#)

### Confirmed invited speakers:

- Klavs Hansen, Tianjin University - Characterizing molecules with power law decays
- Oksana Plekan, Elettra Sincrotrone Trieste - Molecular Dynamics at FERMI/LDM
- Bratislav Marinkovic, Institute of Physics Belgrade - Electron scattering by metal atom vapours
- Paul Scheier, Innsbruck University
- Tomasz Wařowicz, Gdańsk University of Technology - Inner-shell fragmentation of molecules into neutral fragments in high-Rydberg states induced by soft X-ray excitation with pulsed-field ionization
- Sadia Bari, Deutsches Elektronen-Synchrotron DESY - Soft X-ray absorption spectroscopy of isolated biomolecules
- Paulo Limao-Vieira, Universidade NOVA de Lisboa - Methanol negative ions fragmentation probed in electron transfer experiments
- Jesús González-Vázquez, Universidad Autónoma de Madrid
- Mathias Rapacioli, Laboratoire de Chimie et Physique Quantiques - Investigating the dynamical evolution of Polycyclic Aromatic Hydrocarbons (PAHs) and PAH clusters after energy deposition
- Miroslav Polářek, The Czech Academy of Sciences - The reactivity of cyanamide radical cation with simple hydrocarbons: a quest for routes to complex organic molecules in the interstellar medium and Titan's atmosphere
- Shirin Faraji, University of Groningen - Excited state on-the-fly hybrid quantum/classical dynamics
- Noelle Walsh, MAX IV Laboratory
- Michał Kochman, Institute of Physical Chemistry Polish Academy of Science - Excited-state relaxation dynamics of 4-(N,N-Dimethylamino)benzonitrile (DMABN) - from the gas phase to polar solvents
- Moa Kristiansson, Stockholm University - Photodetachment studies of atomic and molecular anions in DESIREE
- Robin Schürmann, University of Potsdam - Insights into plasmon chemistry from gas-phase experiments
- Veljko Vujčić, Astronomical Observatory Belgrade - Characteristics of the atmospheric plasma: experiment and modelling
- Diptesh Dey, University College London - Simulating photo-excitation with a laser pulse beyond the perturbative regime
- Ana Martín Sómer, Universidad Autónoma de Madrid - Photodissociation dynamics of a protonated peptide: the role of microsolvation
- Néstor F. Aguirre, Software for Chemistry & Materials
- Nicolas Sisourat, Université Pierre et Marie Curie - On the Iodine plasma chemistry for space propulsion
- Tomislav Pitesa, Ruder Boskovic Institute - Mixed quantum-classical approach to the simulation and assignment of the time-resolved photoelectron spectra
- Emelie Olsson, University of Gothenburg - Unimolecular double photoionization-induced processes in iron pentacarbonyl

### Selected ECI Speakers:

- Raj Singh, GANIL
- Péter Szabó, Université du Luxembourg
- Giovanna Salvitti, University of Bologna
- Krishnendu Gope, The Hebrew University of Jerusalem
- Dhanoj Gupta, Weizmann Institute of Science
- Hernán Velásquez, University of Amsterdam
- Musab Al-Ajaleen, Institute for Nuclear Research (ATOMKI)
- Vinitha Meloottayil, Université de Toulouse III - Paul Sabatier
- Andrés Ordoñez, The Institute of Photonic Sciences
- Patricia Vindel Zandbergen, Rutgers University

### Organising Committee:

- Ewa Erdmann: [ewa.erdmann@pg.edu.pl](mailto:ewa.erdmann@pg.edu.pl)
- Henning Zettergren: [henning@fysik.su.se](mailto:henning@fysik.su.se)
- Alicja Domaracka: [domaracka@ganil.fr](mailto:domaracka@ganil.fr)

### Scientific Committee:

Thomas Schlathöf, Paola Bolognesi, Sergio Diaz-Tendero, Sanja Tošić, Marta Łabuda, Amanda Steber, Dariusz G. Piekarski, Sylvain Maclot, Mattea C. Castrovilli



# CA18212 - Molecular Dynamics in the GAS phase

Downloads

Home > Browse Actions > Molecular Dynamics in the GAS phase

Description Management Committee **Main Contacts and Leadership** Working Groups and Membership

## Main Contacts

### Action Contacts



**Prof Henning ZETTERGREN**  
Action Chair  
+46855378634  
[henning@fysik.su.se](mailto:henning@fysik.su.se)



**Dr Alicja DOMARACKA**  
Action Vice Chair  
+0033231454503  
[domaracka@ganil.fr](mailto:domaracka@ganil.fr)

### COST Staff



**Dr Fatima BOUCHAMA**  
Science Officer  
+3225333832  
[fatima.bouchama@cost.eu](mailto:fatima.bouchama@cost.eu)



**Ms Cassia AZEVEDO**  
Administrative Officer  
+3225333844  
[cassia.azevedo@cost.eu](mailto:cassia.azevedo@cost.eu)

### Action Details

- MoU - 029/19
- CSO Approval date - 04/06/2019
- Start date - 12/11/2019
- End date - 11/11/2023
- <http://www.mdgas.eu/>

### How can I participate?

- Read the Project Description [MoU](#)
- Inform the Main Proposer/Chair of your interest [\(email\)](#)
- [Apply](#) to join your Working Groups of interest
- Please note, Management Committee nominations are carried out through the [COST National Contact Points](#)

## Leadership

Role	Leader
Action Chair	Prof Henning ZETTERGREN ▾
Action Vice Chair	Dr Alicja DOMARACKA ▾
Grant Holder Scientific Representative	Prof Henning ZETTERGREN ▾
Science Communication Coordinator	Dr Marta LABUDA ▾
Grant Awarding Coordinator	Dr Sanja TOSIC ▾
WG1 Leader	Dr Thomas SCHLATHÖLTER ▾
WG2 Leader	Dr Paola BOLOGNESI ▾
WG3 Leader	Dr Sergio DIAZ-TENDERO ▾

## Additional roles

Role	Leader
ITC CG Coordinator	Dr Sanja TOSIC ▾
STSM Coordinator	Dr Sanja TOSIC ▾



# POSMOL 2019

XX International Workshop on Low-Energy Positron and Positronium Physics  
XXI International Symposium on Electron-Molecule Collisions and Swarms  
18 - 20 JULY 2019  
Belgrade, Serbia

HOME

NEWS

PROGRAM

PHOTO GALLERY

VENUE

REGISTRATION

ABSTRACTS AND PAPERS

ACCOMMODATION

TRAVEL

COMMITTEES

HISTORY

CONTACTS

WORKSHOP

## SPONSORS



MINISTRY OF EDUCATION, SCIENCE  
AND TECHNOLOGICAL DEVELOPMENT

EPJ.org

EUROPEAN PHYSICAL JOURNAL D

## Committees

### Local Organising Committee

- Zoran Lj. Petrović (SASA, IPB) **Chair**
- Bratislav Marinković (IPB) **Co-Chair**
- Saša Dujko (IPB) **Co-Chair**
- Sanja Tošić (IPB) **Secretary**
- Dragana Marić (IPB) **Conference Manager**
- Gordana Malović (IPB)
- Danko Bošnjaković (IPB)
- Andrej Bunjac (IPB)
- Jelena Sivoš (IPB)
- Marija Puač (IPB)
- Ilija Simonović (IPB)
- Vladan Simić (IPB)
- Nenad Selaković (IPB)
- Dejan Maletić (IPB)
- Kosta Spasić (IPB)
- Olivera Jovanović (IPB)
- Anđelija Petrović (IPB)
- Goran Poparić (FP)
- Biljana Grozdanić (SASA)
- Aleksandra Hreljac (SASA)

### Positron International Advisory Committee

- David Cassidy (University College London), **Chair**
- Gustavo Garcia (Consejo Superior de Investigaciones Científicas)
- Michael Bromley (University of Queensland)
- Marcio Varella (Universidade de São Paulo)
- Masanori Tachikawa (Yokohama City University)
- Roberto Brusa (Università di Trento)
- James Danielson (University of California, San Diego)
- Laszlo Liskay (University of Paris, Saclay)

### Electron International Advisory Committee

- Michael J. Brunger (Flinders University), **Chair**
- Ilya I. Fabrikant (University of Nebraska, Lincoln)
- Roman Čurik (J. Heyrovsky Institute of Physical Chemistry)
- Roma da Costa (Universidade Federal do Espírito Santo)
- Paulo Limao-Vieira (Universidade Nova de Lisboa)
- Dragana Maric (Institute of Physics Belgrade)
- Sylwia Ptasinska (University of Notre Dame)
- Petra Swiderek (University of Bremen)
- Hajime Tanuma (Tokyo Metropolitan University)
- Ronald D. White (James Cook University)

## ORGANIZERS



Serbian Academy of  
Sciences and Arts



Institute of Physics  
University of Belgrade



PanaComp Wonderland  
Travel

- Home >
- About XLIC >
- Committee >
- News >
- Deadlines >
  
- Topics & Program >
- Invited Lectures >
- List of Participants >
- Registration >
- Abstracts >
  
- Meeting Venue >
- Travel Information >
- Social program >
- Partners >
  
- Contact >
- Links >
- XLIC WG2 1st Meeting >
- Meeting Poster >

#### COMMITTEE

##### Meeting chairs

Aleksandar Milosavljević (*Institute of Physics Belgrade, University of Belgrade, Serbia*)

Paola Bolognesi (*CNR-Istituto di Struttura della Materia, Roma, Italy*)

##### Scientific Committee

Paola Bolognesi (*CNR-Istituto di Struttura della Materia, Roma, Italy*)

Alicja Domaracka (*CIMAP, Caen, France*)

Henning Zettergren (*Stockholm University, Stockholm, Sweden*)

Aleksandar Milosavljević (*IPB, Belgrade, Serbia*)

Manuel Alcamí (*Universidad Autónoma de Madrid, Departamento de Química, Spain*)

##### Local Organising Committee (IPB, Belgrade, Serbia)

Aleksandar Milosavljević

Nenad Simonović

Sanja Tošić (meeting secretary)

Andrej Bunjac

Miloš Ranković

Iva Bačić

Beatriz Martin, COST XLIC Local Science Manager

#### News

22.04.2015

The book of abstracts is available [HERE](#).

22.04.2015

The list of posters is available [HERE](#).

22.04.2015

The transfer list is available [HERE](#).

06.05.2015

Conference gallery uploaded.

#### Deadlines

Registration - 20th of March

Abstract submission - 12th of April



# 27<sup>th</sup> Summer School and International Symposium on the Physics of Ionized Gases

August 26 – 29, 2014, Belgrade, Serbia

[Home](#) >  
[About SPIG](#) >  
[Committees](#) >  
[News](#) >  
[Deadlines](#) >

[Topics & Program](#) >  
[Invited Lectures](#) >  
[Workshops](#) >  
[Registration](#) >  
[Papers](#) >

[Location](#) >  
[Travel Information](#) >  
[Accommodation](#) >  
[Social program](#) >  
[Sponsors](#) >  
[Links](#) >

[Contact](#) >

[First Announcement](#) >  
[Final Announcement](#) >  
[Conference Poster](#) >

[SPIG 2012 Homepage](#) >  
[SPIG 2010 Homepage](#) >  
[SPIG 2008 Homepage](#) >  
[SPIG 2006 Homepage](#) >

[Previous SPIG Lecturers](#) >

## SPIG SCIENTIFIC COMMITTEE

- Z. Mijatović (Chair), Serbia
- S. Buckman, Australia
- J. Burgdörfer, Austria
- M. Danezis, Greece
- Z. Donko, Hungary
- V. Guerra, Portugal
- M. Ivković, Serbia
- D. Jovanović, Serbia
- K. Lieb, Germany
- I. Mančev, Serbia
- D. Marić, Serbia
- N. J. Mason, UK
- A. R. Milosavljević, Serbia
- K. Mima, Japan
- Z. Mišković, Canada
- B. Obradović, Serbia
- G. Poparić, Serbia
- L. C. Popović, Serbia
- Z. Rakočević, Serbia
- Y. Serruys, France
- N. Simonović, Serbia
- M. Škorić, Japan
- M. Trtica, Serbia

## SPIG 2014 ORGANIZING COMMITTEE

Institute of Physics Belgrade

- D. Marić (Co-chair)
- A. R. Milosavljević (Co-chair)
- S. D. Tošić (Co-Secretary)
- N. Škoro (Co-Secretary)
- Z. Lj. Petrović
- B. P. Marinković
- M. Cvejić
- J. Sivoš
- K. Spasić
- M. Ranković

Serbian Academy of Sciences and Arts

- M. Ivanović

## SPIG ADVISORY COMMITTEE

- D. Belić
- N. Bibić
- M. S. Dimitrijević
- S. Đurović
- N. Konjević
- J. Labat
- B. P. Marinković
- M. Milosavljević
- Z. Lj. Petrović
- J. Purić
- B. Stanić

## News

**Jun 26 2015**  
[SPIG-central website started](#)

**Dec 23 2014**  
[Papers of Invited Lectures - JPCS](#)

**Sep 02 2014**  
[SPIG 2014 Poster prize](#)

**Sep 02 2014**  
[Photos from SPIG 2014](#)

## Deadlines

**Sep 15 2014**  
Full papers of Invited lectures

## Meetings

**August 28 2014**  
[COST Celina WG1 Meeting](#)

Follow us!



Serbian Academy of  
Sciences and Arts





## 5<sup>th</sup> Conference on Elementary Processes in Atomic Systems

Belgrade, Serbia, June 21 - 25, 2011

Committees



- Home >
- Conference History >
- News >
- Important Dates >
  
- Topics & Program >
- Committees >
- Registration >
- Papers >
  
- Conference Site >
- Accommodation >
- Social program & Photos >
- Sponsors >
  
- Contact >
  
- Satellite meeting CEAMPP >

### CEPAS 2011 International Advisory Board:

- Dr Bratislav Marinkovic, Institute of Physics, University of Belgrade (IPB)  
<http://mail.ipb.ac.rs/~marinkov/>, [bratislav.marinkovic@ipb.ac.rs](mailto:bratislav.marinkovic@ipb.ac.rs)
- Prof. Dr Karoly Tokesi, MTA Atomki Debrecen  
[http://www.atomki.hu/index\\_en.html](http://www.atomki.hu/index_en.html), [tokesi@namafia.atomki.hu](mailto:tokesi@namafia.atomki.hu)
- Prof. Dr Zoran Lj. Petrovic, IPB and Serbian Academy of Sciences and Arts  
<http://mail.ipb.ac.rs/~cep/lje/Members/zpetrovic.htm>, [zoran@ipb.ac.rs](mailto:zoran@ipb.ac.rs)
- Prof. Mariusz Zubek, Gdansk University of Technology  
<http://www.mif.pg.gda.pl/kfze/staff/MZubek/MZubek.html>, [mazub@mif.pg.gda.pl](mailto:mazub@mif.pg.gda.pl)
- Prof. Dr Jiri Horacek, Charles University, Prague  
<http://utf.mff.cuni.cz/en/info/people/horacek.html>, [jho@matfyz.cz](mailto:jho@matfyz.cz)
- Prof. Dr Gustavo Garcia Gomez-Tejedor, Instituto de Fisica Fundamental, CSIC Madrid  
<http://www.iff.csic.es/fama/personas/gustavo/gustavo.html>, [g.garcia@iff.csic.es](mailto:g.garcia@iff.csic.es)
- Prof. Dr Joachim Burgdörfer, Vienna University of Technology (TU Wien)  
<http://dollywood.itp.tuwien.ac.at/index.html>, [burg@concord.itp.tuwien.ac.at](mailto:burg@concord.itp.tuwien.ac.at)
- Prof. John A. Tanis, Western Michigan University  
<http://homepages.wmich.edu/~tanis/>, [john.tanis@wmich.edu](mailto:john.tanis@wmich.edu)
- Prof. Dr Friedrich Aumayr, Vienna University of Technology (TU Wien)  
<http://www.iap.tuwien.ac.at/www/atomic/group/aumayr/index>, [aumayr@iap.tuwien.ac.at](mailto:aumayr@iap.tuwien.ac.at)
- Prof. Robert DuBois, University of Missouri-Rolla  
<http://campus.mst.edu/physics/courses/conf/dubois.html>, [dubois@mst.edu](mailto:dubois@mst.edu)
- Prof. Dr Andrey Solov'yov, Frankfurt Institute for Advanced Studies, Goethe University  
<http://fias.uni-frankfurt.de/mfn/index.php/pages/soll>, [solovvov@fias.uni-frankfurt.de](mailto:solovvov@fias.uni-frankfurt.de)
- Prof. Ladislau Nagy, Facultatea de Fizica, Universitatea Babeş-Bolyai  
<http://phys.ubbcluj.ro/~lnagy/>, [lnagy@phys.ubbcluj.ro](mailto:lnagy@phys.ubbcluj.ro)
- Dr Viorica Stancalie, Department of Lasers at National Institute for Laser, Plasma and Radiation Physics  
<http://atomic.inflor.ro/>, [viorica.stancalie@inflor.ro](mailto:viorica.stancalie@inflor.ro)
- Prof. Dr Nigel J. Mason, OBE, The Open University, United Kingdom  
[n.j.mason@open.ac.uk](mailto:n.j.mason@open.ac.uk)
- Prof. Dr Otto B. Shpenik, Institute of Electron Physics, National Academy of Sciences Ukraine  
[oshpenik@gmail.com](mailto:oshpenik@gmail.com)

### CEPAS 2011 Organizing Committee:

- Dr Bratislav Marinkovic, Chair  
<http://mail.ipb.ac.rs/~marinkov/>, [bratislav.marinkovic@ipb.ac.rs](mailto:bratislav.marinkovic@ipb.ac.rs)
- Dr Aleksandar Milosavljevic, Secretary  
<http://mail.ipb.ac.rs/~vrzaj/>, [vrzaj@ipb.ac.rs](mailto:vrzaj@ipb.ac.rs)
- Dr Nenad Simonovic  
[nenad.simonovic@ipb.ac.rs](mailto:nenad.simonovic@ipb.ac.rs)
- Dr Sasa Dujko  
[sasa.dujko@ipb.ac.rs](mailto:sasa.dujko@ipb.ac.rs)
- Mr Nikola Skoro  
[nikola.skoro@ipb.ac.rs](mailto:nikola.skoro@ipb.ac.rs)
- Ms Sanja Tosic  
[seka@ipb.ac.rs](mailto:seka@ipb.ac.rs)
- Ms Maja Rabasovic  
[majao@ipb.ac.rs](mailto:majao@ipb.ac.rs)
- Ms Jelena Maljkovic  
[jelena.maljkovic@ipb.ac.rs](mailto:jelena.maljkovic@ipb.ac.rs)
- Mr Dalibor Radosavljevic
- Mr Branko Petrusovski